The techno-economic stakes associated to the integration of renewables into electric systems

Pierre Cayet

Université Paris Nanterre

200 av. de la République
92001 Nanterre Cedex
www.parisnanterre.fr

École doctorale 396 : Économie, organisation, société
EconomiX

Membre de l'université Paris Lumières

Pierre CAYET

The techno-economic stakes associated to the integration of renewables into electric systems

Thèse présentée et soutenue publiquement le 17/12/2021
en vue de l'obtention du doctorat de Sciences économiques de l'Université Paris Nanterre
sous la direction de M. Lionel RAGOT (Université Paris Nanterre)
et de M. Arash FARNOOSH (codirecteur)

Jury * :

Rapporteur·e :	Mme Katheline SCHUBERT	Professeur, Paris School of Economics
Rapporteur·e :	Mr Gilles LAFFORGUE	Professeur, Toulouse Business School
Membre du jury :	Mr Marc BAUDRY	Professeur, Université Paris Nanterre
Membre du jury :	Mr Ramteen SIOSHANSI	Professeur, The Ohio State University
Directeur de thèse :	Mr Lionel RAGOT	Professeur, Université Paris Nanterre
Codirecteur :	Mr Arash FARNOOSH	Professeur, IFP School

* *Vous pouvez rajouter ou enlever des lignes au tableau, ou modifier les fonctions (remplacer Membre du jury par Rapporteur·e par exemple). N'oubliez pas de supprimer ces deux lignes de texte à la fin de votre rédaction.*

Cette thèse a été conjointement réalisée :

- Au laboratoire EconomiX – UMR 7235, à l'Université Paris Nanterre
- Dans le cadre de la Chaire « Economie de l'Electricité et de la Transition Digitale » à l'IFP School

Remerciements

J’ai eu la chance d’être particulièrement bien entouré et soutenu au cours de cette thèse, alors je ne me risquerai pas à essayer de remercier individuellement chacune des personnes qui ont fait de ce long voyage une expérience si enrichissante.

Je tiens à remercier tout particulièrement mes directeurs de thèse, Lionel Ragot et Arash Farnoosh, pour leurs commentaires et réflexions toujours pertinentes, ainsi que pour la confiance et la grande liberté intellectuelle qu’ils m’ont accordées tout au long de ce travail. Je remercie tout spécialement Frédéric Lantz, pour avoir été toujours disponible à chacune de mes interrogations, ainsi que pour nos longs échanges pleins de créativité mathématique et algorithmique. Je remercie également Patrick Criqui et Nadia Maïzi pour leurs remarques pertinentes et constructives lors de ma présentation de mi-thèse.

Je remercie chaleureusement l’ensemble des membres du jury, pour le temps consacré à ce travail qui constitue littéralement un chapitre de ma vie.

Je remercie aussi sincèrement mes collègues et amis de l’IFPEN, de l’IFP School et du Centre Economie et Management de l’Energie, pour leur bonne humeur et leur bienveillance constante, ainsi que l’équipe des secrétaires, toujours prêtes à m’aider lorsque j’en ai eu besoin. Merci également à la direction Economie et Veille pour avoir contribué à nourrir mes réflexions et améliorer ce travail.

Enfin, je tiens à remercier ma famille et Sandrine, ma relectrice la plus attentive, sans lesquels tout le temps et les efforts consacrés à cette aventure n’auraient eu guère de sens.

Contents

Résumé en français ……...…… **1**

Glossary ……..…….…….…… **13**

Introduction …….……. **15**

Chapter I – A robust structural model of the electric system with significant share of renewables under auto-correlated residual demand ……..……..... **23**

1. Introduction ……...…….……. 24
2. Formulation of the structural model of the electricity system ..…….. 25
3. Dynamic robust reformulation of the optimization model …….....….. 29
4. Application to the case of Auvergne-Rhône-Alpes …….……..... 40
5. Conclusion …….……...….. 63
6. Appendix …….…… 65
7. Bibliography …….……...…… 73

Chapter II- Optimization of electricity mix with high penetration of renewables: A robust methodology derived from Bayesian inference and graph theory …….…….…..… **75**

1. Introduction ……...…….……. 76
2. Definition of the "(ϵ, M) certainty set" …….……..…… 78
3. Definition of a path generation algorithm for constructing the set of worst-case trajectories …….…..…….……...…. 88
4. Application to the case of Auvergne-Rhône-Alpes ……..……...…… 92
5. Conclusion …….……...…… 108
6. Appendix …….…..... 110

7. Bibliography ……..……..... 125

Chapter III- Exploring the paradoxes of the French energy transition and nuclear policy: A techno-economic analysis ……..... **129**

1. Introduction ……..……. 130
2. Methodology ……..... 133
3. Optimal capacity mix and cost analysis ……..... 147
4. Comparative analysis of operational performances …….. 169
5. Conclusion and policy implications……...…. 212
6. Appendix ……...… 213
7. Bibliography …….. 229

Chapter IV- Towards future electricity market designs: Ensuring cost-effectiveness and efficiency under significant RES penetration ……...… **233**

1. Introduction ……... 234
2. Market remuneration analysis under marginal-cost bidding ……. 236
3. Alternative price-formation mechanisms for adequate resource and scarcity pricing ……..…….. 257
4. Alternative off-market compensation mechanisms ……..... 277
5. Conclusion and policy implications ……..... 288
6. Appendix ……...… 290
7. Bibliography …….. 299

Résumé en français

Introduction

La récente Loi pour la Transition Energétique et la Croissance Verte (LTECV) de 2015 a introduit un nouvel outil de pilotage de la politique énergétique française, appelé Programmation Pluriannuelle de l'Energie (PPE). Celle-ci exprime les grandes orientations et les priorités des pouvoirs publics en matière de technologies et d'investissements afin de décarboner l'ensemble des secteurs d'activité. Elle s'inscrit dans le cadre du Paquet Européen Energie-Climat 2030, lequel impose aux Etats membres un objectif de 20% d'énergies renouvelables (ENR) dans la consommation finale en 2020, et 27% en 2030.

À la suite de la catastrophe de Fukushima et afin de diversifier le mix électrique nationale, la sortie partielle du nucléaire est devenue un enjeu de taille de la transition énergétique française, avec une place à part dans la PPE. Plus précisément, cette dernière a fixé l'objectif de ramener la part du nucléaire dans la production totale d'électricité à 50% d'ici 2035. Deux scénarios proposés par RTE ont été retenus dans la PPE de 2017 (voir [1]), à savoir les scénarios « Volt » et « Ampère ». Le scénario « Volt » préconise un fort développement des investissements dans les ENR (116 GWe en 2035), ainsi qu'une sortie modérée du nucléaire avec la fermeture de seulement 9 réacteurs de 900 MWe, celle-ci étant conditionnée par les perspectives d'exportations. Le scénario « Ampère » soumet explicitement la sortie du nucléaire au rythme des investissements dans les ENR. La décision de fermer une centrale ne sera ainsi prise que si la perte de production de l'unité mise hors service peut être compensée, en moyenne, par la production des nouvelles capacités renouvelables. Bien qu'aucun besoin d'investissements dans des centrales thermiques de pointe ne soit identifié, l'équilibre du système électrique dans le scénario « Ampère » requiert des capacités d'interconnexion croissantes avec les voisins européens, ainsi qu'un fort développement de la gestion active de la demande et de l'efficacité énergétique.

La transformation du secteur électrique, associée au développement des énergies renouvelables (ENR), soulève de nombreux défis économiques, techniques, politiques et sociaux. En effet, le système électrique doit assurer en permanence l'équilibre en l'offre et la

demande, or le caractère intermittent de la production d'électricité renouvelables, tributaire des conditions météorologiques, requiert une flexibilité croissante de la part du système et des moyens de production conventionnels (thermiques et hydraulique), qui doit accompagnée par un investissement massif dans les technologies de stockage.

Contrairement aux centrales électriques classiques, la production des ENR est non pilotable et intermittente. Cette absence de « pilotabilité » nécessite des unités de production flexibles en back-up et éventuellement l'utilisation du stockage pour assurer la stabilité du réseau. Les conditions météorologiques deviennent un facteur déterminant du volume et de la dynamique de la production d'électricité. La demande résiduelle (DR), qui correspond à la différence entre la consommation d'électricité et la production des ENR, est la mesure pertinente à prendre en compte pour évaluer l'impact de la pénétration des ENR sur les besoins de flexibilité des centrales pilotables. L'augmentation des capacités ENR est généralement associée à une plus grande volatilité de la DR. Une modélisation correcte de ses dynamiques est donc essentielle pour estimer correctement les besoins en flexibilité du futur système électrique. La flexibilité étant liée à la gestion des variations de la DR, des méthodes formelles de modélisation de ses trajectoires sont nécessaires pour définir la combinaison d'investissements optimale tant sur le plan économique que technique. L'élaboration d'un ensemble de trajectoires de DR correspondant aux pires des cas, notamment les plus volatiles et chaotiques, est essentielle pour garantir des niveaux de fiabilité et de sécurité du système élevés en cas de forte pénétration des ENR. À court terme, les centrales conventionnelles ayant des rampes de puissance faibles et des niveaux de production minimum élevés pourraient être incapables d'adapter leur production aux fluctuations rapides de la DR. On s'attend à ce que les batteries et les véhicules électriques (VE) jouent un rôle important dans la gestion des ENR et la flexibilité du système, en stockant l'excédent de production des ENR durant les périodes de faible demande et en le restituant pendant les périodes de pointe de consommation. Bien que leurs coûts actuels empêchent pour l'instant un déploiement à grande échelle, ces technologies devraient générer une valeur ajoutée importante provenant d'une large gamme de services auxiliaires avec des externalités positives, qui doivent être prises en compte dans leur tarification (voir [2]-[3]).

La problématique des centrales nucléaires joue un rôle unique dans la transition énergétique française. Tandis que la part du nucléaire dans la production électrique n'était que de 8% en 1973, les chocs pétroliers des années 1970 ont considérablement accéléré le programme électronucléaire français, basé sur la technologie des réacteurs à eau pressurisée

(REP). Suivant le Plan Mesmer, le premier REP est raccordé au réseau à Fessenheim, en avril 1977. Correspondant à une puissance installée totale de 55 GWe, 54 réacteurs nucléaires supplémentaires sont construits entre la fin des années 1970 et le début des années 1990, pour un coût de construction estimé à 65 milliards d'euros (en euros courants de 2012, voir [4]). Bien que critiqué pour les risques d'accidents majeurs et le problème des déchets nucléaires, le nucléaire pourrait jouer un rôle central dans l'atténuation du changement climatique (voir [5]). L'électricité d'origine nucléaire n'est pas émettrice de CO_2 et pourrait donc s'inscrire dans le futur mix électrique aux côtés des ENR. Par ailleurs, [6] estime que les coûts de remplacement des réacteurs déclassés par des technologies alternatives pourraient être extrêmement élevés, surtout si les ENR sont le principal substitut. Enfin, en raison du faible coût variable du nucléaire, [7] estime que son abandon progressif pourrait plus que quadrupler les coûts totaux de production d'électricité, ainsi que faire augmenter les émissions de CO_2. Repousser la fermeture de certaines centrales pourrait enfin permettre de gagner du temps, afin de permettre l'émergence et la maturation de technologies alternatives (hydrogène, fusion nucléaire), ainsi que la diminution des coûts d'investissements des ENR. Toutefois, cette stratégie pourrait aggraver le risque d' « effet falaise », correspondant à l'effondrement de la capacité de production d'électricité après la fermeture rapide de plusieurs réacteurs nucléaires, avec des risques potentiellement élevés de rupture d'approvisionnement électrique.

Par ailleurs, l'essentiel des coûts des énergies renouvelables étant fixes et leurs coûts marginaux quasiment nuls, l'introduction de capacités ENR a tendance à faire baisser le prix de l'électricité sur le marché spot, ce qui menace à la fois la rentabilité des centrales conventionnelles, nécessaires à l'équilibre de marché lorsque la production ENR est insuffisante, mais aussi celle des ENR en créant paradoxalement les conditions contraires à leur propre rentabilité. Selon le design actuel des marchés de gros de l'électricité (de type EPEX SPOT), les offres de production sont soumises au gestionnaire de réseau de transport (GRT, correspondant à RTE en France), qui les classe par ordre croissant sur la base de leurs coûts marginaux selon la règle dite du « merit order ». Le prix spot se trouve à l'intersection des courbes d'offre et de demande, et correspond en théorie au coût marginal de la dernière unité de production appelée par le GRT. Comme les ENR ont un coût de production quasi nul, elles sont appelées les premières et elles contribuent ainsi à faire baisser le prix spot en poussant hors du marché les centrales de pointe plus coûteuses. Ce phénomène, connu sous le nom de « merit order effect » (voir [8]), nuit à la viabilité financière à long terme de l'ensemble des unités de production, y compris les ENR. Par un effet d'« auto

cannibalisation » [9], celles-ci contribuent à décourager les investissements nécessaires à leur propre expansion. Il est donc nécessaire de mettre en place des mécanismes de soutien hors-marché, tels que le FiT et le FiP, afin de de rémunérer correctement les ENR et inciter les futurs investisseurs. Ces mécanismes génèrent toutefois une charge budgétaire importante (5.5 milliards d'euros en France en 2018[1]), et laissent de côté la question du déficit structurel des centrales électriques conventionnelles.

Ce problème, connu sous le nom de « Missing Money » (voir [10]), n'est toutefois pas causé mais seulement aggravé par la pénétration croissante des ENR. Le design du marché spot ne permettant pas aux prix de dépasser un seuil légalement fixé (égal à 3000 €/MWh sur la bourse EPEX SPOT et pris pour référence dans cette thèse), la rente de rareté nécessaire pour couvrir les coûts opérationnels et variables de certains producteurs n'est pas intégrée dans le prix. Adapter le design du marché afin d'accroitre l'efficacité du signal prix est donc une direction prometteuse (voir [11]), notamment par la tarification en temps réel de la disponibilité et de la rareté (dans les situations où les capacités de production sont insuffisantes pour garantir une sécurité d'approvisionnement élevée) des ressources. Les ENR déplaçant la valeur de l'électricité de la production d'énergie vers les services de réserve et services auxiliaires, valoriser en temps réel les besoins en réserves pourrait également contribuer à restaurer l'efficacité du signal prix. Une adaptation des règles institutionnelle du marché spot semble donc nécessaire pour capturer les bénéfices économiques des technologies ENR (voir [12]), mais aussi corriger les défauts des marchés spot tel qu'ils existent actuellement en France et en Europe.

Ce travail de thèse est divisé en quatre chapitres, qui peuvent se lire de manière indépendante. Toutefois, les méthodes et modèles présentés dans les deux premiers chapitres constituent la base formelle requise pour comprendre les modèles d'investissement et de dispatching utilisés tout au long de ce travail. En raison de la complexité informatique des modèles ainsi que du temps nécessaire à leur résolution, les analyses empiriques et applications fournies dans ce travail sont circonscrites à la région Auvergne-Rhône-Alpes, choisie pour sa représentativité du mix national.

Les chapitres I et II adoptent une structure très similaire, avec d'abord la présentation théorique d'une méthode originale puis son application dans un second temps. Celles-ci permettent de modéliser les dynamiques de DR et déterminer les pires trajectoires (entendues

[1] Commission de la Régulation de l'Energie (CRE), 2018

comme succession de valeurs d'un processus aléatoire) possibles, afin de déterminer les besoins en capacité de production et en flexibilité permettant de garantir un niveau de fiabilité et de stabilité maximal du futur système électrique, pour différents niveaux de pénétration ENR. Chacune des méthodologies est appliqué à un modèle d'optimisation du système électrique, intégrant les contraintes thermiques et les contraintes de stockage de chaque unité de production. L'emploi d'un cadre identique, dans l'application des méthodes introduites dans chaque chapitre, permet une comparaison fine des avantages et inconvénients associés à chacune d'entre elles.

Le chapitre III s'intéresse aux paradoxes et contradictions inhérentes à la transition énergétique et la politique nucléaire française. On note que la totalité de la littérature étudiant la sortie du nucléaire ainsi que la pénétration des ENR s'appuie sur la constitution de scénarios, dans lesquels les décisions d'investissement sont fixées et exogènes. Utilisant une version améliorée du modèle d'investissement et de dispatching présenté dans les premiers chapitres, la décision de fermer ou prolonger les centrales nucléaires de plus de 40 ans est modélisée de façon endogène, de même que le niveau d'investissement dans les ENR. Nos résultats viennent confirmer la grande majorité des analyses existantes, et suggèrent qu'aucune base économique (ni écologique) ne vient justifier la fermeture à court-terme de centrales nucléaires.

Enfin, le quatrième et dernier chapitre est consacré à l'analyse des futurs revenus des différents types de producteurs d'électricité, dans un mix avec une forte proportion d'ENR. Ceci permet d'étudier un ensemble de designs de marché et de mécanismes de rémunération originaux, et de voir comment ceux-ci transforment la distribution des prix spot et la rémunération associée aux différentes technologies de production présentes dans le mix.

Chapitre I - Un modèle d'optimisation structurel et robuste du système électrique avec autocorrélation de la demande résiduelle

Le premier chapitre s'intéresse tout d'abord à l'élaboration d'un modèle d'optimisation robuste intégrant l'ensemble des contraintes opérationnelles et thermiques des moyens de production conventionnels, ainsi que les contraintes associées aux différents moyens de stockage disponibles. La modélisation de ces contraintes au niveau des centrales permet d'analyser de façon détaillée et précise comment un mix de production donné peut

s'adapter à une demande résiduelle de plus en plus volatile. En effet, la formulation robuste du modèle permet de déterminer l'ensemble de décisions d'investissement, mais aussi de production (le dispatching), permettant de garantir à moindre coût la fiabilité et la stabilité du système électrique dans un ensemble de conditions extrêmes. Cette approche s'inscrit dans le cadre de l'optimisation robuste ([13]), qui cherche à résoudre un problème d'optimisation en prenant en compte l'incertitude relative aux paramètres du modèle. Plus précisément, l'optimisation robuste cherche à minimiser les coûts totaux qui peuvent être observé lorsqu'un ensemble de paramètres, lesquels prennent leurs valeurs dans un ensemble d'incertitude borné (voir [14]), prend les valeurs les plus élevées (ou les plus faibles) possibles. Cette approche garantit la faisabilité des contraintes associées au problème d'optimisation pour toutes les valeurs de paramètres dans l'ensemble d'incertitude.

Toutefois, l'incertitude associée aux paramètres du modèle a reçu un traitement essentiellement statique dans la littérature existante, à l'exception de [15] qui propose un ensemble d'incertitude dynamique pour un problème d'optimisation multi-période. En utilisant les méthodes de l'Analyse en Composantes Principales (ACP) et la régression polynomiale, ce chapitre propose une méthode d'approximation robuste des variations d'un processus aléatoire entre plusieurs périodes, conditionnellement aux valeurs qu'il peut prendre. Cette méthode est appliquée à la DR, laquelle correspond à un vecteur aléatoire avec trois composantes (la demande d'électricité, la production solaire et la production d'origine éolienne), et qui peut donc s'exprimer comme un processus aléatoire en trois dimensions. L'ACP permet ici de décorréler chacune des composantes de la DR et d'étudier séparément leurs dynamiques. Associé à une méthode de binning, la régression polynomiale permet d'estimer les quantiles associés à la distribution des variations de chaque composante, conditionnellement à son niveau. Un intervalle de prévision est également fourni pour les variations estimées, dont la précision peut être configurée en fonction de la qualité et de la structure de l'échantillon utilisé pour l'estimation. On peut ainsi définir une approximation continue des variations de la DR et l'inclure directement au modèle d'optimisation robuste. Ceci permet de définir un ensemble de trajectoires extrêmes de DR, telles que celle-ci prend la série de valeurs les plus élevées, les plus basses ou les plus variables possibles.

En appliquant cette méthode à la région Auvergne-Rhône-Alpes, les analyses suggèrent que la prise en compte de la variabilité de la DR dans le modèle d'optimisation augmente fortement le niveau optimal d'investissement dans les technologies de stockage et les centrales de pointe. Toutefois, bien que moins flexibles, les mix électriques dominés par le

nucléaire présentent systématiquement de meilleures performances en termes de coût de production moyen, tant dans des conditions d'opération extrêmes que normales. Ils sont également moins émetteurs de CO_2, mais présentent des coûts fixes très élevés, ce qui peut les rendre plus sensible à des prix spot faibles en cas de forte croissance des ENR. Enfin, les résultats obtenus suggèrent que, comme la pression sur les centrales nucléaires risque d'augmenter avec la croissance des ENR, un mix basé sur le nucléaire peut rapidement devenir trop coûteux et inefficace, même si les réacteurs sont utilisés dans une moindre mesure pour le suivi de charge.

Chapitre II - Optimisation du mix électrique dans le cas d'une forte pénétration des énergies renouvelables : Une méthode robuste basée sur l'inférence bayésienne et la théorie des graphes

La méthodologie introduite au chapitre I, bien que flexible et paramétrable, n'offre toutefois pas la garantie théorique que les trajectoires les plus volatiles, générées par le modèle théorique, correspondent effectivement à la séquence de valeurs de DR la plus variable qui soit possible. En d'autres termes, la première méthode proposée dans cette thèse propose un *extremum* conditionnel, ou encore local, mais ne garantit pas que les trajectoires trouvées constituent un *extremum* global[2]. Le chapitre II propose ainsi une approche complémentaire permettant de dépasser cette limite, mais est toutefois plus difficile à mettre en pratique à cause de besoins élevés en termes de données. Par ailleurs, il n'a pas été possible d'obtenir une reformulation du modèle d'optimisation intégrant cette méthode complémentaire, ce qui pourra faire l'objet de recherches futures.

Cette seconde méthode s'appuie sur les outils de l'inférence bayésienne, ainsi que de concepts de base issus de la théorie des graphes. En m'appuyant sur la terminologie de l'optimisation robuste, j'introduits le concept de « l'ensemble des certitudes », défini pour un processus aléatoire en référence à un couple de paramètres strictement positifs (ϵ, M), où ϵ est inférieur ou égal à 1. La construction de cet ensemble requiert tout d'abord l'ajustement des données à un modèle théorique (multivarié), par l'utilisation d'outils issus des statistiques

[2] L'usage du terme *extremum* est justifié par le fait qu'une séquence de points (ici, la valeur de la RD à chaque pas de temps) n'est rien d'autre qu'un unique point dans un espace multidimensionnel.

bayésiennes. Du fait de la complexité de l'approche développée et de la difficulté computationnelle liée à son implémentation, une version simplifiée en est présentée pour faciliter sa compréhension. Le modèle estimé est ensuite utilisé pour déterminer, pour M observations du processus aléatoire modélisé, le sous-ensemble des trajectoires ayant une probabilité supérieure ou égale à $1 - \epsilon$ d'être observées au moins une fois.

Ensuite, un opérateur mathématique original, nommé « opérateur de chemin », est introduit. Il permet d'écrire de manière rigoureuse, sous forme matricielle, l'ensemble des chemins discrets possibles associés à plusieurs ensembles de sommets dans un graphe. Plus précisément, pour deux ensembles de sommets avec chacun K sommets, il permet de représenter les K^2 chemins possibles entre chaque paire de sommets issus des deux ensembles, ainsi que le poids associé à chaque arrête. Cet opérateur sert de base théorique à la conception d'un algorithme permet de trouver en temps polynomial le sous ensemble des trajectoires d'un processus aléatoire qui maximisent une fonction objectif donnée. Il offre également la garantie théorique que la trajectoire correspondant à l'optimum global est incluse dans ce sous-ensemble. Cet algorithme est appliqué à la DR, et permet de déterminer les trois trajectoires qui respectivement maximisent et minimisent globalement la somme des valeurs prises par le processus, mais aussi maximisent ses variations.

Enfin, cette seconde méthode est appliquée à un modèle d'optimisation de l'investissement et du dispatch, identique à celui présenté au Chapitre I, toujours dans le cas de la région Auvergne-Rhône-Alpes. Des résultats très similaires sont trouvés, bien que légèrement moins prudents concernant les besoins en flexibilité ainsi que la part des capacités de pointe, de type turbine à gas à cycle-combiné et thermique à flamme, nécessaires pour assurer l'équilibre en cas de forte pénétration des ENR.

Chapitre III – Les paradoxes de la transition énergétique et de la politique nucléaire françaises : une analyse technico-économique

Contrairement à la majorité des analyses, ce chapitre propose un modèle dans lequel les décisions relatives au niveau investissement dans les ENR et à la politique nucléaire sont définies de manière endogène. En effet, la littérature existante étudie généralement ces questions par la constitution des scénarios exogènes de sortie du nucléaire et de progression

des ENR dans le mix électrique. Une version améliorée du modèle d'optimisation introduit dans les chapitres précédents est construite, prenant en compte les capacités initiales déjà présentes dans le mix. On identifie ensuite un sous-ensemble des réacteurs nucléaires candidats pouvant être mis hors service. Les réacteurs sont contraints à être fermés par paires, chacune d'entre elles étant associé à une décision binaire : payer un ensemble d'investissements de maintenance pour prolonger la durée de vie des réacteurs, ou bien payer les coûts de déclassement et retirer les réacteurs du mix. Les conclusions obtenues confirment la plupart des résultats trouvés dans la littérature : une sortie rapide du nucléaire est susceptible d'augmenter de manière significative les coûts du système et les émissions de carbone. Aucune justification économique n'est trouvée pour la sortie immédiate du nucléaire, car le remplacement des réacteurs déclassés par des investissements dans les énergies renouvelables est toujours sous-optimal en termes de coûts totaux, même si les coûts de prolongation du nucléaire sont plus élevés que les estimations initiales ou si les coûts d'investissement et les coûts fixes des énergies renouvelables diminuent fortement. Le remplacement des réacteurs nucléaires par un ensemble de turbines à gaz à cycle combiné (CCGT) est économiquement optimal mais incompatible avec l'objectif de réduction des émissions de CO_2. Ce chapitre fournit également une analyse approfondie des performances opérationnelles de divers types de mix électriques dans des conditions opérationnelles extrêmes et représentatives. Afin de rendre la comparaison la plus complète possible, 4 mix sont sélectionnés : 2 mix sans diminution des capacités nucléaires avec pénétration des ENR faible et modéré, et 2 mix avec diminution d'un quart de flotte nucléaire, avec également un niveau faible et modéré de capacité ENR. On constate que l'abandon partiel du nucléaire peut menacer la stabilité du système mais pourrait permettre de conserver le nucléaire comme principale technologie produisant en base en cas de forte pénétration des ENR. Les coûts d'exploitation et les émissions de carbone augmentent considérablement lorsqu'on remplace des réacteurs déclassés par des centrales à cycle combiné, même en ajoutant une part élevée d'ENR dans le mix électrique. La question de la gestion des déchets nucléaires et des conditions de sécurité suffisantes, en ce qui concerne les réacteurs prolongés, n'entre toutefois pas dans le cadre de cette analyse.

Chapitre IV – Vers de nouveaux designs des marchés de l'électricité : assurer l'efficacité et la rentabilité des producteurs en cas de forte pénétration des ENR

Ce quatrième et dernier chapitre propose une analyse détaillée des futurs revenus, en cas de pénétration importante des ENR, perçus par les différentes technologies de production disponibles dans le mix français. L'introduction d'outils méthodologiques originaux permet d'étudier la structure des distributions jointes optimales de production et de prix spot, spécifiques à chaque technologie, qui seraient nécessaires pour la couverture totale des coûts fixes et variables annuels. Cela fournit une base pour analyser plusieurs propositions de réforme et designs originaux du marché spot, et la façon dont ils peuvent répondre aux problèmes actuels de rentabilité des producteurs mieux que le marché spot français. Plus précisément, il s'agit d'étudier comment la tarification de la rareté, comme dans [16], et un mécanisme d'enchères sur la base des coûts moyen pour les ENR (voir [17]), impactent le dispatching optimal, mais aussi la distribution des prix spot et la structure des revenus des producteurs. L'application de tels designs de marché peut toutefois contribuer à fortement désavantager les ENR et faire monter les prix à des niveaux politiquement inacceptables. Le modèle du Contract-for-Difference (CfD) est également étudié comme une alternative possible au FiP. Les résultats sont mitigés : les avantages du CfD dépendent de la corrélation de la production rémunérée par contrat et du prix spot. Enfin, en s'appuyant sur le concept d'"assureur en dernier ressort" proposé dans [18], ce chapitre se clôt par l'étude des prérequis théoriques et des outils nécessaires pour la mise en place d'un mécanisme assurantiel superposé au marché de gros, basé sur les préférences révélées par les consommateurs en matière de fiabilité et de stabilité du système électrique. Une mesure adéquate de la valeur attribuée à l'électricité par chaque consommateur pourrait être une étape nécessaire au bon fonctionnement futur des marchés de l'électricité. Inciter les individus à révéler leurs préférences en matière de fiabilité et de stabilité, par le biais de mécanismes de type assurantiels, pourrait à la fois contribuer à combler le fossé du "Missing Money" et rapprocher le coût de l'électricité payé par les consommateurs de leurs évaluations individuelles, améliorant ainsi l'équité dans le partage des coûts du système.

Références

[1] “Bilan Prévisionnel de l’équilibre offre-demande d’électricité en France”, RTE, Edition 2017, 44 p.

[2] FUCHS Georg, LUNZ Benedikt, LEUTHOLD Matthias, UWE SAUER Dirk, “Technology Overview on Electricity Storage”, Institut für Stromrichtertechnik und Elektrische Antriebe, June 2012

[3] BITAR Eilyan, KHARGONEKAR Pramod, POOLLA Kameshwar, “On the marginal value of electricity storage”, *Systems & Control Letters*, vol. 123, 2019, pp. 151-159

[4] “Les coûts de la filière électronucléaire”, Rapport Cour des Comptes, January 2012, 430 p.

[5] BOCCARD Nicolas, “The cost of nuclear electricity: France after Fukushima”, *Energy Policy*, vol. 66, 2014, pp. 450-461

[6] MALISCHEK Raimund & TRÜBY Johannes, “The future of nuclear power in France: an analysis of the costs of phasing-out”, *Energy*, vol. 116, 2016, pp. 908-921

[7] KOMIYAMA Ryoichi & FUJII Yasumasa, “Long-term scenario analysis of nuclear energy and variable renewables in Japan’s power generation mix considering flexible power resources”, *Energy Policy*, vol. 83, 2015, pp. 169-184

[8] SENSFUSS Frank, RAGWITZ Mario, GENOESE Massimo, “The merit-order effect: a detailed analysis of the spot price effect of renewable electricity generation on spot market prices in Germany”, Working Paper Sustainability and Innovation, n°7, 2007

[9] HIRTH Lion, “The market value of variables renewables: The effect of solar wind power variability on their relative price”, *Energy Economics*, vol. 38, 2013, pp. 218-236

[10] SHANKER R., “Comments on standard market design: resource adequacy requirements”, *FERC*, Docket RM-01-12-000, 2003

[11] PAPAVASILIOU Anthony, “Scarcity pricing and the missing European market for real-time reserve capacity”, *The Electricity Journal*, vol. 33, 2020

[12] NORTH Douglas, “Institutions”, *The Journal of Economic Perspectives*, vol. 5, n°1, 1991, pp. 97-112

[13] SOYSTER A.L., “Convex programming with set-inclusive constraints and applications to inexact linear programming”, *Operations Research*, vol. 21, 1973, pp. 1154-1157

[14] BABONNEAU F., VIAL J.-P., APPARIGLIATO R., “Robust Optimization for Environmental and Energy Planning” in *Uncertainty and Environmental Decision Making: A Handbook of Research and Best Practice*, 2009, pp.79-126

[15] LORCA Alvaro & SUN Xu Andy, “Adaptive Robust Optimization with Dynamic Uncertainty Sets for Multi-Period Economic Dispatch under Significant Wind”, *IEEE Transactions on Power Systems*, vol.30, n°4, 2015, pp.1702-1713

[16] HOGAN William H., “Electricity Scarcity Pricing Through Operating Reserves”, *Economics of Energy & Environmental Policy*, vol. 2, n°2, 2013

[17] DAMBRINE Fabrice, “Analyse micro-économique de l’intégration des EnR électriques intermittentes dans un système de production électrique”, *Responsabilité & Environnement*, Annales des Mines, n°93, 2019, pp. 7-14

[18] BILLIMORIA Farhad, POUDINEH Rahmatallah, “Decarbonized Market Design: An Insurance Overlay on Energy-Only Electricity Markets”, The Oxford Institute for Energy Studies, OEIS Paper: EL 30, 2018, 26 p.

Glossary

Definitions:

Baseload: The minimum level of load that a power supply system must serve over a given period.

Curtailment: The voluntary reduction of output below the maximum possible load factor of a wind or solar generation unit, in order to balance the electric system.

Electric load: The amount of power that is required by the electric system and must be supplied by generation units.

Electricity mix: The repartition of different energy sources in the total electricity generation fleet.

Load factor: A measure of the utilization rate, i.e. the instantaneous proportion of its nominal power that a generator uses when supplying electricity to the grid.

Residual demand: The difference between the electric load and the volume of electricity produced by renewable energy sources, i.e. photovoltaic and wind power units.

Spot market: A trading platform where generators and retailers (or, directly, electricity customers) submit orders for selling/buying power. The market operator matches supply and demand and determines the equilibrium spot price.

Spot price: The equilibrium price at which selling and buying bids for power are exchanged.

Abbreviations:

ARMA: Auto-Regressive Moving-Average

CfD : Contract-for-Difference

CCGT: Combined-Cycle Gas Turbine

RD: Residual demand

GT: (Oil-fired) Gas Turbine

FiT: Feed-in-Tariff

FiP: Feed-in-Premium

LOLP: Loss of Load Probability

LTECV: Loi Relative à la Transition Energétique pour la Croissance Verte du 17 août 2015

PPE : Programmation Pluriannuelle de l'Energie

RES: Renewable Energy Sources

VOLL: Value of Lost Load

Introduction

The recent French Law for the Energy Transition and Green Growth (LTECV, 2015) has introduced a new tool for steering the energy policy called Programmation Pluriannuelle de l'Energie (PPE). The PPE expresses the main orientations and priorities of public authorities in the management of energy sources in order to meet the energy policy targets set by the law. The PPE comes within the scope of the European Paquet Energie-Climat 2030, which sets for member states a target of 20% of renewable energy in the final consumption of 2020 and 27% in 2030. France proved even more ambitious as it enshrined in the LTECV targets corresponding to 23% and 32% for 2020 and 2030 respectively. In the wake of the Fukushima accident and to diversify the electricity mix, the partial phasing out of nuclear is also a central stake in the French energy transition. More precisely, the PPE has set the objective of bringing the share of nuclear to 50% of total electricity production by 2035. Two main scenarios have been retained in the PPE (see [1]), namely the "Volt" and the "Ampere" scenarios.

In essence, the energy transition of electric production systems can be described as the progressive replacement of existing power plants by new technologies using solely the potentially unlimited forces of the sun, wind, tides and gravity to produce electricity. Investment in new storage technologies, to complement renewable energy sources (RES), also plays a pivotal role. Conventional power plants indeed rely on exhaustible fossil fuels and reject carbon dioxide into the atmosphere, massively contributing to climate change. On the contrary, wind and solar plants produce at almost zero cost carbon-free electricity. This bright picture of renewables is however rapidly tarnished by several technical and economic issues linked to their very nature.

Contrary to conventional power plants, their production is non-dispatchable and intermittent. This lack of dispatchability requires flexible production units as back-up and possibly electricity storage to ensure the stability of the network. Weather becomes a prominent determinant of the volume and dynamics of electricity supply. Residual demand (RD), which corresponds to the difference between electricity consumption and RES

generation, is the relevant metric to consider when assessing the impact of RES penetration on flexibility requirements from dispatchable units. A higher RES capacity is usually associated with a higher RD volatility. A proper modelling of RD dynamics is thus pivotal to correctly estimate flexibility requirements of the future electric system. As flexibility pertains to the management of RD variations, formal methods for modeling the trajectories[3] of RD are necessary to define the optimal future generation mix. Deriving a set of worst-case RD trajectories, especially the most variable ones, is crucial for guaranteeing a higher level of system reliability under strong RES penetration. In the short-term, conventional plants with low ramping rates and high minimum production levels could be unable to adapt their production to quick residual demand fluctuations. Batteries and electric vehicles (EV) are also expected to play a significant role in storing RES and ensuring system flexibility, by storing RES production surplus in low-demand periods and releasing it in peak-demand periods. Though their current costs prevent large deployment for the moment, these technologies should generate significant value added from a large range of ancillary services with positive externalities, that should be taken into account in their pricing (see[2]-[3]).

Nuclear holds a specific place in the French energy transition, because of its dominant share in the electricity mix. While nuclear accounted for only 8% of the electricity production in 1973, the first petrol shock drastically accelerated the French electronuclear program based on Pressurized Water Reactors (PWR). Following the Mesmer Plan, the first PWR was connected to the grid at Fessenheim in April 1977. 54 additional reactors, corresponding to a cumulated power of 55 GWe, were built by 1990 for an estimated total construction cost of 65€ billion in 2012 euros (see [4]). In 2019 in France, 70.6% of electricity was produced by nuclear power plants. While it is pointed out for the risks of major accidents, such as in Fukushima, and the issue of nuclear waste management, [5] suggests nuclear may be a central player in climate change mitigation. A large body of literature also shows that the total costs of phasing out of nuclear and replacing decommissioned reactors by alternative technologies might be extremely costly, especially if RES are the main substitute technologies ([6]). As nuclear electricity has low variable costs, [7] show that nuclear phase out may significantly increase total system costs, in addition to CO_2 emissions. On the one hand, postponing nuclear phase out may allow for alternative technologies to emerge and RES sectors to decrease investment costs. Yet, on the other hand, it may worsen the "cliff effect", corresponding to the collapse of generation capacity following a rapid nuclear phase out, with potentially high risks

[3] Trajectories are throughout defined as a sequence of values for a random process.

for security of supply. The adequate timing of both nuclear phase out and RES capacity investment thus depends on a series of economic, ecological, and political factors regarding the risks and costs associated to available options.

Because of their capital-intensive nature (see [8]), RES have dire consequences on the functioning of the spot market and the determination of the spot price of electricity. Under the current market design, generation bids are submitted to the Transmission System Operator (TSO) and are ranked by increasing production cost to form a supply curve, based on the "merit order rule". The spot price is found at the intersection of the supply and demand curves, and thus corresponds to the marginal cost of the market clearing power plant. Yet, as renewable technologies have quasi-null costs of production, they are called first by the market operator and depress the spot price by pushing the more expensive production units out of the market. In the case of high penetration of renewables, this phenomenon, known as the "merit order effect" (see [9]), may harm the long-term financial viability of back-up units that remain necessary for periods with quasi null RES production. Moreover, by depressing spot prices, RES discourage investments required for their own expansion. This calls for off-market subsidy mechanisms (such as the Feed-in-Tariffs – FiT, Feed-in-Premiums – FiP) to properly remunerate RES, which generate high additional costs borne by electricity customers and taxpayers. However, considering the significant budgetary burden represented by RES (5.5€ billion in France in 2018[4]), adapting the market design to increase the efficiency of the price signal is a promising option. However, although RES penetration reduces the profitability of all power plants, the structural remuneration deficit of electricity generator, known as the "Missing Money" issue (see [10]), is not caused but only worsened by RES. As the wholesale market design does not allow prices to spike above a legal threshold, the rarity annuity required to cover fixed costs is not received by peaking generators. [11] identifies this issue as one of the major elements questioning the economic efficiency of liberalized electricity markets.

It can be argued that RES shift the value of the electricity market from energy to reserve and ancillary services, which requires adapting market design as exposed in [12]. Flexibility becomes a central element of the stability of future electric systems and needs to be rewarded as a system service. Following the guidelines from the European Commission expressed in [13], accurately pricing real-time resource availability and scarcity conditions

[4] Commission de Régulation de l'Energie (CRE), 2018

(corresponding to situations when the system is short on generation capacity), coupled with the introduction of a real-time market for reserve capacity, might help restoring the efficiency of short-term electricity markets. Institutional and market design adaptation is thus required to capture the economic benefits of RES technologies (see [14]) but also correct the flaws of the current wholesale French electricity market, which was originally designed for conventional dispatchable production units.

This thesis deals with several of the aspects mentioned above, from original methods for modeling RD dynamics in a robust optimization framework, to an in-depth investigation of the future remuneration issues of electricity generators under significant RES penetration and alternative market designs and subsidy mechanisms. Most of the work carried out in the thesis is both theoretical and empirical. It is divided into four chapters that can be read independently, although the methods presented in the first two chapters constitute the formal basis for understanding the investment and dispatching models used throughout this work. Because of the high computational complexity and resolution time of the models built in this thesis, the empirical analysis provided in this thesis focus on the French region Auvergne-Rhône-Alpes.

In the first chapter, I propose a robust structural model of the electric system incorporating the autocorrelation of RD. More precisely, my model is formulated as a robust Mixed Integer Linear Programming (MILP) model, integrating storage and commitment constraints at the individual plant level. Then, using Principal Component Analysis and polynomial approximation, I estimate the order statistics of the variations of RD between successive time periods, conditional on its level. This framework allows the estimation of a continuous approximation function, which shape and prevision interval can be tightly configured depending on the quality and structure of the training dataset. Moreover, we can directly include it to a dynamic robust optimization model. This allows defining a set of limiting, or "worst-case", residual demand trajectories. In an application to the case of Auvergne Rhône-Alpes, we show that hedging against trajectories with extremely high short-term variability globally increases the optimal storage and peaking capacities. Although they are less flexible, nuclear based electricity mixes consistently have better performance in terms of average generation costs and CO_2 emissions. However, our results suggest that, as the stress on nuclear plants may increase with renewable penetration, a nuclear-based mix may rapidly become too costly and inefficient for high renewable capacities.

In chapter II, I develop an original and complementary robust approach built from Bayesian inference methods and tools from graph theory. Using terminology from robust optimization (see [15]), I introduce the data-driven concept of "certainty set", which includes the set of paths of a random process that are observed with a probability superior to a given threshold over a limited number of trials. Then, using an original mathematical operator named the "path operator", I design a polynomial-time algorithm allowing me to find the trajectories, followed by a random process, which maximize globally a given objective function. Like in chapter I, I derive a subset of worst-case RD but with the theoretical guarantee that the trajectory maximizing the objective globally is included in the it. However, contrary to the method introduced in chapter I, this one has high data requirements and could not be directly reformulated to be included in an optimization model. Using the same empirical framework on Auvergne-Rhône-Alpes, I find similar results to chapter I, although slightly less conservative regarding flexibility and minimum peaking capacity requirements under strong RES penetration.

In the third chapter, I investigate the paradoxes of the French energy transition and nuclear policy, from an economic and technical perspective. RES investment and nuclear policy decisions are defined as endogenous variables, contrary to the existing literature which investigates exogenous nuclear and RES scenarios. Applying an enhanced version of the optimization model introduced in previous chapters, I select a subset of candidate nuclear reactors to be decommissioned by pairs. My findings confirm most results found in the literature: phasing out nuclear rapidly is likely to significantly increase both system costs and carbon emissions. No economic justification is found for the immediate phasing out of nuclear, as replacing decommissioned reactors by RES investment is always suboptimal in terms of total costs, even under higher nuclear prolongation costs or lower investment and fixed costs for renewables. Replacing nuclear reactors by combined-cycle gas turbines (CCGT) is economically optimal but incompatible with the objective of decreasing CO_2 emissions. I also provide a thorough analysis of the operational performances of various electricity mixes under both extreme and representative operational conditions. I find that partial nuclear phase out may threaten system stability but might allow to keep nuclear as the main 'baseload' technology under high RES penetration. The operational costs and carbon emissions drastically increase when replacing decommissioned reactors by CCGT plants, even when adding a high share of RES in the mix. The issues of nuclear waste management

and safety conditions, regarding prolonged reactors, are however outside of the scope of this chapter.

Finally, in the fourth and last chapter, I provide a detailed analysis of the future revenues of technologies available in the French mix under significant RES penetration. Then, I study the optimal joint production and spot prices distribution that would be required for each type of generator to cover its annual fixed and variable costs. This provides a basis for analyzing how some new market designs may better address these cost-effectiveness issues than the current French wholesale spot market. More precisely, I investigate how scarcity pricing, like in [16], and average cost bidding for RES (see [17]), impact the optimal dispatching, spot prices distribution and remuneration patterns of generators. As these designs, if not finely tuned, may fail to provide sufficient remuneration, or may require lengthy institutional transformations, I also investigate the Contract-for-Difference (CfD) as an alternative to the FiP. Finally, following the "insurer-of-last-resort" design proposed in [18], I also investigate theoretical grounds for an insurance overlay on the wholesale spot market based on customers' revealed preferences for reliability and system stability. Adequately measuring the value attributed to electricity by different customers might be a necessary step towards future well-functioning electricity markets. Incentivizing individuals to reveal their preferences for reliability and stability, through insurance-type mechanisms, may both help bridging the "Missing Money" gap and bring the electricity cost paid by customers closer to their individual valuations, thus improving equity in system cost-sharing.

References

[1] "Bilan Prévisionnel de l'équilibre offre-demande d'électricité en France", RTE, Edition 2017, 44 p.

[2] FUCHS Georg, LUNZ Benedikt, LEUTHOLD Matthias, UWE SAUER Dirk, "Technology Overview on Electricity Storage", Institut für Stromrichtertechnik und Elektrische Antriebe, June 2012

[3] BITAR Eilyan, KHARGONEKAR Pramod, POOLLA Kameshwar, "On the marginal value of electricity storage", *Systems & Control Letters*, vol. 123, 2019, pp. 151-159

[4] "Les coûts de la filière électronucléaire", Rapport Cour des Comptes, January 2012, 430 p.

[5] BOCCARD Nicolas, “The cost of nuclear electricity: France after Fukushima”, *Energy Policy*, vol. 66, 2014, pp. 450-461

[6] MALISCHEK Raimund & TRÜBY Johannes, “The future of nuclear power in France: an analysis of the costs of phasing-out”, *Energy*, vol. 116, 2016, pp. 908-921

[7] KOMIYAMA Ryoichi & FUJII Yasumasa, “Long-term scenario analysis of nuclear energy and variable renewables in Japan’s power generation mix considering flexible power resources”, *Energy Policy*, vol. 83, 2015, pp. 169-184

[8] HIRTH Lion & STECKEL Jan Christoph, “The role of capital costs in decarbonizing the electricity sector”, *Environmental Research Letters*, vol. 11, 2016

[9] SENSFUSS Frank, RAGWITZ Mario, GENOESE Massimo, “The merit-order effect: a detailed analysis of the spot price effect of renewable electricity generation on spot market prices in Germany”, Working Paper Sustainability and Innovation, n°7, 2007

[10] SHANKER R., “Comments on standard market design: resource adequacy requirements”, *FERC*, Docket RM-01-12-000, 2003

[11] JOSKOW P., “Lessons Learned from Electricity Market Liberalization”, *The Energy Journal*, Special Issue, 2008, pp. 9-42

[12] PAPAVASILIOU Anthony, “Scarcity pricing and the missing European market for real-time reserve capacity”, *The Electricity Journal*, vol. 33, 2020

[13] European Commission, 2020. Commission Opinion of 30/04/2020 Pursuant to Article 20 (5) of Regulation (EC) n°2019/943 on the Implementation Plan of Belgium. Brussels: European Commission

[14] NORTH Douglas, “Institutions”, *The Journal of Economic Perspectives*, vol. 5, n°1, 1991, pp. 97-112

[15] SOYSTER A.L., “Convex programming with set-inclusive constraints and applications to inexact linear programming”, *Operations Research*, vol. 21, 1973, pp. 1154-1157

[16] HOGAN William H., “Electricity Scarcity Pricing Through Operating Reserves”, *Economics of Energy & Environmental Policy*, vol. 2, n°2, 2013

[17] DAMBRINE Fabrice, “Analyse micro-économique de l’intégration des EnR électriques intermittentes dans un système de production électrique”, *Responsabilité & Environnement*, Annales des Mines, n°93, 2019, pp. 7-14

[18] BILLIMORIA Farhad, POUDINEH Rahmatallah, “Decarbonized Market Design: An Insurance Overlay on Energy-Only Electricity Markets”, The Oxford Institute for Energy Studies, OEIS Paper: EL 30, 2018, 26 p.

Chapter I:

A robust structural model of the electric system with significant share of intermittent renewables under auto-correlated residual demand

***Abstract* – In this paper, we propose a robust structural investment and dispatch model of electric systems, including commitment and storage constraints, with auto-correlated residual demand. We associate it to a novel approach to robust optimization focusing on uncertain parameter trajectories. Using Principal Component Analysis, we approximate conditional order statistics for the distribution of residual demand variations using parametric polynomial approximation. This flexible method allows us to derive a set of extreme trajectories maximizing the level and variability of residual demand. Finally, we apply our dynamic robust model to the electric system of the French region Auvergne Rhône-Alpes and discuss the implications in terms of investment decisions and cost performance.**

***Keywords* –** Optimal electricity mix; Robust optimization; Dynamic uncertainty; Renewable energy

1. Introduction

Robust optimization provides a natural modeling technique for quantifying uncertainties affecting future weather and electric systems. Increasing the penetration of renewables increases the volatility of residual demand [1], which in turns requires higher system flexibility through technical solutions including battery and electric vehicle storage, gas fired power plants, demand-side management (DSM) and curtailment [2]. As underlined by [3], reserves are increasingly used to cover fluctuations of power output as the share of renewables increase, which may require stochastic decision-making tools. In the absence of reliable probabilistic description of the joint distribution of residual demand at various point of time and locations in the grid, robust optimization provides a non-probabilistic tool allowing to minimize the dispatch and recourse cost under the worst-case realization of the uncertainty.

First introduced by [4], robust optimization provides a non-probabilistic formulation of uncertainty as in [5]. The uncertainty set, defined in the real space, corresponds to the set of values the uncertain parameters can take (see [6]-[7]). Recent developments introduce correlation between uncertain parameters (see [8]-[9]) and dynamic uncertainty sets for multi-period optimization problems (see [10]). For each time period, the value of the uncertain parameter determines the set of values included in the uncertainty set corresponding to the following period. Proposing a similar dynamic approach, our method allows us, like in [11], to model distributional asymmetries of the uncertain parameters. However, contrary to the traditional robust approach, our method does not explicitly require the definition of uncertainty sets.

First, we propose a robust structural model of the electric system including transmission, thermic constraints and storage with auto correlated and spatially cross-correlated residual demand parameters. Then, similarly to [12], we use Principal Component Analysis in order to capture correlations between residual demand parameters and create a decorrelated vector by projection along principal components. Then, we generate a set of bins for the training data and estimate the order statistics of the “differential” distribution of the decorrelated vector, defined as the conditional distribution of its first-difference, using a tailored parametric polynomial regression. Our method can be related to quantile regression and autoregressive models but allows greater flexibility in the usage of the training data when it is sparse. Section II presents the formulation of our structural electric system model. Our polynomial regression

method is described in Section III. Then, our model is applied in Section IV to the case of the French region Auvergne Rhône-Alpes, with interesting results regarding flexibility requirements for electricity mixes with strong renewable penetration, before concluding in Section V.

2. Formulation of the structural model of the electric system

Modern electric systems including renewable generation technologies can be broken down into a series of simple components: the electric load, renewable production units, dispatchable production units with thermal limits, storage units and a transmission network. For simplicity, we consider a single region and neglect transmission constraint in the following model.

2.1. Formulation of the model

The structural cost-minimization problem for an electricity generation system, neglecting spatial transfers and transmission network, can then be defined as follows:

$$\min_{\boldsymbol{U},\boldsymbol{q},\boldsymbol{\kappa},\boldsymbol{z}} \sum_{j>1} \left(A_j + c_j^{FOM}\right) U_j + \sum_g \left(A_g + c_g^{FOM}\right) D_g U_g + \left(A_e + c_e^{FOM}\right) U_e + \Theta\left(\sum_{s\in\mathcal{S}} \sum_{t\in\mathcal{T}} \left(\sum_g \left(c_g^V + \pi^{CO_2} E_g\right) q_{gst} + c_g^{STUP} z_{gst} + \sum_j c_j^{\kappa} \kappa_{jst}\right)\right) \quad (\mathbf{1})$$

Such that :

$$\overline{\xi_{1st}} + \widehat{\xi_{1st}}\eta_{1st} - \kappa_{1st} - \sum_{j>1} \left(\left(\overline{\xi_{jst}} + \widehat{\xi_{jst}}\eta_{jst}\right) U_j - \kappa_{jst}\right) - \sum_g q_{gst} + e_{st}^{+} - e_{st}^{-} \leq \gamma \quad (\mathbf{2})$$

$$-\overline{\xi_{1st}} - \widehat{\xi_{1st}}\eta_{1st} + \kappa_{1st} + \sum_{j>1} \left(\left(\overline{\xi_{jst}} + \widehat{\xi_{jst}}\eta_{jst}\right) U_j - \kappa_{jst}\right) + \sum_g q_{gst} - e_{st}^{+} + e_{st}^{-} \leq \gamma \quad (\mathbf{3})$$

$$u_{gst} - u_{gst-1} = z_{gst} - v_{gst} \quad ,\forall g \in \mathcal{G} \quad (\mathbf{4a})$$

$$z_{gst} + v_{gst} \leq 1 \quad ,\forall g \in \mathcal{G} \quad (\mathbf{4b})$$

$$\omega_{gst}^1 = q_{gst} - \omega_{gst}^2 \quad ,\forall g \in \mathcal{G} \quad (\mathbf{5})$$

$$\omega_{gst}^1 - \omega_{gst-1}^1 \leq \overline{r_g} \quad ,\forall g \in \mathcal{G} \quad (\mathbf{6a})$$

$$\omega^1_{gst-1} - \omega^1_{gst} \leq \underline{r_g} \qquad ,\forall g \in \mathcal{G} \ (\mathbf{6b})$$

$$\omega^1_{gst} \leq U_g D_g \left(\overline{q_g} - \underline{q_g}\right) \qquad ,\forall g \in \mathcal{G} \ (\mathbf{7a})$$

$$\omega^1_{gst} \leq u_{gst}\mathrm{K} \qquad ,\forall g \in \mathcal{G} \ (\mathbf{7b})$$

$$\omega^2_{gst} \leq U_g D_g \underline{q_g} \qquad ,\forall g \in \mathcal{G} \ (\mathbf{8})$$

$$\omega^2_{gst} = U_g D_g \underline{q_g} - \left(1 - u_{gst}\right)\mathrm{K} + s_{gst} \qquad ,\forall g \in \mathcal{G} \ (\mathbf{9})$$

$$s_{gst} \leq \left(1 - u_{gst}\right)\mathrm{K} - U_g D_g \underline{q_g} + u_{gst}\mathrm{K} \qquad ,\forall g \in \mathcal{G} \ (\mathbf{10})$$

$$u_{gst} \geq \sum_{t' > t - M_j^U} z_{gst} \qquad ,\forall g \in \mathcal{G} \ (\mathbf{11a})$$

$$1 - u_{gst} \geq \sum_{t' > t - M_j^D} v_{gst} \qquad ,\forall g \in \mathcal{G} \ (\mathbf{11b})$$

$$\kappa_{jst} \leq \left(\overline{\xi_{jst}} + \widehat{\xi_{jst}}\eta_{jst}\right)U_j \qquad ,\forall j \in \mathcal{J} \ (\mathbf{12})$$

$$e_{st} = e_{st-1} + \sqrt{\eta_e}e^+_{st} - \frac{e^-_{st}}{\sqrt{\eta_e}} \qquad (\mathbf{13})$$

$$e_{st} \leq \overline{e}U_e \qquad (\mathbf{14})$$

$$e_{st} \geq \underline{e}U_e \qquad (\mathbf{15})$$

$$e^+_{st} \leq l_{st}(\overline{e}U_e - e_{st}) \qquad (\mathbf{16})$$

$$e^-_{st} \leq (1 - l_{st})\left(e_{st} - \underline{e}U_e\right) \qquad (\mathbf{17})$$

$$u_{gst} \in \{0\ ,1\} \qquad ,\forall g \in \mathcal{G} \ (\mathbf{18})$$

$$v_{gst} \in \{0\ ,1\} \qquad ,\forall g \in \mathcal{G} \ (\mathbf{19})$$

$$z_{gst} \in \{0\ ,1\} \qquad ,\forall g \in \mathcal{G} \ (\mathbf{20})$$

$$l_{st} \in \{0\ ,1\} \qquad (\mathbf{21})$$

2.2. Description of the model

2.2.1. Indices and sets

We define the set $\mathcal{T}$ used to index hours of the week, with element $t \in \mathcal{T}$, and the set of seasons $\mathcal{S}$ with element $s \in \mathcal{S}$. We define the set of residual demand components $\mathcal{J}$, where the first element of $\mathcal{J}$ corresponds to the electric load and the remaining elements are available renewable technologies. Residual demand can be expressed as a linear combination of electric load and production from renewable generation units. The latter can be decomposed into subsets $\mathcal{W} \subset \mathcal{J}$ and $\mathcal{P} \subset \mathcal{J}$, which respectively denote wind and photovoltaic technologies.

The set of thermal generation units is noted $\mathcal{G}$, with unit $g \in \mathcal{G}$. The set $\mathcal{G}$ can be decomposed into the subsets of nuclear units $\mathcal{N} \subset \mathcal{G}$, combined cycle gas turbines (CCGT) $\mathcal{C}^1 \subset \mathcal{G}$, and gas turbines (GT) $\mathcal{C}^2 \subset \mathcal{G}$.

2.2.2. Investment variables and parameters

For each unit $g \in \mathcal{G}$, we define the binary building decision $U_g \in \{0; 1\}$. The parameter $D_g \geq 0$ corresponds to the "block" size of unit g, or equivalently, its nominal power. For simplicity, we assume D_g is equal for all units of the same technology. Each unit $g \in \mathcal{G}$ is characterized by minimum and maximum output levels $\underline{q_g} \geq 0$ and $\overline{q_g} \geq 0$, in addition to maximum ramp-up and ramp-down capacities $\overline{r_g} \geq 0$ and $\underline{r_g} \geq 0$. The commitment status of g is constrained by minimum uptime $M_g^U \geq 0$ and minimum downtime $M_g^D \geq 0$. Finally, each thermal generation unit is characterized by a ratio of CO_2 emissions per unit output E_g, expressed in ton per unit generated.

We define the investment level for $j \in \mathcal{J}$ as $U_j \geq 0$, with the convention that $U_1 = 1$, and note $\boldsymbol{U} = (U_i)_{1 \leq i \leq |\mathcal{J}|}$ the vector of installed capacities for residual demand components. We define the level of investment in storage as $U_e \geq 0$. We assume the variables U_j and U_e are continuous, while U_g is binary.

Renewable technologies, thermal generation technologies and storage respectively have annuitized unit investment costs A_j, A_g and A_e, with $A_j, A_g, A_e \geq 0$. Similarly, both renewable

and thermal generation technologies exhibit yearly fixed and operation maintenance (FOM) costs c_j^{FOM}, c_g^{FOM} and c_e^{FOM}, with $c_j^{FOM}, c_g^{FOM}, c_e^{FOM} \geq 0$.

2.2.3. Operational variables and parameters

For any season $s \in \mathcal{S}$ and hour $t \in \mathcal{T}$, we define the uncertain capacity factor $\xi_{jst} = \overline{\xi_{jst}} + \widehat{\xi_{jst}}\eta_{jst} \in \mathbb{R}^+$ for $j = 1$, and $\xi_{jst} = \overline{\xi_{jst}} + \widehat{\xi_{jst}}\eta_{jst} \in [0,1]$ for $j > 1$, with nominal or average value noted $\overline{\xi_{jst}}$ and standard deviation $\widehat{\xi_{jst}}$. The parameter η_{jst} follows a random variable with zero mean and standard deviation equal to one. The variable $\kappa_{jst} \geq 0$ is equal to volume of curtailed production for renewable technology $j \in \mathcal{J}$. Using this notation, κ_{1st} can naturally be interpreted as the volume of non-served load (VOLL).

We define the variable $q_{gst} \geq 0$, equal to the production of generation unit $g \in \mathcal{G}$. For any hour $t \in \mathcal{T}$ and season $s \in \mathcal{S}$, $\omega_{gst}^2 \geq 0$ corresponds to the minimum-production level of generator $g \in \mathcal{G}$, while $\omega_{gst}^1 \geq 0$ is an auxiliary variable equal to the generation volume above minimum-production level. We introduce the scalar $K \gg 0$ and define the slack variable $s_{gst} \geq 0$. u_{gst}, v_{gst} and z_{gst} are all binary variables respectively corresponding to the commitment state, start-up and shut-down decision of generator $g \in \mathcal{G}$.

The variable $e_{st} \geq 0$ corresponds to the stock of electricity stored in hour t and season s, while $e_{st}^+ \geq 0$ and $e_{st}^- \geq 0$ are flux variables respectively equal to the quantity of electricity stored and released. η_e is the round-trip efficiency of the battery storage technology, with $0 \leq \eta_e \leq 1$, such that $\sqrt{\eta_e}$ can be interpreted as the efficiency of charge or discharge. Finally, $\overline{e}$ and $\underline{e}$ respectively correspond to the maximum and minimum state of charge, and l_{st} corresponds to the charging state of storage devices, with l_{st} equal to one when batteries store electricity.

We respectively note $c_g^V \geq 0$ and $c_g^{STUP} \geq 0$ the variable and start-up costs of the unit $g \in \mathcal{G}$. We note $c_j^\kappa \geq 0$ the curtailment cost of renewable technology $j \in \mathcal{J}$, where c_1^κ corresponds to the Value of Lost Load (VOLL). Finally, we define the price of a carbon ton as $\pi^{CO_2} \geq 0$.

2.3. Description of the model equations

Each constraint must hold for each hour $t \in \mathcal{T}$ and season $s \in \mathcal{S}$. The expression in **(1)** corresponds to the sum of the annuitized investment costs of the electricity mix and short-term generation, start-up, load-shedding and curtailment costs. We introduce a scaling parameter Θ equal to the number of weeks per season, so the total variable costs are expressed on an annual basis. **(2)** and **(3)** correspond to the upper and lower limits of the primary frequency control constraint: net generation, which is the sum of electricity generation minus electric load and storage, must lie in the interval $[-\gamma, \gamma]$. We may further define $\gamma = \iota \Delta f$, where ι is proportional to the physical inertia of the electric system and Δf corresponds to the maximum feasible absolute deviation of frequency from its nominal value.

(4a) to **(11b)** together formalize, as a set of linear constraints, the commitment state, starting-up decisions and output limits for dispatchable generators. We combine the "big-M" method with the use of slack variables in order to linearize minimum generation level constraints[5]. **(12)** constrains the volume of electricity curtailed (respectively non-served load) to be inferior or equal to the generation of renewable technology $j \in \mathcal{J}$ (respectively inferior or equal to the electric load). Finally, **(13)** to **(17)** correspond to the power balance of the storage technology, with constraints on the state of charge lower and upper limits and upper bounds on electricity inflows and outflows, in addition to charging status.

3. Dynamic robust reformulation of the optimization model

For clarity of presentation, we drop the seasonal subscript s within Section III. For each t, we define the random vector $\boldsymbol{\eta}_t = (\eta_{1t}, \dots, \eta_{nt})^T \in \mathbb{R}^{(1\times n)}$, where n is the number of uncertain parameters. We set $n = |\mathcal{J}|$, so the first component of $\boldsymbol{\eta}_t$ corresponds to electric load. We assume that the random process $\{\boldsymbol{\eta}_t\}_{t\in\mathcal{T}}$ is (weakly) stationary. Using the variance-covariance matrix of $\boldsymbol{\eta}_t$, we compute its corresponding matrix of eigenvectors $\boldsymbol{\Phi}$ so that $\boldsymbol{\mu}_t = \boldsymbol{\Phi}^T \boldsymbol{\eta}_t$ has a diagonal variance-covariance matrix, ie has uncorrelated components.

[5] For K big enough, $\omega^1_{gst} \leq U_g D_g \left(\overline{q_g} - \underline{q_g}\right)$ if u_{gst} is equal to 1 and $\omega^1_{gst} \leq 0$ otherwise. Similarly, $\omega^2_{gst} = U_g D_g \underline{q_g} - (1 - u_{gst})\mathrm{K} + s_{gst}$ if u_{gst} is equal to 1 and $\omega^2_{gst} = 0$ otherwise. Indeed, if $u_{gst} = 0$, as ω^2_{gst} is positive by definition and $s_{gst} \leq \mathrm{K} - U_g D_g \underline{q_g}$, we necessarily have $s_{gst} = \mathrm{K} - U_g D_g \underline{q_g}$ so ω^2_{gst} is null. On the contrary, if $u_{gst} = 1$, we must have $s_{gst} = 0$ as s_{gst} is positive.

3.1. Decorrelation procedure of the autocorrelated vector and motivation for using polynomials

We start by defining the variance-covariance matrix of $\boldsymbol{\eta}_t$ as $\boldsymbol{\Sigma}_\eta \in \mathbb{R}^{n\times n}$. We define $\boldsymbol{\Lambda} \in \mathbb{R}^{n\times n}$ the matrix of its eigenvalues and $\boldsymbol{\Phi} \in \mathbb{R}^{n\times n}$ the corresponding matrix of eigenvectors. Then, using the orthogonality of $\boldsymbol{\Phi}$, we have $\boldsymbol{\Phi}^T = \boldsymbol{\Phi}^{-1}$ so that:

$$\boldsymbol{\Sigma}_\eta \boldsymbol{\Phi} = \boldsymbol{\Phi}\boldsymbol{\Lambda} \Leftrightarrow \boldsymbol{\Phi}^T\boldsymbol{\Sigma}_\eta\boldsymbol{\Phi} = \boldsymbol{\Phi}^T\boldsymbol{\Phi}\boldsymbol{\Lambda} = \boldsymbol{\Lambda} \in \mathbb{R}^{n\times n} \quad (\mathbf{22})$$

Our transformed random vector $\boldsymbol{\mu}_t = \boldsymbol{\Phi}^T\boldsymbol{\eta}_t$ has the following diagonal variance-covariance matrix, noted $\boldsymbol{\Sigma}_\mu$:

$$\boldsymbol{\Sigma}_\mu = \boldsymbol{\Phi}^T\boldsymbol{\Sigma}_\eta\boldsymbol{\Phi} = \boldsymbol{\Lambda} \in \mathbb{R}^{n\times n} \quad (\mathbf{23})$$

It is possible to show that for any lag value $p \in \mathbb{N}$, the autocovariance matrix of $\boldsymbol{\mu}_t$ of order p, noted $\boldsymbol{K}_p = \mathbb{E}(\boldsymbol{\mu}_t\boldsymbol{\mu}_{t-p})$ is diagonal. As $\boldsymbol{\Sigma}_\mu$ is diagonal, we have by construction $\mathrm{cov}(\mu_{it}, \mu_{jt}) = 0, \forall (i,j) \in [1,n]^2, i \neq j$. We start by assuming that $\mathrm{cov}(\mu_{it}, \mu_{i,t-p}) \neq 0$ and $\mathrm{cov}(\mu_{it}, \mu_{j,t-p}) \neq 0$. Then, there exists a couple $(\phi_{jj,p}, \phi_{ij,p}) \in (\mathbb{R}^*)^2$ such that:

$$\mu_{jt} = \phi_{jj,p}\mu_{j,t-p} + \varepsilon_{j,t-p} \quad (\mathbf{24a})$$

$$\mu_{it} = \phi_{ij,p}\mu_{j,t-p} + \varepsilon_{i,t-p} \quad (\mathbf{24b})$$

We can reformulate the above equations as follows:

$$\mu_{it} = \phi_{ij,p}\phi_{jj,p}^{-1}(\mu_{jt} - \varepsilon_{j,t-p}) + \varepsilon_{i,t-p} = \phi_{ij,p}\phi_{jj,p}^{-1}\mu_{jt} + \varepsilon'_{i,t-p} \quad (\mathbf{25})$$

Where $\varepsilon'_{i,t-p} = \varepsilon_{i,t-p} - \phi_{ij,p}\phi_{jj,p}^{-1}\varepsilon_{j,t-p}$. By assumption, $\phi_{ij,p}\phi_{jj,p}^{-1} \neq 0$ so $\mathrm{cov}(\mu_{it}, \mu_{jt}) \neq 0$. We reach a contradiction, so $\mathrm{cov}(\mu_{it}, \mu_{jt}) = 0 \Longrightarrow \mathrm{cov}(\mu_{it}, \mu_{j,t-p}) = 0$. There exists a diagonal matrix $\boldsymbol{\phi} = \mathrm{diag}(\phi_{ii})_{i\leq n} \in \mathbb{R}^{n\times n}$ and a vector $\boldsymbol{\epsilon}_{t-1} \in \mathbb{R}^{n\times 1}$ such that we have the following VAR(1) model:

$$\boldsymbol{\mu}_t = \boldsymbol{\phi}\boldsymbol{\mu}_{t-1} + \boldsymbol{\epsilon}_t \quad (\mathbf{26})$$

Using a similar VAR model, [10] build an adaptive uncertainty set where the random vector is equal to a linear combination of its previous values plus an error term, which is subjected to a budgeted uncertainty set.

As $\{\boldsymbol{\eta}_t\}_{t\in\mathcal{T}}$ is stationary by assumption, we further drop the subscript t. For all $i \leq n$, we define the real-valued random variables $\Delta\mu_i$ and μ_i. We call the distribution of $\Delta\mu_i$ the "differential" distribution of μ_i. We assume that their relationship is non-linear, which makes linear autoregressive models unfit as we would have $\mathbb{E}(\epsilon_{it}\epsilon_{it'}) \neq 0$ for $t \neq t'$. Non-linear autoregressive models using data mining algorithms such as ARMAX may provide superior forecasting performances, as shown in [13]. GARCH processes and non-linear ARMA-GARCH models might also be used to capture dynamic changes in the mean and volatility of the process when the variance of the error term changes over time (see [14] for a comprehensive evaluation).

We further assume the variance of $\Delta\mu_i$ is a (possibly non-linear) function of μ_i. Although the above-cited methods may be used to simulate a collection of trajectories for μ_i and identify a subset of extreme trajectories, such an approach may be cumbersome in practice. We propose a different approach where we estimate the bounds within which the uncertain random variable μ_i can vary between successive periods. For any value of $q \in [0,1]$, we seek to compute for any μ_i the value $\beta_q(\mu_i)$ that verifies:

$$\beta_q(\mu_i) = \inf_z \left\{z \in \mathbb{R} \middle| F_{\Delta\mu_i|\mu_i}(z) \geq q\right\} \tag{27}$$

$F_{\Delta\mu_i|\mu_i}(z) = \mathbb{P}(\Delta\mu_i \leq z|\mu_i)$ is the cumulative distribution function of the random variable $\Delta\mu_i|\mu_i$, corresponding to the distribution of $\Delta\mu_i$ conditional on μ_i. Thus, assuming μ_i is continuous, we can define a set of application φ_i^q, $0 \leq q \leq 1$, such that $\varphi_i^q(\mu_i)$ corresponds to the value of the q^{th} quantile of $\Delta\mu_i$ conditional on μ_i. Using polynomial regression, we can approximate the set of application φ_i^q, $0 \leq q \leq 1$ such that the polynomial $P_{n_i^q}(\mu_i)$ verifies:

$$P_{n_i^q}(\mu_i) = \underset{P\in\mathbb{R}_{n_i^q}[\mu_i]}{\arg\min} \left\|P - \varphi_i^q(\mu_i)\right\|_{\infty,[\inf\mu_i,\sup\mu_i]} \tag{28}$$

Then, there exists sets of real coefficients $\left(\mathfrak{a}_{in}^q\right)_{n\leq n_i^q}$ such that:

$$P_{n_i^q}(\mu_i) = \sum_{n=0}^{n_i^q} \mathfrak{a}_{in}^q \, \mu_i^n \tag{29}$$

3.2. Estimation of the polynomial approximation for the distribution of $\Delta\boldsymbol{\mu_i}$

We estimate the transformed random vector $\boldsymbol{\mu}_t$ and the set of parameters $\left(\mathfrak{a}_{in}^{q}\right)_{n\leq n_i^q}$ using a training sample S of size N, such that $S = \{(\boldsymbol{\eta}_m)_{1\leq m\leq N}\}$. In order to mitigate the expected sampling error for extreme values of $\Delta\mu_i$ conditional on μ_i, we cut the interval $[\inf\mu_i, \sup\mu_i]$ into $|\mathcal{B}_i|$ bins of equal length. For each bin $b_i \in \{1, \dots, |\mathcal{B}_i|\}$, we note N_{b_i} the number of observations included into the bin b_i, with $\sum_{b_i} N_{b_i} = N$. For any $m \in \{1, \dots, N_{b_i}\}$, $\Delta\mu_{im}^{b_i}$ corresponds to the m^{th} observation for the random variable $\Delta\mu_i$ within bin b_i. For any $q \in [0,1]$, we define the empirical q^{th} quantile value $\Delta\mu_i^{(b_i,q)}$ such that, with $\Delta\mu_{i1}^{b_i} \leq \cdots \leq \Delta\mu_{im}^{b_i} \leq \cdots \leq \Delta\mu_{iN_{b_i}}^{b_i}$:

$$\Delta\mu_i^{(b_i,q)} = \inf_{\substack{\Delta\mu_i \\ \Delta\mu_{i1}^{b_i}\leq\Delta\mu_i\leq\Delta\mu_{iN_{b_i}}^{b_i}}} \left\{\Delta\mu_i : \frac{1}{N_{b_i}}\left(\sum_{m=1}^{N_{b_i}} \mathbb{1}\{\Delta\mu_{im}^{b_i} \leq \Delta\mu_i\}\right) \geq q\right\} \qquad (\mathbf{30})$$

By noting $\sigma_{\Delta\mu_i}^{q}$ the empirical sampling error of the q^{th} quantile of $\Delta\mu_i$ estimated from the training sample, the expected sampling error $\sigma_{\Delta\mu_i^{(b_i,q)}}$ of any quantile q, $0 \leq q \leq 1$, can be expressed as $\sigma_{\Delta\mu_i^{(b_i,q)}} \cong K\left(\left|q-\frac{1}{2}\right|\right)\sigma_{\Delta\mu_i}^{q} N_{b_i}^{-\frac{1}{2}}$, where $K\left(\left|q-\frac{1}{2}\right|\right)$ is a function[6] satisfying $K(0) \geq 1$ and $K'\left(\left|q-\frac{1}{2}\right|\right) \geq 0$. Then, by noting M_{b_i} the median value of the bin b_i, we estimate the following systems of equations:

$$\boldsymbol{Y}_q = \boldsymbol{X}_q\boldsymbol{A}_q + \boldsymbol{\epsilon}_q \qquad (\mathbf{31})$$

, where:

$$\boldsymbol{Y}_q = \begin{pmatrix} \Delta\mu_i^{(1,q)} \\ \Delta\mu_i^{(2,q)} \\ \vdots \\ \Delta\mu_i^{(|\mathcal{B}_i|,q)} \end{pmatrix}, \boldsymbol{X}_q = \begin{pmatrix} 1 & M_1 & M_1^2 & \cdots & M_1^{n_i^q} \\ 1 & M_2 & M_2^2 & \cdots & M_2^{n_i^q} \\ \vdots & \vdots & \vdots & \ddots & \vdots \\ 1 & M_{|\mathcal{B}_i|} & M_{|\mathcal{B}_i|}^2 & \dots & M_{|\mathcal{B}_i|}^{n_i^q} \end{pmatrix}, \boldsymbol{A}_q = \begin{pmatrix} \mathfrak{a}_{i0} \\ \mathfrak{a}_{i1} \\ \mathfrak{a}_{i2} \\ \vdots \\ \mathfrak{a}_{in_i^q} \end{pmatrix}, \boldsymbol{\epsilon}_q = \begin{pmatrix} \epsilon_{0q} \\ \epsilon_{1q} \\ \epsilon_{2q} \\ \vdots \\ \epsilon_{|\mathcal{B}_i|q} \end{pmatrix}$$

[6] These properties simply reflect that fact that the expected sampling error increases for quantiles distant from the median.

Yet, as the number of observations per bin b_i is expected to be non-constant, the MCO assumption of constant variance of the error terms is violated. Assuming the $\epsilon_{b_i q}$ are normally distributed, we introduce a diagonal weighting matrix $\boldsymbol{W}_q$, with diagonal entry $\omega_{b_i,b_i} = \left(\sigma^2_{\Delta\mu_i^{(b_i,q)}}\right)^{-1}$. The MCO estimators are then equal to:

$$\widehat{\boldsymbol{A}_q} = \left(\boldsymbol{X}_q^T \boldsymbol{W}_q \boldsymbol{X}_q\right)^{-1} \boldsymbol{X}_q^T \boldsymbol{W}_q \boldsymbol{Y}_q$$

The standard errors associated to each estimated coefficient $\widehat{\mathfrak{a}_{in}^q}$ are given by the following expression:

$$\sigma_{\widehat{\mathfrak{a}_{in}^q}} = \sqrt{\frac{\boldsymbol{Y}_q^T \boldsymbol{Y}_q - \widehat{\boldsymbol{A}_q}^T \boldsymbol{X}_q^T \boldsymbol{W}_q \boldsymbol{X}_q \widehat{\boldsymbol{A}_q}}{|\mathcal{B}_i| - n_i^q - 1}} \times \sqrt{\left(\boldsymbol{X}_q^T \boldsymbol{W}_q \boldsymbol{X}_q\right)^{-1}_{n+1}} \qquad (\mathbf{32})$$

$\left(\boldsymbol{X}_q^T \boldsymbol{W}_q \boldsymbol{X}_q\right)^{-1}_{n+1}$ is the $n+1$-th diagonal element of the matrix $\left(\boldsymbol{X}_q^T \boldsymbol{W}_q \boldsymbol{X}_q\right)^{-1}$. We observe that both expressions for standard error decrease with the number of bins $|\mathcal{B}_i|$. Simultaneously, increasing $|\mathcal{B}_i|$ decreases the number of observations per bins, which mechanically increases $\sigma_{\Delta\mu_i^{(b_i,q)}}$. If $\sigma_{\Delta\mu_i^{(b_i,q)}} \approx \sigma_{\Delta\mu_i^{(b_i',q)}}$ for any couple $(b_i, b_i') \in \mathcal{B}_i^2$, then all weight coefficients in matrix $\boldsymbol{W}_q$ decrease in similar proportions. Yet, if $\sigma_{\Delta\mu_i^{(b_i,q)}} \neq \sigma_{\Delta\mu_i^{(b_i',q)}}$, bins with a large error will have a low weight in the estimation of the polynomial coefficients and the polynomial approximation may thus be poorly reliable for forecasting limiting variations of $\Delta\mu_i$ within these bins intervals. In order to maximize the reliability of our approximation polynomials for all bins intervals, we chose the number of bins $|\mathcal{B}_i|^*$ which minimizes the variance of $N_{\mathcal{B}_i}$.

Assuming that the number of observations is higher around the mean value of $\Delta\mu_i$ (ie small variations occur more frequently than large ones), the number of observations is inversely proportional to the distance to the mean value $\overline{\Delta\mu_i}$. Under this behavioral assumption, quantile estimates corresponding to extreme values of $\Delta\mu_i$ will be associated to a higher standard error. This feature will be captured by the prediction intervals of the estimated polynomial $\widehat{P_{n_i^q}(\mu_i)}$. Indeed, using the propagation of uncertainty method, the standard error of $\widehat{P_{n_i^q}(\mu_i)}$ can be expressed as follows:

$$\sigma_{P_{n_i^q}\widehat{(\mu_i)}} = \sqrt{\sum_{n=0}^{n_i^q} \sigma^2_{\widehat{a_{in}^q}}\, \mu_i^{2n}} = \sqrt{\sum_{n=0}^{n_i^q} \frac{\boldsymbol{Y}_q^T\boldsymbol{Y}_q - \widehat{\boldsymbol{A}_q}^T\boldsymbol{X}_q^T\boldsymbol{W}_q\boldsymbol{X}_q\widehat{\boldsymbol{A}_q}}{|\mathcal{B}_i|^* - n_i^q - 1} \times \left(\boldsymbol{X}_q^T\boldsymbol{W}_q\boldsymbol{X}_q\right)^{-1}_{n+1} \mu_i^{2n}} \quad (\mathbf{33a})$$

Assuming normality of the coefficients estimators $\widehat{\boldsymbol{A}_q}$, ie $\widehat{\boldsymbol{A}_q} \sim N\left(\boldsymbol{A}_q, \sigma^q_{\Delta\mu_i}\left(\boldsymbol{X}_q^T\boldsymbol{W}_q\boldsymbol{X}_q\right)^{-1}\right)$, we can compute exact confidence intervals and prediction intervals. We define $\sigma^q_{\Delta\mu_i}$ the standard error associated to the estimation of the q^{th} quantile of $\Delta\mu_i$. Considering the polynomial $P_{n_i^q}\widehat{(\mu_i)}$ as a linear combination, the variance of the predicted values $P_{n_i^q}\widehat{(\mu_i)}$ are given by:

$$\sigma^q_{\Delta\mu_i} + \boldsymbol{X}^T\, \frac{\boldsymbol{Y}_q^T\boldsymbol{Y}_q - \widehat{\boldsymbol{A}_q}^T\boldsymbol{X}_q^T\boldsymbol{W}_q\boldsymbol{X}_q\widehat{\boldsymbol{A}_q}}{|\mathcal{B}_i|^* - n_i^q - 1} \times \left(\boldsymbol{X}_q^T\boldsymbol{W}_q\boldsymbol{X}_q\right)^{-1}\boldsymbol{X} \quad (\mathbf{33b})$$

We define $\boldsymbol{X} = \left(1, \mu_i, \mu_i^2, \dots, \mu_i^{n_i^q}\right)^T \in \mathbb{R}^{(n_i^q+1)\times 1}$. The prediction interval for the value of the q^{th} quantile of $\Delta\mu_i$, conditional on $\boldsymbol{X}$, can thus be expressed as:

$$\mathcal{U}_i(q, \alpha, |\mathcal{B}_i|^*|\boldsymbol{X}) = \left[\widehat{\boldsymbol{A}_q}\boldsymbol{X} \pm t_{1-\frac{\alpha}{2};|\mathcal{B}_i|^*-n_i^q} \times \sqrt{\sigma^q_{\Delta\mu_i} + \boldsymbol{X}^T\, \frac{\boldsymbol{Y}_q^T\boldsymbol{Y}_q - \widehat{\boldsymbol{A}_q}^T\boldsymbol{X}_q^T\boldsymbol{W}_q\boldsymbol{X}_q\widehat{\boldsymbol{A}_q}}{|\mathcal{B}_i|^* - n_i^q - 1} \times \left(\boldsymbol{X}_q^T\boldsymbol{W}_q\boldsymbol{X}_q\right)^{-1}\boldsymbol{X}}\right] \quad (\mathbf{34})$$

$t_{1-\frac{\alpha}{2};|\mathcal{B}_i|^*-n_i^q}$ is the upper critical value of a Student distribution with $|\mathcal{B}_i|^* - n_i^q$ degrees of liberty for quantile $1 - \frac{\alpha}{2}$.

The prediction interval is wider than the confidence interval as it accounts for the fluctuations of $\Delta\mu_i$. Our prediction intervals can be interpreted as follows: if we observe the variation of $\Delta\mu_i$ conditional on μ_i and repeat the experiment, the q^{th} quantile of the distribution of variations will be included in the prediction interval $\mathcal{U}_i(q, \alpha, |\mathcal{B}_i|^*|\boldsymbol{X})$ in $1 - \alpha\%$ of the cases. Taking $\alpha = 0.05$, there is only a probability of 5% that $\Delta\mu_i^q \notin \mathcal{U}_i(q, \alpha, |\mathcal{B}_i|^*|\boldsymbol{X})$. Assuming that the prediction error is normally distributed around the mean predicted value, it is straightforward to see that:

$$\mathbb{P}(\Delta\mu_i \leq \sup \mathcal{U}_i(q, \alpha, |\mathcal{B}_i|^*|\boldsymbol{X})) = q - \frac{\alpha}{2} \quad (\mathbf{35a})$$

$$\mathbb{P}(\Delta\mu_i \geq \inf \mathcal{U}_i(1 - q, \alpha, |\mathcal{B}_i|^*|\boldsymbol{X})) = 1 - q + \frac{\alpha}{2} \quad (\mathbf{35b})$$

So we have:

$$\mathbb{P}(\Delta\mu_i \notin [\inf \mathcal{U}_i(1-q,\alpha,|\mathcal{B}_i|^*|\boldsymbol{X}) ; \sup \mathcal{U}_i(q,\alpha,|\mathcal{B}_i|^*|\boldsymbol{X})]) = 2-2q+\alpha \qquad (\mathbf{35c})$$

Finally, we can provide "worst-case" lower and upper bounds for φ_i^q using the following empirical approximation:

$$\widehat{\varphi_i^q}(\alpha,|\mathcal{B}_i|^*|\boldsymbol{X}) = \widehat{\boldsymbol{A}}_q\boldsymbol{X} + (-1)^{\mathbb{1}\left\{q\geq\frac{1}{2}\right\}} t_{1-\frac{\alpha}{2};|\mathcal{B}_i|^*-n_i^q} \times \sqrt{\sigma^q_{\Delta\mu_i} + \boldsymbol{X}^T \frac{\boldsymbol{Y}_q^T\boldsymbol{Y}_q - \widehat{\boldsymbol{A}}_q^T\boldsymbol{X}_q^T\boldsymbol{W}_q\boldsymbol{X}_q\widehat{\boldsymbol{A}_q}}{|\mathcal{B}_i|^*-n_i^q-1} \times \left(\boldsymbol{X}_q^T\boldsymbol{W}_q\boldsymbol{X}_q\right)^{-1}\boldsymbol{X}} \qquad (\mathbf{36a})$$

And:

$$\widehat{\varphi_i^{0.5}}(\alpha,|\mathcal{B}_i|^*|\boldsymbol{X}) = \widehat{\boldsymbol{A}}_q\boldsymbol{X} \qquad (\mathbf{36b})$$

As this empirical approximation is computed for each season, we define $\widehat{\varphi_{is}^q}(\alpha,|\mathcal{B}_i|^*|\boldsymbol{X})$ as the approximation function corresponding to season $s \in \mathcal{S}$ and further note the corresponding matrix of eigenvectors $\boldsymbol{\Phi}_s$. Our method actually mimics a polynomial quantile regression, as we model the conditional dependence of quantiles of the endogenous variable $\Delta\mu_i$. However, as the density of the dependent variable is expected to be higher around its mean value, conditional quantiles of $\Delta\mu_i$ associated to extreme values of μ_i are expected to be highly noisy. This would likely bias the conditional quantile regression estimator.

Our binning strategy allows us to decrease the overall variance of the sample conditional quantiles of $\Delta\mu_i$. Then, using weights reduces the influence of bins with high conditional quantile variance on the estimator value. Finally, the larger prediction interval associated to a bin with lower weight accounts for its smaller contribution to the estimation of the polynomial and the higher probability of forecasting error for values included in the bin. Though parametric, our method allows us to account for differences in the density of observations, especially for extreme values, so we provide robust predictions of the conditional interval within which our unknown parameter can vary.

3.3. Dynamic robust reformulation of the optimization model

As there may exist no single set of dispatching decisions which simultaneously verify thermal constraints for all worst-case trajectories, we introduce superscripts **L**, **H** and **V** which respectively index dispatching variables associated to the lower, upper and most volatile conditional trajectories of residual demand. Applying the above results, the optimization model becomes:

$$\min_{\boldsymbol{U},\boldsymbol{q},\boldsymbol{\kappa},\boldsymbol{z}} \sum_{j>1}\left(A_j + c_j^{FOM}\right)U_j + \sum_g \left(A_g + c_g^{FOM}\right)U_g + \left(A_e + c_e^{FOM}\right)U_e + \frac{\Theta}{N^R}\left(\sum_{s\in\mathcal{S}}\sum_{t\in\mathcal{T}}\left(\sum_g \left(c_g + \pi^{CO_2}E_g\right)\left(q_{gst}^H + q_{gst}^L + q_{gst}^V\right) + c_g^{STUP}\left(z_{gst}^H + z_{gst}^L + z_{gst}^V\right) + \sum_j c_j^{\kappa}\left(\kappa_{jst}^H + \kappa_{jst}^L + \kappa_{jst}^V\right)\right)\right) \quad (37)$$

such that **(4a)**-**(21)** hold for each subset of dispatching decision variables and :

$$\bar{\xi}_{1st} + \widehat{\xi}_1\pi_{1st}^{+} - \kappa_{1st}^H - \sum_{j>1}\left(\left(\bar{\xi}_{jst} + \widehat{\xi_{jst}}\pi_{jst}^{+}\right)U_j - \kappa_{jst}^H\right) - \sum_g q_{gst}^H + \Delta e_{st}^{+H} - e_{st}^{-H} \leq \gamma \quad (38a)$$

$$-\bar{\xi}_{1st} - \widehat{\xi}_1\pi_{1st}^{+} + \kappa_{1st}^H + \sum_{j>1}\left(\left(\bar{\xi}_{jst} + \widehat{\xi_{jst}}\pi_{jst}^{+}\right)U_j - \kappa_{jst}^H\right) + \sum_g q_{gst}^H - \Delta e_{st}^{+H} + e_{st}^{-H} \leq \gamma \quad (38b)$$

$$\bar{\xi}_{1st} + \widehat{\xi}_1\pi_{1st}^{-} - \kappa_{1st}^L - \sum_{j>1}\left(\left(\bar{\xi}_{jst} + \widehat{\xi_{jst}}\pi_{jst}^{-}\right)U_j - \kappa_{jst}^L\right) - \sum_g q_{gst}^L + \Delta e_{st}^{+L} - e_{st}^{-L} \leq \gamma \quad (39a)$$

$$-\bar{\xi}_{1st} - \widehat{\xi}_1\pi_{1st}^{-} + \kappa_{1st}^L + \sum_{j>1}\left(\left(\bar{\xi}_{jst} + \widehat{\xi_{jst}}\pi_{jst}^{-}\right)U_j - \kappa_{jst}^L\right) + \sum_g q_{gst}^L - \Delta e_{st}^{+L} + e_{st}^{-L} \leq \gamma \quad (39b)$$

$$\bar{\xi}_{1st} + \widehat{\xi}_1\pi_{1st}^{V} - \kappa_{1st}^V - \sum_{j>1}\left(\left(\bar{\xi}_{jst} + \widehat{\xi_{jst}}\pi_{jst}^{V}\right)U_j - \kappa_{jst}^L\right) - \sum_g q_{gst}^V + \Delta e_{st}^{+V} - e_{st}^{-V} \leq \gamma \quad (40a)$$

$$-\bar{\xi}_{1st} - \widehat{\xi}_1\pi_{1st}^{V} + \kappa_{1st}^V + \sum_{j>1}\left(\left(\bar{\xi}_{jst} + \widehat{\xi_{jst}}\pi_{jst}^{V}\right)U_j - \kappa_{jst}^V\right) + \sum_g q_{gst}^V - \Delta e_{st}^{+V} + e_{st}^{-V} \leq \gamma \quad (40b)$$

$$\boldsymbol{\pi}_{st}^{+} = \boldsymbol{\pi}_{st-1}^{+} + \boldsymbol{\Phi}_s^{-T}\widehat{\boldsymbol{\varphi}_s^{q}}\left(\alpha, |\boldsymbol{\mathcal{B}}|^{*}|\boldsymbol{\Phi}_s^T\boldsymbol{\pi}_{st-1}^{+}\right) \quad (41a)$$

$$\boldsymbol{\pi}_{st}^{-} = \boldsymbol{\pi}_{st-1}^{-} + \boldsymbol{\Phi}_s^{-T}\widehat{\boldsymbol{\varphi}^{1-q}}_s\left(\alpha, |\boldsymbol{\mathcal{B}}|^{*}|\boldsymbol{\Phi}_s^T\boldsymbol{\pi}_{st-1}^{-}\right) \quad (41b)$$

$$\boldsymbol{\pi}_{st}^{V} = \boldsymbol{\pi}_{st-1}^{V} + \left(\mathbf{1}^{(n\times 1)} - \boldsymbol{w}_{st}\right)\circ\left(\boldsymbol{\Phi}_s^{-T}\widehat{\boldsymbol{\varphi}_s^{q}}\left(\alpha, |\boldsymbol{\mathcal{B}}|^{*}|\boldsymbol{\Phi}_s^T\boldsymbol{\pi}_{st-1}^{V}\right)\right) + \boldsymbol{w}_{st}\circ\left(\boldsymbol{\Phi}_s^{-T}\widehat{\boldsymbol{\varphi}_s^{1-q}}\left(\alpha, |\boldsymbol{\mathcal{B}}|^{*}|\boldsymbol{\Phi}_s^T\boldsymbol{\pi}_{st-1}^{V}\right)\right) \quad (41c)$$

$$-\Delta\bar{\boldsymbol{\xi}}_{st} \circ \boldsymbol{U} - \left(\widehat{\bar{\boldsymbol{\xi}}_{st}} \circ \boldsymbol{\Phi}_s^{-T} \widehat{\boldsymbol{\varphi}_s^{q}}\,(\alpha, |\boldsymbol{\mathcal{B}}|^* | \boldsymbol{\Phi}_s^T \boldsymbol{\pi}_{st-1}^V)\right) \circ \boldsymbol{U}$$
$$\leq \Delta\bar{\boldsymbol{\xi}}_{st} \circ \boldsymbol{U} + \left(\widehat{\bar{\boldsymbol{\xi}}_{st}} \circ \boldsymbol{\Phi}_s^{-T} \widehat{\boldsymbol{\varphi}_s^{1-q}}(\alpha, |\boldsymbol{\mathcal{B}}|^* | \boldsymbol{\Phi}_s^T \boldsymbol{\pi}_{st-1}^V)\right) \circ \boldsymbol{U} + \boldsymbol{M} \circ \left(\boldsymbol{1}^{(n\times 1)} - \boldsymbol{w}_{st}\right) \quad (\boldsymbol{42a})$$

$$-\Delta\bar{\boldsymbol{\xi}}_{st} \circ \boldsymbol{U} - \left(\widehat{\bar{\boldsymbol{\xi}}_{st}} \circ \boldsymbol{\Phi}_s^{-T} \widehat{\boldsymbol{\varphi}_s^{q}}(\alpha, |\boldsymbol{\mathcal{B}}|^* | \boldsymbol{\Phi}_s^T \boldsymbol{\pi}_{st-1}^V)\right) \circ \boldsymbol{U}$$
$$\geq \Delta\bar{\boldsymbol{\xi}}_{st} \circ \boldsymbol{U} + \left(\widehat{\bar{\boldsymbol{\xi}}_{st}} \circ \boldsymbol{\Phi}_s^{-T} \widehat{\boldsymbol{\varphi}_s^{1-q}}(\alpha, |\boldsymbol{\mathcal{B}}|^* | \boldsymbol{\Phi}_s^T \boldsymbol{\pi}_{st-1}^V)\right) \circ \boldsymbol{U} - \boldsymbol{M} \circ \boldsymbol{w}_{st} \quad (\boldsymbol{42b})$$

$$\boldsymbol{w}_{st} \in [0\,;1]^{(n\times 1)} \quad (\boldsymbol{43})$$

$$\boldsymbol{\Phi}_s^T \circ \boldsymbol{\pi}_0^+ \geq \boldsymbol{\Psi}^+ \quad (\boldsymbol{44a})$$

$$\boldsymbol{\Phi}_s^T \circ \boldsymbol{\pi}_0^- \leq \boldsymbol{\Psi}^- \quad (\boldsymbol{44b})$$

$$\boldsymbol{\Phi}_s^T \circ \boldsymbol{\pi}_0^V = \boldsymbol{\Psi}^V \quad (\boldsymbol{44c})$$

As three different worst-case scenarios, or "trajectories", are simultaneously considered in the cost function, we divide the variable costs by $N^R = 3$ and multiply them by the scaling factor Θ in **(37)**, so the variable part of the expression corresponds to the average yearly variable cost.

(41a) and **(41b)** model the dynamics of the uncertain positive and negative projected vectors $\boldsymbol{\pi}_{st}^+$ and $\boldsymbol{\pi}_{st}^-$, where $\boldsymbol{\pi}_{st}^+ - \boldsymbol{\pi}_{st-1}^+$ corresponds to the maximum positive variation conditional on $\boldsymbol{\pi}_{st-1}^+$ with probability inferior or equal to $q - \frac{\alpha}{2}$. This means that, for each time period, there is a probability inferior to $1 - q + \frac{\alpha}{2}$ that the observed variations of the uncertain parameters are larger than $\boldsymbol{\pi}_{st}^+ - \boldsymbol{\pi}_{st-1}^+$. The same reasoning applies to the largest negative variation of the uncertain parameters. **(41C)** is a weighted sum of the maximum and minimum variations possible given the couple (q, α), where $w_{ist} = 1$ if $\widehat{\boldsymbol{\varphi}_s^{q}}(\alpha, |\boldsymbol{\mathcal{B}}|^* | \boldsymbol{\Phi}_s^T \boldsymbol{\pi}_{st-1}^V)$ is superior or equal to the absolute value of $\widehat{\boldsymbol{\varphi}_s^{1-q}}(\alpha, |\boldsymbol{\mathcal{B}}|^* | \boldsymbol{\Phi}_s^T \boldsymbol{\pi}_{st-1}^V)$. Thus, our model chooses the direction of the variation such that for each parameter, the total absolute variation of its nominal and uncertain parts is maximized. By noting that, for any pair $(a, b) \in \mathbb{R}^2$, $a \geq |b| \Leftrightarrow -a \leq b \leq a$, we have the following term by term system of inequalities:

$$\Delta\bar{\boldsymbol{\xi}}_{st} \circ \boldsymbol{U} + \left(\widehat{\bar{\boldsymbol{\xi}}_{st}} \circ \boldsymbol{\Phi}_s^{-T} \widehat{\boldsymbol{\varphi}_s^{q}}(\alpha, |\boldsymbol{\mathcal{B}}|^* | \boldsymbol{\Phi}_s^T \boldsymbol{\pi}_{st-1}^+)\right) \circ \boldsymbol{U}$$
$$\geq \left|\Delta\bar{\boldsymbol{\xi}}_{st} \circ \boldsymbol{U} + \left(\widehat{\bar{\boldsymbol{\xi}}_{st}} \circ \boldsymbol{\Phi}_s^{-T} \widehat{\boldsymbol{\varphi}_s^{1-q}}(\alpha, |\boldsymbol{\mathcal{B}}|^* | \boldsymbol{\Phi}_s^T \boldsymbol{\pi}_{st-1}^-)\right) \circ \boldsymbol{U}\right| \quad (\boldsymbol{45})$$

$$\Leftrightarrow \begin{cases} -\Delta\bar{\boldsymbol{\xi}}_{st} \circ \boldsymbol{U} - \left(\widehat{\bar{\boldsymbol{\xi}}_{st}} \circ \boldsymbol{\Phi}_s^{-T} \widehat{\boldsymbol{\varphi}_s^{q}}\left(\alpha, |\boldsymbol{\mathcal{B}}|^* \left| \boldsymbol{\Phi}_s^T \boldsymbol{\pi}_{st-1}^V \right.\right)\right) \circ \boldsymbol{U} \leq \Delta\bar{\boldsymbol{\xi}}_{st} \circ \boldsymbol{U} + \left(\widehat{\bar{\boldsymbol{\xi}}_{st}} \circ \boldsymbol{\Phi}_s^{-T} \widehat{\boldsymbol{\varphi}_s^{1-q}}\left(\alpha, |\boldsymbol{\mathcal{B}}|^* \left| \boldsymbol{\Phi}_s^T \boldsymbol{\pi}_{st-1}^V \right.\right)\right) \circ \boldsymbol{U} \\ \Delta\bar{\boldsymbol{\xi}}_{st} \circ \boldsymbol{U} + \left(\widehat{\bar{\boldsymbol{\xi}}_{st}} \circ \boldsymbol{\Phi}_s^{-T} \widehat{\boldsymbol{\varphi}_s^{q}}\left(\alpha, |\boldsymbol{\mathcal{B}}|^* \left| \boldsymbol{\Phi}_s^T \boldsymbol{\pi}_{st-1}^V \right.\right)\right) \circ \boldsymbol{U} \geq \Delta\bar{\boldsymbol{\xi}}_{st} \circ \boldsymbol{U} + \left(\widehat{\bar{\boldsymbol{\xi}}_{st}} \circ \boldsymbol{\Phi}_s^{-T} \widehat{\boldsymbol{\varphi}_s^{1-q}}\left(\alpha, |\boldsymbol{\mathcal{B}}|^* \left| \boldsymbol{\Phi}_s^T \boldsymbol{\pi}_{st-1}^V \right.\right)\right) \circ \boldsymbol{U} \end{cases}$$

The operator $\circ$ corresponds to the Hadamard product. We note $\Delta\bar{\bar{\boldsymbol{\xi}}}_{st} = \bar{\bar{\boldsymbol{\xi}}}_{st} - \bar{\bar{\boldsymbol{\xi}}}_{st-1}$. By definition, we have $\widehat{\boldsymbol{\varphi}_s^q}(\alpha, |\boldsymbol{\mathcal{B}}|^* | \boldsymbol{\Phi}_s^T \boldsymbol{\pi}_{st-1}^V) \geq \widehat{\boldsymbol{\varphi}_s^{1-q}}(\alpha, |\boldsymbol{\mathcal{B}}|^* | \boldsymbol{\Phi}_s^T \boldsymbol{\pi}_{st-1}^V)$ so we are only interested in the first inequality. Then, by defining the vector $\boldsymbol{w}_{st} \in [0\,;1]^{(n\times 1)}$, the latter can be reformulated as the following equivalent system of constrains, corresponding to **(42a-42b)**:

$$\begin{cases} -\Delta\bar{\bar{\boldsymbol{\xi}}}_{st} \circ \boldsymbol{U} - \left(\widehat{\bar{\bar{\boldsymbol{\xi}}}_{st}} \circ \boldsymbol{\Phi}_s^{-T} \widehat{\boldsymbol{\varphi}_s^q}\left(\alpha, |\boldsymbol{\mathcal{B}}|^* \middle| \boldsymbol{\Phi}_s^T \boldsymbol{\pi}_{st-1}^V\right)\right) \circ \boldsymbol{U} \leq \Delta\bar{\bar{\boldsymbol{\xi}}}_{st} \circ \boldsymbol{U} + \left(\widehat{\bar{\bar{\boldsymbol{\xi}}}_{st}} \circ \boldsymbol{\Phi}_s^{-T} \widehat{\boldsymbol{\varphi}_s^{1-q}}\left(\alpha, |\boldsymbol{\mathcal{B}}|^* \middle| \boldsymbol{\Phi}_s^T \boldsymbol{\pi}_{st-1}^V\right)\right) \circ \boldsymbol{U} + \boldsymbol{M} \circ (\mathbf{1}^{(n\times 1)} - \boldsymbol{w}_{st}) \\ -\Delta\bar{\bar{\boldsymbol{\xi}}}_{st} \circ \boldsymbol{U} - \left(\widehat{\bar{\bar{\boldsymbol{\xi}}}_{st}} \circ \boldsymbol{\Phi}_s^{-T} \widehat{\boldsymbol{\varphi}_s^q}\left(\alpha, |\boldsymbol{\mathcal{B}}|^* \middle| \boldsymbol{\Phi}_s^T \boldsymbol{\pi}_{st-1}^V\right)\right) \circ \boldsymbol{U} \geq \Delta\bar{\bar{\boldsymbol{\xi}}}_{st} \circ \boldsymbol{U} + \left(\widehat{\bar{\bar{\boldsymbol{\xi}}}_{st}} \circ \boldsymbol{\Phi}_s^{-T} \widehat{\boldsymbol{\varphi}_s^{1-q}}\left(\alpha, |\boldsymbol{\mathcal{B}}|^* \middle| \boldsymbol{\Phi}_s^T \boldsymbol{\pi}_{st-1}^V\right)\right) \circ \boldsymbol{U} - \boldsymbol{M} \circ \boldsymbol{w}_{st} \end{cases}$$

We use the "big-M" method where $\boldsymbol{M} \in \mathbb{R}^{n\times 1}$ and $\boldsymbol{M} \gg \mathbf{0}^{n\times 1}$. Finally, equations **(44a)-(44c)** control the initial values of the uncertain vectors $\boldsymbol{\pi}_0^+, \boldsymbol{\pi}_0^-$ and $\boldsymbol{\pi}_0^V$, where $\boldsymbol{\Psi}^+$, $\boldsymbol{\Psi}^-$ and $\boldsymbol{\Psi}^V$ are adjustable positive vectors included in $\mathbb{R}^{n\times 1}$. As $\boldsymbol{\Phi}_s^T$ is a matrix of parameters, we may equivalently formulate a set of constraints controlling the initial values taken by the projected parameters.

Under this model formulation, we can derive for each point of time the value of the uncertain vector that maximizes residual demand, conditional on its previous value. Similarly, we compute the trajectory of the uncertain vector than minimize residual demand values, and the trajectory which maximizes its variations in absolute terms. As each possible value for variation can be associated to a positive probability, it is possible to compute the joint probability of any trajectory of the uncertain vector. We may further introduce a probabilistic threshold so that we restrict ourselves to the worst-case residual demand trajectories which satisfy it. We propose in Appendix a linear programming approach in order to derive the worst-case set of trajectories with a minimum probability of occurrence superior or equal to a given threshold. The variability-maximizing trajectory of uncertain parameters is computed using a quadratic formulation, which can easily be reformulated into an equivalent linear form.

However, the above model formulation maximizes the variability of the uncertain parameters separately. There is no theoretical guarantee that it simultaneously maximizes the total variability of residual demand. Yet, by noticing that $\forall i \leq n, \widehat{\varphi_{is}^q}(\alpha, |\boldsymbol{\mathcal{B}}|^* | \boldsymbol{X}_t) \geq \widehat{\varphi_{is}^{1-q}}(\alpha, |\boldsymbol{\mathcal{B}}|^* | \boldsymbol{X}_t)$, we can deduce that $\widehat{\boldsymbol{\varphi}_s^q}(\alpha, |\boldsymbol{\mathcal{B}}|^* | \boldsymbol{\Phi}_s^T\, \boldsymbol{\pi}_{st}^V)^T \boldsymbol{U}$ corresponds to the largest positive variation of residual demand in t. Similarly, $\widehat{\boldsymbol{\varphi}_s^{1-q}}\,(\alpha, |\boldsymbol{\mathcal{B}}|^* | \boldsymbol{\Phi}_s^T\, \boldsymbol{\pi}_{st}^V)^T \boldsymbol{U}$ yields the largest negative variation of residual demand. Thus, it bowls down to only comparing the absolute values of two terms. Again, as we are interested in the total absolute variation of the

residual demand, we must account for its average variation. As previously, we can reformulate the resulting inequality in order to evacuate the absolute term:

$$\left|\Delta\bar{\boldsymbol{\xi}}_{st}^{T}\boldsymbol{U}+\left(\widehat{\bar{\boldsymbol{\xi}}_{st}}\circ\boldsymbol{\Phi}_{s}^{-T}\widehat{\boldsymbol{\varphi}_{s}^{q}}(\alpha,|\boldsymbol{\mathcal{B}}|^{*}|\boldsymbol{\Phi}_{s}^{T}\,\boldsymbol{\pi}_{st-1}^{V})\right)^{T}\boldsymbol{U}\right|\geq\left|\Delta\bar{\boldsymbol{\xi}}_{st}^{T}\boldsymbol{U}+\left(\widehat{\bar{\boldsymbol{\xi}}_{st}}\circ\boldsymbol{\Phi}_{s}^{-T}\widehat{\boldsymbol{\varphi}_{s}^{1-q}}\,(\alpha,|\boldsymbol{\mathcal{B}}|^{*}|\boldsymbol{\Phi}_{s}^{T}\boldsymbol{\pi}_{st-1}^{V})\right)^{T}\boldsymbol{U}\right| \quad (\mathbf{46})$$

$$\Leftrightarrow\begin{cases}-\Delta\bar{\boldsymbol{\xi}}_{st}^{T}\boldsymbol{U}-\left(\widehat{\bar{\boldsymbol{\xi}}_{st}}\circ\boldsymbol{\Phi}_{s}^{-T}\widehat{\boldsymbol{\varphi}_{s}^{q}}(\alpha,|\boldsymbol{\mathcal{B}}|^{*}|\boldsymbol{\Phi}_{s}^{T}\boldsymbol{\pi}_{st-1}^{V})\right)^{T}\boldsymbol{U}\leq\Delta\bar{\boldsymbol{\xi}}_{st}^{T}\boldsymbol{U}+\left(\widehat{\bar{\boldsymbol{\xi}}_{st}}\circ\boldsymbol{\Phi}_{s}^{-T}\widehat{\boldsymbol{\varphi}_{s}^{1-q}}(\alpha,|\boldsymbol{\mathcal{B}}|^{*}|\boldsymbol{\Phi}_{s}^{T}\boldsymbol{\pi}_{st-1}^{V})\right)^{T}\boldsymbol{U}\\ \Delta\bar{\boldsymbol{\xi}}_{st}^{T}\boldsymbol{U}+\left(\widehat{\bar{\boldsymbol{\xi}}_{st}}\circ\boldsymbol{\Phi}_{s}^{-T}\widehat{\boldsymbol{\varphi}_{s}^{q}}(\alpha,|\boldsymbol{\mathcal{B}}|^{*}|\boldsymbol{\Phi}_{s}^{T}\boldsymbol{\pi}_{t-1}^{V})\right)^{T}\boldsymbol{U}\geq\Delta\bar{\boldsymbol{\xi}}_{st}^{T}\boldsymbol{U}+\left(\widehat{\bar{\boldsymbol{\xi}}_{st}}\circ\boldsymbol{\Phi}_{s}^{-T}\widehat{\boldsymbol{\varphi}_{s}^{1-q}}(\alpha,|\boldsymbol{\mathcal{B}}|^{*}|\boldsymbol{\Phi}_{s}^{T}\boldsymbol{\pi}_{st-1}^{V})\right)^{T}\boldsymbol{U}\end{cases}$$

By introducing the binary variable w_{st}, we have $w_{st}=1$ when **(46)** holds true with:

$$\begin{cases}-\Delta\bar{\boldsymbol{\xi}}_{st}^{T}\boldsymbol{U}-\left(\widehat{\bar{\boldsymbol{\xi}}_{st}}\circ\boldsymbol{\Phi}_{s}^{-T}\widehat{\boldsymbol{\varphi}_{s}^{q}}\left(\alpha,|\boldsymbol{\mathcal{B}}|^{*}\left|\boldsymbol{\Phi}_{s}^{T}\boldsymbol{\pi}_{st-1}^{V}\right.\right)\right)^{T}\boldsymbol{U}\leq\Delta\bar{\boldsymbol{\xi}}_{st}^{T}\boldsymbol{U}+\left(\widehat{\bar{\boldsymbol{\xi}}_{st}}\circ\boldsymbol{\Phi}_{s}^{-T}\widehat{\boldsymbol{\varphi}_{s}^{1-q}}\left(\alpha,|\boldsymbol{\mathcal{B}}|^{*}\left|\boldsymbol{\Phi}_{s}^{T}\boldsymbol{\pi}_{st-1}^{V}\right.\right)\right)^{T}\boldsymbol{U}+M(1-w_{st})\\ -\Delta\bar{\boldsymbol{\xi}}_{st}^{T}\boldsymbol{U}-\left(\widehat{\bar{\boldsymbol{\xi}}_{t}}\circ\boldsymbol{\Phi}_{s}^{-T}\widehat{\boldsymbol{\varphi}_{s}^{q}}\left(\alpha,|\boldsymbol{\mathcal{B}}|^{*}\left|\boldsymbol{\Phi}_{s}^{T}\boldsymbol{\pi}_{st-1}^{V}\right.\right)\right)^{T}\boldsymbol{U}\geq\Delta\bar{\boldsymbol{\xi}}_{st}^{T}\boldsymbol{U}+\left(\widehat{\bar{\boldsymbol{\xi}}_{st}}\circ\boldsymbol{\Phi}_{s}^{-T}\widehat{\boldsymbol{\varphi}_{s}^{1-q}}\left(\alpha,|\boldsymbol{\mathcal{B}}|^{*}\left|\boldsymbol{\Phi}_{s}^{T}\boldsymbol{\pi}_{st-1}^{V}\right.\right)\right)^{T}\boldsymbol{U}-Mw_{st}\end{cases}$$

Thus, we can replace equations **(40a)**,**(40b)**, **(40c)** and **(41c)-(43)** by the following subset of constraints:

$$\bar{\xi}_{1st}-\kappa_{1st}^{V}-\sum_{j>1}\left(\bar{\xi}_{jst}U_{j}-\kappa_{jst}^{V}\right)+\vartheta_{st}-\sum_{g}q_{gst}^{V}+\Delta e_{st}^{V}\leq\gamma \quad (\mathbf{47a})$$

$$-\bar{\xi}_{1st}+\kappa_{1st}^{V}+\sum_{j>1}\left(\bar{\xi}_{jst}U_{j}-\kappa_{jst}^{V}\right)-\vartheta_{st}+\sum_{g}q_{gst}^{V}-\Delta e_{st}^{V}\leq\gamma \quad (\mathbf{47b})$$

$$\vartheta_{st}=(1-\omega_{st})\left(\widehat{\bar{\boldsymbol{\xi}}_{st}}\circ\left(\boldsymbol{\Phi}_{s}^{-T}\widehat{\boldsymbol{\varphi}_{s}^{q}}\,(\alpha,|\boldsymbol{\mathcal{B}}|^{*}|\boldsymbol{\Phi}_{s}^{T}\boldsymbol{\pi}_{st-1}^{V})\right)\right)^{T}\boldsymbol{U}$$
$$+\omega_{st}\left(\widehat{\bar{\boldsymbol{\xi}}_{st}}\circ\left(\boldsymbol{\Phi}_{s}^{-T}\widehat{\boldsymbol{\varphi}_{s}^{1-q}}(\alpha,|\boldsymbol{\mathcal{B}}|^{*}|\boldsymbol{\Phi}_{s}^{T}\boldsymbol{\pi}_{st-1}^{V})\right)\right)^{T}\boldsymbol{U} \quad (\mathbf{48})$$

$$\boldsymbol{\pi}_{st}^{V}=\boldsymbol{\pi}_{st-1}^{V}+\left(\mathbf{1}^{(n\times1)}-\boldsymbol{\omega}_{st}\right)\circ\left(\boldsymbol{\Phi}_{s}^{-T}\widehat{\boldsymbol{\varphi}_{s}^{q}}(\alpha,|\boldsymbol{\mathcal{B}}|^{*}|\boldsymbol{\Phi}_{s}^{T}\boldsymbol{\pi}_{st-1}^{V})\right)+\boldsymbol{\omega}_{st}$$
$$\circ\left(\boldsymbol{\Phi}_{s}^{-T}\widehat{\boldsymbol{\varphi}_{s}^{1-q}}(\alpha,|\boldsymbol{\mathcal{B}}|^{*}|\boldsymbol{\Phi}_{s}^{T}\boldsymbol{\pi}_{st-1}^{V})\right) \quad (\mathbf{49})$$

$$-\Delta\bar{\boldsymbol{\xi}}_{st}^{T}\boldsymbol{U}-\left(\widehat{\bar{\boldsymbol{\xi}}_{st}}\circ\boldsymbol{\Phi}_{s}^{-T}\widehat{\boldsymbol{\varphi}_{s}^{q}}(\alpha,|\boldsymbol{\mathcal{B}}|^{*}|\boldsymbol{\Phi}_{s}^{T}\boldsymbol{\pi}_{st-1}^{V})\right)^{T}\boldsymbol{U}$$
$$\leq\Delta\bar{\boldsymbol{\xi}}_{st}^{T}\boldsymbol{U}+\left(\widehat{\bar{\boldsymbol{\xi}}_{st}}\circ\boldsymbol{\Phi}_{s}^{-T}\widehat{\boldsymbol{\varphi}_{s}^{1-q}}(\alpha,|\boldsymbol{\mathcal{B}}|^{*}|\boldsymbol{\Phi}_{s}^{T}\boldsymbol{\pi}_{st-1}^{V})\right)^{T}\boldsymbol{U}+M(1-w_{st}) \quad (\mathbf{50a})$$

$$-\Delta\bar{\boldsymbol{\xi}}_{st}^{T}\boldsymbol{U}-\left(\widehat{\bar{\boldsymbol{\xi}}_{st}}\circ\boldsymbol{\Phi}_{s}^{-T}\widehat{\boldsymbol{\varphi}_{s}^{q}}(\alpha,|\boldsymbol{\mathcal{B}}|^{*}|\boldsymbol{\Phi}_{s}^{T}\boldsymbol{\pi}_{st-1}^{V})\right)^{T}\boldsymbol{U}$$
$$\geq\Delta\bar{\boldsymbol{\xi}}_{st}^{T}\boldsymbol{U}+\left(\widehat{\bar{\boldsymbol{\xi}}_{st}}\circ\boldsymbol{\Phi}_{s}^{-T}\widehat{\boldsymbol{\varphi}_{s}^{1-q}}(\alpha,|\boldsymbol{\mathcal{B}}|^{*}|\boldsymbol{\Phi}_{s}^{T}\boldsymbol{\pi}_{st-1}^{V})\right)^{T}\boldsymbol{U}-Mw_{st} \quad (\mathbf{50b})$$

$$w_{st}\in[0;1] \quad (\mathbf{51})$$

This formulation however raises some issues regarding the modeling of load-shedding and curtailment. As residual demand is now modelled at the aggregate level, the maximum volumes of generation and load that can be curtailed for each component of residual demand cannot be computed directly anymore. Indeed, residual demand can be interpreted as a multilinear function, which is unlikely to be bijective. We leave this issue open for further research.

4. Application to the case of Auvergne-Rhône-Alpes

4.1. Estimation of the model parameters

In the following section, we apply the above model to the case of the French region Auvergne Rhône-Alpes. This administrative region is located in the South-East of France and enjoys strong solar irradiation compared to the national average. It is the first French region in terms of electricity generation. In addition, it accounts for roughly 11.6% of French GDP, while its mean share of national electricity load equals to 13.8%.

We assume no initial generation capacities in order to better disentangle the impact of each worst-case trajectories on investment decisions. For convenience, we further assume that no investment occurs in hydroelectric production. Moreover, we constrain the variable for capacity investment to take only discrete values for nuclear, gas turbines (GT) and combined cycle gas turbine plants (CCG), and continuous values for other production and storage technologies. Nuclear investment is performed by blocks of 1.6 GW, corresponding to the rated power of the EPR Flamanville plant (the most recent nuclear power project in France), while CCG investments are made by blocs of 0.45 GW, which is equal to the average nominal power of General Electric's 9HA.01/.02 gas turbine. Finally, GT investments are performed by blocks of 0.3 GW. Flexibility and cost assumptions for generation units can be found in **Table 1.A** and **Table 1.B.** in Appendix. We set the price of CO2 to 50 €/t. We use a discount factor of 5% for the computation of annuities corresponding to investment costs. Finally, following the CRE (CRE, 2018)[7], we choose a VOLL equal to 13 000 €/MWh.

[7] Public consultation from the French Energy Regulatory Commission (CRE), Public consultation No. 2018-015 of 20 December 2018 on the investment request relating to the Celtic project, including a cross-border cost allocation

When considering the technical characteristics of generation technologies presented in **Table 1.A.**, one actually notices that ramping rates are high enough for each online generation unit to very its output entirely between its minimum and maximum generation level within an hour. Indeed, as the model is defined with an hourly time resolution, nuclear plants may vary their production by up to 100% of their rated power between successive time periods. Thus, ramping constraints are actually not binding.

Using RTE database on the electricity consumption, solar and wind power generation on the period 2013-2018[8], we start by normalizing each variable by subtracting its mean and dividing by its normal deviation, both defined at the hourly level. The normalized variables can be interpreted as the number of standard deviations by which the original variable deviates from its mean. Then, we use the eigenvector matrix of the variance-covariance matrix of residual demand components in order to obtain a set of three decorrelated variables.

4.1.1. Performance analysis of the polynomial approximation

The illustrations provided in the subsection are restricted to the case of Winter only, as it exhibits the highest values of residual demand. However, we apply our methodology for all seasons. We thus have to compute a total of 12 "worst-case" trajectories, i.e. 3 trajectories for each season.

Using this new set of projected variables, we estimate the optimal number of bins for each residual demand component. **Figures 1.A., 1.B.** and **1.C.** plot the number of bins against the variance of the number of observations per bins for electricity demand, photovoltaic and wind power data respectively. In all three figures, the variance of the number of observations per bin is a strictly decreasing function of the number of bins. Unsurprisingly, as we define bins of equal length, the average number of observations per bins decreases. Yet, we can notice from **Figure 1.A.** that the variance of N_{b_i} for demand exhibits a steeper decrease that in the case of photovoltaic and wind power.

[8] Consumption and generation data was not available for years beyond 2018.

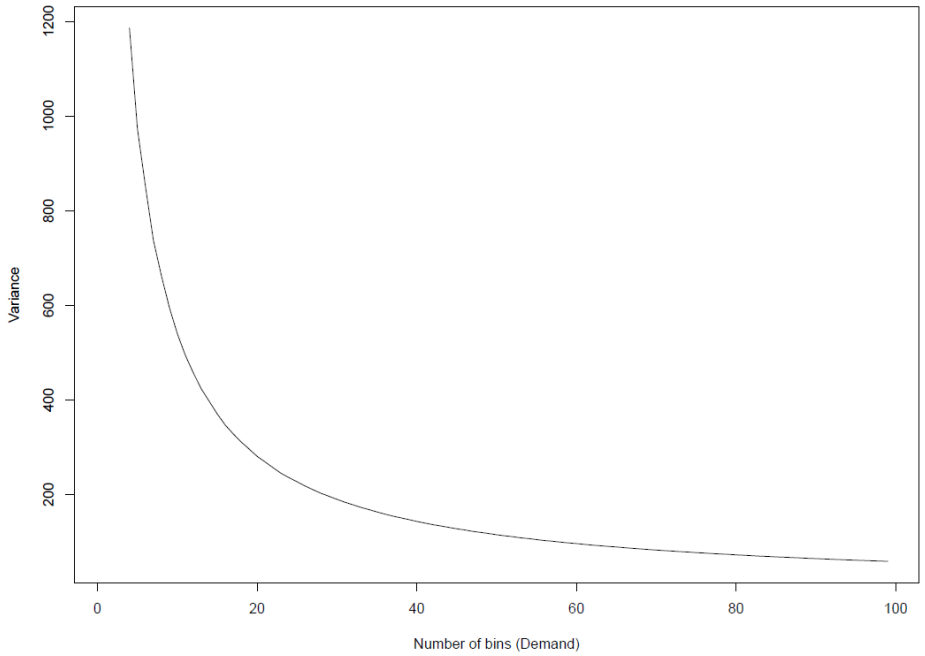

Figure 1.A.: Variance of the number of per bin observations against the number of bins (Demand)

Recalling the inverse relationship between the number of bins and the standard deviation of our polynomial regression estimators, we chose a number of bins such that increasing it by one unit would not significantly decrease the variance of N_{b_i}. This ensures that increasing the number of bins would most likely increase the standard error of our estimators without improving the average accuracy of the empirical quantile estimate within each bin. Setting $|\mathcal{J}| = 3$ with $i = 1$ for electricity load, $i = 2$ for photovoltaic power and $i = 3$ for wind power, we chose $|\mathcal{B}_1| = 60$ and $|\mathcal{B}_2| = |\mathcal{B}_3| = 50$.

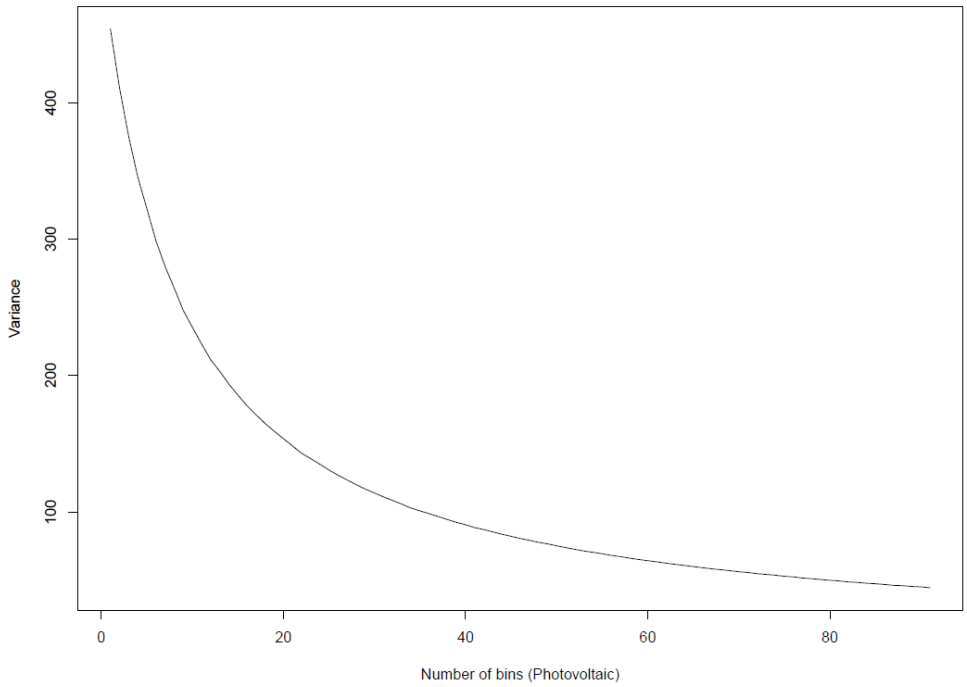

Figure 1.B.: Variance of the number of per bin observations against the number of bins (Photovoltaic)

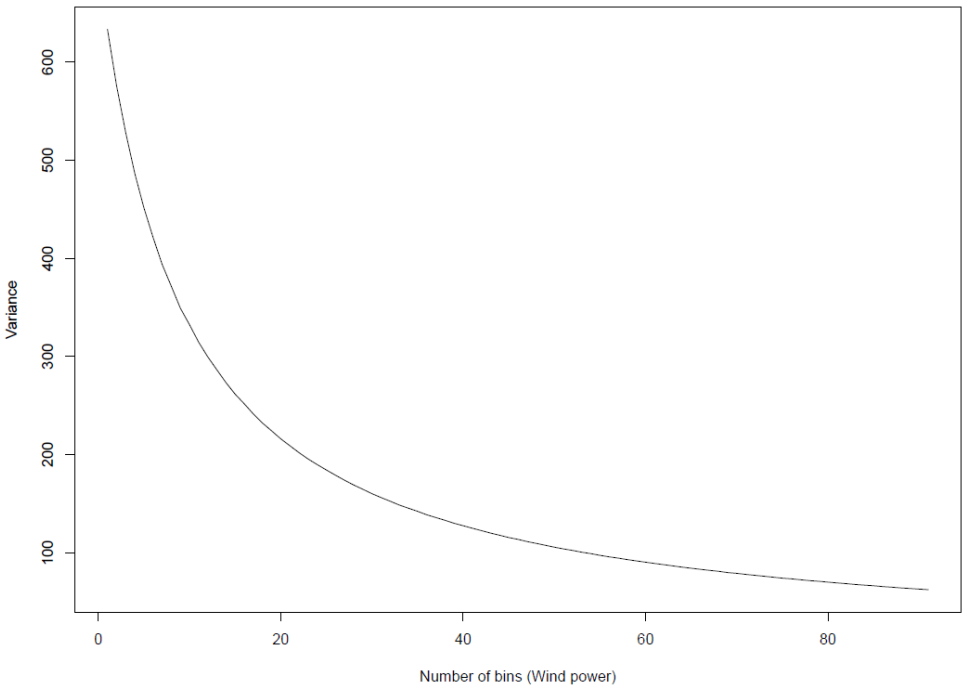

Figure 1.C.: Variance of the number of per bin observations against the number of bins (Wind power)

Then, for each $i \in \mathcal{J}$ and $b_i \in \mathcal{B}_i$, we estimate the empirical q^{th} quantile of $\Delta\mu_i$, in addition to its standard error and the empirical median value of μ_i, for $q = 0.95$. Then, we estimate the equations **(25a)** and **(25b)**, setting n_i^* between 3 and 4 for all residual demand components. We finally compute the prediction interval associated to each set of estimators resulting from our polynomial regressions, setting $\alpha = 0.05$. **Figures 2.A., 2.B.** and **2.C.** respectively plot the polynomial fit corresponding to the q^{th} and $1 - q^{\text{th}}$ quantiles, with prediction interval, for demand, photovoltaic and wind capacity factors.

Figure 2.A. shows a mean-reversing tendency for strongly negative values of the projected uncertain deviation of demand. This tendency is robust as the prediction intervals of both polynomial fitting curves are strictly positive. On the contrary, the convergence of the polynomial fitting curves for the q^{th} and $1 - q^{\text{th}}$ quantiles for high positive values indicates the possibility of a sustained regime of high demand, as there is a probability superior or equal to q that $\Delta\mu_1$ is positive for μ_1 around 3.

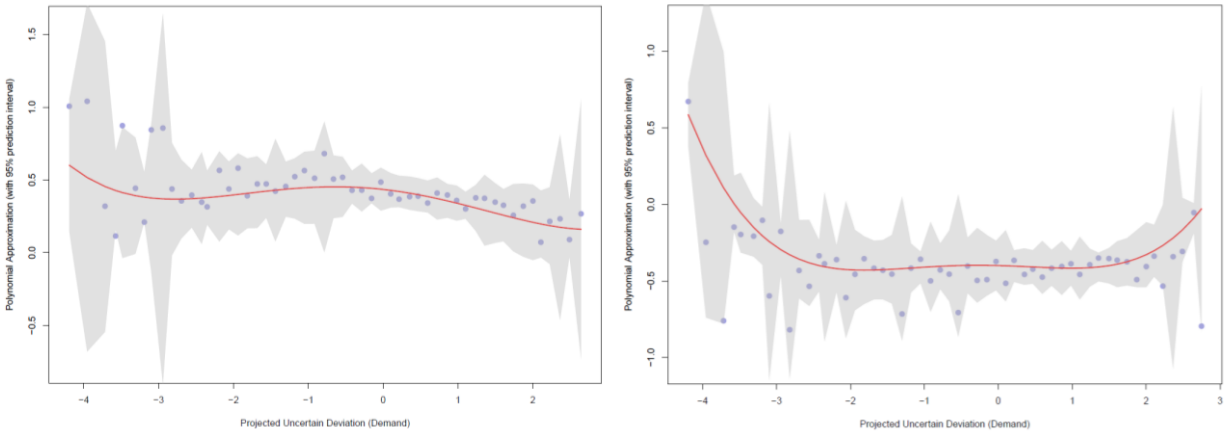

Figure 2.A.: Upper and lower quantile polynomial approximation for electricity demand

Note: The blue dots correspond to the empirical q^{th} quantile (left figure) and $1 - q^{\text{th}}$ quantile (right figure) associated to the median empirical value of each bin. It can be read as follows: for a projected uncertain deviation of demand equal to 0, $\Delta\mu_1 \in [-0.35, 0.5]$ approximately with a probability $2q - 1 - \alpha$.

Similar observations can be made for **Figures 2.B.** and **2.C.**. A mean-reversing behavior can be observed for extremely low levels of photovoltaic load factor, yet no straightforward conclusions can be drawn regarding the sign of $\Delta\mu_2$ when μ_2 increases. This tendency is against robust as both prediction intervals are positive for extreme negative values of μ_2. Wind capacity factor exhibits a slightly different behavior. While the prediction intervals are both strictly positive for extreme left-tail values, the probability of observing a sustained regime of extremely high wind capacity factor, corresponding to the right tail of μ_3, is quasi null. Indeed, the values in both prediction intervals are mostly negative for μ_3 superior or equal to 2.5, which implies $\Delta\mu_3$ must be decreasing. This suggests extreme values of wind capacity factor may only occur as temporary spikes and not as a stable state.

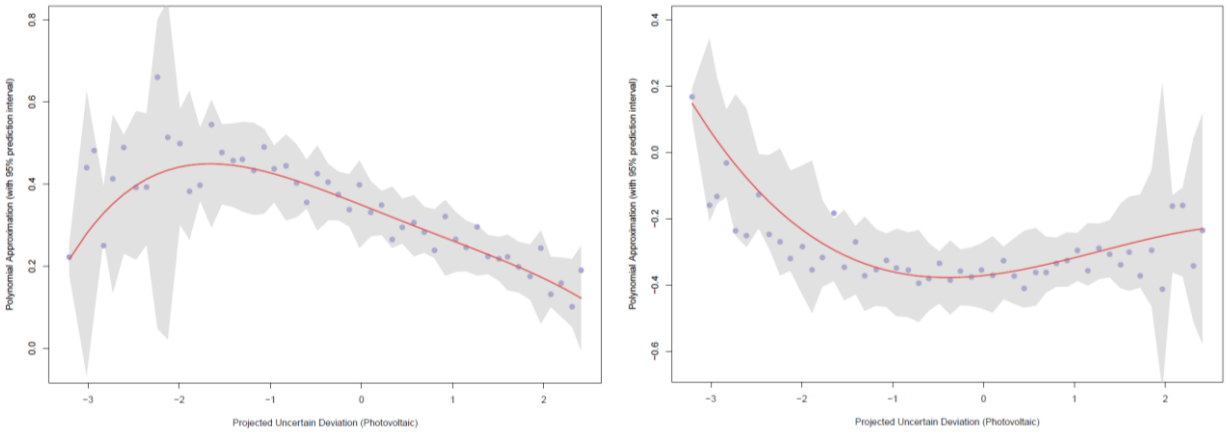

Figure 2.B.: Upper and lower quantile polynomial approximation for photovoltaic capacity factor

It may finally be noticed that our prediction intervals behave as expected: their width generally increases with the distance with respect to the median projected uncertain deviation, which translates the higher sampling error for extreme bins as they contain on average less observations than bins closer to the median. Moreover, the average width of prediction intervals decreases when estimating polynomial approximations of variations for more intermediate values of q. **Figures 3.A., 3.B.** and **3.C.** in Appendix respectively plot the polynomial fit corresponding to the q^{th} and $1-q^{\text{th}}$ quantiles for demand, photovoltaic and wind capacity factors, with $q = 0.75$. For all residual demand components, we observe a net decrease in the width of the prediction interval in the neighborhood of extreme values.

Finally, the fact that almost all empirical quantile values are included into prediction intervals is an indicator of good performance.

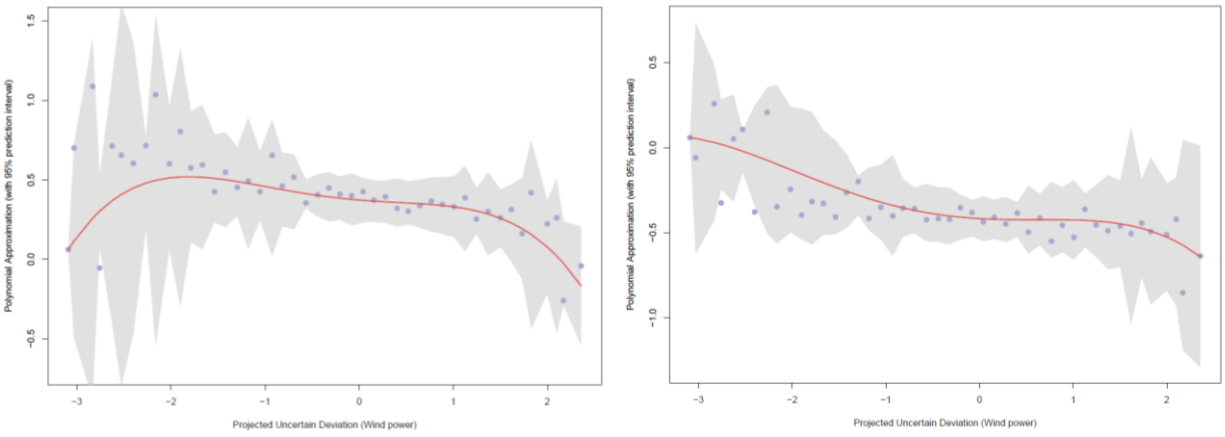

Figure 2.C.: Upper and lower quantile polynomial approximation for wind capacity factor

4.1.2. Dynamics and convergence regimes of worst-case residual demand trajectories

We now turn to the study of the dynamics of equations **(36a)** and **(36b)**. As polynomial regression provides a smooth approximation curve of $\Delta\mu_i$ that cancels for some values, we can expect $\boldsymbol{\pi}_t^+$ and $\boldsymbol{\pi}_t^-$ to converge to steady-states.

Figures 4.A., 4.B. and **4.C.** respectively plot the trajectories, or sequences, generated by **(36a)** and **(36b)**, for various starting values for projected demand, photovoltaic and wind capacity factors. We set $q = 0.95$.[9] We first note that for all projected variables, the trajectories converge to a unique trajectory whatever the starting value.

[9] The software R does not allow us to predict future values of $\widehat{\boldsymbol{\varphi}^q}(\alpha, |\boldsymbol{\mathcal{B}}|^* | \boldsymbol{\Phi}^T \boldsymbol{\pi}_{t-1}^V)$ for other values than those included in the training sample. In order to circumvent this issue, we observe that $\exists \lambda \in [0,1]$, $\pi_i^+ = \lambda M_{\pi_i^+}^+ + (1-\lambda) M_{\pi_i^+}^-$, where $M_{\pi_i^+}^+$ and $M_{\pi_i^+}^-$ are the nearest bin median values such that $M_{\pi_i^+}^- \leq \pi_i^+ \leq M_{\pi_i^+}^+$. We impose $\lambda = 1$ if $\pi_i^+ > \sup M_{b_i}$ and $\lambda = 0$ if $\pi_i^+ < \inf M_{b_i}$. Then, by linearity of the prediction interval, we have $\widehat{\boldsymbol{\varphi}^q}(\alpha, |\boldsymbol{\mathcal{B}}|^* | \boldsymbol{\Phi}^T \boldsymbol{\pi}_{t-1}^V) = \lambda \widehat{\boldsymbol{\varphi}^q}\left(\alpha, |\boldsymbol{\mathcal{B}}|^* \middle| \boldsymbol{\Phi}^T M_{\pi_i^+}^+\right) + (1-\lambda)\widehat{\boldsymbol{\varphi}^q}\left(\alpha, |\boldsymbol{\mathcal{B}}|^* \middle| \boldsymbol{\Phi}^T M_{\pi_i^+}^-\right)$. We apply the same approximation method for $\widehat{\boldsymbol{\varphi}^{1-q}}(\alpha, |\boldsymbol{\mathcal{B}}|^* | \boldsymbol{\Phi}^T \boldsymbol{\pi}_{t-1}^V)$.

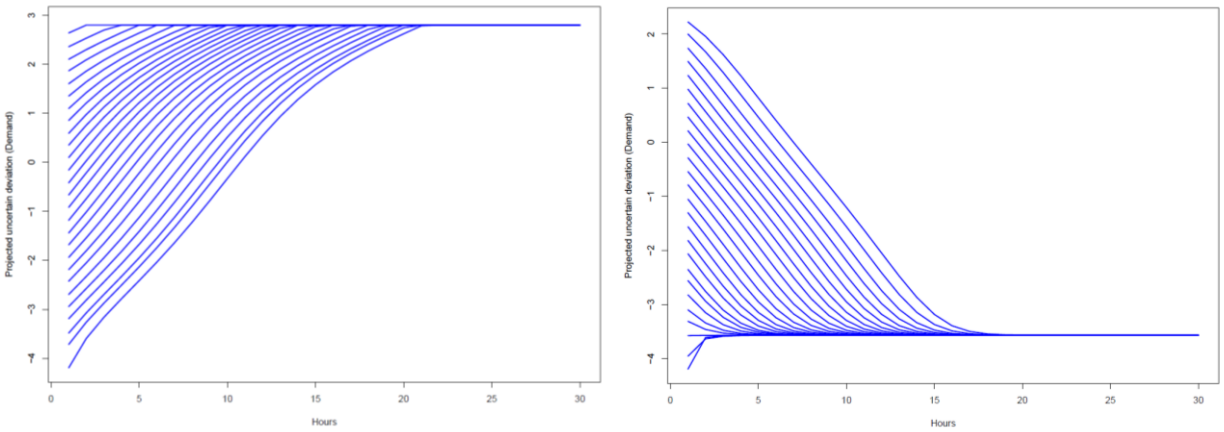

Figure 4.A.: q worst-case convergence patterns for π_{1t}^{+} and π_{1t}^{-}

Note: The left figure (resp. right figure) corresponds to the demand-maximizing (resp. demand minimizing) trajectory when $\Delta\mu_1$ is equal to the value of the q^{th} (resp. $1-q^{\text{th}}$) empirical quantile of its conditional distribution.

We observe from **Figures 4.A.** and **4.B.** that for any starting value, the projected uncertain deviation converges towards an upper and lower trajectory respectively within less than 20 hours. Interestingly, the sequence of projected deviations generated by equation **(36b)** starting from extremely low values monotonically increases, while higher starting values generate non-increasing sequences. This implies that, in our framework, there exist no stable trajectories such that the projected demand and solar capacity factor parameters remain at their minimum observable level.

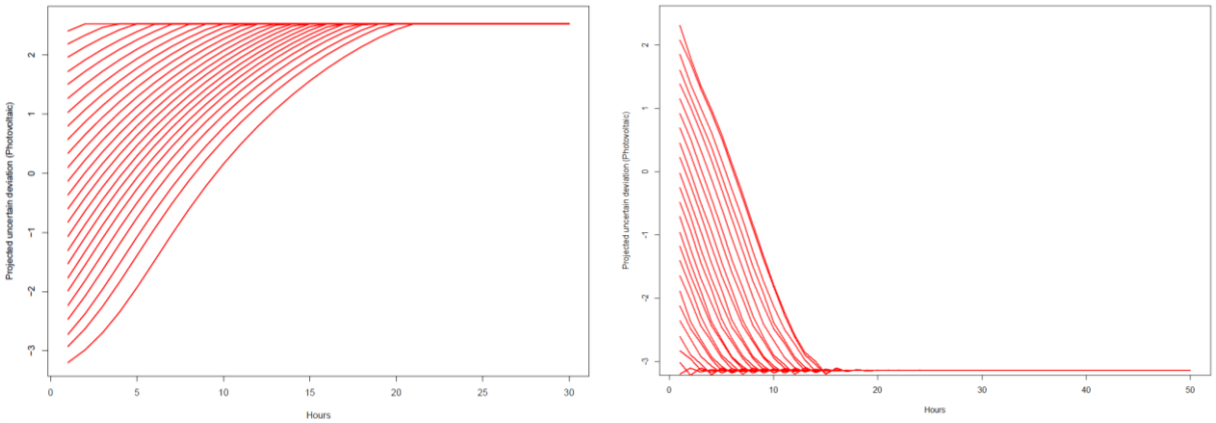

Figure 4.B.: q worst-case convergence patterns for π_{2t}^{+} and π_{2t}^{-}

Wind capacity factor exhibits a slightly different behavior. We observe from **Figure 4.C.** that **(36a)** generates decreasing sequences for the highest starting values, while **(37b)** generates cyclical sequences for any initial value. This implies that the lowest trajectory of the wind capacity factor exhibits a reversive behavior and cannot take its most extreme values for successive periods. This can translate the "spiking" behavior of wind generation. Overall, our approach is thus likely to generate less conservative solutions than a static robust methodology.

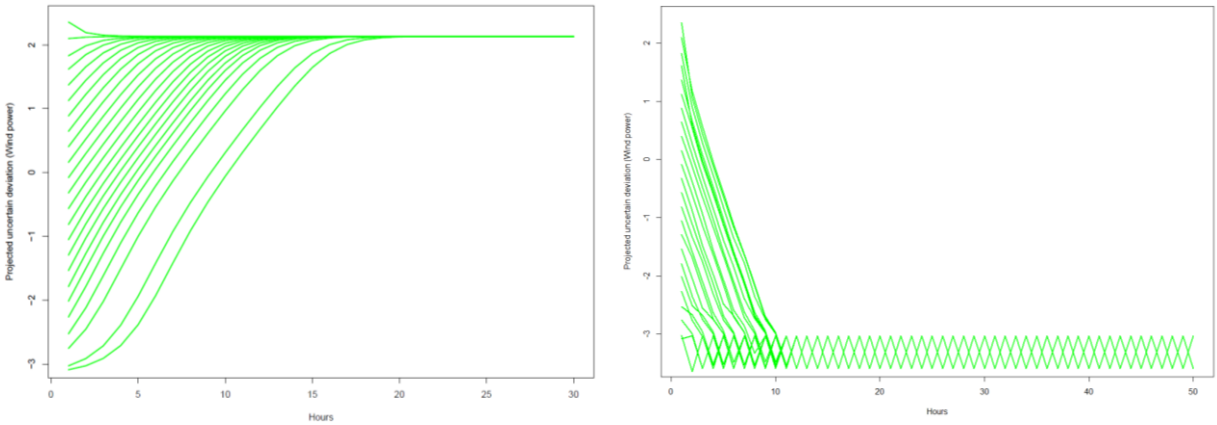

Figure 4.C.: q worst-case convergence patterns for π_{3t}^{+} and π_{3t}^{-}

The same convergence analysis can be carried out for equation **(36c)**. **Figures 5.A., 5.B.** and **5.C.** respectively plot the trajectories generated by **(36c)** for various starting values for projected demand, photovoltaic and wind capacity factors respectively. When letting the value of the projected deviation vary such that we maximize its absolute variations between successive time periods, we observe the convergence towards "oscillatory regimes" for wind and solar units. We note the emergence of stable trajectories for which the projected deviation displays a cyclic pattern and its moving average tends towards a constant value. Quite strikingly, all sequences rapidly converge towards oscillatory regimes within a small number of steps and for any starting value.

On the contrary, the projected deviation for demand exhibits a chaotic behavior overall, with cyclical sequences for a subset of starting values only.

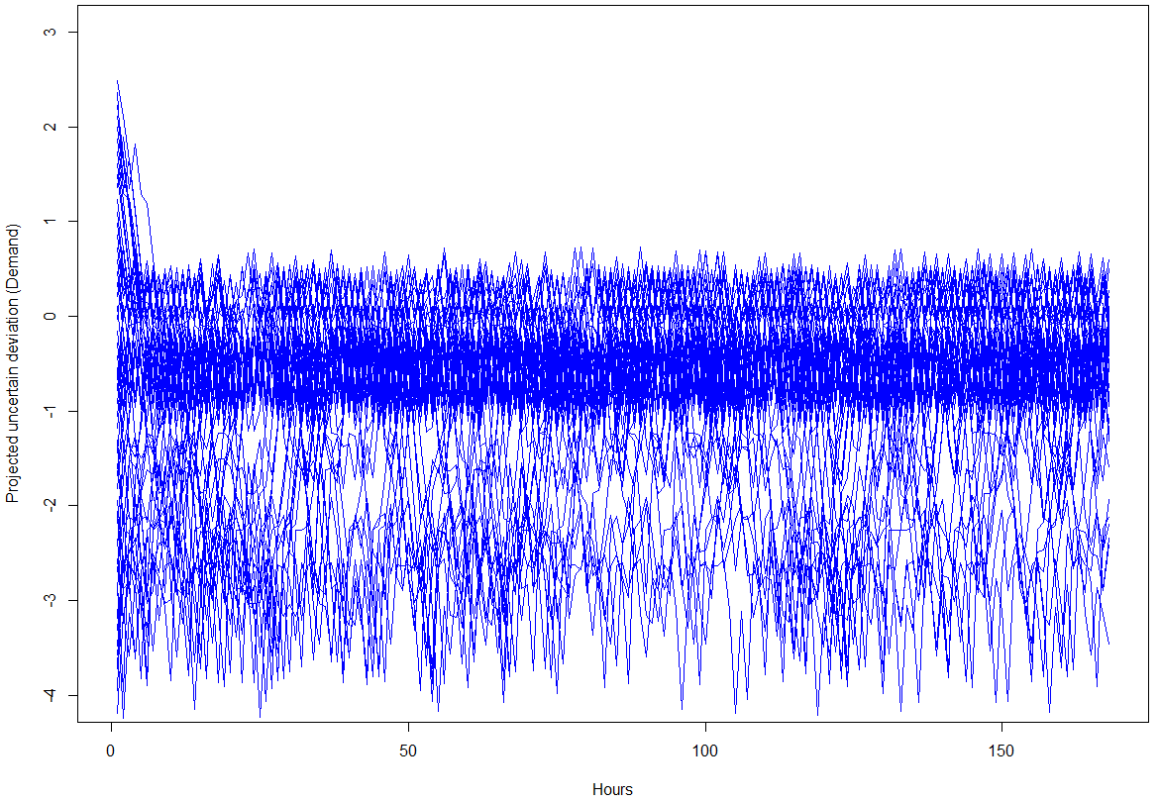

Figure 5.A.: q worst-case convergence patterns for π_{1t}^{V}

Yet, recalling that for each time step, our algorithm selects the maximum absolute variation possible, conditional on the value of the deviation from the mean for each parameter, there is no guarantee that the sequences generated by such chaotic or oscillatory regimes actually correspond to the theoretical trajectories maximizing variability within all possible trajectories.

The same calculations are carried for all four seasons, keeping constant the chosen values for parameters q and $|\mathcal{B}_i|^*$.

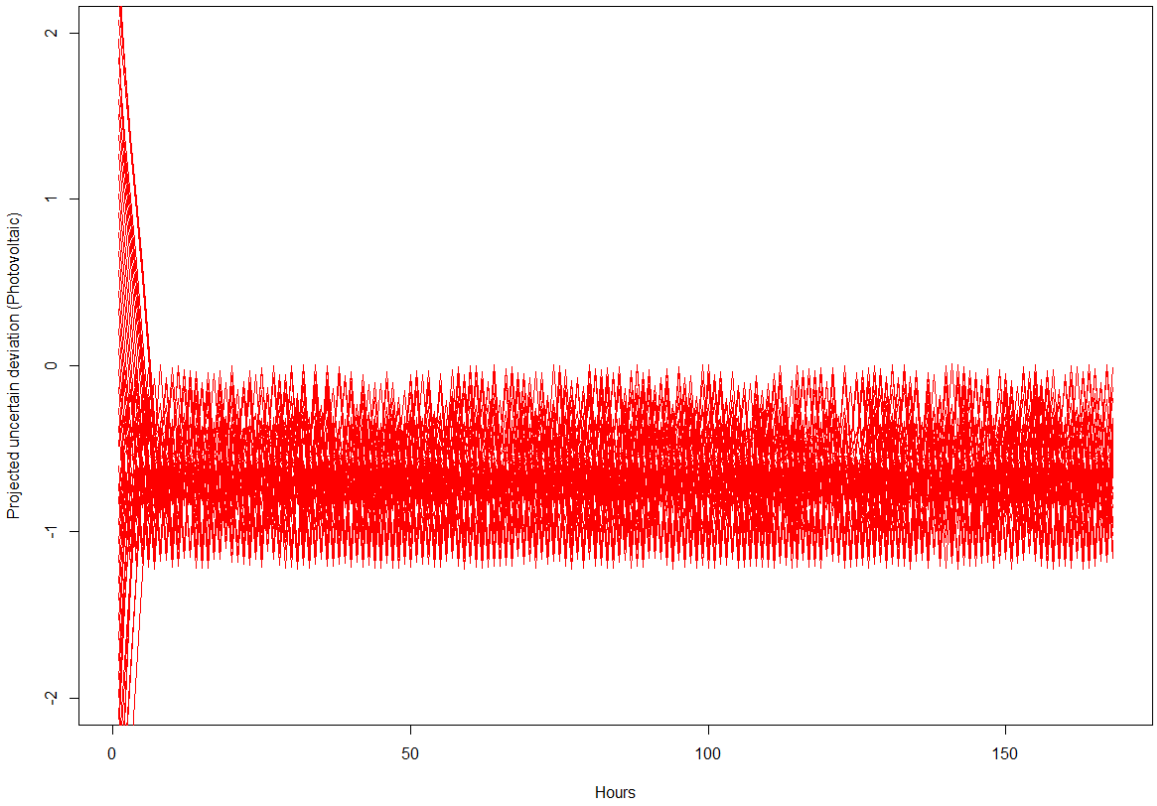

Figure 5.B.: q worst-case convergence patterns for π_{2t}^{V}

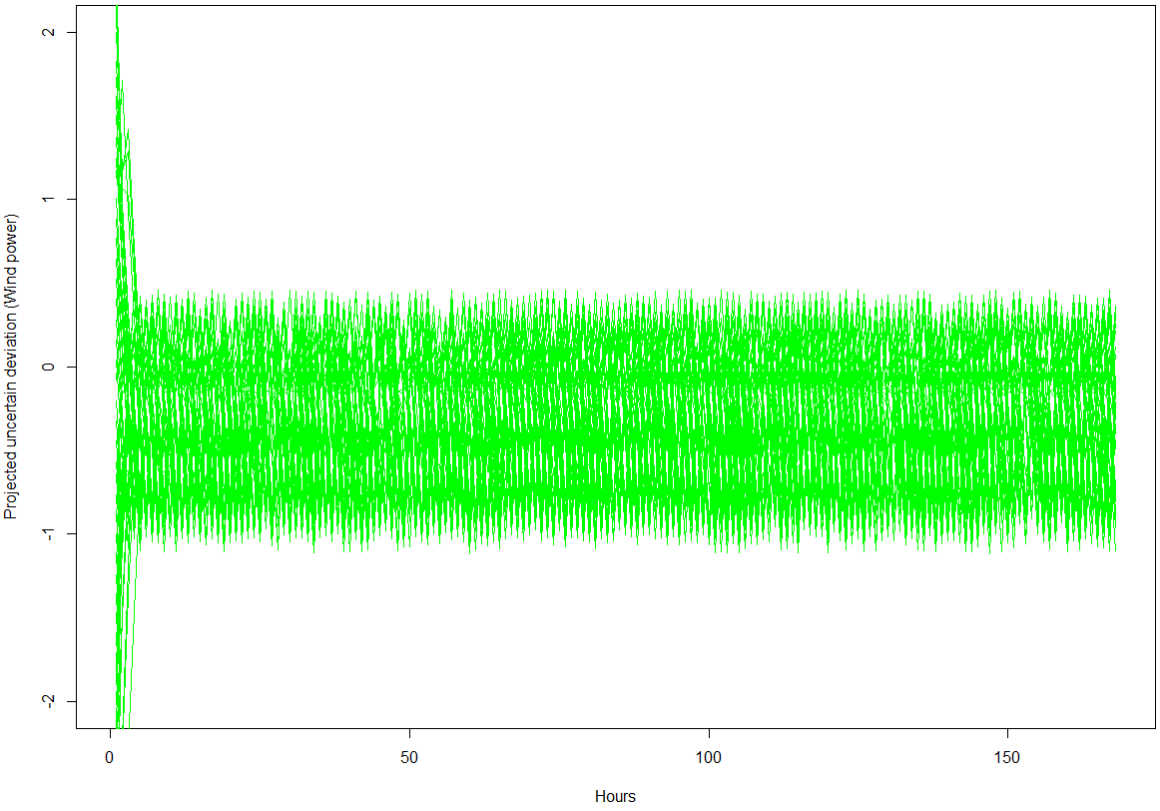

Figure 5.C.: q worst-case convergence patterns for π_{3t}^{V}

4.2. Baseline simulation results

We compare the investment levels and cost performance of the optimal mix obtained when hedging against a variety of extreme trajectories. We respectively note **L**, **H** and **V** the trajectories for which residual demand takes its lowest, highest and most volatile values. When hedging only against **H** or against the couple of trajectories **L** and **H**, we set N^R respectively equal to 1 and 2. Hedging against **L**,**H** and **V** consists in simultaneously hedging against all types of worst-case trajectories, with $N^R = 3$. We respectively refer to these three different hedging strategies as investment scenarios I_1, I_2 and I_3. As the variability of residual demand variability increases with renewable capacities, we may reasonably assumed that without any constraints on renewable capacity, it may be less costly to minimize investment in renewable capacity, so that additional costs required for enhancing system flexibility are avoided. In order to clearly observe the effects of renewable penetration on investment levels and cost performance, we constraint the wind and photovoltaic capacities to be equal to $\boldsymbol{S}$ GWe, where $\boldsymbol{S} \in \{0; 2; 4; 6\}$.

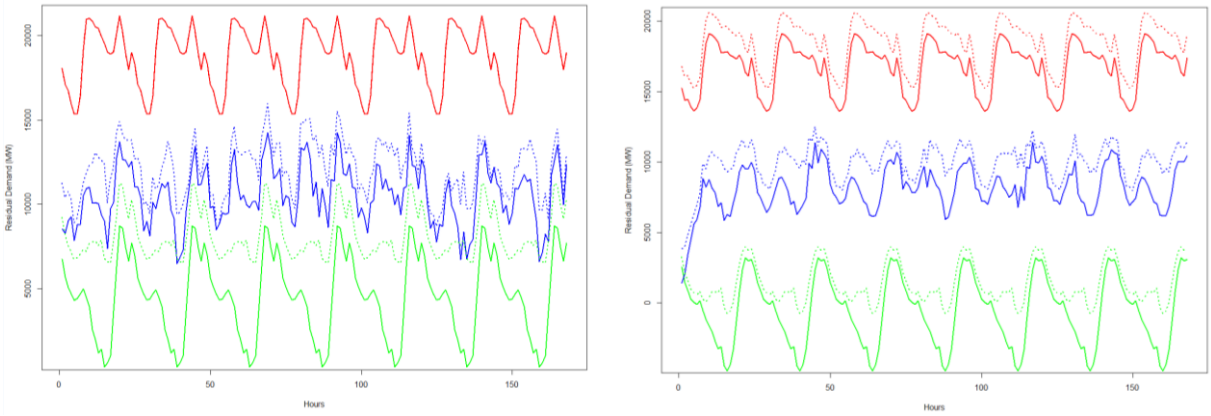

Figure 6: Extreme residual demand trajectories for Winter (left) and Summer (right), $q = 0.95$

Note: The red, green and blue plain curve corresponds to trajectory **H**, **L** and **V** for $\boldsymbol{S} = 6$. The dotted lines correspond to residual demand trajectories for $\boldsymbol{S} = 2$.

As illustrated in **Figure 6**, our method provides an interval for the set of values within which residual demand can fluctuate. As there exists a unique trajectory maximizing variability for each initial residual demand value, we compute the corresponding trajectory for different initial values and select the one with the maximum variability. In an extreme fashion, the

difference between the green dotted and plain lines strikingly shows how increasing renewable capacities reshapes the residual demand curve and increases the depth of the "duck dive" [15], which describes the timing imbalance between peak load in the evening and the solar generation peak in the afternoon. The difference between successive peaks and valleys on the green plain curve translates into a ramp need of approximately 10 GW within a few hours, for both seasons. This indicates an adequate generation mix under high renewable penetration requires production units with high ramping capacities and low minimum production levels, associated with an active management of renewable output, including energy storage, curtailment, and demand response. Finally, the rapid oscillations of the blue curves, which reflect residual demand short term variability, make visible the need for generation units with both moderate to high ramping capacities and low minimum uptime and downtime.

The optimal investment levels corresponding to a robustness level of $q = 0.95$ are reported in **Table 2.A**. First, the nuclear capacity is superior when hedging against trajectory **H** only (scenario I_1), while the investment in storage capacity is generally significantly lower compared to scenarios I_2 and I_3. Second, the optimal nuclear capacity decreases with renewable penetration, while the sum of CCGT and GT capacities increase in almost all scenarios. This confirms a higher renewable penetration requires higher generation flexibility from conventional plants, which translates into higher investment in peaking units with low minimum generation level and high ramping rates.

$q = 0.95$	I_1	I_2	I_3	I_1	I_2	I_3
	$S = 0$			$S = 2$		
Combined cycle gas turbine	2.7	12.15	9.45	2.7	12.15	10.8
Gas turbine	0	0	2.7	0	0.9	0
Nuclear	19.2	9.6	9.6	19.2	9.6	12.8
Wind	0	0	0	2	2	2
PV	0	0	0	2	2	2
Battery storage	3663.06	8472.327	8454.993	3541.751	3392.070	6388.972
	$S = 4$			$S = 6$		
Combined cycle gas turbine	6.75	14.85	10.8	5.4	12.15	12.15
Gas turbine	0	0.9	1.8	0	1.8	0.9
Nuclear	16	6.4	9.6	16	9.6	9.6
Wind	4	4	4	6	6	6
PV	4	4	4	6	6	6
Battery storage	2890.556	5030.130	9575.962	7302.519	3534.021	6928.550

Table 2.A.: Optimal investment level by technology for various levels of renewables capacity (in GWe)

Note: For any level of $\boldsymbol{S}$, the investment levels corresponding to column I_1 (resp. I_2) are obtained when hedging against the highest residual demand trajectory (resp. when hedging both against the lowest and highest residual demand trajectories).

Finally, no clear pattern regarding the complementarity or substitutability of storage and peaking units can be identified. While CCGT and storage capacities move in opposite directions in I_1, a weak positive correlation may be observed for I_2 and I_3 when $\boldsymbol{S} \geq 2$ GWe. This complementarity is explained by the fact that, while higher capacities in battery storage allow the smoothing of highly variable renewable production, thermal peaking technologies remain necessary as the capacity factors of wind and solar units are quasi null in **H**. This pattern of substitutability and complementarity of peaking units and storage, conditional on residual demand trajectories, generates a non-linear relationship between the level of renewable penetration and the required level of peaking capacities.

$q = 0.95$	I_1				I_2				I_3			
$S = 0$												
Total investment costs (B€)	75.48				47.07				46.11			
Average unit cost (week **H**, €/MWh)	9.907	8.282	8.282	12.01	35.33	27.74	33.51	36.56	38.20	27.73	33.54	43.72
Average unit cost (week **L**, €/MWh)	8.359	8.361	9.916	8.303	12.14	8.322	8.373	8.303	12.15	8.322	8.373	8.303
Average unit cost (week **V**, €/MWh)	8.296	8.304	8.286	8.330	28.78	20.31	12.37	16.35	28.77	20.30	12.37	16.35
$S = 2$												
Total investment costs (B€)	79.65				50.48				61.76			
Average unit cost (week **H**, €/MWh)	9.817	8.282	7.928	12.03	35.15	27.73	30.76	36.56	26.01	16.12	21.02	27.78
Average unit cost (week **L**, €/MWh)	6.971	6.116	7.966	7.043	7.847	6.611	8.674	6.686	6.973	5.668	6.541	5.500
Average unit cost (week **V**, €/MWh)	7.784	7.810	7.775	8.130	24.98	16.97	9.642	15.25	15.42	7.757	7.775	8.094
$S = 4$												
Total investment costs (B€)	84.28				44.54				54.77			
Average unit cost (week **H**, €/MWh)	16.87	8.282	10.03	19.14	44.11	39.39	37.76	45.78	35.01	27.73	28.02	38.69
Average unit cost (week **L**, €/MWh)	5.626	8.621	19.36	6.001	9.889	6.673	15.37	4.533	5.626	4.016	7.929	4.058
Average unit cost (week **V**, €/MWh)	7.292	7.301	7.268	7.945	32.44	26.67	21.03	28.62	21.14	13.54	7.248	14.70
$S = 6$												
Total investment costs (B€)	77.82				58.67				58.88			
Average unit cost (week **H**, €/MWh)	16.57	8.282	7.606	19.10	34.79	27.73	25.27	36.56	34.79	27.73	25.27	36.56
Average unit cost (week **L**, €/MWh)	4.666	26.86	39.44	17.33	4.823	29.58	45.18	20.43	4.453	27.07	39.31	17.69
Average unit cost (week **V**, €/MWh)	6.780	6.885	6.735	7.694	17.54	12.22	7.033	12.40	17.49	10.93	6.736	11.81

Table 2.B.: Total investment costs and average unit cost by worst-case trajectory for various levels of renewables capacity (in GWe)

Note: For each column I_1, I_2 and I_3, sub-columns respectively correspond to the average unit cost obtained for Winter, Spring, Summer and Autumn.

Table 2.B. summarizes the average unit generation cost, in €/MWh, and the total investment cost, in billion €, associated to each optimal mix presented in **Table 2.A**. When hedging against **H** only in scenario I_1, the significantly higher nuclear capacity entails consistently higher investment costs compared to I_2 and I_3. Yet, as we assume nuclear plants to have a higher minimum generation level and uptime/downtime compared to peaking units, mixes with significant nuclear capacities may not be flexible enough to accommodate large residual demand fluctuations if they are not adapted to the level of renewable capacities. The minimum generation level may be too high to keep plants running during periods with high renewable generation, leading to generation surpluses, curtailment or even infeasibilities (i.e. blackouts).

Surprisingly, in terms of average unit cost, the optimal mixes obtained in I_1 consistently outperforms the more flexible ones obtained in the I_2 and I_3 investment scenarios, for all three types of worst-case trajectories. Although the average unit cost for trajectory **H** increases with renewable penetration and for all seasons, it remains almost 60 % lower on average. While the average unit cost for trajectory **L** is higher for low renewable penetration levels, compared to values found for I_2 and I_3, this difference seems to vanish for high renewable capacities.

However, we may expect that a higher share of nuclear may result in higher curtailment levels for trajectory **L**. This is not confirmed by our simulations. When taking $\boldsymbol{S} = 6$, 17.3%, 17% and 7% of total wind generation is curtailed in Spring, Summer and Autumn respectively. Regarding photovoltaic generation, 29.5% of production is curtailed in Spring, 38.2% in Summer and 28.3% in Autumn. By comparison, respectively 22.3%, 19.9% and 9.1% of wind output is curtailed for I_2, while 26.4%, 43.8% and 32.4% of photovoltaic generation is curtailed. Finally, although I_3 is by construction the most flexible generation mix for any level of renewable penetration, 16.6%, 15.7% and 7.3% of wind generation are curtailed and photovoltaic curtailment levels remain above 30%. In theory, more flexible generation mixes with higher peaking capacities would result in lower curtailment levels as they can better accommodate rapid fluctuations of renewable output than nuclear plants. However, curtailment may be the less costly option overall, as renewable demand dynamics may require a succession of start-ups and shutdowns to accommodate their variability, which would be very costly for CCGT and GT technologies. In conclusion, we observe a clear trade-off between high fixed-low variable costs and low fixed-high variable costs mixes, depending on the targeted level of system flexibility.

However, comparing generation mixes in terms of cost performance over a sample of extreme scenario, with a potentially low probability of occurrence, has little relevance in terms of average cost performance. In order to approximate the yearly distribution of production cost associated with a given capacity mix, we approximate the yearly Net Load Duration Curve (NLDC) with a 4-week sample drawn from a set of 52 weeks, corresponding to a full year of demand and renewable production data. We then scale up the sample, so it matches the number of hours contained in one year, and sort the resulting residual demand distribution by decreasing order so we obtain an Approximate NLDC. This method is introduced in [16]. We select the sample of weeks (one week for each season) that minimizes the distance between the NLDC and Approximate NLDC, measured in terms of Root-Mean-Square-Error (RMSE) and normalized RMSE. Using 2018 as a reference year for our cost analysis, our optimal 4-

week sample has a RMSE of 93.53 and a normalized RMSE of 0.46 %, which corresponds to a highly accurate approximation. The approximate average yearly unit cost of generation is presented in **Table 2.C**.

$q = 0.95$	I_1	I_2	I_3
$S = 0$			
Approximate average unit cost (€/MWh)	8.320	20.41	20.83
$S = 2$			
Approximate average unit cost (€/MWh)	7.836	17.97	9.994
$S = 4$			
Approximate average unit cost (€/MWh)	7.417	27.15	14.74
$S = 6$			
Approximate average unit cost (€/MWh)	6.881	13.00	12.61

Table 2.C.: Approximate yearly average unit cost for various levels of renewables capacity (in GWe)

Again, for all levels of S, the optimal mix corresponding to the investment scenario I_1 outperforms other ones in terms of production cost performance. Moreover, while the approximate average unit generation cost decreases with renewable penetration, no clear trend can be observed for I_2 and I_3. The latter performs better than I_2 but remains on average twice as costly as I_1.

Overall, optimal generation mixes obtained when hedging against all three types of worst-case trajectories systematically exhibit lower investment costs, as they include a high share of peaking units with low overnight costs. However, these mixes systematically exhibit higher average unit production costs, both for extreme and representative trajectories, in addition to higher curtailment levels. In the absence of CO2 emission targets, our results entail a trade-off between investment and FOM costs on the one side, and production costs on the over side. Their respective importance depends on the life-duration of generation units, the probability of occurrence of extreme weeks and the distribution of costs between consumer categories.

4.3. Sensitivity analysis

4.3.1. Sensitivity to nuclear technical assumptions

As stated above, ramping constraints are not binding when using an hourly time step. While extremely volatile residual demand trajectories remain feasible with a large share of nuclear power in the mix, this may not be the case anymore using a minute time step. Moreover, as underlined in [17], a higher RES penetration increases the frequency of extreme nuclear power ramps and annual required shut downs/start-up events, which may eventually damage reactors.

Even though nuclear plants can technically be operated in load-following mode (see [18]), nuclear plants are traditionally operated in 'baseload' mode with low to moderate output variations. In order to capture the effect of this operation mode on investment and dispatching decisions, we constrain the absolute nuclear power ramp of each individual plant, denoted $\boldsymbol{r_{NUC}}$, to be inferior to 25% and 15% of the difference of the maximum and minimum generation level. The optimal investment and cost performance results are shown in **Table 3.A.**, **3.B**, **3.C.** and **Table 4.A.**, **4.B.** and **4.C.** respectively.

A comparison between **Table 3.A.** and **Table 2.A.** immediately shows that, for investment scenario I_1, the capacity of CCGT and GT units increases for any level of renewable penetration. This confirms that nuclear units were previously used in load-following and peaking modes. Except for null values of renewable penetration, the installed capacities of storage and peaking units are also generally higher for I_2 and I_3.

However, for any given investment case, a clear negative correlation between peaking units and storage capacities can be noted: an increase in storage capacities is associated with a decrease in peaking capacities. This negative correlation is even more marked in **Table 4.A.** in Appendix. This suggests that the magnitude of the elasticity of substitution between storage and peaking technologies (CCG and GT) depends of the technical characteristics of other technologies available in the mix.

$q = 0.95$ $r_{NUC} = 25\ \%$	I_1	I_2	I_3	I_1	I_2	I_3
	$S = 0$			$S = 2$		
Combined cycle gas turbine	6.75	12.150	8.1	6.75	12.150	10.8
Gas turbine	0	0	1.8	0	0.9	1.8
Nuclear	16	9.6	12.8	16	9.6	9.6
Wind	0	0	0	2	2	2
PV	0	0	0	2	2	2
Battery storage	8112.999	6219.146	7992.364	4399.080	9431.786	13850.776
	$S = 4$			$S = 6$		
Combined cycle gas turbine	6.75	12.150	14.85	6.75	12.15	12.15
Gas turbine	0	0.9	0.9	0	0.9	0.9
Nuclear	16	9.6	6.4	16	9.6	9.6
Wind	4	4	4	6	6	6
PV	4	4	4	6	6	6
Battery storage	4573.590	6419.424	6609.16	2890.556	9320.521	10627.595

Table 3.A.: Optimal investment level by technology for $r_{NUC} = 25\%$ and various levels of renewables capacity (in GWe)

The results in **Table 3.A.** confirm the idea that, in the absence of affordable Carbon Capture and Storage (CCS) technologies, diminishing the share of CO2 emitting capacities would be economically optimal from a social planner perspective only if mature, clean and flexible alternative dispatchable technologies are available[10].

In terms of physical constraints, the degree of substitutability of storage and peaking technologies is limited by a specific subset of residual demand sequences, which correspond to prolonged periods of low renewable generation, during which a minimum peaking capacity remains necessary. The substitutability of storage and peaking technologies must also be evaluated by the ability of storage units to balance residual demand variations at all time. The optimal storage capacity should indeed allow system balance for any residual demand trajectory. If storage technologies are too costly or do not allow system balance by

[10] Demand-side management, which is not treated in this paper, is a special case, as its elasticity of substitution with storage is a possible time-varying function of the correlation (and cross-correlations) of demand and renewable generation. If the correlation is negative, a share of demand (which is expected to be high) during low renewable generation periods may be transferred to high generation ones with lower demand.

compensating its variations in most situations, flexible peaking technologies remain necessary. The sequence of values taken by residual demand is greatly relevant to evaluate the feasibility of any storage decision sequence. This limitation is not explicitly accounted for in our model formulation but can easily be alleviated by adding an extra constraint on the moving average of residual demand net of storage inflows and outflows.

Moreover, our methodology maximizes residual demand variability locally, conditional on the value of residual demand, but offers no guarantee that it globally maximizes its total variability along its trajectory. Our model allows investment decisions hedging against residual demand trajectories that maximize short-term conditional volatility only. This limitation shall be the topic of the next chapter.

Table 3.B. and **4.B.** (see in Appendix) both show that even by decreasing nuclear units ramping rate, the average unit generation cost of nuclear based mixes remains unambiguously lower for all seasons, all investment cases and all levels of renewable penetration. Yet, decreasing nuclear flexibility increases the utilization rate of CCGT and GT units, which increases the average unit cost as they have higher marginal cost. Moreover, this flexibility loss translates into higher curtailment rates for I_1 compared to alternative investment scenarios. For trajectory **L**, with a nuclear ramping rate of 25% and $\boldsymbol{S} = 6$, 22.8%, 13.5% and 2.2% of wind generation are curtailed in Spring, Summer and Autumn respectively. Furthermore, 24.2% of photovoltaic production is now curtailed in Spring, 49.2% in Summer and 46.2% in Autumn. By comparison, respectively 16.2%, 14.5% and 5.2% of wind output is curtailed for I_3, while 28%, 31.4% and 25.2% of photovoltaic generation is curtailed.

As nuclear flexibility diminishes, the costs of renewable integration become comparatively higher for a mix with a high share of nuclear capacity. For scenario I_1, the decrease in nuclear flexibility is not counterbalanced by adaptation to low residual values trajectories, which results in higher curtailment rates for all seasons. However, for any level of renewable penetration, the economic performance of nuclear based mixes remains better, except for trajectory **L**, which consistently exhibits a higher average unit generation cost due to higher curtailment rates.

Finally, **Table 3.C.** and **Table 4.C.** in Appendix clearly show that, even when restricting nuclear units to strictly ‘baseload’ operation mode, nuclear based mixes remain on average the least expensive investment choice in terms of average unit cost.

$q = 0.95$ $r_{NUC} = 25\ \%$	I_1				I_2				I_3			
$S = 0$												
Total investment costs (B€)	67.25				46.69				56.82			
Average unit cost (week **H**, €/MWh)	17.09	8.282	14.10	19.06	35.33	27.73	33.51	36.56	26.20	16.13	23.77	28.69
Average unit cost (week **L**, €/MWh)	8.291	8.322	8.382	8.303	15.25	8.322	8.383	8.303	8.291	8.322	8.382	8.303
Average unit cost (week **V**, €/MWh)	8.287	8.306	8.288	8.295	28.77	20.36	12.76	16.42	17.49	8.620	8.288	8.295
$S = 2$												
Total investment costs (B€)	70.54				51.50				51.58			
Average unit cost (week **H**, €/MWh)	16.91	8.282	12.05	19.06	35.15	27.73	30.77	36.56	35.19	27.73	30.76	37.89
Average unit cost (week **L**, €/MWh)	6.972	6.258	9.511	5.502	6.949	5.185	6.637	5.502	6.949	5.180	6.412	5.502
Average unit cost (week **V**, €/MWh)	7.784	7.784	7.818	8.130	24.95	16.82	8.742	14.80	24.95	16.74	8.844	14.79
$S = 4$												
Total investment costs (B€)	74.47				54.89				44.80			
Average unit cost (week **H**, €/MWh)	16.73	8.282	9.803	19.06	34.97	27.73	28.02	36.56	44.11	39.39	37.76	45.52
Average unit cost (week **L**, €/MWh)	5.628	7.524	16.47	4.698	5.770	5.859	13.06	5.392	9.511	6.694	13.03	5.238
Average unit cost (week **V**, €/MWh)	7.292	7.303	7.312	7.914	21.14	13.60	7.623	13.27	32.44	26.63	21.08	28.62
$S = 6$												
Total investment costs (B€)	78.09				59.29				59.51			
Average unit cost (week **H**, €/MWh)	16.82	8.282	8.125	19.14	34.79	27.73	25.27	36.56	34.79	27.73	25.27	36.56
Average unit cost (week **L**, €/MWh)	5.113	30.59	46.54	21.63	8.884	25.76	33.97	15.79	4.703	25.05	36.14	38.72
Average unit cost (week **V**, €/MWh)	6.802	6.950	6.806	7.768	17.51	10.54	6.817	11.77	17.45	10.27	6.770	11.78

Table 3.B.: Total investment costs and average unit cost by worst-case trajectory for $r_{NUC} = 25\%$ and various levels of renewables capacity (in GWe)

$q = 0.95$ $r_{NUC} = 25\ \%$	I_1	I_2	I_3
$S = 0$			
Approximate average unit cost (€/MWh)	8.443	20.93	11.51
$S = 2$			
Approximate average unit cost (€/MWh)	7.869	17.63	17.57
$S = 4$			
Approximate average unit cost (€/MWh)	7.354	14.95	27.12
$S = 6$			
Approximate average unit cost (€/MWh)	6.911	12.46	12.35

Table 3.C.: Approximate yearly average unit cost for $r_{NUC} = 25\%$ and various levels of renewables capacity (in GWe)

4.3.2. Sensitivity to robustness parameter q

We can finally study the sensitivity of our results to the degree of robustness of our model, controlled by parameter q. By definition, for $q = 1$, the set of extreme residual demand trajectories, defined by our simulation method, includes trajectories with the most extreme variations and is thus expected to be the most conservative. The conservativeness of solutions can then be diminished by decreasing q, but the proportion of infeasible trajectories might increase. The value of q can be chosen by defining a probabilistic threshold so that values of q that generate trajectories with a joint probability below this threshold are ruled out.

We set $q = 0.75$. The optimal investment levels are shown in **Table 5.A.**. We note that for scenario I_1, the capacity of CCGT increases while the capacity of nuclear decreases for low renewable penetration. As the cost advantage of nuclear technology decreases with the required volume of generation, CCGT become comparatively less costly, in terms of total overnight and generation costs. Unsurprisingly, the total installed capacity decreases for all investment case and level of renewable penetration.

$q = 0.75$	I_1	I_2	I_3	I_1	I_2	I_3
	$S = 0$			$S = 2$		
Combined cycle gas turbine	4.050	9.45	6.75	4.050	12.15	9.45
Gas turbine	0	0	0	0	0	0.9
Nuclear	16	9.6	12.8	16	6.4	9.6
Wind	0	0	0	2	2	2
PV	0	0	0	2	2	2
Battery storage	1131.393	6680.721	10858.910	1211.035	13952.555	9866.306
	$S = 4$			$S = 6$		
Combined cycle gas turbine	4.050	13.5	9.45	4.050	10.8	9.45
Gas turbine	0	0	0.9	0	2.7	0.9
Nuclear	16	6.4	9.6	16	6.4	9.6
Wind	4	4	4	6	6	6
PV	4	4	4	6	6	6
Battery storage	4081.681	2184.314	984.991	4317.095	3287.598	10798.593

Table 5.A.: Optimal investment level by technology for $q = 0.75$ and various levels of renewables capacity (in GWe)

These observations translate into lower investment costs for all mixes, as shown in **Table 5.B.**. Simultaneously, the average unit generation costs associated with trajectory **L** are

generally lower compared to **Table 2.B.**, while the unit cost associated with trajectory **H** are consistently higher. The lower share of nuclear and storage capacities translates into a higher utilization rate of peaking units during high demand periods, while less curtailment is necessary during periods with strong renewable generation.

This finally translates into higher approximate average unit costs for all investment cases and renewable installed capacity level. A higher degree of conservativeness, associated to a higher q, thus automatically results in higher total installed capacities and investment costs, but may result in better unit cost performance depending on the mix composition.

$q = 0.75$	I_1				I_2				I_3			
$S = 0$												
Total investment costs (B€)	64.04				44.73				55.56			
Average unit cost (week **H**, €/MWh)	14.84	7.617	14.94	12.58	32.60	22.55	33.85	28.86	23.40	11.41	24.07	20.08
Average unit cost (week **L**, €/MWh)	8.649	8.847	11.62	8.661	14.66	8.877	11.48	8.601	8.633	8.816	9.201	8.601
Average unit cost (week **V**, €/MWh)	8.462	8.379	8.837	7.783	26.95	20.64	17.15	12.86	15.68	8.372	8.837	7.765
$S = 2$												
Total investment costs (B€)	67.96				39.74				49.53			
Average unit cost (week **H**, €/MWh)	14.83	7.616	12.39	13.88	41.80	34.21	40.45	37.65	32.60	22.54	30.69	28.86
Average unit cost (week **L**, €/MWh)	7.455	6.924	26.38	6.508	22.11	5.931	6.218	5.983	7.818	5.931	10.16	5.983
Average unit cost (week **V**, €/MWh)	7.522	7.792	8.326	7.337	34.24	30.09	28.96	24.28	22.92	16.62	13.53	9.805
$S = 4$												
Total investment costs (B€)	72.35				42.68				51.94			
Average unit cost (week **H**, €/MWh)	14.51	7.598	9.554	12.20	41.66	34.21	37.31	37.57	34.22	22.54	27.57	29.45
Average unit cost (week **L**, €/MWh)	6.194	5.352	12.32	5.000	13.83	16.98	15.80	5.395	6.963	7.237	20.08	17.17
Average unit cost (week **V**, €/MWh)	6.985	7.172	7.778	6.859	30.21	26.09	25.57	21.05	19.06	13.38	11.50	9.504
$S = 6$												
Total investment costs (B€)	76.30				45.81				57.50			
Average unit cost (week **H**, €/MWh)	14.48	7.598	11.13	12.20	49.59	34.21	34.20	42.78	32.60	22.54	24.45	28.86
Average unit cost (week **L**, €/MWh)	5.548	21.31	37.95	16.00	8.731	21.93	39.72	16.96	4.970	16.60	25.43	11.21
Average unit cost (week **V**, €/MWh)	6.467	6.804	7.263	6.412	26.19	22.36	21.99	18.04	15.11	9.481	7.360	6.399

Table 5.B.: Total investment costs and average unit cost by worst-case trajectory for $q = 0.75$ and various levels of renewables capacity (in GWe)

$q = 0.75$	I_1	I_2	I_3
$S = 0$			
Approximate average unit cost (€/MWh)	8.757	20.92	11.47
$S = 2$			
Approximate average unit cost (€/MWh)	8.369	30.70	17.62
$S = 4$			
Approximate average unit cost (€/MWh)	7.360	27.22	15.64
$S = 6$			
Approximate average unit cost (€/MWh)	6.932	23.86	12.34

Table 5.C.: Approximate yearly average unit cost for $q = 0.75$ and various levels of renewables capacity (in GWe)

5. Conclusion

This paper presents an original approach to robust optimization, that does not require the definition of any uncertainty set contrary to more traditional approaches. As the dynamics of robustness have received little attention so far, we approximate the variations of uncertain parameters between successive periods using a flexible polynomial approximation method. This framework allows the estimation of a continuous approximation function, the shape of which and prevision interval can be tightly configured depending on the quality and distribution of the training data. This allows defining a set of limiting residual demand trajectories. However, the variability maximizing trajectory only maximizes locally the variations of residual demand. We leave for further research the definition a solution for determining the trajectory which globally maximizes residual demand trajectory over its full length.

Finally, we showed the usefulness of our enriched robust optimization method with an application to the case of Auvergne Rhône-Alpes. Hedging against trajectories with extremely high short-term variability globally increased the optimal storage and peaking capacities. Our results show that mixes with a high share of nuclear globally performed generally economically better, with significantly lower variable costs than theoretically more “flexible” and adapted mixes. Still, due to the significant share of CCGT and GT capacities, more “flexible” have lower investment and fixed costs. Moreover, our results suggest that, as the stress on nuclear plants may increase with renewable penetration, a nuclear-based mix may

rapidly become too costly and inefficient for high renewable capacities. In the absence of low cost and non-CO2 emitting alternative peaking technology, increasing renewable penetration while significantly decreasing the share of carbon emitting capacities seems economically suboptimal and technically difficult without harming the stability of the electric system balance or requiring frequent curtailment. Yet, the increase in curtailment costs associated to higher renewable penetration may provide a cost-effective strategy to maintain a significant nuclear base load production, thereby keeping the average generation cost low. Moreover, we show that curtailment does not necessarily decrease with peaking capacities: the high start-up costs of CCGT and GT turbines may make curtailment more cost-effective and increase balancing costs if they must be turned on and off more often.

Yet, decreasing the share of conventional generators may decrease the physical inertia of the electric system, which may further increase the likelihood of frequency deviations and damage to low flexibility units. Moreover, our methodology does not take into account very short-term ramping limitations and residual demand uncertainty. This would question the observed advantages of nuclear based mixes. Intensive demand-side management and hydrogen based inter-seasonal storage, in addition to stability solutions such as synchronous condensers, fast frequency responses and grid-forming converters [19] offer a panel of promising options to be studied in further research.

6. Appendix

Appendix to 3.3.:

We define the matrix $\boldsymbol{\pi}_{0\to|\mathcal{T}|}^{+} = \left(\boldsymbol{\pi}_{0}^{+}, \boldsymbol{\pi}_{1}^{+}, \dots, \boldsymbol{\pi}_{|\mathcal{T}|}^{+}\right) \in \mathbb{R}^{n\times(|\mathcal{T}|+1)}$ and the probability threshold $\rho > 0$ such that we must have:

$$\mathbb{P}\left(\boldsymbol{\pi}_{0\to|\mathcal{T}|}^{+}\right) = \prod_{t'=0}^{|\mathcal{T}|} \mathbb{P}(\boldsymbol{\pi}_{t'}^{+}) = \mathbb{P}(\boldsymbol{\pi}_{0}^{+}) \prod_{t'=1}^{|\mathcal{T}|} \mathbb{P}(\boldsymbol{\pi}_{t'}^{+}|\boldsymbol{\pi}_{t'-1}) \geq \rho \qquad (\mathbf{52a})$$

For clarity and without loss of generality, we drop the subscript s corresponding to seasons. Using the Frechet's inequality twice, we have:

$$\mathbb{P}\left(\boldsymbol{\pi}_{0\to|\mathcal{T}|}^{+}\right) = \prod_{t'=0}^{|\mathcal{T}|} \mathbb{P}(\boldsymbol{\pi}_{t'}^{+}) \geq \max\left(0, \sum_{t'=0}^{|\mathcal{T}|} \mathbb{P}\left(\boldsymbol{\pi}_{t'}^{+}\right) - |\mathcal{T}|\right) \geq \max\left(0, \sum_{t'=1}^{|\mathcal{T}|} \max\left(0, \sum_{i=1}^{n} \mathbb{P}\left(\pi_{it'}^{+}\right) - (n-1)\right) - |\mathcal{T}|\right) \qquad (\mathbf{52b})$$

Without loss of generality, assuming that for π_t^+ strictly positive, we have for any real vector $\boldsymbol{\epsilon}$ that $\mathbb{P}(\boldsymbol{\pi}_t^+|\boldsymbol{\pi}_{t-1}) \leq \mathbb{P}(\boldsymbol{\pi}_t^+ + \boldsymbol{\epsilon}|\boldsymbol{\pi}_{t-1}) \Leftrightarrow \boldsymbol{\epsilon} \geq 0$. We introduce auxiliary variables $\eth_{it}^{+}$ such that we have the following set of constraints for all $i \leq n$:

$$\pi_{it}^{+} = \pi_{it-1}^{+} + \eth_{it}^{+} \qquad (\mathbf{53})$$

$$\eth_{it}^{+} \leq \lambda_{i0t} \boldsymbol{\Phi}_{i,*}^{-T} \widehat{\boldsymbol{\varphi}^{0}}\left(\alpha, |\boldsymbol{\mathcal{B}}|^{*} \middle| \boldsymbol{\Phi}_{i,*}^{T} \boldsymbol{\pi}_{t-1}^{V}\right) + \sum_{q\in\mathcal{Q}\setminus\{0\}} \lambda_{iqt} \left(\boldsymbol{\Phi}_{i,*}^{-T} \widehat{\boldsymbol{\varphi}^{q}}\left(\alpha, |\boldsymbol{\mathcal{B}}|^{*} \middle| \boldsymbol{\Phi}_{i,*}^{T} \boldsymbol{\pi}_{t-1}^{V}\right) - \boldsymbol{\Phi}_{i,*}^{-T} \widehat{\boldsymbol{\varphi}^{q-|\mathcal{Q}|}}^{-1}\left(\alpha, |\boldsymbol{\mathcal{B}}|^{*} \middle| \boldsymbol{\Phi}_{i,*}^{T} \boldsymbol{\pi}_{t-1}^{V}\right)\right) \qquad (\mathbf{54})$$

$$\max\left(0, \sum_{t'=0}^{|\mathcal{T}|} \left(\max\left(0, \sum_{i=1}^{n} \left(1 - \sum_{q\in\mathcal{Q}\setminus\{0\}} \lambda_{iqt'} |\mathcal{Q}|^{-1}\right) - (n-1)\right)\right) - |\mathcal{T}|\right) \geq \rho \qquad (\mathbf{55})$$

$$\lambda_{iqt} \in [0; 1] \qquad (\mathbf{56})$$

$\boldsymbol{\Phi}_{i,*}^{T}$ corresponds to the i-th line of $\boldsymbol{\Phi}^{T}$. Using the monotonicity of $\mathbb{P}\left(\boldsymbol{\pi}_{0\to|\mathcal{T}|}^{+}\right)$, the probability of any given trajectory will decrease when $\boldsymbol{\pi}_{0\to|\mathcal{T}|}^{+}$ increases. However, due to the multidimensionality of $\boldsymbol{\pi}_{0\to|\mathcal{T}|}^{+}$, there exists an infinity of "worst-case" vectors which saturate **(55)**. To see this, we can reformulate **(55)** as follows:

$$\max\left(0,\sum_{t'=0}^{\tau}\left(\max\left(\sum_{i=1}^{n}\left(1-\sum_{q\in\mathcal{Q}\setminus\{0\}}\lambda_{iqt'}|\mathcal{Q}|^{-1}\right)-(n-1)\right)\right)\right.$$
$$\left.+\sum_{t'=\tau+1}^{|\mathcal{T}|}\left(\max\left(0,\sum_{i=1}^{n}\left(1-\sum_{q\in\mathcal{Q}\setminus\{0\}}\lambda_{iqt'}|\mathcal{Q}|^{-1}\right)-(n-1)\right)\right)-|\mathcal{T}|\right)\geq\rho \quad (\mathbf{57})$$

An increase in the left-hand side is associated with a decrease in the right-side one. In order to define the sequence $\{\eth_{it}^{+}\}_{t\in\mathcal{T}}$ that maximizes the vector length of $\boldsymbol{\pi}_{0\to|\mathcal{T}|}^{+}$, we solve the following linear binary optimization problem:

$$\max_{\eth}\sum_{i=1}^{n}\sum_{t=1}^{|\mathcal{T}|}\eth_{it}^{+}$$

s.t. **(53)-(56)** hold. Likewise, the trajectory $\{\eth_{it}^{-}\}_{t\in\mathcal{T}}$ that minimizes the vector length of $\boldsymbol{\pi}_{0\to|\mathcal{T}|}^{-}$ is the solution to the following linear optimization problem:

$$\min_{\eth}\sum_{i=1}^{n}\sum_{t=1}^{|\mathcal{T}|}\eth_{it}^{-}$$

s.t. **(56)** holds and:

$$\pi_{it}^{-}=\pi_{it-1}^{-}+\eth_{it}^{-} \quad (\mathbf{58})$$

$$\eth_{it}^{-}\geq\lambda_{i0t}\boldsymbol{\Phi}_{i,*}^{-T}\widehat{\boldsymbol{\varphi}^{1}}\left(\alpha,|\boldsymbol{\mathcal{B}}|^{*}\middle|\boldsymbol{\Phi}_{i,*}^{T}\boldsymbol{\pi}_{t-1}^{V}\right)$$
$$+\sum_{q\in\mathcal{Q}\setminus\{0\}}\lambda_{iqt}\left(\boldsymbol{\Phi}_{i,*}^{-T}\widehat{\boldsymbol{\varphi}^{1-q}}\left(\alpha,|\boldsymbol{\mathcal{B}}|^{*}\middle|\boldsymbol{\Phi}_{i,*}^{T}\boldsymbol{\pi}_{t-1}^{V}\right)-\boldsymbol{\Phi}_{i,*}^{-T}\widehat{\boldsymbol{\varphi}^{1-q+|\mathcal{Q}|^{-1}}}\left(\alpha,|\boldsymbol{\mathcal{B}}|^{*}\middle|\boldsymbol{\Phi}_{i,*}^{T}\boldsymbol{\pi}_{t-1}^{V}\right)\right) \quad (\mathbf{59})$$

$$\max\left(0,\sum_{t'=0}^{|\mathcal{T}|}\left(\max\left(0,\sum_{i=1}^{n}\left(1-\sum_{q\in\mathcal{Q}\setminus\{0\}}\lambda_{iqt'}|\mathcal{Q}|^{-1}\right)-(n-1)\right)\right)-|\mathcal{T}|\right)\geq\rho \quad (\mathbf{60})$$

In a similar fashion, we can express the trajectory $\{\eth_{it}^{V}\}_{t\in\mathcal{T}}$ that maximizes the variability of the vector $\boldsymbol{\pi}_{0\to|\mathcal{T}|}^{V}$ such that $\mathbb{P}\left(\boldsymbol{\pi}_{0\to|\mathcal{T}|}^{V}\right)$ as the solution of the following quadratic optimization problem:

$$\max_{\eth}\sqrt{\sum_{i=1}^{n}\sum_{t=1}^{|\mathcal{T}|}{\eth_{it}^{V}}^{2}}$$

s.t. **(56)** holds and:

$$\pi_{it}^{V}=\pi_{it-1}^{V}+\eth_{it}^{V} \quad (\mathbf{61})$$

$$\eth_{it}^{V} \leq \lambda_{imt}\boldsymbol{\Phi}_{i,*}^{-T}\widehat{\boldsymbol{\varphi}^{m}}\left(\alpha, |\boldsymbol{\mathcal{B}}|^{*}\middle|\boldsymbol{\Phi}_{i,*}^{T}\boldsymbol{\pi}_{t-1}^{V}\right) + \sum_{q\in\mathcal{Q}\setminus\mathcal{Q}_{m}^{-}} \lambda_{iqt}\left(\boldsymbol{\Phi}_{i,*}^{-T}\widehat{\boldsymbol{\varphi}^{q}}\left(\alpha, |\boldsymbol{\mathcal{B}}|^{*}\middle|\boldsymbol{\Phi}_{i,*}^{T}\boldsymbol{\pi}_{t-1}^{V}\right) - \boldsymbol{\Phi}_{i,*}^{-T}\widehat{\boldsymbol{\varphi}^{q-|\mathcal{Q}|^{-1}}}\left(\alpha, |\boldsymbol{\mathcal{B}}|^{*}\middle|\boldsymbol{\Phi}_{i,*}^{T}\boldsymbol{\pi}_{t-1}^{V}\right)\right) \quad (\mathbf{62a})$$

$$\eth_{it}^{V} \geq \lambda_{imt}\boldsymbol{\Phi}_{i,*}^{-T}\widehat{\boldsymbol{\varphi}^{m}}\left(\alpha, |\boldsymbol{\mathcal{B}}|^{*}\middle|\boldsymbol{\Phi}_{i,*}^{T}\boldsymbol{\pi}_{t-1}^{V}\right) + \sum_{q\in\mathcal{Q}\setminus\mathcal{Q}_{m}^{+}} \lambda_{iqt}\left(\boldsymbol{\Phi}_{i,*}^{-T}\widehat{\boldsymbol{\varphi}^{m-q}}\left(\alpha, |\boldsymbol{\mathcal{B}}|^{*}\middle|\boldsymbol{\Phi}_{i,*}^{T}\boldsymbol{\pi}_{t-1}^{V}\right) - \boldsymbol{\Phi}_{i,*}^{-T}\widehat{\boldsymbol{\varphi}^{m-q+|\mathcal{Q}|^{-1}}}\left(\alpha, |\boldsymbol{\mathcal{B}}|^{*}\middle|\boldsymbol{\Phi}_{i,*}^{T}\boldsymbol{\pi}_{t-1}^{V}\right)\right) \quad (\mathbf{62b})$$

$$\max\left(0, \sum_{t'=0}^{|\mathcal{T}|}\left(\max\left(\sum_{i=1}^{n}\left(\left(m - \left(\sum_{q\in\mathcal{Q}\setminus\mathcal{Q}_{m}^{-}} \lambda_{qt'}|\mathcal{Q}|^{-1} + \sum_{q\in\mathcal{Q}\setminus\mathcal{Q}_{m}^{+}} \lambda_{qt'}|\mathcal{Q}|^{-1}\right)\right)\right) - (n-1)\right)\right) - |\mathcal{T}|\right) \geq \rho \quad (\mathbf{63})$$

$$m - \left(\sum_{q\in\mathcal{Q}\setminus\mathcal{Q}_{m}^{-}} \lambda_{qt}|\mathcal{Q}|^{-1} + \sum_{q\in\mathcal{Q}\setminus\mathcal{Q}_{m}^{+}} \lambda_{qt}|\mathcal{Q}|^{-1}\right) \geq 0 \quad (\mathbf{64})$$

Where we define the subsets $\mathcal{Q}_{m}^{+} \subset \mathcal{Q}$ and $\mathcal{Q}_{m}^{-} \subset \mathcal{Q}$ such that $\mathcal{Q}_{m}^{+} \cap \mathcal{Q}_{m}^{-} = \emptyset$ and $\mathcal{Q}_{m}^{+} \cup \mathcal{Q}_{m}^{-} \cup q_m = \mathcal{Q}$, with q_m corresponding to the median. As $\lambda_{qt} = 0$ for the subset of quantiles that does not maximize the objective function in period $t \in \mathcal{T}$, **(64)** may be redundant. Yet, in order to ensure proper behavior of the model, we further impose **(64)** so that $\eth_{it}^{V}$ is always associated to a positive probability.

Appendix to 4:

Technology	Minimum generation level (% nominal power)	Ramping rate (% of nominal power/min)	Minimum uptime/downtime (hours)	Average CO_2 emission factor (ton/MWh)
Combined cycle gas turbine	20	20	0	0.352
Gas turbine	15	8	2	0.777
Nuclear	50	2-5	10	0

Table 1.A.: Technical characteristics of main thermal technologies

Sources : Gonzalez-Salazar et al. (2018), IAEA (2018), Schill et al. (2016), IEA (2015), Schröder et al. (2013), EC JRC (2010), RTE Bilan Electrique 2019 (RTE, 2019)

Technology	Overnight cost (€/kWe)	Annual fixed & maintenance costs (€/kWe)	Unit variable cost (€/MWh)	Unit starting cost (€/MWh)	Average lifetime (years)
Combined cycle gas turbine	754	20	45	235	30
Gas turbine	400	6.4	135	542.8	30
Nuclear	3800	137	8	90	60
Photovoltaic	669	19	0	0	25
Wind power	1284	45	0	0	20
Battery storage	169	5.1	0	0	10

Table 1.B.: Cost assumptions for generation technologies for 2021

Sources : Le Cout des ENR en France, ADEME (2016) ; CRE (2018) ; "Coûts et rentabilité du grand photovoltaïque en métropole continentale", CRE (2019) ; IEA (2015) ; "Current and Prospective Costs of Electricity Generation until 2050", DIW (2013) ; OECD/IEA-NEA (2015)

Appendix to 4.1.1. :

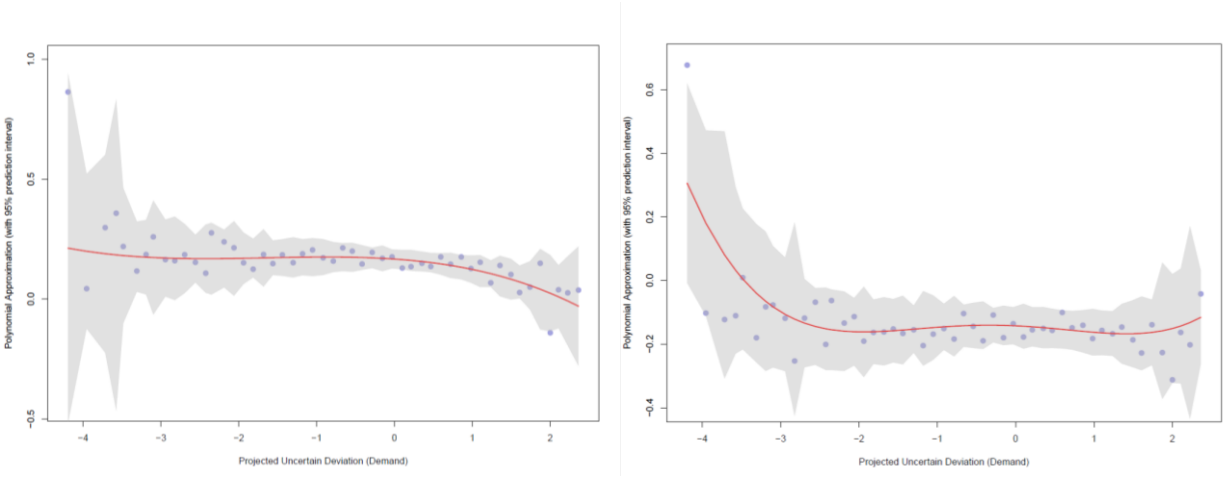

Figure 3.A.: Upper and lower quantile polynomial approximation for electricity demand for $q = 0.75$

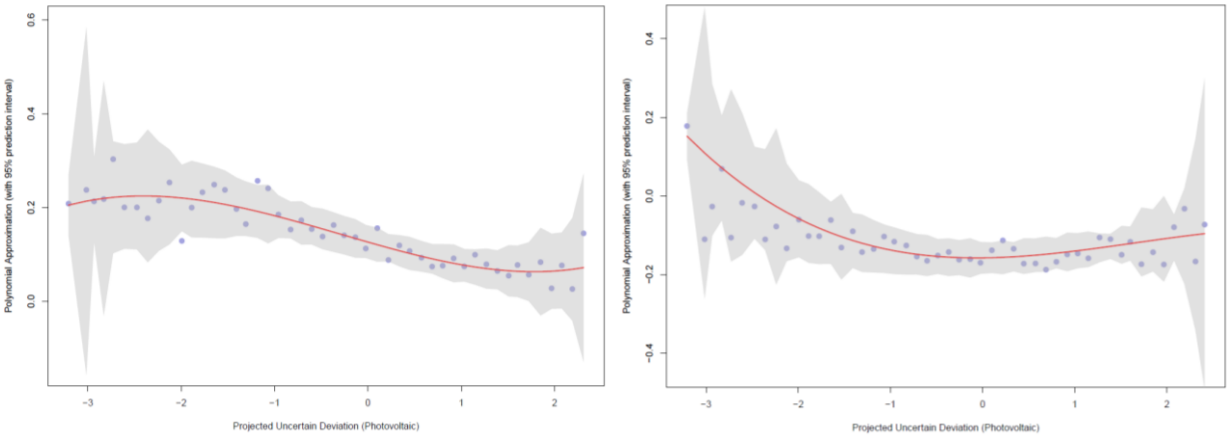

Figure 3.B.: Upper and lower quantile polynomial approximation for photovoltaic capacity factor for $q = 0.75$

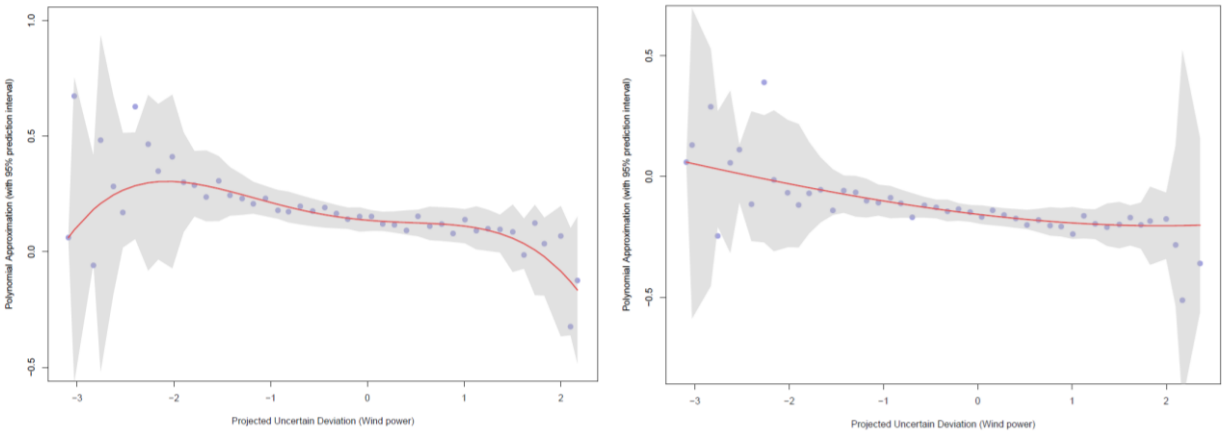

Figure 3.C.: Upper and lower quantile polynomial approximation for wind capacity factor for $q = 0.75$

Appendix to 4.3.1.:

$q = 0.95$ $r_{NUC} = 15\ \%$	I_1	I_2	I_3	I_1	I_2	I_3
	$S = 0$			$S = 2$		
Combined cycle gas turbine	2.7	12.15	8.1	6.75	12.150	14.85
Gas turbine	0	0	0	0	0.9	0
Nuclear	19.2	9.6	12.8	16	9.6	6.4
Wind	0	0	0	2	2	2
PV	0	0	0	2	2	2
Battery storage	3743.083	10434.345	11884.191	2890.556	4511.516	7044.852
	$S = 4$			$S = 6$		
Combined cycle gas turbine	2.7	12.150	10.8	5.4	14.850	13.5
Gas turbine	0	0.9	0.9	0	1.8	2.7
Nuclear	19.2	9.6	9.6	16	6.4	6.4
Wind	4	4	4	6	6	6
PV	4	4	4	6	6	6
Battery storage	2444.324	5503.534	8590.854	5035.049	2277.660	2335.401

Table 4.A.: Optimal investment level by technology for $r_{NUC} = 15\%$ and various levels of renewables capacity (in GWe)

$q = 0.95$ $r_{NUC} = 15\ \%$	I_1				I_2				I_3			
$S = 0$												
Total investment costs (B€)	75.63				47.70				56.75			
Average unit cost (week **H**, €/MWh)	9.899	8.282	8.282	12.05	35.33	27.73	33.51	36.56	26.20	16.16	23.77	27.90
Average unit cost (week **L**, €/MWh)	8.320	8.373	9.799	8.306	24.93	8.389	8.400	8.306	8.291	8.324	8400	8.306
Average unit cost (week **V**, €/MWh)	8.298	8.375	8.366	11.35	28.77	20.25	12.61	16.34	17.49	8.297	8.291	8.295
$S = 2$												
Total investment costs (B€)	70.28				50.67				40.61			
Average unit cost (week **H**, €/MWh)	17.03	8.282	12.27	19.14	35.15	27.73	30.76	36.56	44.29	39.39	40.51	45.35
Average unit cost (week **L**, €/MWh)	6.975	7.020	10.42	6.557	7.524	6.079	13.05	6.178	18.63	6.340	6.943	5.510
Average unit cost (week **V**, €/MWh)	7.823	8.014	9.172	8.170	24.95	16.95	9.971	15.21	36.27	30.19	24.94	30.19
$S = 4$												
Total investment costs (B€)	83.22				54.74				54.60			
Average unit cost (week **H**, €/MWh)	9.823	8.306	7.579	12.16	34.97	27.73	28.02	36.56	35.01	27.73	28.02	38.87
Average unit cost (week **L**, €/MWh)	5.923	9.459	21.19	6.819	5.635	11.44	15.66	4.462	5.883	5.240	9.732	4.499
Average unit cost (week **V**, €/MWh)	7.303	7.398	7.354	7.973	21.14	13.68	7.955	13.44	21.29	13.70	7.525	13.27
$S = 6$												
Total investment costs (B€)	77.44				48.34				47.69			
Average unit cost (week **H**, €/MWh)	16.56	8.282	7.900	19.10	43.93	39.39	35.01	45.69	44.81	39.39	35.01	50.60
Average unit cost (week **L**, €/MWh)	5.346	28.98	60.54	19.42	7.136	28.74	41.88	19.00	9.053	46.11	77.82	22.24
Average unit cost (week **V**, €/MWh)	6.808	6.895	6.845	7.702	28.62	23.49	20.61	27.06	28.62	25.03	17.69	27.10

Table 4.B.: Total investment costs and average unit cost by worst-case trajectory for $r_{NUC} = 15\%$ and various levels of renewables capacity (in GWe)

$q = 0.95$ $r_{NUC} = 15\ \%$	I_1	I_2	I_3
$S = 0$			
Approximate average unit cost (€/MWh)	8.323	21.67	11.46
$S = 2$			
Approximate average unit cost (€/MWh)	8.324	17.87	30.70
$S = 4$			
Approximate average unit cost (€/MWh)	7.439	14.97	15.45
$S = 6$			
Approximate average unit cost (€/MWh)	6.974	23.80	23.97

Table 3.C.: Approximate yearly average unit cost for $r_{NUC} = 15\%$ and various levels of renewables capacity (in GWe)

7. Bibliography

[1] ENGELAND Kolbjørn et al. “Space-time variability of climate variables and intermittent renewable electricity production- A review”, *Renewable and Substainable Energy Reviews*, vol. 79, 2017, pp. 600-617

[2] NOURAI Ali & SCHAFER Chris, “Changing the electricity game”, *IEEE Power and Energy Magazine*, vol.7, n°4, 2009

[3] ZUGNO Marco, CONEJO Antonio J., “A Robust Optimization Approach to Energy and Reserve Dispatch in Electricity Markets”, Technical University of Denmark. Technical Report-2013, n°5

[4] SOYSTER A.L., “Convex programming with set-inclusive constraints and applications to inexact linear programming”, *Operations Research*, vol. 21, 1973, pp. 1154-1157

[5] BABONNEAU F., VIAL J.-P., APPARIGLIATO R., “Robust Optimization for Environmental and Energy Planning” in *Uncertainty and Environmental Decision Making: A Handbook of Research and Best Practice*, 2009, pp.79-126

[6] BEN-TAL A. & NEMIROVSKI A., “Robust solutions of linear programming problems contaminated with uncertain data”, *Mathematical Programming*, vol.88, 2000, pp.411-424

[7] BERTSIMAS D. & SIM M., “Price of robustness”, *Operations Research*, vol.52, 2004, pp.35-53

[8] YUAN Yuan, LI Zukui, HUANG Biao, “Robust optimization under correlated uncertainty: Formulations and computational study”, *Computers and Chemical Engineering*, vol.85, 2016, pp.58-71

[9] JALILVAND-NEJAD Amir, SHAFAEI Rasoul, SHAHRIARI Hamid, “Robust optimization under correlated polyhedral uncertainty set”, *Computers & Industrial Engineering*, vol.92, 2016, pp.82-94

[10] LORCA Alvaro & SUN Xu Andy, “Adaptive Robust Optimization with Dynamic Uncertainty Sets for Multi-Period Economic Dispatch under Significant Wind”, *IEEE Transactions on Power Systems*, vol.30, n°4, 2015, pp.1702-1713

[11] CHEN Xin, SIM Melvyn, SUN Peng, “A Robust Optimization Perspective on Stochastic Programming”, *Operations Research*, vol. 55, n°6, 2007, pp. 1058-1071

[12] NING Chao & YOU Fengqui, “Data-driven decision under uncertainty integrating robust optimization with principal component analysis and kernel smoothing methods”, *Computers and Chemical Engineering*, vol. 112, 2018, pp. 190-210

[13] LYDIA M., SURESH KUMAR S., IMMANUEL SELVAKUMAR A., EDWIN PREM KUMAR G., “Linear and non-linear autoregressive models for short-term wind speed forecasting”, *Energy Conversion and Management*, vol. 112, 2016, pp. 115-124

[14] LIU Heping, ERDEM Ergin, SHI Jing, “Comprehensive evaluation of ARMA-GARCH(-M) approaches for modelling the mean and volatility of wind speed”, *Applied Energy*, vol. 88, n°3, 2011, pp. 724-732

[15] HOU Qingchun, ZHANG Ning, DU Ershun, MIAO Miao, PENG Fei, KANG Chongqing, “Probabilistic duck curve in high PV penetration power system: Concept, modeling, and empirical analysis in China”, *Applied Energy*, vol. 242, 2019, pp. 205-215

[16] DE SISTERNES Fernando, “Risk Implications of the Deployment of Renewables for Investments in Electricity Generation”, MIT, May 2014

[17] CANY C., MANSILLA C., MATHONNIERE G., DA COSTA P., “Nuclear contribution to the penetration of variable renewable energy sources in a French decarbonized mix”, *Energy*, vol. 150, 2018, pp. 544-555

[18] MORILHAT Patrick, FEUTRY Stéphane, LE MAITRE Christelle, MELAINE FAVENNEC Jean, “Nuclear Power Plant flexibility at EDF”, 2019, hal-01977209

[19] IAE-RTE, “Conditions and requirements for the technical feasibility of a power system with a high share of renewables in France towards 2050”, IEA Publications, 2021

Chapter II:

Optimization of electricity mix with high penetration of renewables: A robust methodology derived from Bayesian inference and graph theory

***Abstract* – In this paper, we propose a two-part approach to robust optimization to derive the set of worst-case trajectories of any random process. First, we approximate its distribution using a set of concurrent multivariate distributions and tools from Bayesian inference. This allow us to introduce the "(ϵ, M) certainty set", which corresponds to the set of paths for the random process which have a probability greater than $1-\epsilon$ to be observed at least once after M trials. Second, using elementary matrix algebra and graph theory, we use the "(ϵ, M) certainty set" to derive in polynomial time a family of "worst-case" trajectories, including the most volatile path that can be generated by the random process. We apply this robust approach to an investment and dispatching model of the electric system of the French region Auvergne Rhône-Alpes, formulated as a MILP with commitment constraints.**

***Keywords*-** Optimal electricity mix; Robust optimization; Uncertainty; Bayesian inference; Graph

1. Introduction

Due to the necessarily incomplete nature of sampling, some rare events can be attributed a null probability although they are theoretically possible. Our prior knowledge of an uncertain parameter is encoded in the assumptions we make in assigning probabilities to its possible outcomes. This pivotal issue was given consideration by [1], in his famous "sunrise problem". When having very little prior knowledge of a system, Laplace's rule of succession assigns a non-null probability that the sun will not rise tomorrow, which decreases with each new observation of sunrise. Still, in a Bernoulli trial process where a given event has a probability n^{-1}, $n > 0$, the limit probability that the event is not observed after n trials has been shown to tend to e^{-1} as $n \to +\infty$. Thus, it does not seem reasonable to assign *a priori* a null probability to a given possible but never occurring event subjected to uncertainty. Similarly, an event with an *a priori* positive probability may never occur in a finite sequence of trials.

Stochastic optimization (SO) and robust optimization (RO) are two of the main traditional approaches to optimization under uncertainty (see [2]), along with chance-constrained programming ([3], [4]). First introduced by [5], SO is a risk-neutral approach which seeks to optimize the expected value of the objective function over a given probability distribution of the uncertain parameters (see [6]-[7]). The combinations of successive values than can be taken by parameters are usually modeled using a scenario tree. Parameters can both exhibit exogenous and endogenous uncertainty, the latter being decision dependent as in [8]. However, this method requires assumptions about the underlying joint distribution of the parameters in addition to accurately measuring it, which is likely to introduce measurement errors. Introduced by [9], RO seeks to optimize the objective function under the worst-case scenario over a pre-defined uncertainty set. In order to avoid over-conservative solutions, recent work focused on the development of more elaborate uncertainty sets of parameters ([10]-[11]), introducing uncertainty budgets, asymmetries in the distribution of uncertainties as in [12] and correlated uncertainties ([13]-[15]). However, to the noticeable exception of [16], which introduce dynamic uncertainty sets, the uncertainty remains essentially modeled as a static phenomenon. Our paper aims at addressing this shortfall by constructing a robust optimization approach of uncertain dynamical systems.

The state of knowledge of an uncertain system can also be described using the Bayesian framework. This approach has strong ties with optimization, as it allows us to quantify how the observed information for this system influences the optimal decision (see [17]). Bayesian

statistics particularly apply to robust optimization (RO) and distributionally robust optimization (DRO), which seeks to optimize the objective under the worst-case distribution of uncertain parameters with an ambiguity set satisfying some statistical criterion. With the aim of improving computational efficiency, [18] analyzes the Bayesian networks constructed with a Bayesian optimization algorithm to extract the patterns of non-robust solutions and discard them. In order to circumvent limitations of moment based DRO, the authors in [19] define a *likelihood robust optimization* method associated to an accessible distribution set that contains only distributions which make the observed data reach a given likelihood threshold. In this respect, DRO methods may yield over-conservative results as extreme realizations of the uncertain parameters with positive probability may never occur with certainty within a quasi-finite time horizon. In a similar fashion, [20] introduces a novel Bayesian robustness guarantee, which allows the author to define an asymptotical optimal set as the smallest convex set satisfying this guarantee. These Bayesian near-optimal ambiguity sets are tractable and significantly smaller than the traditional ambiguity sets.

Using tools from Bayesian inference and Bayesian Model Averaging, we define a "local" *posterior* probability distribution associated to each value of the uncertain dynamical system, described by the random process $\{\boldsymbol{\xi}_t\}_{t\in\mathcal{T}}$, for a set of concurrent theoretical models. Our method is thus essentially data-driven and develops the intuition that hedging against specific events, with a very low probability of almost-surely occurring within the optimization period, may be suboptimal. Indeed, for a given probability distribution $\mathcal{P}$ associated to a random variable $\boldsymbol{\xi}_t \in \Xi_t \subseteq \mathbb{R}$, the probability associated to each value $\xi \in \Xi_t$ is traditionally described by a singleton. Yet, the probability $\mathbb{P}_{\mathcal{P}}(\boldsymbol{\xi}_t = \xi)$ of observing ξ can be better described as the expected value of an infinite Bernoulli process, where $\mathbb{P}_{\mathcal{P}}(\boldsymbol{\xi}_t = \xi)$ is the theoretical probability of observing ξ if $\boldsymbol{\xi}_t$ follows the probability distribution $\mathcal{P}$. As the number of trials tends to infinity, the proportion of successes tends to $\mathbb{P}_{\mathcal{P}}(\boldsymbol{\xi}_t = \xi)$. However, as illustrated in the above "sunrise problem", there is a non-null probability that an event with a positive probability is never observed when the number of trials tends to infinity. To quantify this phenomenon, we define for any sample of size $M \gg 0$ the smallest set of events that occur almost-surely with probability $1 - \epsilon$ with $0 \leq \epsilon \leq 1$. We call this set the "(ϵ, M)-certainty set". This original concept and the method associated to its computation are described in Section II.

In Section III, we use our "(ϵ, M)-certainty set" to formulate a set of trajectories that can be taken by the random process $\{\boldsymbol{\xi}_t\}_{t\in\mathcal{T}}$. This allows us to formulate a dynamic definition of robustness, which corresponds to the optimal policy that minimizes an objective function when the uncertain random process follows its "worst-case" trajectories. For any $\{\Delta^k\boldsymbol{\xi}_t\}_{t\in\mathcal{T}}$, where $\Delta^k\boldsymbol{\xi}_t = \boldsymbol{\xi}_t - \boldsymbol{\xi}_{t-k}, k \in \mathbb{N}$, the set of worst-case trajectories corresponds to the subset of paths for which $\{\Delta^k\boldsymbol{\xi}_t\}_{t\in\mathcal{T}}$ reaches the greatest number of local maxima (or minima) within a given time window. Under this formulation, the worst-case trajectories of $\{\Delta\boldsymbol{\xi}_t\}_{t\in\mathcal{T}}$ correspond to the subset of paths which maximize (or minimize) the first-difference of the initial random process $\{\boldsymbol{\xi}_t\}_{t\in\mathcal{T}}$. Similarly, the worst-case trajectories of $\{\boldsymbol{\xi}_t\}_{t\in\mathcal{T}}$ either maximize or minimize the level of $\{\boldsymbol{\xi}_t\}_{t\in\mathcal{T}}$. Using basic matrix algebra and a newly introduced "path operator", we propose a polynomial time algorithm, named the "N-Summit Algorithm", which allows us to compute the subset of all "worst-case" trajectories for a given couple (M, ϵ).

Finally, Section IV proposes an empirical application of the methods introduced in the previous sections to the case of the French Region Auvergne Rhône-Alpes. We formulate a robust multiple time-scale investment and dispatching model with unit commitment constraints, formulated as a MILP, and provide some sensitivity analysis. We compare our main findings to those of Chapter I before concluding in Section V.

2. Definition of the "$(\boldsymbol{\epsilon}, \boldsymbol{M})$ certainty set"

We define the real-valued random variable $\boldsymbol{\xi}_t \in \mathbb{R}$, and the corresponding random process $\{\boldsymbol{\xi}_t\}_{t\in\mathcal{T}}$, where $\mathcal{T}$ is a set of successive time periods indexed by t. We further consider $\mathcal{T}$ as the set of hours in a week, so it has cardinal $|\mathcal{T}| = 168$. No assumptions are required about the stationarity of $\{\boldsymbol{\xi}_t\}_{t\in\mathcal{T}}$. $\{\boldsymbol{\xi}_t\}_{t\in\mathcal{T}}$ may equivalently be partitioned as the union of shorter random processes such that, for instance:

$$\{\boldsymbol{\xi}_t\}_{t\in\mathcal{T}} = \bigcup_{t\in\mathcal{T}\setminus\{|\mathcal{T}|\}} \{\boldsymbol{\xi}_t, \boldsymbol{\xi}_{t+1}\} \qquad (\mathbf{1a})$$

This partition allows us to approximate the behavior of $\{\boldsymbol{\xi}_t\}_{t\in\mathcal{T}}$ by investigating the statistical properties of its shorter components. We assume the true support $\boldsymbol{\Xi}_t$ of $\boldsymbol{\xi}_t$ is unknown. For

each $t \geq 0$, we observe the sample $\mathcal{S}_{N,t}$ with $N \geq 0$ observations, $N \in \mathbb{N}$, that we define as follows:

$$\mathcal{S}_{N,t} = \left\{\left(\xi_{1,t}, \xi_{1,t+1}\right), \left(\xi_{2,t}, \xi_{2,t+1}\right), \dots, \left(\xi_{N,t}, \xi_{N,t+1}\right)\right\} \qquad (\mathbf{1b})$$

By abuse of notation, we define $\mathcal{S}_{N,t} \cap \mathcal{S}_{N,t+1} = \left\{\xi_{1,t+1}, \xi_{2,t+1}, \dots, \xi_{N,t+1}\right\}$, since the second element of each pair in $\mathcal{S}_{N,t}$ corresponds to the first element of each pair included in $\mathcal{S}_{N,t+1}$. By definition, $\mathcal{S}_{N,t}$ is finite so there exists a sample $\mathcal{S}_{N,t}{}'$ such that $\mathcal{S}_{N,t} \subseteq \mathcal{S}_{N,t}{}'$. $\mathcal{S}_{N,t}$ is therefore a subsample of $\mathcal{S}_t{}'$, for which we can infer statistical properties by resampling with replacement $\mathcal{S}_t$ using bootstrapping. In the following section, we fit the empirical distribution of $\{\boldsymbol{\xi}_t\}_{t \in \mathcal{T}}$ with theoretical distribution from a set of concurrent models using tools from Bayesian inference.

2.1. Multivariate model specification

For any $t \geq 0$, we define the vectors $\boldsymbol{\xi}_{t \to t+1} = \begin{pmatrix} \xi_t \\ \xi_{t+1} \end{pmatrix}$ and $\boldsymbol{\mu}_{t \to t+1} = \begin{pmatrix} \mathbb{E}(\xi_t) \\ \mathbb{E}(\xi_{t+1}) \end{pmatrix}$. For clarity of the exposition, we approximate the partial random process $\boldsymbol{\xi}_{t \to t+1}$ using the unique model $\mathcal{M}_t$. We assume that $\mathcal{M}_t$ is a bivariate normal distribution which parameters need to be estimated. The joint density function of a bivariate normal distribution with mean vector $\boldsymbol{\mu}_{t \to t+1}$ and variance-covariance matrix $\boldsymbol{\Sigma}_{t \to t+1}$ is equal to:

$$f_{\boldsymbol{\mu}_{t \to t+1}, \boldsymbol{\Sigma}_{t \to t+1}}(\boldsymbol{\xi}_{t \to t+1}) = \frac{1}{2\pi\sqrt{|\boldsymbol{\Sigma}_{t \to t+1}|}} e^{-\frac{1}{2}\left[\left(\boldsymbol{\xi}_{t \to t+1} - \boldsymbol{\mu}_{t \to t+1}\right)^T \boldsymbol{\Sigma}_{t \to t+1}^{-1} \left(\boldsymbol{\xi}_{t \to t+1} - \boldsymbol{\mu}_{t \to t+1}\right)\right]} \qquad (\mathbf{2})$$

$|\boldsymbol{\Sigma}_{t \to t+1}|$ is the determinant of the variance-covariance matrix. We define the vector of parameters $\boldsymbol{\theta}_t = \left(\mathbb{E}(\xi_t), \mathbb{E}(\xi_{t+1}), \sigma_{\xi_t}^2, \sigma_{\xi_{t+1}}^2, \rho_{t \to t+1}\sigma_{\xi_t}\sigma_{\xi_{t+1}}\right) = \left(\widehat{\boldsymbol{\theta}_{\imath t}}\right)_{i \leq I}$, where $\sigma_{\xi_t}^2$ is the variance of ξ_t and $\rho_{t \to t+1}$ is the coefficient of correlation between ξ_t and ξ_{t+1}. I is the number of parameters used for the specification of $\mathcal{M}_t$. For conveniency, we note the density of the bivariate normal distribution associated to parameters $\boldsymbol{\theta}_t$ as $f_{\boldsymbol{\theta}_t}(\boldsymbol{\xi}_{t \to t+1})$.

Using consumption and generation records for the region Auvergne Rhône Alpes over the period 2013-2018[11], **Figure 1.A.** displays the distribution of residual demand values for various hours in Winter, with an installed solar and wind capacity of 2 GWe each. For each

[11] From RTE Eco2mix, https://www.rte-france.com/eco2mix

couple of hours t and $t+1$, residual demand values are normalized by removing the geometric median. We notice a strong positive correlation for residual demand value from consecutive hours. The density of the scatter plot decreases with the distance from the geometric median. This suggests a bivariate normal distribution with a positive coefficient of correlation is an accurate model specification for $\mathcal{S}_{N,t}$.

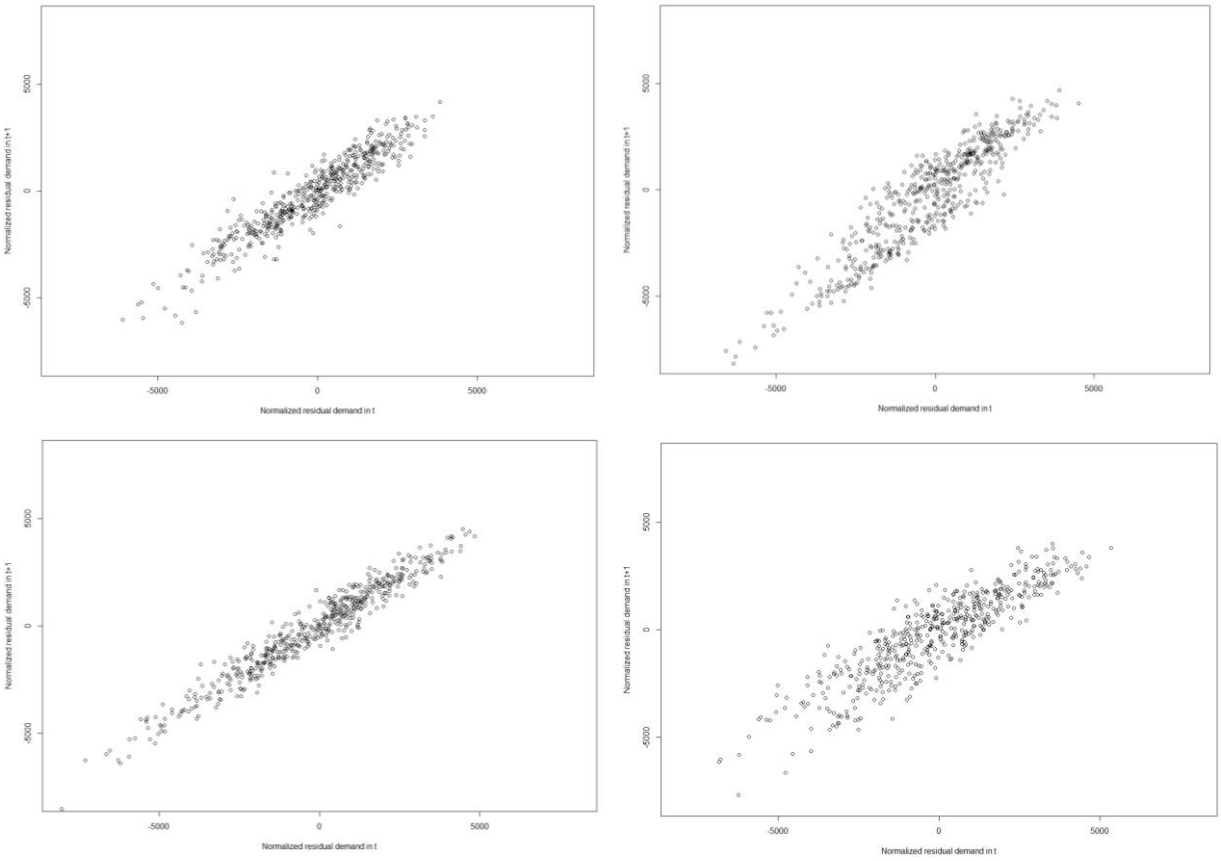

Figure 1.A.: Residual demand scatter plot with 2 GWe of wind and photovoltaic installed capacity, in Winter

Note: Each point corresponds to a couple of residual demand values for t and $t+1$. This figure shows the distributions of residual demand values for 12 p.m. (top-left), 6 a.m (top-right), 12 a.m (bottom-left) and 6 p.m (bottom-right).

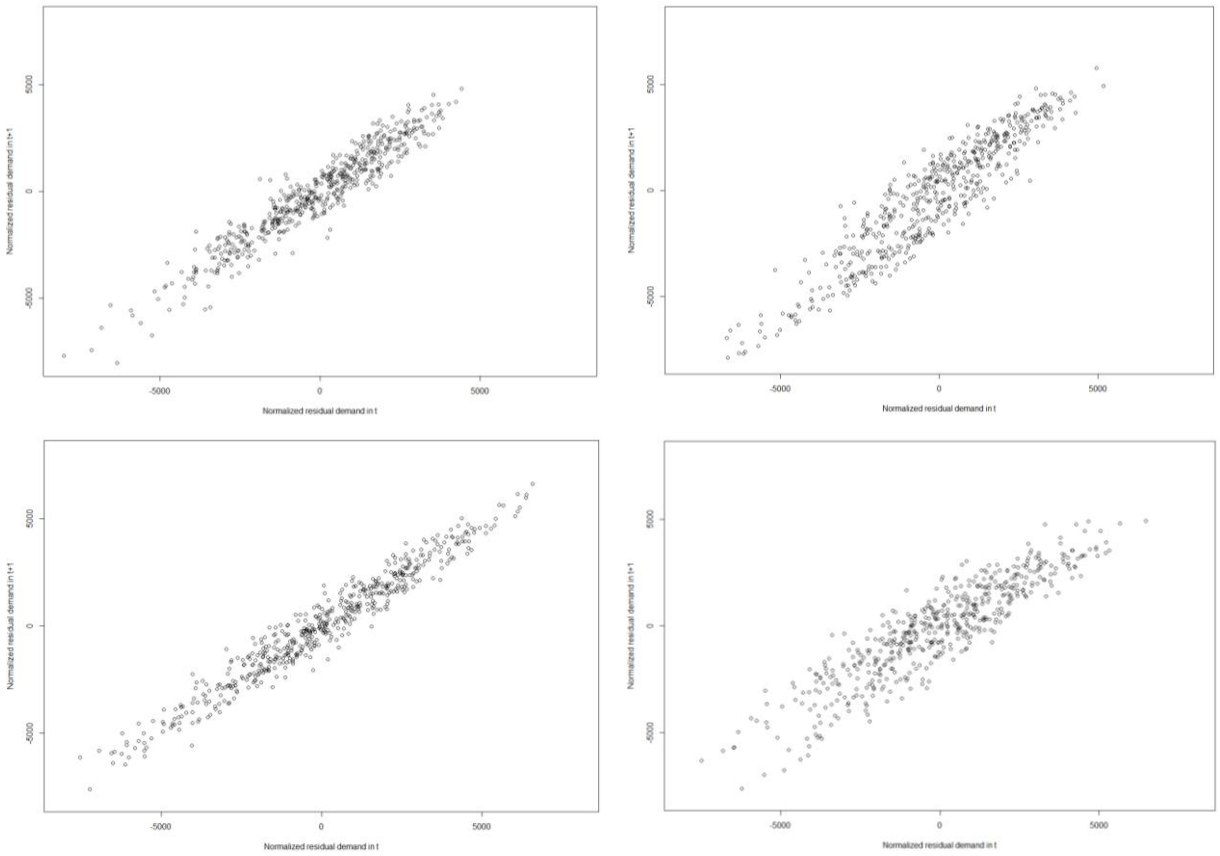

Figure 1.B.: Residual demand scatter plot with 6 GWe of wind and photovoltaic installed capacity, in Winter

We notice from **Figure 1.B.** that the width of the scatter plot, which corresponds to the diffusion of residual demand couples, increases with wind and photovoltaic installed capacity. However, it does not seem that the coefficient of correlation between the distribution of consecutive residual demand changes with installed capacities, at least for the subset of hours selected in the graph. Finally, we see from **Figure 1.C.** in Appendix that the scatter plots follow closely similar diffusion patterns in Summer, with a higher concentration of observations around the median. This confirms our bivariate Gaussian approximation of the diffusion of residual demand for successive periods of time is relevant for all seasons. We introduce the "expected sample" concept and estimate the vector of parameters which maximizes its *posterior* distribution (for tractability issues, we do not compute the full *posterior* distribution).

2.2. Inference of the optimal model parameters

Before bootstrapping $\mathcal{S}_{N,t}$, we first discretize the uncertain vector space by building a grid approximation. For $(\alpha, \beta) \in \mathbb{Z}^2$ and real increment $\Delta_{\alpha,\beta} > 0$, we define the square:

$$\Xi_t(\alpha, \beta) = \left\{ (\xi_t, \xi_{t+1}) \in \mathbb{R}^2 \middle| \begin{matrix} \alpha\Delta_{\alpha,\beta} \leq \xi_t < (\alpha+1)\Delta_{\alpha,\beta} \\ \beta\Delta_{\alpha,\beta} \leq \xi_{t+1} < (\beta+1)\Delta_{\alpha,\beta} \end{matrix} \right\} \quad (\mathbf{3})$$

We verify that $\bigcup_{(\alpha,\beta)\in\mathbb{Z}^2} \Xi_t(\alpha, \beta) = \mathbb{R}^2$. Without loss of generality and for tractability issues, the reunion of squares $\Xi_t(\alpha, \beta)$ can be defined on a subset of $\mathbb{R}^2$. Then, for any random sample of size N, we define the probability $p_N(\alpha, \beta)$ as the share of observations included in $\Xi_t(\alpha, \beta)$:

$$p_{N,t}(\alpha, \beta) = N^{-1}\left\{ (\xi_t, \xi_{t+1}) \subseteq \mathcal{S}_{N,t} \middle| (\xi_t, \xi_{t+1}) \subset \Xi_t(\alpha, \beta) \right\} \quad (\mathbf{4})$$

The choice of square size $\Delta_{\alpha,\beta}$ is both dependent on the number of observations N and the variance of the sample scatter plot (measured for instance with respect to its geometric median). It is straightforward to see that for any pair $(\alpha, \beta) \in \mathbb{Z}^2$, $p_{N,t}(\alpha, \beta)$ is non-decreasing with $\Delta_{\alpha,\beta}$ since the size of the square $\Xi_t(\alpha, \beta)$ increases with $\Delta_{\alpha,\beta}$. Yet, $p_{N,t}(\alpha, \beta)$ becomes less informative as the uncertainty regarding the exact location of observations in the space of values increases. Thus, we can choose $\Delta_{\alpha,\beta}$ as a decreasing function of N and of the variance of $\boldsymbol{\xi}_{t\to t+1}$.

We then use bootstrap resampling to measure how the proportion of observations included in each subspace $\Xi_t(\alpha, \beta)$ varies when resampling from the original sample. We note $p_{N,t}(\alpha, \beta)_\gamma$ the share of observations included in $\Xi_t(\alpha, \beta)$ associated to sample γ and $\Gamma \in \mathbb{N}^*$, $\gamma \leq \Gamma$, the total number of bootstrap samples which are drawn. This allows us to define the expected probability of observations made in the square $\Xi_t(\alpha, \beta)$ as:

$$\mathbb{E}\left(p_{N,t}(\alpha, \beta)\right) = \Gamma^{-1} \sum_{\gamma=1}^{\Gamma} p_{N,t}(\alpha, \beta)_\gamma \quad (\mathbf{5})$$

The total number of possible resampling with replacement is exactly $\binom{2N-1}{N}$, which grows exponentially with N. However, increasing the number of bootstrap samples does not increase the amount of information available from the original sample. [21] suggests that increasing the number of bootstrap resamples above 100 does not significantly improve the estimated

standard errors. Finally, we may similarly "bootstrap" the sample behavior by defining an "expected sample", which mimics the asymptotic behavior of the original sample when the number of bootstrap resamples tends to infinity. For each subspace $\Xi_t(\alpha, \beta)$, its average value $\overline{\Xi_t(\alpha, \beta)}$ is repeated in the expected sample a number of times equal to the expected number of observations found in $\Xi_t(\alpha, \beta)$ after Γ boostrap resamples. We formally define the expected sample as:

$$\mathbb{E}[\mathcal{S}_{N,t}] = \bigcup_{(\alpha,\beta)\in\mathbb{Z}^2} \mathfrak{X}_{\alpha,\beta,t} \qquad (6)$$

$I\left(\mathrm{N}\mathbb{E}\left(p_{N,t}(\alpha, \beta)\right)\right)$ is the expected number of observations made in the square $\Xi_t(\alpha, \beta)$, rounded to the nearest integer. $\overline{\Xi_t(\alpha, \beta)} = \left(\frac{(2\alpha+1)\Delta_{\alpha,\beta}}{2}, \frac{(2\beta+1)\Delta_{\alpha,\beta}}{2}\right)$ corresponds to the coordinates of the intersection of the diagonals of $\Xi_t(\alpha, \beta)$, which is interpreted as the average value of observations made in $\Xi_t(\alpha, \beta)$.

The multiset $\mathfrak{X}_{\alpha,\beta,t} = \langle \Xi_t(\alpha, \beta), I\left(\mathrm{N}\mathbb{E}\left(p_{N,t}(\alpha, \beta)\right)\right)\rangle$ can be defined as the set in which the element $\Xi_t(\alpha, \beta)$ has multiplicity $I\left(\mathrm{N}\mathbb{E}\left(p_{N,t}(\alpha, \beta)\right)\right)$. The expected sample $\mathbb{E}[\mathcal{S}_{N,t}]$ is simply the union of the multisets associated to each grid cell.

Our concept of expected sample allows us to better capture the uncertainty pertaining to the original sample. For instance, assume that the probability $p_{N,t}(\alpha, \beta)$ associated to a given subspace equals 0.2 when using the initial sample, but $p_{N,t}(\alpha, \beta)_\gamma$ varies between 0.15 and 0.30 when generating bootstrap resamples. This means that for some samples, the share of all observations included in $\Xi_t(\alpha, \beta)$ may vary from 15% to 30%, or equivalently, that we can formulate a probability distribution associated to the proportion of all observations found in $\Xi_t(\alpha, \beta)$. The expected sample takes advantage of this uncertainty by associating to each square $\Xi_t(\alpha, \beta)$ its expected number of observations. This can be seen as a limiting case to the set of bootstrap resamples generated by resampling.

Finally, for each bootstrap sample γ, we note the corresponding vector of parameters $\widehat{\boldsymbol{\theta}_{t_\gamma}} = \left(\widehat{\boldsymbol{\theta}_{it_\gamma}}\right)_i$, which allows us to define the empirical parameter space $\widehat{\boldsymbol{\Theta}_t} = \otimes_i \left[\wedge_\gamma \widehat{\boldsymbol{\theta}_{it_\gamma}}, \vee_\gamma \widehat{\boldsymbol{\theta}_{it_\gamma}}\right]$ and derive the empirical joint distribution of the model parameters on $\widehat{\boldsymbol{\Theta}_t}$, noted $p\left(\widehat{\boldsymbol{\theta}_t}\right)$. We note $p\left(\mathbb{E}[\mathcal{S}_{N,t}] \middle| \boldsymbol{\theta}_t\right)$ the likelihood of $\boldsymbol{\theta}_t \in \widehat{\Xi_t}$ with respect to the expected sample. For

tractability issues, we do not compute the full *posterior* distribution of $\boldsymbol{\theta}_t$ but chose its maximum *a posteriori* estimator, noted $\boldsymbol{\theta}_t^*$. The maximum a posteriori estimation (MAP) corresponds to the mode of the posterior distribution. It estimates the optimal set of parameters which maximizes the posterior distribution of the estimated quantity based on the observations. By noting $p\left(\boldsymbol{\theta}_t \middle| \mathbb{E}\left[\mathcal{S}_{N,t}\right]\right)$ the posterior probability of $\boldsymbol{\theta}_t \in \widehat{\boldsymbol{\Theta}_t}$, the MAP set of parameters $\boldsymbol{\theta}_t^*$ formally writes as:

$$\boldsymbol{\theta}_t^* = \underset{\boldsymbol{\theta}_t \in \widehat{\boldsymbol{\Theta}_t}}{\arg\max}\, p\left(\boldsymbol{\theta}_t \middle| \mathbb{E}\left[\mathcal{S}_{N,t}\right]\right) = \underset{\boldsymbol{\theta}_t \in \widehat{\boldsymbol{\Theta}_t}}{\arg\max}\, p\left(\mathbb{E}\left[\mathcal{S}_{N,t}\right] \middle| \boldsymbol{\theta}_t\right) p(\boldsymbol{\theta}_t) \qquad (\mathbf{7}\boldsymbol{a})$$

The likelihood $p\left(\mathbb{E}\left[\mathcal{S}_{N,t}\right] \middle| \boldsymbol{\theta}_t\right)$ is estimated using $f_{\boldsymbol{\theta}_t}(\boldsymbol{\xi}_{t\to t+1})$ as our model follows a bivariate normal distribution. As the marginal likelihood $p\left(\mathbb{E}\left[\mathcal{S}_{N,t}\right]\right)$ is independent from $\boldsymbol{\theta}_t$, we have:

$$p\left(\mathbb{E}\left[\mathcal{S}_{N,t}\right] \middle| \boldsymbol{\theta}_t\right) p(\boldsymbol{\theta}_t) \propto \frac{p\left(\mathbb{E}\left[\mathcal{S}_{N,t}\right] \middle| \boldsymbol{\theta}_t\right) p(\boldsymbol{\theta}_t)}{p\left(\mathbb{E}\left[\mathcal{S}_{N,t}\right]\right)} = \frac{p\left(\mathbb{E}\left[\mathcal{S}_{N,t}\right] \middle| \boldsymbol{\theta}_t\right) p(\boldsymbol{\theta}_t)}{\int p\left(\mathbb{E}\left[\mathcal{S}_{N,t}\right] \middle| \boldsymbol{\theta}_t{}'\right) p(\boldsymbol{\theta}_t{}') d\boldsymbol{\theta}_t{}'} \qquad (\mathbf{7}\boldsymbol{b})$$

The density of a bivariate Gaussian distribution with parameters $\boldsymbol{\theta}_t^*$ is equal to $f_{\boldsymbol{\theta}_t^*}(\boldsymbol{\xi}_{t\to t+1})$. In order to diminish the computational cost, we discretize the parameter space $\widehat{\boldsymbol{\Xi}_t}$ using a Bayesian-grid approximation. We can further define the probability $f(\alpha, \beta | \boldsymbol{\theta}_t^*)$ of being in the square $\boldsymbol{\Xi}_t(\alpha, \beta)$, formally defined noted as $f(\alpha, \beta | \boldsymbol{\theta}_t^*) = \mathbb{P}\left(\left(\alpha\Delta_{\alpha,\beta} \leq \xi_t < (\alpha+1)\Delta_{\alpha,\beta}\right) \cap \left(\beta\Delta_{\alpha,\beta} \leq \xi_{t+1} < (\beta+1)\Delta_{\alpha,\beta}\right)\right)$, using the bivariate Gaussian cumulative distribution function, noted $\Phi_{\boldsymbol{\theta}_t^*}(x, y)$, where $(x, y) \in \mathbb{R}^2$. Simple computations yield the following expression:

$$f(\alpha, \beta | \boldsymbol{\theta}_t^*) = \left(\Phi_{\boldsymbol{\theta}_t^*}\left((1+\alpha)\Delta_{\alpha,\beta}, \beta\Delta_{\alpha,\beta}\right) - \Phi_{\boldsymbol{\theta}_t^*}\left(\alpha\Delta_{\alpha,\beta}, \beta\Delta_{\alpha,\beta}\right)\right)$$

$$\times \left(\Phi_{\boldsymbol{\theta}_t^*}\left(\alpha\Delta_{\alpha,\beta}, (1+\beta)\Delta_{\alpha,\beta}\right) - \Phi_{\boldsymbol{\theta}_t^*}\left(\alpha\Delta_{\alpha,\beta}, \beta\Delta_{\alpha,\beta}\right)\right) \qquad (\mathbf{8})$$

2.3. Formal expression of the "(ϵ, M)-certainty set"

For $M \in \mathbb{N}$ fixed and any couple $(\alpha, \beta) \in \mathbb{Z}^2$, we define the associated Poisson parameter $\lambda(\alpha, \beta|M) = Mf(\alpha, \beta|\boldsymbol{\theta}_t^*)$. The probability that $m \in \mathbb{N}$ observations are made in the square $\Xi_t(\alpha, \beta)$, with $m \leq M$, is assumed to follow a Poisson distribution $\text{Pois}\big(\lambda(\alpha, \beta|M)\big)$. It is formally expressed as follows:

$$p_{\lambda(\alpha,\beta|M),t}(m) = \frac{M^m f(\alpha, \beta|\boldsymbol{\theta}_t^*)^m}{m!} e^{-Mf(\alpha,\beta|\boldsymbol{\theta}_t^*)} \quad (\mathbf{9})$$

If the model specification is correct, $f(\alpha, \beta|\boldsymbol{\theta}_t^*)$ can be interpreted as the probability of the observation (ξ_t, ξ_{t+1}) of being included in the subspace $\Xi_t(\alpha, \beta)$. However, the concept of probability is only valid asymptotically. In finite sample settings, the probability that an event with non-null asymptotic probability is never observed is positive. Considering the event $(\xi_t, \xi_{t+1}) \in \Xi_t(\alpha, \beta)$, $f(\alpha, \beta|\boldsymbol{\theta}_t^*)$ may be interpreted as the limit probability of success associated to this event, when the number of trials tends to infinity. Letting $M \gg 0$ be the total number of trials, the number of successes can accurately be approximated by a binomial distribution of parameter $f(\alpha, \beta|\boldsymbol{\theta}_t^*)$. The finite-sample "behavior" of the probability $f(\alpha, \beta|\boldsymbol{\theta}_t^*)$ can thus be described by a distribution. More precisely, for $\Delta_{\alpha,\beta}$ small enough, we can further approximate this distribution with a Poisson distribution of parameter $\lambda(\alpha, \beta|M)$.

Then, for any subspace $\Xi_t(\alpha, \beta)$ and threshold ϵ, $0 \leq \epsilon \leq 1$, we can compute the number of trials necessary for m observations to be included in $\Xi_t(\alpha, \beta)$ with probability $1 - \epsilon$. In the context of rare event modeling, we can compute the minimum number of trials $M_\epsilon^*(\alpha, \beta)$ such that at least one observation is included in $\Xi_t(\alpha, \beta)$ with probability $1 - \epsilon$. This is formally expressed as follows:

$$M_{\epsilon,t}^*(\alpha, \beta) = \arg\min_M \left\{ M \in \mathbb{N} \,\middle|\, p_{\lambda(\alpha,\beta|M),t}(m > 0) \geq 1 - \epsilon \right\}$$

$$\Leftrightarrow M_{\epsilon,t}^*(\alpha, \beta) = \arg\min_M \left\{ M \in \mathbb{N} \,\middle|\, 1 - \frac{M^0 f(\alpha, \beta|\boldsymbol{\theta}_t^*)^0}{0!} e^{-Mf(\alpha,\beta|\boldsymbol{\theta}_t^*)} \geq 1 - \epsilon \right\}$$

$$\Leftrightarrow M_{\epsilon,t}^*(\alpha, \beta) = \arg\min_M \left\{ M \in \mathbb{N} \,\middle|\, e^{-Mf(\alpha,\beta|\boldsymbol{\theta}_t^*)} \leq \epsilon \right\} \quad (\mathbf{10})$$

If $M_{\epsilon,t}^*(\alpha, \beta) > M$, there is a probability at least $1 - \epsilon$ that no observations are made in the square $\Xi_t(\alpha, \beta)$ after exactly M trials. Equivalently, for $\epsilon \ll 1$, it is quasi-certain that the event "$(\xi_t, \xi_{t+1}) \in \Xi_t(\alpha, \beta)$" does not occur at least once after M observations.

We can eventually define the "(ϵ, M)-certainty set", $\mathcal{C}_{M,\epsilon,t}$, which is equal to the reunion of all subspaces $\Xi_t(\alpha, \beta)$ for which the event "$(\xi_t, \xi_{t+1}) \in \Xi_t(\alpha, \beta)$" occurs at least once after M trials:

$$\mathcal{C}_{M,\epsilon,t} = \bigcup_{\substack{(\alpha,\beta)\in\mathbb{Z}^2 \\ M_\epsilon^*(\alpha,\beta)\leq M}} \Xi_t(\alpha, \beta) \qquad (\mathbf{11a})$$

By definition, $M_{\epsilon,t}^*(\alpha, \beta)$ decreases with ϵ and with $f(\alpha, \beta|\boldsymbol{\theta}_t^*)$[12]. This has two main implications for the behavior of the "(ϵ, M)-certainty set": first, for fixed $M > 0$, square subspaces with a higher probability of including sample observations are more likely to be included in the set. This captures the intuitive fact that a lower number of trials is necessary to observe at least once events with a high asymptotic probability. Moreover, if the event "$(\xi_t, \xi_{t+1}) \in \Xi_t(\alpha, \beta)$" fails to occur after M trials with $M \gg M_\epsilon^*(\alpha, \beta)$, this might indicate that the theoretical model use in the computation data generating process is poorly specified. Second, this implies that the size of $\mathcal{C}_{M,\epsilon,t}$ increases with ϵ, which can reformulated as $\epsilon' \geq \epsilon \Leftrightarrow \mathcal{C}_{M,\epsilon',t} \supseteq \mathcal{C}_{M,\epsilon,t}$. These elementary properties are illustrated in the following section. They imply that, in order to keep the size of $\mathcal{C}_{M,\epsilon,t}$ constant when $\epsilon \to 1$, we must have $M \to +\infty$ for subspaces where $f(\alpha, \beta|\boldsymbol{\theta}_t^*)$ is strictly positive.

The concept of "(ϵ, M)-certainty set" is an intuitive concept that can easily be generalized. For instance, in $\mathbb{R}^3$, the square approximation becomes a cubic approximation. In higher dimensions, any sequence of uncertain parameters of length $|\mathcal{T}| \in \mathbb{N}^*$ can be approximated using a multivariate distribution, where the real space $\mathbb{R}^T$ is partitioned into a set of hypercubes in $|\mathcal{T}|$ dimensions. However, the computation of the likelihood $p\left(\mathbb{E}\left[\mathcal{S}_{N,t}\right]\middle|\boldsymbol{\theta}_t\right)$ would be increasingly costly as the number of permutations of $\boldsymbol{\theta}_t$ increases exponentially with the size of $\boldsymbol{\theta}_t$. We leave this issue for further research.

Furthermore, for a given model $\mathcal{M}_t$ and corresponding vector of model parameters $\boldsymbol{\theta}_t$, we may compute its full *posterior* distribution $p\left(\boldsymbol{\theta}_t\middle|\mathbb{E}\left[\mathcal{S}_{N,t}\right], \mathcal{M}_t\right)$ in order to better account for parameter uncertainty, which may increase the risk of incorrect model specification. Its computation may rapidly become intractable in high dimensions though. We may also directly

[12] The proof is straightforward as the logarithm is an increasing function and we have, for $0 \leq \epsilon \leq 1$:

$$e^{-Mf(\alpha,\beta|\boldsymbol{\theta}_t^*)} \leq \epsilon \Leftrightarrow -Mf(\alpha, \beta|\boldsymbol{\theta}_t^*) \leq \ln\epsilon \Leftrightarrow M \geq -\frac{\ln\epsilon}{f(\alpha,\beta|\boldsymbol{\theta}_t^*)} \geq 0$$

express $M^*_{\epsilon,t}(\alpha,\beta)$ as a function of $\boldsymbol{\theta}_t$ and $\mathcal{M}_t$, noted $M^*_{\epsilon,t}(\alpha,\beta|\boldsymbol{\theta}_t,\mathcal{M}_t)$. Then, given a set of candidate models $\boldsymbol{\mathcal{M}}_t = \{\mathcal{M}_t^1, \mathcal{M}_t^2, \dots, \mathcal{M}_t^\ell\}$, we directly compute the *posterior* probability $p\left(\mu_{\alpha,\beta}(M,\epsilon)\right)$ of observing at least one observation in $\Xi_t(\alpha,\beta)$ after M trials. In a similar fashion to Bayesian Model Averaging, we weight the *posterior* probability $p\left(\mu_{\alpha,\beta}\left(M,\epsilon\middle|\mathcal{M}_t^l\right)\right)$ by the *posterior* probability of model $\mathcal{M}_t^l$, noted $p\left(\mathcal{M}_t^l\middle|\mathbb{E}[\mathcal{S}_{N,t}]\right)$, for each $\mathcal{M}_t^l \subseteq \boldsymbol{\mathcal{M}}_t$[13]. Then, for a given positive probability threshold $p^{\mathcal{C}} \leq 1$, we compute the reunion of all subspaces of $\Xi_t(\alpha,\beta)$ such that $p\left(\mu_{\alpha,\beta}(M,\epsilon)\right)$ is superior or equal to $p^{\mathcal{C}}$:

$$\mathcal{C}_{M,\epsilon,t} = \bigcup_{\substack{(\alpha,\beta)\in\mathbb{Z}^2 \\ p\left(\mu_{\alpha,\beta}(M,\epsilon)\right)\geq p^{\mathcal{C}}}} \Xi_t(\alpha,\beta) \qquad (\mathbf{11b})$$

Intuitively, $\mathcal{C}_{M,\epsilon,t}$ corresponds to the reunion of all events that have an expected probability of being observed at least once superior to $p^{\mathcal{C}}$ after exactly M trials. Our method may be interpreted as a Bayesian application of the "law of truly large numbers" [22]. Once $\mathcal{C}_{M,\epsilon,t}$ is estimated for all $t \in \mathcal{T}\backslash\{|\mathcal{T}|\}$, we can use this information to formulate the set of possible trajectories of the partial random process for any pair $(\boldsymbol{\xi}_t, \boldsymbol{\xi}_{t+1})$. Then, using simple matrix algebra and graph theory concepts, we propose an original algorithm allowing us to estimate the most extreme and volatile trajectories that can be observed for the full random process $\{\boldsymbol{\xi}_t\}_{t\in\mathcal{T}}$.

[13] We define the function $\mu_{\alpha,\beta}(M,\epsilon|\boldsymbol{\theta}_t,\mathcal{M}_t^l)$ equal to 1 if $M^*_{\epsilon,t}(\alpha,\beta|\boldsymbol{\theta}_t,\mathcal{M}_t^l) \leq M$ and 0 otherwise. Then, for a given model $\mathcal{M}_t^l$, the probability $p\left(\mu_{\alpha,\beta}(M,\epsilon|\mathcal{M}_t^l)\right)$ is equal to:

$$p\left(\mu_{\alpha,\beta}(M,\epsilon|\mathcal{M}_t^l)\right) = \int \mu_{\alpha,\beta}(M,\epsilon|\boldsymbol{\theta}_t{}',\mathcal{M}_t^l)\, p(\boldsymbol{\theta}_t{}'|\mathbb{E}[\mathcal{S}_{N,t}],\mathcal{M}_t^l)\, d\boldsymbol{\theta}_t{}'$$

Finally, we take the weighted sum over all concurrent models in $\boldsymbol{\mathcal{M}}_t = \{\mathcal{M}_t^1, \mathcal{M}_t^2, \dots, \mathcal{M}_t^\ell\}$ to obtain the probability that at least one observation is made in $\Xi_t(\alpha,\beta)$ for the couple (M,ϵ):

$$p\left(\mu_{\alpha,\beta}(M,\epsilon)\right) = \sum_{l=1}^{\ell} p\left(\mu_{\alpha,\beta}(M,\epsilon|\mathcal{M}_t^l)\right) \times p\left(\mathcal{M}_t^l\middle|\mathbb{E}[\mathcal{S}_{N,t}]\right)$$

3. Definition of a path generation algorithm for constructing the set of worst-case trajectories

3.1. Motivation and main notations

Set $Q \in \mathbb{N}^*$. We start by discretizing the "ϵ-certainty set" so that we can formulate a finite set of trajectories, or paths, of the uncertain vector. A trajectory corresponds to a tuple that has each element included in the "(ϵ, M)-certainty set". For instance, we consider the couple $(\xi_t, \xi_{t+1}) \in \mathbb{R}^2$ is an eligible trajectory if $(\xi_t, \xi_{t+1}) \in \mathcal{C}_{M,\epsilon,t}$.

More generally, any trajectory $(\xi_t, \xi_{t+1} \dots, \xi_{t+T+1}) \in \mathbb{R}^{T+1}$ of length $T+2$, $T \geq 0$, is eligible if $(\xi_{t+\tau}, \xi_{t+\tau+1}) \in \mathcal{C}_{M,\epsilon,t+\tau}$ for any $\tau \in \{0, \dots, T\}$. Then, for any $t \geq 0$, we partition $\mathcal{C}_{M,\epsilon,t}$ into exactly $(Q+1)$ subsets of equal length. Setting $\xi_t^- = \inf\left\{\xi_t \middle| (\xi_t, \xi_{t+1}) \in \mathcal{C}_{M,\epsilon,t}\right\}$ and $\xi_t^+ = \sup\left\{\xi_t \middle| (\xi_t, \xi_{t+1}) \in \mathcal{C}_{M,\epsilon,t}\right\}$, we generate for each t the set of equally spacd discrete values $\boldsymbol{V}_Q^t$ such that:

$$\boldsymbol{V}_Q^t = \{v_i^t | v_i^t = \xi_t^- + iQ^{-1}(\xi_t^+ - \xi_t^-), i \in \{0, \dots, Q\}\} \qquad (\mathbf{12})$$

In terms of graph theory, $\boldsymbol{V}_Q^t$ corresponds to a set of $(Q+1)$ vertices. For any pair of subsets $\left(\boldsymbol{V}_Q^t, \boldsymbol{V}_Q^{t+1}\right)$, we are interested in computing all possible pairs, or "paths", of successive vertices. In the case of robust optimization, we may wish to know which "path" generates the highest or lowest residual demand trajectories. We propose an original method for estimating both the set of trajectories for which residual demand takes its most extreme values, but also the set of trajectories with the most volatile behavior. In terms of graph theory, the most volatile trajectory exactly corresponds to the longest path, as the variations of its level are maximized. The set of all possible combinations is finite and can be expressed using the Cartesian product as follows:

$$\boldsymbol{V}_Q^t \times \boldsymbol{V}_Q^{t+1} = \begin{pmatrix} (v_1^t, v_1^{t+1}) & (v_1^t, v_2^{t+1}) & \cdots & \left(v_1^t, v_{Q+1}^{t+1}\right) \\ (v_2^t, v_1^{t+1}) & (v_2^t, v_2^{t+1}) & \cdots & \left(v_2^t, v_{Q+1}^{t+1}\right) \\ \vdots & \vdots & \ddots & \vdots \\ \left(v_{Q+1}^t, v_1^{t+1}\right) & \left(v_{Q+1}^t, v_2^{t+1}\right) & \cdots & \left(v_{Q+1}^t, v_{Q+1}^{t+1}\right) \end{pmatrix} \qquad (\mathbf{13})$$

We count $(Q+1)^2$ possible pairs. Following the same logic, for any $(T+2)$-uplet of subsets $\left(\boldsymbol{V}_Q^t, \boldsymbol{V}_Q^{t+1}, \dots, \boldsymbol{V}_Q^{t+T+1}\right)$, there exists $(Q+1)^{T+1}$ possible simple "paths" with $(T+2)$ vertices from the set of vertices $\boldsymbol{V}_Q^t$ to $\boldsymbol{V}_Q^{t+T+1}$. In terms of graph theory, the resulting graph can be

interpreted as the union of T undirected complete bipartite graphs, as illustrated in **Figure 2** below.

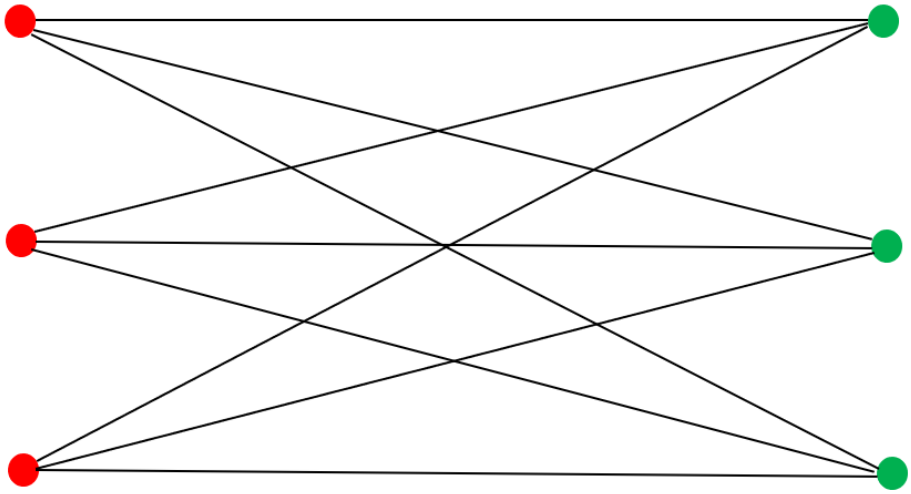

Figure 2: A complete bipartite graph

The above graph is fully connected. Each possible pair of vertices $\left(v_i^t, v_j^{t+1}\right)$, $1 \leq i, j \leq n$ belonging to consecutive sets $\left(\boldsymbol{V}_Q^t, \boldsymbol{V}_Q^{t+1}\right)$, is connected by an edge with a positive weight. We may define the weight associated to the edge $\left(v_i^t, v_j^{t+1}\right)$ as the distance between the two vertices, which we note $\ell\left(v_i^t, v_j^{t+1}\right) = \left|v_i^t - v_j^{t+1}\right| \in \mathbb{R}^+$. Then, we define the length of a given "path" as the sum of the weights associated to its edges. For any $t < |\mathcal{T}|$, we define the matrix of weights associated to the pair of sets $\left(\boldsymbol{V}_Q^t, \boldsymbol{V}_Q^{t+1}\right)$ as follows:

$$X^t = \begin{pmatrix} \ell(v_1^t, v_1^{t+1}) & \ell(v_1^t, v_2^{t+1}) & \cdots & \ell\left(v_1^t, v_{Q+1}^{t+1}\right) \\ \ell(v_2^t, v_1^{t+1}) & \ell(v_2^t, v_2^{t+1}) & \cdots & \ell\left(v_2^t, v_{Q+1}^{t+1}\right) \\ \vdots & \vdots & \ddots & \vdots \\ \ell\left(v_{Q+1}^t, v_1^{t+1}\right) & \ell\left(v_{Q+1}^t, v_2^{t+1}\right) & \cdots & \ell\left(v_{Q+1}^t, v_{Q+1}^{t+1}\right) \end{pmatrix} \in \mathbb{R}^{(Q+1)\times(Q+1)} \quad (\mathbf{14})$$

3.2.Formulation and complexity of the *N*-Summits Algorithm

As Q and T increase, the number of all possible "paths" grows exponentially, which may rapidly make the computation of their set intractable. Similarly, finding the longest "path" in a weighted graph, that is the graph which maximizes the sum of weights of its edges, is NP-

hard. However, instead of directly searching for the simple path of maximum length in a complete multipartite graph, we may instead drastically reduce the set of candidate paths, with the guarantee that the longest path is included within this set. We propose such a solution, which generates the subset in polynomial time.

Our method is constructed based on intuitions derived from a new operator, that we call "path operator", which allows us to generate the set of all discrete paths of maximum length QT, with their corresponding length, associated to a given graph with QT vertices. Our operator exhibits nice recursive properties. However, because of its rather technical formulation, we let the reader refer to the Appendix for a full description. In this section, we consider without loss of generality a fully connected graph with non-null weights. By taking advantage of the peculiar structure of our "path operator", we identify and build an algorithm for finding the longest path in a multipartite complete graph in polynomial time. Using backward induction, we simultaneously compute the longest path originating for each vertex of each set of vertices. This allows us to keep the set of candidate paths of constant size, as the latter only varies with Q'. Due to the parallel nature of our algorithm, we call it the "N-Summits Algorithm".

For simplicity and without loss of generality, we consider the $(m+2)$-uplet of sets $(\boldsymbol{V}^0, \boldsymbol{V}^1, \dots, \boldsymbol{V}^{m+1})$. For $m > 0$ and $i \leq m$, we define the matrix $\Omega^i \in \mathbb{R}^{(Q' \times Q')}$ as follows:

$$\Omega^i = \begin{pmatrix} X_{1,1}^{m-i} + \sup \Omega_{1,*}^{i-1} & X_{1,2}^{m-i} + \sup \Omega_{2,*}^{i-1} & \cdots & X_{1,Q'}^{m-i} + \sup \Omega_{Q',*}^{i-1} \\ X_{2,1}^{m-i} + \sup \Omega_{1,*}^{i-1} & X_{2,2}^{m-i} + \sup \Omega_{2,*}^{i-1} & \cdots & X_{2,Q'}^{m-i} + \sup \Omega_{Q',*}^{i-1} \\ \vdots & \vdots & \ddots & \vdots \\ X_{Q',1}^{m-i} + \sup \Omega_{1,*}^{i-1} & X_{Q',2}^{m-i} + \sup \Omega_{1,*}^{i-1} & \cdots & X_{Q',Q'}^{m-i} + \sup \Omega_{Q',*}^{i-1} \end{pmatrix} \in \mathbb{R}^{+(Q' \times Q')} \quad (\mathbf{15})$$

Where $\Omega^0 = X^m$ and $\Omega_{j,*}^i$ corresponds to the elements on the j-th line of Ω^i. Let us denote by $\mathbb{T}(\Omega^i)$ the set of all paths generated by recursively applying $\Omega^{i'}$ from 0 to i, $i' \leq i$. Finally, for j such that $1 \leq j \leq Q'$ and $i \leq m$, we note $\mathbb{T}(\Omega_{j,*}^i)^+$ the $i+2$-uplet that maximizes $\Omega_{j,*}^i$ and define the ordered set $\mathbb{T}(\Omega^i)^+ = \left(\mathbb{T}(\Omega_{1,*}^i)^+, \dots, \mathbb{T}(\Omega_{Q',*}^i)^+\right)$. We can recursively express $\mathbb{T}(\Omega^i)$ under matrix form using the Cartesian product:

$$\mathbb{T}(\Omega^i) = \boldsymbol{V}^{m-i} \times \mathbb{T}(\Omega^i)^+ \quad (\mathbf{16})$$

Where $\mathbb{T}(\Omega^0) = \boldsymbol{V}^m \times \boldsymbol{V}^{m+1}$. We note $\mathfrak{P}_{i'=m-i}^{m+1} \boldsymbol{V}^{i'}$ the set of all paths with $(i+2)$ vertices from Then, we can express the following central result:

Fundamental theorem: For any path with $(i+2)$ vertices $\mathfrak{t}^i = \left(v^{m-i}_{t^i_{m-i}}, \dots, v^{m}_{t^i_m}, v^{m+1}_{t^i_{m+1}}\right) \in \mathfrak{P}^{m+1}_{i\prime=m-i}\boldsymbol{V}^{i\prime}$ such that $\mathfrak{t}^i \notin \mathbb{T}(\Omega^i)$, then the length of $\mathfrak{t}^i$ is inferior or equal to the length of the longest path included in $\mathbb{T}(\Omega^i)$, ie $\ell(\mathfrak{t}^i) \leq \sup \Omega^i$.

Proof:

The property is trivial for $i = 0$, since by definition, for any $(j,k) \in \{1, \dots, Q'\}^2$, we have $X^m_{j,k} \leq \sup X^m_{j,*} = \sup \Omega^0_{j,*}$, which implies that $X^m_{j,k} \leq \sup X^m$ so $\ell(\mathfrak{t}^0) \leq \sup \Omega^0$.

For any $j \in \{1, \dots, Q'\}$, assume that $v^{m-i}_j \in \mathfrak{t}^i \Longrightarrow \ell(\mathfrak{t}^i) \leq \sup \Omega^i{}_{j,*}$. For any couple $(j,k) \in \{1, \dots, Q'\}^2$ and $i > 0$, we have by definition:

$$X^{m-(i+1)}_{j,k} + \sup \Omega^i_{k*,} \leq \sup\left(X^{m-(i+1)}_{*,k} + \sup \Omega^i{}_{k,*}\right) = \sup X^{m-(i+1)}_{*,k} + \sup \Omega^i{}_{k,*} \leq \sup \Omega^{i+1}$$

As this condition is true for any couple, then for any trajectory $\mathfrak{t}^{i+1} \notin \mathbb{T}(\Omega^{i+1})$, $\exists (j', k') \in \{1, \dots, Q'\}^2$ such that for $\left(v^{m-i-1}_{j\prime}, v^{m-i}_{k\prime}\right) \in \mathfrak{t}^{i+1}$. It follows that:

$$\ell(\mathfrak{t}^{i+1}) \leq \ell\left(\left(v^{m-i-1}_{j\prime}, v^{m-i}_{k\prime}\right)\right) + \sup \Omega^i{}_{k\prime,*} \leq \sup X^{m-(i+1)}_{*,k\prime} + \sup \Omega^i{}_{k\prime,*} \leq \sup \Omega^{i+1}$$

Thus, we have $\mathfrak{t}^{i+1} \notin \mathbb{T}(\Omega^{i+1}) \Longrightarrow \ell(\mathfrak{t}^{i+1}) \leq \sup \Omega^{i+1}$.

For any $m > 0$ and $i \leq m$, we can recursively compute the matrix Ω^i and the associated path matrix $\mathbb{T}(\Omega^i)$ with the guarantee that the longest path with $i+1$ edges is included in $\mathbb{T}(\Omega^i)$. For any $j \in \{1, \dots, Q'\}$, computing the supremum of $\Omega^i_{j,*}$ requires at most Q' operations. Computing $\sup \Omega^i_{j,*}$ for all $j \in \{1, \dots, Q'\}$ thus requires at most Q'^2, plus Q'^2 additions in order to compute each element of Ω^i. Thus, computing matrix Ω^m has a total time complexity of $\mathcal{O}(2mQ'^2)$. Computing $\mathbb{T}(\Omega^i)$ requires exactly the same set of operations, least the identification of $\mathbb{T}(\Omega^i)^+ = \left(\mathbb{T}(\Omega^i_{1,*})^+, \dots, \mathbb{T}(\Omega^i_{Q\prime,*})^+\right)$ as the matrix coordinates of the tuples maximizing each row of Ω^i are identical to the coordinates of $\sup \Omega^i_{j,*}$ for all $j \in \{1, \dots, Q'\}$. Finally, identifying the maximum value of Ω^i requires Q'^2 comparisons. Thus, the total time complexity of our algorithm for finding the longest path with $m+2$ vertices is equal to $\mathcal{O}(Q'^2 + 2mQ'^2 + mQ'^2)$, which is equal to $\mathcal{O}\left(Q'^2(1+3m)\right)$. A graphical illustration of the N-Summit Algorithm is provided in **Figure 3**.

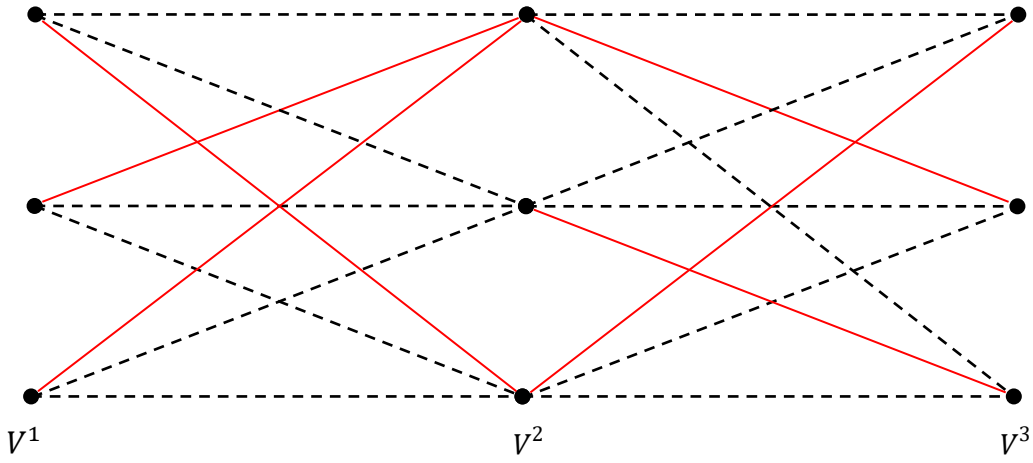

Figure 3: Illustration of the N-Summit Algorithm with 3 sets of vertices

Note: For any set of vertices V^1, V^2 and V^3, the black dotted lines correspond to all possible edges between all vertices of two consecutive sets. The red plain lines represent the longest edges starting from each vertex of V^i for consecutive sets (V^i, V^{i+1}), $i = \{1,2\}$.

4. Application to the case of Auvergne-Rhône-Alpes

In the following section, we use the methodology described introduced in Sections I and II to the case of the French region Auvergne Rhône-Alpes. This administrative region is located in the South-East of France and enjoys strong solar irradiation compared to the national average. In addition, it accounts for roughly 11.6% of French GDP, while its mean share of national electricity load equals to 13.8%.

4.1. Estimation of the model parameters

We model the regional electric system using a robust investment and dispatching model with unit commitment constraints, formulated as a MILP. Neglecting transmission and distribution constraints, it includes short-term thermal constraints with commitment state, start-up and shut-down decisions, minimum and maximum generation levels, in addition to minimum uptime and downtime for operating plants. For conveniency, the mathematical formulation of the model, with the full description of notations and equations, is provided in Appendix. It is

formulated using multiple time scales (diurnal, weekly and seasonal) with an hourly time resolution.

We assume no initial generation capacities in order to better disentangle the impact of each worst-case trajectories on investment decisions. For convenience, we further assume that no investment occurs in hydroelectric capacity. Moreover, we constrain the investment variables to take only discrete values for nuclear, gas turbines (GT) and combined cycle gas turbine plants (CCG), and continuous values for renewable energy sources (RES) and storage technologies. Nuclear investment is performed by blocks of 1.6 GW, corresponding to the rated power of the EPR Flamanville plant (the most recent nuclear power project in France), while CCG investments are made by blocs of 0.45 GW, which corresponds to the average nominal power of General Electric's 9HA.01/.02 gas turbine. Finally, GT investments are performed by blocks of 0.3 GW. Flexibility and cost assumptions for generation units can be found in **Table 1.A** and **Table 1.B.** in Appendix. We set the price of CO2 to 50€/t. We use a discount factor of 5% for the computation of annuities corresponding to investment costs. Finally, following the CRE (CRE, 2018)[14], we choose a VOLL equal to 13 000 €/MWh.

When considering the technical characteristics of generation technologies presented in **Table 1.A.**, one actually notices that ramping rates are high enough for each online generation unit to very entirely between its minimum and maximum generation level. Indeed, as the model is defined with an hourly time resolution, nuclear plants may vary their production by up to 100% of their rated power between successive time periods. Thus, ramping constraints are actually not binding without adding operational restrictions on nuclear units.

Still using the RTE database on the electricity consumption, solar and wind power generation on the period 2013-2018, we apply for all four seasons our methodology. For each hour of the day, the number of observations N in the training sample goes from 541 in Winter and 546 in Autumn to 552 in Spring and Summer.

[14] Public consultation from the French Energy Regulatory Commission (CRE), Public consultation No. 2018-015 of 20 December 2018 on the investment request relating to the Celtic project, including a cross-border cost allocation

4.1.1. Estimation *of the "(ϵ, M)-certainty set"*

In the context of this application, the random vector $\boldsymbol{\xi}$ corresponds to residual demand (RD). RD can be considered as a linear combination, equal to the electricity demand minus renewable generation. Thus, there exists a unique $\boldsymbol{\xi}$ for each combination of wind and photovoltaic capacities. We set wind and solar capacities to be respectively equal to $\boldsymbol{S}$ GWe, where $\boldsymbol{S} \in \{0; 2; 4; 6\}$.

In order to clearly disentangle how the couple(ϵ, M) affects the shape of the "(ϵ, M) certainty set", we fix $\boldsymbol{S} = 2$. For a given increment $\Delta_{\alpha,\beta}$, we restrict the set within which the normalized residual demand couples $\left(\widetilde{\xi_t}, \widetilde{\xi_{t+1}}\right)$ can take values to the restricted square subsample $\Xi^R(x, y)$ such that, for $x \leq y$ and $x \equiv 0 \left(\mathrm{mod}\ \Delta_{\alpha,\beta}\right), y \equiv 0 \left(\mathrm{mod}\ \Delta_{\alpha,\beta}\right)$:

$$\bigcup_{(\alpha,\beta)\in\left\{x\Delta_{\alpha,\beta}^{-1}, y\Delta_{\alpha,\beta}^{-1}\right\}^2} \Xi_t(\alpha, \beta) = \Xi^R(x, y) = \left\{ \left(\widetilde{\xi_t}, \widetilde{\xi_{t+1}}\right) \middle| \begin{matrix} x \leq \widetilde{\xi_t} \leq y \\ x \leq \widetilde{\xi_{t+1}} \leq y \end{matrix}, t \in \mathcal{T} \right\} \subset \mathbb{R}^2 \qquad (\mathbf{17})$$

We choose $\Delta_{\alpha,\beta} = 80$, $x = -8 \times 10^3$ and $y = 6 \times 10^3$.

We compute the *"(ϵ, M)-certainty set"* for size parameters (ϵ, M) varying over a large range of values. Keeping ϵ constant, **Figure 4.A.** shows that the size of $\mathcal{C}_{M,\epsilon,t}$ increases monotonically with M, which confirms our theoretical intuition. As $\epsilon = 10^{-6}$, $1 - \epsilon \sim 1$. This allows us to state that, for instance, we can be almost certain that the couple of residual demand values (7000,7000) at 12 p.m in Winter will not occur at least once for a number of trials lower than 10^8. Equivalently, we observe that the minimum number of trials M required to observe at least once the couple of values (15 000, 15 000) with certainty is below 10^6. Similar patterns for Summer can be observed in **Figure 4.B.** in Appendix.

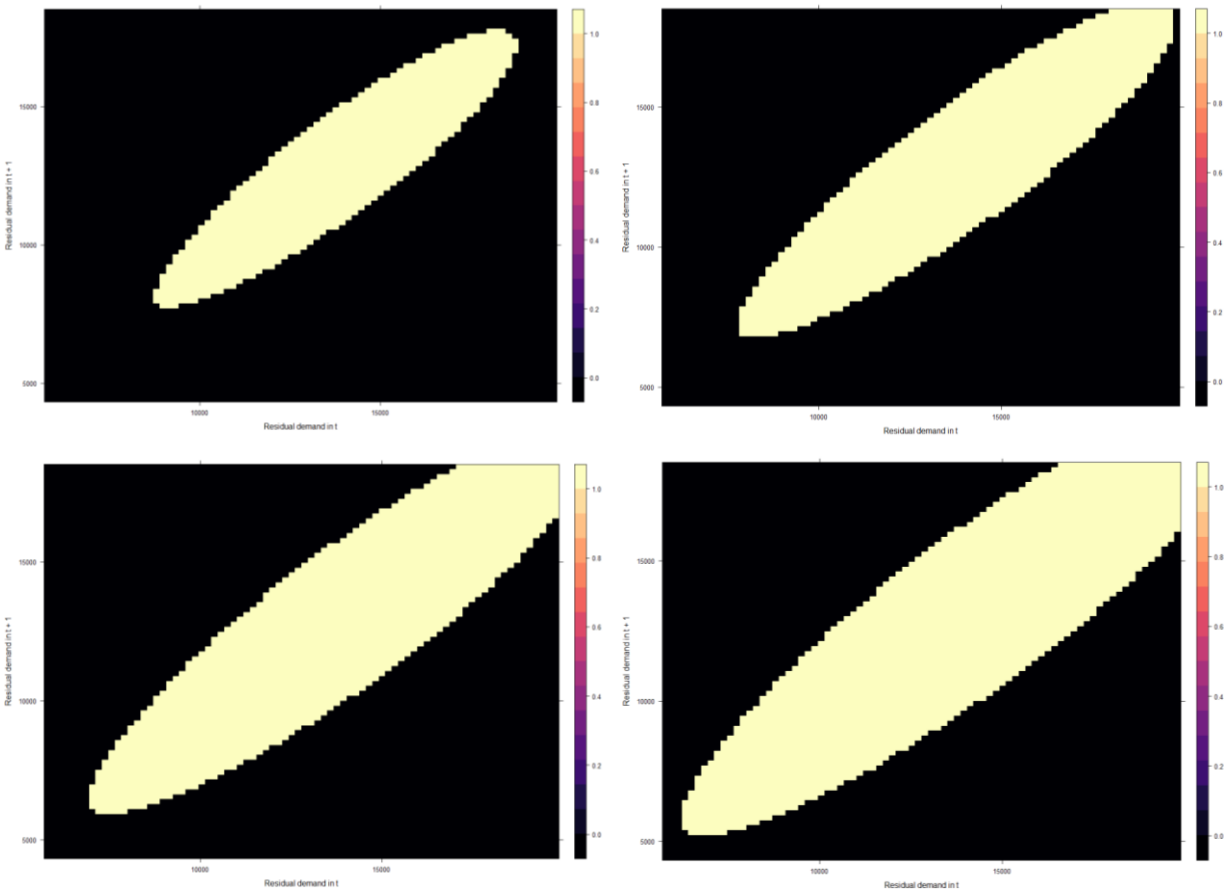

Figure 4.A.: *"*(ϵ, M)-certainty set*"* at 12 p.m in Winter keeping ϵ fixed

Note: We set $\epsilon = 10^{-6}$. We set M respectively equal to 10^6 (top-left), 10^7 (top-right), 10^8 (bottom-left) and 10^9 (bottom-right).

As expected, we observe from **Figure 4.C.** that the size of the *"*(ϵ, M)-certainty set*"* increases with ϵ. As ϵ gets higher, the probability of observing at least once a given event, for M fixed, increases as $M^*_{\epsilon,t}(\alpha, \beta)$ gets smaller for all $(\alpha, \beta) \in \mathbb{Z}^2$. Thus, the probability of never observing any event also decreases for an increasing ϵ.

We set $M = 10^9$ and $\epsilon = 10^{-6}$ and estimate $\mathcal{C}_{M,\epsilon,t}$ for all $t \in \{0, \dots, 23\} \subset \mathcal{T}$ and all seasons. As $\mathcal{T}$ exhibits diurnal cyclicality (i.e. the sequence of hours repeats each day), we make the simplifying assumption that for a given $t \in \{0, \dots, 23\}$ and season, $\mathcal{C}_{M,\epsilon,t}$ is identical for all days of the week. This may be refined in further work as residual demand is likely to exhibit different dynamic patterns during the week and the weekend. For each season and each $t \in \mathcal{T}$, we compute the set $\mathcal{C}_{M,\epsilon,t}$ corresponding to each value of $\boldsymbol{S}$.

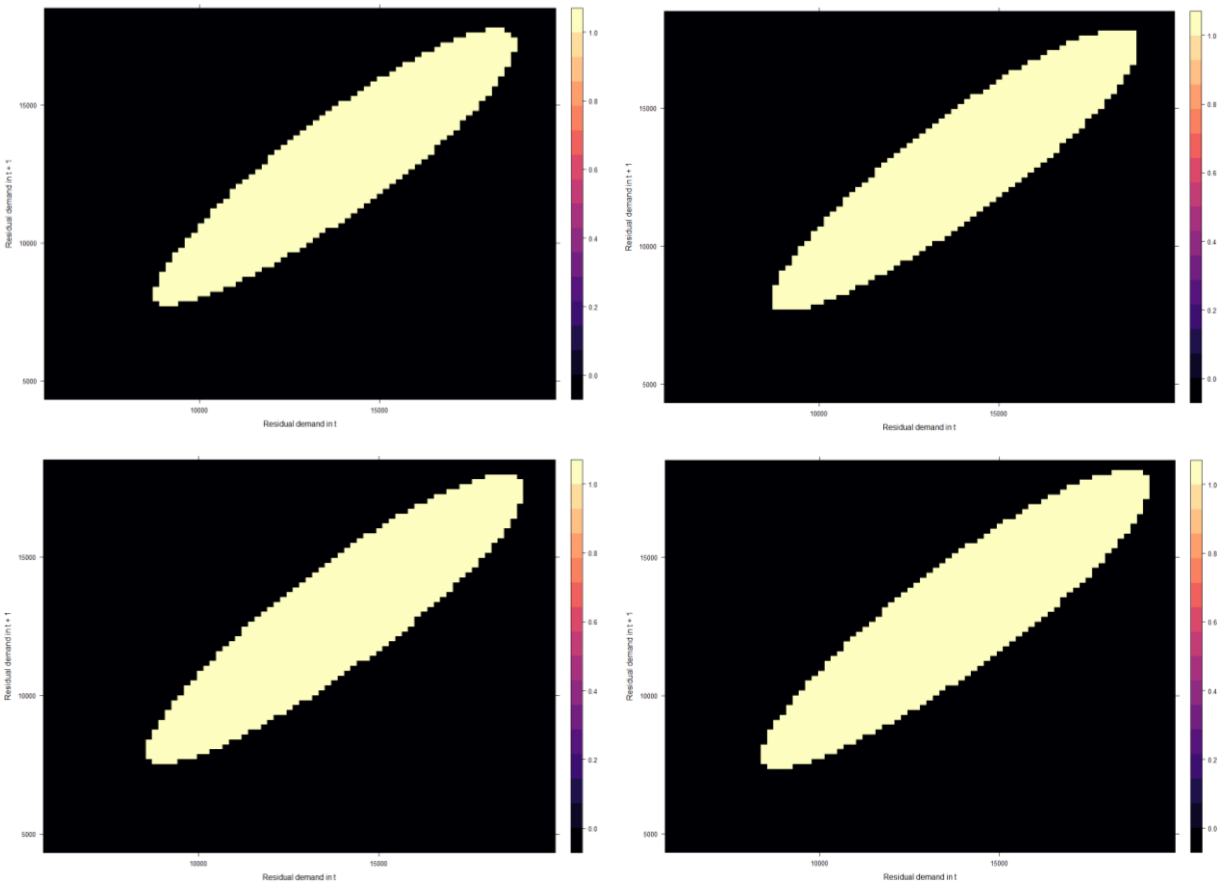

Figure 4.C.: *"*(ϵ, M)-certainty set*"* at 12 p.m in Winter keeping M fixed

Note: We set $M = 10^6$. We set ϵ respectively equal to 10^{-6} (top-left), 10^{-5} (top-right), 10^{-4} (bottom-left) and 10^{-3} (bottom-right).

4.1.2. Estimation of the worst-case set of residual demand trajectories

Using the methodological framework introduced in Section II, we discretize the "(ϵ, M)-certainty sets" for each t into Q segments of equal length, such that $\boldsymbol{V}_Q^t$ contains exactly $Q + 1$ values or "edges". We set $Q = 10$ and $m = |\mathcal{T}| - 2$, such that we estimate worst-case RD trajectories with a length equal to one full week.

We respectively denote by **H**, **L** and **V** the sequences of values that maximize, minimize and maximize the variability of RD. We count a maximum number of $(Q + 1)^{|\mathcal{T}|}$ possible residual demand trajectories, that is 11^{168}. However, there exists some pairs of vertices (couples of residual demand values) that are not linked by any edge, i.e. it is not possible to observe the corresponding sequence of vertices. We observe that for any couple $\left(\boldsymbol{V}_Q^t, \boldsymbol{V}_Q^{t+1}\right)$, each vertex

from $\boldsymbol{V}_Q^t$ shares on average 5 edges with $\boldsymbol{V}_Q^{t+1}$. This restricts the total number of possible residual demand trajectories to roughly 5^{168}.

We apply the N-Summit Algorithm to each season. The elapsed CPU time for computing trajectory **V** is estimated to 0.55 seconds. In order to compute trajectories **H** and **L**, we first replace each element $\ell\left(\left(v_j^i, v_k^{i+1}\right)\right)$ in matrix X^i by the term $\ell\left(\left(v_j^i, v_k^{i+1}\right)\right) = v_j^i - v_k^{i+1} \in \mathbb{R}$. Then, finding **H** consists in finding the trajectory which maximizes residual demand values, or equivalently that increases the most in the interval $[0, m]$. Similarly, computing **L** is equivalent to finding the residual demand trajectory that decreases the most, which requires in addition replacing the supremum by the infimum in the definition of Ω^i. The elapsed CPU times for computing **L** and **H** are both estimated to 0.75 seconds.

Figure 5 shows the set of worst-case trajectories estimated for all seasons and various levels of renewable installed capacity. It can be noted for all seasons that higher RES penetration increases the diurnal variability of RD, following the generation pattern of photovoltaic units. Moreover, we observe that the depth of the "duck dive", described in [23], which describes the timing imbalance between the evening peak load and the afternoon solar generation peak, strongly increases in Spring and Summer. This translates a ramp need of more 10 GWh within a few hours, both in the morning around 9 a.m. and in the afternoon around 7 p.m. This indicates the adequate production mix would require production units with steep ramping capacities and low minimum production levels, associated with an active management of renewable output, including energy storage, curtailment and demand response.

Yet, our method models RD at the aggregate level and thus does not allow to separately observe the values of demand nor RES generation. This makes the exact computation of maximum possible levels of load shedding or curtailment impossible in practice. Using a simple approximation heuristic, we first generate the vector of values of RD that would have been observed in the training sample for each value taken by $\boldsymbol{S}$. Then, for each worst-case trajectory, we match each component with the observation in the generated vector which minimizes their squared distance. This allows us to attribute to each value of the worst-case trajectory a 3-uplet of electricity demand, wind and solar capacity factors found in the training sample. Finally, we gradually modify the values of demand in each 3-uplet in the direction that reduces the most the total mean squared distance with the worst-case trajectory until it falls below a given threshold. We shall further refine this approximation heuristic in further research.

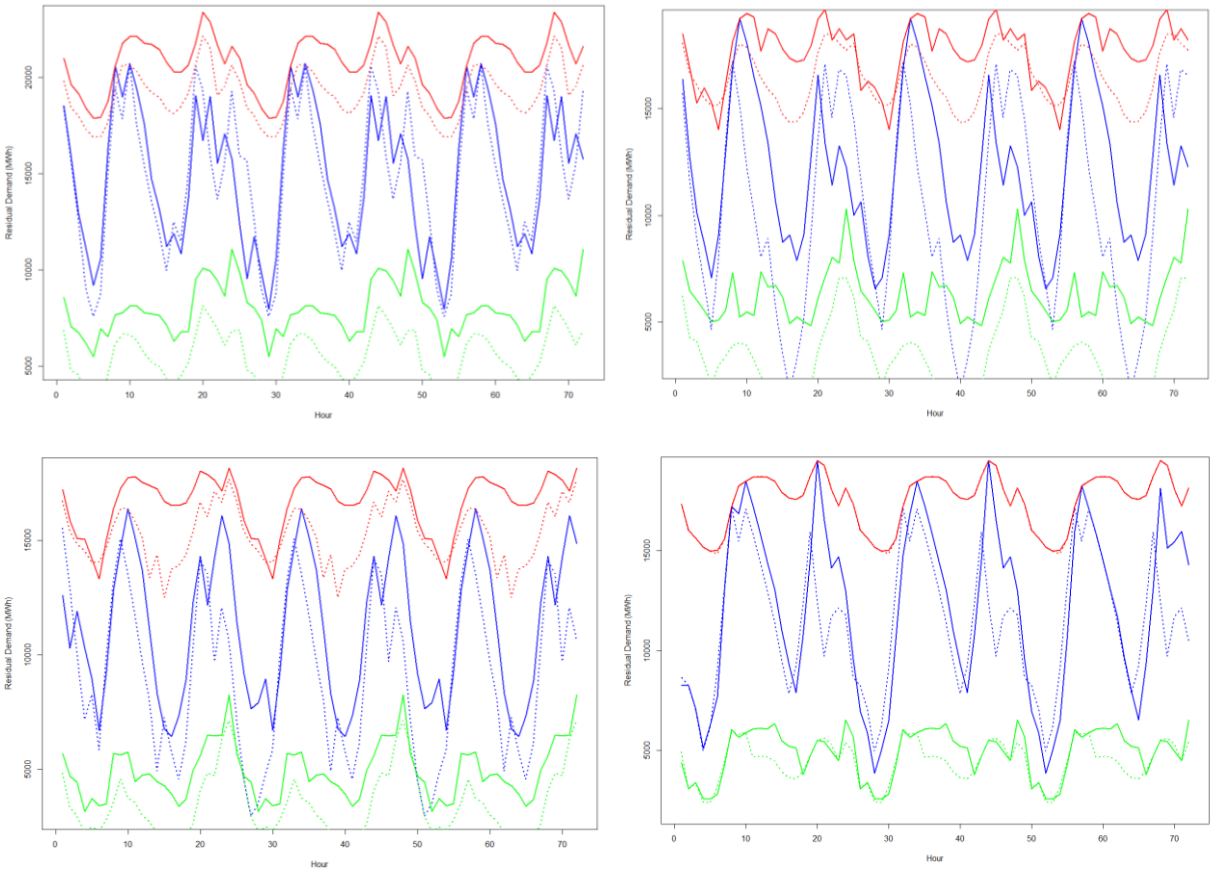

Figure 6: Extreme residual demand trajectories for all seasons

Note: The red, green and blue plain curves respectively correspond to trajectory **H**, **L** and **V** for $\boldsymbol{S} = 2$. The dotted lines correspond to residual demand trajectories for $\boldsymbol{S} = 6$. The top-left (resp. top-right, bottom-left and bottom-right) corresponds to residual demand worst-case trajectories in Winter (resp. Spring, Summer and Autumn).

4.2. Baseline simulation results

We compare the investment levels and cost performance of the optimal mix obtained when hedging against a variety of extreme trajectories. We throughout compare our results to those obtained in Chapter I. When hedging only against **H** or against the couple of trajectories **L**+ **H**, we set N^R respectively equal to 1 and 2. Hedging against **L+H+V** consists in hedging against all types of worst-case trajectories. Like in the previous chapter, we will refer to these three different hedging strategies as scenarios I_1, I_2 and I_3. Similarly, in order to clearly observe the effects of renewable penetration on investment levels and cost performance, we constraint the wind and photovoltaic capacities to be respectively equal to $\boldsymbol{S}$ GWe, where $\boldsymbol{S} \in \{0; 2; 4; 6\}$ as previously.

	I_1	I_2	I_3	I_1	I_2	I_3
	$\boldsymbol{S=0}$			$\boldsymbol{S=2}$		
Combined cycle gas turbine	6.75	12.15	9.45	2.7	13.5	10.8
Gas turbine	0	0.9	0	0	0	2.7
Nuclear	16	9.6	12.8	19.2	9.6	9.6
Wind	0	0	0	2	2	2
PV	0	0	0	2	2	2
Battery storage	2970.199	2564.256	9311.854	1619.789	1838.806	3755.732
	$\boldsymbol{S=4}$			$\boldsymbol{S=6}$		
Combined cycle gas turbine	5.4	13.5	10.8	4.05	13.5	9.45
Gas turbine	0	0.9	0	0	0.9	0.9
Nuclear	16	6.4	9.6	16	6.4	9.6
Wind	4	4	4	6	6	6
PV	4	4	4	6	6	6
Battery storage	7705.299	5204.875	6565.825	10868.865	2680.999	14821.713

Table 2.A.: Optimal investment level by technology for various levels of renewables capacity (in GWe)

Note: For any level of $\boldsymbol{S}$, the investment levels corresponding to column I_1 (resp. I_2) are obtained when hedging against the highest residual demand trajectory (resp. when hedging both against the lowest and highest residual demand trajectories).

We first observe from **Table 2.A.** that nuclear installed capacity is consistently higher in investment scenario I_1. Under this scenario, peaking capacity globally decreases while storage capacity increases with higher RES penetration. For all investment scenarios, we observe a roughly decreasing trend in peaking capacities with U-shaped evolution of storage capacities. Compared to Chapter I, we note CCGT and GT capacities are significantly lower for all investment scenario and do not necessarily increase with renewable penetration. This suggests that, in the presence of storage technologies, there exists no clear linear relationship between renewable penetration and the level of required peaking capacities. Still, the decreasing share of nuclear translates higher requirements for flexible generation units with low minimum generation level and high ramping rates.

Table 2.B. shows the total investment cost and average unit generation costs for each worst-case weekly trajectory associated to each investment scenario. First, despite the increase of investment costs generated by imposed renewable penetration, the total investment costs show

no positive clear trend. We also note investment costs are systematically higher for nuclear based mixes: mixes found in I_2 (resp. I_3) have between 41 % and 64 % (resp. 16% and 58%) lower investment costs.

	I_1				I_2				I_3			
$\boldsymbol{S=0}$												
Total investment costs (B€)	66.39				46.43				57.33			
Average unit cost (week **H**, €/MWh)	19.80	13.18	11.00	12.64	36.98	32.77	31.03	32.28	28.39	22.78	20.48	22.13
Average unit cost (week **L**, €/MWh)	8.311	8.313	8.344	8.320	10.05	8.313	9.045	8.320	8.311	8.313	8.344	8.320
Average unit cost (week **V**, €/MWh)	11.99	8.953	8.511	9.956	28.59	25.86	20.04	24.59	17.92	11.45	8.745	12.93
$\boldsymbol{S=2}$												
Total investment costs (B€)	79.17				50.87				50.24			
Average unit cost (week **H**, €/MWh)	11.65	8.182	8.117	8.246	36.62	31.95	29.78	31.94	38.12	31.95	29.78	31.94
Average unit cost (week **L**, €/MWh)	6.912	6.419	7.341	6.359	6.912	6.419	6.765	6.243	6.912	6.370	6.765	6.238
Average unit cost (week **V**, €/MWh)	8.036	8.295	8.074	9.086	26.15	22.84	18.03	22.83	25.86	19.81	17.33	21.95
$\boldsymbol{S=4}$												
Total investment costs (B€)	73.98				52.49				53.54			
Average unit cost (week **H**, €/MWh)	17.84	10.29	8.055	11.71	44.75	40.90	39.21	41.72	35.64	30.66	28.31	31.53
Average unit cost (week **L**, €/MWh)	5.673	4.404	4.972	4.439	7.663	4.547	4.972	4.439	5.470	4.404	4.972	4.439
Average unit cost (week **V**, €/MWh)	8.144	7.917	7.361	7.737	35.33	30.09	26.11	33.55	24.79	18.87	14.90	22.44
$\boldsymbol{S=6}$												
Total investment costs (B€)	77.40				47.03				58.18			
Average unit cost (week **H**, €/MWh)	16.17	8.377	8.002	11.55	44.02	39.78	37.89	41.67	34.71	29.25	26.53	31.60
Average unit cost (week **L**, €/MWh)	4.014	3.305	3.653	3.758	4.014	3.788	4.704	3.758	4.014	2.829	3.653	3.758
Average unit cost (week **V**, €/MWh)	7.461	7.068	6.736	7.239	33.85	25.70	22.08	27.91	22.94	12.23	7.401	14.74

Table 2.B.: Total investment costs and average unit cost by worst-case trajectory for various levels of renewables capacity (in GWe)

Note: For each column I_1, I_2 andI_3, sub-columns respectively correspond to the average unit generation cost for various worst-case trajectories for Winter, Spring, Summer and Autumn, from the left to the right. Example: the average unit cost in Spring when hedging against **H** only, for $\boldsymbol{S=2}$, is equal to 8.182 €/MWh.

Using average unit generation cost as a proxy for long-term spot prices, we note that for all worst-case trajectories, mixes with significant nuclear capacities clearly outperform more flexible ones. Except for the week **L**, for which lower minimum generation constraints in I_2 and I_3 allow slightly lower average unit cost, the generation cost advantage of nuclear based mixes increases with RES capacities. For $\boldsymbol{S=0}$ and worst-case week **H**, the yearly average unit cost associated to investment scenario I_1 represents only 42% (resp. 59%) of the average

cost associated to I_2 (resp. I_3). For $\boldsymbol{S = 6}$, these ratios further decrease to 27% and 36% respectively. Still, like in Chapter I, we note the cost performances associated to I_3 are in all cases significantly better than that of scenario I_2. This confirms the economic relevance of hedging against the most volatile residual demand trajectories in terms of optimal investment decision.

However, comparing generation mixes in terms of cost performance over a sample of extreme scenario, with a potentially low probability of occurrence, has little relevance in terms of average cost performance. We can thus approximate the yearly distribution of production cost associated with a given generation mix.

Like in Chapter I, we approximate the yearly Net Load Duration Curve (NLDC) with a 4-week sample drawn from a set of 52 weeks, corresponding to a full year of demand and renewable capacity factor data. We use the same subset of representative weeks and method than in Chapter I. The approximate average yearly unit costs of generation are presented in **Table 2.C**.

	I_1	I_2	I_3
$\boldsymbol{S = 0}$			
Approximate average unit cost (€/MWh)	8.631	21.19	11.51
$\boldsymbol{S = 2}$			
Approximate average unit cost (€/MWh)	7.849	18.14	17.94
$\boldsymbol{S = 4}$			
Approximate average unit cost (€/MWh)	7.380	27.14	14.91
$\boldsymbol{S = 6}$			
Approximate average unit cost (€/MWh)	6.887	23.89	12.25

Table 2.C.: Approximate yearly average unit cost for various levels of renewables capacity (in GWe)

Again, nuclear based mixes associated to I_1 outperform other mixes in terms of average generation unit costs. Moreover, average yearly unit costs decrease with renewable penetration, while no such trend can be identified more mixes corresponding to I_2 and I_3. Under these investment scenarios, the decrease in total variable costs entailed by a higher

share of RES generation share fails to compensate the high variable costs of CCGT and GT, which utilization rate increase with renewable penetration.

Overall, simultaneously hedging against **H**, **L** and **V** exhibits significant advantages in terms of total costs and long-term marginal cost. Still, despite higher investment and fixed costs, nuclear based mixes consistently exhibit lower average unit generation costs, both for extreme and representative trajectories. In the absence of CO2 emission targets, our results entail a net trade-off between these two categories of costs, which depends on the life-duration of generation units, distribution of fixed costs among consumers by retailers, probability of occurrence of extreme weeks and the distribution of costs between consumer categories.

However, we show this difference in cost structure does not result in a significant difference in retail prices as nuclear based mixes can allocate their investment costs over a higher number of operating years. Taking the case $\boldsymbol{S} = 6$ and a reference average life duration of the whole mix of 40 years, the total investment cost of 77.4 billion euros in scenario I_1 corresponds to an annuity of roughly 4.5 billion euros. For an annual demand of 100 GWh, equally sharing the annuitized investment costs among consumers would result in a 45 €/MWh add-up. Neglecting network costs, retail costs and additional taxes, the approximate average retail cost would be close to 52 €/MWh. In comparison, the annuitized investment corresponding to I_3 is equal to 3.8 billion euros approximately, taking an average life duration of 30 years because of the significant share of CCGT and GT units. This results in an approximate yearly retail price of 50 €/MWh.

The generation costs of flexible mixes would however be more sensitive to the price of gas and potentially be more volatile. Within a general equilibrium framework, a high electricity generation price would increase the cost of goods using electricity as an input and lower the disposable income of households. This would both likely lower the cost competitiveness of domestic goods and decrease domestic consumption, with negative consequences on social welfare that are not accounted for in our framework.

Still, the true flexibility options of nuclear may be overestimated, which may result in higher than expected operational costs in order to accommodate fluctuations from renewable output.

4.3. Sensitivity analysis

Like in the previous chapter, ramping constraints are not binding using an hourly time step. Moreover, as underlined in [24], increasing renewable penetration increase the frequency of extreme nuclear power ramps and annual required shutdowns/start-up events. These may cause frequent physical damage to the equipment and shorten the expected lifetime of plants.

Again, we constrain the absolute nuclear power ramp of each individual plant, denoted $\boldsymbol{r_{NUC}}$, to be inferior to 25% or 15% of the difference between the maximum and minimum generation level. The optimal investment and cost performance results are shown in **Table 3.A.**, **3.B**, **3.C.** and **Table 4.A.**, **4.B.** and **4.C.** respectively.

First, we notice the optimal CCGT capacity does globally not increase in I_1 and remains stable with high renewable penetration. Surprisingly, the overall storage capacity is also lower than when letting the hourly ramping rate of nuclear units unconstrained. This suggests a more efficient use of storage units, used in association to nuclear units to mitigate the loss in generation flexibility by reallocating nuclear production in time. I_2 and I_3 yield very similar findings to those in Chapter I: the share of CCGT and GT significantly increases in the optimal mix, while optimal storage capacities strongly decrease for high values of renewable penetration.

We notice in **Table 3.B.** that constraining nuclear flexibility preserves the cost advantage of nuclear based mixes. Lowering ramping capability of nuclear units increases the average unit generation cost for all types of mixes and all worst-case trajectories except **L**. This reflects the higher utilization rate of peaking units, in addition to an increase in the number of start-ups and shutdowns required to compensate the loss of nuclear flexibility. These two effects add up significant costs for mixes with large CCGT and GT capacities.

$r_{NUC} = 25\ \%$	I_1	I_2	I_3	I_1	I_2	I_3
	$S = 0$			$S = 2$		
Combined cycle gas turbine	2.7	12.150	13.5	5.4	12.15	14.85
Gas turbine	0	0	0	0	0	0
Nuclear	19.2	9.6	9.6	16	9.6	6.4
Wind	0	0	0	2	2	2
PV	0	0	0	2	2	2
Battery storage	3175.161	4976.634	5081.780	2381.078	1838.806	5359.475
	$S = 4$			$S = 6$		
Combined cycle gas turbine	4.05	13.5	12.15	4.05	13.5	13.5
Gas turbine	0	0	2.7	0	0.9	1.8
Nuclear	16	9.6	6.4	16	6.4	6.4
Wind	4	4	4	6	6	6
PV	4	4	4	6	6	6
Battery storage	4978.830	1891.511	1577.625	2753.524	4486.686	3206.784

Table 3.A.: Optimal investment level by technology for $r_{NUC} = 25\%$ and various levels of renewables capacity (in GWe)

The same conclusions apply to **Table 3.C.**, as the increase in yearly average unit cost is markedly higher for CCGT and GT based mixes than for nuclear based ones. The exact same patterns can be observed in **Tables 4.A.**, **4.B.** and **4.C.** in Appendix when further decreasing nuclear ramping capabilities.

$r_{NUC} = 25\ \%$	I_1				I_2				I_3			
$S = 0$												
Total investment costs (B€)	75.53				46.48				47.52			
Average unit cost (week **H**, €/MWh)	13.03	8.282	8.278	8.293	37.77	33.78	31.52	31.96	37.72	33.79	31.52	31.96
Average unit cost (week **L**, €/MWh)	8.296	8.362	8.306	8.410	8.296	8.362	8.306	8.305	8.296	8.362	8.306	8.305
Average unit cost (week **V**, €/MWh)	8.460	8.382	8.347	9.007	29.69	27.02	19.97	22.15	29.73	27.02	20.01	22.06
$S = 2$												
Total investment costs (B€)	69.18				49.86				40.33			
Average unit cost (week **H**, €/MWh)	19.45	12.59	9.836	12.40	36.62	31.92	29.78	31.94	35.19	27.73	30.76	37.89
Average unit cost (week **L**, €/MWh)	6.914	6.373	6.768	6.245	6.914	6.424	6.779	6.555	6.949	5.180	6.412	5.502
Average unit cost (week **V**, €/MWh)	11.19	9.103	8.195	12.37	26.14	20.89	18.03	23.37	24.95	16.74	8.844	14.79
$S = 4$												
Total investment costs (B€)	72.50				54.79				42.64			
Average unit cost (week **H**, €/MWh)	17.91	10.30	8.055	12.01	35.61	30.66	28.30	31.53	51.15	40.91	39.21	41.72
Average unit cost (week **L**, €/MWh)	5.470	4.787	4.972	4.442	5.506	5.693	5.463	4.442	8.611	6.640	5.686	4.442
Average unit cost (week **V**, €/MWh)	9.085	10.34	8.261	8.209	25.60	22.99	17.86	23.28	36.02	30.99	27.78	34.14
$S = 6$												
Total investment costs (B€)	76.03				47.33				47.48			
Average unit cost (week **H**, €/MWh)	16.17	9.587	8.002	12.18	43.85	39.78	37.89	41.67	43.92	39.78	37.89	41.67
Average unit cost (week **L**, €/MWh)	4.018	4.077	4.580	3.853	4.017	3.915	4.528	3.758	4.017	4.143	4.471	3.759
Average unit cost (week **V**, €/MWh)	10.69	12.50	8.922	7.850	33.81	25.23	21.19	27.67	33.84	26.02	21.77	27.97

Table 3.B.: Total investment costs and average unit cost by worst-case trajectory for $r_{NUC} =$ 25% and various levels of renewables capacity (in GWe)

	I_1	I_2	I_3
$S = 0$			
Approximate average unit cost (€/MWh)	8.328	21.02	20.99
$S = 2$			
Approximate average unit cost (€/MWh)	7.996	18.13	17.94
$S = 4$			
Approximate average unit cost (€/MWh)	7.365	15.44	27.24
$S = 6$			
Approximate average unit cost (€/MWh)	7.144	23.82	23.88

Table 3.C.: Approximate yearly average unit cost for various levels of renewables capacity (in GWe)

As an additional test, we let the installed capacity of renewables vary freely and investigate how the optimal generation mix varies with the price of CO_2. Two main trends can be identified from **Table 5.A.**: the total peaking capacity of CCGT and GT units is strictly decreasing with carbon price, while battery storage capacity monotonically increases with it, which compensates the flexibility loss entailed by lower peaking capacities. Increasing CO_2 price globally increases total renewable capacities although RES penetration remains very low. As photovoltaic generation exhibits diurnal pattern and CCGT capacities decrease, wind power provides a more sustained minimum generation level to supplement peaking generation at nighttime.

	$\pi^{CO2} = 0$	$\pi^{CO2} = 50$	$\pi^{CO2} = 100$	$\pi^{CO2} = 150$
Combined cycle gas turbine	13.5	9.45	5.4	4.05
Gas turbine	2.7	0.9	0	0
Nuclear	6.4	9.6	16	16
Wind	0.568	0	0.353	1.195
PV	0	0	0.803	0.047
Battery storage	2048.989	4372.142	7331.214	9336.769

Table 5.A.: Optimal investment level by technology for various values of carbon price (in €/ton)

The significant drop in average unit costs for all worst-case trajectories in **Table 5.B.** can be attributed to the absence of GT units in the optimal mix for carbon prices superior to 50 €/ton. The extremely high average unit cost for Winter in week **H** for a price of 50 €/ton corresponds to repeated periods of load shedding, with negative macroeconomic consequences on economic activity and social welfare. For higher CO_2 prices, the generation cost increase for carbon emitting technologies is more than compensated by their decreasing share in the optimal mix and generation dispatch.

	$\pi^{CO2} = 0$				$\pi^{CO2} = 50$			
Total investment costs (B€)	36.65				44.70			
Average unit cost (week **H**, €/MWh)	36.94	31.52	30.81	31.38	1871	32.77	31.03	32.28
Average unit cost (week **L**, €/MWh)	17.99	13.62	8.640	9.948	9.587	8.319	77.28	8.339
Average unit cost (week **V**, €/MWh)	29.15	26.08	24.29	26.86	28.36	29.28	19.23	24.43
	$\pi^{CO2} = 100$				$\pi^{CO2} = 150$			
Total investment costs (B€)	67.10				66.99			
Average unit cost (week **H**, €/MWh)	23.43	14.08	10.57	13.29	19.24	8.238	8.258	8.264
Average unit cost (week **L**, €/MWh)	8.011	7.830	7.880	7.833	7.628	7.921	9.231	7.347
Average unit cost (week **V**, €/MWh)	11.51	8.796	8.211	12.53	8.184	8.190	8.206	9.579

Table 5.B.: Total investment costs and average unit cost by worst-case trajectory various values of carbon price (in €/ton)

Finally, **Figure 5.C.** displays the approximate yearly average unit generation cost as a function of CO_2 price. They exhibit a strong negative correlation. Because CCGT capacities decreases and its utilization rate is much lower in representative than in extreme residual load scenarios, the increase in variable cost for emitting technologies is more than compensated by their decreasing share in optimal generation. Surprisingly, increasing carbon price thus tends to lower the spot price by fostering low-carbon technologies with very low marginal costs. The share of fixed costs increases in the cost structure of the optimal mix.

	$\pi^{CO2} = 0$	$\pi^{CO2} = 50$
Approximate average unit cost (€/MWh)	25.55	21.05
	$\pi^{CO2} = 100$	$\pi^{CO2} = 150$
Approximate average unit cost (€/MWh)	8.318	8.140

Table 5.C.: Approximate yearly average unit cost for various values of carbon price (in €/ton)

5. Conclusion

In this methodological paper, we introduced a variety of original concepts aiming at modeling worst-case possible trajectories for a random process with unknown distribution.

First, using Bayesian probability tools, we formalized the concept of "certainty set", which corresponds to the set of values which are observed with quasi-certainty within a given number of trials. This intuitive concept can easily be generalized to the multivariate case, in addition to using the full posterior distribution associated to the parameters of the random vector, in order to formulate a distribution of possible "certainty sets". This is expected to reduce the results conservativeness but may significantly increase computational costs. For a fixed number of periods over which the objective function is computed, the "certainty set" provides a flexible tool in order to select the subset of parameter values that have a probability superior to a given threshold to occur at least once.

Second, using elementary graph theory and matrix algebra, we introduced a new operator called the "path operator". It exhibits nice recursive properties and allows us to derive a polynomial-time algorithm that offers the guarantee to include the trajectory of our random process that maximizes a given criterion within a very reduced set of candidate trajectories. This allows us to compute the set of worst-case trajectories which globally maximize (or minimize) the values and variability of residual demand. This nicely complements the approach of Chapter I, which offered no guarantee that the worst-case trajectories provide a global maximum for the selected criterion.

Third, we applied our methodology using a MILP investment and dispatch model with storage and unit commitment constraints to the case of Auvergne Rhône-Alpes. We confirm the intuition from Chapter I that electricity mixes with a high share of nuclear power globally perform better than more "flexible" mixes in terms of average generation cost. The resulting retail costs for both types of mixes are however similar but ignore the macroeconomic effects and welfare losses from higher generation costs. We also note that the alternative method presented in this chapter provided less conservative results, with significantly lower peaking and storage installed capacities. Yet, like in Chapter I, we did not account for very short-term ramping limitations or residual demand uncertainty and assume the physical inertia of the electric system is constant. We leave for further research the investigation of the impact of alternative technologies such as intensive demand-side management, hydrogen based inter-

seasonal storage, in addition to stability solutions such as synchronous condensers, fast frequency responses and grid-forming converters [25].

6. Appendix

Appendix to 2.1.:

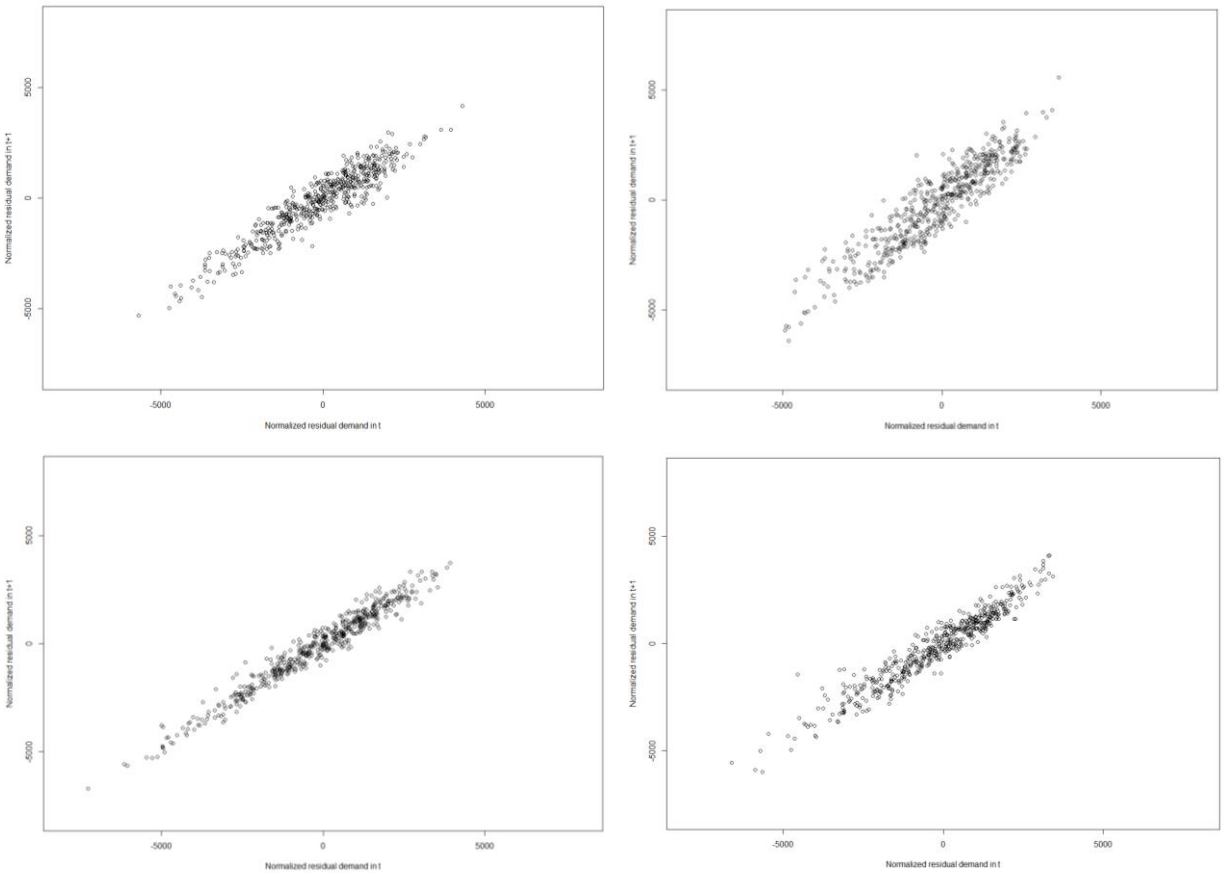

Figure 1.C.: Residual demand scatter plot with 2 GWe of wind and photovoltaic installed capacity, in Summer

Note: Each point corresponds to a couple of residual demand values for t and $t+1$. This figure show the distributions of residual demand values for 12 p.m. (top-left), 6 a.m (top-right), 12 a.m (bottom-left) and 6 p.m (bottom-right).

Appendix to 3.2.: Introduction of the "path operator"

Let us consider a set of vertices $\boldsymbol{V}^i = \left(v_1^i, \dots, v_{Q\prime}^i\right)$, $1 \leq i \leq I$ (let $I = |\mathcal{T}|$ for simplicity) where $\boldsymbol{V}^i$ includes Q' vertices. We set $Q' = Q - 1$. Considering any $(m+2)$-uplet of consecutive sets $\left(\boldsymbol{V}^i, \boldsymbol{V}^{i+1}, \dots, \boldsymbol{V}^{i+m+1}\right)$, $0 \leq m \leq I - i - 1$, we want to define the set of all simple paths of length m in the graph $G^m = \left(\bigcup_{j=0}^{m+1} \boldsymbol{V}^{i+j}, \bigcup_{j=0}^{m} \boldsymbol{V}^{i+j} \times \boldsymbol{V}^{i+j+1}\right)$. We call this operator $\mathfrak{P}$ and note the set of all paths from $\boldsymbol{V}^i$ to $\boldsymbol{V}^{i+1}$ as $\boldsymbol{V}^i \,\mathfrak{P}\, \boldsymbol{V}^{i+1}$.

For any pair $\left(\boldsymbol{V}^i, \boldsymbol{V}^{i+1}\right)$, we simply have $\boldsymbol{V}^i \,\mathfrak{P}\, \boldsymbol{V}^{i+1} = \boldsymbol{V}^i \times \boldsymbol{V}^{i+1}$. However, this simple pattern vanishes for any m-uplet of consecutive sets where m strictly greater than 0. For instance, for $m = 1$, we can represent the set of paths under the following matrix form:

$$\boldsymbol{V}^i \,\mathfrak{P}\, \boldsymbol{V}^{i+1} \mathfrak{P}\, V^{i+2} = \begin{pmatrix} \left(v_1^i, v_1^{i+1}, v_1^{i+2}\right) & \left(v_1^i, v_1^{i+1}, v_2^{i+2}\right) & \cdots & \left(v_1^i, v_{Q\prime}^{i+1}, v_{Q\prime}^{i+2}\right) \\ \left(v_2^i, v_1^{i+1}, v_1^{i+2}\right) & \left(v_2^i, v_1^{i+1}, v_2^{i+2}\right) & \cdots & \left(v_2^i, v_{Q\prime}^{i+1}, v_{Q\prime}^{i+2}\right) \\ \vdots & \vdots & \ddots & \vdots \\ \left(v_{Q\prime}^i, v_1^{i+1}, v_1^{i+2}\right) & \left(v_Q^i, v_1^{i+1}, v_2^{i+2}\right) & \cdots & \left(v_Q^i, v_{Q\prime}^{i+1}, v_{Q\prime}^{i+2}\right) \end{pmatrix} \in \mathbb{R}^{\left(Q' \times Q'^2\right)} \quad (\mathbf{18})$$

By defining the row-vector $\boldsymbol{I}_{Q\prime} = (1,1,\dots,1) \in \mathbb{R}^{(1 \times Q\prime)}$, we can rewrite the above expression recursively as:

$$\boldsymbol{V}^i \,\mathfrak{P}\, \boldsymbol{V}^{i+1} \mathfrak{P}\, \boldsymbol{V}^{i+2} = \left[\left(\boldsymbol{V}^i \,\mathfrak{P}\, \boldsymbol{V}^{i+1}\right) \otimes \boldsymbol{I}_{Q\prime}\right] \times \left[\boldsymbol{V}^{i+2} \otimes \boldsymbol{I}_{Q\prime}\right] = \left[\left(\boldsymbol{V}^i \times \boldsymbol{V}^{i+1}\right) \otimes \boldsymbol{I}_{Q\prime}\right] \times \left[\boldsymbol{V}^{i+2} \otimes \boldsymbol{I}_{Q\prime}\right] \quad (\mathbf{19})$$

Where $\otimes$ is the Kronecker product and the set $\boldsymbol{V}^{i+2}$ is expressed as a row vector such that we have $\boldsymbol{V}^{i+2} \otimes \boldsymbol{I}_{Q\prime} = \left(v_1^{i+2}, v_1^{i+2}, \dots, v_1^{i+2}, v_2^{i+2}, \dots, v_2^{i+2}, \dots, v_{N\prime}^{i+2}, \dots, v_{N\prime}^{i+2}\right) \in \mathbb{R}^{\left(1 \times Q\prime^2\right)}$. We note that the "path operator" is not commutative:

$$\boldsymbol{V}^{i+1} \mathfrak{P}\, \boldsymbol{V}^{i+2} \mathfrak{P}\, \boldsymbol{V}^i = \left[\left(\boldsymbol{V}^{i+1} \,\mathfrak{P}\, \boldsymbol{V}^{i+2}\right) \otimes \boldsymbol{I}_{Q\prime}\right] \times \left[\boldsymbol{V}^i \otimes \boldsymbol{I}_{Q\prime}\right] \neq \boldsymbol{V}^i \,\mathfrak{P}\, \boldsymbol{V}^{i+1} \mathfrak{P}\, \boldsymbol{V}^{i+2} \quad (\mathbf{20})$$

We can deduce a general recursive expression for the set of simple paths generated by any $(m+2)$-uplet $\left(\boldsymbol{V}^i, \boldsymbol{V}^{i+1}, \dots, \boldsymbol{V}^{i+m+1}\right)$, with $m \geq 1$, as:

$$\mathfrak{P}_{j=0}^{m+1} \boldsymbol{V}^{i+j} = \left[\left[\left[\left(\boldsymbol{V}^i \times \boldsymbol{V}^{i+1}\right) \otimes \boldsymbol{I}_{Q\prime}\right] \times \left[\boldsymbol{V}^{i+2} \otimes \boldsymbol{I}_{Q\prime}\right]\right] \otimes \boldsymbol{I}_{Q\prime}\right] \times \dots\right] \times \left[\boldsymbol{V}^{i+m+1} \otimes \left(\otimes_{j=1}^{m} \boldsymbol{I}_{Q\prime}\right)\right] \quad (\mathbf{21})$$

The "path operator" can easily be applied to the computation of the length associated to each possible path for a given $(m+2)$-uplet of vertices. We write $\ell\left(\left(v_j^i, v_k^{i+1}\right)\right) = \left|v_j^i - v_k^{i+1}\right|$ the length of the edge linking the couple of vertices $\left(v_j^i, v_k^{i+1}\right)$ and define $\mathfrak{P}_{j=0}^{m} \ell\left(V^{i+j}\right)$ as the

matrix giving the lengths of all paths generated by the $(m+2)$-uplet of sets $\left(\boldsymbol{V}^i, \boldsymbol{V}^{i+1}, \ldots, \boldsymbol{V}^{i+m+1}\right)$. By noting that the length of any path is additive, ie $\ell\left(\left(v_j^i, v_k^{i+1}, v_l^{i+2}\right)\right) = \ell\left(\left(v_j^i, v_k^{i+1}\right)\right) + \ell\left(\left(v_k^{i+1}, v_l^{i+2}\right)\right)$, we can decompose the length of any path using the following square matrix::

$$X^i = \ell\left((\boldsymbol{V}^i \,\mathfrak{P}\, \boldsymbol{V}^{i+1})\right) = \begin{pmatrix} \ell\left(\left(v_1^i, v_1^{i+1}\right)\right) & \ell\left(\left(v_1^i, v_2^{i+1}\right)\right) & \cdots & \ell\left(\left(v_1^i, v_{Q'}^{i+1}\right)\right) \\ \ell\left(\left(v_2^i, v_1^{i+1}\right)\right) & \ell\left(\left(v_2^i, v_2^{i+1}\right)\right) & \cdots & \ell\left(\left(v_2^i, v_{Q'}^{i+1}\right)\right) \\ \vdots & \vdots & \ddots & \vdots \\ \ell\left(\left(v_{Q,}^i, v_1^{i+1}\right)\right) & \ell\left(\left(v_{Q,}^i, v_2^{i+1}\right)\right) & \cdots & \ell\left(\left(v_{Q,}^i, v_{Q'}^{i+1}\right)\right) \end{pmatrix} \in \mathbb{R}^{+(Q' \times Q')} \qquad (\mathbf{22})$$

Similarly, we may expend this notation to paths with more than 2 edges. For $m = 1$, we have for instance:

$$\mathfrak{P}_{j=0}^{1}\ell(\boldsymbol{V}^{i+j}) = \ell\left((\boldsymbol{V}^i \,\mathfrak{P}\, \boldsymbol{V}^{i+1} \mathfrak{P}\, \boldsymbol{V}^{i+2})\right) = \begin{pmatrix} \ell\left(\left(v_1^i, v_1^{i+1}, v_1^{i+2}\right)\right) & \ell\left(\left(v_1^i, v_1^{i+1}, v_2^{i+2}\right)\right) & \cdots & \ell\left(\left(v_1^i, v_{Q'}^{i+1}, v_{Q'}^{i+2}\right)\right) \\ \ell\left(\left(v_2^i, v_1^{i+1}, v_1^{i+2}\right)\right) & \ell\left(\left(v_2^i, v_1^{i+1}, v_2^{i+2}\right)\right) & \cdots & \ell\left(\left(v_2^i, v_{Q'}^{i+1}, v_{Q'}^{i+2}\right)\right) \\ \vdots & \vdots & \ddots & \vdots \\ \ell\left(\left(v_{Q'}^i, v_1^{i+1}, v_1^{i+2}\right)\right) & \ell\left(\left(v_{Q'}^i, v_1^{i+1}, v_2^{i+2}\right)\right) & \cdots & \ell\left(\left(v_{Q'}^i, v_{Q'}^{i+1}, v_{Q'}^{i+2}\right)\right) \end{pmatrix} \qquad (\mathbf{23})$$

We propose find a closed-form expression for the set of lengths associated to all simple paths over the $m+2$-uplet $(\boldsymbol{V}^1, \boldsymbol{V}^2, \ldots, \boldsymbol{V}^{m+2})$, $m \geq 1$, expressed under matrix form:

$$\mathfrak{P}_{i=1}^{m}\ell(\boldsymbol{V}^i) = X^1 \otimes \left(\otimes_{j=1}^{m-1} \boldsymbol{I}_{Q'}\right) + \sum_{i=2}^{m}\left[\left(\otimes_{j=1}^{i-2} \boldsymbol{I}_{Q'}\right) \otimes \mathrm{vec}(X^i) \otimes \boldsymbol{I}_{Q'}^T \otimes \left(\otimes_{j=1}^{m-i} \boldsymbol{I}_{Q'}\right)\right] \in \mathbb{R}^{+\left(Q' \times Q'^m\right)} \qquad (\mathbf{24})$$

$\boldsymbol{I}_{Q'}^T$ corresponds to the transpose of $\boldsymbol{I}_{Q'}$ and we impose the convention $\left(\otimes_{i=1}^{j} \boldsymbol{I}_{Q'}\right) = 1 \in \mathbb{R}^{(1\times 1)}$ for $j < i$. We note $\mathrm{vec}\left(X^i\right)$ the result of the vectorization operation of matrix X^i. We can give a more general expression for the set of lengths associated to all simple paths generated by the $(m+2)$-uplet of consecutive sets $\left(\boldsymbol{V}^j, \boldsymbol{V}^{j+1}, \ldots, \boldsymbol{V}^{m+j+1}\right)$:

$$\mathfrak{P}_{i=j}^{m+j-1}\ell(\boldsymbol{V}^i) = X^j \otimes \left(\otimes_{j''=1}^{m-1} \boldsymbol{I}_{Q'}\right) + \sum_{i=j+1}^{m+j-1}\left[\left(\otimes_{j'=1}^{i-(j+1)} \boldsymbol{I}_{Q'}\right) \otimes \mathrm{vec}(X^i) \otimes \boldsymbol{I}_{Q'}^T \otimes \left(\otimes_{j'=1}^{m+j-1-i} \boldsymbol{I}_{Q'}\right)\right] \in \mathbb{R}^{+\left(Q' \times Q'^m\right)} \qquad (\mathbf{25})$$

Despite its intricate formulation, the path operator exhibits nice recursive properties which allow it to be computed both forward and backward for a given $(m+2)$-uplet of vertices $\left(\boldsymbol{V}^j, \boldsymbol{V}^{j+1}, \ldots, \boldsymbol{V}^{j+m+1}\right)$. This is summarized in the following property:

Property 1: It is possible to build the matrix $\mathfrak{P}_{i=j}^{m+j-1}\ell(\boldsymbol{V}^i)$ recursively, both forward and backward, by noting that:

$$\mathfrak{P}_{i=j}^{m+j-1}\ell(\boldsymbol{V}^i) = \ell(\mathfrak{P}_{i=j}^{m+j-2}\boldsymbol{V}^i)\otimes\boldsymbol{I}_{Q'} + (\otimes_{j'=1}^{m-2}\boldsymbol{I}_{Q'})\otimes\mathrm{vec}(X^m)\otimes\boldsymbol{I}_{Q'}^T$$

And:

$$\mathfrak{P}_{i=j}^{m+j-1}\ell(\boldsymbol{V}^i) = X^j\otimes\left(\otimes_{j'=1}^{m-1}\boldsymbol{I}_{Q'}\right) + \mathrm{vec}\left(\left(\mathfrak{P}_{i=j+1}^{m+j}\ell(\boldsymbol{V}^i)\right)^T\right)\otimes\boldsymbol{I}_{Q'}^T$$

Proof:

We start by proving the forward recursive decomposition of $\mathfrak{P}_{i=j}^{m}\ell(\boldsymbol{V}^i)$, which can be reformulated as follows by linearity of the Kronecker product:

$$\mathfrak{P}_{i=j}^{m+j-1}\ell(\boldsymbol{V}^i) = \left[X^j\otimes(\otimes_{j'=1}^{m-1}\boldsymbol{I}_{Q'}) + \sum_{i=j+1}^{m+j-1}[(\otimes_{j'=1}^{i-(j+1)}\boldsymbol{I}_{Q'})\otimes\mathrm{vec}(X^i)\otimes\boldsymbol{I}_{Q'}^T\otimes(\otimes_{j'=1}^{m+j-1-i}\boldsymbol{I}_{Q'})]\right]\otimes\boldsymbol{I}_{Q'}$$

$$= \left[X^j\otimes(\otimes_{j'=1}^{m-1}\boldsymbol{I}_{Q'}) + \sum_{i=j+1}^{m+j-2}[(\otimes_{j'=1}^{i-(j+1)}\boldsymbol{I}_{Q'})\otimes\mathrm{vec}(X^i)\otimes\boldsymbol{I}_{Q'}^T\otimes(\otimes_{j'=1}^{m+j-2-i}\boldsymbol{I}_{Q'})]\right]\otimes\boldsymbol{I}_{Q'} - (\otimes_{j'=1}^{m-2}\boldsymbol{I}_{Q'})\otimes\mathrm{vec}(X^{m+j-1})\otimes\boldsymbol{I}_{Q'}^T$$

$$= \ell(\mathfrak{P}_{i=j}^{m+j-2}\boldsymbol{V}^i)\otimes\boldsymbol{I}_{Q'} + (\otimes_{j'=j}^{m-2}\boldsymbol{I}_{Q'})\otimes\mathrm{vec}(X^m)\otimes\boldsymbol{I}_{Q'}^T$$

We prove the recursive backward decomposition property by noting that $\mathfrak{P}_{i=j}^{m}\ell(\boldsymbol{V}^i)$ can be expressed as the sum of two matrices:

$$\mathfrak{P}_{i=j}^{m+j-1}\ell(\boldsymbol{V}^i) = \begin{pmatrix} X_{1,1}^j + X_{1,1}^{j+1} + \cdots + X_{1,1}^{j+m} & X_{1,1}^j + X_{1,1}^{j+1} + \cdots + X_{1,2}^{j+m} & \cdots & X_{1,Q'}^j + X_{Q',Q'}^{j+1} + \cdots + X_{Q',Q'}^{j+m} \\ X_{2,1}^j + X_{1,1}^{j+1} + \cdots + X_{1,1}^{j+m} & X_{2,1}^j + X_{1,1}^{j+1} + \cdots + X_{1,2}^{j+m} & \cdots & X_{2,Q'}^j + X_{Q',Q'}^{j+1} + \cdots + X_{Q',Q'}^{j+m} \\ \vdots & \vdots & \ddots & \vdots \\ X_{Q',1}^j + X_{1,1}^{j+1} + \cdots + X_{1,1}^{j+m} & X_{Q',1}^j + X_{1,1}^{j+1} + \cdots + X_{1,2}^{j+m} & \cdots & X_{Q',Q'}^j + X_{Q',Q'}^{j+1} + \cdots + X_{Q',Q'}^{j+m} \end{pmatrix} = \boldsymbol{A} + \boldsymbol{B}$$

Where $X_{k,l}^j$ corresponds to the element on the k-th row and l-th column of matrix X^j and:

$$\boldsymbol{A} = \begin{pmatrix} X_{1,1}^j & X_{1,1}^j & \cdots & X_{1,1}^j & X_{1,2}^j & X_{1,2}^j & \cdots & X_{1,Q'}^j \\ X_{2,1}^j & X_{2,1}^j & \cdots & X_{2,1}^j & X_{2,2}^j & X_{2,1}^j & \cdots & X_{2,Q'}^j \\ \vdots & \vdots & \ddots & \cdots & \cdots & \cdots & \cdots & \vdots \\ X_{Q',1}^j & X_{Q',1}^j & \cdots & X_{Q',1}^j & X_{Q',2}^j & X_{Q',2}^j & \cdots & X_{Q',Q'}^j \end{pmatrix} \in \mathbb{R}^{+(Q'\times Q'^m)}$$

$$\boldsymbol{B} = \begin{pmatrix} X_{1,1}^{j+1} + \cdots + X_{1,1}^{j+m} & X_{1,1}^{j+1} + \cdots + X_{1,2}^{j+m} & \cdots & X_{Q',Q'}^{j+1} + \cdots + X_{Q',Q'}^{j+m} \\ X_{1,1}^{j+1} + \cdots + X_{1,1}^{j+m} & X_{1,1}^{j+1} + \cdots + X_{1,2}^{j+m} & \cdots & X_{Q',Q'}^{j+1} + \cdots + X_{Q',Q'}^{j+m} \\ \vdots & \vdots & \ddots & \vdots \\ X_{1,1}^{j+1} + \cdots + X_{1,1}^{j+m} & X_{1,1}^{j+1} + \cdots + X_{1,2}^{j+m} & \cdots & X_{Q',Q'}^{j+1} + \cdots + X_{Q',Q'}^{j+m} \end{pmatrix} \in \mathbb{R}^{+(Q'\times Q'^m)}$$

Finally, we note matrices $\boldsymbol{A}$ and $\boldsymbol{B}$ can simply be re-written as follows:

$$\boldsymbol{A} = X^j\otimes(\otimes_{j'=1}^{m-1}\boldsymbol{I}_{Q'})$$

$$\boldsymbol{B} = \text{vec}\left(\left(\mathfrak{P}_{i=j+1}^{m+j-1}\ell(\boldsymbol{V}^i)\right)^T\right)\otimes \boldsymbol{I}_{Q'}^T$$

Where $\mathfrak{P}_{i=j+1}^{m+j-1}\ell(\boldsymbol{V}^i)$ is equal to:

$$\mathfrak{P}_{i=j+1}^{m+j-1}\ell(\boldsymbol{V}^i) = \begin{pmatrix} X_{1,1}^{j+1} + X_{1,1}^{j+2} \dots + X_{1,1}^{j+m} & X_{1,1}^{j+1} + X_{1,1}^{j+2} \dots + X_{1,2}^{j+m} & \cdots & X_{1,Q'}^{j+1} + X_{Q',Q'}^{j+2}, \dots + X_{Q',Q'}^{j+m} \\ X_{2,1}^{j+1} + X_{1,1}^{j+2} \dots + X_{1,1}^{j+m} & X_{2,1}^{j+1} + X_{1,1}^{j+2} \dots + X_{1,2}^{j+m} & \cdots & X_{2,Q'}^{j+1} + X_{Q',Q'}^{j+2}, \dots + X_{Q',Q'}^{j+m} \\ \vdots & \vdots & \ddots & \vdots \\ X_{Q',1}^{j+1} + X_{1,1}^{j+2} \dots + X_{1,1}^{j+m} & X_{Q',1}^{j+1} + X_{1,1}^{j+2} \dots + X_{1,2}^{j+m} & \cdots & X_{Q',Q'}^{j+1} + X_{Q',Q'}^{j+2}, \dots + X_{Q',Q'}^{j+m} \end{pmatrix} \in \mathbb{R}^{+\left(Q'\times Q'^{(m-1)}\right)}$$

We can also easily derive an upper bound for the maximum length included in $\mathfrak{P}_{i=1}^{m}\ell(\boldsymbol{V}^i)$, as expressed in the following property:

Property 2: $\forall m \geq 1, \sup \mathfrak{P}_{i=1}^{m}\ell(\boldsymbol{V}^i) \leq \sum_{i=1}^{m} \sup X^i$

Proof:

We first note that $\forall m \geq 2$, we necessarily have the following inequality:

$$\sup \mathfrak{P}_{i=1}^{m}\ell(V^i) \leq \sup \mathfrak{P}_{i=1}^{m-1}\ell(V^i) + \sup X^m$$

Then, by induction:

$$\sup \mathfrak{P}_{i=1}^{m}\ell(V^i) \leq \sup \mathfrak{P}_{i=1}^{m-1}\ell(V^i) + \sup X^m \leq \sup \mathfrak{P}_{i=1}^{m-2}\ell(V^i) + \sup X^{m+1} + \sup X^m$$

$$\Rightarrow \sup \mathfrak{P}_{i=1}^{m}\ell(V^i) \leq \sum_{i=1}^{m} \sup X^i$$

Appendix to 4.1.: Technical characteristics and cost assumptions:

Technology	Minimum generation level (% nominal power)	Ramping rate (% of nominal power/min)	Minimum uptime/downtime (hours)	Average CO_2 emission factor (ton/MWh)
Combined cycle gas turbine	20	20	0	0.352
Gas turbine	15	8	2	0.777
Nuclear	50	2-5	10	0

Table 1.A.: Technical characteristics of main thermal technologies

Sources : Gonzalez-Salazar et al. (2018), IAEA (2018), Schill et al. (2016), IEA (2015), Schröder et al. (2013), EC JRC (2010), RTE Bilan Electrique 2019 (RTE, 2019)

Technology	Overnight cost (€/kWe)	Annual fixed & maintenance costs (€/kWe)	Unit variable cost (€/MWh)	Unit starting cost (€/MWh)	Average lifetime (years)
Combined cycle gas turbine	754	20	45	235	30
Gas turbine	400	6.4	135	542.8	30
Nuclear	3800	137	8	90	60
Photovoltaic	669	19	0	0	25
Wind power	1284	45	0	0	20
Battery storage	169	5.1	0	0	10

Table 1.B.: Cost assumptions for generation technologies for 2021

Sources : Le Cout des ENR en France, ADEME (2016) ; CRE (2018) ; "Coûts et rentabilité du grand photovoltaïque en métropole continentale", CRE (2019) ; IEA (2015) ; "Current and Prospective Costs of Electricity Generation until 2050", DIW (2013) ; OECD/IEA-NEA (2015)

Investment and dispatching model with commitment constraints

Formulation of the model:

The cost-minimization problem for our electric system, neglecting spatial transfers and transmission network, is defined as a MILP as follows:

$$\min_{\boldsymbol{U},\boldsymbol{q},\boldsymbol{\kappa},\boldsymbol{z}} \sum_{j>1}\left(A_j + c_j^{FOM}\right)U_j + \sum_{g}\left(A_g + c_g^{FOM}\right)D_g U_g + \left(A_e + c_e^{FOM}\right)U_e$$
$$+ \frac{\Theta}{N^R}\left(\sum_{\mathfrak{p}\in\{\boldsymbol{L},\boldsymbol{H},\boldsymbol{V}\}}\sum_{s\in\mathcal{S}}\sum_{t\in\mathcal{T}}\left(\sum_{g}\left(c_g^V + \pi^{CO_2}E_g\right)q_{gst}^{\mathfrak{p}} + c_g^{STUP}z_{gst}^{\mathfrak{p}} + \sum_{j} c_j^{\kappa}\kappa_{jst}^{\mathfrak{p}}\right)\right) \quad (\mathbf{26})$$

Such that :

$$\xi_{1st}^{\mathfrak{p}} - \kappa_{1st}^{\mathfrak{p}} - \sum_{j>1}\left(\xi_{jst}^{\mathfrak{p}}U_j - \kappa_{jst}^{\mathfrak{p}}\right) - \sum_{g} q_{gst}^{\mathfrak{p}} + e_{st}^{+\mathfrak{p}} - e_{st}^{-\mathfrak{p}} \leq \gamma \qquad ,\forall \mathfrak{p} \in \{\boldsymbol{L},\boldsymbol{H},\boldsymbol{V}\}\ (\mathbf{27})$$

$$-\xi_{1st}^{\mathfrak{p}} + \kappa_{1st}^{\mathfrak{p}} + \sum_{j>1}\left(\xi_{jst}^{\mathfrak{p}}U_j - \kappa_{jst}^{\mathfrak{p}}\right) + \sum_{g} q_{gst}^{\mathfrak{p}} - e_{st}^{+\mathfrak{p}} + e_{st}^{-\mathfrak{p}} \leq \gamma \qquad ,\forall \mathfrak{p} \in \{\boldsymbol{L},\boldsymbol{H},\boldsymbol{V}\}\ (\mathbf{28})$$

$$u_{gst}^{\mathfrak{p}} - u_{gst-1}^{\mathfrak{p}} = z_{gst}^{\mathfrak{p}} - v_{gst}^{\mathfrak{p}} \qquad ,\forall \mathfrak{p} \in \{\boldsymbol{L},\boldsymbol{H},\boldsymbol{V}\}, \forall g \in \mathcal{G}\ (\mathbf{29a})$$

$$z_{gst}^{\mathfrak{p}} + v_{gst}^{\mathfrak{p}} \leq 1 \qquad ,\forall \mathfrak{p} \in \{\boldsymbol{L},\boldsymbol{H},\boldsymbol{V}\}, \forall g \in \mathcal{G}\ (\mathbf{29b})$$

$${\omega_{gst}^{1}}^{\mathfrak{p}} = q_{gst}^{\mathfrak{p}} - {\omega_{gst}^{2}}^{\mathfrak{p}} \qquad ,\forall \mathfrak{p} \in \{\boldsymbol{L},\boldsymbol{H},\boldsymbol{V}\}, \forall g \in \mathcal{G}\ (\mathbf{30})$$

$${\omega_{gst}^{1}}^{\mathfrak{p}} - {\omega_{gst-1}^{1}}^{\mathfrak{p}} \leq \overline{r_g} \qquad ,\forall \mathfrak{p} \in \{\boldsymbol{L},\boldsymbol{H},\boldsymbol{V}\}, \forall g \in \mathcal{G}\ (\mathbf{31a})$$

$${\omega_{gst-1}^{1}}^{\mathfrak{p}} - {\omega_{gst}^{1}}^{\mathfrak{p}} \leq \underline{r_g} \qquad ,\forall \mathfrak{p} \in \{\boldsymbol{L},\boldsymbol{H},\boldsymbol{V}\}, \forall g \in \mathcal{G}\ (\mathbf{31b})$$

$${\omega_{gst}^{1}}^{\mathfrak{p}} \leq U_g D_g\left(\overline{q_g} - \underline{q_g}\right) \qquad ,\forall \mathfrak{p} \in \{\boldsymbol{L},\boldsymbol{H},\boldsymbol{V}\}, \forall g \in \mathcal{G}\ (\mathbf{32a})$$

$${\omega_{gst}^{1}}^{\mathfrak{p}} \leq u_{gst}^{\mathfrak{p}}\mathrm{K} \qquad ,\forall \mathfrak{p} \in \{\boldsymbol{L},\boldsymbol{H},\boldsymbol{V}\}, \forall g \in \mathcal{G}\ (\mathbf{32b})$$

$${\omega_{gst}^{2}}^{\mathfrak{p}} \leq U_g D_g \underline{q_g} \qquad ,\forall \mathfrak{p} \in \{\boldsymbol{L},\boldsymbol{H},\boldsymbol{V}\}, \forall g \in \mathcal{G}\ (\mathbf{33})$$

$${\omega_{gst}^{2}}^{\mathfrak{p}} = U_g D_g \underline{q_g} - \left(1 - u_{gst}^{\mathfrak{p}}\right)\mathrm{K} + s_{gst}^{\mathfrak{p}} \qquad ,\forall \mathfrak{p} \in \{\boldsymbol{L},\boldsymbol{H},\boldsymbol{V}\}, \forall g \in \mathcal{G}\ (\mathbf{34})$$

$$s_{gst}^{\mathfrak{p}} \leq \left(1 - u_{gst}^{\mathfrak{p}}\right)\mathrm{K} - U_g D_g \underline{q_g} + u_{gst}^{\mathfrak{p}}\mathrm{K} \qquad ,\forall \mathfrak{p} \in \{\boldsymbol{L},\boldsymbol{H},\boldsymbol{V}\}, \forall g \in \mathcal{G}\ (\mathbf{35})$$

$$u_{gst}^{\mathfrak{p}} \geq \sum_{t'>t-M_j^U} z_{gst}^{\mathfrak{p}} \qquad ,\forall \mathfrak{p} \in \{\boldsymbol{L},\boldsymbol{H},\boldsymbol{V}\}, \forall g \in \mathcal{G}\ (\mathbf{36a})$$

$$1 - u_{gst}^{\mathfrak{p}} \geq \sum_{t'>t-M_j^D} v_{gst}^{\mathfrak{p}} \qquad ,\forall \mathfrak{p} \in \{\boldsymbol{L},\boldsymbol{H},\boldsymbol{V}\}, \forall g \in \mathcal{G} \quad (\mathbf{36b})$$

$$\kappa_{jst}^{\mathfrak{p}} \leq \xi_{jst}^{\mathfrak{p}} U_j \qquad ,\forall \mathfrak{p} \in \{\boldsymbol{L},\boldsymbol{H},\boldsymbol{V}\}, \forall j \in \mathcal{J} \quad (\mathbf{37})$$

$$e_{st}^{\mathfrak{p}} = e_{st-1}^{\mathfrak{p}} + \sqrt{\eta_e} e_{st}^{+\mathfrak{p}} - \frac{e_{st}^{-\mathfrak{p}}}{\sqrt{\eta_e}} \qquad ,\forall \mathfrak{p} \in \{\boldsymbol{L},\boldsymbol{H},\boldsymbol{V}\} \quad (\mathbf{38})$$

$$e_{st}^{\mathfrak{p}} \leq \overline{e} U_e \qquad ,\forall \mathfrak{p} \in \{\boldsymbol{L},\boldsymbol{H},\boldsymbol{V}\} \quad (\mathbf{39})$$

$$e_{st}^{\mathfrak{p}} \geq \underline{e} U_e \qquad ,\forall \mathfrak{p} \in \{\boldsymbol{L},\boldsymbol{H},\boldsymbol{V}\} \quad (\mathbf{40})$$

$$e_{st}^{+\mathfrak{p}} \leq l_{st}^{\mathfrak{p}} (\overline{e} U_e - e_{st}^{\mathfrak{p}}) \qquad ,\forall \mathfrak{p} \in \{\boldsymbol{L},\boldsymbol{H},\boldsymbol{V}\} \quad (\mathbf{41})$$

$$e_{st}^{-\mathfrak{p}} \leq (1 - l_{st}^{\mathfrak{p}}) \left(e_{st}^{\mathfrak{p}} - \underline{e} U_e\right) \qquad ,\forall \mathfrak{p} \in \{\boldsymbol{L},\boldsymbol{H},\boldsymbol{V}\} \quad (\mathbf{42})$$

$$u_{gst}^{\mathfrak{p}} \in \{0,1\} \qquad ,\forall \mathfrak{p} \in \{\boldsymbol{L},\boldsymbol{H},\boldsymbol{V}\}, \forall g \in \mathcal{G} \quad (\mathbf{43})$$

$$v_{gst}^{\mathfrak{p}} \in \{0,1\} \qquad ,\forall \mathfrak{p} \in \{\boldsymbol{L},\boldsymbol{H},\boldsymbol{V}\}, \forall g \in \mathcal{G} \quad (\mathbf{44})$$

$$z_{gst}^{\mathfrak{p}} \in \{0,1\} \qquad ,\forall \mathfrak{p} \in \{\boldsymbol{L},\boldsymbol{H},\boldsymbol{V}\}, \forall g \in \mathcal{G} \quad (\mathbf{45})$$

$$l_{st}^{\mathfrak{p}} \in \{0,1\} \qquad ,\forall \mathfrak{p} \in \{\boldsymbol{L},\boldsymbol{H},\boldsymbol{V}\} \quad (\mathbf{46})$$

Description of the model:

Indices and sets:

We define the set $\mathcal{T}$ used to index hours of the week and the set of seasons $\mathcal{S}$. Residual demand can be expressed as a linear combination of electric load and production from renewable generation units. We define the set of residual demand components $\mathcal{J}$, where the first element of $\mathcal{J}$ corresponds to the electric load and the remaining elements are available renewable technologies. These can be decomposed into subsets $\mathcal{W} \subset \mathcal{J}$ and $\mathcal{P} \subset \mathcal{J}$, which respectively denote wind and photovoltaic technologies.

The set of units of thermal generation technologies is noted $\mathcal{G}$, with unit $g \in \mathcal{G}$. The set $\mathcal{G}$ can be decomposed into the subsets of nuclear units $\mathcal{N} \subset \mathcal{G}$, combined cycle gas turbines (CCGT) $\mathcal{C}^1 \subset \mathcal{G}$ and gas turbines $\mathcal{C}^2 \subset \mathcal{G}$.

Investment variables and parameters:

For each unit $g \in \mathcal{G}$, we define the binary building decision $U_g \in \{0;1\}$. The parameter $D_g \geq 0$ corresponds to the "block" size of unit g, or equivalently, its electricity output capability. For simplicity, we assume D_g is equal for all units of the same technology. Each unit $g \in \mathcal{G}$ is characterized by minimum and maximum output levels $\underline{q_g} \geq 0$ and $\overline{q_g} \geq 0$, in addition to maximum ramp-up and ramp-down capacities $\overline{r_g} \geq 0$ and $\underline{r_g} \geq 0$. The commitment status of g is constrained by minimum uptime $M_g^U \geq 0$ and minimum downtime $M_g^D \geq 0$. Finally, each thermal generation unit is characterized by a ratio of CO_2 emissions per unit output E_g, expressed in ton per unit generated.

We define the installed capacity of $j \in \mathcal{J}$ as $U_j \geq 0$ with the convention that $U_1 = 1$ and note $\boldsymbol{U} = (U_i)_{1 \leq i \leq |\mathcal{J}|}$ the vector of installed capacities for residual demand components. We define the installed capacity of storage as $U_e \geq 0$. We assume the variables U_j and U_e are continuous, while U_g is binary.

Renewable technologies, thermal generation technologies and storage respectively have annuitized unit investment costs A_j, A_g and A_e, with $A_j, A_g, A_e \geq 0$. Similarly, both renewable and thermal generation technologies exhibit yearly fixed and operation maintenance costs c_j^{FOM}, c_g^{FOM} and c_e^{FOM}, with $c_j^{FOM}, c_g^{FOM}, c_e^{FOM} \geq 0$.

Operational variables and parameters:

For any hour $t \in \mathcal{T}$ and season $s \in \mathcal{S}$, we define the uncertain capacity factor $\xi_{jst} \in \mathbb{R}^+$ for $j = 1$ and $\xi_{jst} \in [0,1]$ for $j > 1$. The variable $\kappa_{jst}^{\mathrm{p}} \geq 0$ is equal to volume of curtailed production for renewable technology $j \in \mathcal{J}$. Using this notation, $\kappa_{1st}^{\mathrm{p}}$ can naturally be interpreted as the volume of non-served load (VOLL).

We define the variable $q_{gst}^{\mathrm{p}} \geq 0$ equal to the production of generation technology $g \in \mathcal{G}$. For any hour $t \in \mathcal{T}$ and season $s \in \mathcal{S}$, ${\omega_{gst}^2}^{\mathrm{p}} \geq 0$ corresponds to the minimum-production level of generator $g \in \mathcal{G}$, while ${\omega_{gst}^1}^{\mathrm{p}} \geq 0$ is an auxiliary variable equal to the generation volume above minimum-production level. We set the scalar $\mathrm{K} \gg 0$ and define the slack variable

$s^{\mathfrak{p}}_{gst} \geq 0$. $u^{\mathfrak{p}}_{gst}$, $v^{\mathfrak{p}}_{gst}$ and $z^{\mathfrak{p}}_{gst}$ are all binary variables respectively corresponding to the commitment state, start-up and shut-down decision of generator $g \in \mathcal{G}$.

The variable $e^{\mathfrak{p}}_{st} \geq 0$ corresponds to the stock of electricity stored in hour t and season s, while $e^{+\mathfrak{p}}_{st} \geq 0$ and $e^{-\mathfrak{p}}_{st} \geq 0$ are flux variables respectively equal to the quantity of electricity stored and released. η_e is the round-trip efficiency of the battery storage technology, with $0 \leq \eta_e \leq 1$, such that $\sqrt{\eta_e}$ can be interpreted as the efficiency of charge or discharge. Finally, $\overline{e}$ and $\underline{e}$ respectively correspond to the maximum and minimum state of charge, and $l^{\mathfrak{p}}_{st}$ corresponds to the charging state of batteries, with $l^{\mathfrak{p}}_{st}$ equal to 1 when batteries store electricity.

We respectively note $c^V_g \geq 0$ and $c^{STUP}_g \geq 0$ the variable and start-up costs of the unit $g \in \mathcal{G}$. We note $c^{\kappa}_j \geq 0$ the curtailment cost of renewable technology $j \in \mathcal{J}$, where c^{κ}_1 corresponds to the Value of Lost Load (VOLL). Finally, we define the price of a carbon ton as π^{CO_2}.

Description of the equations:

Each constraint must hold for each hour $t \in \mathcal{T}$ and season $s \in \mathcal{S}$. We define the set of worst-case trajectories $\{\boldsymbol{L}, \boldsymbol{H}, \boldsymbol{V}\}$, where $\xi^{\mathfrak{p}}_{jst}$ is the value of the uncertain capacity factor for $j \in \mathcal{J}$, $t \in \mathcal{T}$, $s \in \mathcal{S}$ and trajectory $\mathfrak{p} \in \{\boldsymbol{L}, \boldsymbol{H}, \boldsymbol{V}\}$. As there may exist no single set of dispatching decisions which simultaneously verify thermal constraints for all worst-case trajectories, our formulation ensures each operational constrain must hold in addition for any $\mathfrak{p} \in \{\boldsymbol{L}, \boldsymbol{H}, \boldsymbol{V}\}$.

As three different worst-case scenario or "trajectories" are simultaneously considered in the cost function, we divide the variable costs by $N^R = 3$ and multiply them by the scaling factor Θ equal to the number of weeks per season in **(26)**, which corresponds to the scaled sum of annuitized investment costs and generation, start-up, load-shedding and curtailment costs. This ensures that the variable part of the expression still corresponds to the average yearly variable cost. **(27)** and **(28)** correspond to the upper and lower limits of the primary frequency control constraint: net generation, which is the sum of electricity generation minus electric load and storage, must lie in the interval $[-\gamma, \gamma]$. We may further define $\gamma = \iota \Delta f$, where ι is proportional to the physical inertia of the electric system and Δf corresponds to the maximum absolute deviation of frequency from its nominal value.

(29a) to **(36b)** together formalize as a set of linear constraints commitment state, starting-up decisions and output limits for dispatchable generators. We combine the "big-M" method with the use of slack variables in order to linearize minimum generation level constraints[15].

(37) constraint the volume of electricity curtailed (respectively non-served load) to be inferior or equal to the generation of renewable technology $j \in \mathcal{J}$ (respectively inferior or equal to the electric load). Finally, **(38)** to **(42)** correspond to the power balance of the storage technology, with state of charge lower and upper limits, upper bounds on electricity inflows and outflows in addition to charging status.

[15] For K big enough, ${\omega^1_{gst}}^{\mathfrak{p}} \leq U_g D_g \left(\overline{q_g} - \underline{q_g}\right)$ if u_{gst} is equal to 1 and ${\omega^1_{gst}}^{\mathfrak{p}} \leq 0$ otherwise. Similarly, ${\omega^2_{gst}}^{\mathfrak{p}} = U_g D_g \underline{q_g} - \left(1 - u^{\mathfrak{p}}_{gst}\right)\mathrm{K} + s^{\mathfrak{p}}_{gst}$ if $u^{\mathfrak{p}}_{gst}$ is equal to 1 and ${\omega^2_{gst}}^{\mathfrak{p}} = 0$ otherwise. Indeed, if $u^{\mathfrak{p}}_{gst} = 0$, as ω^2_{gst} is positive by definition and $s^{\mathfrak{p}}_{gst} \leq \mathrm{K} - U_g D_g \underline{q_g}$, we necessarily have $s_{gst} = \mathrm{K} - U_g D_g \underline{q_g}$ so ω^2_{gst} is null. On the contrary, if $u^{\mathfrak{p}}_{gst} = 1$, we must have $s^{\mathfrak{p}}_{gst} = 0$ as $s^{\mathfrak{p}}_{gst}$ is positive.

Appendix to 4.1.1.:

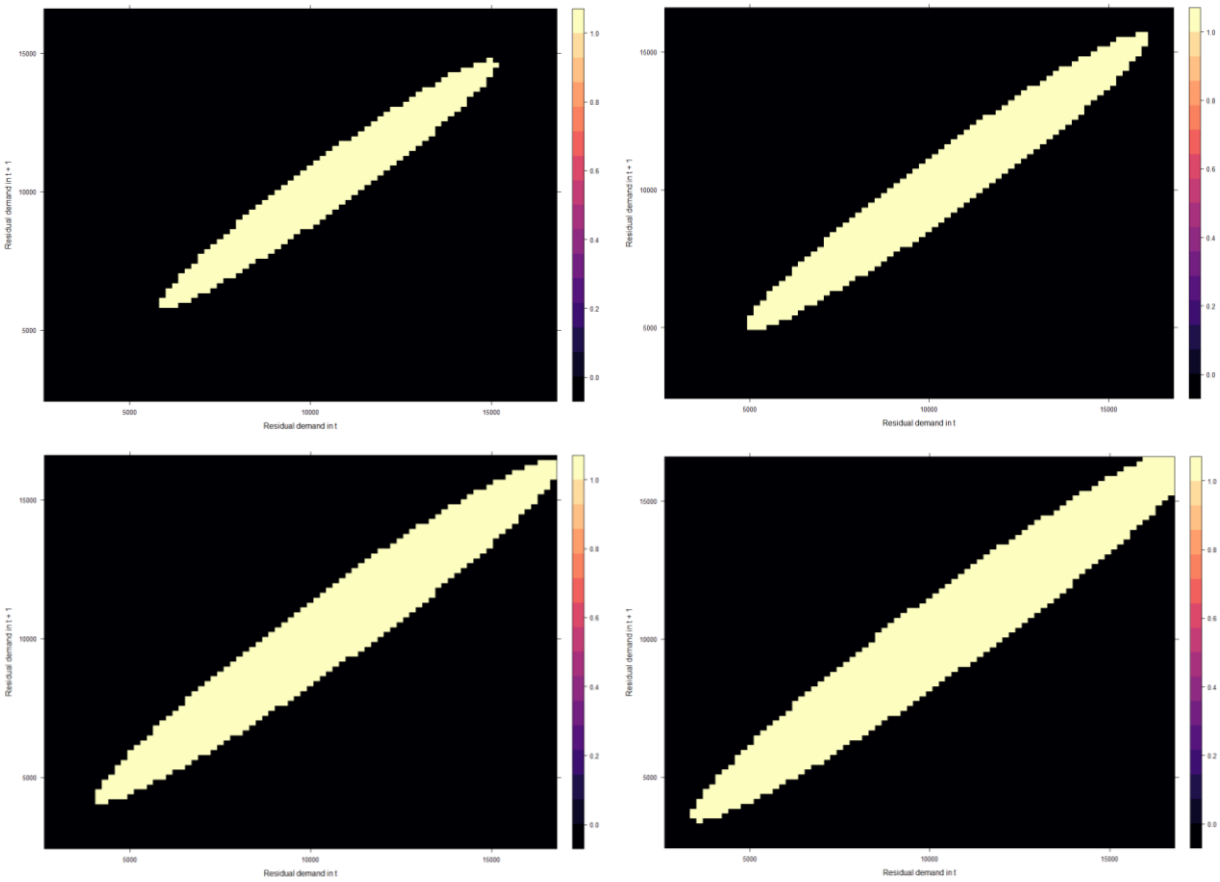

Figure 5: *"*(ϵ, M)-certainty set*"* at 2 p.m in Summer keeping ϵ fixed

Note: We set $\epsilon = 10^{-6}$. We set M respectively equal to 10^6 (top-left), 10^7 (top-right), 10^8 (bottom-left) and 10^9 (bottom-right).

Appendix to 4.3.:

$r_{NUC} = 15\ \%$	I_1	I_2	I_3	I_1	I_2	I_3
	$S = 0$			$S = 2$		
Combined cycle gas turbine	2.7	12.15	9.45	4.05	10.8	12.15
Gas turbine	0	0.9	0.9	0.9	1.8	2.7
Nuclear	19.2	9.6	9.6	19.2	9.6	6.4
Wind	0	0	0	2	2	2
PV	0	0	0	2	2	2
Battery storage	4038.346	8475.958	4372.142	1977.009	4440.072	2852.374
	$S = 4$			$S = 6$		
Combined cycle gas turbine	5.4	14.85	12.15	4.05	13.5	16.2
Gas turbine	0	0.9	2.7	0	0.9	0
Nuclear	16	6.4	6.4	16	6.4	3.2
Wind	4	4	4	6	6	6
PV	4	4	4	6	6	6
Battery storage	4845.312	1920.791	6336.033	4414.305	2680.909	5507.048

Table 4.A.: Optimal investment level by technology for $r_{NUC} = 15\%$ and various levels of renewables capacity (in GWe)

$r_{NUC} = 15\ \%$	I_1				I_2				I_3			
$S = 0$												
Total investment costs (B€)	75.68				47.43				44.70			
Average unit cost (week **H**, €/MWh)	12.95	8.282	8.278	8.294	37.77	33.78	31.52	31.96	1871	32.77	31.03	32.28
Average unit cost (week **L**, €/MWh)	8.299	8.375	8.308	8.317	8.299	8.323	8.308	8.315	9.587	8.319	77.28	8.339
Average unit cost (week **V**, €/MWh)	9.340	8.679	8.362	11.29	29.68	28.18	19.82	22.85	28.36	29.28	19.23	24.43
$S = 2$												
Total investment costs (B€)	80.61				49.99				38.95			
Average unit cost (week **H**, €/MWh)	16.91	8.282	8.105	10.06	38.05	31.95	29.78	31.94	54.71	41.96	40.34	42.09
Average unit cost (week **L**, €/MWh)	6.972	6.258	9.511	5.502	6.921	6.382	6.780	6.250	14.79	8.186	6.781	6.267
Average unit cost (week **V**, €/MWh)	9.784	10.84	8.818	8.130	25.81	19.58	16.90	22.81	36.77	31.46	28.73	33.05
$S = 4$												
Total investment costs (B€)	73.50				44.01				43.44			
Average unit cost (week **H**, €/MWh)	17.84	10.32	8.055	12.06	44.49	40.90	39.21	41.72	50.13	40.90	39.21	41.72
Average unit cost (week **L**, €/MWh)	5.668	5.169	5.118	4.448	8.406	10.49	6.335	4.449	7.549	4.954	4.974	4.448
Average unit cost (week **V**, €/MWh)	10.36	13.55	10.70	10.19	35.44	31.11	27.74	34.12	35.34	29.90	26.36	33.50
$S = 6$												
Total investment costs (B€)	76.31				47.03				37.02			
Average unit cost (week **H**, €/MWh)	16.17	9.158	8.002	11.99	44.02	39.78	37.89	41.67	53.12	50.32	49.24	51.75
Average unit cost (week **L**, €/MWh)	4.025	3.902	4.295	3.764	4.364	5.596	7.726	3.888	14.14	7.280	6.448	9.313
Average unit cost (week **V**, €/MWh)	11.44	14.14	10.37	8.486	33.85	27.38	22.46	28.04	44.77	36.68	34.21	40.79

Table 4.B.: Total investment costs and average unit cost by worst-case trajectory for $r_{NUC} =$ 15% and various levels of renewables capacity (in GWe)

	I_1	I_2	I_3
$S = 0$			
Approximate average unit cost (€/MWh)	8.314	20.85	21.05
$S = 2$			
Approximate average unit cost (€/MWh)	7.996	17.89	30.72
$S = 4$			
Approximate average unit cost (€/MWh)	7.454	27.23	27.12
$S = 6$			
Approximate average unit cost (€/MWh)	6.992	23.93	37.50

Table 4.C.: Approximate yearly average unit cost for various levels of renewables capacity (in GWe)

7. Bibliography

[1] LAPLACE Pierre-Simon, *Essai philosophique sur les probabilités*, Cambridge University Press, 2009, 280 p.

[2] LI Can & GROSSMANN Ignacio E., "A Review of Stochastic Programming Methods for Optimization of Process Systems Under Uncertainty, Li and Grossmann", *Frontiers in Chemical Engineering*, vol.2, 2021, 34 p.

[3] CHARNES A. & COOPER W. W., "Chance-Constrained Programming", *Management Science*, vol.6, n°1, 1959, pp.73-79

[4] PREKOPA Andras, "On Probabilistic Constrained Programming", Proceedings of the Princeton Symposium on Mathematical Programming, Princeton University Press, 1970, pp.113-138

[5] DANTZIG George B., "Linear Programming under Uncertainty", *Management Science*, vol. 1, n°3-4, 1955, pp. 197-281

[6] KALL Peter & WALLACE Stein W., *Stochastic Programming*, John Wiley & Sons, Chichester, 1994

[7] BIRGE J.R. & LOUVEAUX F., *Introduction to stochastic programming*, Springer Science & Business Media, Heidelberg, Germany, 2011

[8] GOEL V. & GROSSMANN I.E., "A class of stochastic programs with decisions dependent uncertainty", *Mathematical Programming.*, vol.108, 2006, pp. 355–394

[9] SOYSTER A.L., "Convex programming with set-inclusive constraints and applications to inexact linear programming", *Operations Research*, vol.21, 1973, pp.1154-1157

[10] BEN-TAL A. & NEMIROVSKI A., "Robust solutions of linear programming problems contaminated with uncertain data", *Mathematical Programming*, vol.88, 2000, pp. 411-424

[11] BERTSIMAS D. & SIM M., "Price of robustness", *Operations Research*, vol.52, 2004, pp. 35-53

[12] CHEN XIN, SIM Melvyn, SUN PENG, “A Robust Optimization Perspective on Stochastic Programming”, *Operations Research*, vol.55, 2007, pp. 1058-1071

[13] YUAN Yuan, LI Zukui, HUANG Biao, “Robust optimization under correlation uncertainty: Formulations and computational study”, *Computers and Chemical Engineering*, vol.85, 2016, pp. 58-71

[14] JALILVAND-NEJAD Amir, SHAFAEI Rasoul, SHAHRIARI Hamid, “Robust optimization under correlated polyhedral uncertainty set”, *Computers and Industrial Engineering*, vol.92, 2016, pp. 82-94

[15] NING Chao & YOU Fengqi, “Data-driven decision making under uncertainty integrating robust optimization with principal component analysis and kernel smoothing methods”, *Computers and Chemical Engineering*, vol.112, 2018, pp. 190-210

[16] LORCA Alvaro & SUN XU Andy, “Adaptive Robust Optimization with Dynamic Uncertainty Sets for Multi-Period Economic Dispatch under Significant Wind”, *IEEE Transactions on Power Systems*, vol.30, n°4, 2015, pp. 1702-1713

[17] MCCANN Brian T., “Using Bayesian Updating to Improve Decisions under Uncertainty”, *California Management Review*, 2020, vol. 63, n°1, pp. 26-40

[18] KAEDI Marjan & WOOK AHN Chang, “Robust optimization using Bayesian optimization algorithm: Early detection of non-robust solutions”, *Applied Soft Computing*, vol. 61, 2017, pp. 1125-1138

[19] WANG Zizhuo, GLYNN Peter W., YE Yinyu, “Likelihood robust optimization for data-driven problems”, *Computational Management Science*, 2016, vol. 13, pp. 241-261

[20] GUPTA Vishal, “Near-Optimal Bayesian Ambiguity Sets”, *Management Science*, vol. 65, n°9, 2019, pp. 3949-4450

[21] GOODHUE Dale L., LEWIS William, THOMPSON Ron, “Does PLS Have Advantages for Small Sample Size or Non-Normal Data?” *MIS Quarterly*, vol. 36, n°3, 2012, pp. 981-1001

[22] DIACONIS Persi & MOSTELLER Frederick, “Methods for Studying Coincidences”, *Journal of the American Statistical Association*, vol. 84, n°408, 1989, pp. 853-861

[23] HOU Qingchun, ZHANG Ning, DU Ershun, MIAO Miao, PENG Fei, KANG Chongqing, “Probabilistic duck curve in high PV penetration power system: Concept, modeling, and empirical analysis in China”, *Applied Energy*, vol. 242, 2019, pp. 205-215

[24] CANY CAMILLE, MANSILLA Christine, MATHONNIERE Gilles, DA COSTA Pascal, “Nuclear contribution to the penetration of variable renewable energy sources in a French decarbonized power mix”, *Energy*, vol. 150, 2018, pp. 544-555

[25] IAE-RTE, “Conditions and requirements for the technical feasibility of a power system with a high share of renewables in France towards 2050”, IEA Publications, 2021

Chapter III:

Exploring the Paradoxes of the French Energy Transition and Nuclear Policy: A Techno-Economic Analysis

***Abstract* – In this chapter, we propose a thorough analysis of the contradictions between the three main objectives of the French energy transition: partially phasing out nuclear by 2035, increasing renewable capacity and reducing carbon emissions to achieve carbon neutrality by 2050. Applying an enhanced version of the optimization model introduced in previous chapters, our findings confirm most results found in the literature: phasing out nuclear rapidly is likely to significantly increase both system costs and carbon emissions. Investments in renewables and nuclear policy decisions are however endogenous, contrary to the existing literature which investigates exogenous nuclear and RES scenarios. No economic justification is found for the immediate phasing out of nuclear, as replacing decommissioned reactors by RES investment is, in all investigated cases, suboptimal in terms of total costs.**

***Keywords*-** Nuclear policy; Renewables; France; Phase out

1. Introduction

Introduced in the LTECV in 2015, the PPE expresses the main orientations and priorities of the French public authorities in the management of energy sources to meet the energy policy targets set by the law. Its content and objectives are re-examined every 5 years. The PPE comes within the scope of the European Paquet Energie-Climat 2030 and 3 × 20 European directive, which set a target of 20% from renewable energy sources (RES) in the final electricity consumption of Member states in 2020 and 27% in 2030. France proved even more ambitious, as it enshrined in the LTECV final consumption targets of 23% and 32% for 2020 and 2030 respectively. Two main scenarios have been retained in the PPE (see [1]), namely the "Volt" and the "Ampere" scenarios. The "Volt" scenario advocates a strong development of RES investment (116 GWe in 2035) and a mild phase out of nuclear with a total shutdown of 9 reactors 900 MWe, conditional on economic and exports prospects. The scenario assumes France remains a strong exporter, based on significant interconnexion capacities and competitive generation costs. The "Ampere" scenario explicitly conditions the extend of nuclear phase out to the pace of RES capacity increase. Decommission decisions are made only when RES production means generate on average as much as decommissioned reactors. Although no additional investment in thermal plants is predicted, system balance requires increasing interconnexion capacities and demand-side management as well as energy efficiency.

The PPE encapsulate quantitative objectives to diversify the French electricity mix, by bringing the share of nuclear to 50% of total electricity production by 2035. While the last version of the PPE, published in April 2020, confirmed this objective, it insisted on the necessity to put into service new reactors should the share of nuclear remain set to 50% by 2050. Moreover, in its examination of the recent Climate law[16], the French Senate voted an article conditioning the phasing out of nuclear to the production of RES and low-carbon electricity in equivalent volumes, such that sufficient reserve margins are available at all time to guarantee the security of supply. Although the progressive phase out of nuclear is legally enacted, the conditions and precise schedule for its proceeding remain hot topics.

The French electricity mix is strongly dominated by nuclear production. It supplies on average 75% of demand, allowing for a very low-carbon production on average. In 2019,

[16] https://www.assemblee-nationale.fr/dyn/15/textes/l15b3875_projet-loi

French nuclear plants accounted for 70.6% of total national production, with approximately 380 TWh. Nuclear plants are mostly used in 'baseload' mode, although their technical characteristics theoretically allow load-following operations. According to [2], pressurized-water reactors currently in service in France can vary their output, from 100% to 50% of their rated power, up to twice a day, with ramping rates ranging from 2% to 5% of nominal capacity per minute. However, the capacity of nuclear to accommodate increasing RES capacities and volatile residual demand is a debated topic. Designing scenarios of nuclear and renewable penetration levels, [3] estimate the impact of load-following operations on nuclear production cost. Under a 50% share of wind and solar generation in the mix, the nuclear annual load factor decreases as low as 40%, with significant profit losses in the long run. A progressive shutdown would permit lower nuclear production costs from 2030 to 2050, even at reduced load factors, while contributing to load following and giving deciders more time before choosing the most sustainable technologies. They further advocate modulating the use of nuclear power instead of modulating production to keep high load factors, by using excess nuclear energy to produce valuable energy carriers such as hydrogen or heat.

Nuclear phase out is also expected to generate a significant increase in CO_2 emissions. Investigating different nuclear policy options from a French perspective, [4] document significant a CO_2 increase for all nuclear exit scenarios with a large drop in electricity exports from 2025. All scenarios induce sustained capacity investment, in order to compensate for the "cliff effect" created by the phasing out of nuclear reactors. They also find a downturn in system reliability and inertia reserves following nuclear exit (see [5], [6]). Using a system dynamics approach, [7] also find that early phasing out of nuclear contributes to a significant increase in fossil-fuel generation capacity, with important drawbacks regarding security of supply and dependency on imports. The authors stress the need for increased imports to control carbon emissions and show delaying shut down would benefit the technical development of RES. [8] reach similar conclusions regarding the case of German nuclear phase out.

Finally, the total costs of both decommissioning and replacing nuclear reactors by alternative generation technologies proves to be extremely costly. [9] find that the costs of nuclear phase out depend crucially on the phase out policy design, reaching a maximum of 76€ billion (in 2010 euros), most of which are borne by the French system with limited repercussions in the rest of the European system. Costs are also found to be higher when phase out occurs immediately after the decommissioning decision without any transition period. Interestingly,

the costs of policy uncertainty are low, which suggests a clear nuclear policy commitment provides little benefit. Replacing ageing nuclear reactors by EPR type or SMR reactors is a possible option. The French Small Modular Reactor (SMR) Nuward, developed as a joint project by EDF, the CEA, TechnicAtome and Naval Group, should be commercialized by 2030. With a projected unit capacity of 340 MW and estimated investment cost of 1€ billion, [10] elaborate on the possible replacement of 900 MW decommissioned nuclear reactors by SMR units, conditional on cost and safety conditions. [11] show the SMR would provide a reliable primary source of electricity generation in a flexible nuclear hybrid energy system and stabilizes short-term and long-term costs. However, due to political preferences in favor of nuclear phase out (although the public opinion appears quite mixed, see [12]), this paper does not consider alternative nuclear technologies nor replacement with last generation nuclear reactors. RES are thus a privileged investment option. [13] finds that, in terms of total costs, nuclear power is more expensive than wind power and natural gas in the absence of carbon pricing. Yet, nuclear remains a relatively affordable technology and its "pros and cons (…) revolve around its contribution to climate change mitigation".

The quasi totality of literature investigates the French energy transition and nuclear policy by the elaboration of a set of scenarios. Each scenario corresponds to the combination of a specific trajectory of nuclear phase out, depending on the exogenous rate at which capacity is decommissioned, in addition to an investment trajectory for RES. Each scenario might be attributed a probability, allowing stochastic optimization approaches like in [9]. We adopt a different methodology, where both the RES investment level and nuclear policy decisions are endogenous. Applying an enhanced version of the optimization model introduced in previous chapters, we include initial installed capacities for each type of technology. Then, we select a subset of candidate nuclear reactors to be decommissioned by pairs, with a binary decision for each pair: either prolonging the life duration of reactors by paying prolongation costs or removing reactors from the nuclear fleet by paying decommissioning costs. Our findings confirm most results found in the literature: phasing out of nuclear rapidly is likely to significantly increase both system costs and carbon emissions. No economic justification is found for the quick phasing out of nuclear, as replacing decommissioned reactors by RES investment is always suboptimal in terms of total costs, even under higher nuclear prolongation costs or lower investment and fixed costs for renewables. When imposing a minimum threshold for the number of decommissioned reactors, we find that massive investment in combined-cycle gas turbines (CCGT) is economically optimal but incompatible

with the objective of decreasing CO_2 emissions. Our results suggest a significant reduction of French 'baseload' electricity demand is a key condition for making nuclear phase out cost-effective. We also provide a thorough analysis of the operational performances of various electricity mixes under both extreme and representative operational conditions. We find that partial nuclear phase out may threaten system stability but might also allow the keep nuclear in a stable 'baseload' mode under high RES penetration. The operational costs and carbon emissions drastically increase when replacing phase out nuclear by CCGT plants, even when adding a high share of RES in the mix. The issue of nuclear and safety conditions regarding prolonged reactors is however outside of our scope.

The methodology, hypothesis and data used in this analysis are presented in Section II. Section III analyses the repartition of the costs of optimal generation mixes between operational, fixed and nuclear policy costs. Section IV provides a complete investigation of how the electric system behaves for extreme and normal operating conditions, under various nuclear phase out and RES penetration levels. Finally, we conclude in Section V.

2. Methodology

2.1. Motivation

Like in the previous chapters, our analysis focuses on the French region Auvergne-Rhône-Alpes. In addition to its significant share in the French national GDP and in the national electricity demand, it is the first region in terms of electricity production. In 2019, it accounted for 22% of national production, with 22.3% from RES including hydroelectric generation (see [14]). This also makes Auvergne-Rhône-Alpes the first producer of electricity from renewable sources in 2019, also including hydroelectricity. However, within a total of 119 TWh generated by the region in 2019, 85.8 TWh and 27.3 TWh were generated by nuclear and hydroelectric utilities respectively. By comparison, the cumulated generation from wind and photovoltaic units amounted to 2.4 TWh. Equivalently, respectively 72% and 23% of total electricity production were generated by nuclear and hydroelectric units, with less than 3% originated from photovoltaic, wind and bioenergy production units. Auvergne-Rhône-Alpes is also the first French region in terms of nuclear capacity: with 13.4 GWe of nuclear installed capacities, the region accounts for 21% of the total French nuclear fleet.

More specifically, the region counts 12 CPO/CPY type and 2 P4/P'4 type nuclear reactors. They respectively have rated power of 900 MWe and 1300 MWe.

The region Auvergne-Rhône-Alpes enjoys a strongly positive net balance of electricity trade: with a positive trade balance of 49.4 TWh, the region has positive exports to Occitanie, Bourgogne-Franche-Comté and Provence-Alpes-Côte-d'Azur, in addition to Italy and Switzerland. Over the 2013-2018 period, the average net exports to Italy and Switzerland respectively represented 2047 MWh and 1495 MWh. Related to the average regional generation, net exports to Italy and Switzerland represent approximately 15.9 % and 11.7 % respectively. Related to total physical exports, these figures increase to 39.2 % and 28.7 %. This suggests that almost 68 % of all physical exchanges are carried out with these two countries, representing approximately 33.6 TWh in 2019, assuming this ratio remained constant.

This makes this region a much relevant laboratory for studying the impacts of nuclear phasing out, both in terms of optimal electricity mix and effects on electricity exchanges with European neighbors. However, the latter topic shall not be investigated in this chapter. Based on the PPE, a subset of oldest CPO/CPY type is selected as candidates for being closed in order to bring the share of nuclear power in the mix to less than 50% by 2035.

2.2. Main parameters and assumptions

Still following the PPE, we constrain nuclear reactors to be closed by pairs. We do not take into account the decennial visit planning established by the Autorité de Sûreté Nucléaire (ASN), as it would require considering complementarities in the maintenance schedule of nuclear units across French regions. Within the subset of potential candidate reactors, we identify Tricastin 2 and 3, which have their visits in 2021 and 2022, while Bugey 5 and 3 respectively have their fourth visit in 2021 and 2023. Finally, the decennial visits Cruas 3 and 1 are planned for 2025 and 2024, while Cruas 2 and 4 respectively will be visited in 2026 and 2027. We leave for further research the inclusion of the nuclear maintenance schedule in an optimal investment model applied to France.

2.2.1. Technology and initial capacities

We make the realistic assumption that the hydroelectric potential is fully saturated in Auvergne-Rhône-Alpes so no additional capacity investment can occur for hydroelectric units and hydroelectric pumped-storage units. Similarly, we assume that no investment in new nuclear capacity can occur for political grounds. Like in previous chapters, we constrain the investment variable to take only discrete values for thermal dispatchable technologies, and continuous values for renewable and storage technologies. Investments in CCGT are made by blocs of 0.45 GW, which is equal to the average nominal power of General Electric's 9HA.01/.02 gas turbine. GT investments are performed by blocks of 0.3 GW.

However, unlike previous chapters, initial regional capacities are included in the optimal investment model. The reported figures correspond to capacities reported in 2020-2021. As stated above, Auvergne-Rhône-Alpes is the first French region in terms of nuclear capacity with 13.4 GWe. It also gathers a significant share of French hydroelectric capacity, which can be broken up into 8.331 GWe of hydroelectric capacity and 3.310 GWe of pumped-storage hydroelectric capacity. We assume the initial CCGT capacity is equal to 450 MWe, corresponding to one turbine. Finally, the vector of initial RES capacities[17], noted $\boldsymbol{U}^0 \in (\mathbb{R}^+)^2$, is equal to 0.583 GWe of wind turbines and 1.19 GWe of photovoltaic generation units.

2.2.2. Cost assumptions

We keep the same technical and cost assumptions made in previous chapters. Technology-wise thermal constraints and cost assumptions can be found in **Table 1.A** and **Table 1.B.** in Appendix. We assume for simplicity that all investments in conventional technologies made before 2021 have been fully amortized, so annuities are null for this subset of technologies. Still following the CRE (CRE, 2018)[18], we choose a VOLL equal to 13 000 €/MWh. The CO2 price for 2021 is obtained from the EU ETS Phase IV (2018), where the baseline price

[17] The figures are directly obtained from the trimestral Panorama de l'Electricité Renouvelable from RTE and Enedis at the regional scale.

[18] Public consultation from the French Energy Regulatory Commission (CRE), Public consultation No. 2018-015 of December the 20th of 2018, on the investment request relating to the Celtic project, including a cross-border cost allocation

trajectory corresponds to the final agreement reached by the European Parliament, Council and Commission. However, as shown by recent developments, the EU ETS carbon price has steadily increased throughout 2021 to reach 60 €/ton for the first time[19]. We thus provide sensitivity analysis with the CO_2 price varying in the 50-150 €/ton interval. Like in previous chapters, we use a reference discount rate of 5% to compute annuities for investments.

As we are interested in measuring how the optimal future electricity mix reacts to demand parameters, we provide some approximate projections for the future distribution of the total demand addressed to Auvergne-Rhône-Alpes. Using a structural decomposition approach, we model changes in the electricity demand distribution as being driven by sector-wise energy efficiency and economic growth rates (replaced by demographic growth rates in the case of residential demand). Average yearly demographic growth rate projections are obtained from INSEE Omphale 2017. Yearly efficiency growth rates for residential, professional (i.e. services) and industrial electricity consumers were computed using energy efficiency indexes on the 2000-2017 period from the ODYSEE-MURE database. For simplicity, we assume a uniform GDP growth rate of 1% for all sectors. Finally, the hourly share of each sector in the total electric load are computed using aggregated consumer data, segmented by sector and power slice, from ENEDIS[20]. Details and calculations are provided in Appendix. Electric vehicles (EVs) are also expected to significantly transform the structure of electricity consumption. We use the technical characteristics of the Renault Zoe as a benchmark for EV, with an average electric consumption of 0.12-0.20 kWh/km and an average battery size of 50 kW with a round trip efficiency of 90 %. The number of EVs is derived from the median RTE scenario for the evolution of EVs in France, scaled by the share of Auvergne-Rhône-Alpes in the total number of vehicles in France [15]. EVs driving patterns and expected driven distance are estimated from [16]. We add the future expected electricity demand from EVs to the projected electricity consumption to get the total projected electricity demand distribution.

The estimation of the costs of nuclear phasing out is a much harder issue: several competing methodologies have been proposed by EDF and the French Cour des Comptes. Yet, the former may have incentives to understate the true costs of nuclear operations and maintenance in order to capture public subsidies and investments projects, especially as the closure of nuclear plants and construction of new nuclear plants in France is a hot topic. An estimation

[19] https://www.reuters.com/article/eu-carbon-idUSL1N2Q10EP

[20] https://data.enedis.fr/pages/accueil/?id=init

of the costs of the "Grand Carénage" program initiated by EDF on the 2014-2030 period can be obtained from [17]. In the wake of the Fukushima nuclear catastrophe, the "Grand Carénage" program is an industrial project aiming at reinforcing the safety of French nuclear units, increasing plant availability and expanding the exploitation of the French nuclear fleet beyond 40 years. The investment and maintenance expenditures are estimated to 100€ billion on the period 2014-2030, with an average of 1.7€ billion per reactor (in current 2014 euros). Correcting for inflation, we estimate the remaining cost for the period 2021-2030 to 1.015€ billion. As pointed by [17], this investment program is expected to have a limited impact on the cost of nuclear electricity: a 50% increase in investment costs would only lead to a 5% increase in production costs. Yet, by comparison, a 50% decrease in nuclear production would double production costs. The industrial project initiated by EDF thus relies of the objective of avoiding a decrease in the production of the existing nuclear fleet. However, maintenance investments would only be economically justified if they can be amortized by sufficiently prolonging the life duration of nuclear plants. A large share of the costs included in the "Grand Carénage" could be avoided by decommissioning plants reaching 40 years or performing cheaper investments that would allow prolonging existing plants for a shorter duration.

Similarly, the evaluation of the actual decommissioning costs of nuclear reactors remains a difficult issue. According to [18], EDF lacks the technical know-how to dismantle its oldest nuclear reactors, while its costs evaluations rely on overoptimistic assumptions on the level of economies of scale and pooling of resources necessary for dismantling operations. More precisely, EDF does not include the following elements in the computation of provisions required for decommission expenditures: reconditioning of the site; deconstruction of underground structures; evacuation of burned fuel during the early decommissioning phase and social costs of decommissioning. On this basis, EDF estimates per reactor decommissioning costs between 350€ and 500€ million. Yet, by comparison, Engie provisioned approximately 1.3€ billion per reactor for its nuclear plant in Belgium. In Germany, E.ON estimates the dismantling cost of a 1 GWe reactor around 1.2€ billion. Thus, we set the decommissioning cost per reactor to 1€ billion, which is likely to provide a lower bound for actual future costs while preserving the order of magnitude. The dismantling of a reactor can be decomposed into three main phases. The first one, corresponding to the evacuation of radioactive and hazardous material, takes between 3 to 6 years. The dismantlement of equipment and tank is the second phase and takes between 10 and 15 years.

Eventually, the sanitation of the site takes up to 5 years. On average, EDF estimates the full expected dismantling duration to 15 years.

2.3. Investment and dispatch model design

We use the robust investment and dispatching model presented in Chapter II with some significant modifications. In order to account for the multiple time scales driving residual demand patterns, it is modeled using both seasonal and hourly time resolution. As previously, we distinguish the set of RES units $\mathcal{J}$ from the set of thermal units $\mathcal{G}$, which level of generation is not stochastic except when plant failure occurs. The set $\mathcal{J}$ can be decomposed into the subsets of wind and photovoltaic units. Similarly, the set $\mathcal{G}$ can be partitioned into the subset of nuclear units, combined-cycle gas turbines (CCGT), gas turbines (GT), hydroelectric plants and hydroelectric pumped-storage plants. Each individual plant in $\mathcal{G}$ is constrained by its commitment state, start-up and shut-down decisions, minimum uptime and down time, ramping limits, and maximum and minimum generation level. As previously stated, our model includes initial installed capacities, which investment costs are assumed to be fully amortized for dispatchable units.

As we focus on the specific role of nuclear phasing-out in the transition to a low-carbon electric generation system, we further divide the subset of nuclear plants between candidate and non-candidate plants for decommissioning. Phasing-out is implicitly considered as a "negative" investment, with lifetime equal to the full duration of decommissioning operations. Similarly, maintenance investments which increase the duration of candidate plants are considered as regular capacity investments with lifetime equal to the subsequent increase. This approach allows us to model endogenous nuclear policy decisions using a classic investment framework.

We make the very simplifying assumption that maintenance investments for ageing nuclear plants occur instantaneously with no physical duration required. Accounting for this issue in the context of optimal prolongation planning would require a multiannual framework in order to define the optimal prolongation and decommissioning schedule allowing to satisfy supply-demand balance for all periods at minimum total cost. In essence, this could easily be achieved by introducing an additional set of time index corresponding to years, in addition to dynamic capacity constraints. This would however drastically increase the model complexity

and computational cost. Still, our model allows us to quantify the costs and benefits of long-term decisions regarding the share of nuclear within the generation mix.

Finally, we introduce electric vehicles (EVs) as an additional storage technology. We assume the number of EVs and the behavior of drivers are exogenous parameters. We model EVs at the fleet level by approximating its aggregate characteristics and constraints. For each time period, we model its aggregate behavior by computing the expected driving distance and electric consumption of the fleet, in addition to the expected share of EVs in circulation. This allows us to approximate the electric demand needed to satisfy the driving requirements of the fleet and the share of vehicles available for transfers with the grid.

The full mathematical formulation of the model, in addition to the complete description of the variables and parameters used, is provided in Appendix.

2.4. Choice of the optimal "security" level and representative weeks

The security level of the French electric system is defined by a failure criterion, which corresponds to an average annual duration of failure of three hours owing to imbalances between supply and electric load. This indicates that, over all possible scenarios and accounting for interconnexions, the expected annual duration for which part of the electric load is cut because of system imbalances must be inferior to three hours (French Energy Code, Art. D141-12-6). However, this security criterion defines no constraint regarding either the frequency nor the scale of load shedding events.

Expressed in probabilistic terms, the French security criterion corresponds to approximately 0.035 % of the total number of hours within a full year. This provides us with a rough benchmark for choosing the appropriate robustness level for our investment model. Using the (ϵ, M)- certainty set methodology introduced in Chapter II, we choose the minimal value of M^* for ϵ fixed such that the probability of load shedding is lower or equal to 0.035 %.

We start by investigating the distribution and order statistics of residual demand for various levels of RES installed capacity. We note $\boldsymbol{R_U}$ the residual demand cumulative distribution function associated to the vector of wind and solar installed capacities $\boldsymbol{U} \in (\mathbb{R}^+)^2$. For $0 \leq q \leq 1$, $\boldsymbol{R_U}(q)$ corresponds to the value of the q-th quantile of $\boldsymbol{R_U}$. In order to observe how

renewable penetration affects $\boldsymbol{R_U}$ and its order statistics, we gradually increase wind and photovoltaic capacities from $\boldsymbol{U}^0$ to 5 GWe.

Table 1.A. shows order statistics for the distribution of residual value over the period 2013-2018. Strikingly, the lower order statistics decrease faster with RES capacities than the higher ones. While the maximum residual demand value decreases by only 2.7% when increasing wind and photovoltaic capacities from $\boldsymbol{U}^0$ to 5 GWe, the median and first decile respectively decrease by 12.5% and 18.9%. The minimum residual demand value becomes negative for wind and solar installed capacities superior to 3 GWe, which requires investment in storage or demand-side management technologies to absorb the electricity surplus. However, even with higher RES installed capacities, negative residual demand values have a probability of occurrence lower than 0.001. The expected net gain from investment in storage is thus likely to be quite low. Similarly, there are roughly 0.1% chances that residual demand takes values beyond 20 GWh. Additional capacity to supply the peak load might be inefficient economically and in terms of generator utilization. In this respect, peak shaving strategies may yield significant benefits for the grid operator and end-users (see [19]).

	Quantile value of $\boldsymbol{R_U}$ associated to q				
Probability threshold q	$\boldsymbol{U}^0$	$\boldsymbol{U} = (2,2)^T$	$\boldsymbol{U} = (3,3)^T$	$\boldsymbol{U} = (4,4)^T$	$\boldsymbol{U} = (5,5)^T$
0	2413	965	- 210	- 1384	- 2559
0.001	4684	4258	3739	3075	2349
0.01	6196	5751	5287	4768	4189
0.1	8841	8410	8023	7610	7166
0.25	10506	10077	9704	9306	8897
0.5	12363	11926	11543	11171	10812
0.75	14277	13836	13495	13173	12849
0.9	16201	15759	15443	15145	14848
0.99	19136	18797	18552	18333	18123
0.999	20440	20186	20044	19891	19738
1	21709	21348	21233	21148	21120

Table 1.A.: Residual demand order statistics under increasing wind and photovoltaic generation capacities (in MWh)

Note: Example: The value associated to the first decile when wind and solar capacities are both equal to 3 GWe is equal to 8023 MWh.

Table 1.B. presents extreme order statistics for the distribution of residual demand, corresponding to the subset of values within the first and last deciles. The negative relationship between the value of q and the variation of $\boldsymbol{R_U}(q)$ under increasing RES penetration appears even more clearly. The distribution of residual demand appears increasingly right-skewed, with most of the total variance being caused by $\boldsymbol{R_U}(q)$ values for $q < 0.01$. We further observe that negative residual demand values and values beyond 20 GWh both have a probability of occurrence strictly lower than 0.05%. Thus, the optimal (ϵ, M)- certainty set for hour $t \in \mathcal{T}$, noted $\mathcal{C}_{M,\epsilon,t}$, is not required to include the full distribution of residual demand to respect the French security criterion.

	Quantile value of R_U associated to q				
Probability threshold q	$\boldsymbol{U}^0$	$\boldsymbol{U} = (2,2)^T$	$\boldsymbol{U} = (3,3)^T$	$\boldsymbol{U} = (4,4)^T$	$\boldsymbol{U} = (5,5)^T$
0	2413	965	- 210	- 1384	- 2559
0.0005	4510	4028	3429	2723	1880
0.001	4684	4258	3739	3075	2349
0.005	5581	5135	4677	4147	3540
0.01	6196	5751	5287	4768	4189
0.99	19136	18797	18552	18333	18123
0.995	19620	19335	19126	18925	18751
0.999	20440	20186	20044	19891	19738
0.9995	20756	20497	20293	20153	20028
1	21709	21348	21233	21148	21120

Table 1.B.: Extreme residual demand order statistics under increasing wind and photovoltaic generation capacities (in MWh)

Setting $\epsilon = 0.001$, we compare the certainty sets corresponding to $M \in \{10^3, 10^6, 10^9\}$. A higher value of M corresponds to a higher robustness level as the probability that extreme residual demand values are included in the (ϵ, M)- certainty set increase. **Figure 1.A.** plots the residual load duration curve with wind and photovoltaic equal to their initial capacities. For each value of M we compute the probability that residual demand over the period 2013-

2018 would have lied outside the set defined by the union of all certainty sets, noted $\mathcal{C}_{M,\epsilon}$[21] For $M = 10^9$, residual demand is inferior to the upper bound in all cases, while it is inferior to the lower bound in only 0.36% of cases. As was to be expected, the level of security diminishes with lower values of M. For $M = 10^6$, there are 0.025 % chances (resp. 0.63%) that residual demand is superior or equal to the upper bound (resp. inferior or equal to the lower bound).

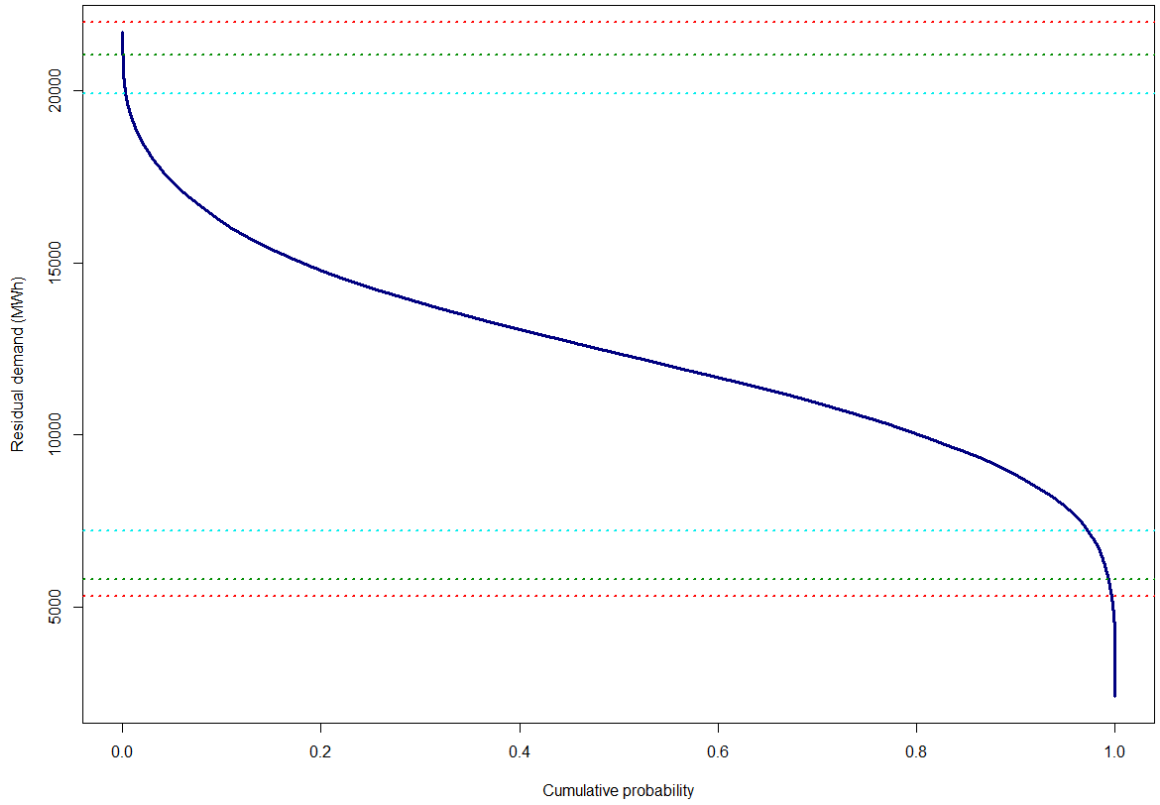

Figure 1.A.: Residual demand duration curve with wind and photovoltaic capacities equal to $\boldsymbol{U}^0$

Note: The red (resp. green and blue) dotted curves corresponds to the lower and upper bounds computed of the union of certainty sets $\mathcal{C}_{M,\epsilon}$ for $M = 10^9$ (resp. $M = 10^6$ and $M = 10^3$).

Similarly, we plot in **Figure 1.B.** the residual load duration curves corresponding to RES capacities ranging from 2 GWe to 5 GWe. Strikingly, the level of security associated to each value of M globally increases with RES capacities. This suggests our method performs

[21] We compute the share of all observations such that residual demand is superior (resp. inferior) to the maximum (resp. minimum) value across all certainty sets $\mathcal{C}_{M,\epsilon,t}$, $t \in \mathcal{T}$.

increasingly well for increasing levels of renewable penetration. With 2 GWe of installed capacities, residual demand has only 0.009 % chances (resp. 0.43% chances) to be above the upper bound (resp. below the lower bound) of $\mathcal{C}_{M,\epsilon}$. For 4 GWe, these figures respectively decrease to 0.005 % and 0.37 %. As the French security criterion only restricts the number of hours during which at least one electric load is cut, $M = 10^6$ is a sufficient robustness level as the hours with extremely low residual demand can be addressed through RES curtailment. The fact that a significant proportion of low residual demand values remains outside $\mathcal{C}_{M,\epsilon}$ suggests fitting data with only a binomial normal distribution model is not optimal. Indeed, residual demand is increasingly skewed to the left with higher RES penetration, which suggests fitting the data with a skewed normal distribution or a logistic distribution would be more appropriate. However, fitting multidimensional data with several concurrent model exhibits high computational costs, as explained in Chapter II.

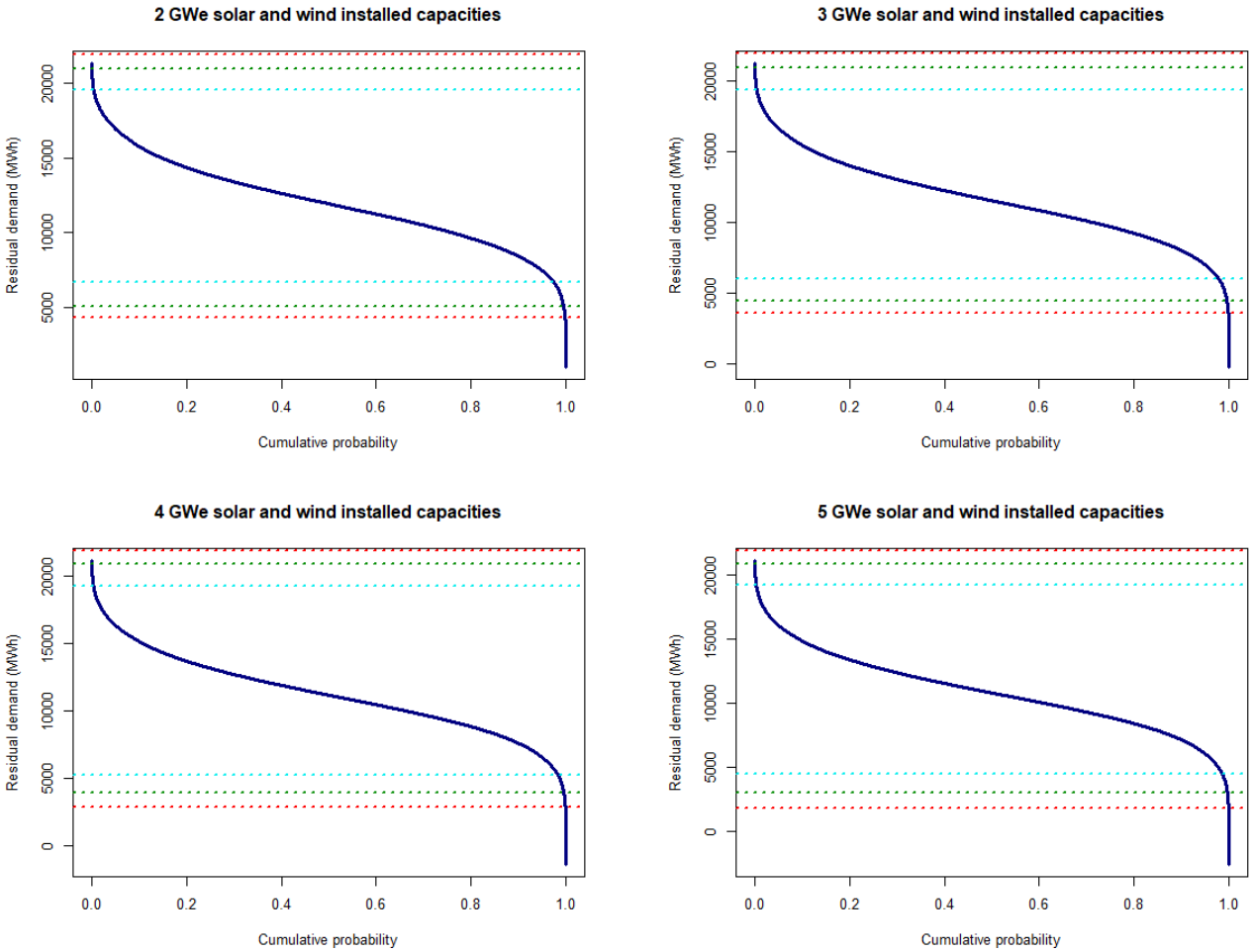

Figure 1.B.: Residual demand duration curve with wind and photovoltaic capacities ranging from 2GWe to 5 GWe

We can also control the level of security of our mix with respect to extreme variations of residual demand. We verify in **Figure 2.A.** and **Figure 2.B.** (see in Appendix) that $M = 10^6$ also guarantees a very high level of system flexibility against residual demand extreme variations. With initial wind and photovoltaic capacities, residual demand variations have only 0.001 % chances to be superior to the most extreme positive variations in $\mathcal{C}_{M,\epsilon}$, and are inferior to the most extreme negative variations in $\mathcal{C}_{M,\epsilon}$ in all cases. Thus, $M = 10^6$ should both guarantee a sufficient level of robustness in terms of security of supply and system flexibility.

Finally, as in previous chapters, we select a subset of representative weeks in order to approximate the representative systems costs and operational behavior associated to a given generation mix.

Still using the RTE database on electricity consumption, solar and wind generation for the period 2013-2018, we approximate seasonal Net Load Duration Curves (NLDC), with a 2-week sample of representative weeks for each season. The number of observations N in the training sample goes from 541 in Winter and 546 in Autumn to 552 in Spring and Summer. **Figure 2.A.** below plots the seasonal NLDCs and the approximate NLDCs obtained by scaling up the number of hours in the 2-week samples to match a full year. Our strategy yields highly accurate performances, with Root-Mean-Square-Error below 1% for all seasons.

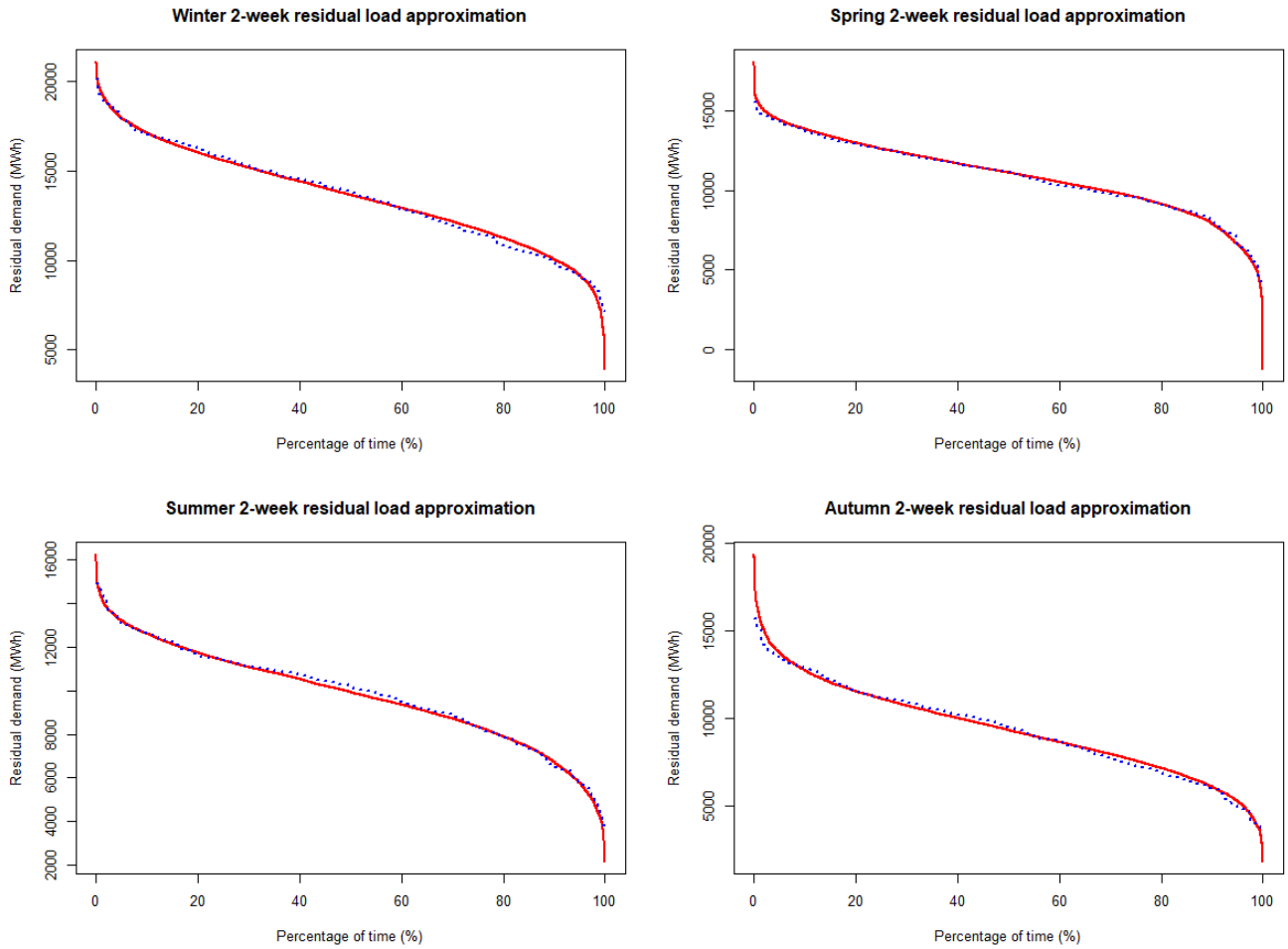

Figure 2.A.: Net Load Duration Curves and 2-week approximation, by season

Note: The red plain lines correspond to the NLDC observed for each season, while the blue dotted lines correspond to the NLDCs obtained by scaling the sample of hours from representative weeks.

Finally, we take historic carbon emissions measured over the 2013-2018 period in Auvergne-Rhône-Alpes as a benchmark for assessing performances in terms of CO_2 emissions. **Table 2.B.** reports the observed distribution. Overall, the region Auvergne-Rhône-Alpes has very low carbon emissions compared to the national average, with respectively 5.7 g/kWh and 48.38 g/kWh over the same period.

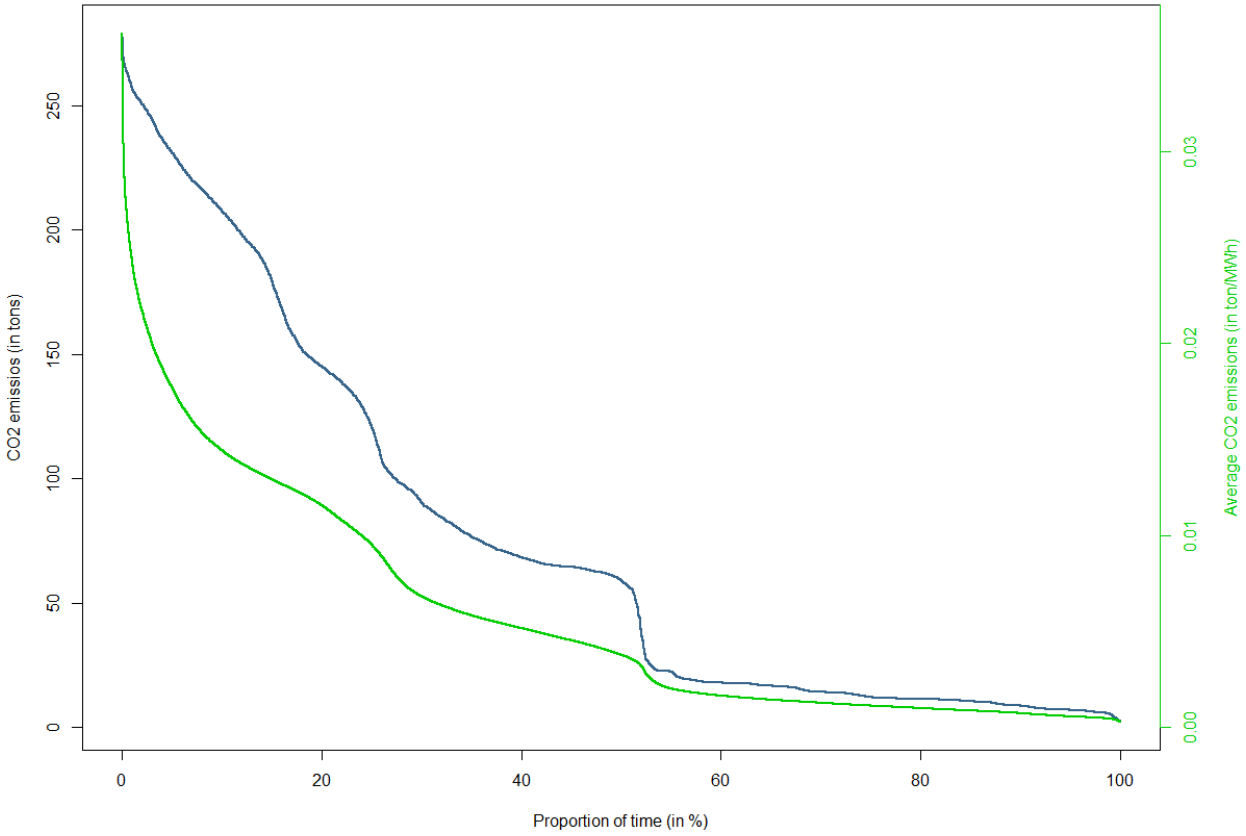

Figure 2.B.: Distribution of regional CO_2 emissions and average CO_2 emissions over the 2013-2018 period

3. Optimal capacity mix and cost analysis

The analysis provided in this section investigates the optimal regional capacity mix under various parameters which affect the total cost of nuclear and RES, but also influence total system cost.

3.1. Optimal capacity mix with endogenous nuclear decommissioning decisions

We investigate the sensitivity of the optimal capacity mix to a set of technical and cost parameters. We focus on parameters which are likely to have a significant impact on the decision of decommissioning nuclear reactors, either by directly changing the costs of phasing out, or by indirectly changing the opportunity cost of keeping nuclear units in the generation mix. We divide the set of parameters selected for sensitivity analysis into two categories:

- Nuclear-related parameters: reactor prolongation unit cost; reactor decommissioning unit cost; reactor total decommissioning time (in years).
- Non-nuclear-related parameters: RES investment and maintenance costs; future electricity demand distribution; carbon cost.

The general conclusion from the following simulations is that nuclear phasing out is never optimal in terms of total system cost. In all cases, the prolongation of the full fleet of 12 CPO/CPY type reactors minimizes both total annual fixed costs, which are decomposed into annuities, fixed operation & maintenance (FOM) costs, and operational costs.

3.1.1. Sensitivity to nuclear-related parameters

	Baseline	**+ 10 %**	**+ 30 %**	**+ 50 %**
Combined cycle gas turbine	**3.15**	2.7	2.7	2.7
Gas turbine	**0**	0	0	0
Nuclear	**13.4**	13.4	13.4	13.4
Wind	**0.665**	2.386	4.158	3.136
PV	**1.190**	4.961	1.190	1.190
Hydroelectric	**8.331**	8.331	8.331	8.331
STEP	**3.310**	3.310	3.310	3.310
Battery storage	**1.384**	1.056	2.150	1.536

Table 2.A.: Optimal capacity by technology with varying prolongation costs (in GWe)

Table 2.A. shows that, while the optimal nuclear capacity remains constant, increasing nuclear prolongation costs shifts the optimal mix towards more RES and battery storage capacities. From a social-planner perspective, the increase in nuclear prolongation costs is mitigated by decreasing operational costs, which is allowed by feeding RES generation into the grid at zero marginal cost. However, this mitigation strategy becomes less effective as prolongation costs increase beyond a certain threshold: the additional RES investment and FOM costs required to increase renewable production is not anymore mitigated by lower operational costs. The total RES and battery storage capacity thus follow an inverse U-shaped curve.

	Baseline	**− 10 %**	**− 30 %**	**− 50 %**
Combined cycle gas turbine	3.15	3.15	3.15	2.7
Gas turbine	0	0	0	0
Nuclear	13.4	13.4	13.4	13.4
Wind	0.665	0.612	0.591	3.670
PV	1.190	1.190	1.262	1.190
Hydroelectric	8.331	8.331	8.331	8.331
STEP	3.310	3.310	3.310	3.310
Battery storage	1.384	0	1.801	2.081

Table 2.B.: Optimal capacity by technology with varying decommissioning costs (in GWe)

On the opposite, we see from **Table 2.B.** that the total RES and battery storage capacity globally increases when decommissioning costs decrease beyond a certain level. For a 50% lower costs, battery storage and RES capacities both increase, while CCGT capacities decrease by one installed unit. This suggests battery storage can effectively complement the variability of renewable generation when sufficient RES capacities are installed, thus partially substituting to CCGT units. Although the blend of renewables and storage operates as 'baseload', a significant share of peaking units remain necessary for ensuring system balance in high residual demand episodes.

Table 2.C. finally shows how the optimal capacity mix varies when extending the total decommissioning time from 15 years to a maximum of 35 years. Assuming that the decommissioning expenditures are allocated over a longer period, we expect the corresponding annuities to decrease. However, this seems to have little impact on the optimal capacity mix. Wind and battery storage are the only technologies with additional investments. However, their capacities both follow an inverted U-shaped curve, with no new investment when extending decommissioning operations to 35 years.

	Baseline	**+5**	**+10**	**+15**	**+20**
Combined cycle gas turbine	3.15	3.15	3.15	3.15	3.15
Gas turbine	0	0	0	0	0
Nuclear	13.4	13.4	13.4	13.4	13.4
Wind	0.665	0.583	1.396	1.033	0.583
PV	1.190	1.190	1.190	1.190	1.190
Hydroelectric	8.331	8.331	8.331	8.331	8.331
STEP	3.310	3.310	3.310	3.310	3.310
Battery storage	1.384	4.516	0.797	0.499	0

Table 2.C.: Optimal capacity by technology with varying total decommissioning time (in GWe) (in years)

It may be noted from **Table 2.A.** to **2.C.** that as the optimal nuclear capacity remains unchanged, the optimal total nuclear retirement and prolongation cost is unaffected by changes in parameters. However, from a mathematical perspective, changing cost coefficients in the objective function mechanically changes the First-Order Conditions (FOC) Lagrangean, in addition to the optimal value of the multipliers. Put differently, changing the value of the parameters modify the shadow price associated to constraint **(2)** in the investment model (see

Appendix). This suggests mixes with low RES-low battery storage capacities and mixes with a high RES-high battery storage are equivalent optimal solutions in terms of total costs, independently of nuclear policy cost parameters.

3.1.2. Sensitivity to non-nuclear-related parameters

We focus our attention on parameters likely to affect the opportunity cost of maintaining a strong share of nuclear in the generation mix. The French nuclear fleet has traditionally been used in 'baseload' mode[22], which means it generates a rather high and stable level of output throughout the year. Before analyzing the optimal capacity mix for the set of chosen parameters, it is fruitful to study how nuclear contributes to total regional production. **Figure 3.A.** shows that, over the 2013-2018 period, the average ratio of nuclear generation to the total electricity demand addressed to Auvergne-Rhône-Alpes (including neighboring regions) is equal to 76.3 %, which is very close to the national average. More specifically, it indicates that the average share of nuclear in total generation (excluding pumping) oscillates between 60% and 90%, while in never drops below 40 % overall. In terms of volume, average nuclear generation is equal to 9.5 GWh roughly, and remains superior to 7.1 GWh in 90 % of hours.

[22] We define the 'baseload' as the minimum electricity demand addressed to the grid over a given time frame (in our case, 2013 to 2018).

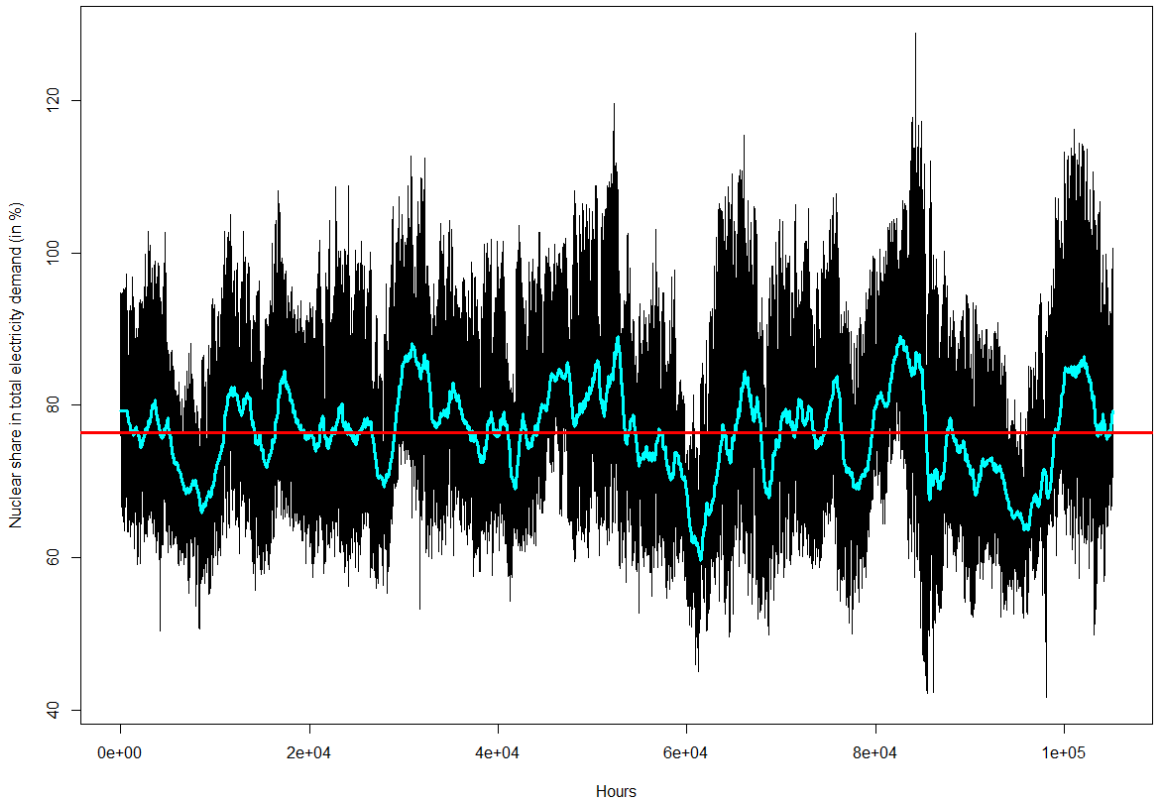

Figure 3.A.: Share and moving-average ratio of nuclear to electricity demand, from 2013 to 2018

Note: The blue plain curve corresponds to the moving-average share of nuclear generation, which computed with a sliding window equal to 15 days. The red line corresponds to the average share computed over the whole period.

Phasing out of nuclear to replace decommissioned units by RES or gas-fired generation units is thus tantamount to changing the very baseload generation technology in the mix.

Our costs projections trends for RES are extrapolated from [20] and [21]. Based on 2016-2019 trends, we assume a 12 % yearly reduction rate of overnight costs and 9% reduction rate of annual FOM costs for solar panels. These trends are however estimated from the evolution of the cost structure of utility-scale solar, which may overestimate the decrease in residential and commercial photovoltaic. Moreover, we expect the costs reduction in the solar sector to be less pronounced in the future as the industry gets increasingly mature. We assume the wind turbine industry is more established, with a yearly overnight and FOM cost reduction rate of 1%. Our results can thus be considered as an illustration of the sensitivity of nuclear decisions to the costs of renewable technologies.

Table 2.D. displays the optimal generation mix corresponding to projected investment and FOM costs for renewables in 2025, 2030 and 2035. We note a slight decrease in CCGT capacities, while the total RES installed capacities increase from 1.773 GWe in the baseline situation (corresponding to 2021 reference costs) to 15.29 GWe under projected costs for 2035. The battery storage capacity is roughly multiplied by 2 but does not increase monotonically with renewable capacities, which illustrates non-linearities in the complementarities between RES and storage. Finally, even when multiplying total RES capacity by more than 8, the optimal nuclear capacity remains unaffected.

	Baseline	**2025**	**2030**	**2035**
Combined cycle gas turbine	3.15	3.15	2.7	2.7
Gas turbine	0	0	0	0
Nuclear	13.4	13.4	13.4	13.4
Wind	0.665	0.583	0.583	2.825
PV	1.190	1.190	11.79	12.47
Hydroelectric	8.331	8.331	8.331	8.331
STEP	3.310	3.310	3.310	3.310
Battery storage	1.384	2.311	3.493	2.760

Table 2.D.: Optimal capacity by technology with varying investment and fixed costs for renewables (in GWe)

As underlined above, nuclear is traditionally operated as 'baseload' technology, which implies the optimal number of operating hours over a typical year is very high. Decreasing the number of hours for which nuclear generation is the least costly option should increase the opportunity cost of prolonging the whole nuclear fleet if a fraction of reactors become unutilized or have a low utilization rate. Thus, we expect decreasing demand to be a factor in favor of nuclear phase out. Using a simple heuristic based on sectoral decomposition of demand (see in Appendix), we approximate the future electricity demand distribution using forecasts for GDP and demographic growth rates and sectoral energy efficiency projections. While leaving the optimal 'baseload' nuclear capacity unchanged, we see from **Table 2.E.** that investment in new CCGT units decreases with electricity demand. While we note an apparent substitution between CCGT units and a blend of RES with battery storage units for 2025 and 2030, all three types of investment see their level decrease in 2035. While the total

regional generation capacity decreases (from 31.4 GWe in the baseline case to 28.4 GWe under 2035 demand distribution), it is economically optimal to decrease total operational costs by reducing investment in CCGT units rather than replacing nuclear units by renewables.

We observe from **Figure 3.B.** in Appendix that, according to our projections, the decrease in demand is more pronounced for higher quantiles. The reduction in the peak load is thus expected to be more pronounced than the reduction in the 'base load'. Over the subset of representative hours, the 9th decile of the distribution decreases from 15.87 GWh in 2021 to 14.25 GWh in 2035 (- 10.2 %), while the 1st decile only decreases from 8.94 GWh to 8.04 GWh (- 10 %). The exact same trends can be observed for the sample of worst-case weeks. The more marked reduction of peaking demand explains the observed decrease in new peaking CCGT units. However, the heuristic used for constructing future demand distribution implicitly assumes the impact of structural parameters, especially energy efficiency gains, uniformly modify the demand distribution.

	Baseline	**2025**	**2030**	**2035**
Combined cycle gas turbine	3.15	2.25	1.8	1.35
Gas turbine	0	0	0	0
Nuclear	13.4	13.4	13.4	13.4
Wind	0.665	2.625	1.835	0.583
PV	1.190	1.190	1.190	1.190
Hydroelectric	8.331	8.331	8.331	8.331
STEP	3.310	3.310	3.310	3.310
Battery storage	1.384	4.751	0.275	0

Table 2.E.: Optimal capacity by technology under future projected electric demand distributions (in GWe)

Although our approach accounts for variations in the structure of electricity demand by computing sectoral shares on an hourly basis (for instance, residential customers account for 41% of load at 9 a.m. against 50% for the evening peak at 8 p.m.), energy efficiency measures are likely to affect differently consumption usages and load dynamics depending on the type of measures (for instance, cavity wall insulation, loft insulation, more efficient heating bowler, see [22]). Still, our analysis suggests that only energy efficiency measures

diminishing significantly the 'baseload' uses of electricity are likely to create optimal economic and technical conditions for phasing out of nuclear.

Increasing carbon price does not challenge our previous conclusions. **Table 2.F.** clearly shows that increasing CO_2 price does not even reduce the optimal level of new CCGT investments but fosters the development and use of storage and RES generation to mitigate the higher cost of gas-powered peaking units. The optimal nuclear capacity remains equal to its initial level as increasing carbon price only affects operational costs of peaking technologies. We may argue that it makes nuclear even more cost competitive as a 'baseload' generator.

	Baseline	$\boldsymbol{\pi^{CO_2} = 50\ €/t}$	$\boldsymbol{\pi^{CO_2} = 100\ €/t}$	$\boldsymbol{\pi^{CO_2} = 150\ €/t}$
Combined cycle gas turbine	3.15	3.15	3.15	3.15
Gas turbine	0	0	0	0
Nuclear	13.4	13.4	13.4	13.4
Wind	0.665	0.583	1.386	0.583
PV	1.190	2.868	1.273	1.190
Hydroelectric	8.331	8.331	8.331	8.331
STEP	3.310	3.310	3.310	3.310
Battery storage	1.384	0.177	0.489	2.570

Table 2.F.: Optimal capacity by technology with varying carbon price (in GWe)

3.2. Optimal capacity mix with constrained nuclear phasing out decisions

To put into perspective the above results, we now impose a minimum number of pairs of reactor to be decommissioned. Unsurprisingly, the optimal number of decommissioned reactors always equals the lower bound imposed to the investment model.

Table 3.A. shows that phased out nuclear capacity is mainly replaced by investments in CCGT units. The total RES installed capacity does not vary linearly with nuclear capacity, reaching a maximum value of 5.5 GWe roughly for 2 pairs of decommissioned reactors. Beyond 3 pairs of decommissioned reactors, CCGT becomes the second most important technology in the mix. With 3 and 4 pairs of decommissioned reactors, CCGT accounts for respectively 22% and 32 % of total capacities respectively. By comparison, solar and wind

capacities only account for 6.5% and 5.9% of total install capacity. According to [23], high capital costs of renewable technologies tend to encourage the use of fossil fuels. Low to moderate capacity factors for renewables require a high volume of new capacity to replace decommissioned reactors, which translate into extremely high investment and fixed costs which favor less capital-intensive technologies. The authors find that only a *combination* of carbon pricing and low RES investment costs achieves significant investment in RES capacity. While a combination of 50 USD carbon price and 3% WACC (Weighted-Average Cost of Capital) leads to significant emission reductions, a 100 USD carbon price combined with a 25 % WACC has virtually no impact. It seems however that WACC reduction has the largest impact in terms of emissions reduction, as carbon pricing is effective only if capital costs are low.

	1	**2**	**3**	**4**
Combined cycle gas turbine	4.5	6.3	8.1	9.9
Gas turbine	0	0	0	0
Nuclear	11.6	9.8	8	6.2
Wind	1.608	4.269	1.222	0.629
PV	1.190	1.190	1.190	1.190
Hydroelectric	8.331	8.331	8.331	8.331
STEP	3.310	3.310	3.310	3.310
Battery storage	4.059	0	6.653	1.277

Table 3.A.: Optimal capacity by technology with imposed minimum number of pairs of decommissioned nuclear reactors (in GWe)

Table 3.B. further shows that lower investment and FOM costs for renewables (corresponding to projected costs for 2025 and 2030) increase the optimal RES capacity without affecting the optimal investment level in CCGT units. Overall, our results suggest that a fraction of CCGT is substituted to decommissioned nuclear and operates as ‘baseload’, while investments in renewables and battery storage are used to mitigate the consequent increase in electricity generation cost.

	$\pi^{CO_2} = 50$ €/t	$\pi^{CO_2} = 100$ €/t	$\pi^{CO_2} = 150$ €/t	2025	2030
Combined cycle gas turbine	6.3	6.75	6.3	6.3	6.3
Gas turbine	0	0	0	0	0
Nuclear	9.8	9.8	9.8	9.8	9.8
Wind	4.269	0.583	1.278	0.911	1.267
PV	1.190	1.190	1.190	2.689	6.639
Hydroelectric	8.331	8.331	8.331	8.331	8.331
STEP	3.310	3.310	3.310	3.310	3.310
Battery storage	0	7.900	1.997	3.821	2.471

Table 3.B.: Optimal capacity by technology with varying carbon price and investment and fixed costs for renewables (in GWe)

Note: For all cases, we impose a minimum of 2 pairs of nuclear reactors to be decommissioned, i.e. 4 reactors.

When considering operational and FOM costs from the perspective of the French nuclear operator only, it appears from **Figure 4.A.** that FOM costs associated to the nuclear fleet decrease with the number of decommissioned pairs of reactors. In other words, phasing out the maximum number of nuclear units is economically optimal in terms of total FOM costs. However, closing nuclear reactors diminishes the maximum available capacity and thus may entail a revenue loss for the nuclear operator. Using panel data for the hourly day-ahead spot market corresponding to the French trading zone BZNFR, over the period 2015-2018[23], we find an average profit of nuclear generation equal to 34.6 €/MWh. The total annual profit earned for each MWe of installed nuclear capacity is estimated to 209 k€ approximately. Thus, *ceteris paribus*, decommissioning a pair of reactors would have entailed an annual profit loss of 376 M€ over the period. By comparison, decommissioning a pair of reactors reduces total annual fixed costs by 317 M€ in the baseline case and respectively 343 M€, 396 M€ and 448 M€ by increasing prolongation costs by 10%, 30% and 50%. Thus, from the sole perspective of the nuclear operator, this simple analysis suggests that for prolongation costs high enough, phasing out of nuclear would reduce the net annual total costs (total FOM and operation costs minus generation revenue) associated to the nuclear fleet. Moreover, we assumed initial nuclear investment costs have been fully amortized so annuities corresponding to these costs are null beyond 40 years of activity. As underlined by [13], many cost items, for

[23] https://transparency.entsoe.eu/

instance “hidden development counts” initially buried in the State’s account, may contribute to inflate the true total costs of nuclear. A careful evaluation thus suggests that nuclear shut down would be beneficial for the nuclear operator, provided dismantling costs have been provisioned to meet back-end commitments.

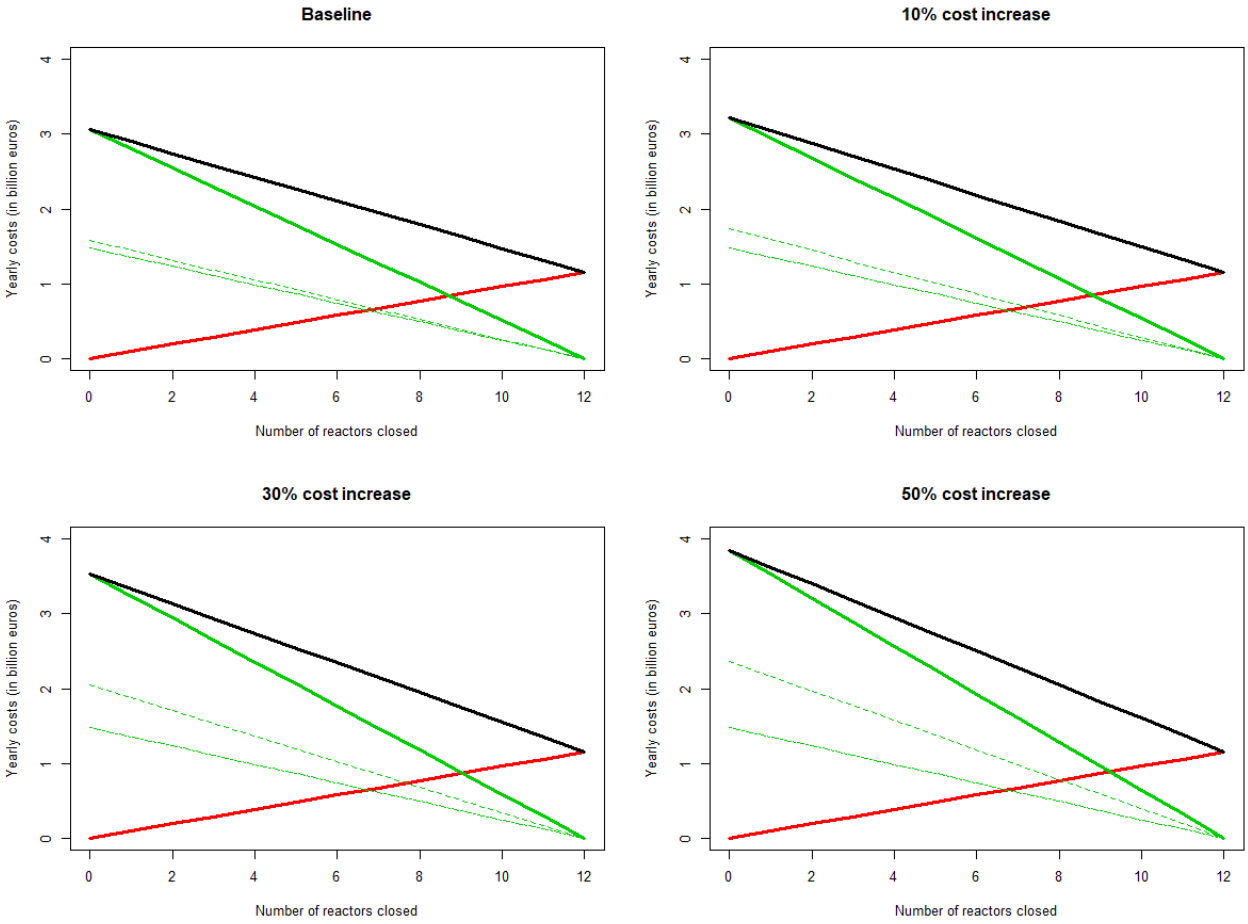

Figure 4.A.: Annual fleet FOM and nuclear policy costs under increasing nuclear prolongation cost

Note: The red plain line corresponds to decommissioning costs. The green dashed (resp. dotted) line corresponds to the prolongation costs (resp. FOM costs) of non-decommissioned reactors, while the green plain line is equal to their sum. Finally, the black plain line is equal to the sum of all costs.

By comparison, **Table 4.B.** shows the rate at which total cost per reactor closed goes down as dismantling costs diminish. Decreasing dismantling costs by 10%, 30% and 50% reduces total annual fixed costs associated to the remaining nuclear capacity, for each decommissioned pair, by 336 M€, 375 M€ and 413 M€. EDF, the owner and operator of the French nuclear fleet, estimated a unit dismantling cost of 320 €/kWe regarding a plant of four 900 MWe

reactors. Equivalently, the estimated cost per 900 MWe reactor amounts to approximately 290 M€, which remains much smaller than the dismantling cost after a 50% decrease. Allocating the costs over a 15-year dismantling period suggests that nuclear phasing out is indeed optimal for the fleet operator.

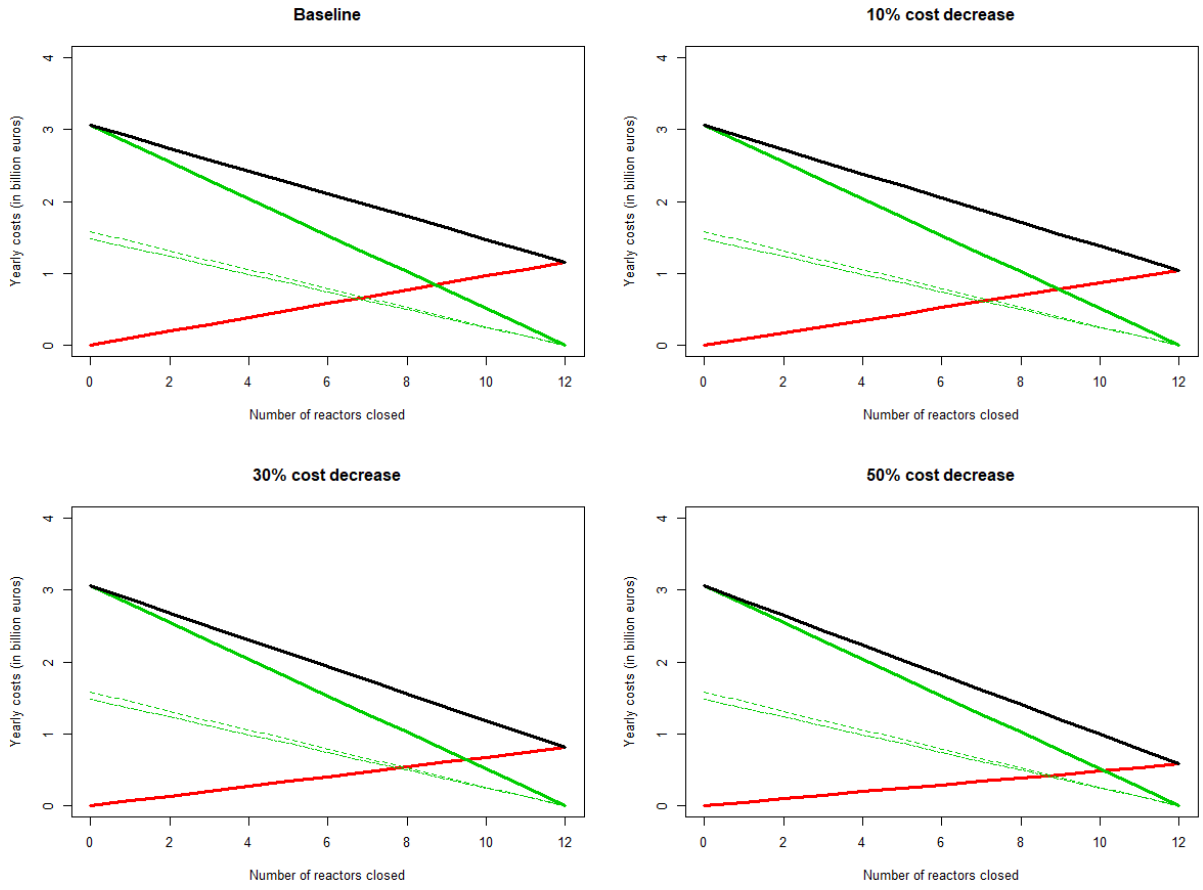

Figure 4.B.: Annual fleet FOM and nuclear policy costs under decreasing dismantling cost

However, from the perspective of a social planner, the gains associated to a partially phased out nuclear fleet remain too low to compensate the extremely high investment costs required to replace decommissioned reactors by RES generation units. Using a simple heuristic, we may compute all combinations of wind and photovoltaic capacity required to replace 1 GWe of nuclear capacity. Given a set of consecutive generation periods τ in the interval $[\tau^-, \tau^+]$, with $(\tau^-, \tau^+) \in (\mathbb{N}^+)^2$, $\tau^- < \tau^+$, we compute the minimum RES capacity such that for any interval $[\tau, \tau^+] \subseteq [\tau^-, \tau^+]$, the cumulated RES generation is superior or equal to the cumulated generation corresponding to 1 GWe of nuclear capacity. Formally, using notations given in Appendix and noting U_1 (resp. U_2) the photovoltaic (resp. wind) installed capacity,

the RES capacity required to replace the whole nuclear fleet amounts to solving the following problem:

$$\min_{U_2 \in \mathbb{R}^+} U_2 : \left(\begin{array}{c} \int_{\tau^-}^{\tau} (\xi_t^1 U_1 + \xi_t^2 U_2) dt \geq \int_{\tau^-}^{\tau} \left(\sum_{g \in \mathcal{N}} q_{gt} \right) dt \, , \forall \tau \in [\tau^-, \tau^+] \\ U_1 \in \mathbb{R}^+ \end{array} \right) \quad (\mathbf{1})$$

ξ_t^1 (resp. ξ_t^2) corresponds to the photovoltaic (resp. wind) capacity factor in $t \in [\tau^-, \tau^+]$. In order to compute each combinations of U_1 and U_2, we arbitrarily fix U_1 exogeously. For simplicity, we assume the storage capacity required to allocate renewable generation between successive periods is avaiable. By linearity assumption, we may directly compute the set of combinations of wind and photovoltaic capacity required to replace 1 GWe of nuclear capacity. Taking historic profiles for nuclear generation, wind and solar capacity factors over the period 2013-2018, we plot the resulting optimal combinations in **Figure 5** below.

Our results help better understand the relatively higher share of wind capacity compared to solar capacity in the optimal mix. While approximately 3.7 GWe of wind capacity and no solar capacity, with the adequate storage capacity, can satisfy the same cumulative profile than 1 GWe of nuclear capacity, 18.7 GWe of photovoltaic are required if wind capacity is null. Consequently, the minimum required wind capacity (resp. photovoltaic capacity) to replace 2 nuclear reactors when photovoltaic (resp. wind) capacity is null is equal to 6.7 GWe (resp. 33.7 GWe). Under 2021 overnight costs, we find the cost minimizing combination comprises 0 GWe of solar installed capacity, for a total annuity cost of 692€ millions neglecting storage investment costs. By comparison, we estimate the sum of the annuitized prolongation cost and FOM costs for 2 nuclear reactors to 510€ millions roughly. Unless the wind turbine industry experiences a strong cost reduction in the following decade (or a sharp increase in average capacity factor), our results show replacing nuclear reactors by renewables is strongly sub-optimal in terms of costs. Furthermore, throughout the previous analysis, the storage investments required for absorbing additional renewable generation are likely to be underestimated, as Auvergne-Rhône-Alpes has significant pumped-storage hydroelectric capacity. The high volume of electricity from hydroelectric sources may also contribute to underestimate the optimal number of CCGT units required to replace decommissioned nuclear units. Overall, it appears clearly throughout our analysis that an early phasing out of nuclear, at least before 2030, is not justified on the basis of costs.

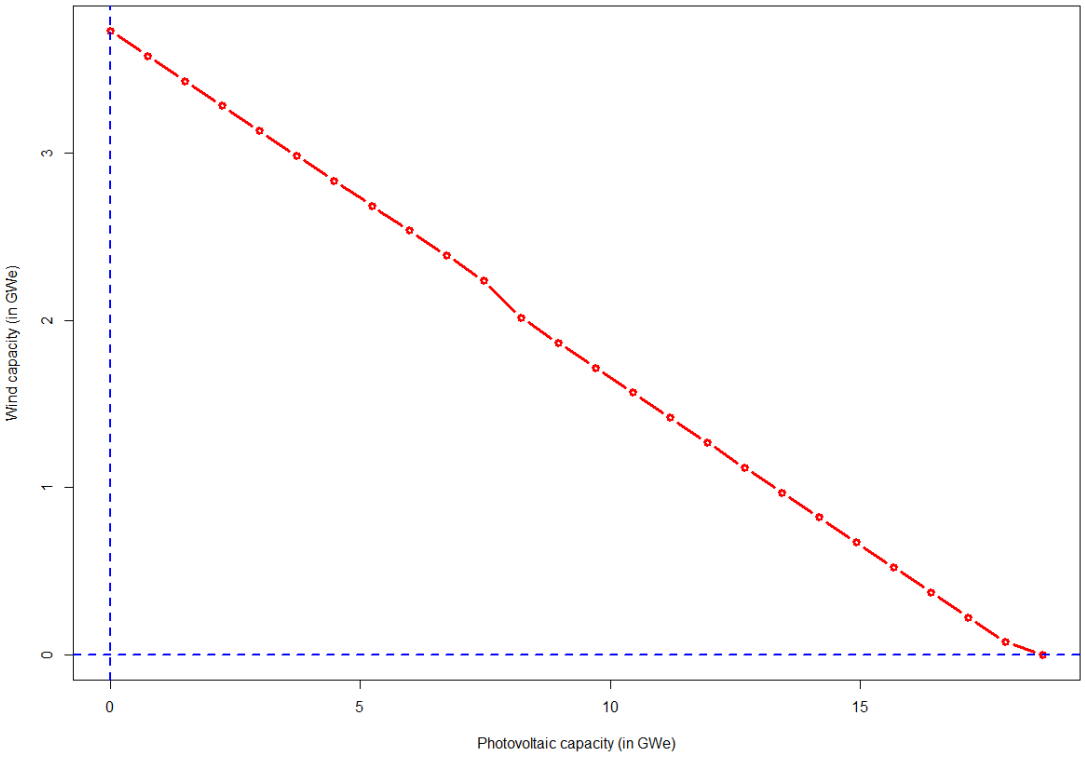

Figure 5.: 'Isoquant' line of photovoltaic and wind capacity combinations equivalent to 1 GWe of nuclear capacity

The French Agency for the Energy Transition (ADEME) estimates the onshore wind potential, for Auvergne-Rhône-Alpes, to 20 GWe for old-generation turbines and 13.3 GWe for new-generation ones[24]. The total regional photovoltaic potential is estimated to 52.1 GWe, which can be decomposed into 31 GWe for residential, 15 GWe for commercial and 6.1 GWe for utility-scale photovoltaic. With an estimated 6.7 GWe of old-generation wind capacity to replace a pair of 900 MWe nuclear reactors, at most 3 pairs of reactors may be replaced by wind turbines. Overall, at most 4 pairs of nuclear reactors could be fully replaced by a combination of wind and photovoltaic at suboptimal investment costs. These results suggest that replacing a higher number of nuclear reactors by a blend of RES might require importing electricity from other French regions with higher wind and solar potentials, possibly triggering additional network reinforcement investments.

[24]https://librairie.ademe.fr/recherche-et-innovation/2881-mix-electrique-100-renouvelable-analyses-et-optimisations.html

3.3. Cost repartition comparisons

As already underlined above, photovoltaic and wind are capital-intensive technologies with null variable costs. Similarly, nuclear is characterized by high investment and maintenance costs but generates carbon-free electricity at a very low variable cost (we estimated the fuel cost to 8 €/MWh). On the contrary, peaking technologies such as CCGT have low capital but high generation costs, increasing with carbon price.

We expect the share of fixed costs to increase with RES penetration, especially if the nuclear capacity remains equal to its initial value. Under the assumption that all annuities have been paid for nuclear and hydroelectric units, **Table 4.A.** shows that a majority of annual costs correspond to FOM and nuclear policy costs. While increasing RES penetration slightly decrease both worst-case and representative operational costs, these gains are counterbalanced by increasing annuities, FOM and nuclear policy costs. Over a representative year, total operational costs only represent 14 % of all costs, while FOM costs and nuclear policy costs respectively account for 48% and 32% of the total. Increasing nuclear prolongation costs further increases the share of fixed costs: under a 50% cost increase, the share of total operational costs drops to 10% while the costs of nuclear prolongation represent approximately 39% of the total.

	Baseline	+10 %	+ 30 %	+ 50 %
Objective function (B€)	5.103	5.802	6.039	6.196
Total overnight costs (B€)	2.036	7.882	6.310	4.899
Worst-case operational costs (B€)	0.207	0.183	0.189	0.191
Representative annual operational costs (B€)	0.691	0.577	0.582	0.603
Annuities (B€)	**0.320**	**0.755**	**0.675**	**0.557**
Combined cycle gas turbine	0.132	0.110	0.110	0.110
Gas turbine	0	0	0	0
Nuclear	0	0	0	0
Wind	0.068	0.246	0.428	0.323
PV	0.090	0.376	0.090	0.090
Hydroelectric	0	0	0	0
STEP	0	0	0	0
Battery storage	0.030	0.023	0.047	0.034
Yearly FOM costs (B€)	**2.343**	**2.519**	**2.494**	**2.445**
Combined cycle gas turbine	0.063	0.054	0.054	0.054
Gas turbine	0	0	0	0
Nuclear	1.836	1.836	1.836	1.836
Wind	0.030	0.107	0.186	0.140
PV	0.034	0.144	0.034	0.034
Hydroelectric	0.267	0.267	0.267	0.267
STEP	0.106	0.106	0.106	0.106
Battery storage	0.007	0.005	0.011	0.008
Nuclear retirement and prolongation costs (B€)	**1.577**	**1.735**	**2.051**	**2.366**

Table 4.A.: Cost allocation by technology and operational conditions with varying prolongation costs

Note: All costs figures correspond to the optimal capacity mixes presented in **Table 2.A**.. The worst-case costs are computed over the subset of worst-case weeks for each season only, while the representative operational costs are computed over the subset of representative weeks and scaled so that they are expressed on a yearly basis.

Similar observations, with a dominant share of fixed costs, can be drawn for the allocation of costs when increasing the lentgh of the dismantling period or decreasing decommissionning costs. We refer to **Table 4.B.** and **Table 4.C.** in Appendix for a comprehensive presentation of the cost allocation. For almost all cases, we note an increase in total annual system costs with respect to the baseline optimal mix.

	Baseline	2025	2030	2035
Objective function (B€)	5.103	5.095	5.309	5.252
Total investment costs (B€)	2.036	2.087	5.789	6.576
Worst-case operational costs (B€)	0.207	0.206	0.177	0.156
Representative annual operational costs (B€)	0.691	0.663	0.554	0.489
Annuities (B€)	**0.320**	**0.246**	**0.544**	**0.599**
Combined cycle gas turbine	0.132	0.132	0.110	0.110
Gas turbine	0	0	0	0
Nuclear	0	0	0	0
Wind	0.068	0.058	0.055	0.252
PV	0.090	0.056	0.303	0.177
Hydroelectric	0	0	0	0
STEP	0	0	0	0
Battery storage	0.030	0.050	0.076	0.060
Yearly FOM costs (B€)	**2.343**	**2.331**	**2.421**	**2.454**
Combined cycle gas turbine	0.063	0.063	0.054	0.054
Gas turbine	0	0	0	0
Nuclear	1.836	1.836	1.836	1.836
Wind	0.030	0.025	0.024	0.109
PV	0.034	0.022	0.116	0.068
Hydroelectric	0.267	0.267	0.267	0.267
STEP	0.106	0.106	0.106	0.106
Battery storage	0.007	0.012	0.018	0.014
Yearly nuclear retirement and prolongation costs (B€)	**1.577**	**1.577**	**1.577**	**1.577**

Table 4.D.: Cost allocation by technology and operational conditions with varying investment and fixed costs for renewables

As illustated in **Table 4.D.**, the increase in RES penetration following lower investment and FOM costs allows for significantly lower operational costs, both in the worst-case and representative weeks. Compared to the baseline, the operational and annual representative costs corresponding to 2035 projected costs are roughly 25% and 29% lower respectively. Yet, the same comparison reveals a 87% increase in annuities and 5% in yearly FOM costs. As previously, an increasing share of total annual costs are fixed, with representative annual operational costs accouning for only 10% of annual system costs. Overall, we note that the value of the objective function is higher or roughly equal to the baseline case in all simulations.

	Baseline	2025	2030	2035
Objective function (B€)	5.103	5.311	4.952	4.708
Total investment costs (B€)	2.036	4.441	2.333	6.447
Worst-case operational costs (B€)	0.207	0.174	0.153	0.148
Representative annual operational costs (B€)	0.691	0.585	0.568	0.560
Annuities (B€)	**0.320**	**0.552**	**0.351**	**0.194**
Combined cycle gas turbine	0.132	0.088	0.066	0.044
Gas turbine	0	0	0	0
Nuclear	0	0	0	0
Wind	0.068	0.270	0.189	0.060
PV	0.090	0.090	0.090	0.090
Hydroelectric	0	0	0	0
STEP	0	0	0	0
Battery storage	0.030	0.104	0.006	0
Yearly FOM costs (B€)	**2.343**	**2.429**	**2.362**	**2.296**
Combined cycle gas turbine	0.063	0.045	0.036	0.027
Gas turbine	0	0	0	0
Nuclear	1.836	1.836	1.836	1.836
Wind	0.030	0.117	0.082	0.026
PV	0.034	0.034	0.034	0.034
Hydroelectric	0.267	0.267	0.267	0.267
STEP	0.106	0.106	0.106	0.106
Battery storage	0.007	0.024	0.001	0
Yearly nuclear retirement and prolongation costs (B€)	**1.577**	**1.577**	**1.577**	**1.577**

Table 4.E.: Cost allocation by technology and operational conditions under future projected electric demand distributions

Table 4.E. shows reducing electricity demand allows for both reducing annual operational and fixed costs. Although higher wind capacities increase total annuities for the cases corresponding to 2025 and 2030 projected demand, results suggest that a sufficient and uniform reduction in electricity demand mecanically decrease the total operating costs, with a smaller utilization of CCGT units (with high variable costs) as peaking demand also diminishes. Our results show similar annual system costs for the baseline optimal mix (4.93 billion €) and the one corresponding to 2030 demand distribution (4.86 billion €), although the latter has both a higher RES penetration and less CO_2-emitting generation units. However, even in the absence of subsidies to renewables, reducing electricity demand without significantly decreasing total fixed cost is likely to increase the average electricity price, as

annuities and annual FOM costs are now allocated over a smaller volume of generation. While decreasing the electricity spot price, some consumers may bear a larger share of the system fixed costs depending on how the latter are allocated. This issue is however outside the scope of this chapter and left for further research.

Finally, **Table 4.F.** shows the impact of increasing carbon price on the repartition of costs for the corresponding optimal mixes. For π^{CO_2} equal to 50€/t and 100€/t, the small reduction in representative annual operational costs is negated by higher annuities and FOM costs following investment in additional RES generation units. Simultaneously, worst-case operational costs steadily increase with carbon price. This is the consequence of the system balance being mainly ensured by CCGT generation, especially in high RD situations.

	Baseline	$\boldsymbol{\pi^{CO_2} = 50\ €/t}$	$\boldsymbol{\pi^{CO_2} = 100\ €/t}$	$\boldsymbol{\pi^{CO_2} = 150\ €/t}$
Objective function (B€)	5.103	5.265	5.333	5.348
Total overnight costs (B€)	2.036	3.520	2.900	2.130
Worst-case operational costs (B€)	0.207	0.208	0.233	0.251
Representative annual operational costs (B€)	0.691	0.654	0.670	0.689
Annuities (B€)	**0.320**	**0.414**	**0.382**	**0.338**
Combined cycle gas turbine	0.132	0.132	0.132	0.132
Gas turbine	0	0	0	0
Nuclear	0	0	0	0
Wind	0.068	0.060	0.143	0.060
PV	0.090	0.218	0.096	0.090
Hydroelectric	0	0	0	0
STEP	0	0	0	0
Battery storage	0.030	0.004	0.011	0.056
Yearly FOM costs (B€)	**2.343**	**2.373**	**2.364**	**2.345**
Combined cycle gas turbine	0.063	0.063	0.054	0.063
Gas turbine	0	0	0	0
Nuclear	1.836	1.836	1.836	1.836
Wind	0.030	0.026	0.062	0.026
PV	0.034	0.083	0.037	0.034
Hydroelectric	0.267	0.267	0.267	0.267
STEP	0.106	0.106	0.106	0.106
Battery storage	0.007	0.001	0.002	0.013
Nuclear retirement and prolongation costs (B€)	**1.577**	**1.577**	**1.577**	**1.577**

Table 4.F.: Cost allocation by technology and operational conditions with varying carbon price

A higher CO_2 price has virtually no effect on the repartition of system costs between operational and fixed costs: while annual representative operational costs represent 14% of total costs in the baseline case, they respectively represent 13% and 13.9% for carbon costs equal to 50€/t and 150€/t. Overall, for all the optimal mixes considered above, FOM costs represent the major part of annual system costs, in addition to nuclear retirement and prolongation costs which consistently account for above 30% of the total.

Imposing a partial nuclear phase out significantly modifies the repartition of system costs. As shown in **Table 4.G.**, annuitized nuclear policy costs decrease by 70 M€ with each pair of closed reactors, while nuclear fixed costs decrease by 246 M€. While nuclear accounts for approximately 78% of annual FOM costs in the baseline case, its share decreases to 65% and 57% with respectively 2 and 4 pairs of decommissioned reactors. Although it remains one of the main contributors to system costs, the sum of nuclear fixed and policy costs accounts for 54% and 37% with 9.8 GWe and 6.2 GWe of installed nuclear capacity, compared to 69% in the baseline case.

Lastly, our results document a significant increase in both worst-case and representative annual operational costs. While closing 4 pairs of reactors multiplies worst-case costs by more than 2, the representative annual cost increases by 230%. This compares to the findings of [24], who simulate Japan's optimal future power generation mix under various nuclear and CO_2 regulations policies. They find a complete nuclear phase out and 80% reduction in carbon emissions entail a quadruple increase in power generation costs. Technical innovation and severe reduction in RES investment costs are shown to be pivotal conditions to guarantee the economic efficiency of a sustainable power supply. Although the optimal capacity mixes found by imposing a minimum level of nuclear phase out are clearly incompatible with CO_2 reduction targets, at least from a cost-minimization perspective, this suggests the existence of a trade-off between an extremely capital-intensive mix based on high RES capacities with low operational costs, and a low capital-intensive mix based on CCGT turbines with high generation costs and a significant increase in carbon emissions. Similar observations in terms of cost allocation can be made for **Table 4.H.** in Appendix, for varying carbon costs and investment and fixed costs for renewables.

The additional cost of carbon capture and storage (CCS) technologies, with the subsequent reduction in CO_2 emissions, should thus be considered and put into balance with the costs of replacing ageing nuclear reactors by a blend of renewables and storage, especially in worst-

case situations with unstable weather or prolonged periods of low renewable production. However, one should also consider the dependency of France to foreign gas imports. Although 50% of the imported gas comes from Europe, with 43% from Norway and 11% from the Netherlands, 21% of the total is imported from Russia[25]. France gas imports have increased by 11% in 2019, which 55% and 39% higher imports from Qatar and Nigeria[26]. Although this diversification strategy limits of the risks of supply rupture, France remains subject to geopolitical risk and dependent from non-EU countries, in addition to the price risk. As documented by the French CRE, the +12.6% increase in gas prices in October 2021 in France uniquely reflects the impact higher gas price on the supply costs of Engie[27]. Properly quantifying the gains from energy independency is thus pivotal for estimating the actual gains from decreasing the share of fossil-fuel generation units in the electricity mix. However, as it has been shown in the first chapters of this thesis, ensuring system balance in worst-case situations with strong RES penetration requires maintaining a fraction of peaking units. Finally, although this topic has received little attention yet, it has recently been estimated that one third of French gas imports directly come from the Arctic zone[28]. Increasing French dependence on gas imports is thus likely to accelerate the exploitation of fragile polar territories and contradicts the French public objectives of environmental preservation. A striking example is the 10% direct financial participation of TotalEnergies in the Arctic LNG 2 Project in Russia, while the grant of an export guarantee by the French Public Bank of Investment (BPI) to TotalEnergies is currently debated[29]. However, the official reluctance to financially back-up this project may not deter Total-Energies from actively pursuing the project development as it may yield significant exports revenue.

[25] https://www.grdf.fr/installateurs/atouts-gaz/consommation-gaz-france

[26] https://www.connaissancedesenergies.org/le-gaz-consomme-en-france-vient-principalement-de-russie-120222

[27] https://www.cre.fr/Actualites/la-cre-constate-une-nouvelle-hausse-du-cout-du-gaz-naturel-importe-entrainant-une-hausse-des-tarifs-reglementes-de-vente-de-gaz-naturel-pour-le-moi

[28] See Mikaa Mered, “Une analyse stratégique et géopolitique des filières de l’hydrogène”, Alters Media, n°4, October 2021

[29]https://www.lemonde.fr/economie/article/2021/09/09/la-france-en-passe-de-renoncer-a-soutenir-un-mega-projet-gazier-dans-l-arctique_6094080_3234.html

	1	2	3	4
Objective function (B€)	5.300	5.599	5.706	5.928
Total investment costs (B€)	4.715	8.804	7.371	7.061
Worst-case operational costs (B€)	0.247	0.295	0.434	0.576
Representative annual operational costs (B€)	0.721	0.845	1.605	2.375
Annuities (B€)	**0.544**	**0.814**	**0.736**	**0.647**
Combined cycle gas turbine	0.199	0.287	0.375	0.464
Gas turbine	0	0	0	0
Nuclear	0	0	0	0
Wind	0.166	0.440	0.126	0.065
PV	0.090	0.090	0.090	0.090
Hydroelectric	0	0	0	0
STEP	0	0	0	0
Battery storage	0.089	0	0.145	0.028
Yearly FOM costs (B€)	**2.179**	**2.067**	**1.723**	**1.489**
Combined cycle gas turbine	0.090	0.126	0.162	0.198
Gas turbine	0	0	0	0
Nuclear	1.589	1.343	1.096	0.849
Wind	0.072	0.191	0.055	0.028
PV	0.034	0.034	0.034	0.034
Hydroelectric	0.267	0.267	0.267	0.267
STEP	0.106	0.106	0.106	0.106
Battery storage	0.021	0	0.003	0.007
Nuclear retirement and prolongation costs (B€)	**1.507**	**1.437**	**1.367**	**1.297**

Table 4.G.: Cost allocation by technology and operational conditions with imposed minimum number of pairs of decommissioned nuclear reactors

4. Comparative analysis of operational performances

Following the analysis of optimal capacity mix and cost allocation performed above, we now study the operational performances of a subset of mixes both in extreme and representative RD conditions. As already mentioned, reducing nuclear generation capacities may shift the generation mode of units traditionally used in peak or semi-peak mode, such as hydroelectric and CCGT units, to 'baseload'. Inversely, the introduction of significant RES generation may both push nuclear into more frequent load-following operations and increase the recourse to flexible generation units to address abrupt RD variations.

To clearly illustrate and disentangle the effects of partial nuclear phase out and increasing RES penetration on operational system performances, we choose a subset of 4 optimal mixes obtained in Section 3. **Table 5** summarizes the optimal capacity for each technology associated to each of the selected mixes. The optimal mixes n°1 and n°2 correspond to the optimal mixes with endogenous nuclear policy under baseline case and under 2030 projected investment and FOM costs for RES. Similarly, optimal mixes n°3 and n°4 correspond to optimal mixes with a compulsory minimum of 2 pairs of decommissioned reactors under baseline case and under 2030 projected RES costs.

	Optimal mix n°1	**Optimal mix n°2**	**Optimal mix n°3**	**Optimal mix n°4**
Combined cycle gas turbine	3.15	2.7	6.3	6.3
Gas turbine	0	0	0	0
Nuclear	13.4	13.4	9.8	9.8
Wind	0.665	0.583	4.269	1.267
PV	1.190	11.79	1.190	6.639
Hydroelectric	8.331	8.331	8.331	8.331
STEP	3.310	3.310	3.310	3.310
Battery storage	1.384	3.493	0	2.471

Table 5: Subset of optimal capacity mixes by technology for operational performances analysis

4.1. Worst-case weeks performances

As explained in the first two chapters of this thesis, worst-case weeks are constructed such that either RD variations are maximized over the simulation period, or RD level is maximized or minimized. The analysis of these extreme situations captures a series of key elements, including the share of each technology in total output under each extreme scenario, in addition to its contribution to maintaining system stability and controlling RD variations, both in relative and absolute terms. All these measures are expressed as probability distributions, computed over the subset of worst-case hours. We keep notations from Chapters I and II and respectively note **H**, **L** and **V** the worst-case weeks corresponding to the maximum, minimum and most variable residual load trajectories. Similarly, we keep the same color coding such each value associated to **H** (resp. **L** and **V**) is represented in red (resp. green and blue).

4.1.1. Energy contribution

Table 6.A. shows the average nuclear share in total generation is equal to 71% in worst-week **H**, against 65% and 75% in worst-weeks **L** and **V**. For 90% of hours, with wind power accounting for less than 6% of total output in **L**, nuclear and hydroelectric generation respectively provide at least 50% and 15%. Highest nuclear shares are observed for **V**, which suggests it is operated quite rigidly during extremely variable RD events, with the largest variations being absorbed by pumped-storage hydroelectric and hydroelectric generation units. Except for **H**, CCGT units remain offline, which suggests worst-case trajectory **H** may be overly conservative with respect to the real-life duration of episodes of sustained high RD with no renewable generation.

Compared to the optimal mix n°1, we note from **Figure 6.B.** that distribution of nuclear share in total generation is shifted downwards in **L** by roughly 20%, indicating a significant proportion of RES replaces nuclear as ‘baseload’ in low RD events. Results also show an additional but small participation of CCGT to total generation in **L** and **V**, contributing up to 8% of total output in less than 5% of hours, corresponding to system-balancing operations. As flexibility requirements grow with RES capacity, CCGT units are increasingly utilized to meet residual load variations although hydroelectric remains the major stabilizer.

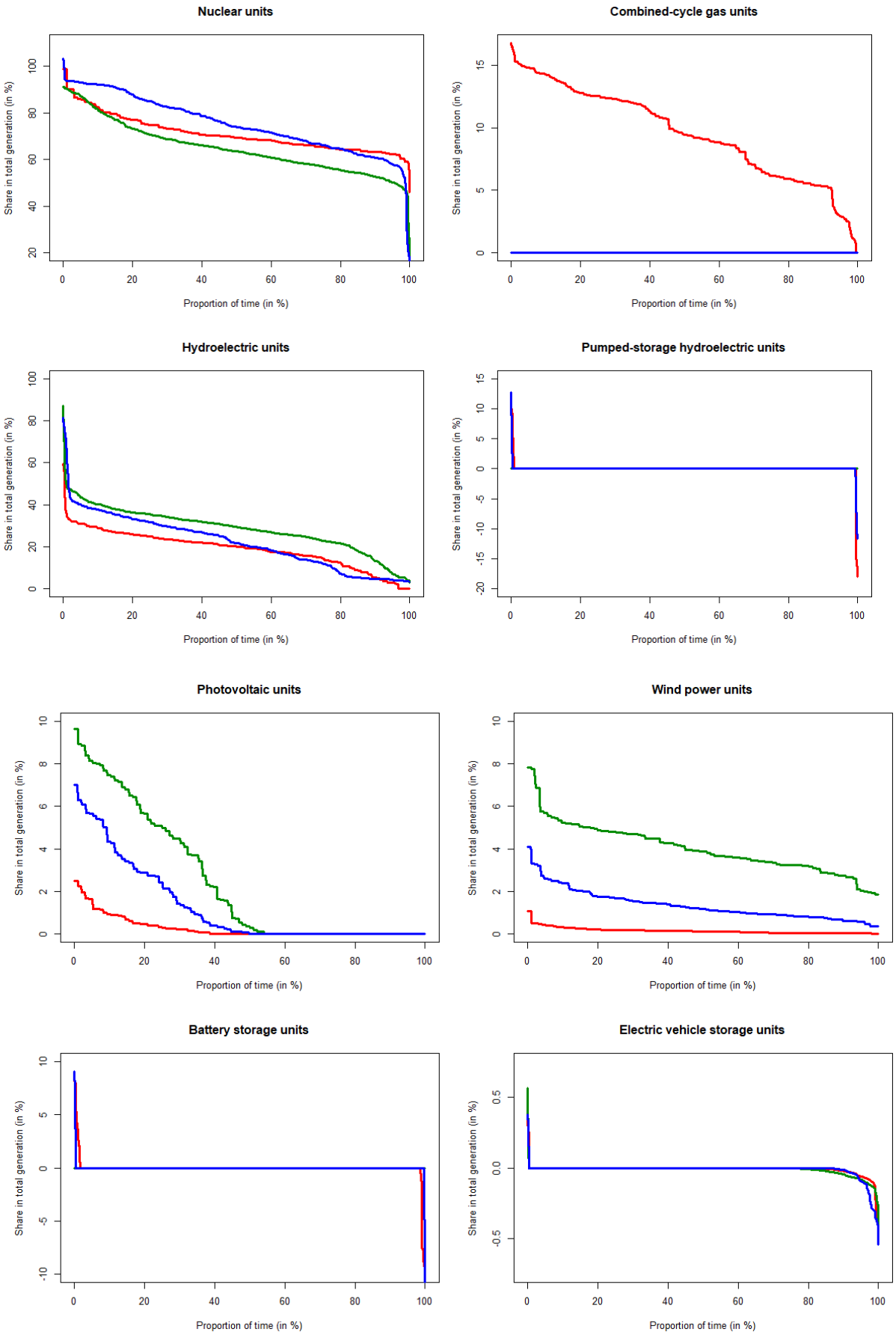

Figure 6.A.: Energy contribution by technology (worst-case weeks, optimal mix n°1)

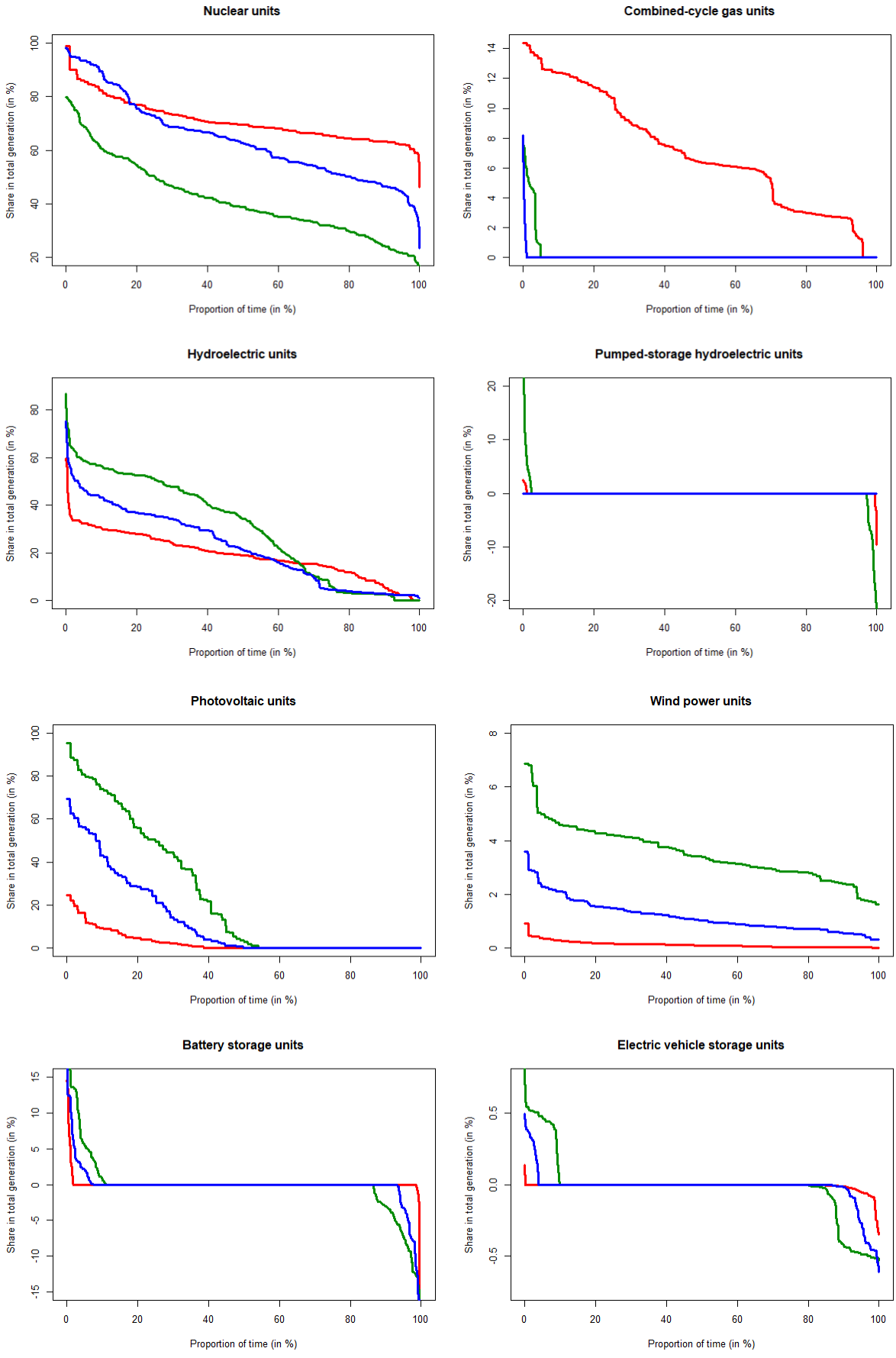

Figure 6.B.: Energy contribution by technology (worst-case weeks, optimal mix n°2)

The upward shift of the hydroelectric generation curve in **L** and **V** indicate a much stronger participation to total generation under high or chaotic RES generation conditions. As solar production may contribute up to 100% of total generation, flexible technologies in addition to storage units play a much more active role in serving total electricity load.

Unsurprisingly, **Figure 6.C.** shows that the average share of nuclear falls to only 52% in **H** and 44% in **L**, as a large fraction of nuclear is being displaced by wind generation. As expected, CCGT is mainly operated as 'baseload', with a share in total generation between 20% and 38% in **H** during 90% of hours, and a significant contribution to production in **V**. The participation profile of hydroelectric units remains much alike the one corresponding to the mix n°1. Finally, we note an increasing participation of pumped-storage and EVs, both in terms of volume of electricity charged and discharged and volume of operating hours.

Finally, compared to mix n°3, we note from **Figure 6.D.** that the average share of nuclear in total generation in **L** is slightly higher, as the diurnal variability of photovoltaic capacity factors only displaces nuclear generation during daylight hours. Overall, even partially phased out, nuclear and hydroelectric generation units remain the major contributors to total generation in **L** and **V**. We further note higher renewable penetration increases the participation of CCGT units for load-following operations in **V**, while battery storage and EVs only participate to total generation in less than 20% of operating hours.

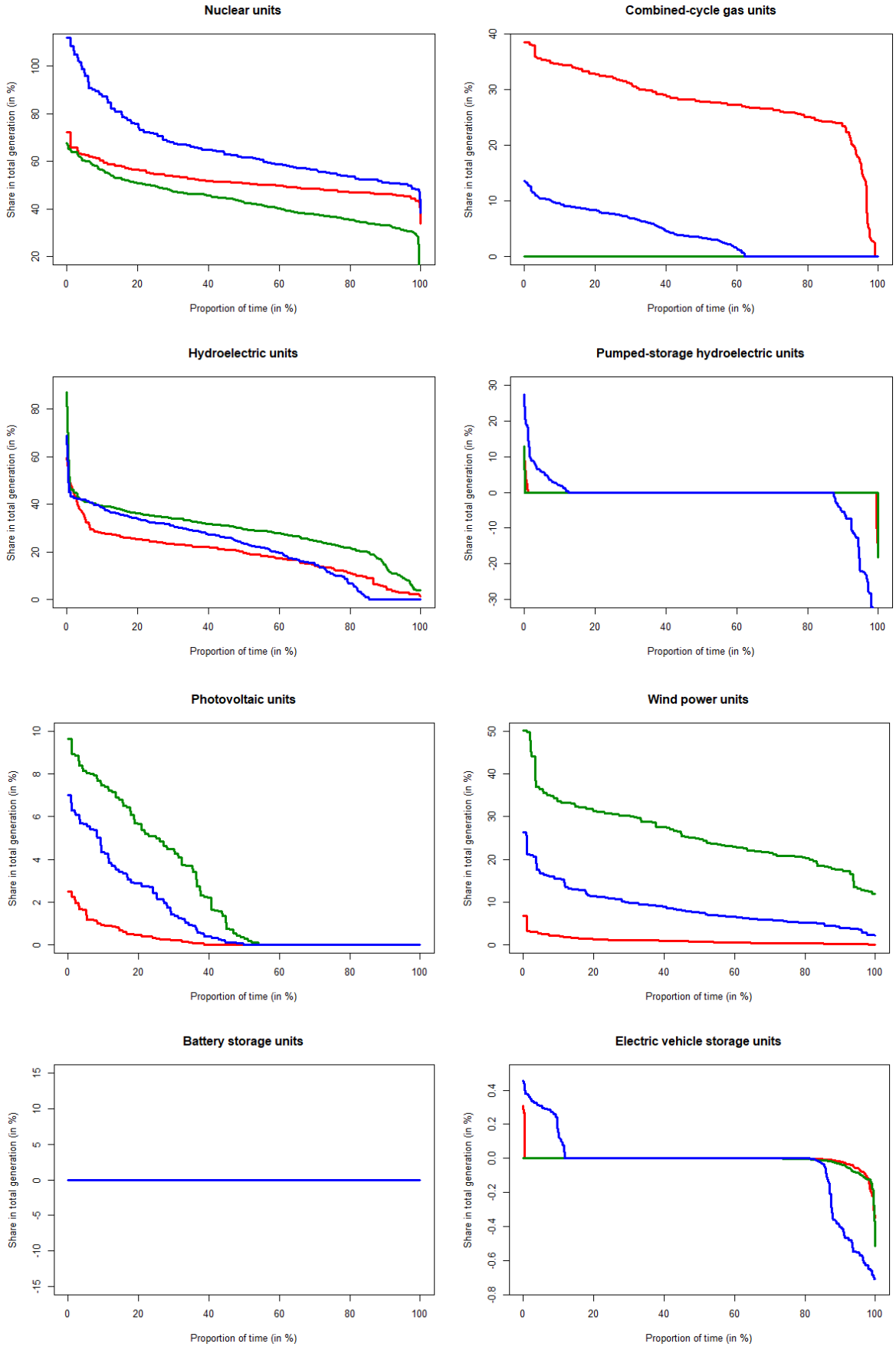

Figure 6.C.: Energy contribution by technology (worst-case weeks, optimal mix n°3)

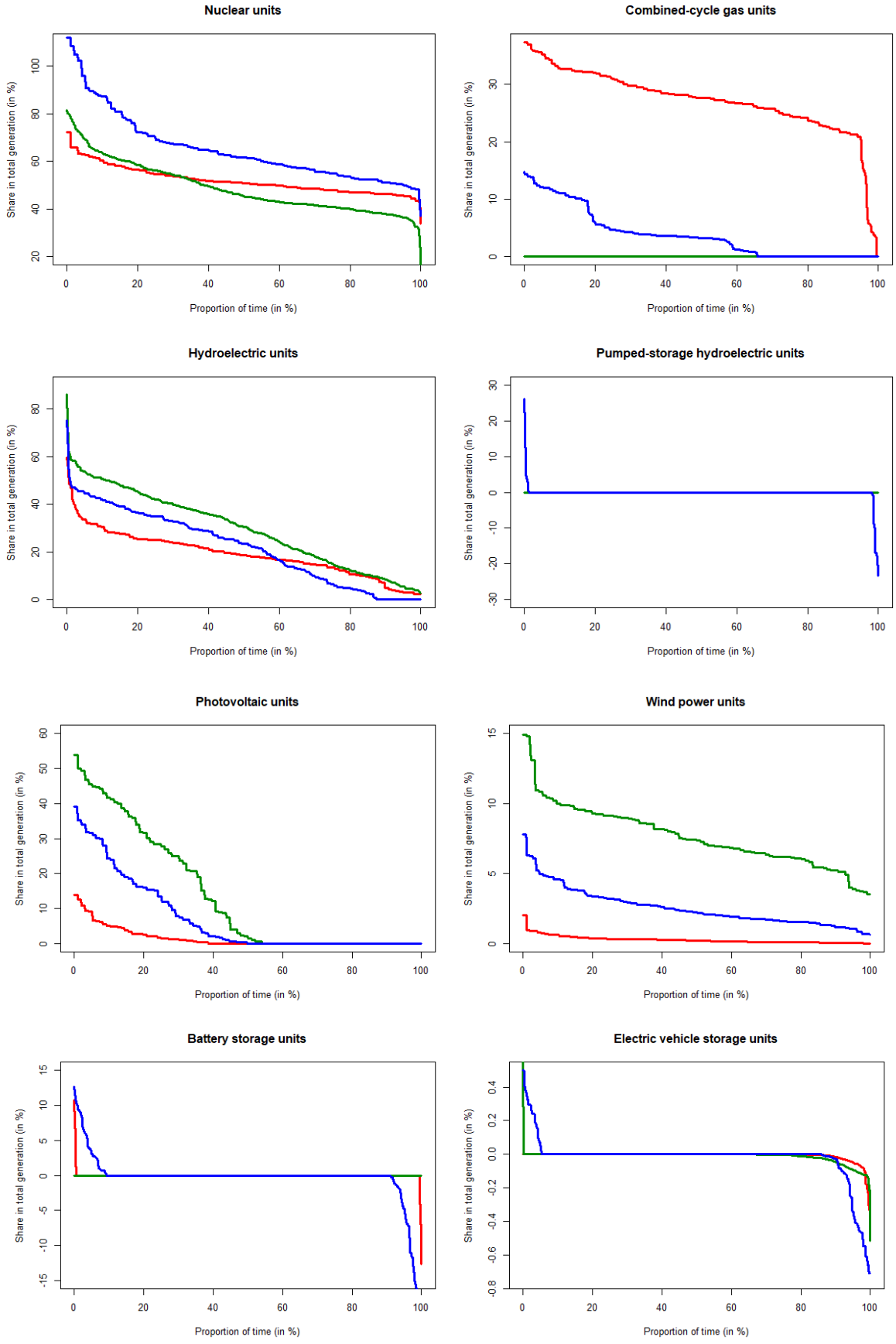

Figure 6.D.: Energy contribution by technology (worst-case weeks, optimal mix n°4)

4.1.2. Contribution to system stability

As expected from its moderate hourly ramping rate and high minimum generation level, nuclear is shown in **Figure 7.A** to be mainly operated in 'baseload' mode in the absence of significant RES penetration in optimal mix n°1. Extreme variations of output correspond to start-ups and shutdowns, with the average absolute hourly variation equal to 196 MWh and 325 MWh in **L** and **V** respectively. With an average nuclear generation of 8.92 GWh over the subset of worst-case hours, the above figures correspond to only 4.4% and 7.2% of the production range over the minimum generation threshold. The significant shares in total variations, superior to 50% (resp. inferior to -50%) in roughly 30% of hours, indicate nuclear power is mostly used to address small RD variations when nuclear units are not producing at maximum capacity in **L** and **V**.

This partial rigidity of nuclear production, with virtually no variations of output in **H**, is compensated by a very active role of hydroelectric generation units and CCGT units to a lesser extent. The hourly variations of output span regularly between 5500 MWh and -6000 MWh, which indicates hydroelectric is operated both in load-following and peaking mode, as the main contributor to "upward" and "downward" system stability over the whole spectrum of RD variations. The almost flat curves with left and right peaks for CCGT, pumped-storage hydroelectric and battery storage correspond to sporadic and brutal RD variations in **V** (yet occurring in less than 5% of hours), or for ensuring system balance a few hours in **H** as hydroelectric units address almost 100% of RD variations the remaining time.

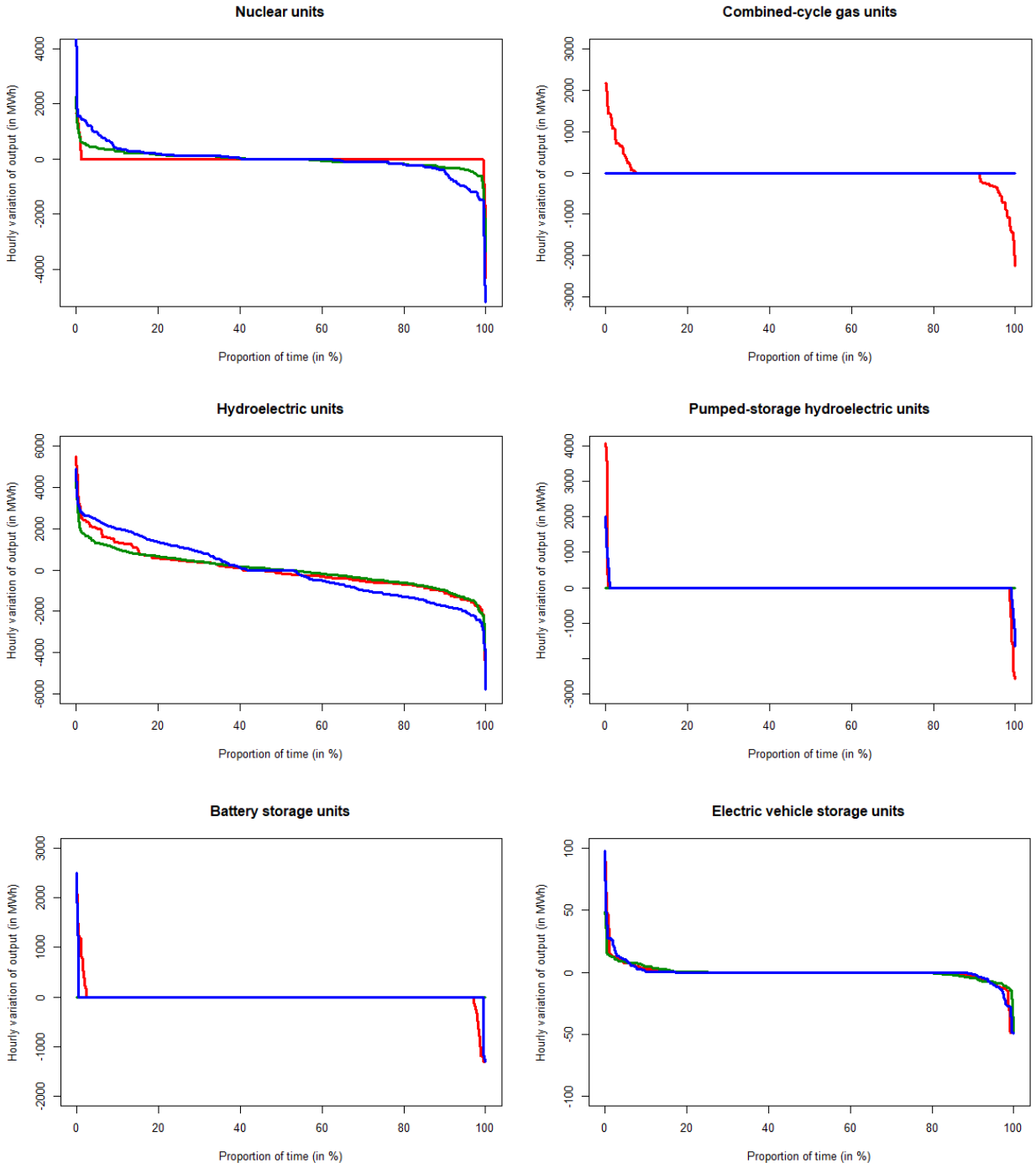

Figure 7.A.: Hourly output variation in MWh, by technology (worst-case weeks, optimal mix n°1)

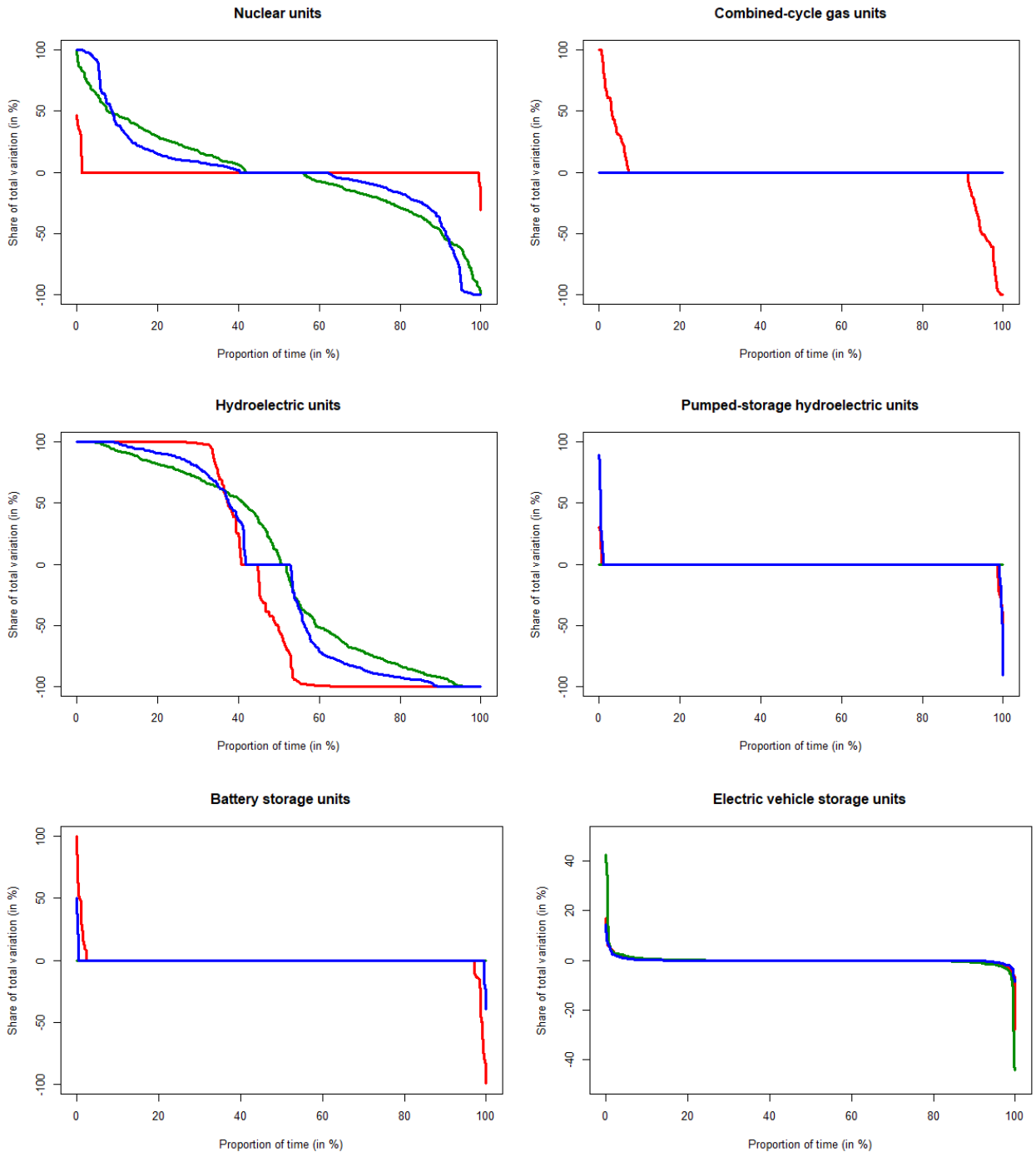

Figure 8.A.: Share in total variation by technology (worst-case weeks, optimal mix n°1)

Under optimal mix n°2, the average absolute hourly output variation of nuclear slightly increases but remains low, with 209 MWh and 362 MWh in **L** and **V**. Even under extremely variable RD in **V**, nuclear variations remain between –600 MWh and 600 MWh more than 90% of operating hours. We observe that the significant penetration of photovoltaic only partially requires using nuclear units for load-following operations, which is allowed by the flexibility services mainly provided by hydroelectric units for all worst-case weeks. It also follows from a more active participation of battery storage to absorbing large RD variations. Finally, the utilization of EVs increases to 40% of operating hours and contributes to system stabilization over a large span of small RD variations.

Compared to optimal mix n°1, CCGT increasingly contributes to providing rapid and large downward output variations in **H**, while pumped-storage units are now used to actively manage large inflows and drops of renewable generation in **L**. Our findings are consistent with [25], who find that flexible generation is increasingly valuable and required as the RES penetration in the mix increases. Different business plans to reward ancillary services, which are increasing provided by flexible generation and storage units, may thus be developed to capture gains from their increasing participation to system stability. However, as underlined by the authors, the European hydroelectric sector is currently under financial stress, mostly because of a surplus of must-run capacity. The partial phase out of nuclear would thus be expected to increase electricity prices in high RES generation periods, by shifting residual demand distribution upwards. However, although the decrease in must-run generation might increase the average RD, the expected increase in spot prices may also be imputed to new investments in CCGT units and their more active role in providing system flexibility.

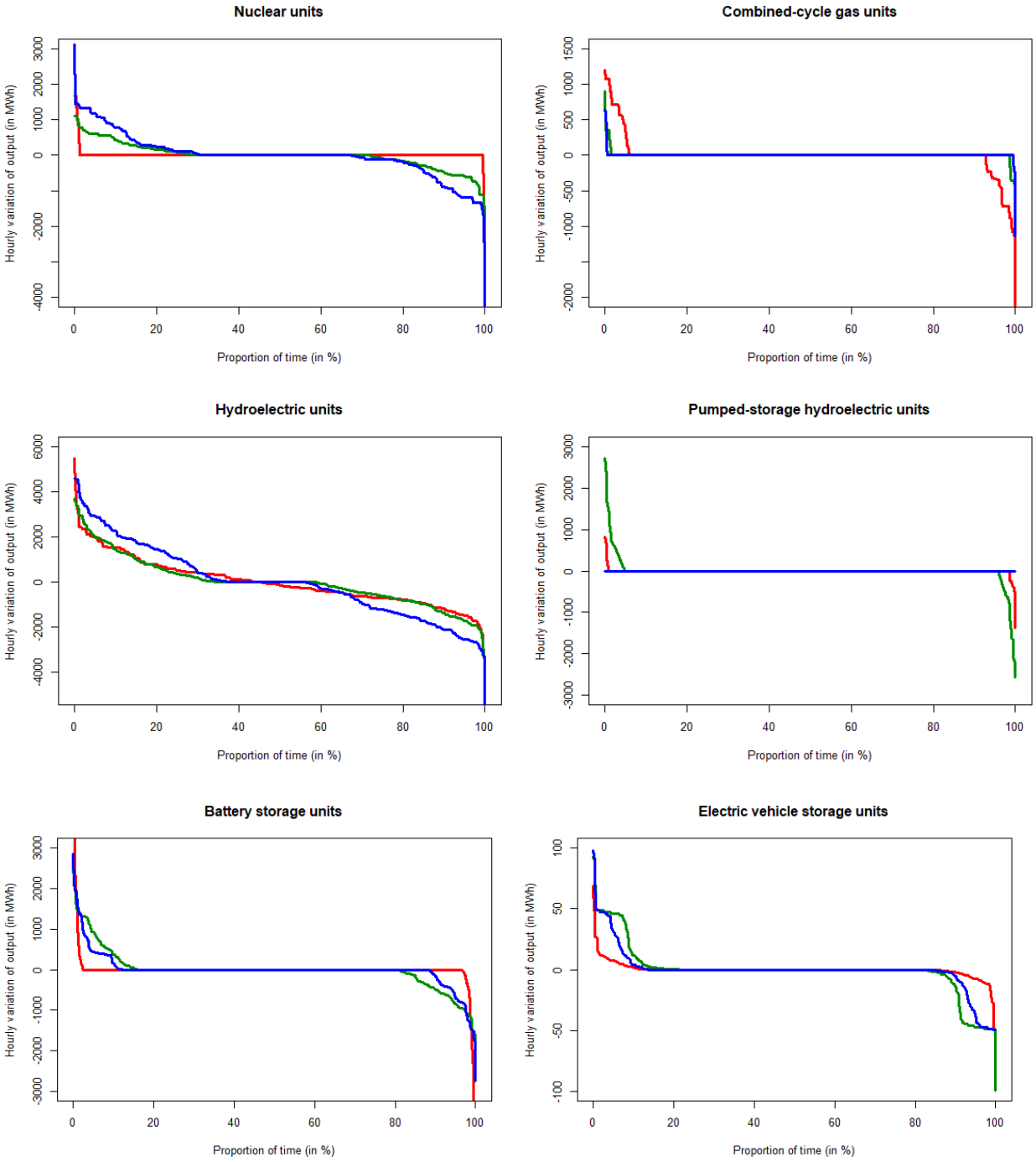

Figure 7.B.: Hourly output variation in MWh, by technology (worst-case weeks, optimal mix n°2)

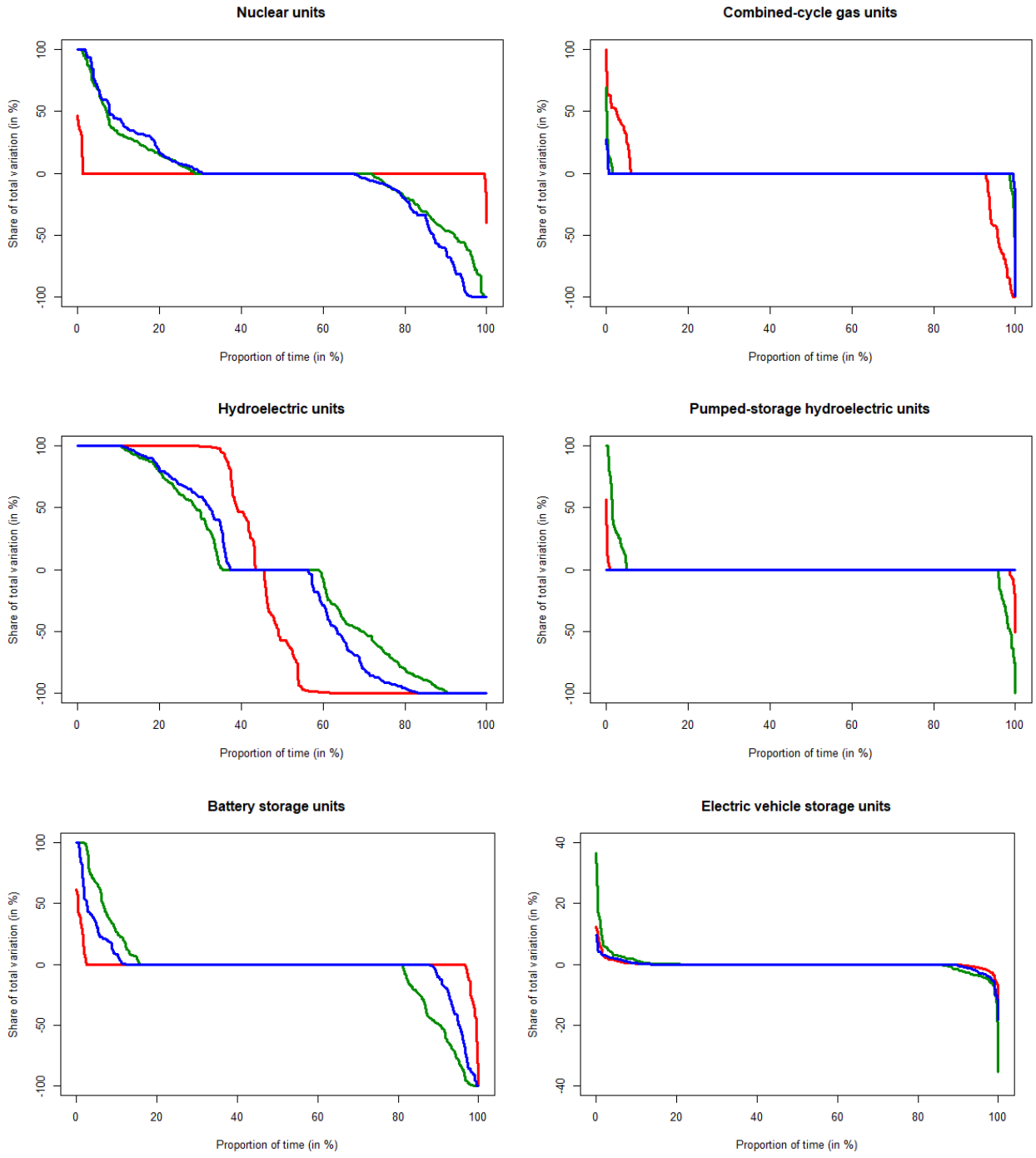

Figure 8.B.: Share in total variation by technology (worst-case weeks, optimal mix n°2)

The phasing out of 4 nuclear reactors in optimal mix n°3 does not significantly alter our previous conclusions. Nuclear is operated in an even more rigid way compared to mix n°1, with its average absolute hourly variation of output equal to 139 MWh and 23 MWh in **L** and **V**. As nuclear production now represents a lower share of total renewable generation, its flexibility requirements are equally lower. Indeed, the decision to operate nuclear flexibly depends on a series specific technical factors : following [26], the grid system operator needs not require nuclear units to operate flexibly if nuclear capacity accounts for a limited fraction of total installed capacities or is significantly lower than the minimum residual demand. However, the growth of RES capacities, combined with a limited or no decrease in nuclear capacity, may significantly lower the minimum residual demand and increase the frequency of nuclear load-following operations. Thus, under increasing RES penetration in the mix, partial nuclear phase out is an option consistent with the choice of maintaining nuclear operating in 'baseload' mode. However, as pointed above, this requires substituting other technologies as 'baseload' during low RES generation periods This might contribute to increase electricity generation costs and carbon emissions if no alternative clean and low-carbon technology is available.

Compared to optimal mix n°1, **Figure 7.C.** shows both increased participation of CCGT and pumped-storage hydroelectric to system stability against very large RD variations. Consistently with the above remarks, the proportion of operating hours for pumped-storage hydroelectric units increases especially in **V**, with an absolute share in total variations above 50% (for variations larger than 1 GWh) more than 30% of operating hours.

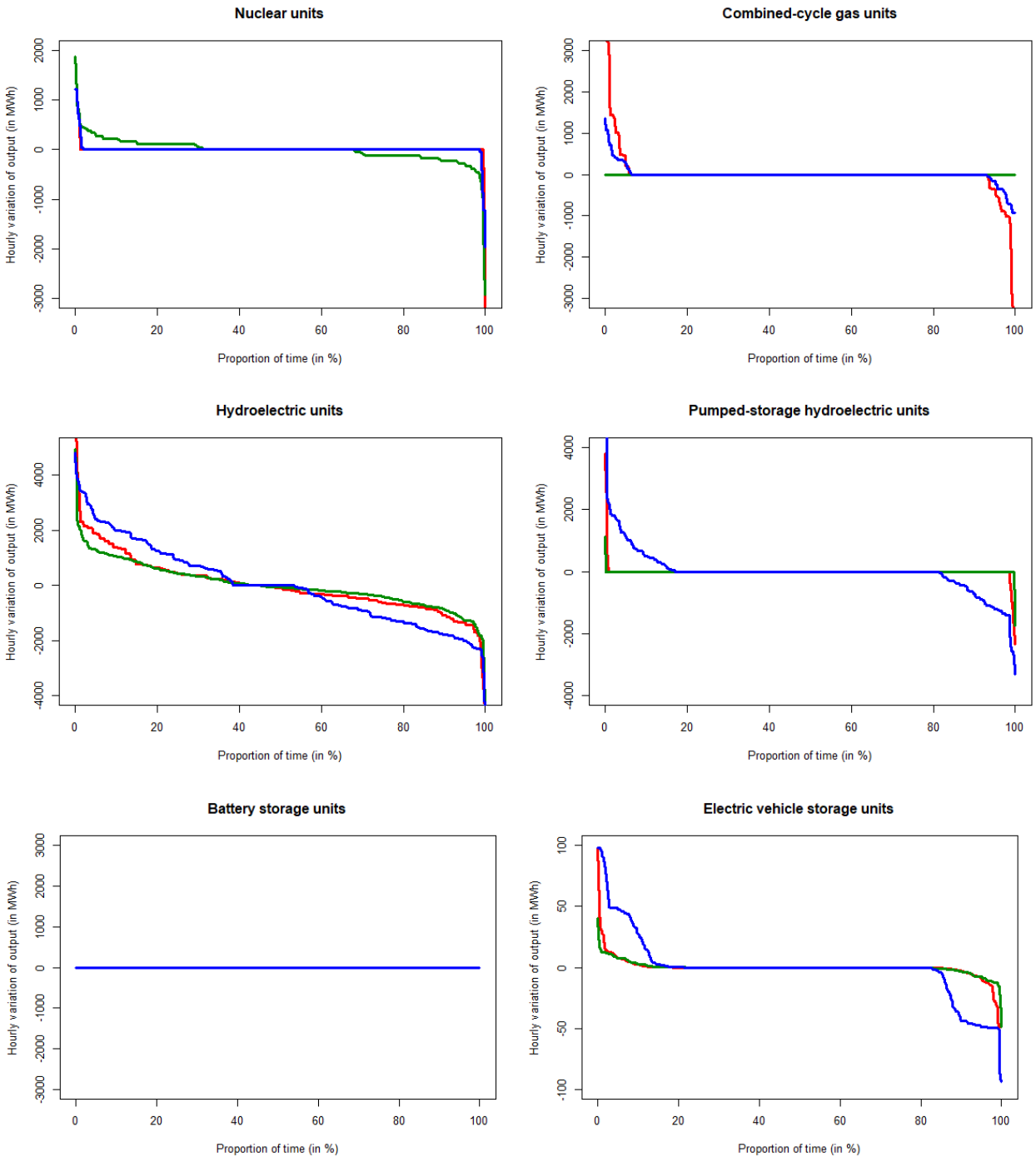

Figure 7.C.: Hourly output variation in MWh, by technology (worst-case weeks, optimal mix n°3)

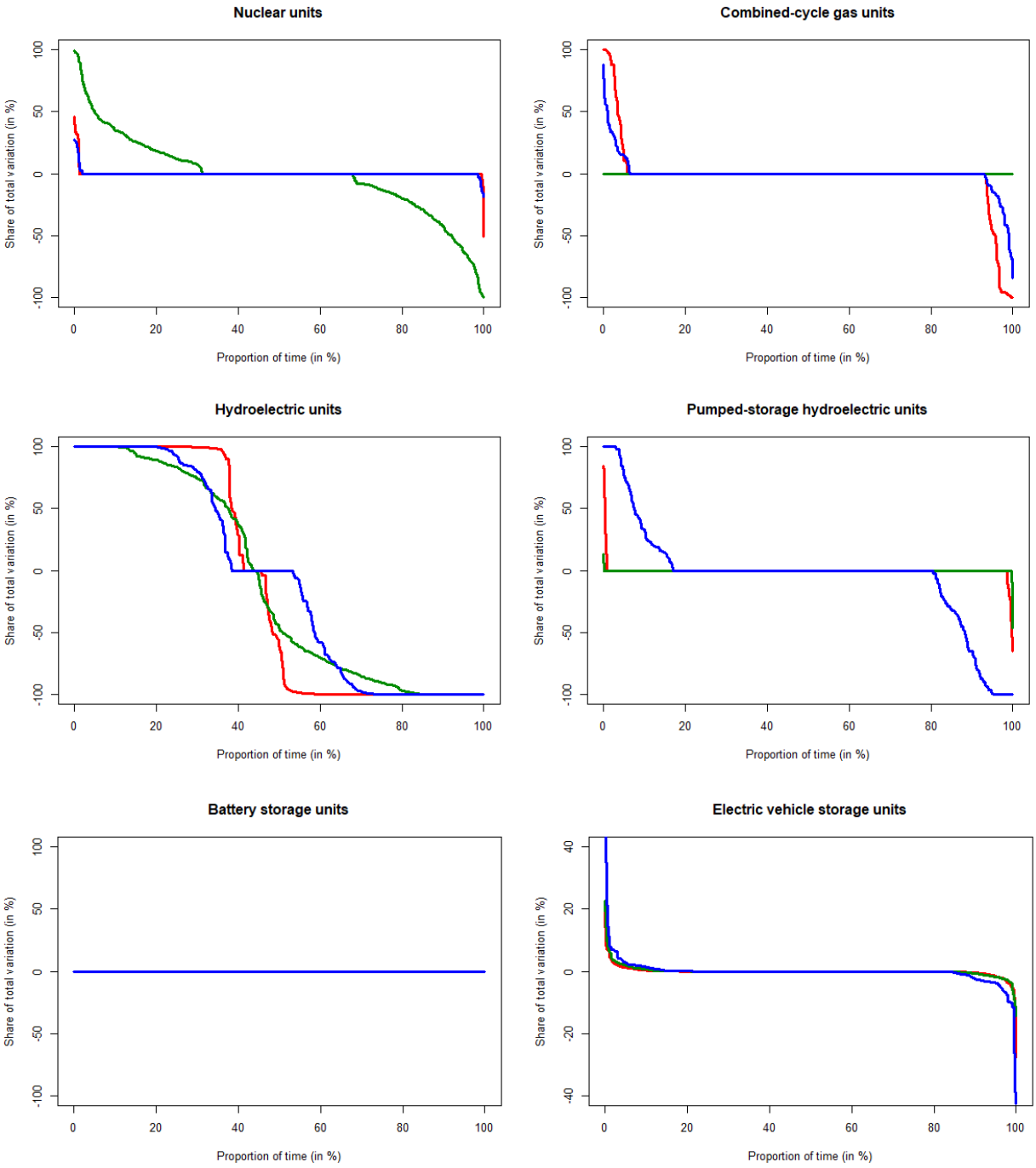

Figure 8.C.: Share in total variation by technology (worst-case weeks, optimal mix n°3)

As expected by comparing optimal mixes n°4 and n°2, **Figures 7.D** and **8.D** show the absolute hourly variation of nuclear output under partial phase out remains quite low on average, even under significant RES penetration (80 MWh and 201 MWh in **L** and **V**). Related to average nuclear generation (6963 MWh), this corresponds to at most 5.8% of the whole production range over the minimum threshold. By comparison and with an average generation of 7681 MWh, the mean nuclear variation with mix n°2 equals 7.5% of the available production range. Our findings thus confirm the intuition that diminishing must-run nuclear capacities allows accommodating larger shares of RES. Moreover, as nuclear load-following operations resulting from RES priority dispatch may reduce its average load factor, maintaining a large nuclear capacity under significant RES penetration may increase average nuclear generation costs. Accordingly, decreasing nuclear capacity at the same pace that RES capacity grows might help keeping nuclear unit generation costs low, by maintaining high average load factors.

However, as shown by [27], the number of extreme nuclear power ramps and amplitude variations, as well as the annually required total start-ups and shutdowns, increase with RES penetration and even with partial nuclear phase out. They find that beyond a 30% share of photovoltaic and wind in the mix, nuclear may not technically face load-following requirements without additional flexibility options. As pointed by the authors, this entails a trade-off regarding the French energy transition by 2030: either partially phasing out nuclear capacity to target a ‘baseload’ operating mode, which entails a higher share of fossil-fuel units in the mix, or maintaining a high nuclear capacity with more frequent load-following operations and lower load factors. Again, Auvergne-Rhône-Alpes is a very specific case as its large hydroelectric capacities allow accommodating large shares of RES generation without changing nuclear operating mode. However, consistently with the authors’ findings, a large fraction of decommissioned nuclear is replaced by CCGT in ‘baseload’ operations, while the latter also increasingly contributes to system balancing operations under higher RES penetration. We further note that more volatile RD increases the total annual number of start-ups and shutdowns for peaking units, which is likely to significantly increase operational costs and carbon emissions due to ignition.

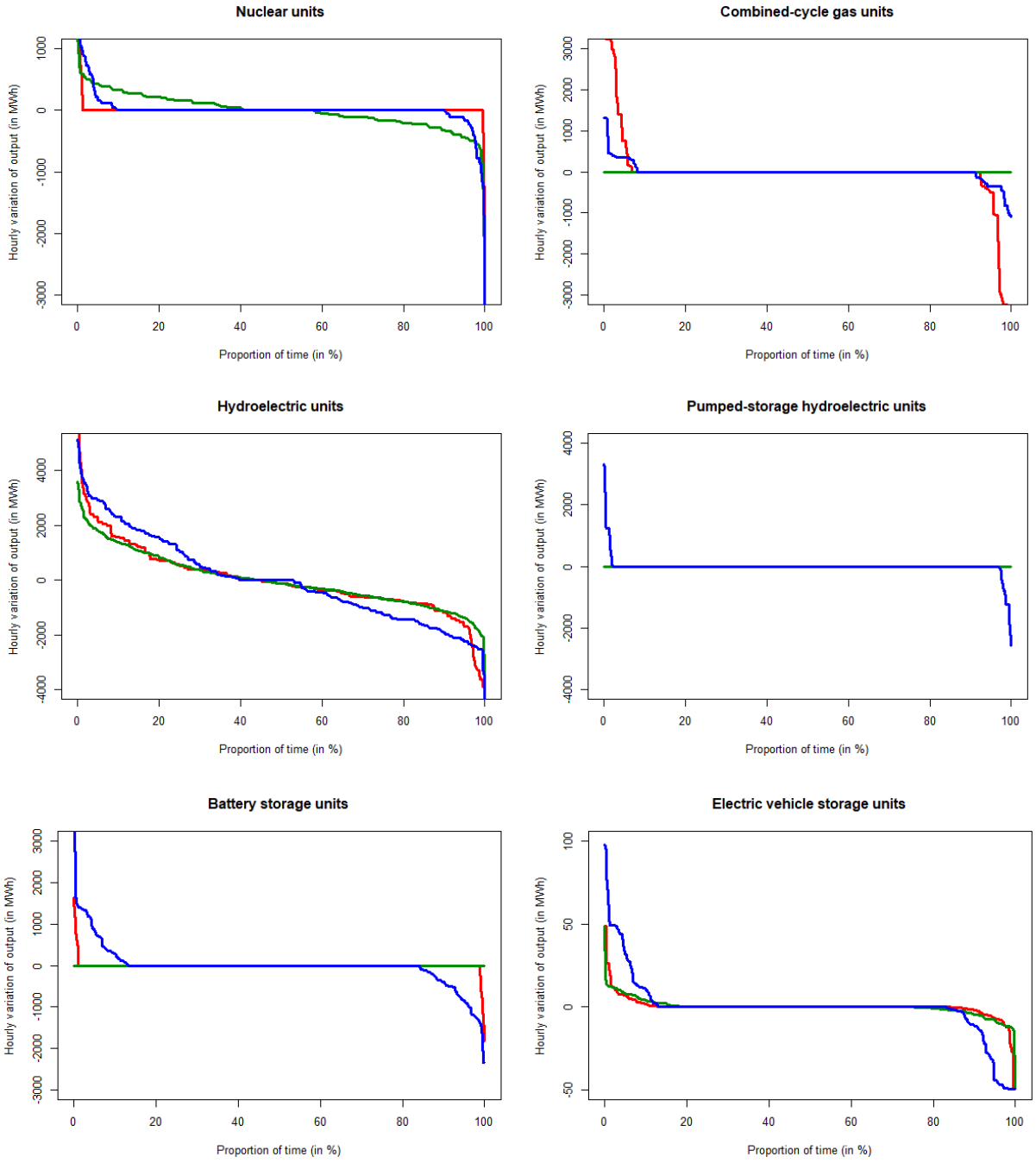

Figure 7.D.: Hourly output variation in MWh, by technology (worst-case week, optimal mix n°4)

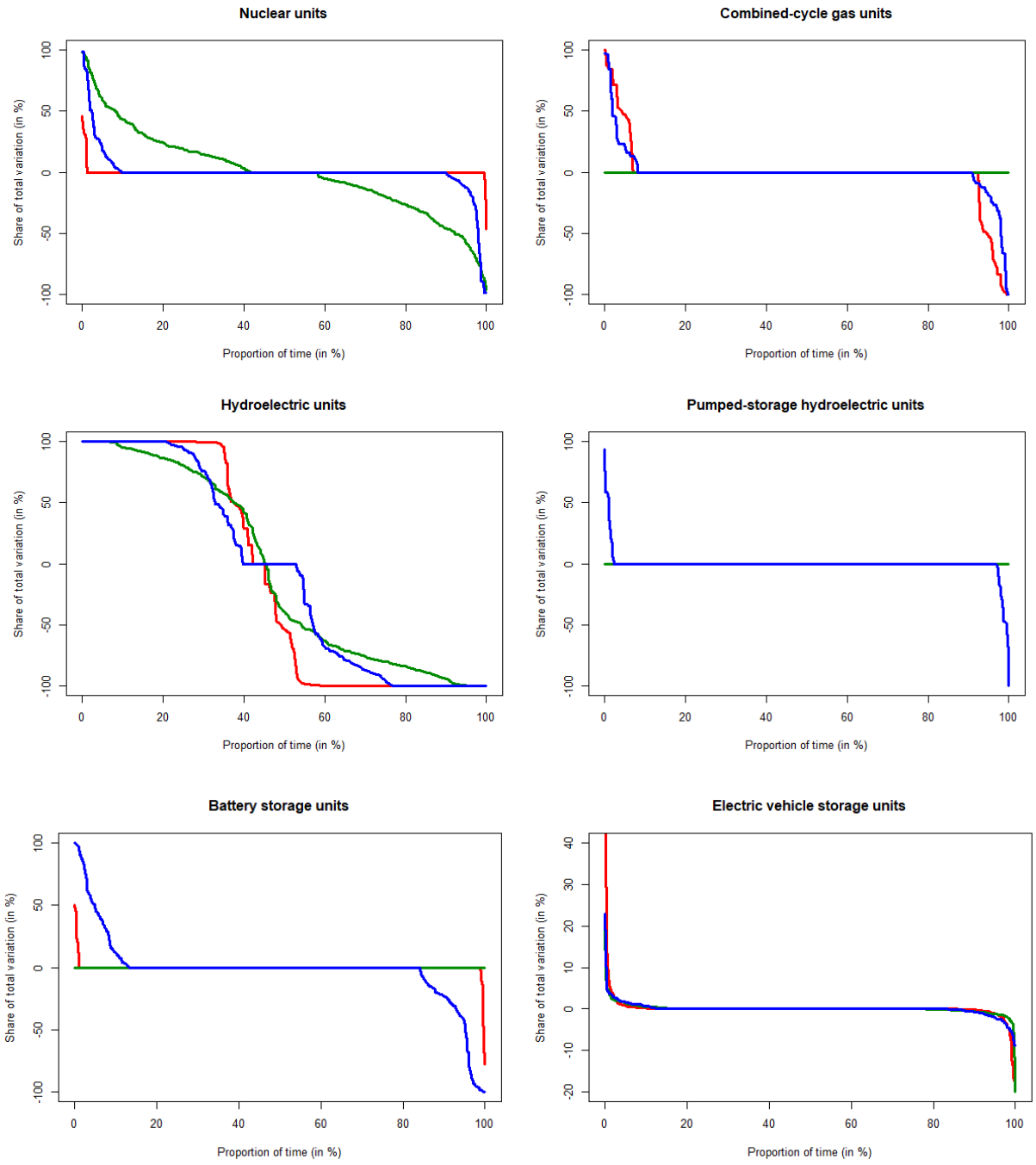

Figure 8.D.: Share in total variation by technology (worst-case weeks, optimal mix n°4)

Under reduced renewables investment and FOM costs, wind and photovoltaic in mix n°2 and n°4 account for a significant share of installed capacities, with 28% and 21% respectively. Although these moderate levels of RES penetration increase flexibility requirements for other generation units, solar and wind generation remain relatively low contributors to total residual load volatility.

Because of their lack of dispatchability and intermittent nature, renewables are generally considered in the literature as the main source of gaps between electricity demand and supply. This approach implicitly considers that load variations are exogenous and "socially" acceptable, in the sense that supply must match demand in real time except when system security requires activation of reserves. Under this paradigm, renewables are criticized as the dynamic pattern of their resources hardly match the dynamics of load. Demand side management (DSM) does not question this paradigm, although it may help controlling demand to match real-time supply, using available resources more efficiently and can even account for resource-constraints in supply (see [28]). However, even under moderate RES penetration levels (between 20% and 30%), we find electricity demand is actually the main contributor to residual load volatility.

Providing an objective measurement of the contribution of each RD component to its total instability is difficult. Indeed, any RD component may contribute to system stability or instability conditionally on how it varies relatively to remaining components. For instance, if renewable generation varies in the same direction than electricity demand, it amplifies RD variations so both electricity demand and renewable generation contribute to increasing system instability. On the contrary, if renewable generation varies in the opposite direction to electricity demand and contributes to lower the absolute RD variation, renewable generation is said to help maintaining system balance.

Using notations given in Appendix, we formally define the total RD variation between $t \in \mathcal{T}$ and $t-1 \in \mathcal{T}$ as follows (we neglect the index for seasons):

$$\Delta\boldsymbol{\xi}_t^{\mathfrak{p}} = \left(\xi_{1t}^{\mathfrak{p}} - \sum_{j>1} \xi_{jt}^{\mathfrak{p}} U_j\right) - \left(\xi_{1t-1}^{\mathfrak{p}} - \sum_{j>1} \xi_{jt-1}^{\mathfrak{p}} U_j\right) = \Delta\xi_{1t}^{\mathfrak{p}} - \sum_{j>1} \Delta\xi_{jt}^{\mathfrak{p}} U_j \qquad (\mathbf{35})$$

Then, we can define the RD variation that would have been observed if the variation of demand was null. Formally, this counterfactual residual demand variation can be expressed as:

$$\Delta\boldsymbol{\xi}_t^{\mathrm{p}D} = \sum_{j>1} \Delta\xi_{jt}^{\mathrm{p}} U_j \tag{36a}$$

Similarly, for any subset $\mathcal{W} \subset \mathcal{J}$ and $\mathcal{P} \subset \mathcal{J}$, we can define the corresponding counterfactual RD variations:

$$\Delta\boldsymbol{\xi}_t^{\mathrm{p}\mathcal{W}} = \Delta\xi_{1t}^{\mathrm{p}} - \sum_{j\in\mathcal{P}} \Delta\xi_{jt}^{\mathrm{p}} U_j \tag{36b}$$

$$\Delta\boldsymbol{\xi}_t^{\mathrm{p}\mathcal{P}} = \Delta\xi_{1t}^{\mathrm{p}} - \sum_{j\in\mathcal{W}} \Delta\xi_{jt}^{\mathrm{p}} U_j \tag{36c}$$

Finally, we introduce a new "stability" metric indicating to which extend each RD component contributes to system balance or imbalance. Intuitively, if any RD component varies in the opposite direction from remaining components but increases total absolute RD variation, such behavior must be captured by our metric as contributing to system instability. Formally, the "stability" metrics respectively associated to electricity demand, wind power generation and photovoltaic generation in $t \in \mathcal{T}$ are defined as:

$$L_t^{\mathrm{p}D} = \frac{1 - e^{-\Delta\xi_t^{\mathrm{p}}\left(\Delta\xi_t^{\mathrm{p}D}\right)^{-1}}}{1 + e^{-\Delta\xi_t^{\mathrm{p}}\left(\Delta\xi_t^{\mathrm{p}D}\right)^{-1}}} \tag{37a}$$

$$L_t^{\mathrm{p}\mathcal{W}} = \frac{1 - e^{-\Delta\xi_t^{\mathrm{p}}\left(\Delta\xi_t^{\mathrm{p}\mathcal{W}}\right)^{-1}}}{1 + e^{-\Delta\xi_t^{\mathrm{p}}\left(\Delta\xi_t^{\mathrm{p}\mathcal{W}}\right)^{-1}}} \tag{37b}$$

$$L_t^{\mathrm{p}\mathcal{P}} = \frac{1 - e^{-\Delta\xi_t^{\mathrm{p}}\left(\Delta\xi_t^{\mathrm{p}\mathcal{P}}\right)^{-1}}}{1 + e^{-\Delta\xi_t^{\mathrm{p}}\left(\Delta\xi_t^{\mathrm{p}\mathcal{P}}\right)^{-1}}} \tag{37c}$$

It is straightforward to see that for any value $\Delta\boldsymbol{\xi}_t^{\mathrm{p}}\left(\Delta\boldsymbol{\xi}_t^{\mathrm{p}D}\right)^{-1} \in \mathbb{R}$, we have $-1 \leq L_t^{\mathrm{p}D} \leq 1$. The same remark applies to both metrics $L_t^{\mathrm{p}\mathcal{W}}$ and $L_t^{\mathrm{p}\mathcal{P}}$. Taking the example of electricity demand, four cases can be distinguished for the description of each "stability" metric:

- $\Delta\boldsymbol{\xi}_t^{\mathrm{p}}\left(\Delta\boldsymbol{\xi}_t^{\mathrm{p}D}\right)^{-1} > 1$: Electricity demand variations amplify RD instabilities and contribute to "additive" system instability. In this case, the "stability" metric associated to electricity demand verifies $L_t^{\mathrm{p}D} > \frac{e-1}{1+e}$.

- $0 \leq \Delta\boldsymbol{\xi}_t^{\mathfrak{p}} \left(\Delta\boldsymbol{\xi}_t^{\mathfrak{p}^D}\right)^{-1} \leq 1$: Electricity demand mitigates total RD variations without changing the sign of $\Delta\boldsymbol{\xi}_t^{\mathfrak{p}}$. It contributes to "additive" system stability and its metric verifies $0 \leq L_t^{\mathfrak{p}^D} \leq \frac{e-1}{1+e}$.
- $0 \geq \Delta\boldsymbol{\xi}_t^{\mathfrak{p}} \left(\Delta\boldsymbol{\xi}_t^{\mathfrak{p}^D}\right)^{-1} \geq -1$: Electricity demand mitigates total RD variations and changes the sign of $\Delta\boldsymbol{\xi}_t^{\mathfrak{p}}$. We say it contributes to "subtractive" system stability and its metric verifies $0 \geq L_t^{\mathfrak{p}^D} \geq \frac{1-e}{1+e}$.
- $\Delta\boldsymbol{\xi}_t^{\mathfrak{p}} \left(\Delta\boldsymbol{\xi}_t^{\mathfrak{p}^D}\right)^{-1} < -1$: Electricity demand variations are superior in absolute terms to renewable generation variation and move in the opposite direction. They contribute to "subtractive" system instability and their metric verifies $L_t^{\mathfrak{p}^D} < \frac{1-e}{1+e}$.

The same four cases and thresholds apply to the "stability" metrics associated to wind generation $L_t^{\mathfrak{p}^{\mathcal{W}}}$ and photovoltaic generation $L_t^{\mathfrak{p}^{\mathcal{P}}}$. For each metric, the distance with respect to the origin is proportional to the contribution to total residual load instability. To give some orders of magnitude, $L_t^{\mathfrak{p}^D} \approx 0.75$ indicates demand correspond to 50% of total residual load variations, or alternatively, amplifies RES generation volatility by a factor 2. $L_t^{\mathfrak{p}^D} \approx 0.9$ and $L_t^{\mathfrak{p}^D} \approx 0.96$ correspond to 66% and 75% shares in total "upward" RD volatility, while $L_t^{\mathfrak{p}^D} = 1$ indicates all RD variation is caused by electric load fluctuations. Negative values of $L_t^{\mathfrak{p}^D}$ provide a different picture, as for $L_t^{\mathfrak{p}^D} < \frac{1-e}{1+e}$, electricity demand moves in the opposite direction from RES generation and is greater in absolute terms. In this case, we interpret $L_t^{\mathfrak{p}^D} \approx -0.75$ as the fact that residual load variability would be twice smaller without electric load variations and would change sign. For instance, if $\Delta\boldsymbol{\xi}_t^{\mathfrak{p}} < 0$, this indicates stabilizing demand would yield a higher but less volatile RD volume addressed to the grid.

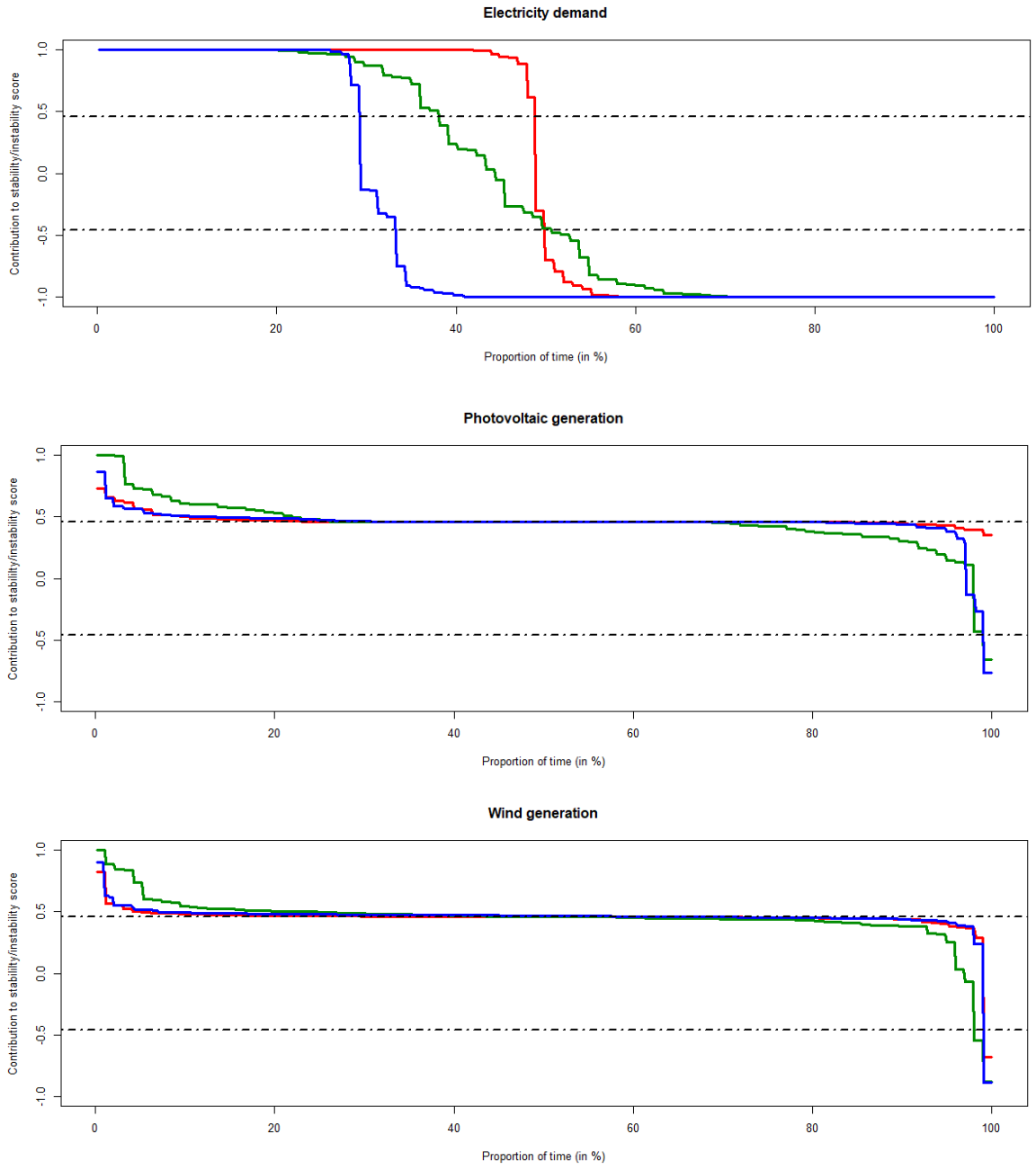

Figure 9.A.: Residual demand components contribution to system stability/instability (worst-case weeks, optimal mix n°1)

Note: The upper and lower black dotted lines respectively correspond to the threshold values $\frac{e-1}{2+2e}$ and $\frac{1-e}{2+2e}$. The above graphs read as follows: for instance, taking the case of worst-case **L**, photovoltaic generation contributes to moderate "upward" system instability in approximately 25% of operating hours, while it brings "upward" system stability almost 20% of time.

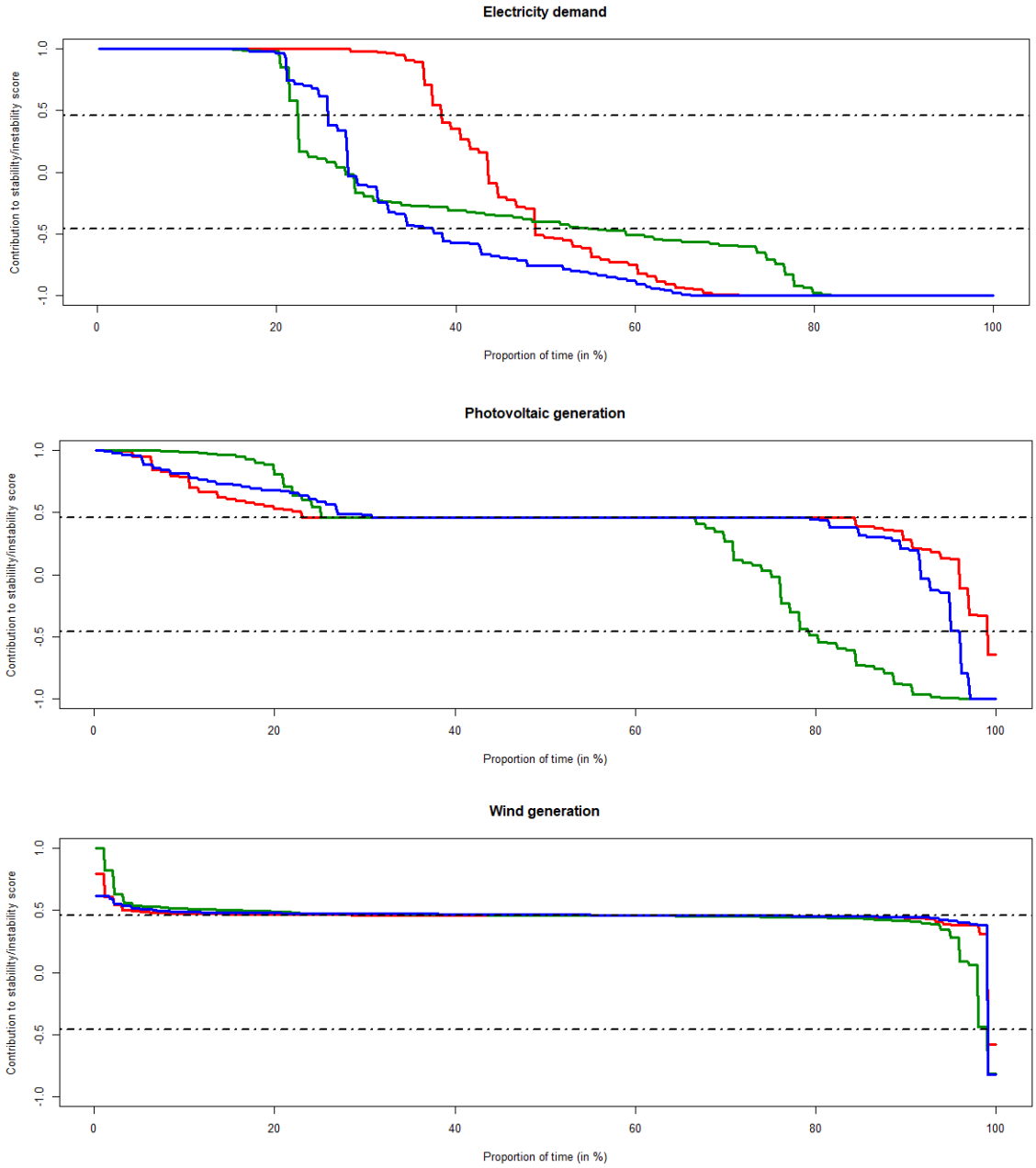

Figure 9.B.: Residual demand components contribution to system stability/instability (worst-case weeks, optimal mix n°2)

As shown in **Figure 9.A.**, electric load is the main contributor to system instability for all worst-case situations. It is almost the sole contributor to "additive" and "subtractive" system instability in respectively 40% and 45% of operating hours. While the effect of demand on both types of stability is quite uniformly distributed in **H**, we notice demand fluctuations annihilate RES output variations in **V** in more than 65% of hours, which could equivalently indicate RES generation is too low to compensate demand fluctuations during episodes of extreme residual load variability. Photovoltaic and wind generation both moderately amplify residual load fluctuations in all cases for roughly 35% of operating hours, and have no effect or a stabilizing effect the remaining time.

With 28% of RES in total installed capacities, clearly dominated by photovoltaic capacity (27%), residual load fluctuations in mix n°2 remain mostly driven by electric load variations. **Figure 9.B.** shows that demand still accounts for 100% of "additive" and "subtractive" system instability in more than 65% of all operating hours. However, contrary to mix n°1, electricity demand mitigates residual load fluctuations in **L**, mainly driven by photovoltaic dynamics, during approximately 40% of time.

Quite surprisingly, solar generation fluctuations drive total residual load variations during a very small fraction of time. $L_t^{\mathfrak{p}\mathcal{P}}$ is above 0.99 only 5% of all operating hours, meaning situations where photovoltaic generation is the only source of instability are quite rare. Moreover, $L_t^{\mathfrak{p}\mathcal{P}}$ is comprised between -0.75 and 0.75 for approximately 75% of operating hours, meaning in contributes to less than two thirds of total variations most of the time. The average absolute value of $L_t^{\mathfrak{p}D}$ in **H**, **L** and **V** respectively equals 0.86, 0.66 and 0.83. By comparison, the mean absolute value of $L_t^{\mathfrak{p}\mathcal{P}}$ is found equal to 0.49, 0.62 and 0.54. Although photovoltaic generation contributes, on average, to amplifying electric load fluctuations, demand remains the major contributor to RD instability even under significant RES penetration.

Most of the above conclusions apply to results in **Figure 9. C..** With more than 4 GWe of installed capacity in optimal mix n°3, wind power contributes to "additive" instability above 20% of operating hours. However, a careful analysis shows it contributes to more than 66% of total fluctuations less than 5% of hours in **H** and **V** and 15% in **L**. Moreover, wind generation mostly contributes to "additive" system stability in more than 40% of worst-case hours on average. Overall, this suggests wind turbines possess the technical ability to provide ancillary

services to the grid, although traditionally not allowed to provide such services. As evidenced by **Rebello et al. (2020)**, commercially available wind turbines may provide ancillary services and participate in the regulation market with gains larger that the energy income loss due to curtailment.

Finally, **Figure 9.D.** provides very similar results to those obtained for optimal mix n°2. Overall, it appears that even with moderate RES penetration in the electricity mix, electric load remains the major contributor of residual demand instability that must be addressed by the generation system. We note that partial nuclear phase out, lowering the share of synchronous generation units in the mix, and increasing RES penetration together participate to decrease the system inertia.

It suggests that DSM and shifting of electricity usages (technically and socially feasible), to periods with high generation resource availability, would efficiently participate to decrease flexibility requirements and thermal stress on both load-following and peaking units.

A more stable electric load would indeed diminish the requirements for fast-ramping generation units as well as the number of start-up and shut-down operations during extreme situations, thus contributing to decrease the average generation cost. Moreover, proper pricing of demand fluctuations in terms of ancillary service cost may be considered in addition to a time-varying price equal to supply instantaneous marginal cost to achieve social optimality (see [29]). However, from an operational perspective, a distinction should be made between residual load components based on the level of uncertainty associated to their respective forecasts. Short-term wind power fluctuations may exhibit less predictable dynamics, although wind generation forecasting errors approach the performances of demand forecasting (see [30] for a comprehensive review of state-of-the-art wind forecasting methods). Moreover, stabilizing electric load might release flexible plants from load-following operations and make them available to for the management of renewable generation, thus decreasing the volume of additional investments in CCGT and storage units to accommodate higher RES shares. Finally, a closer management of demand fluctuations would be consistent with keeping nuclear in ‘baseload’ operation mode, even under increasing RES penetration. We leave these remarks for further research.

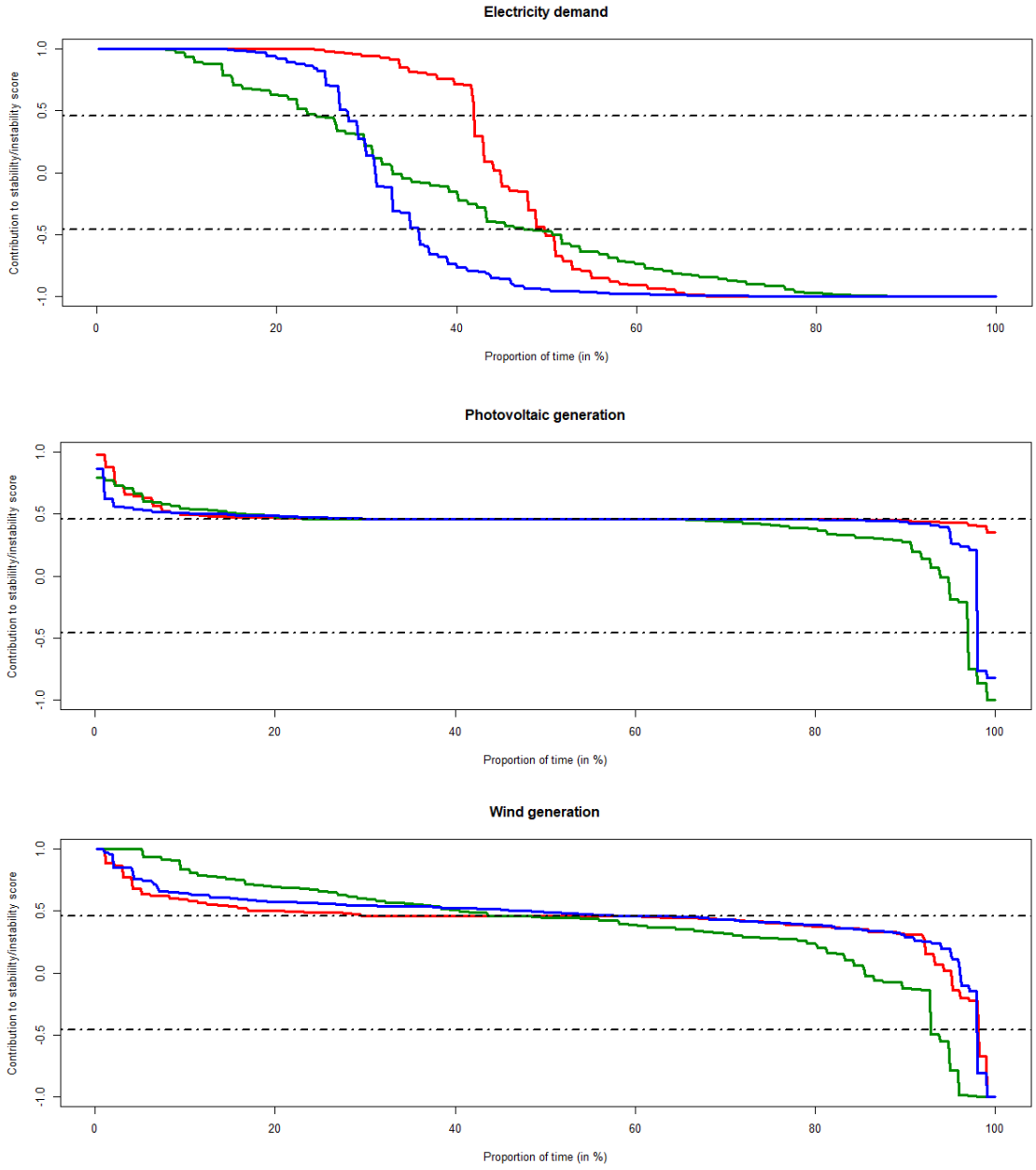

Figure 9.C.: Residual demand components contribution to system stability/instability (worst-case weeks, optimal mix n°3)

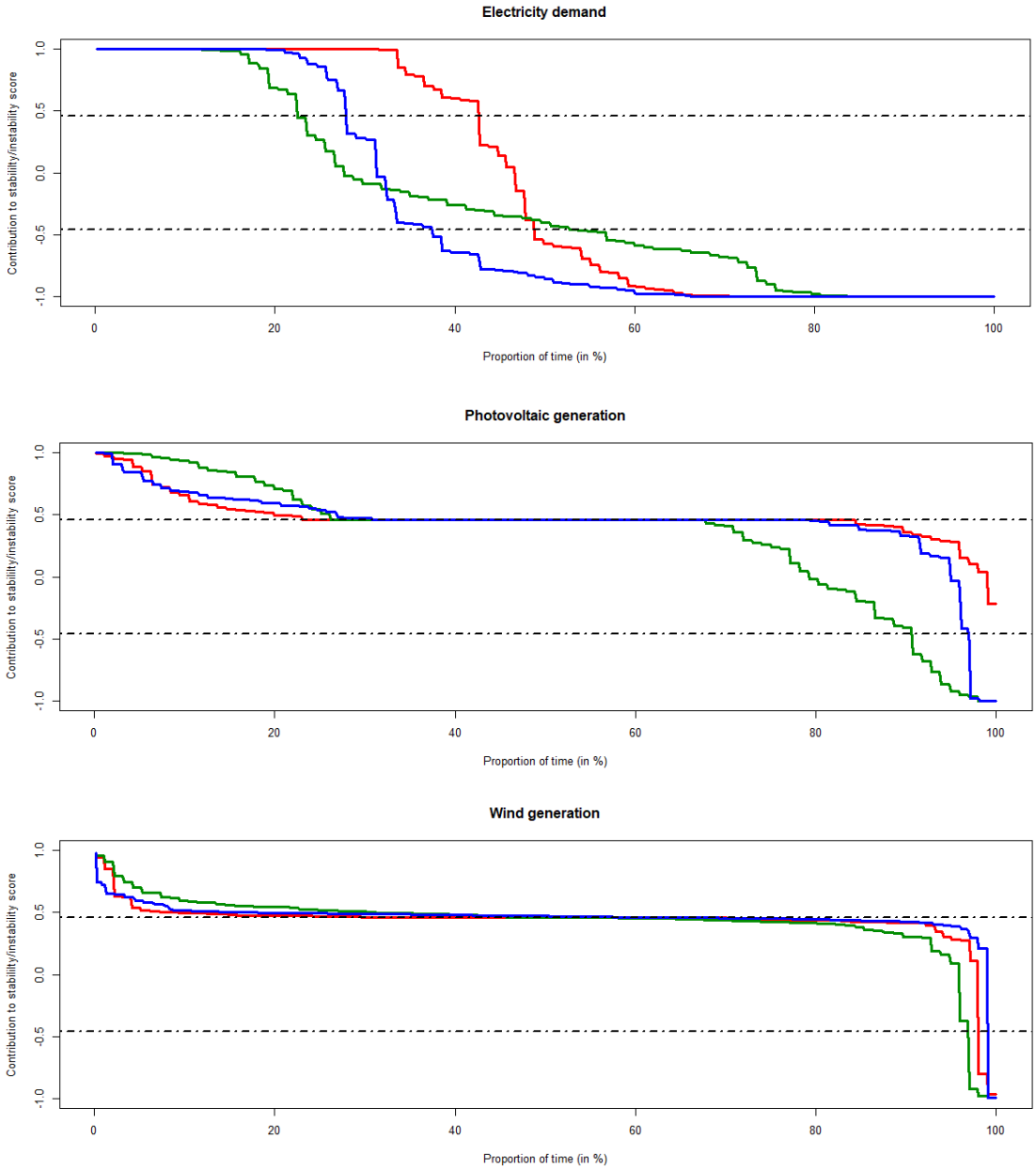

Figure 9.D.: Residual demand components contribution to system stability/instability (worst-case weeks, optimal mix n°4)

4.1.3. Operational cost and spot price profile

As demand goes up, increasingly expensive generation units must be added to the optimal dispatch following the implementation of the "merit-order rule". Subsequently, the worst-case week **H** is characterized by higher average generation costs, while **L** has the lowest generation cost thanks to larger shares of renewable production injected at zero marginal cost. However, a thorough comparison of the costs associated to each optimal mix yields some valuable insights about the effects of partial nuclear phase out.

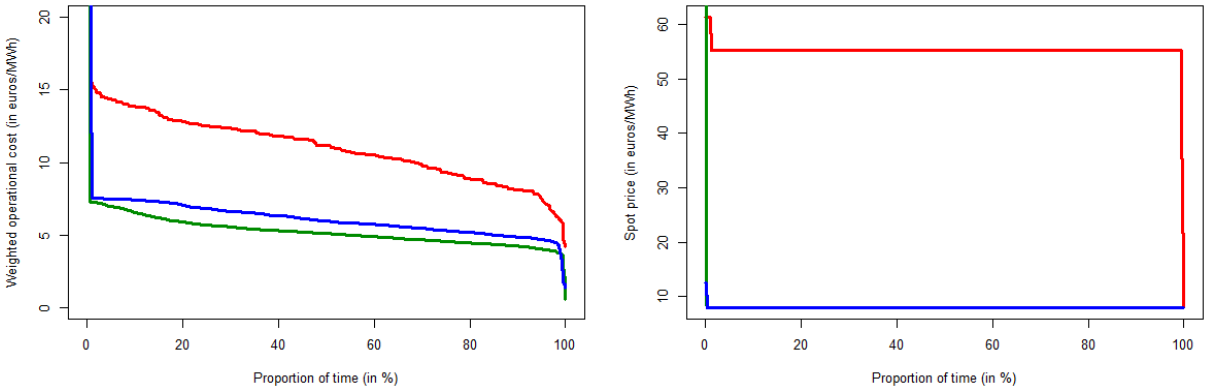

Figure 10.A..: Weighted operational cost and spot price distributions (worst-case weeks,, optimal mix n°1)

Even under extremely high residual load situations, corresponding to **H**, the average weighted operational cost for mix n°1 remains below 11.5 €/MWh, while it falls to 6.63 €/MWh and 6.02 €/MWh in **V** and **L**. The comparison with the distribution of spot prices show that, except for a small fraction of operating hours (less than 0.3%), the market spot price is equal to nuclear marginal costs in **L** and **V** and to CCGT marginal costs (approximately 61 €/MWh) in **H**.

The comparison with **Figure 10.B.** shows that even in high renewable generation periods, corresponding to **L**, spot prices are now equal to CCGT marginal cost in more than 20% of operating hours, while the average weighted operational cost decreases by 37%. The average spot price of electricity increases while its weighted generation cost decreases. Finally, we note the occurrence of negative prices between -5.7 €/MWh and -100 €/MWh in 1.5% of hours.

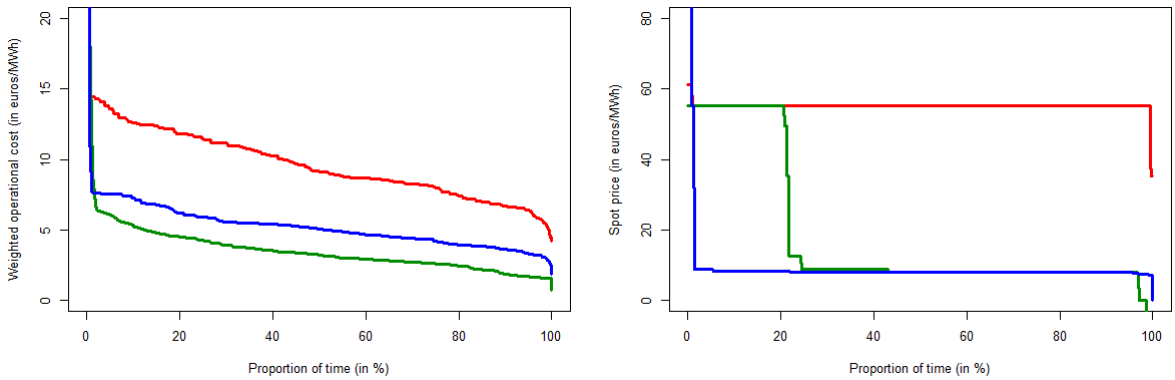

Figure 10.B..: Weighted operational cost and spot price distributions (worst-case weeks, optimal mix n°2)

Partially phasing out nuclear with low replacement investments in RES leads to significant increases in average generation costs and electricity price. The average weighted operational cost increases to 20.1 €/MWh in **H** and 7.75 €/MWh in **V**, while it decreases to 3.81 €/MWh in **L**. **Figure 10.C.** shows the spot market reaches the VOLL (which may be replaced by the +3000 €/MWh price cap legally imposed on the French EPEX SPOT) in **H** for approximately 25% of operating hours. We may consider spot price as a proxy for reserve scarcity, which indicates that even under a robust optimization strategy, the operational reserves in **H** are quasi-null for a quarter of hours. In case of unforeseen residual demand variation or plant failure, the market operator is forced to proceed to load shedding. This suggests minimum reserve constraints should be added to our robust framework, even though it is tailored to respect the French security of supply criterion.

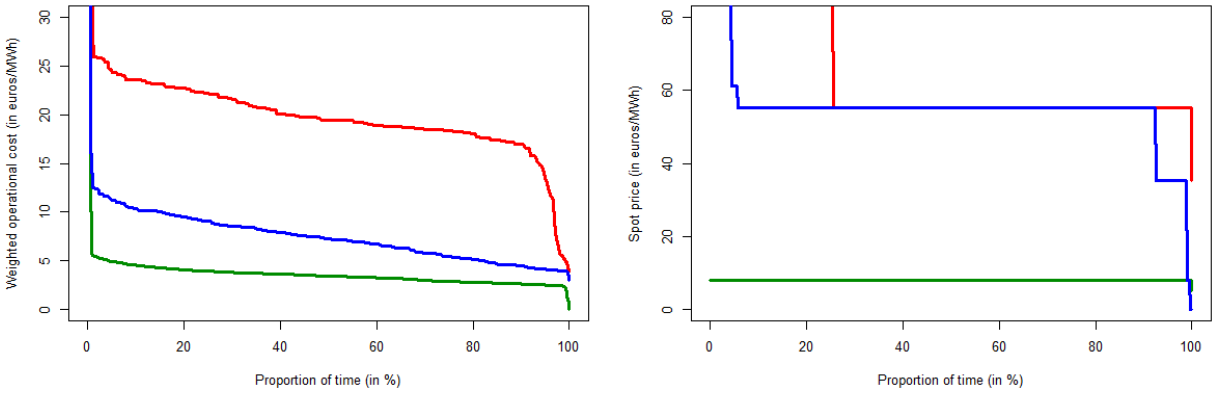

Figure 10.C..: Weighted operational cost and spot price distributions (worst-case weeks, optimal mix n°3)

Increasing the share of renewables in optimal mix n°4 helps suppressing scarcity events by restoring sufficient reserves. By comparison with mix n°3, **Figure 10.D.** shows a 1% lower average weighted operational cost in **V**, while the average spot price distribution is slightly modified: while its average value decreases by 19%, the occurrence probability of spot prices above 60 €/MWh is multiplied by more than 3 (20.4% against 5.7% of hours for mix n°3)

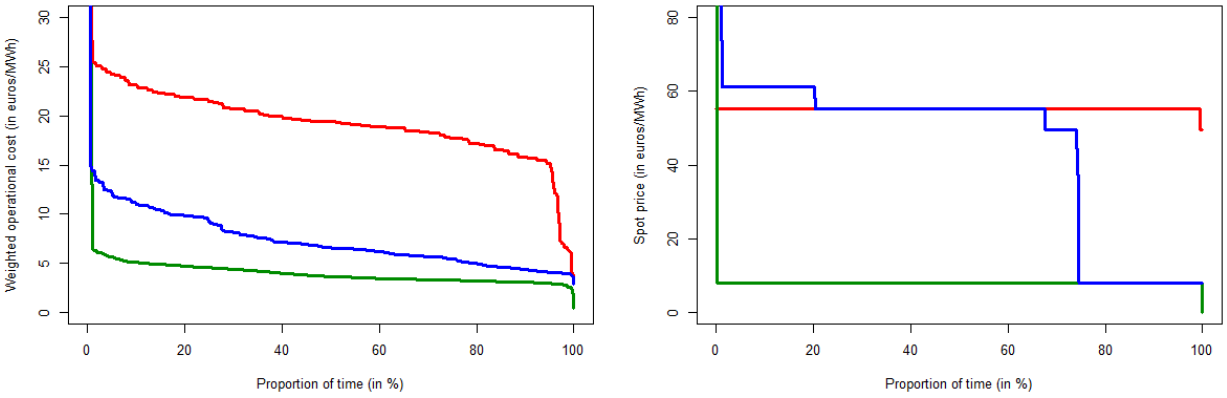

Figure 10.D..: Weighted operational cost and spot price distributions (worst-case weeks, optimal mix n°4)

Overall, the partial phase out of nuclear entails a moderate increase in worst-case weighted operational costs, expect for high residual load week **H** where we note an almost 100% increase. Yet, the average spot price significantly increases (except in **L**), which translates the increasing participation of CCGT units with high marginal costs to 'baseload' generation and load-following operations with more frequent start-ups and shut downs under higher RES penetration in mix n°4.

4.2. Representative weeks performances

Having investigated the behavior of a regional mix with partially phased out nuclear under extreme operational conditions, we now analyze how each type of technology operates in representative conditions. In addition to measuring how increasing RES penetration and partial nuclear phase out impact energy contribution and utilization of all units, we compute

the distribution of carbon emissions and carbon intensity associated to each of the selected optimal mixes.

4.2.1. Energy contribution and utilization rates

With a mean production of 8.903 GWh, **Figure 11.A.** shows a 73% average nuclear participation in the electricity production in mix n°1, with a quite stable share between 60% and 80% more than 80% of operating hours. With an average utilization rate at about 66%, nuclear capacity is under-utilized accounting for its mean annual availability rate of 80%. Hydroelectric maintains a high contribution above 20% for most hours, and significantly participates to covering 'baseload' with an average share of 36%. The participation of CCGT units is clearly restricted to a few hours of the year for balancing operations, with participation sharply increasing over zero for less than 9% of hours.

As more renewable capacity is added in mix n°2, we note from **Figure 11.B.**, that the nuclear mean participation share and utilization rate further decrease to 59% and 55%. As in extremely residual load situations, a large fraction of 'baseload' generation is displaced by renewable generation. Solar power participates on average to 15% of total production, with contributions above 30% in only 20% of all hours however and a low average utilization rate. CCGT utilization declines sharply, with a non-null participation to total output in less than 1% of hours. Our modeling approach of worst-week **H** may thus be overly conservative and overestimate the potential number of consecutive hours with high RD. Hydroelectric generation is also partially replaced by renewables, with an average share falling to 24% although it maintains a 40% participation in 20% of hours. Overall, the electricity mix remains dominated by nuclear generation, followed by a blend of RES and hydroelectric. In both mix n°1 and mix n°2, storage technologies are used only a small fraction of time (less than 20% of hours) and are increasingly used with higher RES penetration.

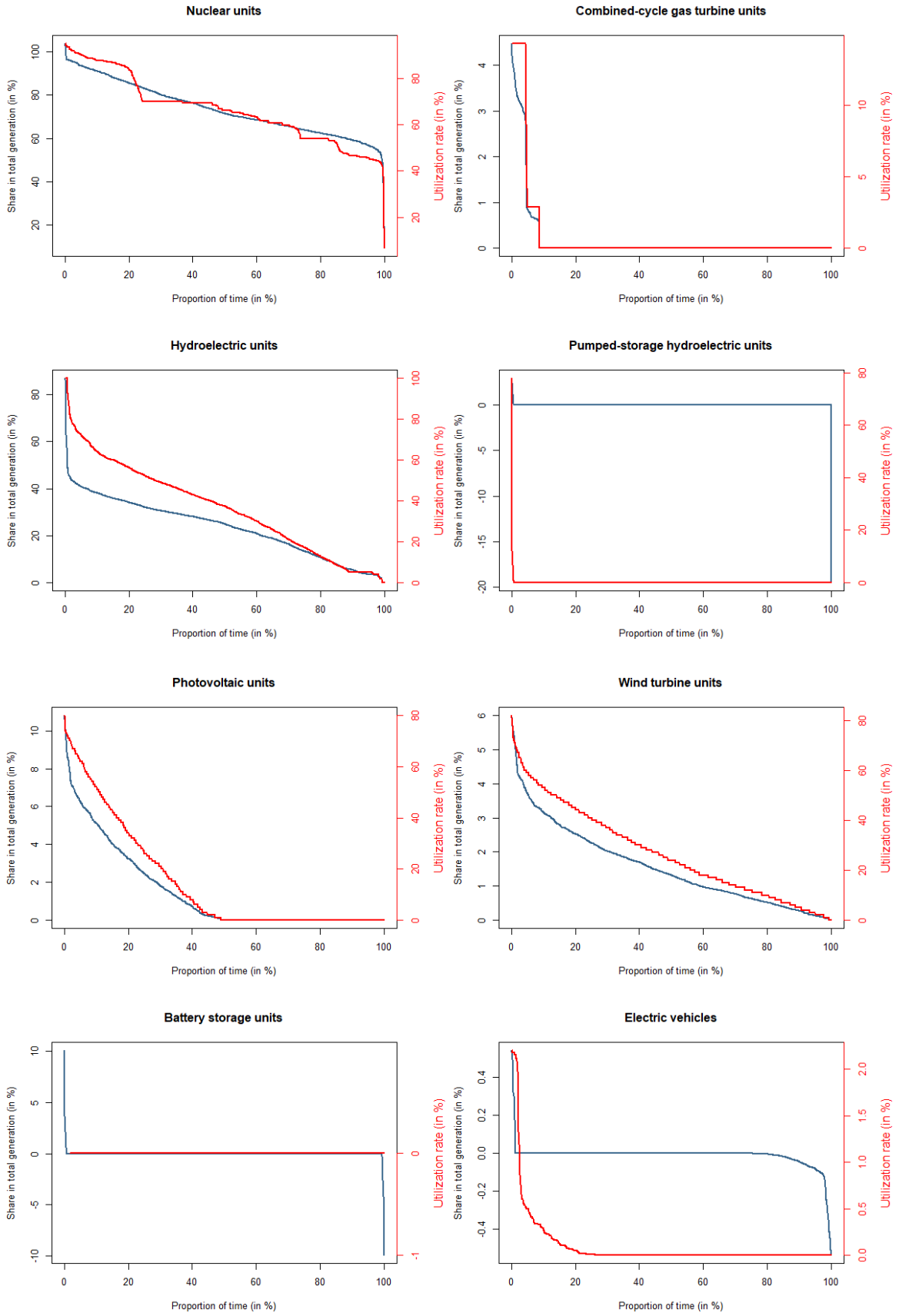

Figure 11.A.: Energy contribution and utilization rate by technology (representative weeks, optimal mix n°1)

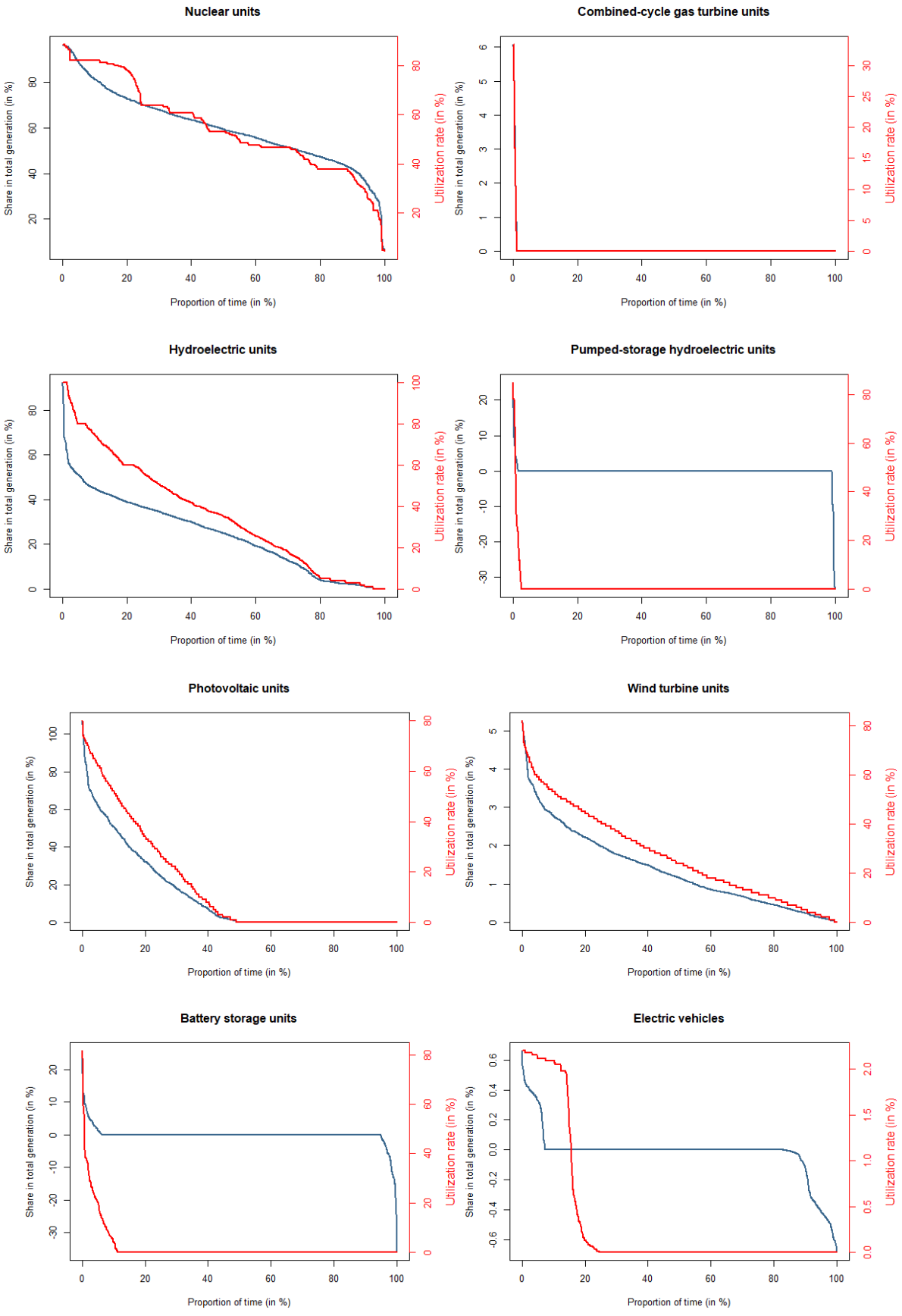

Figure 11.B.: Energy contribution and utilization rate by technology (representative weeks, optimal mix n°2)

By comparison, **Figure 11.C.** shows that nuclear production remains significant even with partial phasing out. It can be observed that while its mean production decreases by almost 17%, its average participation declines to 61%. As expected, the average utilization rate rises from 66% to 75%, which is consistent with the findings of [75]. This amelioration suggests either the initial regional nuclear fleet is over-capacitated, or that 'baseload' operation mode does not allow nuclear to capture the full potential of its large operational range, as load-following operations are traditionally performed by other generation technologies. The participation of CCGT increases sharply with respect to mix n°1, although its utilization rate remains consistently under 30%. A significant share of peaking capacity is thus clearly under-utilized in normal operational conditions. Hydroelectric remains the second largest contributor to total output, with a mean share of 23%, while wind power only contributes 9% on average.

Increasing RES capacity has no effect on the average nuclear participation and utilization rate, which remain stable around 60% and 75%. Interestingly, the decrease in must-run inflexible generation does not increase flexibility requirements even with higher RES penetration. **Figure 11.D.** shows the average CCGT participation remains constant around 4%. Overall, most load-following operations are performed by hydroelectric plants while the contribution of storage and pumped-storage hydroelectric remain small. However, as our model assumes no uncertainty regarding future residual demand values, no unforeseen generation surplus or deficit can occur, which is likely to underestimate the utilization and participation of these units to real-time balancing operations.

Consistent with the literature cited above, our findings show the French energy transition could benefit from phasing out nuclear capacity as new RES generation capacity is added in the mix. Indeed, we find a lower nuclear share in total capacity is associated with a higher and more stable utilizations of generation units. Moreover, the decline in must-run inflexible nuclear generation helps increasing the overall flexibility of the mix, allowing for less frequent use of CCGT for balancing operations when renewable generation is high. However, as pointed above, CCGT remains pivotal for ensuring supply-demand equilibrium when renewable generation is quasi null or when residual load is extremely volatile.

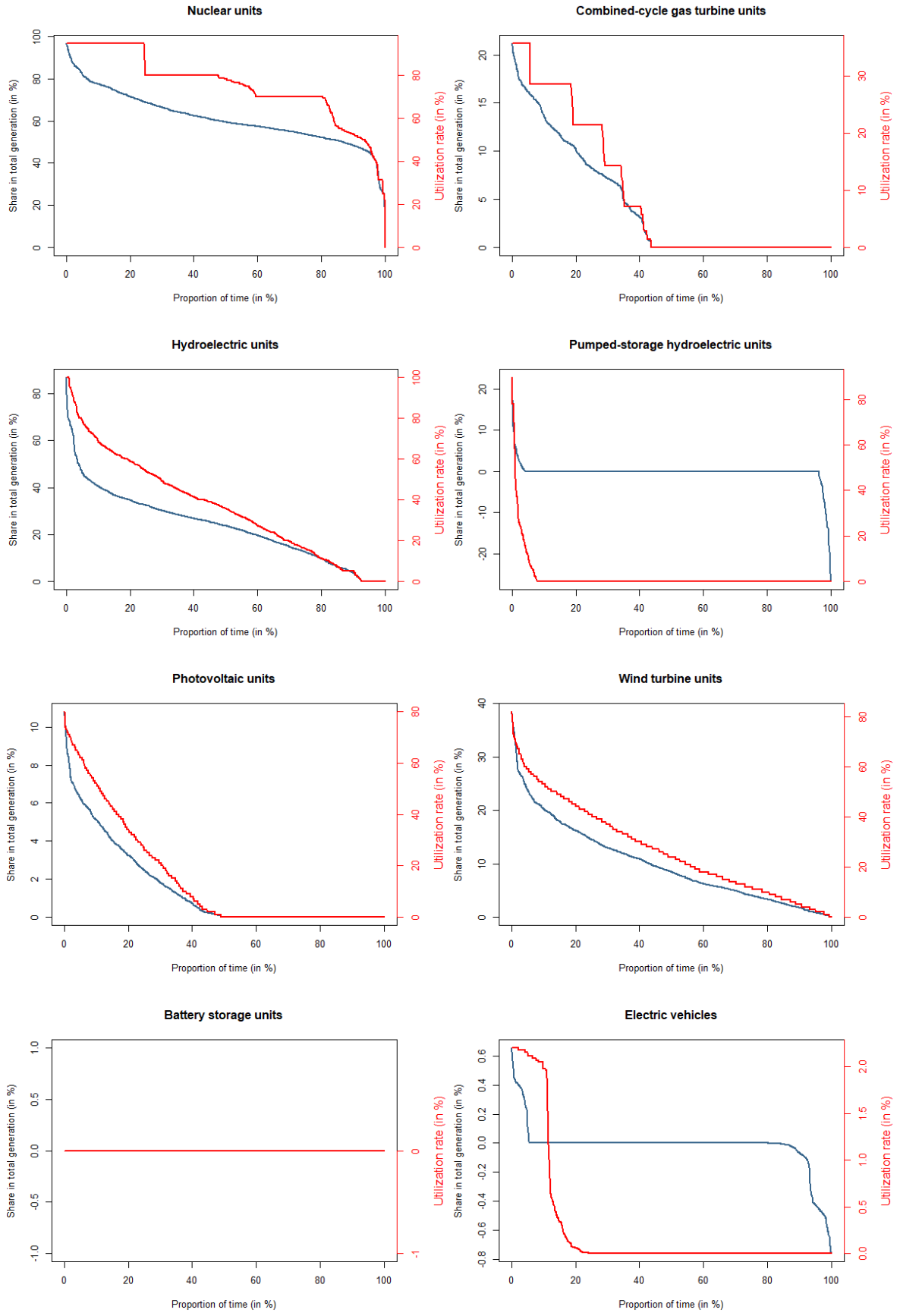

Figure 11.C.: Energy contribution and utilization rate by technology (representative weeks, optimal mix n°3)

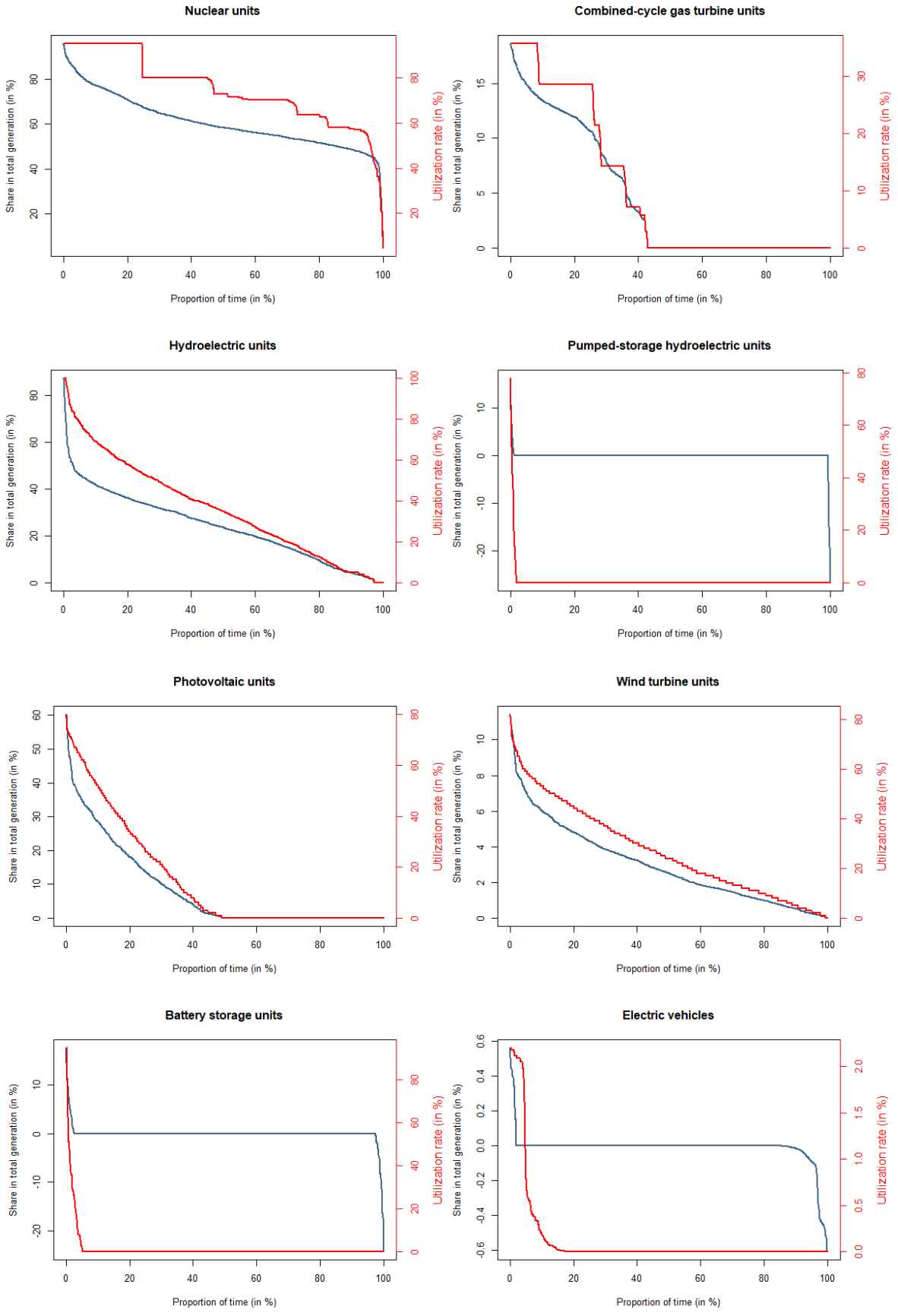

Figure 11.D.: Energy contribution and utilization rate by technology (representative weeks, optimal mix n°4)

4.2.2. Operational cost, spot price and carbon emissions profile

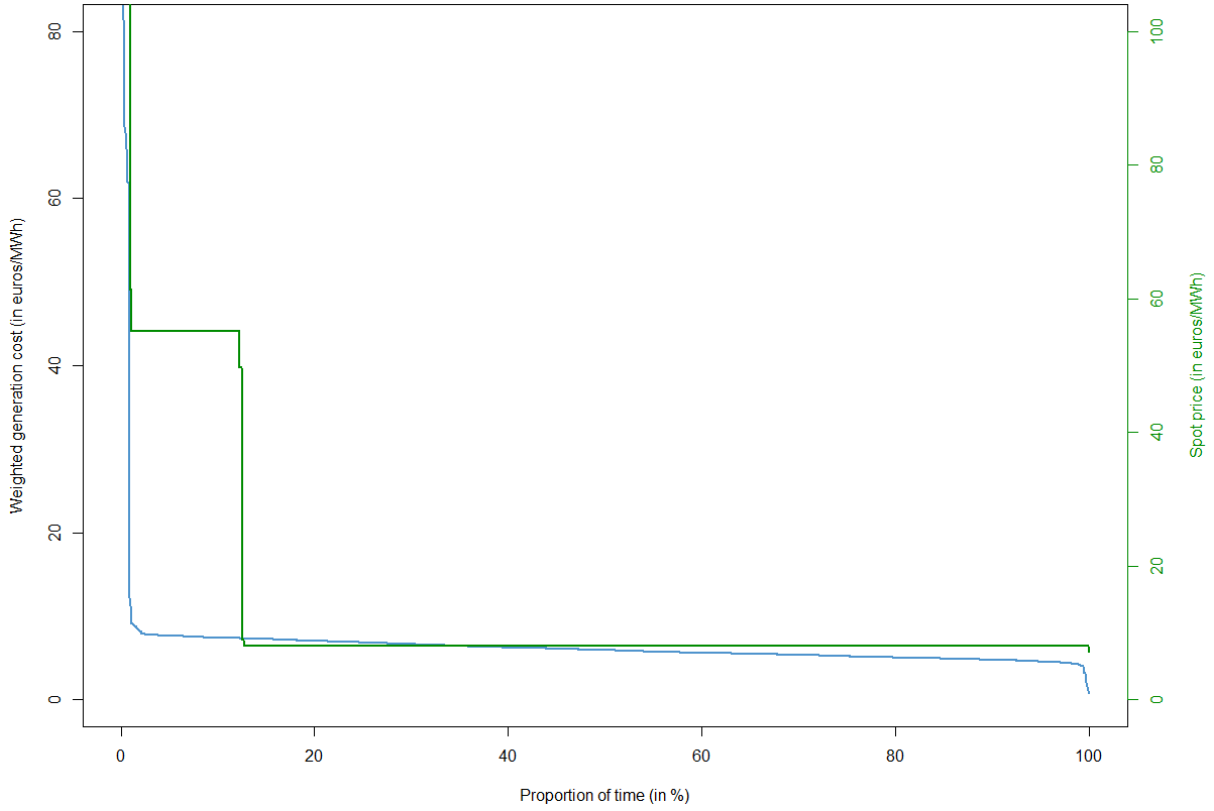

Figure 12.A.: Weighted operational cost and spot price distributions (representative weeks, optimal mix n°1)

Figure 12.A. shows extremely high prices associated to scarcity conditions in less than 1% of operating hours, with spot price lower than 10 €/MWh the remaining time. The average spot price is about 13.5 €/MWh, more than twice the mean weighted generation cost, equal to 5.98 €/MWh.

Under optimal mix n°2, the VOLL is attained in roughly 0.9% of operating hours, indicating a slight amelioration of supply security and system reliability while including higher shares of RES in the electricity mix. Excluding the subset of hours during which spot price equals the VOLL, we find from **Figure 12.B.** that the average value drops to 2.20 €/MWh. This drop is driven by the extremely low participation of CCGT to total output, with spot prices taking values between 2 €/MWh and 10 €/MWh in less than 10% of hours. Finally, the mean weighted generation decreases to 4.82 €/MWh. As expected, with nuclear must-run capacities equal to their initial value, renewable penetration pushes spot prices down.

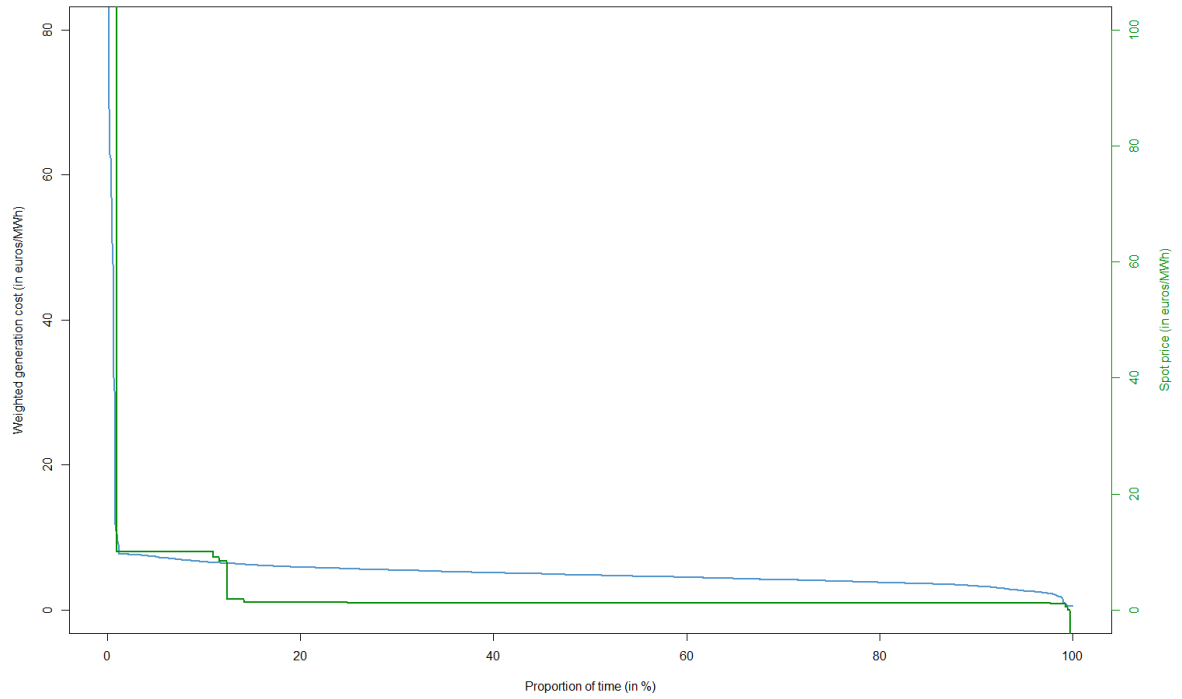

Figure 12.B.: Weighted operational cost and spot price distributions (representative weeks, optimal mix n°2)

Partially phasing out nuclear capacities significantly decreases system reliability, as shown in **Figure 12.C.**, with a VOLL being attained in almost 14% of hours. This is a clear indicator for insufficient security of supply, as no load-shedding occurs in the optimal dispatch. The low CCGT utilization rates suggest capacities are far from being used at maximum capacity and scarcity might thus be addressed by integrating reserve constraints into our model. However, as our optimization model minimizes total dispatching costs, this hints at the sharp increase in operational costs driven by replacing decommissioned nuclear by CCGT in 'baseload' mode, as the model only operates the minimum number of units required to ensure system balance and keeping reserves online might drastically increase operational costs. The rise of average electricity price, equal to 28.2 €/MWh over the subset of spot prices lower than the VOLL, follows from the higher participation of peaking units in 'baseload' operations. While high CCGT marginal costs drive a sharp increase in prices, the significant nuclear energy contribution allows the average weighted generation costs to remain quite low at 6.31 €/MWh.

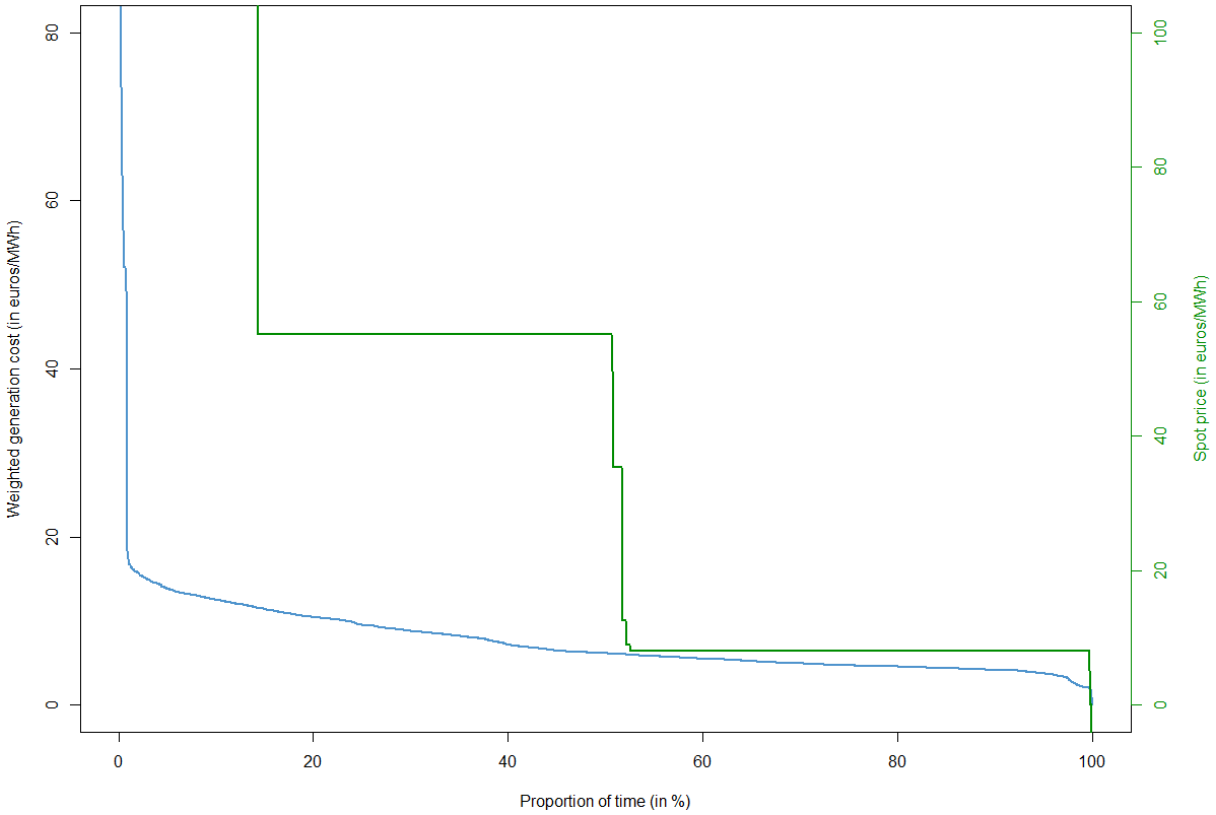

Figure 12.C.: Weighted operational cost and spot price distributions (representative weeks, optimal mix n°3)

Increasing RES penetration in optimal mix n°4 allows the number of scarcity events to drop to less than 0.4% of operating hours. Yet, in comparison with optimal mix n°3, **Figure 12.D.** shows the average spot price increases by almost 11% to reach 31.2 €/MWh. As the system adapts to RES penetration and decommissioned nuclear capacity is replaced by CCGT units, a higher participation of costly peaking units is required to serve a more volatile residual load. It contributes to a moderate increase of the average weighted operational cost, equal to 7.49 €/MWh, as the generation cost structure remains dominated by nuclear, hydroelectric and RES. In the context of increasing RES penetration and nuclear phase out, the expected profitability of generation units may, on the one hand, be improved by the increase in system flexibility and upward shift of residual load, but on the other hand diminish as the number of hours requiring fast-response production may subsequently drop in representative operational conditions. We shall investigate this issue in the next chapter of this work.

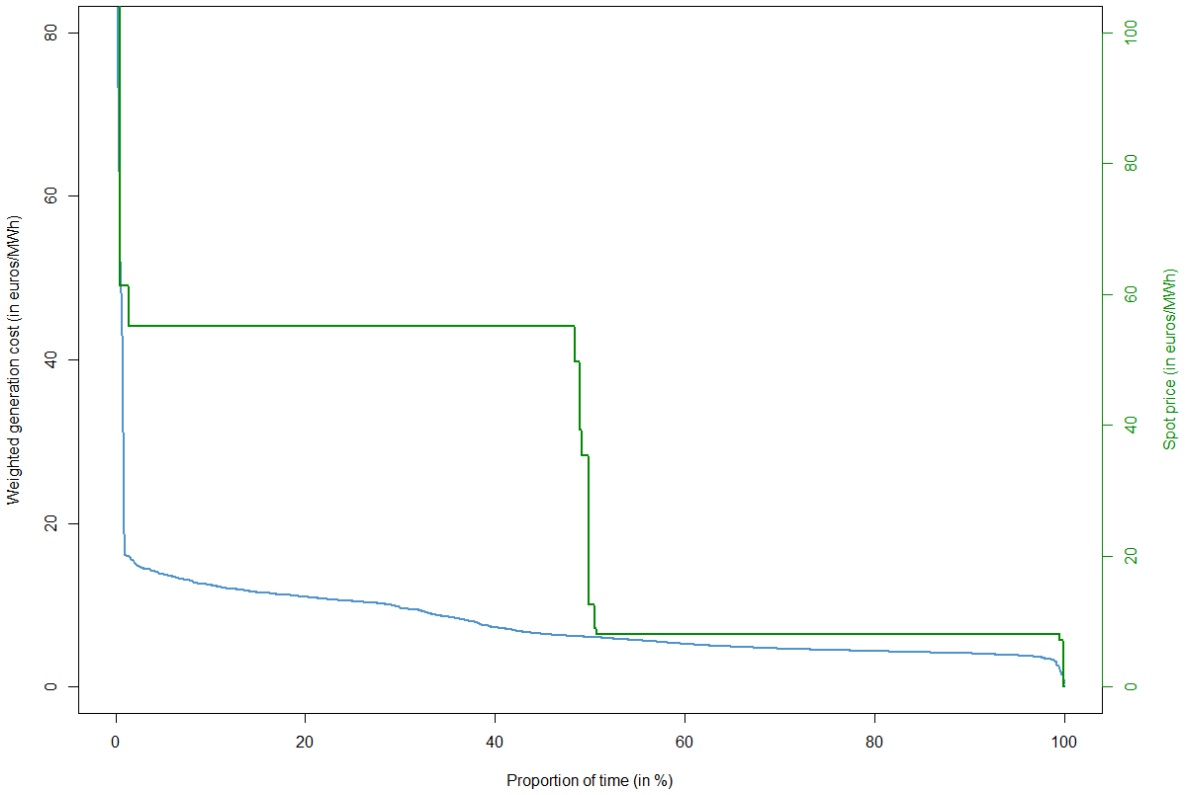

Figure 12.D.: Weighted operational cost and spot price distributions (representative weeks, optimal mix n°4)

The total amount of carbon emissions is directly linked to the participation of CCGT units in the electricity mix. No gas turbine investments occur in our model, which implies all CO_2 emissions related to electricity generation are caused by CCGT. As underlined above, Auvergne-Rhône-Alpes is characterized by a very low carbon intensity compared to the national average.

Figure 13.A. shows positive carbon emissions only during a small fraction of the year, corresponding to CCGT interventions for system security operations. We find an average carbon intensity of 6.3 g/kWh, which is very close to the historic 5.7 g/kWh used for model calibration. With higher RES penetration, total annual carbon emissions drop from 11 334 tons in mix n°1 to 2514 tons in mix n°2. Although CCGT remains necessary for system balance in periods of extreme residual load dynamics, **Figure 13.B.** in Appendix shows the drop of its utilization in representative weeks allows to divide average carbon intensity by 42, with 0.136 kg/MWh.

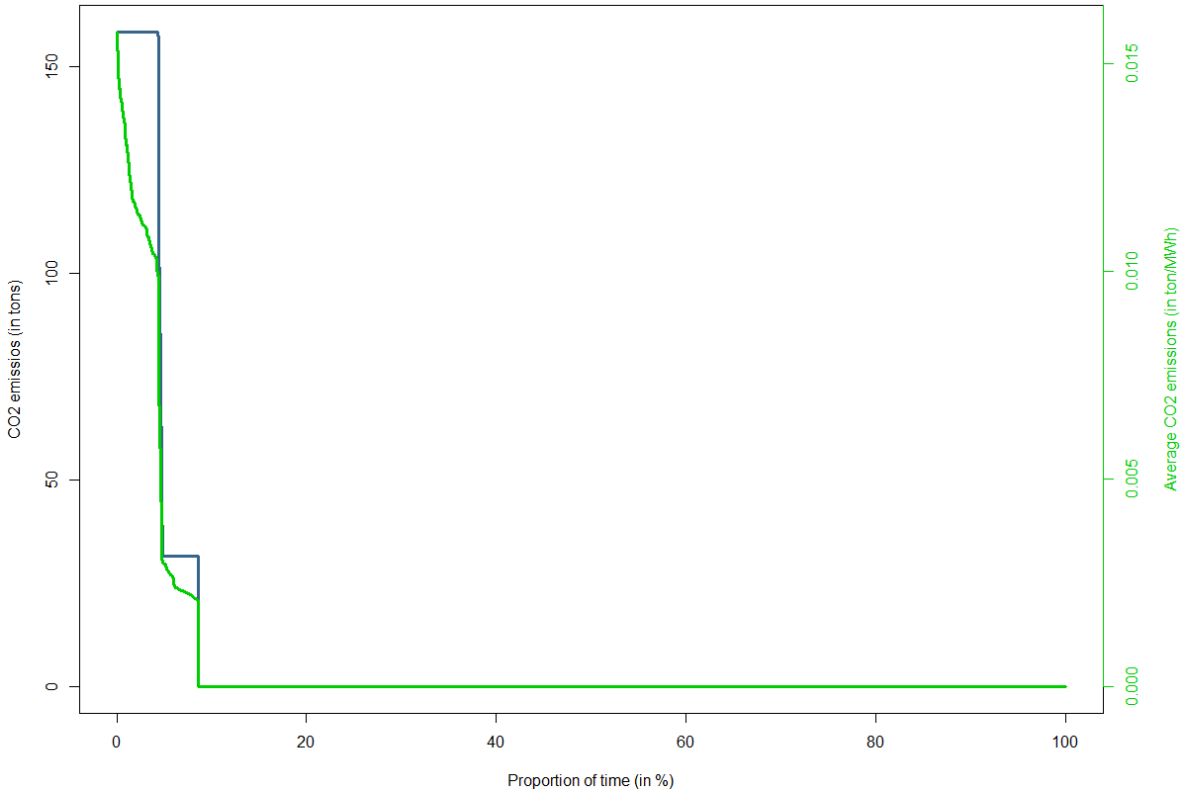

Figure 13.A.: Carbon emissions and carbon intensity distributions (representative weeks, optimal mix n°1)

Partially replacing ‘baseload’ nuclear generation by CCGT in optimal mix n°3 inevitably generates a stark increase in both total carbon emissions and carbon intensity. We see from **Figure 13.C.** a staircase-like curve for carbon emissions, which attain total annual emissions superior to 275 thousand tons of CO_2. Compared to optimal mix n°1, the average carbon intensity is multiplied by 3, with a value of 14.94 g/kWh. Although carbon intensity remains much lower than the national average, this result may not be transposed to other French regions as hydroelectric capacity might participate to underestimate the required CCGT investments to compensate nuclear phase out and accommodate increasing RES penetration at the national scale. Moreover, this would mechanically increase total French carbon emissions and thus contradict reduction targets. Finally, **Figure 13.D.** in Appendix shows an even higher carbon intensity although greater RES penetration in mix n°4, with 15.59 g/kWh. Clearly, although regional emissions remain below the national average, replacing decommissioned reactors by a CCGT to satisfy a share of ‘baseload’ generation does not align with national commitment to reduce carbon emissions. If more nuclear reactors are to be closed in the

coming decade, our results entail a pivotal trade-off between either controlling carbon emissions by massively investing in RES generation units, at extremely high capital costs and provided sufficient potential is available in the region, or replacing a significant share of decommissioned nuclear capacity by CCGT units, which is optimal in terms of system costs but would contribute to increasing CO_2 emissions.

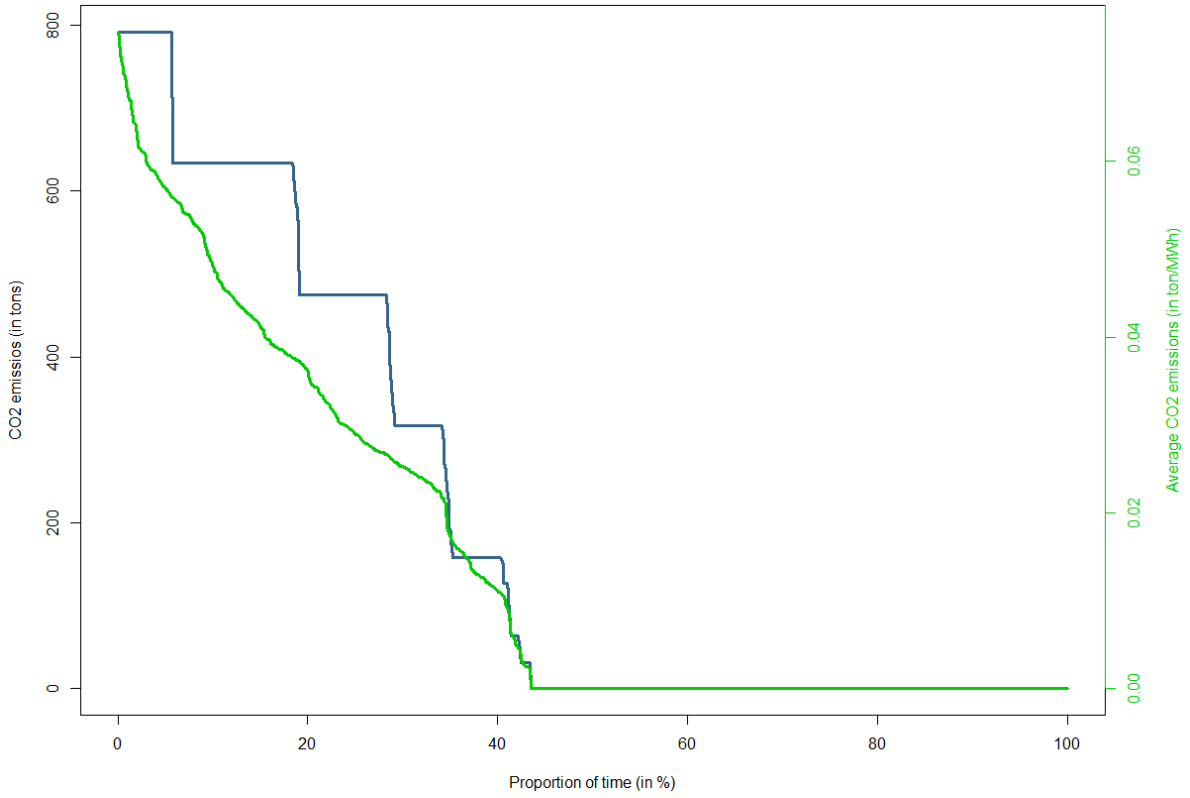

Figure 13.C.: Carbon emissions and carbon intensity distributions (representative weeks, optimal mix n°3)

5. Conclusion and policy implications

No techno-economic analysis has indicated that the 50 % target for the share of nuclear is an optimum, so much regarding the cost of electricity than regarding the security of supply[30]. Such policy decision does neither rely on objective environmental targets nor on a minimization of the costs paid by electricity customers. It most likely results from a political compromise inscribed in the LTECV of 2015. This is confirmed by our findings, which show that phasing out of nuclear in the medium-term is clearly suboptimal in terms of system costs. If the risk levels associated to the prolongation of nuclear reactors reaching 40 years is low and socially acceptable, prolonging the nuclear fleet is the optimal solution, at least until 2030, to keep both CO_2 and electricity generation costs low. As suggested by [3], nuclear may be used as a "buffer" to give deciders, electricity customers and technologies time to adapt. First, it would allow RES sectors to get more mature and continue to decrease investment and FOM costs through innovation. Second, it might give electricity customers and society more time to develop new energy efficient technologies, and more environment-friendly behaviors regarding energy consumption. As the French electricity consumption structured itself along the development of the nuclear fleet since the 1970s, it could make sense to first change electricity consumption patterns and habits before reducing the nuclear fleet, which historically contributed to their emergence. Finally, delaying nuclear phase out may be beneficial to the development of alternative clean technologies, such as hydrogen and nuclear fusion.

However, the static approach adopted in this chapter did not allow us to investigate the "cliff effect" mentioned in introduction, which would be even more pronounced if the decommissioning of most reactors is postponed to the early 2030s. This would indeed require the simultaneous startup and integration to the grid of a significant number of new generation units, with potentially high risks of delay and extreme costs, should prolonged nuclear units be abruptly shut down for safety reasons. Progressively decommissioning nuclear reactors during the coming decade might thus lower these risks, but is suboptimal in terms of system costs and may increase carbon emissions as we have shown. This dilemma should, in our opinion, be the central topic of the French future nuclear policy.

[30] https://www.lemonde.fr/economie/article/2018/05/12/energie-une-reduction-du-nucleaire-a-50-serait-l-amorce-d-une-dynamique-de-pertes-d-apprentissage-technologique-et-industriel_5297976_3234.html

6. Appendix

Appendix to 2.1.: Technical characteristics and cost assumptions

Technology	Minimum generation level (% nominal power)	Ramping rate (% of nominal power/min)	Minimum uptime/downtime (hours)	Average CO_2 emission factor (ton/MWh)
Combined cycle gas turbine	20	20	0	0.352
Gas turbine	15	8	2	0.777
Nuclear	50	2-5	10	0
Hydroelectric	5	15	0.1	0
Hydroelectric pumped storage	5	15	0	0

Table 1.A.: Technical characteristics of thermal technologies

Sources : Gonzalez-Salazar et al. (2018), IAEA (2018), Schill et al. (2016), IEA (2015), Schröder et al. (2013), EC JRC (2010), RTE Bilan Electrique 2019 (RTE, 2019)

Technology	Overnight cost (€/kWe)	Annual fixed & maintenance costs (€/kWe)	Unit variable cost (€/MWh)	Unit starting cost (€/MWh)	Average lifetime (years)
Combined cycle gas turbine	754	20	45	235	30
Gas turbine	400	6.4	135	542.8	30
Nuclear	3800	137	8	90	40
Hydroelectric	3200	32	0	5	80
Photovoltaic	669	19	0	0	25
Wind power	1284	45	0	0	20
Battery storage	169	5.1	0	0	10

Table 1.B.: Cost assumptions for generation technologies for 2021

Sources : "Le Cout des ENR en France", ADEME (2016) ; "La politique de développement des énergies renouvelables", Cour des Comptes (2013) ; CRE (2018) ; "Coûts et rentabilité du grand photovoltaïque en métropole continentale", CRE (2019) ; IEA (2015) ; "Current and Prospective Costs of Electricity Generation until 2050", DIW (2013) ; OECD/IEA-NEA (2015)

Appendix to 2.3.: Investment and dispatching model with endogenous nuclear policy and commitment constraints

Formulation of the model:

The cost-minimization problem for our electric system, neglecting spatial transfers and transmission network, is defined as a MILP as follows:

$$\min_{\boldsymbol{U,Y,q,\kappa,z}} \sum_{j>1} \left(A_j + c_j^{FOM}\right) U_j + \sum_{g \in \mathcal{C}^1, \mathcal{C}^2} \left(A_g + c_g^{FOM}\right) D_g U_g + \sum_{g \in \mathcal{N}} c_g^{FOM} D_g U_g + \sum_{g \in \mathcal{N}^d} \gamma_1 Y_g + \gamma_2 (1 - Y_g)$$
$$+ \frac{\Theta}{N^R} \left(\sum_{\mathfrak{p} \in \{\boldsymbol{L,H,V}\}} \sum_{s \in \mathcal{S}} \sum_{t \in \mathcal{T}} \left(\sum_{g \in \mathcal{G}} \left(c_g^V + \pi^{CO_2} E_g\right) q_{gst}^{\mathfrak{p}} + c_g^{STUP} z_{gst}^{\mathfrak{p}} + \sum_j c_j^{\kappa} \kappa_{jst}^{\mathfrak{p}} \right) \right) \quad (\mathbf{1})$$

Such that :

$$U_g = 1 - Y_g \qquad , \forall g \in \mathcal{N}^d \quad (\mathbf{2})$$

$$\xi_{1st}^{\mathfrak{p}} - \kappa_{1st}^{\mathfrak{p}} - \left(\sum_{j>1} \left(\xi_{jst}^{\mathfrak{p}} U_j - \kappa_{jst}^{\mathfrak{p}} \right) \right) - \left(\sum_{g \in \mathcal{N}, \mathcal{C}^1, \mathcal{C}^2, \mathcal{H}^1} q_{gst}^{\mathfrak{p}} \right) + e_{st}^{+\mathfrak{p}} - e_{st}^{-\mathfrak{p}} + \left(\sum_{g \in \mathcal{H}^2} \varepsilon_{gst}^{+\ \mathfrak{p}} - \varepsilon_{gst}^{-\ \mathfrak{p}} \right) + \Delta_{st}^{+\mathfrak{p}} - \Delta_{st}^{-\mathfrak{p}}$$
$$\leq \alpha \qquad , \forall \mathfrak{p} \in \{\boldsymbol{L,H,V}\} \quad (\mathbf{3a})$$

$$-\xi_{1st}^{\mathfrak{p}} + \kappa_{1st}^{\mathfrak{p}} + \left(\sum_{j>1} \left(\xi_{jst}^{\mathfrak{p}} U_j - \kappa_{jst}^{\mathfrak{p}} \right) \right) + \left(\sum_{g \in \mathcal{N}, \mathcal{C}^1, \mathcal{C}^2, \mathcal{H}^1} q_{gst}^{\mathfrak{p}} \right) - e_{st}^{+\mathfrak{p}} + e_{st}^{-\mathfrak{p}} - \left(\sum_{g \in \mathcal{H}^2} \varepsilon_{gst}^{+\ \mathfrak{p}} - \varepsilon_{gst}^{-\ \mathfrak{p}} \right) + \Delta_{st}^{+\mathfrak{p}}$$
$$- \Delta_{st}^{-\mathfrak{p}} \leq \alpha \qquad , \forall \mathfrak{p} \in \{\boldsymbol{L,H,V}\} \quad (\mathbf{3b})$$

$$u_{gst}^{\mathfrak{p}} - u_{gst-1}^{\mathfrak{p}} = z_{gst}^{\mathfrak{p}} - v_{gst}^{\mathfrak{p}} \qquad , \forall \mathfrak{p} \in \{\boldsymbol{L,H,V}\}, \forall g \in \mathcal{N}, \mathcal{C}^1, \mathcal{C}^2, \mathcal{H}^1 \quad (\mathbf{4a})$$

$$z_{gst}^{\mathfrak{p}} + v_{gst}^{\mathfrak{p}} \leq 1 \qquad , \forall \mathfrak{p} \in \{\boldsymbol{L,H,V}\}, \forall g \in \mathcal{N}, \mathcal{C}^1, \mathcal{C}^2, \mathcal{H}^1 \quad (\mathbf{4b})$$

$$\omega_{gst}^{1\ \mathfrak{p}} = q_{gst}^{\mathfrak{p}} - \omega_{gst}^{2\ \mathfrak{p}} \qquad , \forall \mathfrak{p} \in \{\boldsymbol{L,H,V}\}, \forall g \in \mathcal{N}, \mathcal{C}^1, \mathcal{C}^2, \mathcal{H}^1 \quad (\mathbf{5})$$

$$\omega_{gst}^{1\ \mathfrak{p}} - \omega_{gst-1}^{1\ \mathfrak{p}} \leq \overline{r_g} \qquad , \forall \mathfrak{p} \in \{\boldsymbol{L,H,V}\}, \forall g \in \mathcal{N}, \mathcal{C}^1, \mathcal{C}^2, \mathcal{H}^1 \quad (\mathbf{6a})$$

$$\omega_{gst-1}^{1\ \mathfrak{p}} - \omega_{gst}^{1\ \mathfrak{p}} \leq \underline{r_g} \qquad , \forall \mathfrak{p} \in \{\boldsymbol{L,H,V}\}, \forall g \in \mathcal{N}, \mathcal{C}^1, \mathcal{C}^2, \mathcal{H}^1 \quad (\mathbf{6b})$$

$$\omega_{gst}^{1\ \mathfrak{p}} \leq U_g D_g \left(\overline{q_g} - \underline{q_g} \right) \qquad , \forall \mathfrak{p} \in \{\boldsymbol{L,H,V}\}, \forall g \in \mathcal{N}, \mathcal{C}^1, \mathcal{C}^2, \mathcal{H}^1 \quad (\mathbf{7a})$$

$$\omega_{gst}^{1\ \mathfrak{p}} \leq u_{gst}^{\mathfrak{p}} \mathrm{K} \qquad , \forall \mathfrak{p} \in \{\boldsymbol{L,H,V}\}, \forall g \in \mathcal{N}, \mathcal{C}^1, \mathcal{C}^2, \mathcal{H}^1 \quad (\mathbf{7b})$$

$$\omega_{gst}^{2\ \mathfrak{p}} \leq U_g D_g \underline{q_g} \qquad , \forall \mathfrak{p} \in \{\boldsymbol{L,H,V}\}, \forall g \in \mathcal{N}, \mathcal{C}^1, \mathcal{C}^2, \mathcal{H}^1 \quad (\mathbf{8})$$

$$\omega_{gst}^{2\,\mathfrak{p}} = U_g D_g \underline{q_g} - \left(1 - u_{gst}^{\mathfrak{p}}\right)\mathrm{K} + s_{gst}^{\mathfrak{p}} \qquad ,\forall \mathfrak{p} \in \{\boldsymbol{L},\boldsymbol{H},\boldsymbol{V}\}, \forall g \in \mathcal{N}, \mathcal{C}^1, \mathcal{C}^2, \mathcal{H}^1 \quad (\mathbf{9})$$

$$s_{gst}^{\mathfrak{p}} \le \left(1 - u_{gst}^{\mathfrak{p}}\right)\mathrm{K} - U_g D_g \underline{q_g} + u_{gst}^{\mathfrak{p}}\mathrm{K} \qquad ,\forall \mathfrak{p} \in \{\boldsymbol{L},\boldsymbol{H},\boldsymbol{V}\}, \forall g \in \mathcal{N}, \mathcal{C}^1, \mathcal{C}^2, \mathcal{H}^1 \quad (\mathbf{10})$$

$$u_{gst}^{\mathfrak{p}} \ge \sum_{t'>t-M_j^U} z_{gst}^{\mathfrak{p}} \qquad ,\forall \mathfrak{p} \in \{\boldsymbol{L},\boldsymbol{H},\boldsymbol{V}\}, \forall g \in \mathcal{N}, \mathcal{C}^1, \mathcal{C}^2, \mathcal{H}^1 \quad (\mathbf{11a})$$

$$1 - u_{gst}^{\mathfrak{p}} \ge \sum_{t'>t-M_j^D} v_{gst}^{\mathfrak{p}} \qquad ,\forall \mathfrak{p} \in \{\boldsymbol{L},\boldsymbol{H},\boldsymbol{V}\}, \forall g \in \mathcal{N}, \mathcal{C}^1, \mathcal{C}^2, \mathcal{H}^1 \quad (\mathbf{11b})$$

$$q_{gst}^{\mathfrak{p}} \le \Gamma_{gs}^0 - \sum_{\tau=0}^{t-1}\left(q_{gs\tau}^{\mathfrak{p}} - I_{gs\tau}\right) \qquad ,\forall \mathfrak{p} \in \{\boldsymbol{L},\boldsymbol{H},\boldsymbol{V}\}, \forall g \in \mathcal{H}^1 \quad (\mathbf{12})$$

$$\Gamma_{gs}^0 \le \overline{\Gamma_{gs}} + \sum_{\tau=0}^{t-1}\left(q_{gs\tau}^{\mathfrak{p}} - I_{gs\tau}\right) \qquad ,\forall \mathfrak{p} \in \{\boldsymbol{L},\boldsymbol{H},\boldsymbol{V}\}, \forall g \in \mathcal{H}^1 \quad (\mathbf{13})$$

$$\kappa_{jst}^{\mathfrak{p}} \le \xi_{jst}^{\mathfrak{p}} U_j \qquad ,\forall \mathfrak{p} \in \{\boldsymbol{L},\boldsymbol{H},\boldsymbol{V}\}, \forall j \in \mathcal{J} \quad (\mathbf{14})$$

$$e_{st}^{\mathfrak{p}} = e_{st-1}^{\mathfrak{p}} + \sqrt{\eta_e} e_{st-1}^{+\,\mathfrak{p}} - \frac{e_{st-1}^{-\,\mathfrak{p}}}{\sqrt{\eta_e}} \qquad ,\forall \mathfrak{p} \in \{\boldsymbol{L},\boldsymbol{H},\boldsymbol{V}\} \quad (\mathbf{15})$$

$$e_{st}^{\mathfrak{p}} \le \overline{e} U_e \qquad ,\forall \mathfrak{p} \in \{\boldsymbol{L},\boldsymbol{H},\boldsymbol{V}\} \quad (\mathbf{16})$$

$$e_{st}^{\mathfrak{p}} \ge \underline{e} U_e \qquad ,\forall \mathfrak{p} \in \{\boldsymbol{L},\boldsymbol{H},\boldsymbol{V}\} \quad (\mathbf{17})$$

$$\varepsilon_{gst}^{\mathfrak{p}} = \varepsilon_{gst-1}^{\mathfrak{p}} + \sqrt{\eta_\varepsilon} \varepsilon_{st-1}^{+\,\mathfrak{p}} - \frac{\varepsilon_{st}^{-\,\mathfrak{p}}}{\sqrt{\eta_\varepsilon}} + I_{gst} \qquad ,\forall \mathfrak{p} \in \{\boldsymbol{L},\boldsymbol{H},\boldsymbol{V}\}, \forall g \in \mathcal{H}^2 \quad (\mathbf{18})$$

$$\varepsilon_{gst}^{\mathfrak{p}} \le \overline{\varepsilon_g} D_g U_g \qquad ,\forall \mathfrak{p} \in \{\boldsymbol{L},\boldsymbol{H},\boldsymbol{V}\}, \forall g \in \mathcal{H}^2 \quad (\mathbf{19})$$

$$\varepsilon_{gst}^{\mathfrak{p}} \ge \underline{\varepsilon_g} D_g U_g \qquad ,\forall \mathfrak{p} \in \{\boldsymbol{L},\boldsymbol{H},\boldsymbol{V}\}, \forall g \in \mathcal{H}^2 \quad (\mathbf{20})$$

$$\varepsilon_{gst}^{+\,\mathfrak{p}} \le l_{gst}^{\mathfrak{p}} \overline{\varepsilon_g^+} D_g U_g \qquad ,\forall \mathfrak{p} \in \{\boldsymbol{L},\boldsymbol{H},\boldsymbol{V}\}, \forall g \in \mathcal{H}^2 \quad (\mathbf{21})$$

$$\varepsilon_{st}^{-\mathfrak{p}} \le \left(1 - l_{gst}^{\mathfrak{p}}\right)\overline{\varepsilon_g^-} D_g U_g \qquad ,\forall \mathfrak{p} \in \{\boldsymbol{L},\boldsymbol{H},\boldsymbol{V}\}, \forall g \in \mathcal{H}^2 \quad (\mathbf{22})$$

$$\Delta_{st}^{\mathfrak{p}} = \Delta_{st-1}^{\mathfrak{p}} + \sqrt{\eta_\Delta} \Delta_{st-1}^{+\,\mathfrak{p}} - \frac{\Delta_{st-1}^{-\,\mathfrak{p}}}{\sqrt{\eta_\Delta}} - (1 - \xi_{st-1}^{\Delta}) \psi_{t-1\to t} k^{\Delta} N^{\Delta} \qquad ,\forall \mathfrak{p} \in \{\boldsymbol{L},\boldsymbol{H},\boldsymbol{V}\} \quad (\mathbf{23})$$

$$\Delta_{st}^{\mathfrak{p}} \le \overline{\Delta} k^{\Delta} N^{\Delta} \qquad ,\forall \mathfrak{p} \in \{\boldsymbol{L},\boldsymbol{H},\boldsymbol{V}\} \quad (\mathbf{24})$$

$$\Delta_{st}^{\mathfrak{p}} \ge \underline{\Delta} N^{\Delta} + (1 - \xi_{st}^{\Delta}) \psi_{t\to t+1} \delta^{\Delta} N^{\Delta} \qquad ,\forall \mathfrak{p} \in \{\boldsymbol{L},\boldsymbol{H},\boldsymbol{V}\} \quad (\mathbf{25})$$

$$\Delta_{st}^{+\,\mathfrak{p}} \le \overline{\Delta^+} N^{\Delta} \xi_{st}^{\Delta} \qquad ,\forall \mathfrak{p} \in \{\boldsymbol{L},\boldsymbol{H},\boldsymbol{V}\} \quad (\mathbf{26})$$

$$\Delta_{st}^{-\mathfrak{p}} \leq \overline{\Delta^{-}} N^{\Delta} \xi_{st}^{\Delta} \quad ,\forall \mathfrak{p} \in \{\boldsymbol{L},\boldsymbol{H},\boldsymbol{V}\} \quad (\mathbf{27})$$

$$u_{gst}^{\mathfrak{p}} \in \{0,1\} \quad ,\forall \mathfrak{p} \in \{\boldsymbol{L},\boldsymbol{H},\boldsymbol{V}\}, \forall g \in \mathcal{N}, \mathcal{C}^1, \mathcal{C}^2, \mathcal{H}^1 \quad (\mathbf{28})$$

$$v_{gst}^{\mathfrak{p}} \in \{0,1\} \quad ,\forall \mathfrak{p} \in \{\boldsymbol{L},\boldsymbol{H},\boldsymbol{V}\}, \forall g \in \mathcal{N}, \mathcal{C}^1, \mathcal{C}^2, \mathcal{H}^1 \quad (\mathbf{30})$$

$$z_{gst}^{\mathfrak{p}} \in \{0,1\} \quad ,\forall \mathfrak{p} \in \{\boldsymbol{L},\boldsymbol{H},\boldsymbol{V}\}, \forall g \in \mathcal{N}, \mathcal{C}^1, \mathcal{C}^2, \mathcal{H}^1 \quad (\mathbf{31})$$

$$l_{gst}^{\mathfrak{p}} \in \{0,1\} \quad ,\forall \mathfrak{p} \in \{\boldsymbol{L},\boldsymbol{H},\boldsymbol{V}\}, \forall g \in \mathcal{H}^2 \quad (\mathbf{32})$$

$$Y_g \in \{0,1\} \quad ,\forall g \in \mathcal{N} \quad (\mathbf{33})$$

Description of the model:

Indices and sets

We define the set $\mathcal{T}$ used to index hours of the week and the set of seasons $\mathcal{S}$, with elements $t \in \mathcal{T}$ and $s \in \mathcal{S}$ respectively. We also define the set of worst-case trajectories $\{\boldsymbol{L},\boldsymbol{H},\boldsymbol{V}\}$, with element $\mathfrak{p} \in \{\boldsymbol{L},\boldsymbol{H},\boldsymbol{V}\}$. Finally, we introduce the set of residual demand components $\mathcal{J}$, where the first element of $\mathcal{J}$ corresponds to the electric load and the remaining elements are available renewable technologies (wind and photovoltaic technologies in our case). These can be decomposed into subsets $\mathcal{W} \subset \mathcal{J}$ and $\mathcal{P} \subset \mathcal{J}$, which respectively denote wind and photovoltaic technologies.

The set of units from thermal and dispatchable generation technologies is noted $\mathcal{G}$, with unit $g \in \mathcal{G}$. The set $\mathcal{G}$ can be decomposed into the subsets of nuclear units $\mathcal{N} \subset \mathcal{G}$, combined cycle gas turbines (CCGT) $\mathcal{C}^1 \subset \mathcal{G}$ and oil-powered gas turbines (GT) $\mathcal{C}^2 \subset \mathcal{G}$, hydroelectric generation units $\mathcal{H}^1 \subset \mathcal{G}$ and eventually hydraulic pumped storage units $\mathcal{H}^2 \subset \mathcal{G}$. We further define the subset of nuclear units that are potential candidates for being decommissioned $\mathcal{N}^d \subset \mathcal{N}$. Because they do not have thermal constraints, we consider a single generation unit (equal to the aggregation of all individual units) for each renewable demand component $j \in \mathcal{J}$.

Investment variables and parameters

For each unit $g \in \mathcal{G}$, we define the binary building decision variable $U_g \in \{0;1\}$. The parameter $D_g \geq 0$ corresponds to the "block" size of unit g, or equivalently, its electricity output capability. For simplicity, we assume D_g is equal for all units of the same technology. Each unit $g \in \mathcal{G}$ is characterized by minimum and maximum output levels $\underline{q_g} \geq 0$ and $\overline{q_g} \geq 0$, in addition to maximum ramp-up and ramp-down capacities $\overline{r_g} \geq 0$ and $\underline{r_g} \geq 0$. The commitment status of g is constrained by minimum uptime $M_g^U \geq 0$ and minimum downtime $M_g^D \geq 0$. Finally, we define the installed capacity of storage as $U_e \geq 0$. For any $g \in \mathcal{N}^d$, Y_g is a binary variable equal to 1 if the nuclear unit g is decommissioned. Finally, each thermal generation unit is characterized by a ratio of CO_2 emissions per unit output E_g, expressed in ton per unit generated.

We note the investment level for each residual demand component $j \in \mathcal{J}$ as $U_j \geq 0$ with the convention that $U_1 = 1$ and note $\boldsymbol{U} = (U_i)_{1 \leq i \leq |\mathcal{J}|}$ the vector of installed capacities for residual demand components. We define the investment level in battery storage capacities as $U_e \geq 0$.

We assume the variables U_j and U_e are continuous, while U_g is binary. Renewable technologies, thermal generation technologies and battery storage respectively have annuitized unit investment costs A_j, A_g and A_e, with $A_j, A_g, A_e \geq 0$. Similarly, both renewable and thermal generation technologies exhibit yearly fixed and operation maintenance costs c_j^{FOM}, c_g^{FOM} and c_e^{FOM}, with $c_j^{FOM}, c_g^{FOM}, c_e^{FOM} \geq 0$. Finally, $\gamma_1 \geq 0$ and $\gamma_2 \geq 0$ respectively denote the annuitized unit cost of phasing and prolongation of a nuclear units included in $\mathcal{N}^d$.

Operational variables and parameters

For any season $s \in \mathcal{S}$, hour $t \in \mathcal{T}$ and trajectory $\mathfrak{p} \in \{\boldsymbol{L}, \boldsymbol{H}, \boldsymbol{V}\}$, we define the uncertain capacity factor $\xi_{jst} \in \mathbb{R}^+$ for $j \in \mathcal{J}$, where $\xi_{1st} \in \mathbb{R}^+$ corresponds to electricity demand and $\xi_{1st} \in [0,1]$ for $j > 1$. The variable $\kappa_{jst}^{\mathfrak{p}} \geq 0$ is equal to volume of curtailed production for renewable technology $j \in \mathcal{J}$. Using this notation, $\kappa_{1st}^{\mathfrak{p}}$ can naturally be interpreted as the volume of non-served load (VOLL).

We define the variable $q_{gst}^{\mathfrak{p}} \geq 0$, which corresponds to the production of generation unit $g \in \mathcal{G}$. For any hour $t \in \mathcal{T}$ and season $s \in \mathcal{S}$, the ${\omega_{gst}^{2}}^{\mathfrak{p}} \geq 0$ corresponds to the minimum generation level of plant $g \in \mathcal{G}$, while ${\omega_{gst}^{1}}^{\mathfrak{p}} \geq 0$ is an auxiliary variable equal to the generation volume above minimum-production level. We set $\mathrm{K} \gg 0$ and define the slack variable $s_{gst}^{\mathfrak{p}} \geq 0$. $u_{gst}^{\mathfrak{p}}$, $v_{gst}^{\mathfrak{p}}$ and $z_{gst}^{\mathfrak{p}}$ are all binary variables respectively corresponding to the commitment state, start-up and shut-down decision of generator $g \in \mathcal{G}$.

The volume of electricity that can be produced by hydroelectric generation units is upper bounded by both the generation capacity of each generation unit $g \in \mathcal{H}^1$, but also by the level of its reservoir. We note $\Gamma_{gs}^{0} \geq 0$ the initial storage level of the reservoir for unit $g \in \mathcal{H}^1$ and $\overline{\Gamma_{gs}} \geq 0$ its maximum storage level, for each season $s \in \mathcal{S}$. $I_{gs\tau} \in \mathbb{R}^{+}$ is a random variable corresponding to exogenous energy inflows (typically water received from precipitations and thaw) received by unit $g \in \mathcal{H}^1$ in $s \in \mathcal{S}$ and $t \in \mathcal{T}$. For simplicity, we neglect these inflows and set $I_{gs\tau} = 0$. Moreover, we make the simplifying assumption that each hydroelectric generation unit is operated independently, and its operational decisions have no impact on other units, in particular on the storage level of each individual reservoir.

We must clearly distinguish storage from battery units, electric vehicles and pumped storage units. The variable $e_{st}^{\mathfrak{p}} \geq 0$ (resp. $\varepsilon_{gst}^{\mathfrak{p}} \geq 0$ and $\Delta_{gst}^{\mathfrak{p}} \geq 0$) corresponds to the stock of electricity stored in batteries (resp. in pumped-storage units and EVs) in hour t and season s, while $e_{st}^{+\mathfrak{p}} \geq 0$ (resp. ${\varepsilon_{gst}^{+}}^{\mathfrak{p}} \geq 0$ and $\Delta_{st}^{+\mathfrak{p}} \geq 0$) and $e_{st}^{-\mathfrak{p}} \geq 0$ (resp. ${\varepsilon_{gst}^{-}}^{\mathfrak{p}} \geq 0$ and $\Delta_{st}^{-\mathfrak{p}} \geq 0$) are flux variables respectively equal to the quantity of electricity stored and released by batteries (resp. pumped storage units and EVs). η_e is the round-trip efficiency of the battery storage technology, with $0 \leq \eta_e \leq 1$, such that $\sqrt{\eta_e}$ can be interpreted as the efficiency of charge or discharge. Finally, $\overline{e} \geq 0$ and $\underline{e} \geq 0$ respectively correspond to the maximum and minimum state of charge. In order to decrease the computational complexity of the model, we make the simplifying assumption of atomicity of individual battery storage units, so that on aggregate batteries can both charge and discharge at the same time. No binary commitment variable is thus required.

Similarly, for any $g \in \mathcal{H}^2$, $\sqrt{\eta_\varepsilon}$, $\overline{\varepsilon_g} \geq 0$ and $\underline{\varepsilon_g} \geq 0$ correspond to the round-trip-efficiency, maximum and minimum state of charge. $\overline{\varepsilon_g^{+}}, 0 \leq \overline{\varepsilon_g^{+}} \leq 1$, and $\overline{\varepsilon_g^{-}}$, $0 \leq \overline{\varepsilon_g^{+}} \leq 1$, respectively denote the maximum pumping and generation power ratio of unit g of size D_g. Similarly to

hydroelectric generation units, we assume the level of energy inflows received by pumped-storage units is neglectable, i.e. $I_{gs\tau} = 0$. The binary variable $l^{\mathfrak{p}}_{gst}$ corresponds to the charging state of $g \in \mathcal{H}^2$, with $l^{\mathfrak{p}}_{gst}$ equal to 1 when unit g pumps electricity. $l^{\mathfrak{p}}_{gst}$ corresponds to the charging state of pumped-storage unit $g \in \mathcal{H}^2$, with $l^{\mathfrak{p}}_{gst}$ equal to 1 when the unit is storing electricity.

We adopt a slightly different modeling of electric vehicles in order to account for specific transportation constraints. Like other storage technologies, we define $\sqrt{\eta_{\Delta}}$, $\overline{\Delta} \geq 0$ and $\underline{\Delta} \geq 0$ the round-trip efficiency, maximum and minimum state of charge of EVs respectively. k^{Δ} is the average battery size of individual vehicles and N^{Δ} is equal to the total number of electric vehicles. Parameters $\overline{\Delta^{+}}, 0 \leq \overline{\Delta^{+}} \leq 1$, and $\overline{\Delta^{-}}$, $0 \leq \overline{\Delta^{+}} \leq 1$, correspond to the maximum charging and discharging power ratio of individual electric vehicles. The parameter ξ^{Δ}_{st}, $0 \leq \xi^{\Delta}_{st} \leq 1$, is equal to the expected share of EVs which is parked in $s \in \mathcal{S}$ and $t \in \mathcal{T}$. The difference $1 - \xi^{\Delta}_{st}$ can therefore be interpreted as the coefficient of availability of the EV fleet, while $\xi^{\Delta}_{st} N^{\Delta}$ corresponds to the expected number of EVs in circulation in $s \in \mathcal{S}$ and $t \in \mathcal{T}$. Finally, $\psi_{t \to t+1} \geq 0$ is equal to the expected distance driven by EV drivers between successive hours t and $t+1$ and $\delta^{\Delta} \geq 0$ is the average consumption per unit of distance. The quantity $\left(1 - \xi^{\Delta}_{st}\right) \psi_{t \to t+1} \delta^{\Delta} N^{\Delta}$ thus corresponds to the total expected volume of electricity required for satisfying EVs driving requirements between t and $t+1$. We neglect transportation duration, which is a quite simplifying assumption as in reality travelling cars cannot connect and participate to the grid. In order to mitigate this issue, we assume the share of travelling EVs between t and $t+1$ cannot connect to the grid during this time interval. However, our aggregate approach implicitly allows transfers between individual electric vehicles. Yet, a more accurate modelling would dramatically increase the computational cost of our model. We leave these remarks open for further research.

We respectively note $c^{V}_{g} \geq 0$ and $c^{STUP}_{g} \geq 0$ the variable and start-up costs of the unit $g \in \mathcal{G}$. The parameter $c^{\kappa}_{j} \geq 0$ corresponds to the curtailment cost of renewable technology $j \in \mathcal{J}$, where c^{κ}_{1} is the Value of Lost Load (VOLL). Finally, we define the price of a carbon ton as $\pi^{CO_2} \geq 0$.

Description of the model equations

Each constraint must hold for each hour $t \in \mathcal{T}$ and season $s \in \mathcal{S}$. As there may exist no single set of dispatching decisions which simultaneously verify thermal constraints for all worst-case trajectories, specific variables are defined for each $\mathfrak{p} \in \{\boldsymbol{L}, \boldsymbol{H}, \boldsymbol{V}\}$ so our formulation ensures each operational constrain must hold for each worst-case trajectory.

As three different worst-case scenario or "trajectories" are simultaneously considered in the cost function, we divide the variable costs by $N^R = 3$ and multiply them by the scaling factor Θ equal to the number of weeks per season in **(1)**, so the variable part of the expression still corresponds to the average yearly variable cost. **(2)** simply translates the fact that the capacity of nuclear unit $g \in \mathcal{N}^d$ is set to zero if it is decommissioned. **(3a)** and **(3b)** correspond to the upper and lower limits of the primary frequency control constraint: net generation, which is the sum of electricity generation minus electric load and storage, must lie in the interval $[-\alpha, \alpha]$.

(4a) to **(11b)** together formalize as a set of linear constraints commitment state, starting-up decisions and output limits for dispatchable generators. More precisely, **(4a)** and **(4b)** link commitment status of each thermal plant with its start-up and shut-down decisions. Decomposing total generation as the sum of minimum generation ${\omega^2_{gst}}^{\mathfrak{p}}$ and extra generation ${\omega^1_{gst}}^{\mathfrak{p}}$, we combine the big-M method with the introduction of slack variables **(5)** to **(11b)** to account for mechanical inertia and thermal limitations of plants included in $\mathcal{G}$. **(12)** and **(13)** model the dynamics of the storage level of each hydroelectric generation unit in $\mathcal{H}^1$, while **(14)** imposes an upper bound to the volume of curtailment for each unit $j \in \mathcal{J}$, equal to the generation (or load in the case of electricity demand) of the unit.

The set of equations **(15)-(17)** represent the power balance of battery storage (similarly to renewable technologies, battery storage is treated as a single aggregate unit) with upper and lower bounds on its state of charge and electricity inflows and outflows. Similarly, equations **(18)-(22)** an identical set of constraints imposed to each STEP unit, with additional on the charging and discharging state of each unit $g \in \mathcal{H}^2$. $l^{\mathfrak{p}}_{gst}$ equal to 1 indicates that unit $g \in \mathcal{H}^2$ is in pumping mode. Finally, **(25)-(29)** impose similar constraints to EVs, with the exception that the minimum state of charge for each $t \in \mathcal{T}$ is now equal to $\left(1 - \xi^{\Delta}_{st}\right)\psi_{t \to t+1}\delta^{\Delta}N^{\Delta}$. Equivalently, charging and discharging decisions at each hour must leave enough charge to satisfy expected driving requirement for the next hour.

Appendix to 2.4.:

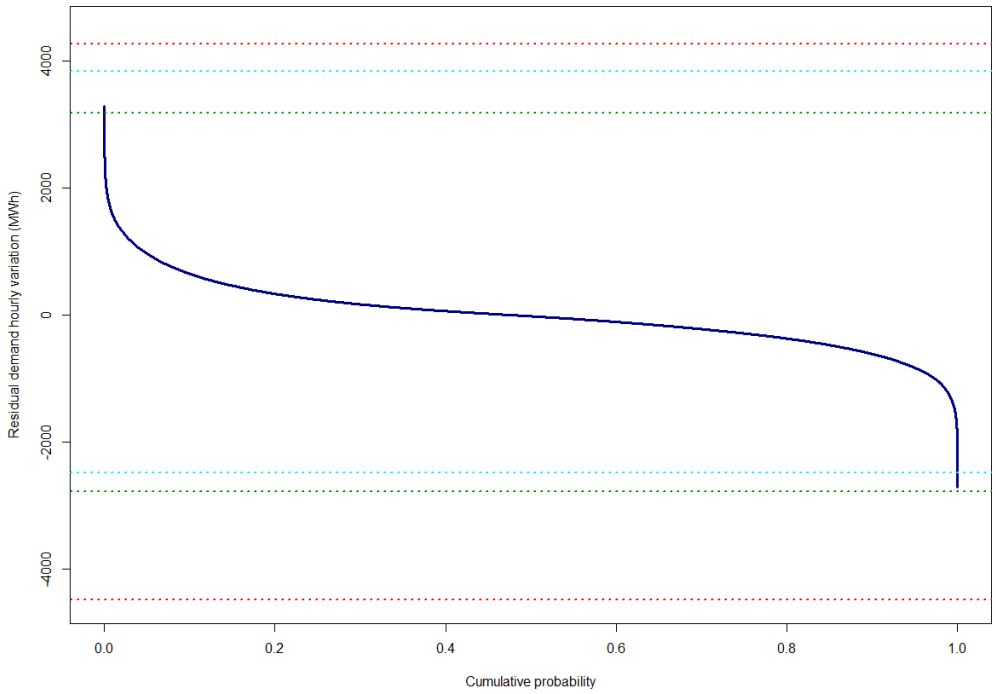

Figure 2.A.: Residual demand variations duration curve with wind and photovoltaic capacities equal to $\boldsymbol{U}^0$

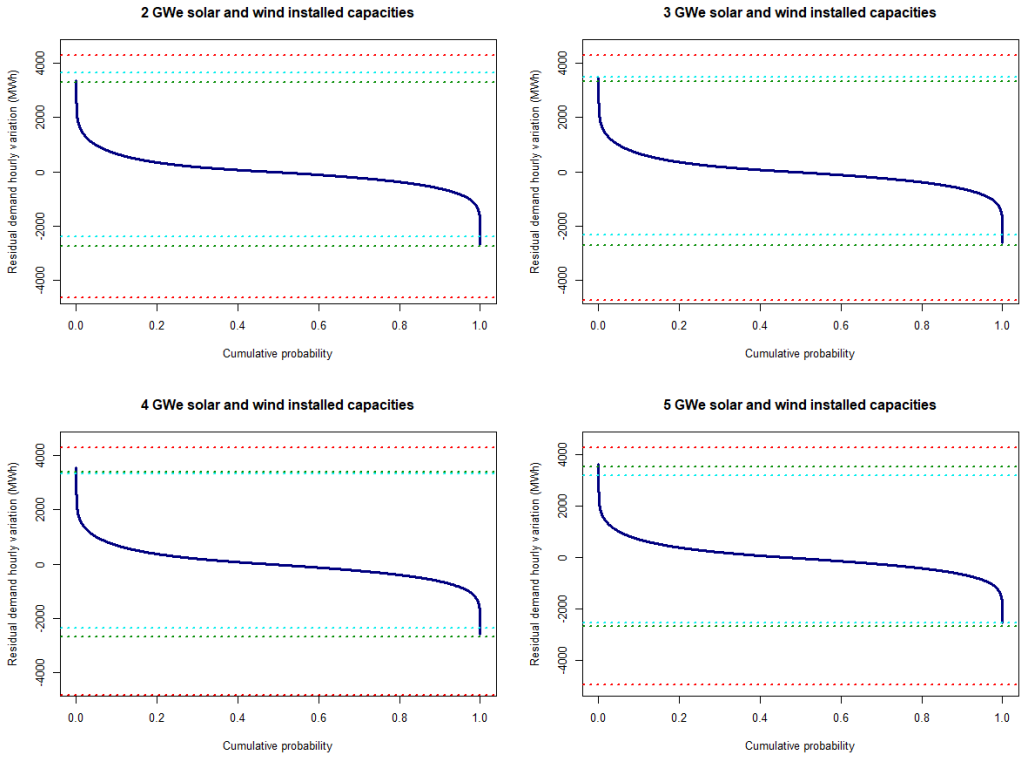

Figure 2.B.: Residual demand variations duration curve with wind and photovoltaic capacities ranging from 2GWe to 5 GWe

Appendix to 3.1.2.: Approximation of future electricity demand distribution

We approximate the future distribution of electricity demand using a structural decomposition model. Similar to [31], we decompose the changes in electricity demand patterns in terms of contributions from final consumer sectors. We distinguish four sectors: industry, transport, services and residential consumers. We assume changes in the non-residential electricity consumption are driven by GDP growth, which is assumed to be equal across all economic sectors for simplicity, while changes in residential electricity consumptions are driven by demographic growth. Finally, the consumption of all sectors is driven by sector-specific energy efficiency growth rate. We define the set of years $\mathcal{Y}$ with element $y \in \mathcal{Y}$ and the set of final consumer sectors $\mathcal{F}$ with element $f \in \mathcal{F}$. The economic growth rate (replaced by the demographic growth rate in the case of the residential sector) of sector $f \in \mathcal{F}$ in year $y \in \mathcal{Y}$ is noted ψ^1_{fy}. Similarly, sector-specific energy efficiency growth rate in year $y \in \mathcal{Y}$ is noted ψ^2_{fy}. Finally, the share of sector $f \in \mathcal{F}$ in total electricity consumption in hour $t \in \mathcal{T}$ is noted ϑ_{ft}. We assume for simplicity that is does vary with year and season. By construction, it verifies $\sum_f \vartheta_{ft} = 1$.

Recalling the definition of electricity demand in hour $t \in \mathcal{T}$ and season $s \in \mathcal{S}$ as the random variable $\boldsymbol{\xi}^{\mathrm{p}}_{1st} \in \boldsymbol{\Xi}^{\mathrm{p}}_{1st}$, we define the transformation $H_y(x)$ such that for $y > 0$:

$$H_y\left(\boldsymbol{\xi}^{\mathrm{p}}_{1st}\right) = \sum_{f \in \mathcal{F}} \left(\vartheta_{ft} \boldsymbol{\xi}^{\mathrm{p}}_{1st} \left[\prod_{y'=1}^{y} \left(\frac{\psi^1_{fy'}}{\psi^2_{fy'}} \right) \right] \right) \qquad (\mathbf{34a})$$

$y = 0$ corresponds to the reference year used for evaluating the parameters ϑ_{ft}, ψ^1_{fy}, ψ^2_{fy} and the distribution function of $\boldsymbol{\xi}^{\mathrm{p}}_{1st}$. Then, for any year $y > 0$, electricity demand follows the random variable $H_y\left(\boldsymbol{\xi}^{\mathrm{p}}_{1st}\right)$ such that $H_y\left(\boldsymbol{\xi}^{\mathrm{p}}_{1st}\right) \in H_y\left(\boldsymbol{\Xi}^{\mathrm{p}}_{1st}\right) = \left\{ H_y\left(\boldsymbol{\xi}^{\mathrm{p}}_{1st}\right) \middle| \boldsymbol{\xi}^{\mathrm{p}}_{1st} \in \boldsymbol{\Xi}^{\mathrm{p}}_{1st} \right\}$. If parameters are identical for each $y \in \mathcal{Y}$, the above expression simplifies to:

$$H_y\left(\boldsymbol{\xi}^{\mathrm{p}}_{1st}\right) = \sum_{f \in \mathcal{F}} \vartheta_{ft} \boldsymbol{\xi}^{\mathrm{p}}_{1st} \left(\frac{\psi^1_{f0}}{\psi^2_{f0}} \right)^y \qquad (\mathbf{34b})$$

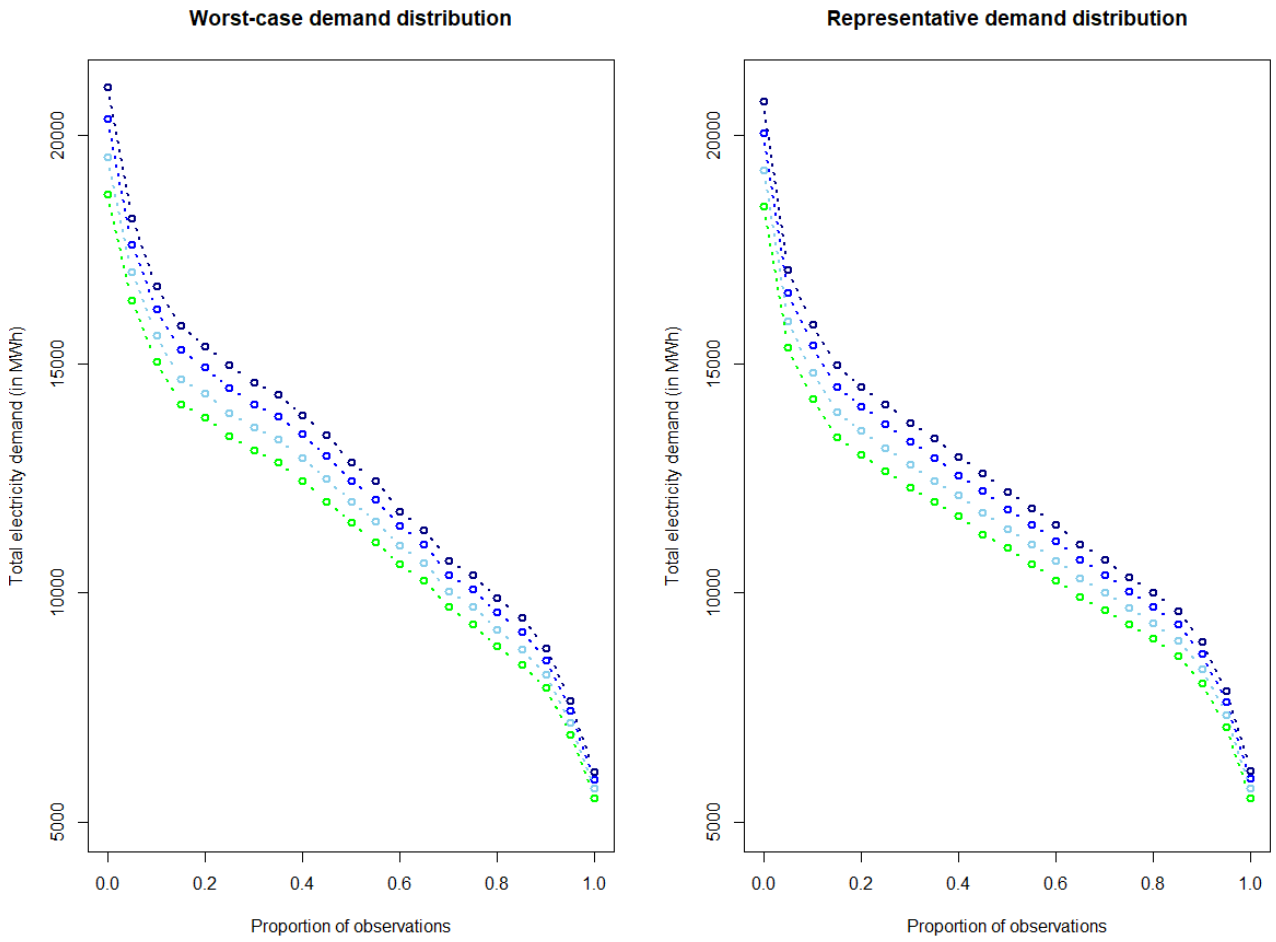

Figure 3.B.: Future worst-case and representative total electricity demand distributions

Note: The navy (resp. blue, light-blue and green) line corresponds to the baseline electricity demand distribution for 2021 (resp. projected electricity demand distribution for 2025, 2030 and 2035).

Appendix to 3.3.:

	Baseline	**− 10 %**	**− 30 %**	**− 50 %**
Objective function (B€)	5.103	5.101	5.138	5.487
Total overnight costs (B€)	2.036	1.734	2.088	5.671
Worst-case operational costs (B€)	0.207	0.210	0.205	0.188
Representative annual operational costs (B€)	0.691	0.664	0.661	0.592
Annuities (B€)	**0.320**	**0.285**	**0.328**	**0.623**
Combined cycle gas turbine	0.132	0.132	0.132	0.110
Gas turbine	0	0	0	0
Nuclear	0	0	0	0
Wind	0.068	0.063	0.061	0.378
PV	0.090	0.090	0.096	0.090
Hydroelectric	0	0	0	0
STEP	0	0	0	0
Battery storage	0.030	0	0.039	0.045
Yearly FOM costs (B€)	**2.343**	**2.333**	**2.345**	**2.472**
Combined cycle gas turbine	0.063	0.063	0.063	0.054
Gas turbine	0	0	0	0
Nuclear	1.836	1.836	1.836	1.836
Wind	0.030	0.027	0.027	0.164
PV	0.034	0.034	0.037	0.034
Hydroelectric	0.267	0.267	0.267	0.267
STEP	0.106	0.106	0.106	0.106
Battery storage	0.007	0	0.009	0.011
Nuclear retirement and prolongation costs (B€)	**1.577**	**1.577**	**1.577**	**1.577**

Table 4.B.: Cost allocation by technology and operational conditions with varying decommissioning costs

	Baseline	+5	+10	+15	+20
Objective function (B€)	5.103	5.206	5.203	5.176	5.083
Total overnight costs (B€)	2036	2.450	2.874	2.359	1.697
Worst-case operational costs (B€)	0.207	0.206	0.201	0.209	0.206
Representative annual operational costs (B€)	0.691	0.663	0.641	0.650	0.664
Annuities (B€)					
Combined cycle gas turbine	0.132	0.132	0.132	0.132	0.132
Gas turbine	0	0	0	0	0
Nuclear	0	0	0	0	0
Wind	0.068	0.060	0.144	0.106	0.060
PV	0.090	0.090	0.090	0.090	0.090
Hydroelectric	0	0	0	0	0
STEP	0	0	0	0	0
Battery storage	0.030	0.099	0.017	0.011	0
Yearly FOM costs (B€)					
Combined cycle gas turbine	0.063	0.063	0.063	0.063	0.063
Gas turbine	0	0	0	0	0
Nuclear	1.836	1.836	1.836	1.836	1.836
Wind	0.030	0.026	0.062	0.046	0.026
PV	0.034	0.034	0.034	0.034	0.034
Hydroelectric	0.267	0.267	0.267	0.267	0.267
STEP	0.106	0.106	0.106	0.106	0.106
Battery storage	0.007	0.023	0.005	0.003	0
Nuclear retirement and prolongation costs (B€)	1.577	1.577	1.577	1.577	1.577

Table 4.C Cost allocation by technology and operational conditions with varying total decommissioning time

	$\pi^{CO_2} = 50$ €/t	$\pi^{CO_2} = 100$ €/t	$\pi^{CO_2} = 150$ €/t	**2025**	**2030**
Objective function (B€)	5.599	5.707	6.152	5.398	5.308
Total investment costs (B€)	5.222	6.083	5.640	6.214	7.268
Worst-case operational costs (B€)	0.295	0.442	0.512	0.325	0.293
Representative annual operational costs (B€)	0.845	1.416	1.494	1.055	0.874
Annuities (B€)	**0.814**	**0.632**	**0.553**	**0.600**	**0.631**
Combined cycle gas turbine	0.287	0.309	0.287	0.287	0.287
Gas turbine	0	0	0	0	0
Nuclear	0	0	0	0	0
Wind	0.087	0.060	0.132	0.091	0.119
PV	0.090	0.090	0.090	0.139	0.171
Hydroelectric	0	0	0	0	0
STEP	0	0	0	0	0
Battery storage	0.105	0.173	0.044	0.083	0.054
Yearly FOM costs (B€)	**2.067**	**1.723**	**1.943**	**1.953**	**1.972**
Combined cycle gas turbine	0.126	0.135	0.126	0.126	0.126
Gas turbine	0	0	0	0	0
Nuclear	1.343	1.343	1.343	1.343	1.343
Wind	0.038	0.026	0.057	0.039	0.052
PV	0.034	0.034	0.034	0.053	0.065
Hydroelectric	0.267	0.267	0.267	0.267	0.267
STEP	0.106	0.106	0.106	0.106	0.106
Battery storage	0.024	0.040	0.010	0.019	0.013
Nuclear retirement and prolongation costs (B€)	**1.437**	**1.437**	**1.437**	**1.437**	**1.437**

Table 4.H.: Cost allocation by technology and operational conditions with varying carbon price and investment and fixed costs for renewables

Note: For all cases, we impose a minimum of 2 pairs of nuclear reactors to be decommissioned.

Appendix to 4.2.2.:

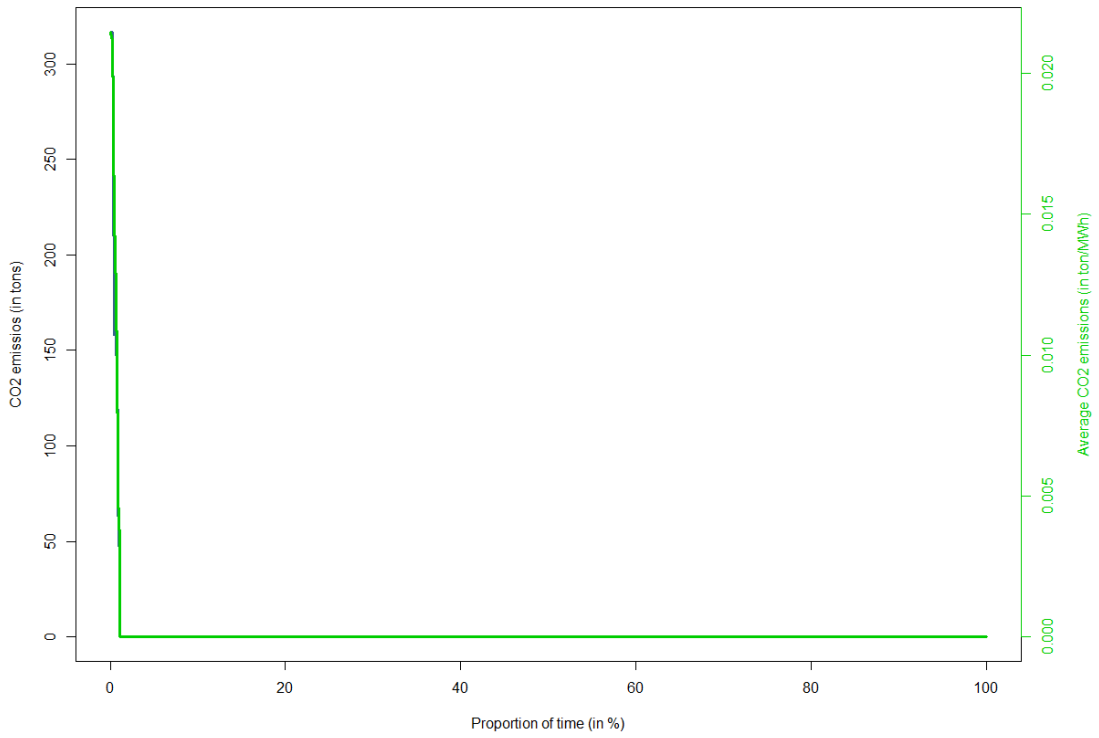

Figure 13.B.: Carbon emissions and carbon intensity distributions (representative weeks, optimal mix n°2)

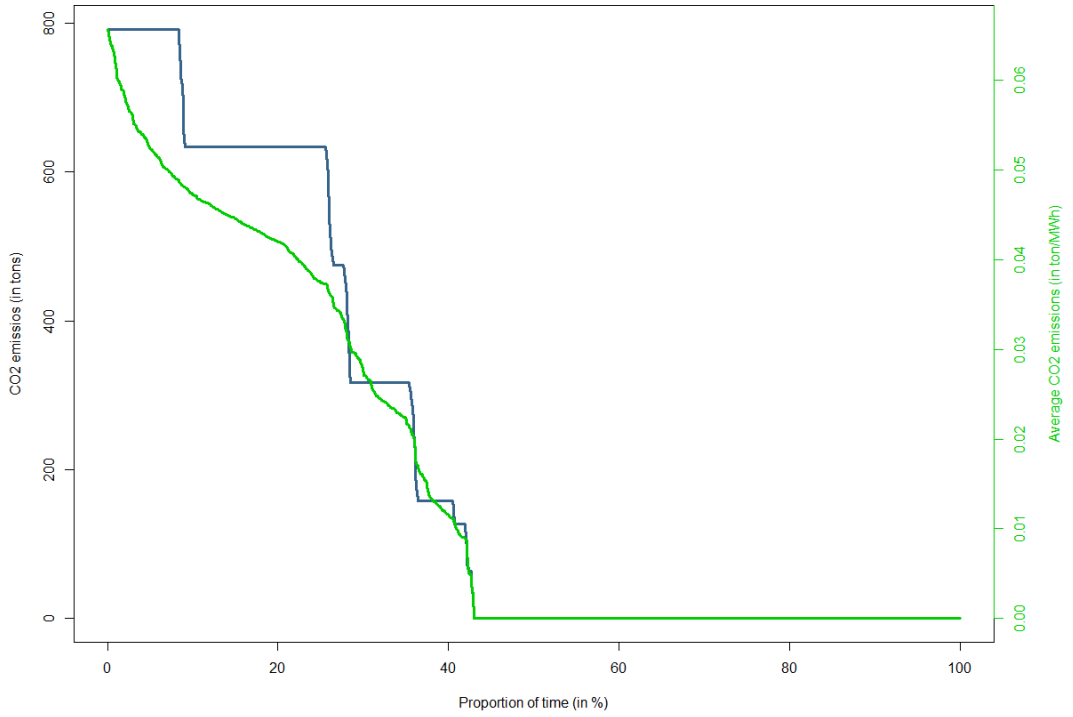

Figure 13.D.: Carbon emissions and carbon intensity distributions (representative weeks, optimal mix n°4)

7. Bibliography

[1] “Bilan Prévisionnel de l’équilibre offre-demande d’électricité en France”, RTE, Edition 2017, 44 p.

[2] “Flexible Nuclear Energy for Clean Energy Systems”, NICE Future, Technical Report NREL/TP-6A50-77088, September 2020

[3] CANY Camille, MANSILLA Christine, DA COSTA Pascal, MATHONNIERE Gilles, DUQUESNOY Thierry, “Nuclear and non-dispatchable renewables: two compatible supply options? The case of the French power mix”, 2015, ffhal-01242310, 38 p.

[4] MAÏZI Nadia, ASSOUMOU Edi, “Future prospects for nuclear power in France”, *Applied Energy*, vol. 136, 2014, pp. 849-859

[5] BRUNINX K., MADZHAROV D., DELARUE E., D’HAESLEER W., “Impact of the German nuclear phase out on Europe’s electricity generation – A comprehensive study”, *Energy Policy*, vol. 60, 2013, pp. 251-261

[6] LOGAN Jeffrey, LOPEZ Anthony, MAI Trieu, BAZILIAN Morgan, ARENT Douglas, “Natural gas scenarios in the US power sector”, *Energy Economics*, vol. 40, 2013, pp. 183-195

[7] KUNSCH Pierre L. & FRIESEWINKEL Jean, “Nuclear energy policy in Belgium after Fukushima”, *Energy Policy*, vol. 66, 2014, pp. 462-474

[8] KNOPF Brigitte, PAHLE Michael, KONDZIELLA Hendrik, JOAS Fabian, EDENHOFER Ottmar, BRUCKNER Thomas, “Germany’s Nuclear Phase Out: Sensitivities and Impacts on Electricity Prices and CO_2 emissions”, *Economics of Energy & Environmental Policy*, vol. 3, n°1, 2014, pp. 89-106

[9] MALISCHEK Raimund & TRÜBY Johannes, “The future of nuclear power in France: an analysis of the costs of phasing-out”, *Energy*, vol. 116, 2016, pp. 908-921

[10] Rapport prévisionnel “L’énergie nucléaire du future et les conséquences de l’abandon du projet de réacteur nucléaire de 4e génération « Astrid »”, enregistré sous le n°4331 à Assemblée Nationale et sous le n°758 au Sénat, 8 July 2021

[11] BAKER T. E., EPINEY A. S., RABITI C., SHITTU E., “Optimal sizing of flexible nuclear hybrid energy system components considering wind volatility”, *Applied Energy*, vol. 212, 2018, pp. 498-508

[12] “Baromètre 2021: La perception des risques et de la sécurité par les Français”, Institut de Radioprotection et de Sûreté Nucléaire (IRSN), 2021

[13] BOCCARD Nicolas, “The cost of nuclear electricity: France after Fukushima”, *Energy Policy*, vol. 66, 2014, pp. 450-461

[14] “Bilan Electrique 2019”, RTE, 2020, 173 p.

[15] “Enjeux du développement de l’électromobilité pour le système électrique”, RTE, May 2019, 80 p.

[16] JRC Scientific and Policy Reports, “Driving and parking patterns of European car drivers – a mobility survey”, Joint Research Centre, European Commission, Report EU 25627, 2012, 112 p.

[17] Cour des Comptes, *Rapport public annuel filière nucléaire :* “La maintenance des centrales nucléaires : une politique remise à niveau, des incertitudes à lever”, February 2016, 33 p.

[18] “Rapport fait au nom de la commission d’enquête sur la sûreté et la sécurité des installations nucléaires”, Assemblée Nationale, rapport n°1122, June 2018, 256 p.

[19] MOSLEM Uddin, MOHD FAKHIZAN Romlie, MOHD FARIS Abdullah, SYAHIRAH Abd Halim, AB HALIM Abu Bakar, TAN CHIA Kwang, “A review on peak load shaving strategies”, *Renewable and Sustainable Reviews*, vol. 82, 2018, pp. 3323-3332

[20] TSIROPOULOS I., TARVYDAS D., ZUCKER A., “Cost development of low carbon technologies : Scenario-based cost, trajectories to 2050, 2017 edition”, EUR 29034 EN, Publications Office of the European Union, Luxembourg, 2018, ISBN 978-92-79-77479-9, doi:10.2760/490059, JRC109894

[21] “Coûts et rentabilité du grand photovoltaïque en métropole continentale”, Rapport de la Commission de Régulation de l’Energie (CRE), Février 2019, 46 p.

[22] ADAN Hassan & FUERST Franz, “Do energy efficiency measures really reduce household energy consumption? A difference-in-difference analysis”, *Energy Efficiency*, vol. 9, 2016, pp. 1207-1219

[23] HIRTH Lion & STECKEL Jan Christoph, “The role of capital costs in decarbonizing the electricity sector”, *Environmental Research Letters*, vol. 11, 2016

[24] KOMIYAMA Ryoichi & FUJII Yasumasa, “Long-term scenario analysis of nuclear energy and variable renewables in Japan’s power generation mix considering flexible power resources”, *Energy Policy*, vol. 83, 2015, pp. 169-184

[25] PAGNIER Laurent, JACQUOD Philippe, “How fast can one overcome the paradox of the energy transition? A physico-economic model for the European power grid”, *Energy*, vol. 157, 2018, pp. 550-560

[26] “Non-baseload Operation in Nuclear Power Plants: Load Following and Frequency Control Modes of Flexible Operation”, IAEA Nuclear Energy Series, n° NP-T-3.23, 2018, 190 p.

[27] CANY CAMILLE, MANSILLA Christine, MATHONNIERE Gilles, DA COSTA Pascal, “Nuclear contribution to the penetration of variable renewable energy sources in a French decarbonized power mix”, *Energy*, vol. 150, 2018, pp. 544-555

[28] NOOR Sana, GUO Miao, VAN DAM Koen H., SHAH Nilay, WANG Xionan, “Energy Demand Side Management with supply constraints: Game theoretic Approach”, *Energy Procedia*, vol. 145, 2018, pp. 368-373

[29] TSITSIKLIS John N., XU Yunjian, “Pricing of fluctuations in electricity demand”, *European Journal of Operational Research*, 2015, pp. 1-10

[30] PINSON Pierre, *Estimation of the uncertainty in wind power forecasting*, Engineering Sciences [Physics], Ecole Nationale Supérieure des Mines de Paris, 2006, English. NNT: 2006ENMP1432ff. ffpastel00002187

[31] MORAL-CARCEDO Julian & PEREZ-GARCIA Julian, “Analysis and long term forecasting of electricity demand through a decomposition model: A case study for Spain”, *Energy*, vol. 97, 2016, 2016, pp. 127-143

Chapter IV:

Towards future electricity market designs: Ensuring cost-effectiveness and efficiency under significant RES penetration

Abstract – **In this last chapter, we investigate the remuneration issues of both conventional and RES generators under significant RES penetration. Then, we study the optimal joint distribution of production and spot prices that would be required for each type of generator to cover its annual fixed and variable costs. This provides a basis for analyzing how original market designs may better address these cost-effectiveness issues than the current French wholesale spot market. We analyze how an average cost bidding rule for RES, and scarcity pricing, by valuing more accurately real-time resources and operational constraints, may address the "Missing Money" issue and impact the remuneration of generators, in addition to the distribution of spot prices. Finally, we investigate the theoretical basis for an efficient Contract-for-Difference and compare its performances and costs with the FiP. Following the "insurer-of-last-resort" design, we also investigate theoretical and methodological grounds for an insurance overlay on wholesale market, based on customers' revealed preferences for reliability and system stability.**

Keywords- Renewable energy, electricity markets, Missing Money, scarcity price, subsidies

1. Introduction

With a growing share in electricity mixes, renewable energy sources (RES) are increasingly pointed out for depressing spot market prices and harming the long-term financial viability of incumbent generators, especially capitalistic ones like nuclear. Although the debt of a group such as EDF must be considered over the long-term to account for the high lifetime and amortization duration of investments, its official debt reached 42€ billion in June 2020[31]. As pointed by [1], most historic European utilities, such as E.ON and RWE, lost more than 50% of their capitalized value between 2015 and late 2016.

Under the existing spot market design, generation bids are submitted to the TSO and are ranked following the "merit order rule". RES technologies, with a quasi-null marginal cost of generation, are called first by the market operator and depress the spot price by pushing the more expensive production units out of the market. This phenomenon is known as the "merit order effect" and is well-studied in several countries. [2] show a significant negative effect on spot prices in addition to wealth transfer from generators to consumers. Furthermore, they find that the negative impact of RES penetration on the distribution of spot prices decisively depends on how fast surplus must-run thermal capacities are phased out. This is in accordance with the findings of [3], who show that the growth rate of RES investments and the rate of must-run units withdrawal are key components in examining the magnitude and duration of the "paradox of the energy transition". Using a two-state Markov switching model, [4] show that a higher RES capacity induces a negative marginal effect on spot prices, which is stronger in relatively high-prices regimes. They also measure how both wind and solar generation significantly impact the distribution of spot prices, in particular the frequency and expected duration of low-prices and high-prices regimes.

These depressed prices call for subsidy mechanisms, such as the FiT and FiP, to adequately remunerate RES generators and incentivize investment. However, the cost burden represented by these subsidies is significant and generates inefficiencies. As explained by [5], electricity customers pay a higher price for electricity that is sold at a loss upstream. Moreover, as the FiP provides a variable total income, it does not suppress the price risk borne by RES generators, especially as RES penetration increases price volatility. Alternative subsidy

[31] https://www.transitionsenergies.com/edf-dette-42-milliards-euros-realite-bien-plus/

mechanisms, such as the Contract-for-Difference (CfD), which may also be adequate for nuclear capacity investments, might provide a more stable source of revenue while simultaneously lowering the tax burden.

However, such off-market mechanisms do not restore the solvency of conventional technologies such as nuclear or combined-cycle gas turbines. Adapting the market design to increase the efficiency of the price signal is thus a preferable direction in the long-term. Although RES penetration reduces the profitability of all power plants, the structural remuneration deficit of electricity generator, known as the "Missing Money" issue [6], is not caused but only worsened by RES. Following [7], RES integration does not modify the fundamental economic principles behind market design. As the wholesale market design does not allow prices to spike above a legal threshold, the rarity annuity required to cover fixed costs is not received by peaking generators. Furthermore, RES shift the value of the electricity market from energy to reserve and ancillary services, which requires adapting the market design. As flexibility becomes a central element of the stability of future electric systems, it needs to be rewarded as a system service. Accurately pricing real-time resource availability and scarcity is thus pivotal in order to restore the efficiency of the price signal. However, such design reform is expected to be incomplete without a real-time and comprehensive valuation of electricity by different customers.

In Section 2, we investigate the remuneration issues of both conventional and RES generators under significant RES penetration. Then, we analyze in Section 3 how average cost bidding rule for RES, and scarcity pricing, by valuing more accurately real-time resources and supply constraints, impact the remuneration of generators and the distribution of spot prices. In Section 4, we investigate the theoretical basis for an efficient CfD and compare its performances and costs with the FiP. Following the "insurer-of-last-resort" design proposed in [8], we also investigate theoretical grounds for an insurance overlay on wholesale market based on customers' revealed preferences for reliability and system stability. Conclusions and policy recommendations are given in Section 5.

2. Market remuneration analysis under marginal-cost bidding

2.1. Econometric model for day-ahead equilibrium price

The mechanism by which the spot market is set in wholesale electricity markets is called the "merit-order" rule. The cheapest offers are thus selected first by the TSO, such as RES, hydroelectric and nuclear generation, followed by more expensive bids made by peaking-units for instance. In theory, the equilibrium price is set at the marginal cost of the last generation unit selected by the TSO in its optimal dispatch.

In the following analysis, we use the optimization model presented in Chapter III, applied to the subset of 8 representative weeks (2 weeks for each season), and fix capacities to their optimal levels corresponding to mix n°2. The dual variables of the demand-balance can be interpreted as shadow prices and correspond to the marginal cost of the last production unit selected to ensure balance of supply and demand. Thus, they provide a good approximation for the theoretical spot price. However, the resulting distribution of spot prices is very flat, and its values are often too low compared to historic prices observed on the EPEX Spot market. In order to obtain a more realistic simulation of market revenues under future electricity mixes and high RES penetration, we couple our optimization model with a simple econometric model linking spot prices, residual demand and market fundamentals, such as dispatched generation volumes by technology and carbon price.

Using 2015 RTE and French EPEX Spot data, [5] quantify the loss of economic value induced by the introduction of RES on historic conventional producers. Overall, they find a negative price effect of RES on conventional generators of 2.7 billion euros and a negative volume effect of 0.2 billion euros over 2015. Their results are based on a simple OLS regression model: their regressors include the average daily level, in addition to the deviation of hourly values from the daily average, for electric load, solar and wind generation. A different set of coefficients is estimated for each season separately. Adopting a similar approach, we use national spot price data with hourly resolution over the period 2015-2019 from ENTSO-E[32]. We merge the vector of spot prices with database on consumption and generation from RTE over the same period and defined at the national scale. Observations are indexed by subscript $m, 0 \leq m \leq N$, where N is the total sample size. We divide it into four season-based subsets. We consider a linear specification of the relationship between spot

[32] https://transparency.entsoe.eu/

prices and market fundamentals, which includes in our case residual demand-based metrics and dispatched generation volume for each thermal technology. For each season $s \in \mathcal{S}$ and observation m, we note $\overline{\boldsymbol{R}_{\boldsymbol{U}_{sm}}}$ the average daily RD, $\overline{\Delta \boldsymbol{R}_{\boldsymbol{U}_{sm}}}$ the deviation of hourly RD from its daily average, and $\Delta \boldsymbol{R}_{\boldsymbol{U}_{sm}}$ the hourly variation of RD.

To avoid confusion with notations adopted in the previous chapters, we define $\mathfrak{T}_{\mathcal{G}}$ the set of thermal technologies, with element $\mathrm{t}_{\mathcal{G}} \in \mathfrak{T}_{\mathcal{G}}$[33]. We further define the subset of carbon-emitting thermal technologies $\mathfrak{T}_{\mathcal{G}}' \subseteq \mathfrak{T}_{\mathcal{G}}$, and the superset $\mathfrak{T}$, with element $\mathrm{t} \in \mathfrak{T}$ and $\mathfrak{T}_{\mathcal{G}} \subset \mathfrak{T}$, such that $\mathfrak{T}$ includes both thermal and renewable technologies[34]. We define the aggregated generation of thermal technology $\mathrm{t}_{\mathcal{G}}$ in season s and observation m as $Q_{sm}^{\mathrm{t}_{\mathcal{G}}}$. Finally, we define the dummy variable $X_{sm}^{\mathrm{t}_{\mathcal{G}}}$ equal to 1 if $Q_{sm}^{\mathrm{t}_{\mathcal{G}}} > 0$, which are multiplied by the carbon price $\pi_s^{CO_2}$. The linear regression model has the following form:

$$P_{sm} = \gamma_s + \gamma_{1s}\overline{\boldsymbol{R}_{\boldsymbol{U}_{sm}}} + \gamma_{2s}\overline{\Delta \boldsymbol{R}_{\boldsymbol{U}_{sm}}} + \gamma_{3s}\Delta \boldsymbol{R}_{\boldsymbol{U}_{sm}} + \sum_{\mathrm{t}_{\mathcal{G}} \in \mathfrak{T}_{\mathcal{G}}} \theta_{\mathrm{t}_{\mathcal{G}}s} Q_{sm}^{\mathrm{t}_{\mathcal{G}}} + \sum_{\mathrm{t}_{\mathcal{G}} \in \mathfrak{T}_{\mathcal{G}}'} \mu_{\mathrm{t}_{\mathcal{G}}s} X_{sm}^{\mathrm{t}_{\mathcal{G}}} \pi_s^{CO_2} + \epsilon_{sm} \quad (\mathbf{1})$$

γ_s is a fixed parameter capturing the effect of seasonality, while $\mu_{\mathrm{t}_{\mathcal{G}}s}$ captures how carbon-emitting technologies influence the spot price depending on the price of carbon. Finally, we note the error term ϵ_{sm}. The above model is estimated via OLS. We note $\left(\widehat{\gamma_s}, \widehat{\gamma_{1s}}, \widehat{\gamma_{2s}}, \widehat{\gamma_{3s}}, \left(\widehat{\theta_{\mathrm{t}_{\mathcal{G}}s}}\right)_{\mathrm{t}_{\mathcal{G}} \in \mathfrak{T}_{\mathcal{G}}}, \left(\widehat{\mu_{\mathrm{t}_{\mathcal{G}}s}}\right)_{\mathrm{t}_{\mathcal{G}} \in \mathfrak{T}_{\mathcal{G}}}\right)$ the vector of estimated coefficients.

Our approach follows a two-step procedure and allows the computation of the spot prices distribution corresponding to a given set of optimal production values. For each type of technology $\mathrm{t}_{\mathcal{G}} \in \mathfrak{T}_{\mathcal{G}}$, we note $Q_{st}^{\mathrm{t}_{\mathcal{G}}^*} \in \mathbb{R}^+$ the optimal aggregated volume of electricity generation in season $s \in \mathcal{S}$ and $t \in \mathcal{T}$. Similarly, $X_{st}^{\mathrm{t}_{\mathcal{G}}^*}$ is the optimal commitment state of $\mathrm{t}_{\mathcal{G}}$. The vector of optimal values is first computed for Auvergne-Rhône-Alpes by applying our optimization model to our set of representative weeks. Then, we plug the equilibrium residual

[33] Recall that $\mathcal{G}$ is the set of individual thermal units. We have by definition $\mathfrak{T}_{\mathcal{G}} = \mathcal{G}$, but $\mathfrak{T}_{\mathcal{G}} = \{\mathcal{N}, \mathcal{C}^1, \mathcal{C}^2, \mathcal{H}^1, \mathcal{H}^2\}$, where $\mathcal{N}, \mathcal{C}_1, \mathcal{C}_2, \mathcal{H}_1, \mathcal{H}_2$ are respectively the subset of nuclear plants, combined-cycle gas turbines, oil-powered gas turbines, , hydroelectric units and pumped-storage hydroelectric defined in the above chapters.

[34] We have $\mathfrak{T} = \{\mathcal{N}, \mathcal{C}^1, \mathcal{C}^2, \mathcal{H}^1, \mathcal{H}^2, \mathcal{P}, \mathcal{W}\}$, where $\mathcal{P}$ and $\mathcal{W}$ are respectively the subset of photovoltaic and wind power generation units.

demand, generation and commitment values in **(1)** to estimate the "recomputed" spot price $\widehat{P_{st}}$, for each $s \in \mathcal{S}$ and $t \in \mathcal{T}$:

$$\widehat{P_{st}} = \widehat{\gamma_s} + \widehat{\gamma_{1s}}\overline{\boldsymbol{R}_{\boldsymbol{U}}{}^{*}_{st}} + \widehat{\gamma_{2s}}\overline{\Delta\boldsymbol{R}_{\boldsymbol{U}}{}^{*}_{st}} + \widehat{\gamma_{3s}}\Delta\boldsymbol{R}_{\boldsymbol{U}}{}^{*}_{st} + \sum_{\mathrm{t}_\mathcal{G} \in \mathfrak{T}_\mathcal{G}} \widehat{\theta_{\mathrm{t}_\mathcal{G} s}} Q_{st}^{\mathrm{t}_\mathcal{G}{}^{*}} + \sum_{\mathrm{t}_\mathcal{G} \in \mathfrak{T}_\mathcal{G}'} \widehat{\mu_{\mathrm{t}_\mathcal{G} s}} X_{st}^{\mathrm{t}_\mathcal{G}{}^{*}} \qquad (\mathbf{2})$$

However, the above model is estimated over national data. The shares of each technology in total regional production may not be comparable to their shares at the national scale. The same remark applies to RD. We define $\omega_{\boldsymbol{R}} < 1$ the average share of RD from Auvergne-Rhône-Alpes in total national RD. Similarly, we note $\omega_{\mathrm{t}_\mathcal{G}} < 1$ the share in national capacities of technology $\mathrm{t}_\mathcal{G} \in \mathfrak{T}_\mathcal{G}$ installed in Auvergne-Rhône-Alpes. The weighted recomputed spot price is defined as follows:

$$\widehat{P_{st}} = \widehat{\gamma_s} + \omega_{\boldsymbol{R}}^{-1}\left(\widehat{\gamma_{1s}}\overline{\boldsymbol{R}_{\boldsymbol{U}}{}^{*}_{st}} + \widehat{\gamma_{2s}}\overline{\Delta\boldsymbol{R}_{\boldsymbol{U}}{}^{*}_{st}} + \widehat{\gamma_{3s}}\Delta\boldsymbol{R}_{\boldsymbol{U}}{}^{*}_{st}\right) + \sum_{\mathrm{t}_\mathcal{G} \in \mathfrak{T}_\mathcal{G}} \omega_{\mathrm{t}_\mathcal{G}}^{-1}\widehat{\theta_{\mathrm{t}_\mathcal{G} s}} Q_{st}^{\mathrm{t}_\mathcal{G}{}^{*}} + \sum_{\mathrm{t}_\mathcal{G} \in \mathfrak{T}_\mathcal{G}'} \widehat{\mu_{\mathrm{t}_\mathcal{G} s}} X_{st}^{\mathrm{t}_\mathcal{G}{}^{*}} \qquad (\mathbf{3})$$

The estimated coefficients are reported in **Table 1**. As spot prices display significant interannual variability, we add yearly dummies for robustness. As shown in **Figure 1.**, the prices predicted by our model closely follow the short-term and long-term trends of historic prices. However, it fails to capture price spikes and drops, especially negative prices. Our simple model also does not account for the formation of price regimes and their transition dynamics. Although it accounts for very short-term hourly and daily dynamics of residual demand, it does not intend to provide a forecasting tool either. Markov regime-switching models [4], threshold panel models with a smooth transition or autoregressive models (see [9]) provide richer specifications of the non-linear relationship between spot price and market fundamentals. Our results however try to give a complete picture of the price distribution associated to a given generation dispatch in representative operational conditions.

Variable	Regression Coefficients (S.E.)			
	Winter	**Spring**	**Summer**	**Autumn**
Residual demand variables (in MWh)				
(Reported coefficients are multiplied by 10^3)				
$\overline{\boldsymbol{R}_{\boldsymbol{U}_{sm}}}$	1.228***	0.562***	0.660***	1.304***
	(0.026)	(0.023)	(0.026)	(0.029)
$\overline{\boldsymbol{\Delta R}_{\boldsymbol{U}_{sm}}}$	1.214***	0.123***	0.272***	1.095***
	(0.038)	(0.028)	(0.027)	(0.041)
$\boldsymbol{\Delta R}_{\boldsymbol{U}_{sm}}$	0.819***	0.759***	0.719***	0.968***
	(0.034)	(0.030)	(0.026)	(0.035)
Generation variables (in MWh)				
(Reported coefficients are multiplied by 10^3 for each $t_{\mathcal{G}} \in \mathfrak{T}_{\mathcal{G}}$)				
Nuclear	- 0.232***	0.683***	0.038	- 1.315***
	(0.037)	(0.030)	(0.025)	(0.035)
Oil	10.11***	- 1.927***	- 0.672	3.724***
	(0.031)	(0.553)	(0.546)	(0.457)
Gas (CCGT)	0.612***	0.545***	2.606***	0.197*
	(0.082)	(0.073)	(0.073)	(0.097)
Hydroelectric	- 1.585***	1.092***	- 0.762***	- 1.053***
	(0.063)	(0.062)	(0.051)	(0.074)
Pumped-storage turbines	1.456***	2.315***	2.875***	3.530***
	(0.106)	(0.080)	(0.083)	(0.112)
Carbon price × Gas (CCGT)	0.835***	2.127***	1.842***	1.883***
	(0.051)	(0.097)	(0.052)	(0.165)
Carbon price × Oil	NA	NA	NA	NA
Year Dummies	Yes	Yes	Yes	Yes
Intercept	- 22.20***	- 44.54***	- 7.322***	26.18***
	(1.632)	(1.432)	(1.024)	(1.737)
Number of observations				
Adjusted R^2 (in %)	76.41	69.41	83.77	75.33

Table 1: Estimated regression coefficients, by season

Note: NA = Non-Available

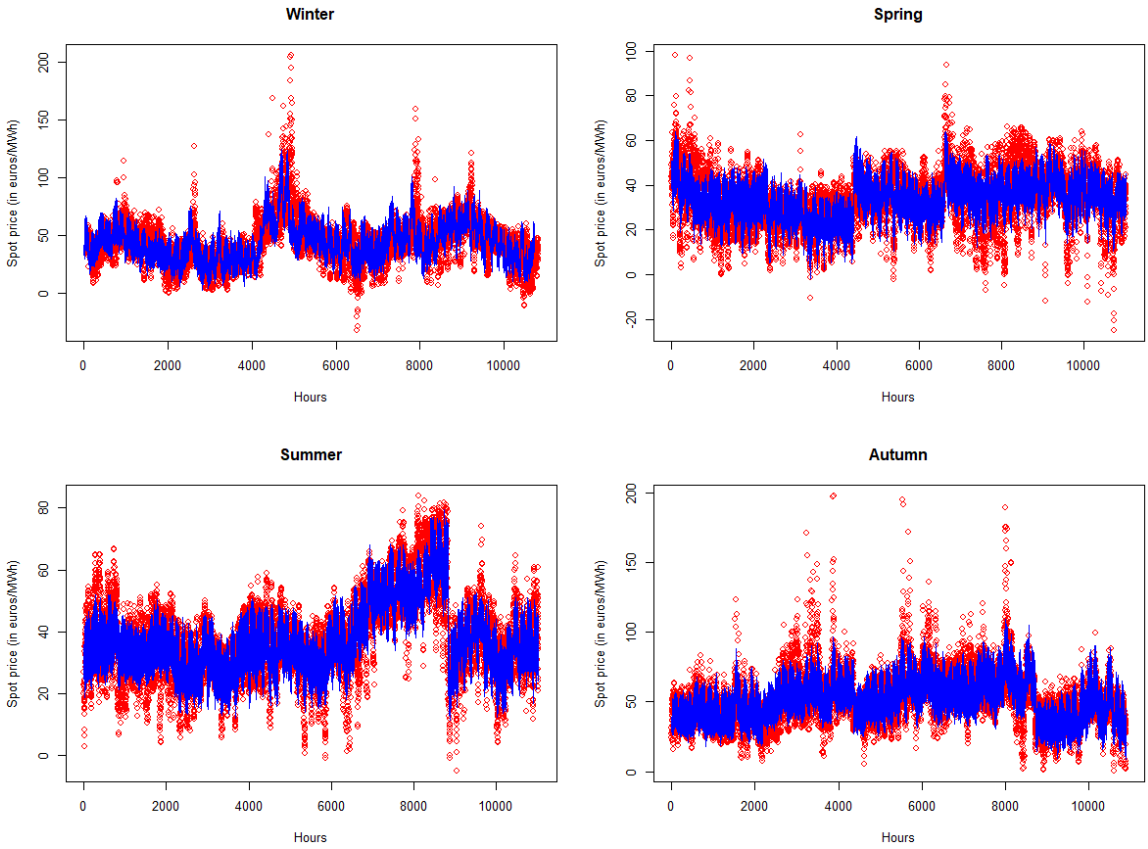

Figure 1: Predicted spot prices versus historic observed spot prices, from 2015 to 2019

Note: Each red dot corresponds to an observation in our sample of spot prices. For each graph, the blue line corresponds to the sequence of predicted spot prices.

2.2. Price-production joint patterns analysis

For each technology $\mathfrak{t} \in \mathfrak{T}$, we note its hourly load factor $u_{st}^{\mathfrak{t}}, 0 \leq u_{st}^{\mathfrak{t}} \leq 1$, which is simply equal to the total generation $Q_{st}^{\mathfrak{t}}$ divided by optimal installed capacity $C_{\mathfrak{t}}^{*}$. To avoid confusion with the index for hours t, we write $\mathfrak{t}$ in the exponent. $u_{st}^{\mathfrak{t}}$ is equivalent to the average utilization rate computed across all generation units of technology $\mathfrak{t} \in \mathfrak{T}$. **Figure 2** plots the optimization model dual values ("model spot price") against the distribution of spot prices recomputed with our econometric approach. We notice the recomputed spot prices distribution closely follows the distribution of the model spot prices, but is systematically higher, with price spikes above the marginal cost of CCGT units a few hours in the year. Finally, the probability of negative spot prices is significantly higher than in the optimization model, occurring in 6.1% of hours.

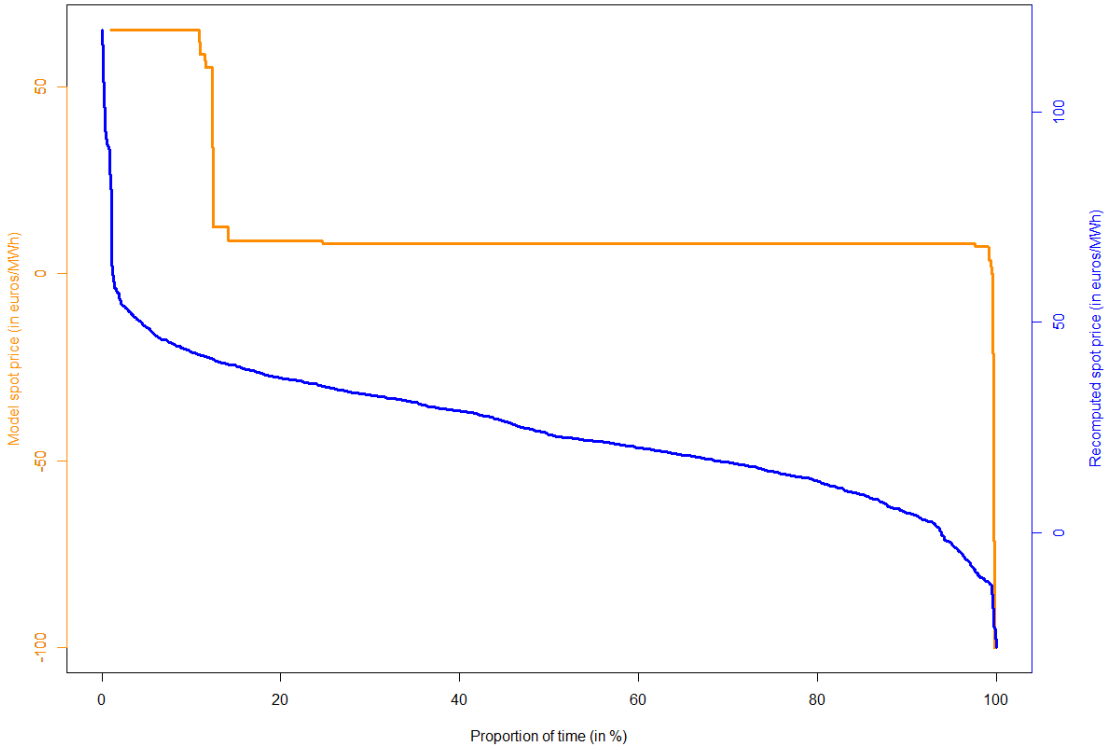

Figure 2: Model and recomputed spot price distribution

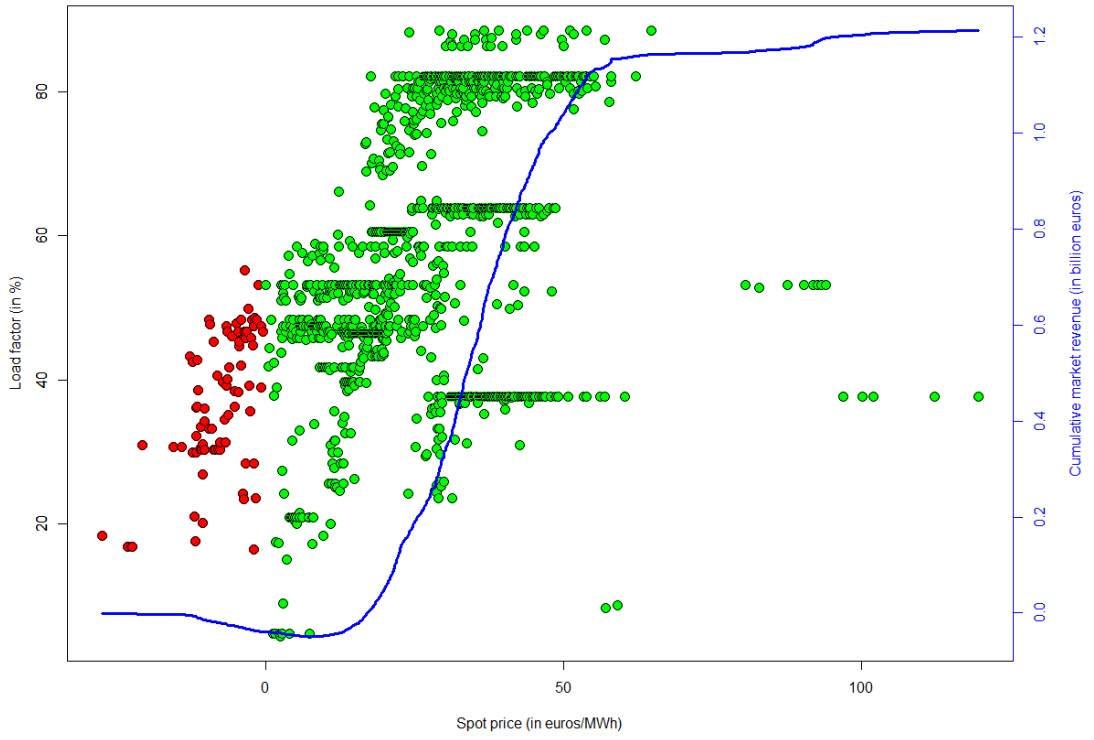

Figure 3.A.: Spot price and load factor patterns for the remuneration of nuclear units

Note: The green (resp. the red) dots correspond to couples of positive (resp. negative) spot price and load factor values. As we select 2 representative weeks for each season in our modeling approach, each point thus represents approximately 6.5 hours in a full year.

As shown by **Table 3.A.**, the cumulated net market revenue of the regional nuclear fleet over a full year equals 1.214€ billion. With a total generation of 64 TWh and without including annuities and FOM costs, nuclear generation units make an average unit profit of 18.93 €/MWh. With 1.836€ billion in FOM costs and 1.577€ billion of reactor prolongation cost, the nuclear operator makes a loss of 2.199€ billion, or equivalently, covers only 36% of total annual costs. Given the above volume of generation, a minimum spot price of 53.21 €/MWh is required to break even. While the average load factor represents 55% of installed capacities, we note it increases with the spot price and reaches an average 64% for prices above 30 €/MWh. However, 97% of generated electricity is sold for a price below the break-even price, which indicates the average prices are generally too low for nuclear to be cost-effective.

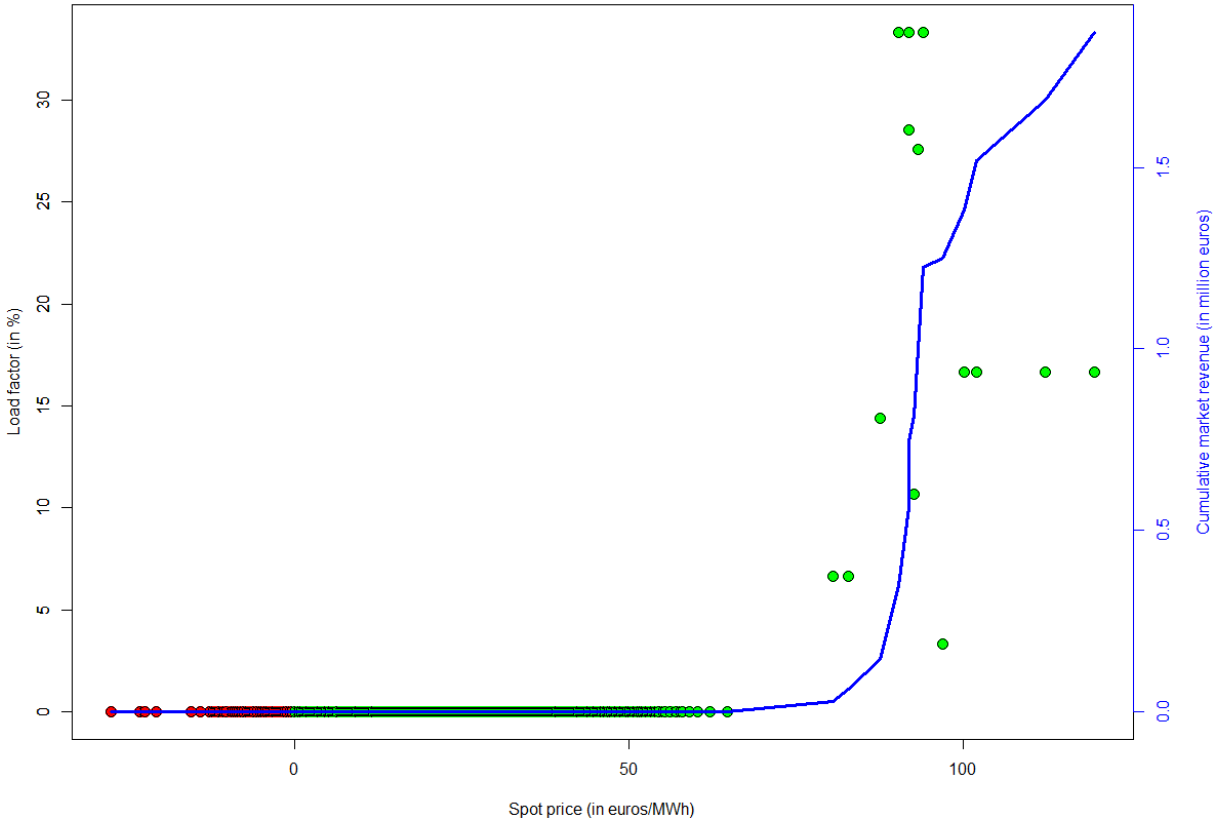

Figure 3.B.: Spot price and load factor patterns for the remuneration of CCGT units

The remuneration pattern of CCGT units draw a completely different picture. **Table 3.B.** shows that their average hourly load factor is null 98.9% of hours. Moreover, within the few hours during which CCGT units are operated, the average hourly load factor remains below 30%, with an average of 19%. With a mean unit profit of 40 €/MWh, the annual volume of

generation is however too low to ensure a proper remuneration. With 0.164€ billion in FOM costs and annuities, the CCGT operator only covers 1.1 % of total annual costs. It may be argued that our econometric model does not capture price spikes and thus contributes to underestimate the market remuneration of peaking units. Indeed, as already noted in **Table 2.A.**, the price ceiling of 3000 €/MWh is attained a few hours in our optimization model, indicating tight supply conditions. Taking the model spot price distribution instead of the recomputed distribution, we find a total market revenue of 35.1€ millions. This remains however too low to break-even, as the minimum price required for the observed levels of generation is superior to 3532 €/MWh, above the legal price ceiling. Recalling our robust methodology applied in Chapter III, this suggests the number of operating hours and load factor of peaking units required to ensure security of supply in very high RD periods is too low in representative operational conditions to ensure cost recovery.

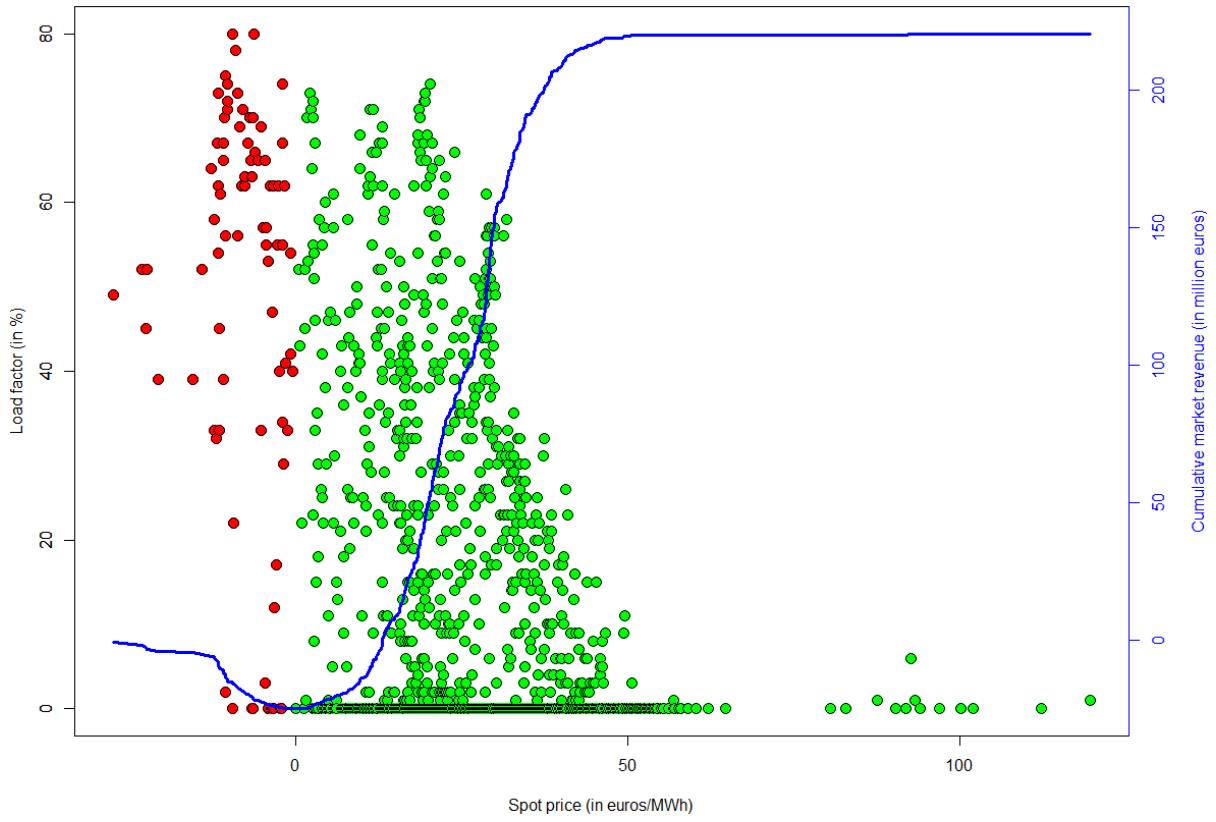

Figure 3.C.: Spot price and load factor patterns for the remuneration of photovoltaic units

As shown in **Figure 3.C.**, the total cumulative market revenue of photovoltaic increases very sharply for intermediate price values to reach 0.220€ billion. Because of the diurnal pattern of solar generation, photovoltaic units have an average hourly load factor of only 14.98%. Yet, it

increases to 30.42% during daylight hours, which can be explained by the south location of Auvergne-Rhône-Alpes and its strong solar irradiation. Still, with an average unit profit of 14.38 €/MWh, the operator of photovoltaic unit covers 52 % of annuities and annual FOM costs. While the break-even price is quite low (approximately 27 €/MWh), the negative correlation between solar production and spot prices prevents the photovoltaic operator to benefit from high price episodes. Indeed, while the average hourly load factor equals 20.7 % for spot prices below 30 €/MWh, it falls to 5.02 % above this threshold. This illustrates the self-cannibalizing effect (see [10]) of RES already mentioned in the literature: by decreasing the marginal cost of electricity, RES push spot prices down and undermine the conditions necessary for their own cost-effectiveness.

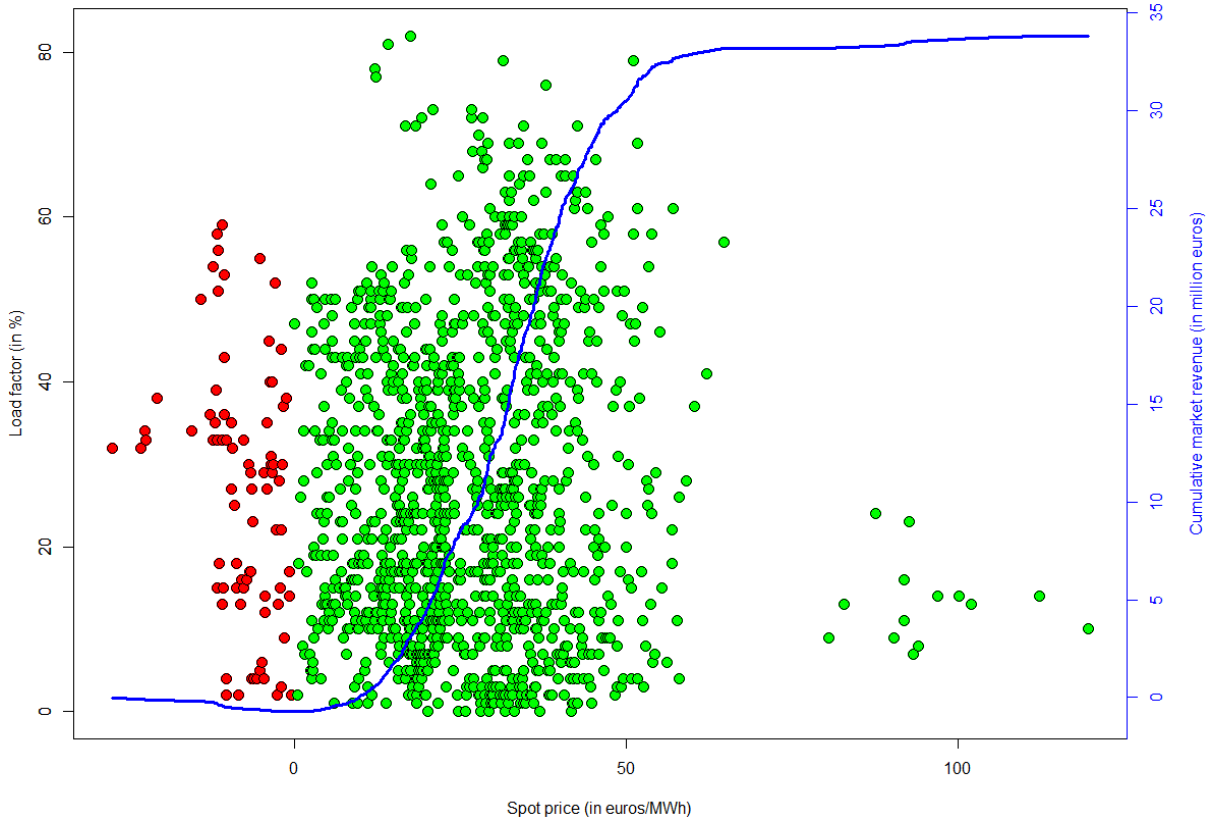

Figure 3.D.: Spot price and load factor patterns for the remuneration of wind units

Similar conclusions can be made for the market remuneration of wind generation units. With a total cumulated generation of 1.366 TWh, the operator of wind turbines fails to achieve cost recovery. With an average unit profit of 24.77 €/MWh, wind units only cover 41% of their annual total fixed costs. While they enjoy a higher average hourly load factor than photovoltaic units, equal to 27.2%, we find a minimum break-even spot price of 60.8 €/MWh

for wind turbines. Following the assumptions made in Chapter III, the costs of photovoltaic units are expected to decrease much faster than those of wind turbines, as the latter is assumed to be a more mature sector. Moreover, while wind generation does not seem to significantly decrease spot prices due to its reduced share in the electricity mix (slightly more than 1% of the total installed capacity), wind turbines are far more likely to operate under low to moderate spot price regimes than under high ones (above 40 €/MWh).

[11] suggest a higher CO_2 price could help RES generators become economically viable without requiring subsidies. The authors stress that the carbon price necessary for wind power to become profitable is significantly higher than the price required for making wind generation competitive based on levelized costs. However, following the above results, it appears that photovoltaic and wind generation is quasi null under the high spot prices regime observed when CCGT units participate to production.

Still, as future RD values are known, there is no uncertainty related to demand and RES production in our model, so reserve requirements are null. We would expect CCGT total generation to be higher, because of its participation in system balancing operations and reserve capacity especially.

2.3. ‘Missing-money’ diagnosis

As illustrated in the previous section, the remuneration patterns and related issues are very specific to each technology. While spot prices are on average too low to cover nuclear costs, we showed both the price ceiling and their very reduced number of operating hours prevent CCGT units to break even. It may thus be valuable to analyze the specific causes and remedies to insufficient market remuneration for each type of technology present in the mix.

For each technology $\mathrm{t} \in \mathfrak{T}$, we note $F_\mathrm{t} \geq 0$ the sum of total annual FOM costs and annuities. By definition, a generation technology is profitable if the cumulative market revenue received during the year is superior to the sum of F_t and its operational costs. Assuming variable costs and carbon emission factors are equal for all units of a given technology, we further define $V_\mathrm{t} \geq 0$ the variable cost of $\mathrm{t} \in \mathfrak{T}$. Using notations from previous chapters, we can decompose V_t as the sum of fuel costs $c_\mathrm{t}^V \geq 0$ and CO_2-related emission costs $\pi^{CO_2} E_\mathrm{t}$, where E_t is measured in tons/MWh, such that $V_\mathrm{t} = c_\mathrm{t}^V + \pi^{CO_2} E_\mathrm{t}$. Without loss of generality, we neglect

non-convex start-up costs for simplicity. Finally, we note the total number of hours within a year H.

For each couple of spot market price $\lambda \in \mathbb{R}$ and average load factor $u^{\mathfrak{t}}$, there exists a value $\Psi_{\mathfrak{t}}(\lambda, u^{\mathfrak{t}}) \in \mathbb{R}$ such that $u^{\mathfrak{t}} C_{\mathfrak{t}}^{*} H \Psi_{\mathfrak{t}}(\lambda, u^{\mathfrak{t}})(\lambda - V_{\mathfrak{t}}) \geq F_{\mathfrak{t}}$, with $\Psi_{\mathfrak{t}}(\lambda, u^{\mathfrak{t}}) \geq F_{\mathfrak{t}} \left(u^{\mathfrak{t}} C_{\mathfrak{t}}^{*} H(\lambda - V_{\mathfrak{t}})\right)^{-1}$. It is straightforward to see that $\Psi_{\mathfrak{t}}(\lambda, u^{\mathfrak{t}}) \to +\infty$ when $u^{\mathfrak{t}} \to 0$ or $\lambda \to^{+} V_{\mathfrak{t}}$, and $\Psi_{\mathfrak{t}}(\lambda, u^{\mathfrak{t}}) = -\infty$ when $\lambda \leq V_{\mathfrak{t}}$. The quantity $H\Psi_{\mathfrak{t}}(\lambda, u^{\mathfrak{t}})$ can naturally be interpreted as the minimum number of hours within a year that is necessary to gain a market revenue at least equal to $F_{\mathfrak{t}}$ if the spot market price and average load factor remain equal to λ and $u^{\mathfrak{t}}$. Furthermore, we note that for values such that $0 \leq \Psi_{\mathfrak{t}}(\lambda, u^{\mathfrak{t}}) \leq 1$, $\Psi_{\mathfrak{t}}(\lambda, u^{\mathfrak{t}})$ can be interpreted as the probability of making non-negative profits given λ and $u^{\mathfrak{t}}$. Then, it is possible to define the "sufficient remuneration set", noted $\mathfrak{Z}_{\mathfrak{t}}^{\Psi}$, as the set of all triplets $\left(\lambda, u^{\mathfrak{t}}, \Psi_{\mathfrak{t}}(\lambda, u^{\mathfrak{t}})\right)$ such that :

$$\mathfrak{Z}_{\mathfrak{t}}^{\Psi} = \left\{ \begin{matrix} \lambda \in \mathbb{R} \\ u^{\mathfrak{t}} \in [0,1] \\ \Psi_{\mathfrak{t}}(\lambda, u^{\mathfrak{t}}) \in \mathbb{R} \end{matrix} \middle| \Psi_{\mathfrak{t}}(\lambda, u^{\mathfrak{t}}) \geq F_{\mathfrak{t}} \left(u^{\mathfrak{t}} C_{\mathfrak{t}}^{*} H(\lambda - V_{\mathfrak{t}})\right)^{-1} \right\} \quad (\mathbf{4})$$

$\mathfrak{Z}_{\mathfrak{t}}^{\Psi}$ simply corresponds to the set of all combinations of spot market price, utilization rate and joint annual probability of occurrence such that the expected net market remuneration exceeds yearly FOM costs and annuities. For a constant utilization rate $u^{\mathfrak{t}}$, a lower number of operating hours is required to achieve cost-recovery if the spot price λ is high than if it is low. Similarly, if λ is kept constant, then generation units of technology $\mathfrak{t} \in \mathfrak{T}$ must be operated at a higher average load factor $u^{\mathfrak{t}}$ over the year if the joint probability $\Psi_{\mathfrak{t}}(\lambda, u^{\mathfrak{t}})$ is low.

We can easily prove the convexity of the set $\mathfrak{Z}_{\mathfrak{t}}^{\Psi}$. Let us define the triplets $\left(\lambda_1, u_1^{\mathfrak{t}}, \Psi_{\mathfrak{t}}(\lambda, u^{\mathfrak{t}})_1\right)$ and $\left(\lambda_2, u_2^{\mathfrak{t}}, \Psi_{\mathfrak{t}}(\lambda, u^{\mathfrak{t}})_2\right)$ such that $\left(\lambda_1, u_1^{\mathfrak{t}}, \Psi_{\mathfrak{t}}(\lambda, u^{\mathfrak{t}})_1\right) \in \mathfrak{Z}_{\mathfrak{t}}^{\Psi}$ and $\left(\lambda_2, u_2^{\mathfrak{t}}, \Psi_{\mathfrak{t}}(\lambda, u^{\mathfrak{t}})_2\right) \in \mathfrak{Z}_{\mathfrak{t}}^{\Psi}$. Thus, by definition of $\mathfrak{Z}_{\mathfrak{t}}^{\Psi}$, $u_1^{\mathfrak{t}} \Psi_{\mathfrak{t}}(\lambda, u^{\mathfrak{t}})_1 (\lambda_1 - V_{\mathfrak{t}}) \geq \frac{F_{\mathfrak{t}}}{C_{\mathfrak{t}}^{*} H}$ and $u_2^{\mathfrak{t}} C_{\mathfrak{t}}^{*} H \Psi_{\mathfrak{t}}(\lambda, u^{\mathfrak{t}})_2 (\lambda_2 - V_{\mathfrak{t}}) \geq \frac{F_{\mathfrak{t}}}{C_{\mathfrak{t}}^{*} H}$. For any couple $(\alpha_1, \alpha_2) \in [0,1]^2$ such that $\alpha_2 = 1 - \alpha_1$, we can use the above expression to see that $\alpha_1 u_1^{\mathfrak{t}} \Psi_{\mathfrak{t}}(\lambda, u^{\mathfrak{t}})_1 (\lambda_1 - V_{\mathfrak{t}}) + (1 - \alpha_1) u_2^{\mathfrak{t}} \Psi_{\mathfrak{t}}(\lambda, u^{\mathfrak{t}})_2 (\lambda_2 - V_{\mathfrak{t}}) \geq \frac{F_{\mathfrak{t}}}{C_{\mathfrak{t}}^{*} H}$. Thus, the weighted triplet $\alpha_1 \left(\lambda_1, u_1^{\mathfrak{t}}, \Psi_{\mathfrak{t}}(\lambda, u^{\mathfrak{t}})_1\right) + (1 - \alpha_1)\left(\lambda_2, u_2^{\mathfrak{t}}, \Psi_{\mathfrak{t}}(\lambda, u^{\mathfrak{t}})_2\right)$ is included in $\mathfrak{Z}_{\mathfrak{t}}^{\Psi}$ so $\mathfrak{Z}_{\mathfrak{t}}^{\Psi}$ is convex.

For each $\mathfrak{t} \in \mathfrak{T}$, we estimate the empirical joint distribution of its average hourly load factor and spot prices. As both variables are continuous, we split the intervals in which observed

spot prices and load factor take values into a finite number of bins and approximate the empirical frequency of each couple of spot price and load factor. Similarly, we approximate the "sufficient remuneration set" $\mathfrak{Z}_t^{\Psi}$ by constructing a grid-approximation for each technology. Then, we can compare the empirical joint probability of load factor and spot price combinations with the set of combinations that would be required for each technology to cover its total costs. This allows us to investigate how the distribution of spot prices and dispatch decisions should be transformed to allow generators to break-even, without resulting to off-market compensation mechanisms such as capacity markets. The "sufficient remuneration set" may be associated to optimal transport notations to yield fruitful intuitions. In terms of graphical interpretation, if the "sufficient remuneration set" and empirical joint distribution intersect at least once, then the nuclear operator earns sufficient revenue to cover her total annual costs. Thus, we may use $\mathfrak{Z}_t^{\Psi}$ to determine the minimum transformation of the joint density of generation and price that would be required to ensure cost-effectiveness.

Figure 4.A. shows both the estimated joint distribution of nuclear load factor and market spot price. We first note the "sufficient remuneration set" does not appear in the figure: for each value of spot price and load factor represented, $\Psi_t(\lambda, u^t)$ is consistently superior to 40%. As already suggested above, under strong RES penetration, nuclear generation units would mainly be operated with load factors below 60% and spot prices below 50 €/MWh. Two directions can be suggested to improve nuclear remuneration: the first one consists in moving the probability mass in red, corresponding to moderate load factors (below 60%) to high load factor region, by increasing the utilization of units. However, this would require drastically increasing the number of hours with moderate to high prices during which nuclear operates at full capacity, which only correspond to period of tight supply conditions. This high utilization of nuclear capacities may be incompatible with operational and thermal constraints, that must be respected by the nuclear operator and the TSO. The second direction, which may be more "realistic", consists in increasing the spot price for high load factor values. Indeed, for a load factor above 70%, while a minimum of 6982 hours of operations are necessary to recover costs for a spot price above 60 €/MWh, it falls to 3950 hours (45% of the year) when the latter increases to 100 €/MWh.

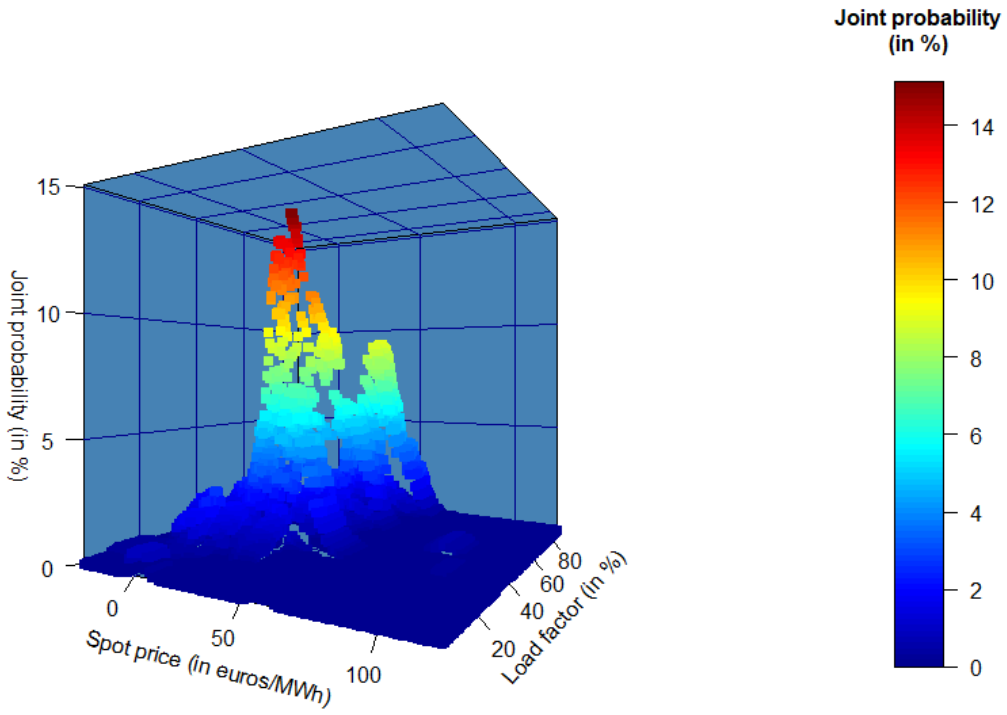

Figure 4.A.: Empirical load factor and spot price joint distribution for nuclear

Note: Each dot corresponds to a bin combining discretized values of load factor and spot price.

Again, the joint pattern of spot price and hourly load factor for CCGT draws an entirely different picture. **Figure 4.B.** shows that hourly load factors are null too often over the year to compensate for the high average unit profit when CCGT plants are dispatched. Again, the "sufficient remuneration set" is not represented. Increasing the participation of CCGT units, i.e. the joint probability of non-null load factors, is a first option to increase market revenue. With a spot price above 95 €/MWh (which corresponds to the average price observed when CCGT is dispatched), at least 14839 hours and 5002 hours of operations are required to cover total annual costs with hourly load factors above 10% and 30% respectively. Following the "merit-order" rule, dispatching CCGT a higher number of hours would increase average annual spot price, thus potentially benefiting to other technologies if load requirements are high. Yet, it may also significantly increase the electricity cost to final customers, in addition to expanding carbon emissions. A second option would then consist in letting spot prices spike when CCGT participates to supply, if it is consistent with scarcity conditions justifying price increases beyond the marginal cost of CCGT. However, this would require lifting the price ceiling of 3000 €/MWh and may expose unhedged electricity customers, if their bill is indexed on real-time spot prices, to potential price spikes.

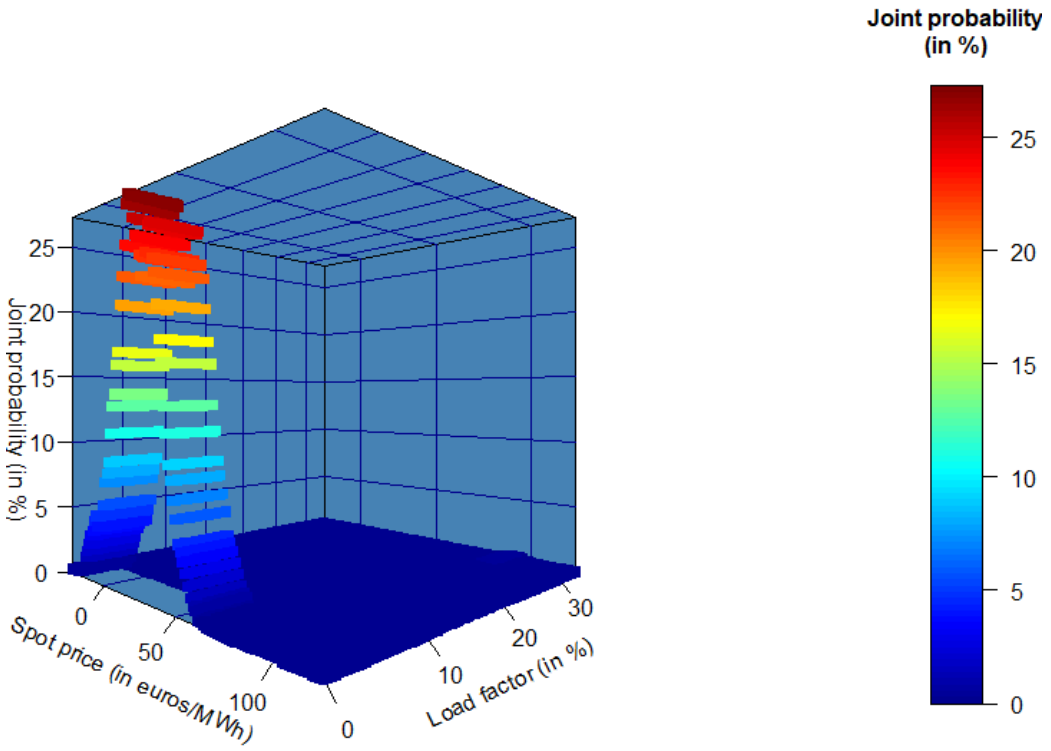

Figure 4.B.: Empirical load factor and spot price joint distribution for combined-cycle gas turbines

Compared to nuclear and CCGT, **Table 4.C.** shows the joint distribution of spot price and hourly load factor for photovoltaic generation is much "closer" to the "sufficient remuneration set" for the operator of solar panels. We might further define the distance between the empirical joint distribution and $\Im_t^{\Psi}$ using metrics like the Euclidian or the Hausdorff distance. This is however outside the topic of this chapter and might be left for further research. Contrary to dispatchable technologies, the probability mass corresponding to high load factors cannot be displaced as it is exogenous for RES. Indeed, RES load factors are determined by weather conditions and can only be adjusted downward using curtailment. Thus, it is only possible to move the probability mass to the right by increasing the spot price for values corresponding to positive hourly load factors. Interestingly, we note that under the stark decrease in photovoltaic investment and FOM costs assumed in our model for 2030, only moderate modifications might be necessary to achieve cost-effectiveness. Indeed, given a load factor above 30% and spot price above 50 €/MWh, a minimum of 2386 hours is necessary to earn a sufficient market remuneration. Taking a spot price above 60 €/MWh drives this number down to 1974 hours (22% of the year), which suggests the annual costs could be

amortized within slightly more than 24 weeks (3948 successive hours as no production occurs at night) with average load factor conditions and moderately high spot prices.

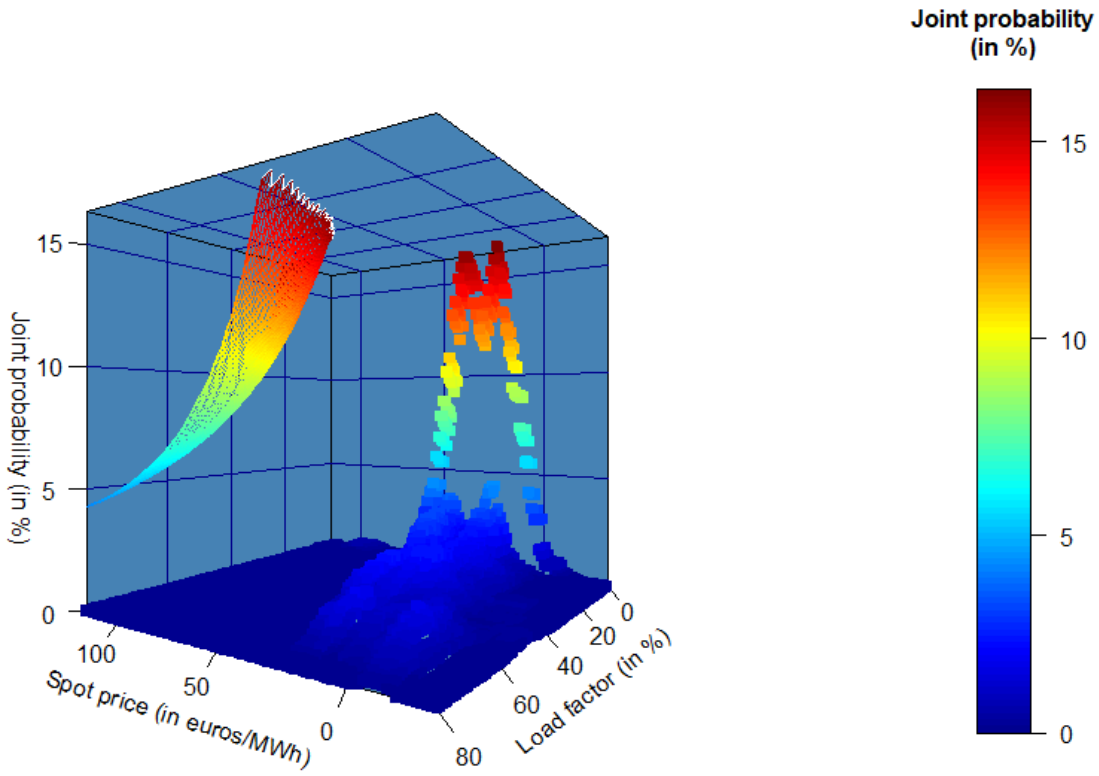

Figure 4.C.: Empirical load factor and spot price joint distribution for solar

Note: The multicolor grid corresponds to the grid approximation of the "sufficient remuneration set" for the nuclear operator.

Similar conclusions can be drawn from **Table 4. D.**. However, the significantly higher annuities and FOM costs of wind turbines, even under the cost assumptions made in Chapter III, require a much larger shift of the marginal price distribution to the right compared to the case of photovoltaic. The generation of wind turbines is quasi null for spot prices superior to 50 €/MWh, with small load factors below 20%. We further note that the load factor of wind turbines is superior to its average value, equal to 27%, approximately 46% of the year. Yet, maintaining a minimum spot price above 112 €/MWh roughly half of the year would be necessary ensure cost-effectiveness.

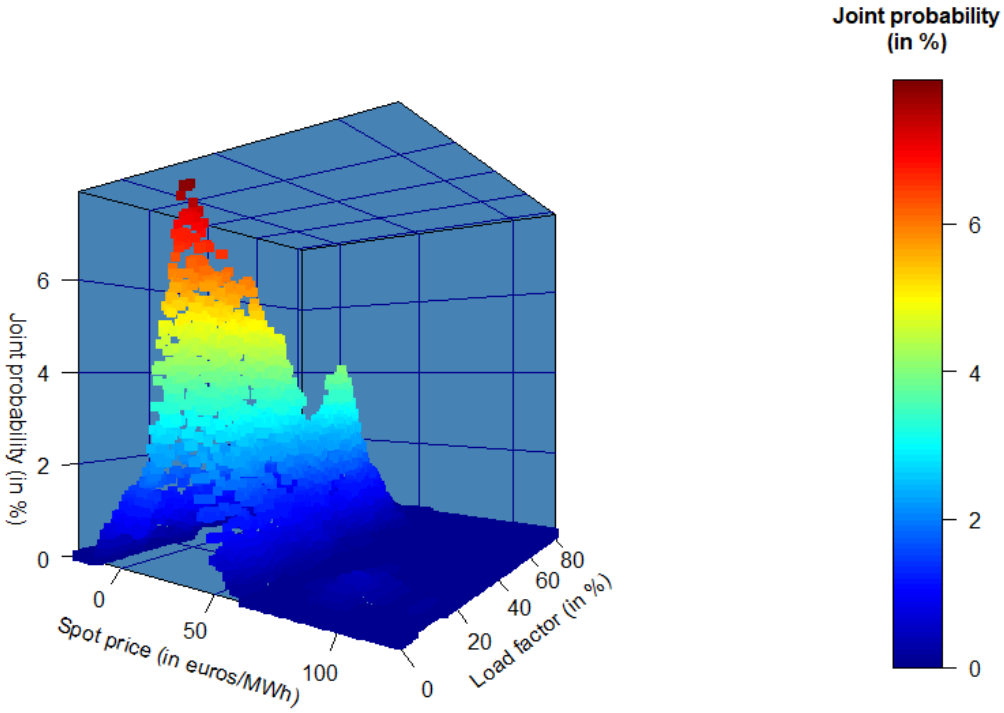

Figure 4.D.: Empirical load factor and spot price joint distribution for wind power

In the above analysis of photovoltaic and wind operator remuneration patterns, we assumed the marginal distribution of load factors is fixed, i.e. the probability mass cannot be moved towards higher load factor regimes. This is however untrue in the presence of storage, as it allows the transfer of RES generation from periods with high load factors to periods with low ones, and inversely. Considering **Figure 4.D.**, a strategic operator equipped with both wind power and storage units would maximize her profit by storing electricity produced during low load factor and low price periods, and sell it during high price periods to inflate her total load factor. The convexity of $\mathfrak{Z}_t^{\Psi}$ is in this case a key property to define the set of equivalent optimal storage strategies. This is however outside the scope of this research, as the social planner approach considered in our optimization model does not account for the allocation of generation and storage assets between different operators and customers, who may install residential or commercial photovoltaic for instance.

We further investigate the optimal transformation of spot price distribution which would allow cost-effectiveness more each technology with minimum "transport" of probability mass. We propose two complementary approaches. For each technology $t \in \mathfrak{T}$, we note $\Omega_{Q_t^*}$ the sorted set of optimal generation volumes obtained after solving our optimization model (it

may be sorted in decreasing or increasing order). Noting Ω_{λ^*} the set of observed spot price values, $\lambda_t^*(Q_t^*): \Omega_{Q_t^*} \mapsto \Omega_{\lambda^*}$ corresponds to the optimal spot price observed when the optimal generation of $t \in \mathfrak{T}$ equals $Q_t^* \in \Omega_{Q_t^*}$[35]. We further define the transport map $\nu_t(Q_t^*): \Omega_{Q_t^*} \mapsto \mathbb{R}$, which associates to each value Q_t^* a (possibly negative) price add-up $\nu_t(Q_t^*)$, such that $\lambda^- \leq \nu_t(Q_t^*) \leq \lambda^+$, with $(\lambda^-, \lambda^+) \in \mathbb{R}^2$. These bounds define the maximum quantity of spot price probability mass that can be removed or added for each value Q_t^*. For instance, for $\lambda^+ = 5$ and $\lambda^- = -\lambda^+$, the maximum price variation must be inferior to 5 €/MWh and superior to – 5 €/MWh. Finally, the total probability mass of the new price distribution must be equal to the mass of the initial one.

Under the first approach we investigate the optimal transport map that maximizes profits for each technology $t \in \mathfrak{T}$, where (λ^-, λ^+) are fixed. Formally, this can be written as the corresponding problem:

$$\max_{\nu_t} \int_{\Omega_{Q_t^*}} Q_t^* \left(\nu_t(Q_t^*) + \lambda_t^*\left(Q_t^*\right)\right) dQ_t^* \ : \ \begin{pmatrix} \int_{\Omega_{Q_t^*}} \nu_t(Q_t^*) dQ_t^* = 0 \\ \lambda^- \leq \nu_t(Q_t^*) \leq \lambda^+ \end{pmatrix} \qquad (\mathbf{5})$$

Figures 5.A. and **5.B.** reveal interesting similarities regarding the spot prices distribution maximizing nuclear and solar market remuneration. Both new distributions move mass from low to high price regimes, without significantly altering distribution tails. This transformation is however more important for nuclear, as the average nuclear load factor increases with spot price. For λ^+ equal to 20 €/MWh, the average unit spot price for values above 22 €/MWh increases by 13.66 €/MWh. Overall, we find that the average unit price paid for nuclear electricity increases from 26.93 €/MWh to 32.33 €/MWh, for λ^+ equal to 20.

Contrary to nuclear, the extreme values for negative prices are slightly higher under optimal distributions for solar. For λ^+ equal to 20, the average unit spot price paid by electricity customers for photovoltaic generation increases from 14.48 €/MWh to 34.48 €/MWh. However, we can prove lower values of λ^+ are sufficient to ensure photovoltaic cost-effectiveness.

[35] For example, if the spot price is equal to 15 €/MWh when $Q_t^* = 500$ MWh and to 30 €/MWh when $Q_t^* = 1000$ MWh, then we note $\lambda_t^*(500) = 15$ and $\lambda_t^*(1000) = 30$.

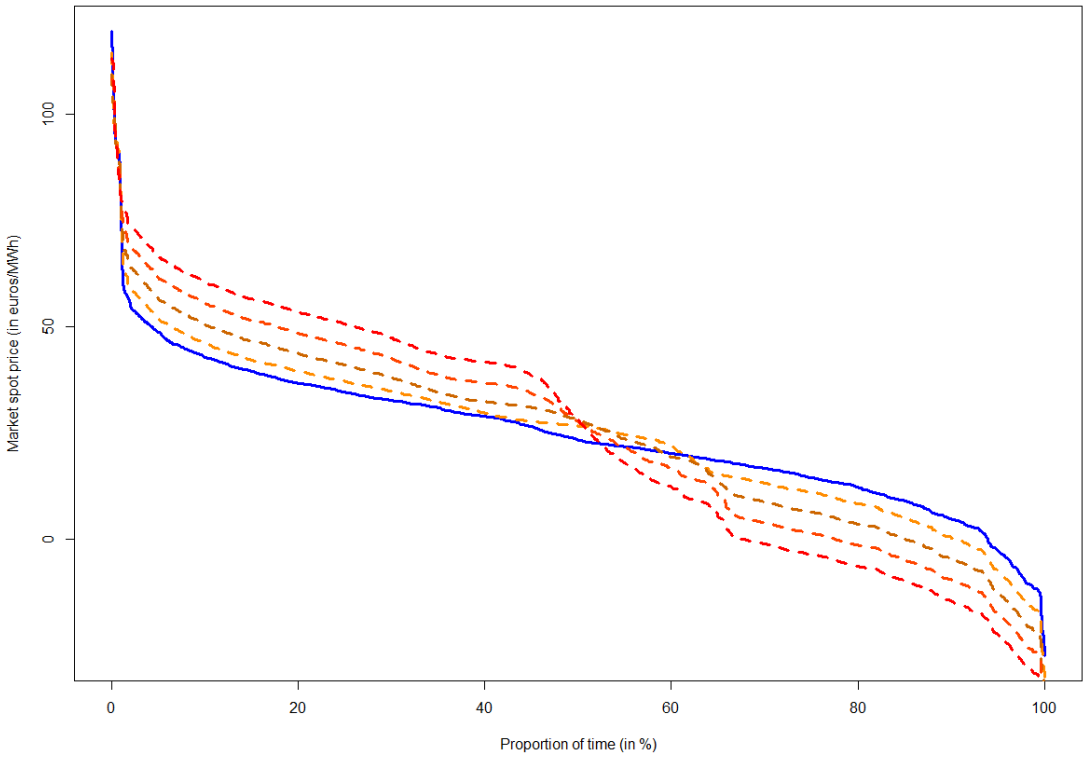

Figure 5.A.: Profit-maximizing transport maps of the initial spot price distribution for nuclear

Note: The plain blue line corresponds to the original spot price distribution. The orange, (resp. dark-orange, orange-red and red) dotted line corresponds to the optimal price distributions respectively obtained with λ^+ equal to 5 (resp. 10, 15 and 20), and $\lambda^- = -\lambda^+$.

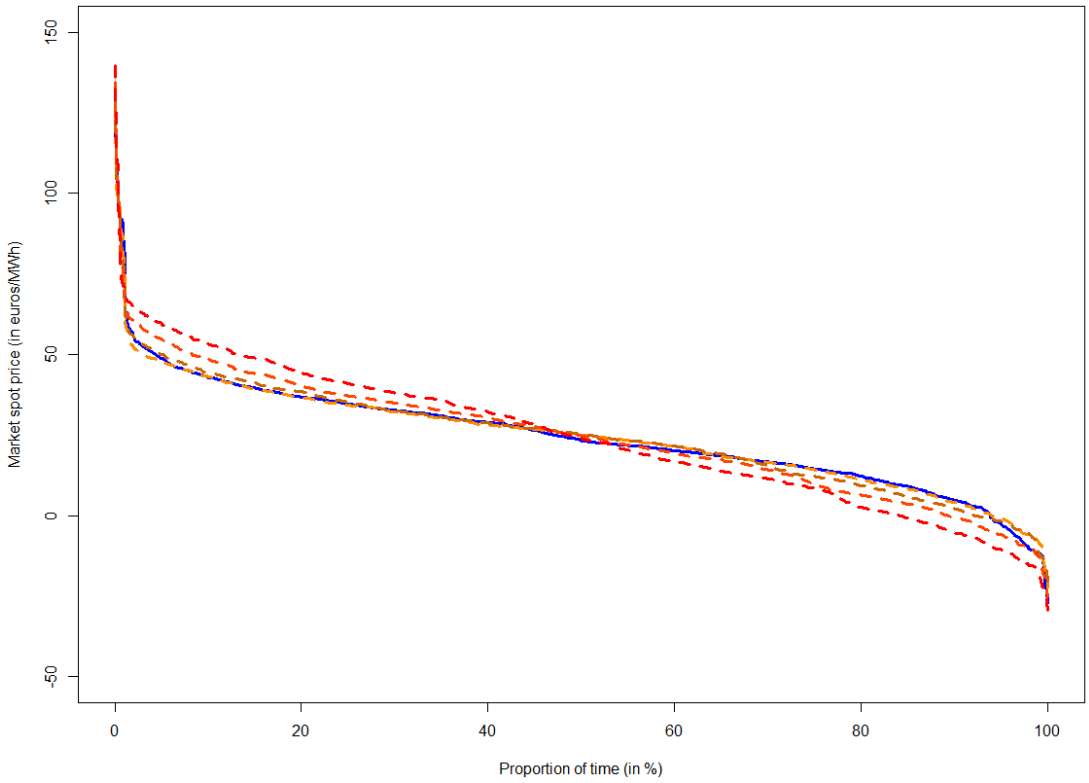

Figure 5.B.: Profit-maximizing transport maps of the initial spot price distribution for photovoltaic

In the second approach, we reformulate the above problem as a minimization one, which consists in finding for each technology the optimal transport map that minimizes the maximum distance between the initial and the new spot price distribution while ensuring cost-effectiveness for each $t \in \mathfrak{T}$. Given the pair of variables $(\lambda_t^-, \lambda_t^+) \in \mathbb{R}^2$ such that $\lambda_t^- \leq \lambda_t^+$, we minimize the distance $\lambda_t^+ - \lambda_t^-$ for each technology. Again, we consider the set of optimal generation values $\Omega_{Q_t^*}$ which is fixed and exogenous. This is formally equivalent to the following optimization problem:

$$\min_{\lambda_t^+, \lambda_t^-} \sum_t \lambda_t^+ - \lambda_t^- : \begin{pmatrix} \int_{\Omega_{Q_t^*}} Q_t^* \left(v_t(Q_t^*) + \lambda_t^*(Q_t^*) \right) dQ_t^* \geq F_t \\ \int_{\Omega_{Q_t^*}} v_t(Q_t^*) dQ_t^* = 0 \\ \lambda_t^- \leq v_t(Q_t^*) \leq \lambda_t^+ \end{pmatrix} \quad (6)$$

As shown in **Figure 6.A.**, the optimal spot price distribution for the nuclear operator entails an average 129 €/MWh increase of the initial spot price distribution, for values above 26

€/MWh. While the average spot price remains unchanged by definition, the average unit price paid by customers to the nuclear operator starkly increases to 60.75 €/MWh. Thus, multiplying by almost three the price paid for nuclear electricity would be necessary at least 50% of the year, under already moderate to high price regimes. The extremely flat left-portion of the new price curve suggest that long-term contracts, such as Contracts for Difference, would be justified to guarantee a stable high revenue to the nuclear operator without having to modify the spot price market. This issue is further investigated in the next Section.

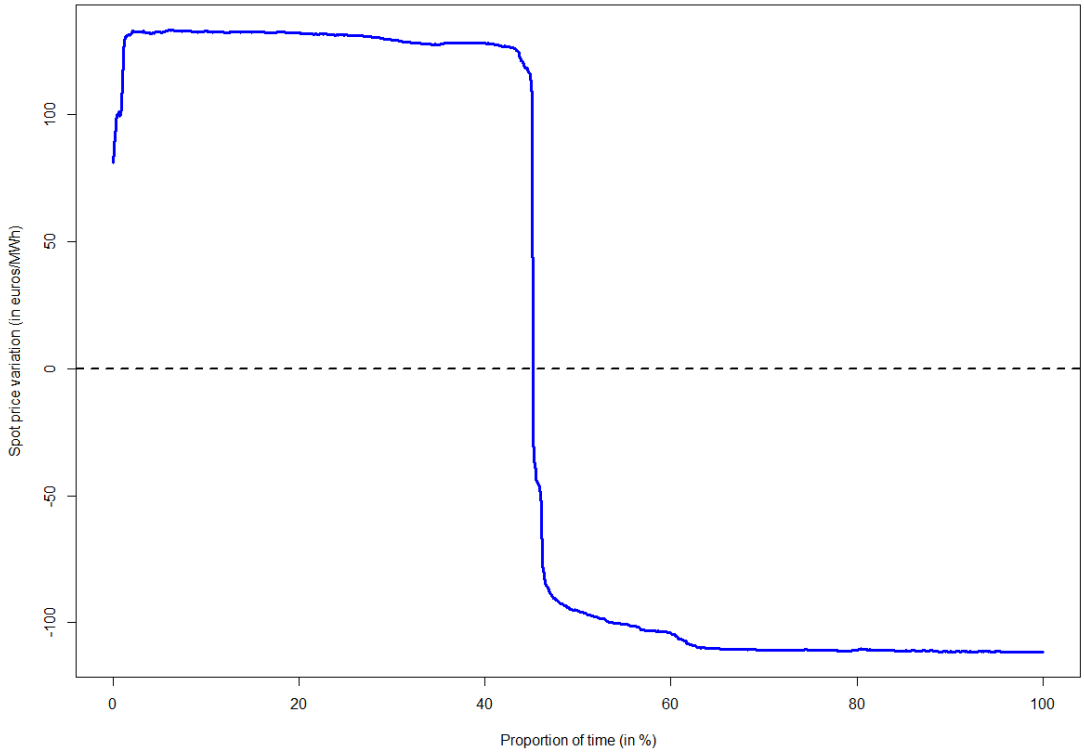

Figure 6.A.: Optimal spot price transportation map required for ensuring nuclear cost-effectiveness

Note: The blue line is obtained by taking the difference between the optimal spot price distribution and the initial one.

Figure 6.B. confirms the findings already foreshadowed by our previous results: moderate modifications of the spot price distribution would be required to make photovoltaic generation cost-effective, assuming investment and FOM costs strongly decrease. Indeed, the optimal values for λ_t^- and λ_t^+ corresponding to solar technology are respectively equal to 7.400 €/MWh and 13.82 €/MWh. The average unit price paid by customers to the photovoltaic operator increases from 14.48 €/MWh to 27.08 €/MWh. The 8.14 €/MWh price difference

(corresponding to a total of 0.029€ million), might be compared to the level of premiums paid to photovoltaic producers under subsidy mechanisms such as the Feed-in-Tariff and Feed-in-Premium. This may provide a benchmark for assessing the relative costs efficiency of revenue support mechanisms against market-based solutions modifying the price paid to generators for their energy.

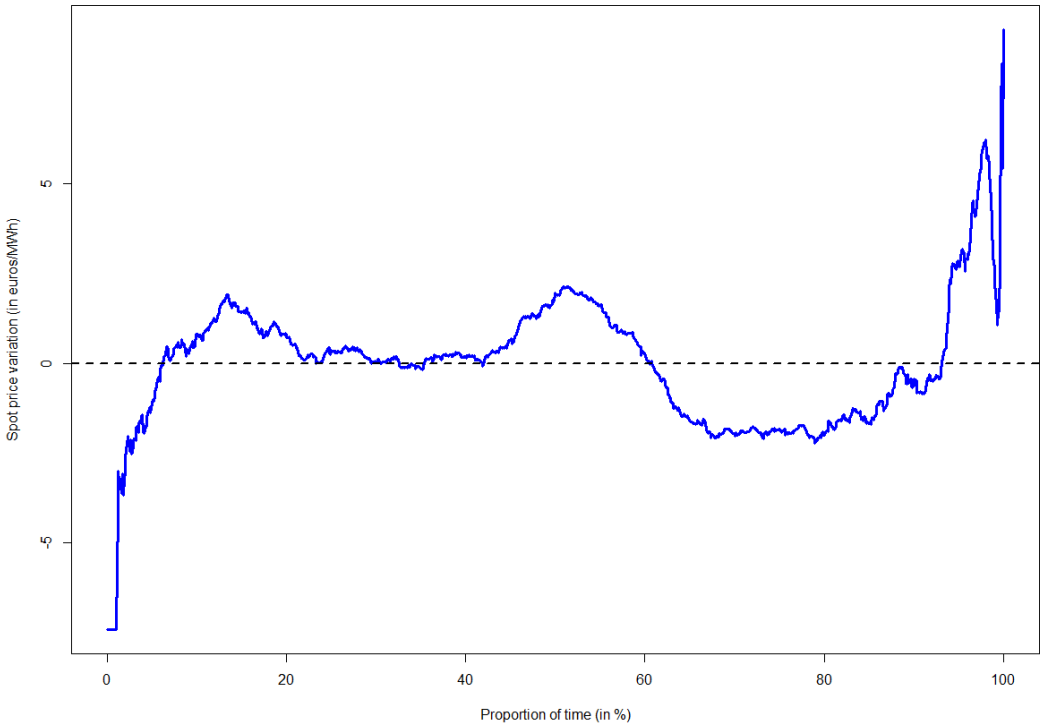

Figure 6.B.: Optimal spot price transportation map required for ensuring photovoltaic cost-effectiveness

3. Alternative price-formation mechanisms for adequate resource and scarcity pricing

In this section, we quickly review the main limits of current electricity market and compensation mechanism designs, in addition to the issues that they raise regarding the remuneration of producers. Then, we investigate the theoretical basis of a mixed-bidding rule for RES and of scarcity price, before analyzing their impact on the spot prices distribution and generator remuneration.

3.1. Limits of classical market and off-market remuneration designs

3.1.1. A review of market design objectives and main challenges

Following [12], electricity market design rests on two key objectives: short-run efficiency, consisting in making the best use of existing resources provided truthful bidding and no market distortions, and long-run efficiency by providing proper incentives for long-term investments.

However, as shown by [13], setting the volumetric price of electricity equal to its short-run social marginal cost will not raise sufficient revenue to cover utilities' total cost, in addition to avoiding the debate about which costs are fixed. The idea that economic efficiency is maximized when price equals short-run marginal cost can be invalidated by the existence of externalities, market power of sellers and failure to cover fixed costs. The optimal pricing mechanism would require real-time pricing with a scarcity signal, which in principle would generates sufficient revenue for producers to cover their variable costs. As put by [14], when the demand for electricity generation exceeds available resources, it is required that prices exceed the marginal cost of the peaking unit in order to justify its investment. In a well-functioning market, the spot price increases up to the Value of Lost Load (VOLL) in scarcity conditions when peaking unit cannot fully cover the electricity load. This sends a signal to customers, which allows peaking units to cover their fixed costs if the value of scarcity is translated in the electricity price. This may however fail to occur if electricity customers cannot react to real-time market conditions, making the demand curve inelastic, or if the spot price is capped. This may indeed protect consumers from price spikes and protect the market from price manipulations, which can result from strategic capacity retention from generators

with market power. More specifically, reflecting the real-time scarcity conditions might significantly increase the price of electricity in underinvestment conditions. Consequently, alternative mechanisms are required to cover the fixed costs of generators and remunerate investment.

As an alternative, average-cost pricing, which is inclusive of both variable and fixed costs, appears at first as an equitable solution. Yet, on equity grounds, it seems doubtful that a customer A consuming twice as much electricity as a customer B should contribute twice as much to fixed costs. The introduction of a fixed charge, which is independent of the quantity consumed, provides an attractive way to minimize deadweight loss. Tiered pricing (known as block-pricing) can allocate more of the additional revenue needed to high-demand consumers, with the price per kWh increasing or decreasing with each "tranche". Yet, tiering pricing implies above average-cost pricing for low-quantity customers, who face a very high marginal price and may respond by inefficiently self-restricting their consumption. Overall, [15] shows that increasing block-pricing, mostly prevalent in U.S. residential tariffs, has modest redistributive effects, with many low-income households being made worst-off by this tariff structure. Overall, the author estimated the introduction of increasing-block pricing in one California utility increased deadweight loss by 3% of the revenues received from customers compared to average-cost pricing. The adequate definition of blocks and corresponding tariffs also requires the regulator to measure the value associated to each use of electricity by each category of customers, which is non-trivial.

The short-run efficiency requirement for the wholesale electricity markets must also allow generators to cover their operational costs. The latter include not only generation costs, but also non-convex costs such as start-up costs. While US day-ahead markets allow generators to simultaneously bid an energy offer curve, start-up and minimum-energy costs, generators on the French EPEX Spot Day-Ahead market only submit orders reflecting their willingness to sell a given volume for all price ticks between minimum and maximum prices of each auction. Generators must then internalize start-up and minimum-energy costs in their offers, based on their expectations of how concurrent bids might be scheduled, which would often distort the energy offer curve.

Out of market make-whole payment mechanisms, such as uplift payments and side payments, may thus be required to cover non-convex operating costs not reflected in the marginal cost and yield the maximum attainable social welfare. Side payments are allocated by computing

the difference between daily operating costs and market remuneration. They are implemented in some power markets such as the PJM and NY-ISO which include a revenue sufficiency guarantee. Price-uplifts are computed *ex post*, i.e. after the daily unit commitment decisions are made, and correspond to the minimum additional payment such that online power plants recover their operating costs. We refer to [16] for an application of those two payment mechanisms to a MILP dispatching model. However, as pointed by (see [17]), make-whole payments may create price discrimination among market participants and generate inadequate market signals. This suggests price signals do not adequately reflect operational costs and may impact long-term investment decisions as in [18]. [19] present a novel and exact methodology for reformulating a revenue and network-constrained day-ahead market model, expressed as a mixed-integer nonlinear bilevel program, as an equivalent single level MILP with bilinear terms. They formulate a general price-based market clearing procedure. By taking locational marginal prices as decision variables, the authors provide a non-discriminatory model which maintain desirable economic properties of marginal pricing. Their framework is however developed for deterministic market clearing procedures. [20] address this shortcoming with a stochastic market clearing algorithm and locational marginal prices accounting for revenue-sufficiency constraints. This new framework may prove especially relevant under increasing share of RES in the electricity mix.

The latter also requires adequate valuation of real-time resources and flexibility requirements, which would justify simultaneously dispatching reserves and energy while accounting for RES uncertainty ([21]-[22]**)**. One may question the market priority legally given to RES generators, which are guaranteed to be dispatched. Indeed, under alternative bidding rules such as average cost bidding, RES would be likely to dispatched after hydroelectric and nuclear units, which might mitigate the ancillary costs associated to renewable priority.

3.1.2. Capacity markets and their limits

Introduced in 2017, the French capacity market aims both at encouraging adequate investment in generation and demand response capacities, while incentivizing changes in consumer behavior during peak hours and providing sufficient revenue to peaking units with very low load factors[36]. After estimating power requirements for a set of peak hours (labelled as PP2

[36] See https://www.powernext.com/french-capacity-guarantees-rte

hours), RTE allocates capacity certificates (each certificate representing 0.1 MW) to generators and demand-side management operators, corresponding to the capacity they can make available during these specific hours. Suppliers are then required to acquire enough capacity certificates to serve all their customers consumption during peak periods. RTE, with the support of the EEX Group, is responsible for the operation of the capacity market and the registry of capacity guarantees. Investment and fixed costs are thus treated as a discrete product, namely "capacity".

Similarly to a FitBit, [23] show the number of MWs purchased in a capacity auction neglects factors determining the location and type of new investments to be made for meeting a predefined reliability target. First, purchasing years in advance undifferentiated MWs does not reflect customer or policy preferences about desired types of generation. Regional resource adequacy requirements may better reflect the preferences of end-users and local natural resources used in the construction and operation of new generation units. Moreover, it may fail to consistently address its two objectives, i.e. supplying "Missing Money", required for resources owners to cover their fixed costs, and providing an efficient "price signal" to incentivize the development of new capacity. Furthermore, the indirect nature of the capacity mechanism makes its evaluation difficult. Generators may both receive revenue from selling capacity certificates and from sales in the energy-markets, so measuring the exact contribution of the capacity mechanism to the cost recovery may be tricky and subject to political manipulations. It might be difficult to strike an equitable and efficient balance between the benefits offered to investors by capacity mechanisms and the long-term investment risks shifted back to consumers. Capacity mechanisms offer limited scope to value certified resources based on their flexibility.

According to [24], capacity markets administered by a central agency are a third-best option. They require monitoring practices to ensure certified capacities perform when needed, and penalties if capacity providers fail to fulfil their obligations. A well-designed capacity mechanism should also accommodate all capacity-equivalent resources equitably (which is currently not the case), to better acknowledge the value of relatively more flexible resources with respect to less flexible ones. Finally, it should supplement rather than substitute more efficient options. Indeed, capacity mechanisms remunerate generators based on their quantity of capacity but not the quantity of energy they produce. They are disconnected from real-time operational constraints and payments to certified capacities do not reflect their actual contribution to system flexibility and reliability. Adjusting the energy and balancing services

markets, so they accurately reflect the real-time cost of these services and supply scarcity, would contribute to remunerate generators based on the real-time energy and reserve levels they provide to the electric system, but also incentivize investment if the system is often short of generation capacity. This is the purpose of scarcity pricing, which restores flexibility in electricity load by pricing reserves based on the expected cost of lost load.

3.2. Ensuring adequate resource pricing: bidding renewables based on their average cost

3.2.1. Definition and formal framework

Under short-term marginal pricing, the injection of renewable generation in the grid has priority and renewable operators are compensated by the Transmission System Operator (TSO) if system balance requires curtailing their production. However, as reminded by [25], RES erase dispatchable production intermittently but do not substitute to them. Investing in additional RES capacity is thus economically justified only if the cost of renewable energy is lower than the marginal cost of dispatchable units and reduce carbon emissions. As proven by the author, this requires comparing RES on the basis of their average production cost (including investment and FOM costs) to the marginal cost of generation electricity with dispatchable technologies. The classic "merit-order rule" can be modified to a mixed-bidding rule, such that RES generators bid their production based on their average cost, while dispatchable units still submit bids based on marginal costs.

If non-dispatchable renewable generators bid their production according to their average costs, the latter may be higher than the marginal cost of dispatchable conventional technologies during low capacity factor periods, and thus push renewable producers down the "merit-order" curve. On the opposite, renewable producers would have high probability be dispatched first by the market operator when their production is high, as it would decrease their average cost. Under this new bidding rule, RES generators bear the costs of curtailment and are not compensated anymore by the TSO.

While the author computes average costs taking the annual expected load factor, the time basis for this computation may be chosen to match the statistical variations of the generation patterns of each renewable technology. Under the assumption that annuities and FOM costs can be allocated uniformly in time, they may computed on a seasonal, weekly or even hourly basis. Indeed, the author implicitly assumes the capacity factor of each renewable technology

to be constant and independent of the time basis used for its computation. A shorter time basis may better reflect the real-time generation costs of solar and wind units. Annual average costs may fail to capture the economic gains associated to high capacity factor periods, which cancel out with low production periods when taking the yearly average. Still, using average cost on short computation time windows is technically challenging as this measure can only be obtained *ex post*. Average-costs computed on the basis of past generation, for whatever computation window, may not exactly correspond the present average cost. An adequate measure of average costs for bidding renewable operators would rely on forecasted generation, with computation error decreasing with the length of the time basis and the inverse of the volatility of generation.

As in the previous chapters, we assume $\boldsymbol{\xi}_{jt}$ is a random variable with real positive values, with $\boldsymbol{\xi}_{jt} \in \boldsymbol{\Xi}_{jt}$. We define the average generation on an annual basis cost for technology $j \in \mathcal{P} \cup \mathcal{W}$ in hour $t \in \mathcal{T}$ as:

$$\Xi_j = F_j C_j \left(\theta C_j \mathbb{E}(\xi_j)\right)^{-1} = F_j \left(\theta \mathbb{E}(\boldsymbol{\xi}_{jt})\right)^{-1} \quad (\mathbf{7a})$$

We may respectively define it on a seasonal, weekly and hourly basis:

$$\Xi_{js} = \frac{F_j C_j}{|\mathcal{S}|}\left(\theta_s C_j \mathbb{E}(\xi_{js})\right)^{-1} = \frac{F_j}{|\mathcal{S}|}\left(\theta_s \mathbb{E}_s(\boldsymbol{\xi}_{jt})\right)^{-1} \quad (\mathbf{7b})$$

$$\Xi^k_{js} = \frac{F_j C_j}{|\mathcal{SK}|}\left(\theta_k C_j \mathbb{E}(\xi^k_{js})\right)^{-1} = \frac{F_j}{|\mathcal{SK}|}\left(\theta_k \mathbb{E}_{s,k}(\boldsymbol{\xi}_{jt})\right)^{-1} \quad (\mathbf{7c})$$

$$\Xi^k_{jst} = \frac{F_j C_j}{|\mathcal{SKT}|}\left(\theta_t C_j \mathbb{E}(\xi^k_{jst})\right)^{-1} = \frac{F_j}{|\mathcal{SKT}|}\left(\theta_t \mathbb{E}_{s,k,t}(\boldsymbol{\xi}_{jt})\right)^{-1} \quad (\mathbf{7d})$$

In the above formulation, $\mathbb{E}_s(\boldsymbol{\xi}_{jt})$ corresponds to the expectation of $\boldsymbol{\xi}_{jt}$ taken in season s, with probabilities computed over the corresponding subperiod. The same rationale applies to $\mathbb{E}_{s,k}(\boldsymbol{\xi}_{jt})$ and $\mathbb{E}_{s,k,t}(\boldsymbol{\xi}_{jt})$. We introduce the scaling parameters $(\theta, \theta_s, \theta_k, \theta_t)$ such that expected generation coincides with the length of the period over which $(\Xi_j, \Xi_{js}, \Xi^k_{js}, \Xi^k_{jst})$ are computed[37]. The objective function in the dispatching optimization problem becomes:

[37] Formally, we have $\theta = |\mathcal{SKT}|$, $\theta_s = |\mathcal{SKT}||\mathcal{S}|^{-1} = |\mathcal{KT}|$, $\theta_k = |\mathcal{SKT}||\mathcal{SK}|^{-1} = |\mathcal{T}|$ and $\theta_k = 1$.

$$\min_{\boldsymbol{q},\boldsymbol{\kappa},\boldsymbol{z}} \sum_{s\in\mathcal{S}}\sum_{t\in\mathcal{T}}\left(\sum_{g\in\mathcal{G}}\left(c_g^V + \pi^{CO_2}E_g\right)q_{gst} + c_g^{STUP}z_{gst} + c_1^{\kappa}\kappa_{1st} + \sum_{j>1}\Xi\left(\xi_{jst}C_j - \kappa_{jst}\right)\right) \quad (8)$$

Where $\Xi = \Xi_j, \Xi_{js}, \Xi_{js}^k, \Xi_{jst}^k$.

Figure 7 shows that the recomputed spot price increases to 31.53 €/MWh, against 24.51 €/MWh under the classic marginal-cost bidding rule. Comparing the spot price distributions, the probability of negative prices under our mixed bidding rule decreases from 0.061 to 0.026, while the probability of prices above 80 €/MWh increases from 0.010 to 0.098. Overall, the mixed bidding rule with an annual computation basis both shifts the price distribution up and reduces the occurrence of negative prices. This is the direct result of extremely high curtailment rates for both photovoltaic and wind power production: over a full year, solar generation is almost fully curtailed (with a curtailment rate of 99.99%), while 92.48% of wind generation is cut. The more frequent occurrence of high spot prices translates the higher participation and utilization rate of CCGT turbines to generation.

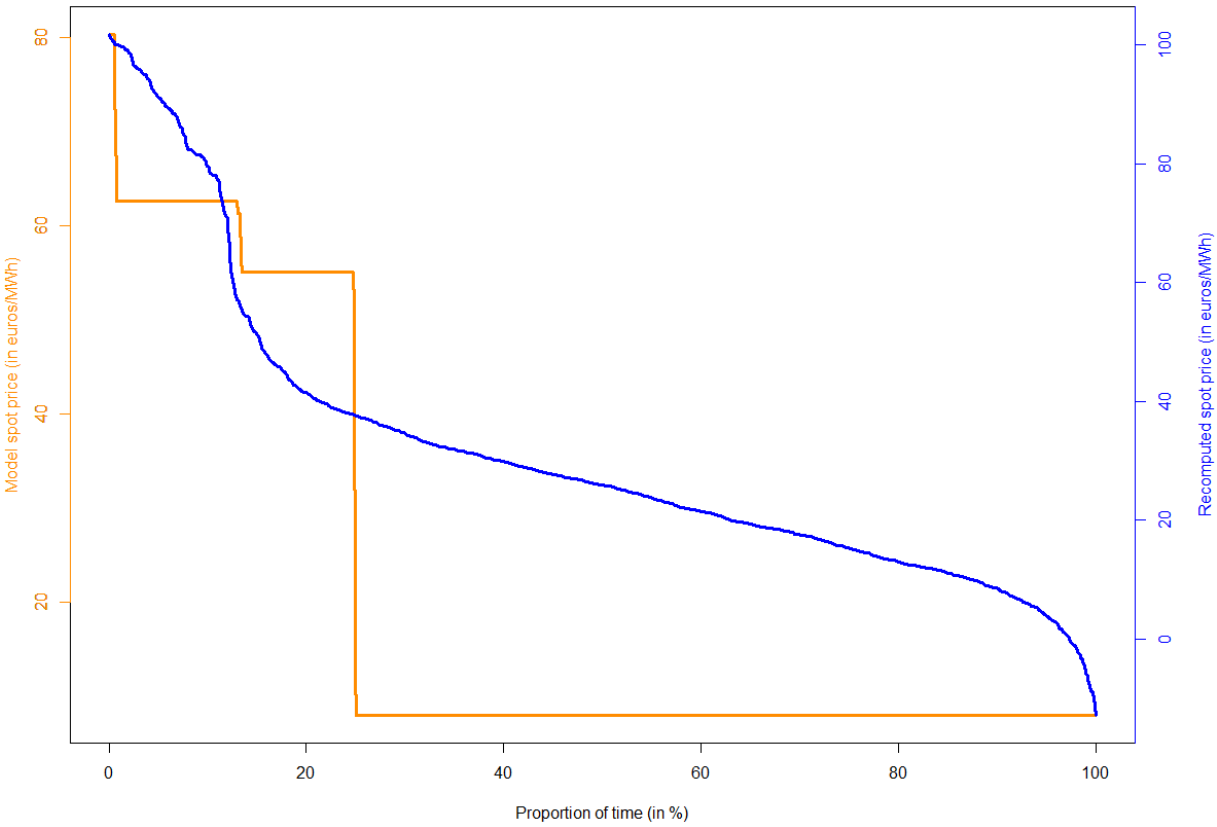

Figure 7: Model and recomputed spot price distributions, annual computation basis

We can see from **Figure 8.A.** that the cumulated nuclear revenue strongly increases compared to the reference case in Section 2. Compared to the marginal-cost bidding rule, the total annual revenue increases by 64%, reaching 1.988€ billion. The increase in total revenue can be split into a 0.182€ billion price effect and 0.592€ billion volume effect. Indeed, with a higher total generation equal 80 TWh, the average profit per unit sold picks up to 24.82 €/MWh. The nuclear still makes a loss of 1.415€ billion euros but covers 58% of her yearly expanses, which is 22% more than under simple marginal-cost bidding. This average load factor improves to 69%. Given this overall higher electricity generation, the break-even price falls to 42.65 €/MWh. Although 81% of nuclear generation is sold for an inferior spot price, the higher number of operational hours, combined with higher average load factor and spot price, significantly improved the profitability of nuclear generation.

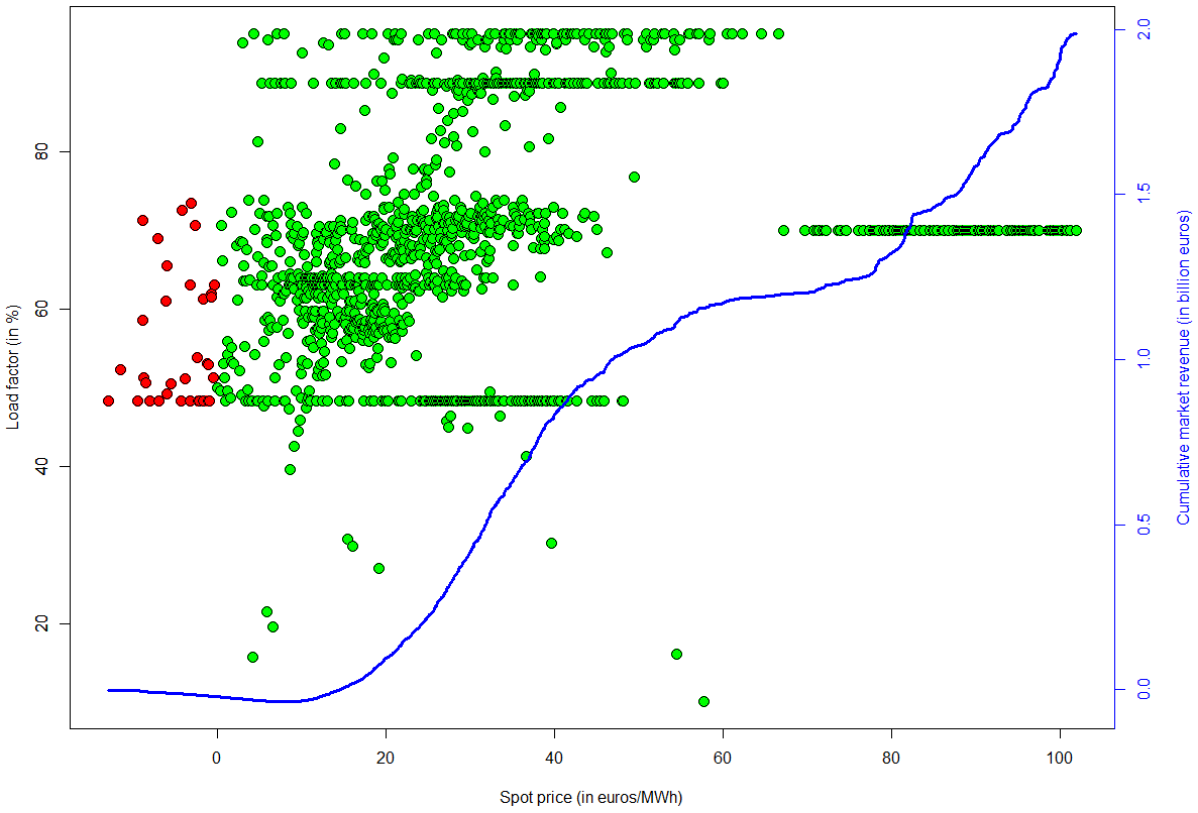

Figure 8.A.: Spot price and load factor patterns for the remuneration of nuclear units under mixed bidding rule, annual computation basis

The remuneration of CCGT units also significantly improves under our mixed bidding rule. **Figure 8.B.** shows that cumulative market remuneration is multiplied by more than 12 with respect to the reference marginal-cost bidding rule. The number of operating hours also

significantly increases as is positive during 12.1% of the year. The average hourly load factor during operating hours also climbs to 23%. The break-even price of CCGT drops to 245.7 €/MWh, which is below the legal price ceiling but remains very high because of the low utilization of CCGT capacities, even under mixed-bidding rule. The CCGT operator still only covers 15% of her total annual costs. While spot prices remain too low to ensure cost-effectiveness by producing only a few hours per year, this new bidding rule may significantly increase carbon emissions. As such, it may thus be poorly compatible with CO_2 emission targets if the average cost bid by RES generators is more expensive than the marginal cost of CCGT units.

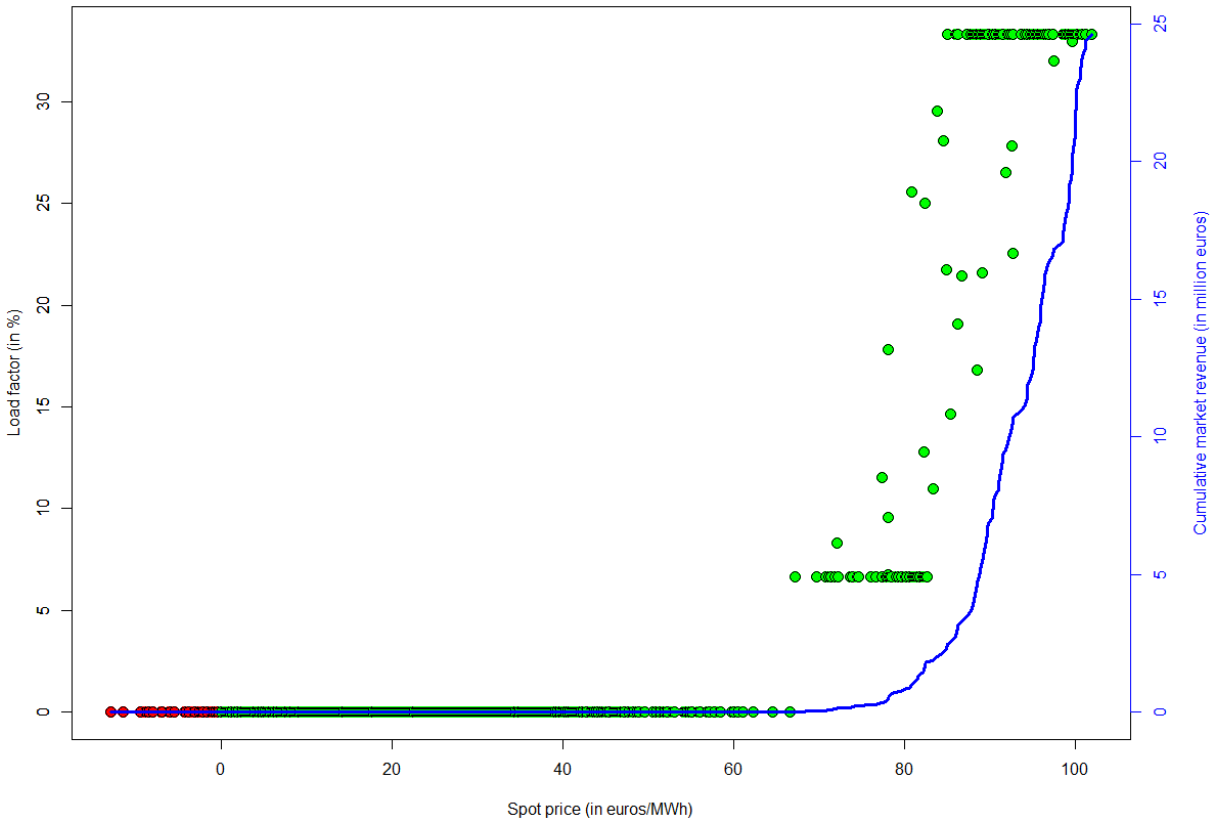

Figure 8.B.: Spot price and load factor patterns for the remuneration of nuclear units under mixed bidding rule, annual computation basis

As shown in **Figures 8.C.** and **8.D.**, the market remuneration of photovoltaic and wind production units collapses under this new bidding rule. Indeed, on an annual computation basis, the average costs of solar and wind generation are respectively equal to 80.37 €/MWh and 62.63 €/MWh. This explains the quasi full curtailment of solar generation units, as their

annual average cost is even higher than the marginal cost of CCGT, equal to 55.5 €/MWh under the carbon cost assumptions made in Chapter III. Choosing an annual basis for RES is thus likely to completely exclude them from participating in the optimal mix, while strong curtailment levels are obviously inefficient in economic terms considering their null marginal cost.

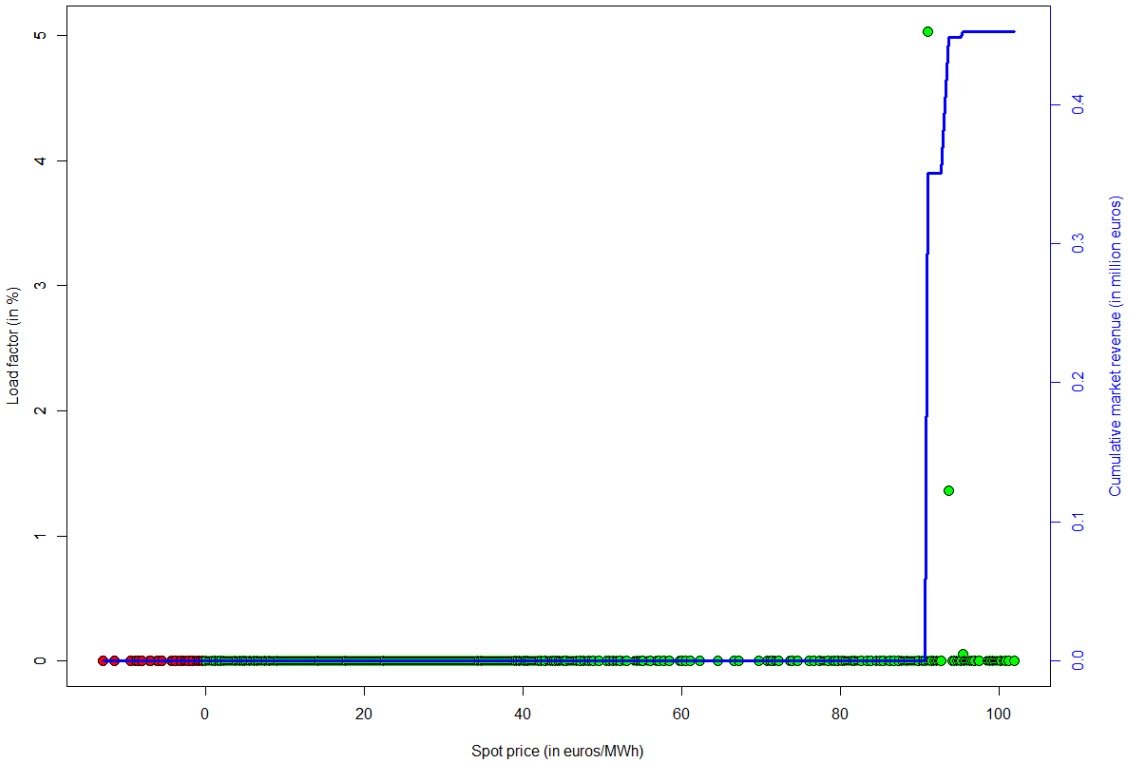

Figure 8.C.: Spot price and load factor patterns for the remuneration of photovoltaic units under mixed bidding rule, annual computation basis

Although the main objective of the mixed bidding rule is to better relate and compare the respective values of renewable and dispatchable resources, this market design both fails to include RES in the optimal dispatch. It also increases the average price of electricity and requires off-market compensation mechanisms to cover the quasi-totality of investment and FOM costs. Dispatchable technologies, such as nuclear and CCGT, are better-off while renewable generators and electricity customers are clearly worse-off.

Moreover, while computing RES average cost on an annual basis facilitates computations, it fails to accurately reflect real-time resources availability. Because of the intermittency of renewables, their load factor is variable and exhibits cyclical patterns both at the daily and

seasonal scales. Accurately reflecting the real-time value of renewables is required to properly evaluate the economic benefits of investing in renewables. Thus, in order to illustrate how the choice of a different computation basis for RES average cost impacts the optimal dispatch under mixed-bidding rule, we now take photovoltaic and wind average cost on a weekly basis.

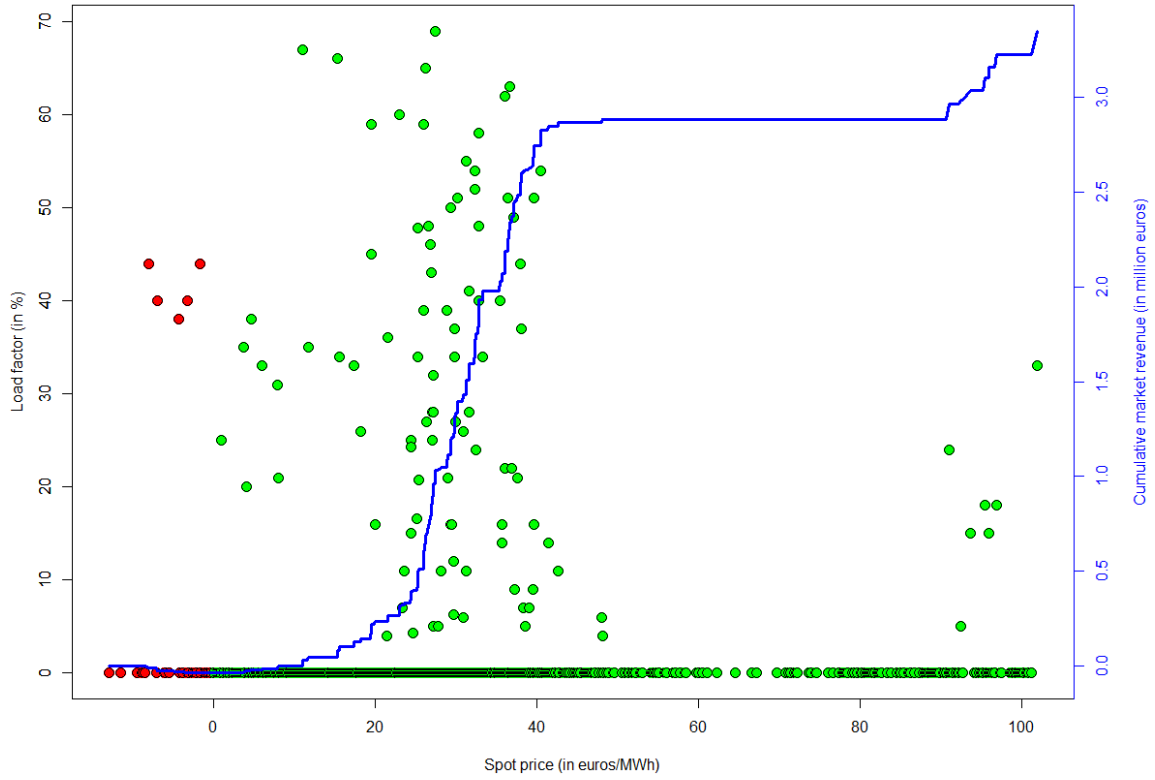

Figure 8.D.: Spot price and load factor patterns for the remuneration of wind power units under mixed bidding rule, annual computation basis

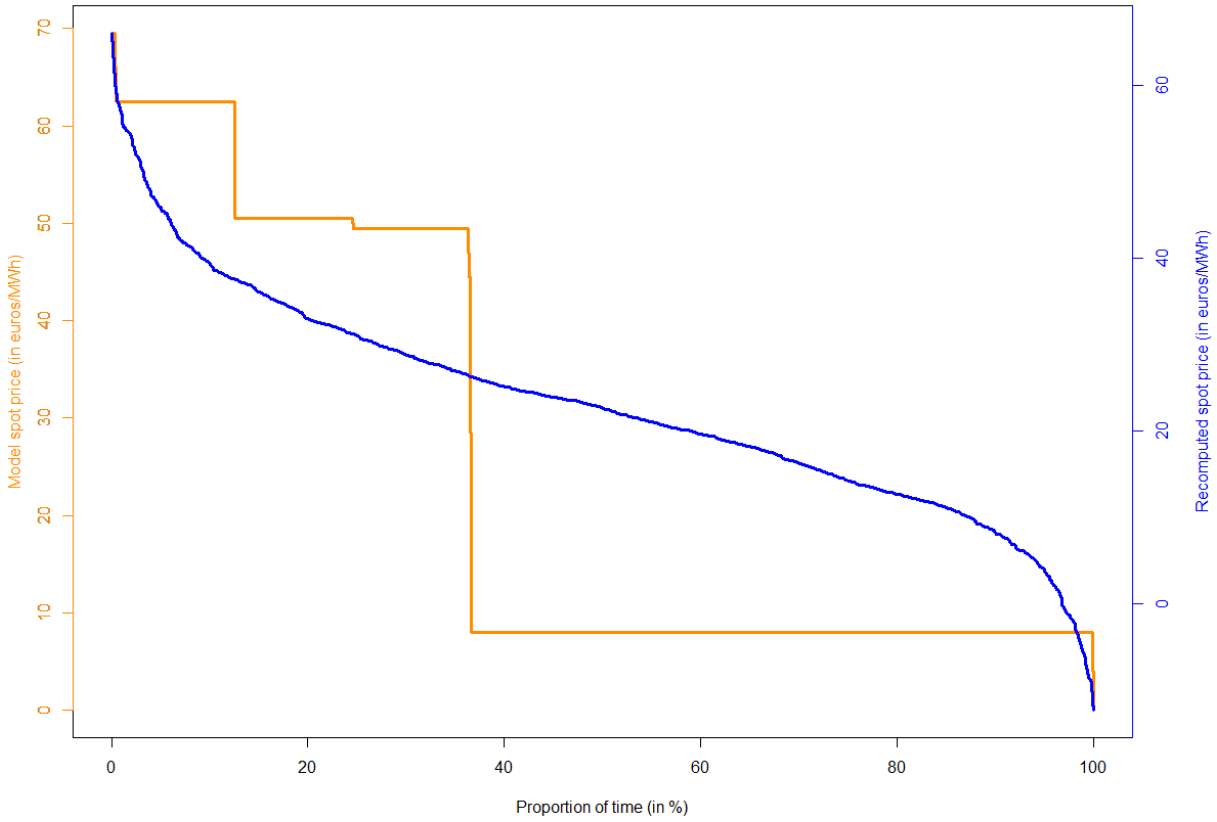

Figure 9: Model and recomputed spot price distributions, weekly computation basis

Looking at the distribution of model spot prices, **Figure 9** shows the number of hours during which the dual values of the model are above 8 €/MWh increases by almost 15%, while the maximum value diminishes from 80 €/MWh to less than 70 €/MWh. These changes are mainly driven by the average cost patterns of RES, which range from 49.46 €/MWh to 163.5 €/MWh for solar generation, and 40.76 €/MWh to 88.25 €/MWh for wind generation. However, 96% solar production is still curtailed, while the curtailment rate of wind generation units slightly decreases to 87%. An infra-daily computational basis is required to neutralize the diurnal pattern of photovoltaic, as it doubles the average cost when taking a lower resolution. Finally, we note the recomputed spot price curve is mostly below the model marginal price, which suggests our econometric model may fail to capture how average cost bidding may impact the equilibrium spot price. More elaborate models integrating market fundamentals and submitted bids, with an explicit modeling of the mixed-bidding rule, might be required to correct this feature.

With a total generation of also 80 TWh and cumulated net market revenue equal to 1.307€ billion, **Figure 10.A.** shows nuclear generation units make an average profit of 16.35 €/MWh (without including FOM costs and annuities). The 0.093€ billion difference with total market revenue obtained under the traditional marginal-cost bidding rule can be decomposed between a negative -0.089€ billion price effect and a 0.182€ billion volume effect. Indeed, compared to the reference case, average unit profit is 2.58 €/MWh lower. Nuclear generation increases but is sold at a smaller price. The total revenue is also 0.681€ billion lower than under annually computed average RES costs, for a similar total generation volume. While solar generation is likely to be fully curtailed in Winter because of its low capacity factor, it contributes to significantly lower spot prices in Spring and Summer.

Independently of the observed load factor, nuclear units have 73% chances to operate for prices below 30 €/MWh, that is they are quite unlikely to be dispatched during periods with high prices. In terms of cumulated annual generation, 70% of generated electricity is sold for a price under 30 €/MWh.

Figure 10.B. in Appendix shows CCGT units are not started-up a single hour, yielding a null market remuneration. Finally, even though choosing a weekly computation basis slightly reduces curtailment, the utilization rates of photovoltaic and wind installed capacities, net of curtailment, remain extremely low. The annual average load factors of solar and wind units are respectively equal to 1% and 3.7%, with total generation of 678 GWh and 190 GWh. Although **Figures 10.C.** and **10.D.** (also in Appendix) display a slight increase in cumulative market revenues compared to the case of annual average costs, the higher number of operating hours for RES units is offset by the lower spot price paid to generators.

3.2.2. Limits of the average cost based mixed-bidding rule

Three kinds of limits can be identified from the previous results: first, while mixed-bidding rule may significantly restore margins of dispatchable generators, it is likely to generate high curtailment rates for wind and solar production. Introducing this new market rule *per se* would generate sunk costs for RES investments made *ex ante*. To minimize inefficiencies, real-time computation of average costs would be required, with some assumptions on the allocation of annual FOM costs and annuities. Only a part of total annual fixed costs (annuities for instance) could be used in the computation of the average cost if RES

generators already benefit from off-market subsidy mechanisms. Finally, the positive externality of RES, which reduce CO_2 emissions, might be accounted for in the computation of average costs and the cost comparison with dispatchable units. Yet, this mixed bidding mechanism may be difficult to implement. [26] advocates considering the storage cost of non-dispatchable renewables as a negative externality, that would be proportional to the installed capacity of renewable generators and added to the marginal cost of renewable technologies. This option is further explored in [27].

Second, the mechanism of average cost bidding may unavoidably introduce estimation errors due to the stochastic nature of renewable generation. It is likely to generate perverse effects. Indeed, while average costs are estimated on historic generation data, the expected load factor used for submitting bids relies on forecasts, as it is computed before the realization of RES generation. On the one hand, the shorter the time frame used for computing Ξ, the closer the reported costs of renewable generation is from their real-time costs. On the other hand, real-time measurement is more likely to generate large estimation errors than when renewable capacity factors are measured over longer periods. Under the assumption that $\{\boldsymbol{\xi}_{jt}\}_{t\geq 0}$ is cyclostationary and the $(\boldsymbol{\xi}_{jt}, \boldsymbol{\xi}_{jt+1}, \dots \boldsymbol{\xi}_{jt+T})$, $T > 0$, are iid with mean μ_{ξ_j} and variance $\sigma^2_{\xi_j}$ (after correcting for diurnal and seasonal non-stationarity and potentially non-Gaussian distribution (see [28])), the normalized variable $\boldsymbol{Z}_j = \left(\overline{\boldsymbol{\xi}_{J_T}} - \mu_{\xi_j}\right)\sigma_{\xi_j}^{-1} T^{-\frac{1}{2}}$ converges in law towards a normal distribution with zero mean when $T \to +\infty$[38]. Thus, the expected value of $\boldsymbol{\xi}_{jt}$ will tend towards its average annual or seasonal value if it is computed over enough observations. Relaxing the assumption that the $(\boldsymbol{\xi}_{jt}, \boldsymbol{\xi}_{jt+1}, \dots \boldsymbol{\xi}_{jt+T})$ are iid, we might model the normalized random process $\{\boldsymbol{Z}_j\}_{t\geq 0}$using an ARMA model to show that it is eventually mean-reverting with normal forecasting errors with zero mean. Under these assumptions, the expectations of $\boldsymbol{Z}_j$ and $\boldsymbol{\xi}_{jt}$ computed over a sufficiently high number of observations coincides with their mode. Computing the expected average generation cost over the year or seasons might thus decrease the estimation error. We refer to [29] for a comprehensive review of forecasting methods used for renewable and especially wind power predictions.

We note $\left(\widetilde{\mathbb{E}(\boldsymbol{\xi}_{jt})}, \widetilde{\mathbb{E}_s(\boldsymbol{\xi}_{jt})}, \widetilde{\mathbb{E}_{s,k}(\boldsymbol{\xi}_{jt})}, \widetilde{\mathbb{E}_{s,k,t}(\boldsymbol{\xi}_{jt})}\right)$ the vector of expected load factors reported by the producer of renewable generation unit $j \in \mathcal{J}$. The vector of estimation error can be

[38] We define $\overline{\boldsymbol{\xi}_{J_T}} = \frac{\boldsymbol{\xi}_{jt}+\boldsymbol{\xi}_{jt+1}+\cdots+\boldsymbol{\xi}_{jt+T}}{T}$ as the sample average corresponding to the sample of observations

decomposed into a random error vector $\boldsymbol{\varepsilon}_j = \left(\varepsilon_j, \varepsilon_{js}, \varepsilon_{js}^k, \varepsilon_{jst}^k\right)$ and systematic error vector $\boldsymbol{\eta}_j = \left(\eta_j, \eta_{js}, \eta_{js}^k, \eta_{jst}^k\right)$[39]. By assumption, the expected random error is null, i.e. $\mathbb{E}\left(\varepsilon_j\right) = \mathbb{E}\left(\varepsilon_{js}\right) = \mathbb{E}\left(\varepsilon_{js}^k\right) = \mathbb{E}\left(\varepsilon_{jst}^k\right) = 0$. Similarly, if the measurement process is unbiased and the producer of renewable generation unit $j \in \mathcal{J}$ truthfully reports expected generation, we have $\mathbb{E}\left(\eta_j\right) = \mathbb{E}\left(\eta_{js}\right) = \mathbb{E}\left(\eta_{js}^k\right) = \mathbb{E}\left(\eta_{jst}^k\right) = 0$. The verification of the cost estimates provided by the RES generators may be difficult. Under a high-resolution computation basis, the deviation of RES load factors from their average value is likely to be both more frequent and larger than under a low-resolution basis. Many observations, adjusted for diurnal and seasonal patterns in RES load factors, might be required to detect systematic false reporting of load factor and eventually average production cost. As verification is only possible *ex post*, RES generators would be incentivized to underreport their average cost to maximize their probability of being dispatched. The optimal choice of reporting would be weighted by the expected imbalance cost that might be paid by the RES operator as her observed generation deviates from her reported forecasts. This may result in increased system instability and balancing costs, with no obvious gains for RES generators as they would have to buy electricity in the balancing market to compensate for their generation deficit.

Finally, this mixed-bidding rule may generate inequalities within RES generators. It is also likely to disincentivize investment. Indeed, assuming one MWe has the same load factor distribution for successive generations (resulting from innovations) of a given technology, older generations are more likely to be curtailed that newer ones. Therefore, we expect new entrants to push incumbent RES operators down the "merit-order" curve. Such pricing system would thus require increasing subsidies paid to incumbent generators, which could raise issues of fairness between entrants and incumbents, but also significantly increase the tax burden for consumers. On the one hand, average cost bidding could provide incentives for technical innovation and lowering the total costs of renewables. On the other hand, investments with long payback periods may fail to break-even if the entry rate of new entrants

[39] The estimated error for the expected generation under each various computation basis can respectively be defined as follows:

$$C_j\left(\mathbb{E}\widetilde{\left(\boldsymbol{\xi}_{jt}\right)} - \mathbb{E}\left(\boldsymbol{\xi}_{jt}\right)\right) = \varepsilon_j + \eta_j \quad , \qquad C_j\left(\mathbb{E}_s\widetilde{\left(\boldsymbol{\xi}_{jt}\right)} - \mathbb{E}_s\left(\boldsymbol{\xi}_{jt}\right)\right) = \varepsilon_{js} + \eta_{js}$$

$$C_j\left(\mathbb{E}_{s,k}\widetilde{\left(\boldsymbol{\xi}_{jt}\right)} - \mathbb{E}_{s,k}\left(\boldsymbol{\xi}_{jt}\right)\right) = \varepsilon_{js}^k + \eta_{js}^k \quad , \qquad C_j\left(\mathbb{E}_{s,k,t}\widetilde{\left(\boldsymbol{\xi}_{jt}\right)} - \mathbb{E}_{s,k,t}\left(\boldsymbol{\xi}_{jt}\right)\right) = \varepsilon_{jst}^k + \eta_{jst}^k$$

into the electricity market is too rapid. Moreover, geographical sites with lower expected capacity factors would consistently exhibit high average costs, which would only make most productive sites financially viable in the absence of subsidies, and further disincentive investment.

At a microeconomic scale, such bidding system may disincentivize investment in RES units. Indeed, if investors anticipate decreasing investment costs, they expect the average cost of future RES technologies to decrease. As previously noticed, the risk of failing to break-even both increases with the rate of entry of new participants and the rate at which investment and FOM costs decrease. Investors would thus have an incentive to delay capacity investments, as units with higher investment and FOM costs would be more likely to be curtailed. Yet, these effects may be mitigated under the assumption that productivity of sites diminishes with installed capacities. We leave these theoretical remarks open for further research. A finely tuned mechanism, simultaneously accounting for the entry rate of new capacities, the evolution of investment costs and seasonal patterns, thus seems to be a promising alternative to marginal-cost pricing to ensure a higher remuneration to generators. A two-market solution as the one proposed by [30], which differentiate electricity market price based on the source of generation, might also be explored.

3.3. Ensuring adequate scarcity pricing: implementation of an operating reserves demand curve

Fundamentally, the US Standard Market Design is characterized by coordination, allowing markets to trade various products consistent with real-time operational constraints, and the anchoring of forward markets against real-time prices (see [22]). As the total amount of capacity imposes a limit on the joint provision of reserve capacity and energy, the profit margins on the energy-only and reserve markets should be equal, resulting in a non-arbitrage condition. As a result, energy and reserve dispatches are optimized simultaneously in the US. By comparison, the European market design segments markets between energy-only and reserve markets. Thus, asset owners decide how to auction their production of energy or provision of reserves based on the anticipated opportunity cost of participating in each market. The trading of energy and reserves is thus not co-optimized, and day-ahead and real-time markets are weakly coupled. However, as underlined by [31], simultaneously clearing

energy and reserves in the same auction would add significant computational complexity to the market, in additional to data collection requirements and new organizational challenges.

Yet, as a high RES penetration significantly increases uncertainty in real-time operations, adequately valuing reserves and flexibility sources is pivotal. Renewables shift market value from energy to reserves, thus requiring an evolving design market closer to real-time scarcity and operational constraints. A combination of scarcity pricing with a real-time reserve market, co-optimized with the energy dispatch, seems to be a promising direction to both better integrate RES and mitigate the "missing-money" problem.

Following [32], the Operating Reserve Demand Curve (ORDC) addresses the scarcity pricing requirement by introducing flexibility in reserve capacity procurement. It is based on a combination of the VOLL and the Loss of Load Probability (LOLP), which corresponds to the probability that load will be curtailed in tight supply conditions, given a certain level of reserve capacity carried by the system. For a given reserve capacity $R_t \geq 0$, a positive LOLP indicates that there is a positive probability that that system imbalance exceeds R_t. As the LOLP decreases with the volume of reserves, adding more reserves decreases the probability of system unbalance, which translates in a lower incremental value of reserves. According to [32], the ORDC has various interesting properties. First, it increases reliability by reflecting immediate supply conditions. Second, it is compatible with an "energy only" market design and forward-markets, and may incentive the development of the latter as customer would seek to hedge against high scarcity prices. ORDC would not automatically translate into higher prices as investment in responsive generation and demand-side management (DSM) devices may lower average costs. Finally, scarcity pricing may incentivize flexible demand participation and developing energy-efficiency, especially for electricity usages observed in peak demand periods.

The first step in computing an ORDC requires the estimation of the probability of failure associated to each generation unit in the mix. For simplicity, we assume that each generation unit belonging to technology $\mathfrak{t} \in \mathfrak{T}$ has the same rate of failure. We use the historic 2015-2019 dataset from EDF listing, for each individual plant the duration and type of each event associated its provisional unavailability. We compute the share of hours during which each technology has at least one generation unit unavailable because of unforeseen failure. The resulting probability of failure for nuclear (resp. CCGT, hydroelectric and pumped-storage hydroelectric) units is equal to 4.22% (resp. 2.65%, 0.91% and 3.67%).

Then, we compute the probability associated to each possible discrete level of non-available power in the mix. Considering the failure associated to each individual generation unit as the result of a Bernoulli trial, we can use iterated convolution products to progressively construct the non-available power probability curve as shown in **Figure 10**. For instances, let us consider two generation units, with rated power C_1 and C_2 and probability of failure q_1 and q_2. Then, there exist four possible combinations of available power, namely $C_1 + C_2$, C_1, C_2 and 0 MW, with respective probabilities of occure $(1 - q_1)(1 - q_2)$, $q_2(1 - q_1)$, $q_1(1 - q_2)$ and $q_1 q_2$. We make the assumption that probabilities of failure are independent across generation units. For two units of the same technology $t \in \mathfrak{T}$, $C_{1t} = C_{2t}$ and $q_{1t} = q_{2t}$, so failure events are symmetric across plants. We note the LOLP has both first and second derivatives decreasing, indicating the probability of non-available power rapidly decreases and approaches zero for values superior to 3 GW.

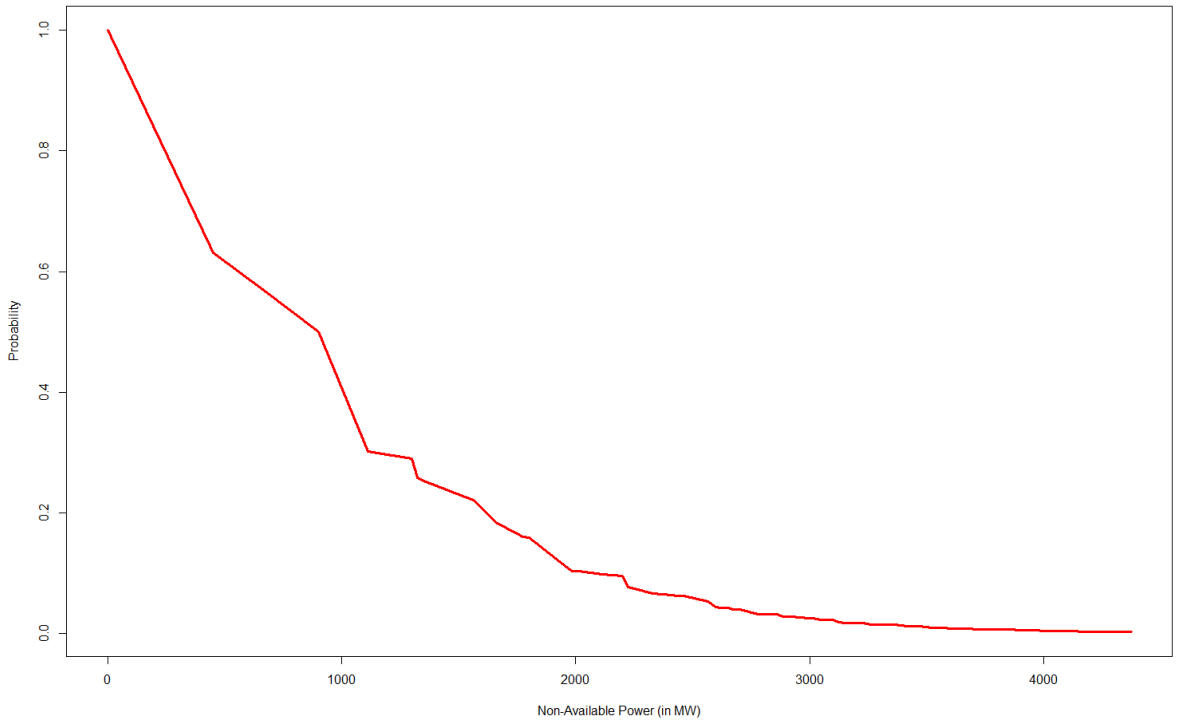

Figure 10: Non-available power cumulative distribution, sorted in decreasing order

As a reminder, the total thermal installed capacity in our optimal mix (neglecting RES and battery storage capacity) equals 27.74 GWe. While the probability of 1 GW (3.6% of total installed capacity) being non-available is quite high with roughly 50% chances of occuring, the non-availability of more than 3GW (10.8 % of capacities) is smaller than 2.6%. Overall,

we find a 99.9% probability that at least 79% of capacities are available. Indeed, as we assumed failure events are independent, the joint probability of simultaneous failures rapidly becomes negligeable although it remains strictly positive. For instance, we find a 2.23×10^{-14} probability that at least 50% of total capacities are unavailable.

The final step in the computation of the ORDC requires using the non-available power probability distrbution to model the LOLP associated to a given level of reserves R_t, and integrate it within the dispatch model. First, we approximate the non-available power probability distribution using a piecewise linear approximation. We chose the set of line segments that minimize the squared distance with the original distribution, and note $\widetilde{l(X)}$ the approximate probability associated to X GW of non-available power. We note Q_t^+ the maximum aggregate power that can be supplied in $t \in \mathcal{T}$, which is the computed by summing the maximum aggregate power than can be served by each online units for $\mathfrak{t} \in \mathfrak{T}$, accounting for ramping limits. Finally, the value of reserves, or scarcity price, can be defined as a function of residual demand $\boldsymbol{R}_{\boldsymbol{U}_t}^*$, maximum aggreate available power and reserve capacity, as follows:

$$V_t^R\left(Q_t^+, \boldsymbol{R}_{\boldsymbol{U}_t}^*\right) = \left(VOLL - \bigvee_{\mathfrak{t} \in \mathfrak{T}} V_{\mathfrak{t}}\right) \times l\left(\widetilde{Q_t^+ - \boldsymbol{R}_{\boldsymbol{U}_t}^*}\right) \approx VOLL \times l\left(\widetilde{Q_t^+ - \boldsymbol{R}_{\boldsymbol{U}_t}^*}\right) \qquad (\boldsymbol{9a})$$

If the difference $Q_t^+ - \boldsymbol{R}_{\boldsymbol{U}_t}^*$ is small, the probability that system imbalance exceeds available reserves is large. Supply is tight as the system is short of capacity in case of unforeseen plant failures, which uplifts the value of reserves. On the contrary, if $Q_t^+ - \boldsymbol{R}_{\boldsymbol{U}_t}^*$ is large, the probability that more than $Q_t^+ - \boldsymbol{R}_{\boldsymbol{U}_t}^*$ GW is non-available due to sudden failure is small, which drive the price of reserves down. We may further add minimum reserve requirements $\underline{R} \geq 0$, such that $\widetilde{l(X)} = 1$ for $X \leq \underline{R}$. The scarcity price now writes as follows:

$$V_t^R\left(Q_t^+, \boldsymbol{R}_{\boldsymbol{U}_t}^* | \underline{R}\right) \approx VOLL \times \left(\mathbb{1}\left\{Q_t^+ - \boldsymbol{R}_{\boldsymbol{U}_t}^* \leq \underline{R}\right\} + \mathbb{1}\left\{Q_t^+ - \boldsymbol{R}_{\boldsymbol{U}_t}^* > \underline{R}\right\} \times l\left(\widetilde{Q_t^+ - \boldsymbol{R}_{\boldsymbol{U}_t}^*}\right)\right) \quad (\boldsymbol{9b})$$

$\mathbb{1}\left\{Q_t^+ - \boldsymbol{R}_{\boldsymbol{U}_t}^* \leq \underline{R}\right\}$ is equal to 1 if $Q_t^+ - \boldsymbol{R}_{\boldsymbol{U}_t}^* \leq \underline{R}$ and 0 otherwise. The objective function in the dispatching optimization problem becomes:

$$\min_{\boldsymbol{q},\boldsymbol{\kappa},\boldsymbol{z}} \sum_{s \in \mathcal{S}} \sum_{t \in \mathcal{T}} \left(\sum_{g \in \mathcal{G}} \left(c_g^V + \pi^{CO_2} E_g\right) q_{gst} + c_g^{STUP} z_{gst} + \sum_{j \in \mathcal{J}} c_j^{\kappa} \kappa_{jst} + V_t^R\left(Q_t^+, \boldsymbol{R}_{\boldsymbol{U}_t}^* | \underline{R}\right) \times \left(Q_t^+ - \boldsymbol{R}_{\boldsymbol{U}_t}^*\right) \right) \qquad (\boldsymbol{10})$$

(10) introduces some non-linearities in the objective function, as the optimal level of reserves and the subsequent scarcity price are both functions of the commitment decisions of dispatchable units that can provide reserves (for simplicity, we assume that only dispatchable units can offer reserve capacity). This problem might be formulated as a Mixed-Integer Non-Linear Problem (MINLP) and solved with GAMS using the solver BARON. However, the computational complexity of this problem makes it intractable, even for small instances of the model. We thus leave the reformulation and resolution of this problem under a tractable form for further research.

Yet, by first solving for the optimal dispatching like in Section 2, it is possible to compute *ex post* the subsequent volumes of spinning reserves and the corresponding scarcity prices using **(9b)**. Although reserves and prices are not included in the decisions variables and are exogenous, this provides information on the periods for which supply is tight. **Figure 11.A.** plots both the values obtained for reserve capacity and scarcity prices for Winter and Summer. While the average scarcity prices are high in both seasons, with 180.8 €/MWh and 131 €/MWh in Winter and Summer respectively, the occurrence of price spikes is quite rare. Indeed, in both Winter and Summer, scarcity prices remain below the average values roughly 94% of hours and exceed 10 €/MWh in only 22% of them. We verify in **Figure 11.B.** and **11.C.** (see in Appendix) that the number of scarcity price spikes, as well as the average scarcity price, both increase with the minimum reserve capacity requirement.

In a model with endogenous computation of scarcity prices and reserves, we would expect the energy price to spike more frequently, but simultaneously take generally lower values, thus creating a favorable environment for investment in resources providing reserve capacity and flexibility services. As explained by [22], the existence of a real-time market for reserve capacity is a necessary condition for scarcity prices to back-propagate to the day-ahead energy market. Because of the non-arbitrage condition between energy and reserve markets, the scarcity price add-up, corresponding to the real-time value of reserve capacity, inflates the energy price. During the settlement of reserve imbalances, the agent selling reserves must buy back, at the real-time scarcity price, the amount of reserves sold to the TSO in the day-ahead reserve market. This condition ensures the backpropagation of scarcity prices to day-ahead reserve and energy markets. However, although the European Commission encourages the introduction of such mechanisms, most European countries have recently favored the choice of capacity markets. With ORDC scarcity prices computed since October 2019, Belgium is a noticeable European exception. Yet, the high prices potentially resulting from an ORDC, at

least in the short-run, may be politically unacceptable. Reaping the benefits of the latter would require the development of more active DSM practices, in addition to long-term forward contracts transferring the price risk from consumers to electricity retailers.

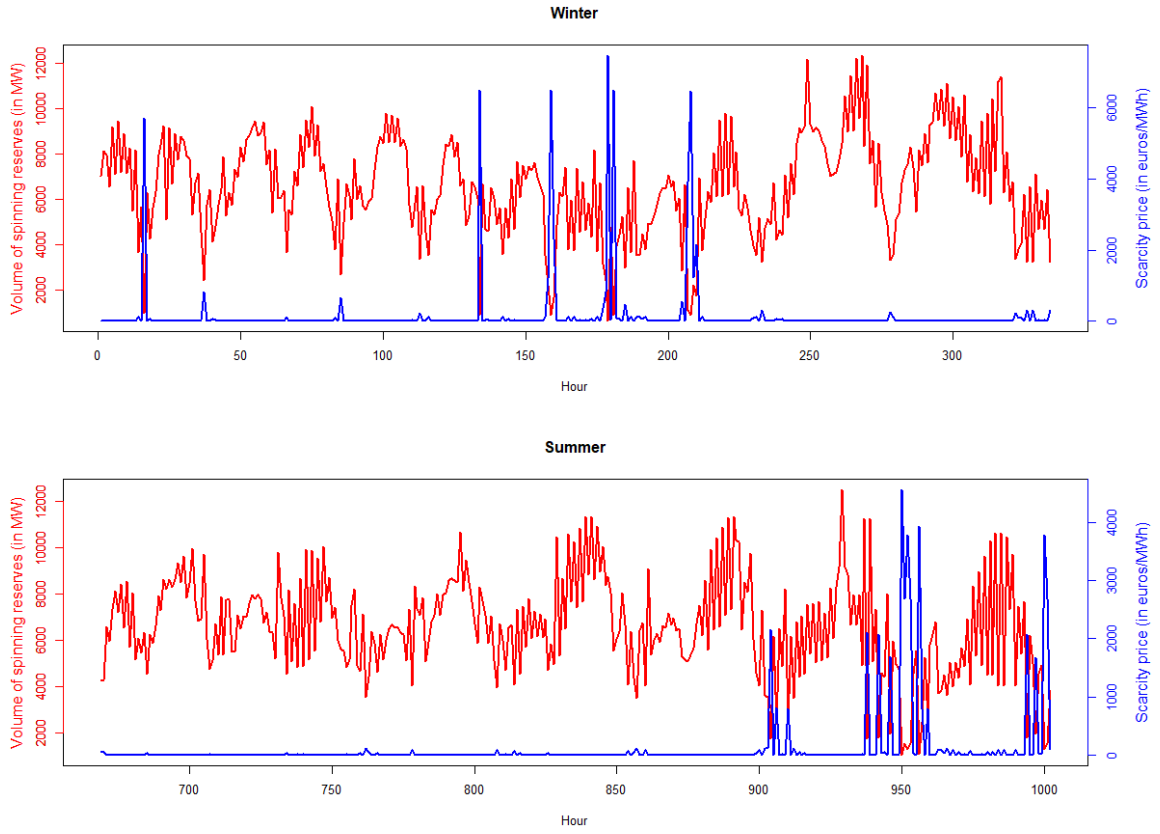

Figure 11.A.: Reserves and scarcity price, with no minimum reserve requirement

4. Alternative off-market compensation mechanisms

The Feed-in-Tariff (FiT) and Feed-in-Premium (FiP) are the two main subsidy schemes for renewables currently applied in France. For each kWh injected in the grid, the FiT contract guarantees the recipient a fixed tariff in €/MWh, generally superior to the average market price and fixed in advance. The tariff guarantees the contract recipient a normal profitability. In France, renewable producers with a FiT contract have a legal obligation to sell all their production to national electricity suppliers (EDF and local distribution companies). Introduced by the LTECV in 2015, the FiP offers the recipient a complementary revenue, on top of the spot price, equal to the difference between a reference tariff, in €/MWh, and a reference market price. The latter is usually set to the monthly average spot price. If the FiP recipient earns a market revenue superior to the contracted reference price, she may refund the

difference. The FiP contract is allocated either through guaranteed contracts or tender procedures conditional on the technology and installation size. The contract duration for the FiT and FiP spans from 12 to 20 years depending on technolog types and maturity. Legal dispositions relative to both the FiT and FiP are stipulated in the French Energy Code (Art. R. 314-1, R. 314-14).

Like the FiP, Contracts-for-Difference (CfD) guarantee the producer a stable revenue during the contract duration. In addition to capacity certificates, RTE provides long-term tenders (in French "Appel d'offres long term", AOLT) which offer visibility on future revenue for new capacities, thus theoretically encouraging investment[40]. Tenders are organized by the Ministry of Energy four years prior to the delivery year. Candidates with offer prices below the equilibrium tender price, or "strike price", are awarded a Contract-for-Difference (CfD). If the "strike price" is above the market price, the selected candidate receives the difference. On the opposite, it pays the difference to a dedicated fund. CfDs are only made available to new capacities which do not benefit from alternative support mechanism, which are committed to make a contracted amount of power available during PP2 hours. The Hinkley Point C nuclear plant located in Sommerset (England), composed of two EPR-type reactors for a total of 3.2 GWe, will benefit from a CfD with a "strike price" of £92.50 (2012 prices) for a 35 year term from its date of commissioning[41].

Interesting similarities and differences between the FiP and the CfD can be noted [33]. First, similarly to the FiP, the CfD entails a choice between taxpayers and electricity customers to fund the difference between the "strike price" and the reference market price. Charging the taxpayer is equivalent to granting public subsidy to generators with a FiP contract or a CfD. On the contrary, making the customer pay the extra may be costly if market prices are durably low, with potential negative macroeconomic effects. Second, generators remain exposed to market prices as the bulk of their remuneration comes from sales on the spot market. However, for a given volume of electricity injected into the grid, the total revenue is fixed under the CfD while it is variable under the FiP. The premium may be negotiated *ex ante* or *ex post*, but the latter exposes the producer to a greater risk as she ignores the future premium when injecting electricity. On the contrary, *ex ante* negotiation may result in a premium too low to generate sufficient remuneration if the future spot prices or generation are lower than

[40] https://www.services-rte.com/fr/decouvrez-nos-offres-de-services/participez-au-mecanisme-de-capacite/appel-d-offres-long-terme.html

[41] https://www.gov.uk/government/collections/hinkley-point-c

expected. The premium may also be defined as a function of the capacity installed in MWe. It is independent of the quantity of electricity injected into the grid and allows the generator to cover a share of its fixed cost. Again, the capacity premium of the FiP can be computed *ex ante* or *ex post*, where the former decreases the risk of not amortizing the investment, while the latter allows the computation of the exact remuneration complement required for the generator to cover her costs.

The CfD might be particularly well-suited for technologies with high investment and FOM costs, such as nuclear and RES technologies, as it allows a stable income while letting the generator exposed to the spot price signal. We provide a formal analysis of the optimal "strike price" and CfD design, in addition to the structure of costs paid by the public authority issuing the contract. We show the CfD generally provides a higher remuneration than the FiP, but at a higher cost for the issuer. Accounting for the joint distribution of spot prices and generation, although rather technical, is shown to be pivotal to design an efficient and cost-effective remuneration mechanism.

4.1. Contract for Difference: theoretical implications and practical implementation

We define the subset of eligible technologies/generation units $\mathcal{D} \subseteq \mathcal{P} \cup \mathcal{W} \cup \mathcal{G}$ based on some measurable criteria. The issuer of the CfD, which is a public entity, compensates the contract holder if the market price received is below a contracted "strike price" $K_{\mathfrak{t}} \geq 0$. In exchange for bearing the price risk, the issuer may in exchange receive a share of abnormal profits made when the spot price is above $K_{\mathfrak{t}}$. The CfD thus smoothes the market revenue received by the contract holder, for a given production profile. In the following subsection, random variables are written in bold to avoid confusion.

We define the random variable $\boldsymbol{\Upsilon}_{\boldsymbol{P},\boldsymbol{K}_{\mathfrak{t}}} = \boldsymbol{P} + (K_{\mathfrak{t}} - \boldsymbol{P})^{+} - \rho(\boldsymbol{P} - K_{\mathfrak{t}})^{+}$, where $\rho \leq 1$ corresponds to the share of extra profits received by the CfD issuer. We further define the functions of random variables $h_1(\boldsymbol{Q}_{\mathfrak{t}}, \boldsymbol{\Upsilon}_{\boldsymbol{P},\boldsymbol{K}_{\mathfrak{t}}}) = \boldsymbol{Q}_{\mathfrak{t}}\boldsymbol{\Upsilon}_{\boldsymbol{P},\boldsymbol{K}_{\mathfrak{t}}}$ and $h_2(\boldsymbol{Q}_{\mathfrak{t}}, \boldsymbol{P}) = \boldsymbol{Q}_{\mathfrak{t}}\boldsymbol{P}$. We assume the spot price P is generated by a random variable $\boldsymbol{P}$ defined on the probability space $(\Omega_{\boldsymbol{P}}, \mathcal{A}_{\boldsymbol{P}}, \mathbb{P}_{\boldsymbol{P}})$. Similarly, the total volume of electricity $Q_{\mathfrak{t}}$ injected in the grid by units of technology $\mathfrak{t} \in \mathcal{D}$ is assumed to follow a random variable $\boldsymbol{Q}_{\mathfrak{t}}$ with probability space

$\left(\Omega_{\boldsymbol{Q}_\mathrm{t}}, \mathcal{A}_{\boldsymbol{Q}_\mathrm{t}}, \mathbb{P}_{\boldsymbol{Q}_\mathrm{t}}\right)$. We respectively note their densities $g_{\boldsymbol{P}}$ and $g_{\boldsymbol{Q}_\mathrm{t}}$, cumulative distribution functions $G_{\boldsymbol{P}}$ and $G_{\boldsymbol{Q}_\mathrm{t}}$, and finally their expected values $\mathbb{E}_{\mathbb{P}_{\boldsymbol{P}}}[\boldsymbol{P}]$ and $\mathbb{E}_{\mathbb{P}_{Q_g}}[\boldsymbol{Q}_\mathrm{t}]$. Furthermore, we define the joint probability distribution $\boldsymbol{P} \times \boldsymbol{Q}_\mathrm{t}$ with probability space $\left(\Omega_{\boldsymbol{P}} \times \Omega_{\boldsymbol{Q}_\mathrm{t}}, \mathcal{A}_{\boldsymbol{P}} \times \mathcal{A}_{\boldsymbol{Q}_\mathrm{t}}, \mathbb{P}_{\boldsymbol{P}} \times \mathbb{P}_{\boldsymbol{Q}_\mathrm{t}}\right)$, with joint density $g_{\boldsymbol{P},\boldsymbol{Q}_\mathrm{t}}$, joint cumulative distribution $G_{\boldsymbol{P},\boldsymbol{Q}_\mathrm{t}}$ and expectation $\mathbb{E}_{\mathbb{P}_{\boldsymbol{P}} \times \mathbb{P}_{\boldsymbol{Q}_\mathrm{t}}}[\boldsymbol{P}\boldsymbol{Q}_\mathbf{t}]$. The participation constraints for each eligible technology $\mathrm{t} \in \mathcal{D}$ can be written as follows:

$$\mathbb{E}_{\mathbb{P}_{\boldsymbol{P}} \times \mathbb{P}_{\boldsymbol{Q}_\mathrm{t}}}\left[h_1\left(\boldsymbol{Q}_\mathrm{t}, \boldsymbol{\Upsilon}_{\boldsymbol{P},\boldsymbol{K}_\mathrm{t}}\right)\right] - \mathbb{E}_{\boldsymbol{Q}_\mathrm{t}}[\boldsymbol{Q}_\mathrm{t}] c_\mathrm{t}^V - F_\mathrm{t} \geq 0 \qquad (\mathbf{11a})$$

$$\mathbb{E}_{\mathbb{P}_{\boldsymbol{P}} \times \mathbb{P}_{\boldsymbol{Q}_\mathrm{t}}}\left[h_1\left(\boldsymbol{Q}_{\boldsymbol{g}}, \boldsymbol{\Upsilon}_{\boldsymbol{P},\boldsymbol{K}_\mathrm{t}}\right)\right] \geq \mathbb{E}_{\boldsymbol{Q}_\mathrm{t},\boldsymbol{P}}[h_2(\boldsymbol{Q}_\mathrm{t}, \boldsymbol{P})] \qquad (\mathbf{11b})$$

Then, it can be proven that the optimal K_t^* satisfies the following constraint:

$$K_\mathrm{t}^* \geq \frac{c_\mathrm{t}^V + F_\mathrm{t}\mathbb{E}_{\mathbb{P}_{\boldsymbol{Q}_\mathrm{t}}}[\boldsymbol{Q}_\mathrm{t}]^{-1} - (1-\rho)\left(1 - G_{\boldsymbol{P}}(K_\mathrm{t})\right)\mathbb{E}_{\mathbb{P}_{\boldsymbol{P}} \times \mathbb{P}_{\boldsymbol{Q}_\mathrm{t}}}[h_2(\boldsymbol{Q}_\mathrm{t}, \boldsymbol{P}) | \boldsymbol{P} > K_\mathrm{t}]}{\left(G_{\boldsymbol{P}}(K_\mathrm{t})\mathbb{E}_{\mathbb{P}_{\boldsymbol{P}}}[\boldsymbol{P} | \boldsymbol{P} < K_\mathrm{t}] + \rho\left(1 - G_{\boldsymbol{P}}(K_\mathrm{t})\right)\mathbb{E}_{\mathbb{P}_{\boldsymbol{P}}}[\boldsymbol{P} | \boldsymbol{P} > K_\mathrm{t}]\right)} \qquad (\mathbf{12a})$$

Moreover, we show that the above expression greatly simplifies when the totality of abnormal profits is received by the emitter of the CfD, i.e. $\rho = 1$:

$$K_\mathrm{t}^* \geq c_\mathrm{t}^V + F_\mathrm{t}\mathbb{E}_{\mathbb{P}_{\boldsymbol{Q}_\mathrm{t}}}[\boldsymbol{Q}_\mathrm{t}]^{-1} \qquad (\mathbf{12b})$$

Proof: See Appendix (Proof 1)

Choosing an appropriate reference period for computing the expected generation is delicate. As the representative sample of weeks is selected to approximate the RD distribution over the period 2013-2018 in Auvergne-Rhône-Alpes, we take it as baseline. We compare the resulting optimal "strike price" for each technology with the "strike prices" found when respectively taking 2014-2018, 2015-2018, 2016-2018, 2017-2018 and 2018 as reference computation periods. Using **(12b)**, **Table 1** shows the corresponding "strike prices" for photovoltaic and wind generation unit:

Computation period	**Photovoltaic** (in €/MWh)	**Wind** (in €/MWh)
2013-2018 (Baseline)	30.95	66.08
2014-2018	30.15	66.13
2015-2018	29.62	66.28
2016-2018	29.90	66.00
2017-2018	29.81	65.19
2018	30.14	67.55

Table 1: Optimal "strike price" values for different computations periods

As the assumed reduction in investment and FOM costs for 2030 is much larger for photovoltaic units than wind turbines, "strike prices" for solar units are consistently more than 50% smaller than those for wind turbines, even with diurnal seasonality. The total annual fixed costs (corresponding to the sum of annuities and FOM costs) per MWe are equal to 35.54€ thousand and 135.5€ thousand for solar and wind power units respectively. For simplicity, we assume the reference tariff used for computing the FiP is also equal to the "strike price". We set $\rho = 1$.

Figure 12.A. plots the cumulative annual revenue for one MWe of photovoltaic capacity, both with CfD and FiP subsidy mechanisms. For all computation periods, we note the total remuneration under CfD is consistently higher than under FiP. In the baseline case, total annual remuneration under CfD completely covers fixed costs and is 18% higher than under FiP. While the total remunerations are very similar in Winter, most of the gap in total remuneration between CfD and FiP originates in Spring. Because of the large share of photovoltaic capacity in the mix, high volumes of solar production push down prices during the day, which are lower than during night hours. While CfD exactly compensates the low price per MWh received by photovoltaic generators, the average price used in the FiP is mechanically higher than spot prices during the day and yields a lower revenue.

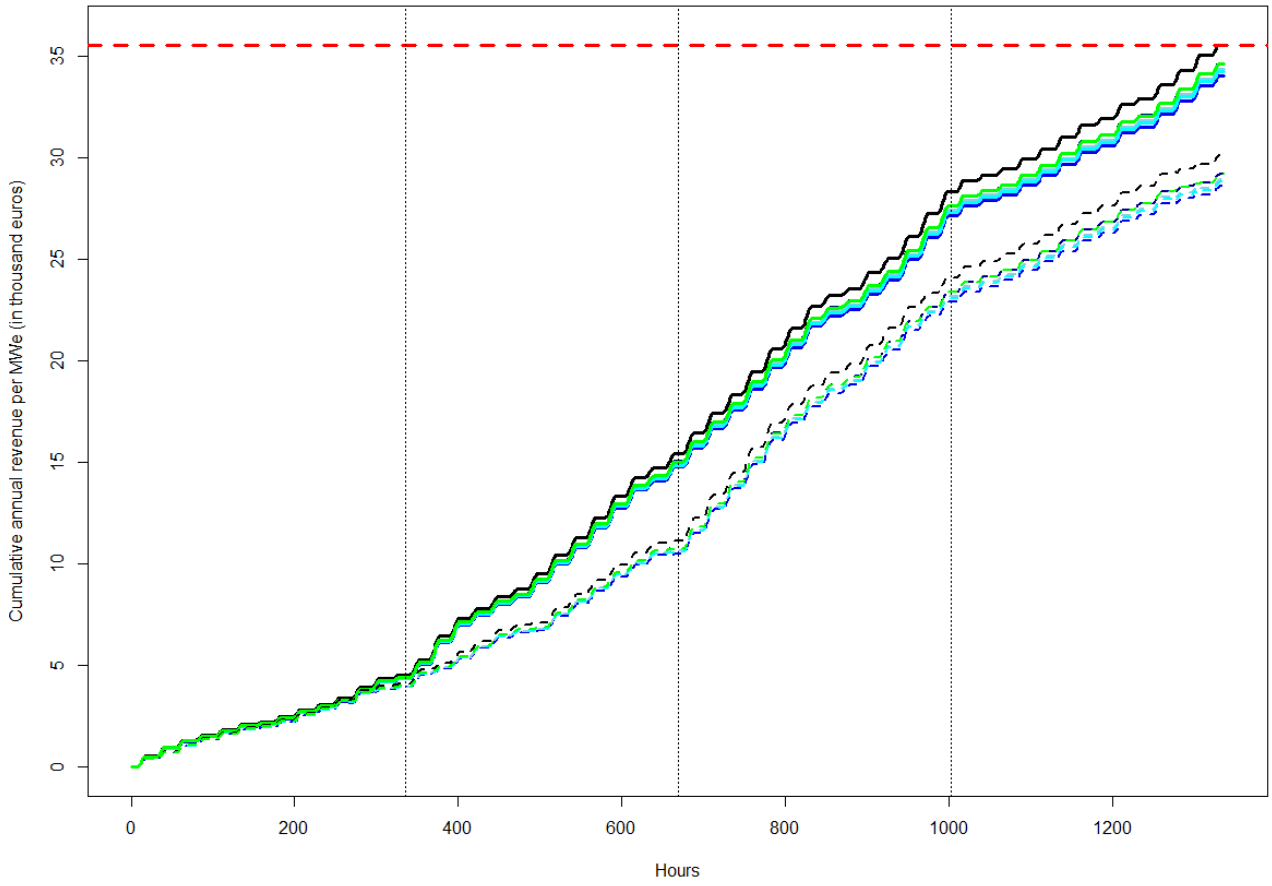

Figure 12.A.: Cumulative total revenue per MWe of installed solar, under both CfD and FiP

Note: The plain black (resp. dark blue, blue, clear blue, cyan and green) line corresponds the cumulative sum of total revenues, including both market remuneration and CfD remuneration, when taking the computation period 2013-2018 (resp. 2014-2018, 2015-2018, 2016-2018, 2017-2018 and 2018). The dotes lines correspond the same information with a FiP instead of a CfD. The red dotted line corresponds to the total annual fixed costs, while the vertical black dotted lines mark out seasons.

Because the "strike price" for wind units is high for all computation basis, most of the revenue of wind generators is derived from subsidies. As shown in **Figure 12.B.**, the FiP yields a slightly higher total remuneration than the CfD. In the baseline case, the CfD brings a 3.5% lower total revenue than the FiP and allows positive profits. Indeed, wind production basically exhibits an inverse pattern with respect to solar production: it is lower during the day, especially in Spring and Summer, and higher at night. Using a FiP thus increases the add-up received for electricity generated during the night when spot prices are high, while the difference between the "strike price" and spot price received under the CfD is small.

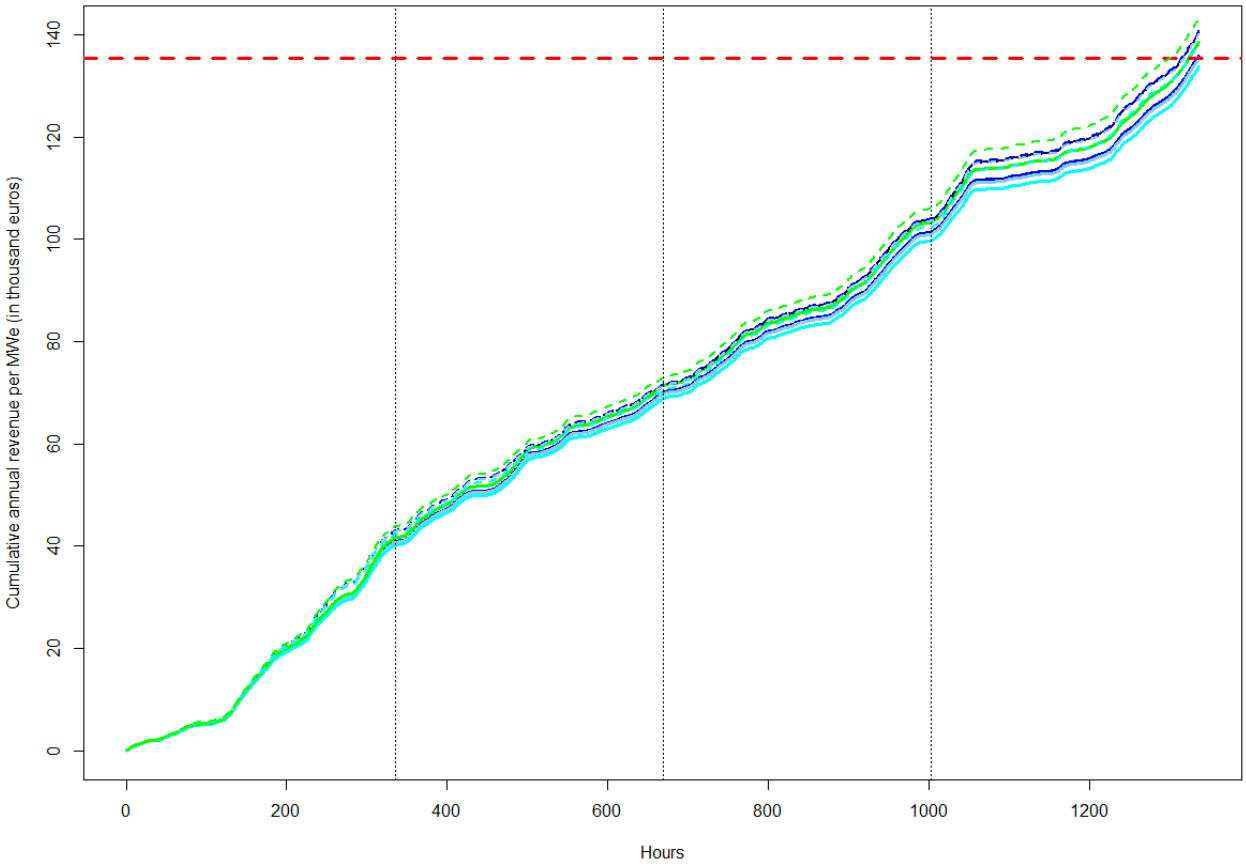

Figure 12.B.: Cumulative total revenue per MWe of installed wind power, under both CfD and FiP

The choice of a CfD or a FiP as a complementary remuneration scheme thus depends on the impact of the recipient on the market price: the comparative advantage of the CfD in terms of total remuneration becomes more preeminent as RES penetration increase and drive prices down. However, as shown in the case of wind generation units, technologies which production level is positively correlated with prices may reap higher benefits from a FiP. However, the positive profits earned under the FiP may lead to contract renegotiation if the abnormal returns are too high with respect to some reference profit rate. Moreover, while the CfD brings a fixed total revenue, generators under FiP receive a variable revenue and are thus subjected to a higher risk of not covering their total fixed costs. Finally, the computation of a fair FiP for each RES requires to know the future aggregate renewable capacity during contract duration, and to precisely estimate its impact on the expected generation of each RES technology and on the spot prices distribution (see [34]). The CfD is simpler as it only

requires knowledge about the future expected generation of renewables, which is quite simple if they are guaranteed priority dispatch.

Yet, the CfD holder is insured against price uncertainty but remains subject to quantity risk. In the above formulation, the optimal value of K_g is determined using estimated values for $\mathbb{P}_{\boldsymbol{Q}_t}$ and $\mathbb{P}_{\boldsymbol{P}}$, which are measured based on available data. We note $\mathbb{P}^K_{\boldsymbol{Q}_t}$ and $\mathbb{P}^K_{\boldsymbol{P}}$ the distributions used for the estimation of K_g^*. The duration of the contract must encompass a period long enough for the *ex post* distribution of $\boldsymbol{Q}_t$ and $\boldsymbol{P}$ to converge to $\mathbb{P}^K_{\boldsymbol{Q}_t}$ and $\mathbb{P}^K_{\boldsymbol{P}}$. Indeed, if the distribution of $\boldsymbol{Q}_t$ observed *ex post*, i.e. after the CfD is signed, differs from $\mathbb{P}^K_{\boldsymbol{Q}_t}$, the contracted "strike price" may be too high or too low, thus yielding losses or abnormal profits to the contract holder. Moreover, if the total annual remuneration is below the annual fixed costs, the CfD issuer might fail to break-even without *ex post* contract renegotiation. We illustrated how the choice of the initial computation period influences total annual remuneration in **Figure 12.C.** and **12.D.** in Appendix.

It is also possible to give a formal definition of the optimal contract design for the CfD issuer. Assuming the public authority proposes a CfD contract to each eligible technology $t \in \mathcal{D}$, it seeks to minimize the expected total cost associated to CfDs while satisfying the participation constraint for each technology, where $W(\vec{K})$ is the cost function of the CfD issuer and $\vec{K} = (K_t)_{t\in\mathcal{D}}$. By defining the function $h_3(\boldsymbol{Q}_t, \boldsymbol{\Upsilon}_{\boldsymbol{P},\boldsymbol{K}_t}) = \boldsymbol{Q}_t(\boldsymbol{\Upsilon}_{\boldsymbol{P},\boldsymbol{K}_t} - \boldsymbol{P})$, we have the following optimization program:

$$\min_{\vec{K}} W(\vec{K}) = \sum_{t\in\mathcal{D}} \left(\mathbb{E}_{\mathbb{P}_{\boldsymbol{P}}\times\mathbb{P}_{\boldsymbol{Q}_t}}\left[h_3(\boldsymbol{Q}_t, \boldsymbol{\Upsilon}_{\boldsymbol{P},\boldsymbol{K}_t})\right]\right) \tag{13}$$

$$\text{s.t. } \mathbb{E}_{\mathbb{P}_{\boldsymbol{P}}\times\mathbb{P}_{\boldsymbol{Q}_t}}\left[h_1(\boldsymbol{Q}_t, \boldsymbol{\Upsilon}_{\boldsymbol{P},\boldsymbol{K}_t})\right] - \mathbb{E}_{\mathbb{P}_{\boldsymbol{Q}_t}}[\boldsymbol{Q}_t]c_t^V - F_t \geq 0$$

The CfD issuer minimizes the total annual volume of subsidies allocated to recipients, under the constraint that they recover their total annual costs. The above formulation does not span for the full contract duration and thus implicitly assumes that the joint distribution $\mathbb{P}_{\boldsymbol{P}} \times \mathbb{P}_{\boldsymbol{Q}_t}$ is identical across years. For $\rho = 1$, the optimal annual transfer to each $t \in \mathcal{D}$ simply corresponds to the product of the optimal "strike price" K_t^* and the expected generation minus its expected market revenue. By plugging the value of K_t^* in the expression of $W(\vec{K})^*$, we further show that the optimal monetary transfer made to each CfD recipient simplifies to the difference between expected annual total costs and market revenue. Formally, we show that:

$$W(\vec{K})^{*} = \sum_{t\in\mathcal{D}} \left(K_t^{*} \mathbb{E}_{\mathbb{P}_{\boldsymbol{Q}_t}}[\boldsymbol{Q}_t] - \mathbb{E}_{\mathbb{P}_{\boldsymbol{P}}\times\mathbb{P}_{\boldsymbol{Q}_t}}[h_2(\boldsymbol{Q}_t, \boldsymbol{P})] \right) = \sum_{t\in\mathcal{D}} \left(c_t^{V} \mathbb{E}_{\mathbb{P}_{\boldsymbol{Q}_t}}[\boldsymbol{Q}_t] + F_t - \mathbb{E}_{\mathbb{P}_{\boldsymbol{P}}\times\mathbb{P}_{\boldsymbol{Q}_t}}[h_2(\boldsymbol{Q}_t, \boldsymbol{P})] \right) \quad (\mathbf{14})$$

Proof: See Appendix (Proof 2)

Figure 13 decomposes the cumulative annual cost of CfD and FiP per installed MWe, both for photovoltaic and wind power units. With a total of 96.73€ thousand, the cost of CfD for wind units if more than 4 times higher than for solar units (21.56€ thousand). While the cumulated costs of CfD and FiP are quite similar for wind power, the total cost of CfD is 67% higher than under a FiP for photovoltaic. The correlation between production and spot prices, in addition to the impact of generated volumes of each eligible technology, both have a significant influence on the respective costs of CfD and FiP paid by the public authority. Choosing a value $\rho < 1$ may lower the optimal "strike price", thus increasing the probability that the CfD recipient reimburses a share of abnormal returns to the public authority. However, setting $\rho < 1$ requires knowing the joint distribution of production and spot prices for all recipient technologies, in addition to future distributions and installed capacities during the contract duration. This may be difficult to implement as it relies on high data requirements, complex electricity market modelling and a full knowledge of future investments. We leave this issue for further research.

The concept of CfD may be extended to other applications. [35] propose a Carbon Contract for Difference (CCfD), applicable to investors in pilot commercial-scale low carbon projets. Following [36], the CCfD would guarantee producers of ultra-low-carbon materials a carbon "strike price" K_{CO_2}, such that at the end of any given period, the investor receives the difference between K_{CO_2} and the average EU ETS carbon price over the period for each ton of avoided CO_2 from her project. If the average EU ETS price is significantly above K_{CO_2}, then the allocation rule of the abnormal profits between the emitter of the CCfD contract and the investor must be determined in the contract design. In return for bearing the downside risk in relation to carbon price, the CCfD emitter would receive a contracted share of the extra profits. Proposing a CfD to carbon emitting generation units, such as CCGT, for investing in Carbon Capture and Storage (CCS) technologies, might significantly contribute to reducing the risk associated to such investments. Moreover, especially if the price of CO_2 is high, CCS

technologies would increase the utilization rate and load factor of CCGT plants, eventually increasing their market revenue. We leave these remarks for further research.

Figure 13: Cumulative annual cost of CfD and FiP for wind power and photovoltaic, under both CfD and FiP

4.2. Designing a customer preference-based insurance overlay on wholesale electricity markets

As illustrated in the case of scarcity pricing, adequately valuing the reliability and flexibility services provided by generators is an important feature of an efficient wholesale electricity market. Although such market design is expected to uplift energy prices, it questions the actual value that electricity customers attribute to their consumption. In this respect, if the willingness to pay of a customer is below the scarcity price, this would suggest her preferences for power reliability are overestimated by the market operator. The VOLL, which is an aggregate measure, might fail to reflect the diversity of individual preferences regarding power supply.

As underlined by [8], existing capacity mechanisms require that the central authority infers customer preferences for reliability, which may be especially challenging in practice. They propose an "insurer-of-last-resort model", functioning as a risk overlay on top of wholesale energy-only markets. While reliability refers to the ability of the generation and transmission system to satisfy electricity demand, security corresponds to the resilience of the system to unforeseen disturbances and frequency deviations. The theoretical basis for the "insurer-of-last-resort" model is the provider insurance model proposed by [37]. Insured customers pay a premium to the central insurer (mandated by the TSO), which compensates the insured agents in the event of power outage. Estimating the individual valuations for power reliability and stability by revealed preferences is theoretically possible if a complete insurance market is available, allowing customers to voluntarily participate to the market and elect the level of coverage that maximizes their utility. For instance, customers with a high VOLL choose a high coverage and thus pay a high premium. The central issuer can then engage in loss-limiting activities such as investing in new generation resources or provide missing money to incumbent generators. It weights the costs of additional capacity contracting and payments to generators making losses against the benefits resulting from lower reliability transfers made to insured customers. Finally, to mitigate potential free-riding issues, [8] propose that customers who decline to participate in insurance market would be automatically eligible for disconnection by the TSO in case of reliability event. This may however generated fairness issues. Alternative incentive mechanisms, such as Grove's schemes and Vickrey auctions (see [38]), may incentivize customers to participate to the insurance scheme and truthfully reveal their preferences.

This approach is justified by the assumption that power reliability and stability are quasi-public goods as in [39]. It can be argued that power reliability is a partial non-rival good, as the consumption of electricity by some customers does not reduce the consumption of others. Yet, in tight supply conditions, a large deviation from subscribed power may threaten system stability, which may reduce the consumption of all electricity customers in case of power outage. Although there is a limited ability to measure the infinitesimal impact of customers on system stability, reliability and stability may not be separable, at least for hours with tight reserves. In this respect, the individual VOLL, under its current definition, may fail to reflect potentially time-dependent joint preferences for reliability and system stability.

Following [40], the individual costs associated to power outages can be derived either from direct methods (blackout studies as in [41], willingness to pay/avoid power outage, scenario

ranking) using questionnaires or interviews, or indirect computation methods (macroeconomic approaches, production function estimation as [42], average household income, revealed preferences approach). A new and more complex measure would however be required to accurately value preferences. Time-differentiation, that is the assumption of heterogenous valuations depending on the hour of power outage, would be critical as it relates preferences for reliability to stability. Indeed, for leisure and economic activities that require a stable and uninterrupted electricity supply for several consecutive time periods (hours or even days, for instance for solving an optimization program), the value of stability increases with the duration of the activity. On the contrary, reliability may be more valuable during peak hours, during which customers require a significant power but over a short period of time. Estimating the frequency of power outages is also insufficient to correctly value customer preferences. For instance, extremely frequent power interruptions during a few hours per year are clearly not equivalent to less frequent but regular power interruptions throughout the year. Thus, the new measure would require the knowledge of the annual distribution of power interruptions and their dynamics, using for instance survival analysis tools, by considering the reliability events as a counting process.

Equipped with this new measurement tool, the central insurer would then propose to customers a complete menu of coverage and premiums, corresponding to various the types of preferences. It would run counterfactual long-run dispatching analysis to determine the optimal level and allocation of premiums between generators, so that it that minimize the compensation transfers made to insured customers during power shortage events. We leave these theoretical remarks and modelling issues for further research.

5. Conclusion and policy implications

By aggravating the existing “Missing Money” problem by depressing spot prices, the growing penetration of RES in the electricity mix requires the adaptation of the market design to better address these new challenges. It has been shown that a higher renewable production increases spot price volatility, which may further deter future investments by inflating the price risk. Better accounting for resources availability and scarcity, though mixed-bidding rules and ORDC as investigated in this chapter, may contribute to better reflect real-time operational conditions, and value flexibility and reserve capacities more accurately. Yet, average cost

bidding for RES may generate significant curtailment and economic inefficiencies. A fined-tune rule, based on a fraction of annual costs and real-time computation of RES load factors, may yield better economic performances, and preserve investment incentives in RES technologies. Scarcity pricing based on the construction of an ORDC may help restoring the efficiency of the price signal on day-ahead and real time wholesale markets, but may generate politically inacceptable price spikes. Its implementation in France would also require the introduction of a real-time reserve capacity market, which turns to be quite unlikely in the short-run with the introduction of a capacity market in 2017.

Subsidy mechanisms thus remain necessary to ensure the cost-effectiveness of RES technologies, but may also prove adapted to other capital-intensive technologies such as nuclear. We have shown that, under certain conditions, the CfD may perform better than the FiP in terms of total remuneration provided to the contract recipient, but it is expected to generate a significantly higher tax burden imposed on electricity customers and taxpayers. Diminishing the volume of subsidies while preserving economic efficiency of the CfD would require high data requirements and intricate modelling of future electricity markets.

Overall, adequately measuring the value attributed to electricity by individual customers might be a necessary step towards future well-functioning electricity markets. Incentivizing individuals to reveal their preferences for reliability and stability, through insurance-type mechanisms, may both help bridging the “Missing Money” gap and bring the electricity price paid by customers closer to their individual valuations, thus improving equity in system cost-sharing.

6. Appendix

Appendix to 2.2.:

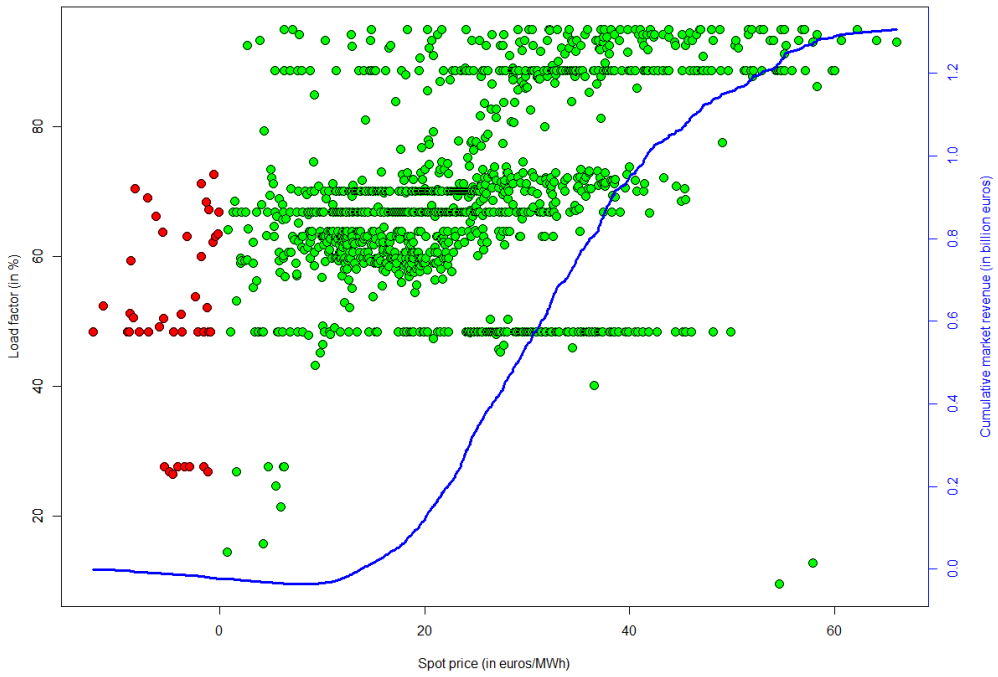

Figure 10.A.: Spot price and load factor patterns for the remuneration of nuclear units under mixed bidding rule, weekly computation basis

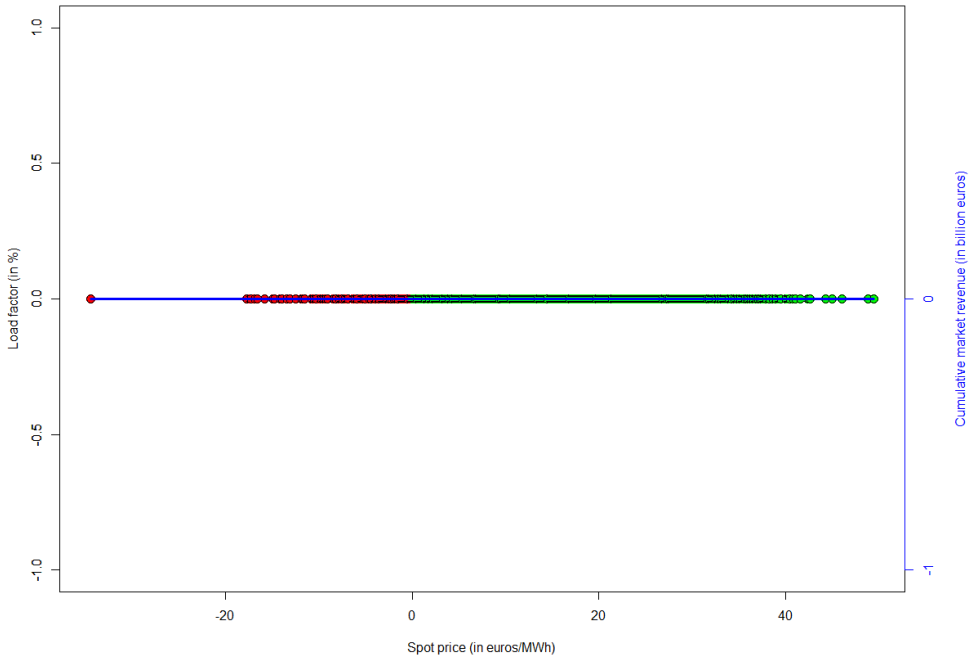

Figure 10.B.: Spot price and load factor patterns for the remuneration of CCGT units under mixed bidding rule, weekly computation basis

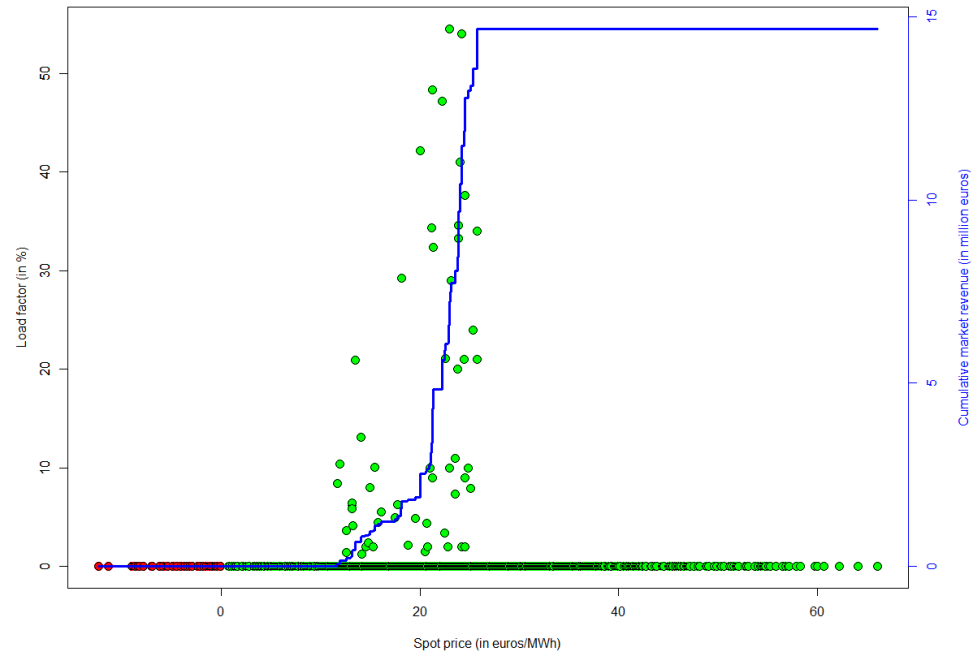

Figure 10.C.: Spot price and load factor patterns for the remuneration of photovoltaic generation units under mixed bidding rule, weekly computation basis

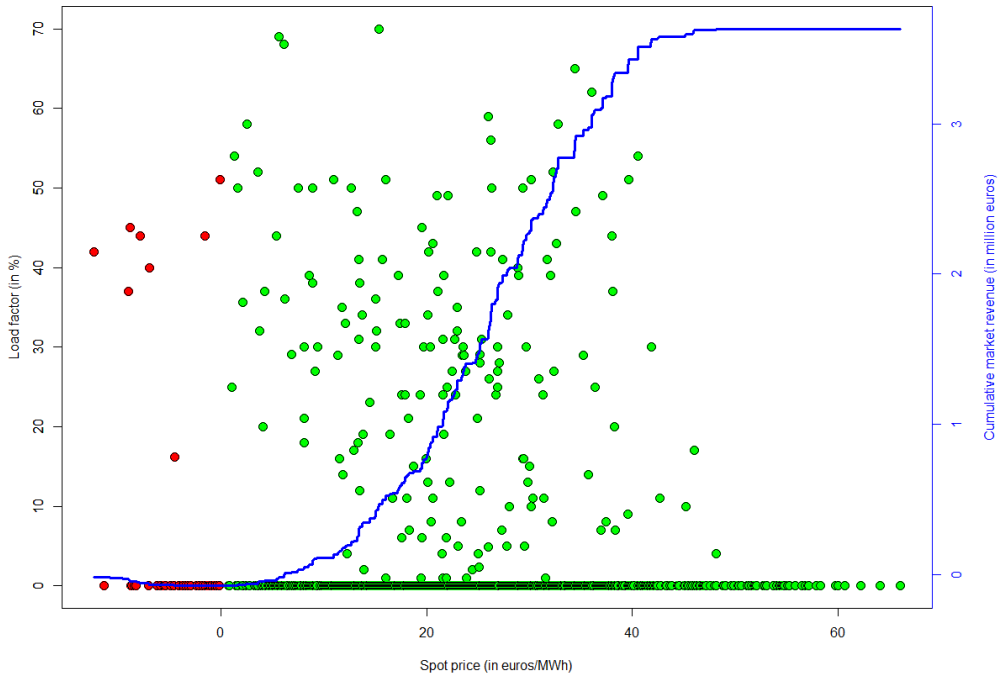

Figure 10.D.: Spot price and load factor patterns for the remuneration of photovoltaic generation units under mixed bidding rule, weekly computation basis

Appendix to 3.3.:

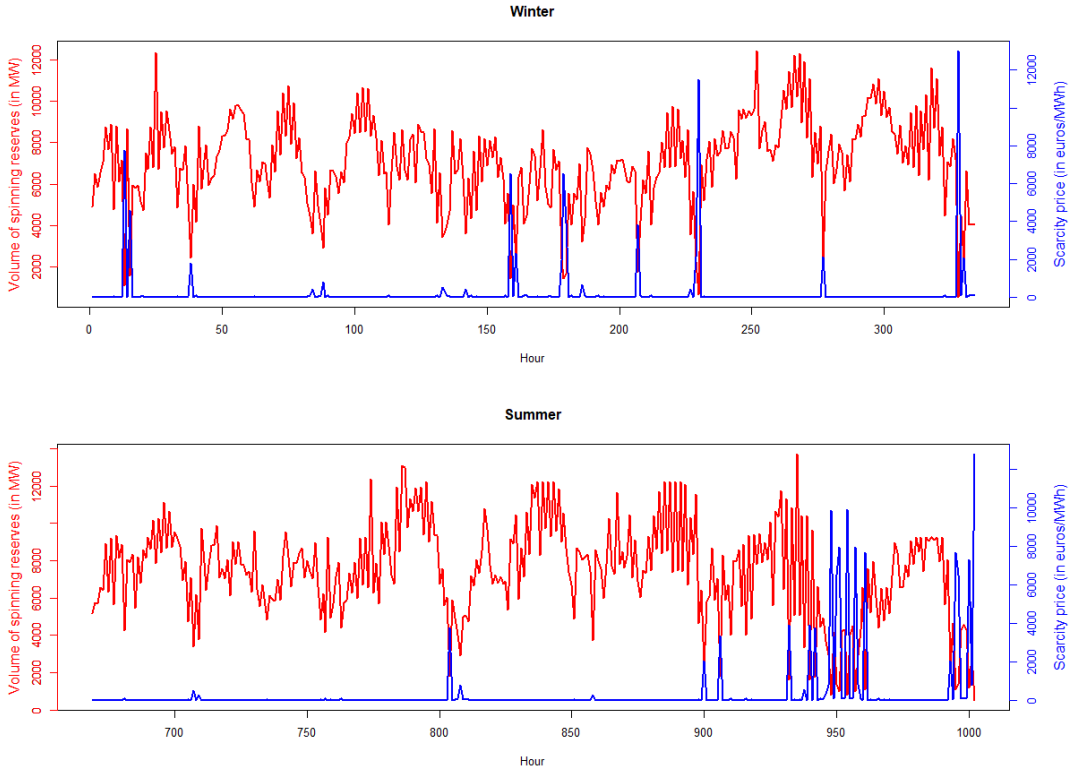

Figure 11.B.: Reserves and scarcity price, with minimum reserve requirement of 500 MW

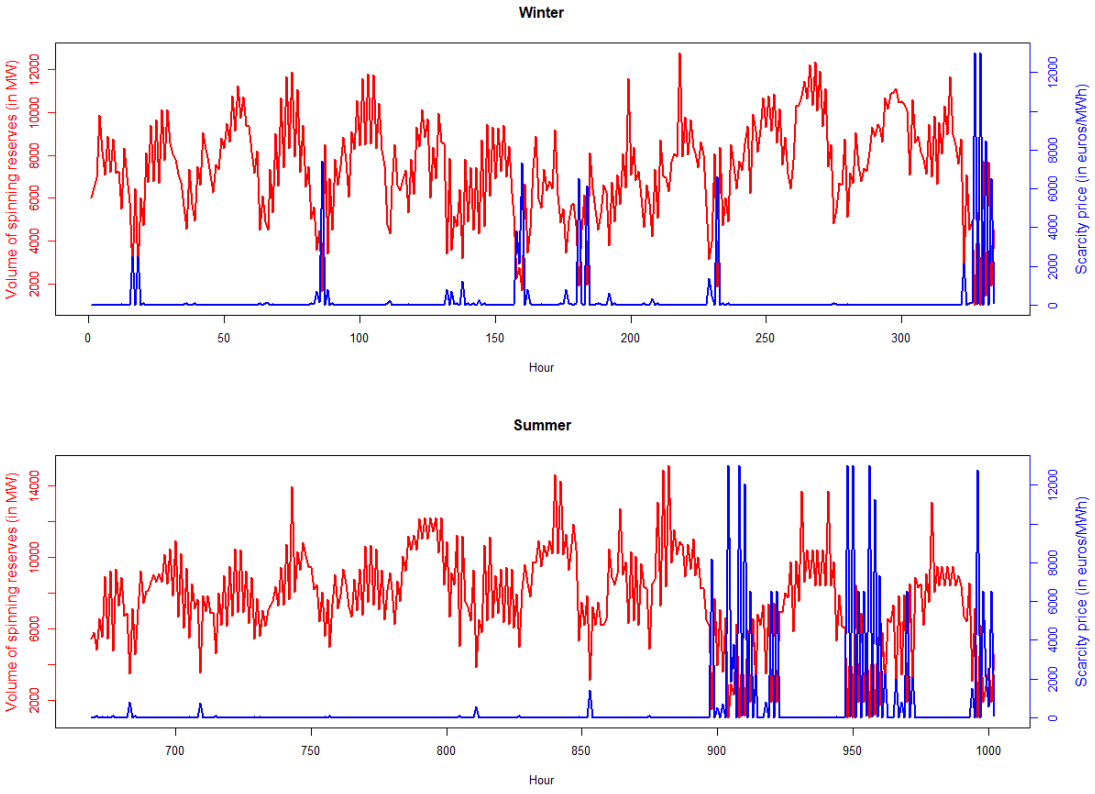

Figure 11.C.: Reserves and scarcity price, with minimum reserve requirement of 1000 MW

Appendix to 4.1.:

Proof 1:

We reformulate the initial condition in terms of integrals:

$$\mathbb{E}_{\mathbb{P}_{\boldsymbol{P}}\times\mathbb{P}_{\boldsymbol{Q}_\mathrm{t}}}\left[h_1\left(\boldsymbol{Q}_\mathrm{t},\boldsymbol{\Upsilon}_{\boldsymbol{P},\boldsymbol{K}_\mathrm{t}}\right)\right]-\mathbb{E}_{\mathbb{P}_{\boldsymbol{Q}_\mathrm{t}}}[\boldsymbol{Q}_\mathrm{t}]c_\mathrm{t}^V-F_\mathrm{t}\geq 0$$

$$\Leftrightarrow \iint_{\Omega_{\boldsymbol{Q}_\mathrm{t}}\times\Omega_{\boldsymbol{P}}} Q_\mathrm{t}\Upsilon_{P,K_\mathrm{t}}d\mathbb{P}_{\boldsymbol{Q}_\mathrm{t},\boldsymbol{P}}(Q_\mathrm{t},P)-c_\mathrm{t}^V\mathbb{E}_{\mathbb{P}_{\boldsymbol{Q}_\mathrm{t}}}[\boldsymbol{Q}_\mathrm{t}]-F_\mathrm{t}\geq 0$$

$$\Leftrightarrow \iint_{\Omega_{\boldsymbol{Q}_\mathrm{t}}\times\Omega_{\boldsymbol{P}}} Q_\mathrm{t}\Upsilon_{P,K_\mathrm{t}}g_{\boldsymbol{P},\boldsymbol{Q}_\mathrm{t}}(P,Q_\mathrm{t})dPdQ_\mathrm{t}-c_\mathrm{t}^V\mathbb{E}_{\mathbb{P}_{\boldsymbol{Q}_\mathrm{t}}}[\boldsymbol{Q}_\mathrm{t}]-F_\mathrm{t}\geq 0$$

It is straightforward to see that as $\int\left|Q_\mathrm{t}\Upsilon_{P,K_\mathrm{t}}g_{\boldsymbol{P},\boldsymbol{Q}_\mathrm{t}}\left(P,Q_g\right)\right|dPdQ_\mathrm{t}<+\infty$, we can use Fubini's theorem to see that the optimal "strike price" must verify the following inequality:

$$\Leftrightarrow \int_{\Omega_{\boldsymbol{P}}}\left[\int_{\Omega_{\boldsymbol{Q}_\mathrm{t}}} Q_\mathrm{t}\Upsilon_{P,K_\mathrm{t}}g_{\boldsymbol{P},\boldsymbol{Q}_\mathrm{t}}(P,Q_\mathrm{t})dQ_\mathrm{t}\right]dP-c_\mathrm{t}^V\mathbb{E}_{\mathbb{P}_{\boldsymbol{Q}_\mathrm{t}}}[\boldsymbol{Q}_\mathrm{t}]-F_\mathrm{t}\geq 0$$

$$\Leftrightarrow \int_{\Omega_{\boldsymbol{P}}<K_\mathrm{t}} K_\mathrm{t}\left[\int_{\Omega_{\boldsymbol{Q}_\mathrm{t}}} Q_\mathrm{t}g_{\boldsymbol{P},\boldsymbol{Q}_\mathrm{t}}(P,Q_\mathrm{t})dQ_\mathrm{t}\right]dP+\int_{\Omega_{\boldsymbol{P}}>K_\mathrm{t}}\left[\int_{\Omega_{\boldsymbol{Q}_\mathrm{t}}} Q_\mathrm{t}\left((1-\rho)P+\rho K_\mathrm{t}\right)g_{\boldsymbol{P},\boldsymbol{Q}_\mathrm{t}}(P,Q_\mathrm{t})dQ_\mathrm{t}\right]dP-c_\mathrm{t}^V\mathbb{E}_{\mathbb{P}_{\boldsymbol{Q}_\mathrm{t}}}[\boldsymbol{Q}_\mathrm{t}]-F_\mathrm{t}$$
$$\geq 0$$

$$\Leftrightarrow \int_{\Omega_{\boldsymbol{P}}<K_\mathrm{t}} K_\mathrm{t}\left[\int_{\Omega_{\boldsymbol{Q}_\mathrm{t}}} Q_\mathrm{t}g_{\boldsymbol{Q}_\mathrm{t}|\boldsymbol{P}=P}(Q_\mathrm{t}|P)g_{\boldsymbol{P}}(P)dQ_\mathrm{t}\right]dP+\int_{\Omega_{\boldsymbol{P}}>K_\mathrm{t}}\left[\int_{\Omega_{\boldsymbol{Q}_\mathrm{t}}} Q_\mathrm{t}\left((1-\rho)P+\rho K_\mathrm{t}\right)g_{\boldsymbol{Q}_\mathrm{t}|\boldsymbol{P}=P}(Q_\mathrm{t}|P)g_{\boldsymbol{P}}(P)dQ_\mathrm{t}\right]dP$$
$$-c_\mathrm{t}^V\mathbb{E}_{\mathbb{P}_{\boldsymbol{Q}_\mathrm{t}}}[\boldsymbol{Q}_\mathrm{t}]-F_\mathrm{t}\geq 0$$

$$\Leftrightarrow \int_{\Omega_{\boldsymbol{P}}<K_\mathrm{t}} K_\mathrm{t}g_{\boldsymbol{P}}(P)\mathbb{E}_{\mathbb{P}_{\boldsymbol{Q}_\mathrm{t}|\boldsymbol{P}=P}}[\boldsymbol{Q}_\mathrm{t}|\boldsymbol{P}=P]dP+\int_{\Omega_{\boldsymbol{P}}>K_\mathrm{t}}\rho K_\mathrm{t}g_{\boldsymbol{P}}(P)\mathbb{E}_{\mathbb{P}_{\boldsymbol{Q}_\mathrm{t}|\boldsymbol{P}=P}}[\boldsymbol{Q}_\mathrm{t}|\boldsymbol{P}=P]dP+(1-\rho)\int_{\Omega_{\boldsymbol{P}}>K_\mathrm{t}} Q_g P g_{\boldsymbol{P},\boldsymbol{Q}_\mathrm{t}}(P,Q_\mathrm{t})dPdQ_\mathrm{t}$$
$$-c_\mathrm{t}^V\mathbb{E}_{\mathbb{P}_{\boldsymbol{Q}_\mathrm{t}}}[\boldsymbol{Q}_\mathrm{t}]-F_\mathrm{t}\geq 0$$

$$\Leftrightarrow K_\mathrm{t}G_{\boldsymbol{P}}(K_\mathrm{t})\mathbb{E}_{\mathbb{P}_{\boldsymbol{P}}}[\boldsymbol{P}|\boldsymbol{P}<K_\mathrm{t}]+\rho K_\mathrm{t}\left(1-G_{\boldsymbol{P}}(K_\mathrm{t})\right)\mathbb{E}_{\mathbb{P}_{\boldsymbol{P}}}[\boldsymbol{P}|\boldsymbol{P}>K_\mathrm{t}]+(1-\rho)\left(1-G_{\boldsymbol{P}}(K_\mathrm{t})\right)\mathbb{E}_{\mathbb{P}_{\boldsymbol{P}}\times\mathbb{P}_{\boldsymbol{Q}_\mathrm{t}}}[h_2(\boldsymbol{Q}_\mathrm{t},\boldsymbol{P})|\boldsymbol{P}>K_\mathrm{t}]$$
$$-c_\mathrm{t}^V\mathbb{E}_{\mathbb{P}_{\boldsymbol{Q}_\mathrm{t}}}[\boldsymbol{Q}_\mathrm{t}]-F_\mathrm{t}\geq 0$$

$$\Leftrightarrow K_\mathrm{t}\left(G_{\boldsymbol{P}}(K_\mathrm{t})\mathbb{E}_{\mathbb{P}_{\boldsymbol{P}}}[\boldsymbol{P}|\boldsymbol{P}<K_\mathrm{t}]+\rho\left(1-G_{\boldsymbol{P}}(K_\mathrm{t})\right)\mathbb{E}_{\mathbb{P}_{\boldsymbol{P}}}[\boldsymbol{P}|\boldsymbol{P}>K_\mathrm{t}]\right)$$
$$\geq c_\mathrm{t}^V+F_\mathrm{t}\mathbb{E}_{\mathbb{P}_{\boldsymbol{Q}_\mathrm{t}}}[\boldsymbol{Q}_\mathrm{t}]^{-1}-(1-\rho)\left(1-G_{\boldsymbol{P}}(K_\mathrm{t})\right)\mathbb{E}_{\mathbb{P}_{\boldsymbol{P}}\times\mathbb{P}_{\boldsymbol{Q}_\mathrm{t}}}[h_2(\boldsymbol{Q}_\mathrm{t},\boldsymbol{P})|\boldsymbol{P}>K_\mathrm{t}]$$

$$\Leftrightarrow K_g\geq\frac{c_\mathrm{t}^V+F_\mathrm{t}\mathbb{E}_{\mathbb{P}_{\boldsymbol{Q}_\mathrm{t}}}[\boldsymbol{Q}_\mathrm{t}]^{-1}-(1-\rho)\left(1-G_{\boldsymbol{P}}(K_\mathrm{t})\right)\mathbb{E}_{\mathbb{P}_{\boldsymbol{P}}\times\mathbb{P}_{\boldsymbol{Q}_\mathrm{t}}}[h_2(\boldsymbol{Q}_\mathrm{t},\boldsymbol{P})|\boldsymbol{P}>K_\mathrm{t}]}{\left(G_{\boldsymbol{P}}(K_\mathrm{t})\mathbb{E}_{\mathbb{P}_{\boldsymbol{P}}}[\boldsymbol{P}|\boldsymbol{P}<K_\mathrm{t}]+\rho\left(1-G_{\boldsymbol{P}}(K_\mathrm{t})\right)\mathbb{E}_{\mathbb{P}_{\boldsymbol{P}}}[\boldsymbol{P}|\boldsymbol{P}>K_\mathrm{t}]\right)}$$

For $\rho=1$, we can easily verify that $K_\mathrm{t}^*\geq c_\mathrm{t}^V+F_\mathrm{t}\mathbb{E}_{\mathbb{P}_{\boldsymbol{Q}_\mathrm{t}}}[\boldsymbol{Q}_\mathrm{t}]^{-1}$ such that it yields a null expected profit for technology $\mathrm{t}\in\mathcal{D}$:

$$\mathbb{E}_{\mathbb{P}_{\boldsymbol{P}}\times\mathbb{P}_{\boldsymbol{Q}_\mathrm{t}}}\left[h_1\left(\boldsymbol{Q}_\mathrm{t},\boldsymbol{\Upsilon}_{\boldsymbol{P},\boldsymbol{Q}_\mathrm{t}}\right)\right]-\mathbb{E}_{\mathbb{P}_{\boldsymbol{Q}_\mathrm{t}}}[\boldsymbol{Q}_\mathrm{t}]c_\mathrm{t}^V-F_\mathrm{t}\geq 0$$

$$\Leftrightarrow \int_{\Omega_{Q_t}} \left[\int_{\Omega_P} Q_t Y_{P,K_t} g_{\boldsymbol{P},\boldsymbol{Q}_t}(P, Q_t) dP \right] dQ_t - c_t^V \mathbb{E}_{\mathbb{P}_{\boldsymbol{Q}_t}}[\boldsymbol{Q}_t] - F_t \geq 0$$

$$\Leftrightarrow \int_{\Omega_{Q_t}} \left[\int_{\Omega_P} Q_t (P + (K_t - P)^+ - (P - K_t)^+) g_{\boldsymbol{P},\boldsymbol{Q}_t}(P, Q_t) dP \right] dQ_t - c_t^V \mathbb{E}_{\mathbb{P}_{\boldsymbol{Q}_t}}[\boldsymbol{Q}_t] - F_t \geq 0$$

$$\Leftrightarrow K_t \int_{\Omega_{Q_t}} Q_t \left[\int_{\Omega_P} g_{\boldsymbol{P},\boldsymbol{Q}_t}(P, Q_t) dP \right] dQ_t - c_t^V \mathbb{E}_{\mathbb{P}_{\boldsymbol{Q}_t}}[\boldsymbol{Q}_t] - F_t \geq 0$$

$$\Leftrightarrow K_t \int_{\Omega_{Q_t}} Q_t g_{\boldsymbol{Q}_t}(Q_t)\, dQ_t - c_t^V \mathbb{E}_{\mathbb{P}_{\boldsymbol{Q}_t}}[\boldsymbol{Q}_t] - F_t \geq 0$$

$$\Leftrightarrow K_t \mathbb{E}_{\mathbb{P}_{\boldsymbol{Q}_t}}[\boldsymbol{Q}_t] - c_t^V \mathbb{E}_{\mathbb{P}_{\boldsymbol{Q}_t}}[\boldsymbol{Q}_t] - F_t \geq 0$$

$$\Leftrightarrow K_t \geq c_t^V + F_t \mathbb{E}_{\mathbb{P}_{\boldsymbol{Q}_t}}[\boldsymbol{Q}_t]^{-1}$$

By plugging $K_t^* = c_t^V + F_t \mathbb{E}_{\mathbb{P}_{\boldsymbol{Q}_t}}[\boldsymbol{Q}_t]^{-1}$, we have:

$$\int_{\Omega_{Q_t}} \left[\int_{\Omega_P} Q_t Y_{P,K_t} d\mathbb{P}_{\boldsymbol{P},\boldsymbol{Q}_t}(P, Q_t) \right] - c_t^V \int_{\Omega_{Q_t}} Q_t d\mathbb{P}_{\boldsymbol{Q}_t}(Q_t) - F_t$$

$$= \int_{\Omega_{Q_t}} Q_t \left(c_t^V + F_t \mathbb{E}_{\mathbb{P}_{\boldsymbol{Q}_t}}[\boldsymbol{Q}_t]^{-1} \right) \left[\int_{\Omega_P} d\mathbb{P}_{\boldsymbol{P}}(P) \right] d\mathbb{P}_{\boldsymbol{Q}_t}(Q_t) - c_t^V \int_{\Omega_{Q_t}} Q_t d\mathbb{P}_{\boldsymbol{Q}_t}(Q_t) - F_t$$

$$= \left(c_t^V + F_t \mathbb{E}_{\mathbb{P}_{\boldsymbol{Q}_t}}[\boldsymbol{Q}_t]^{-1} \right) \mathbb{E}_{\mathbb{P}_{\boldsymbol{Q}_t}}[\boldsymbol{Q}_t] - c_t^V \mathbb{E}_{\mathbb{P}_{\boldsymbol{Q}_t}}[\boldsymbol{Q}_t] - F_t$$

$$= 0$$

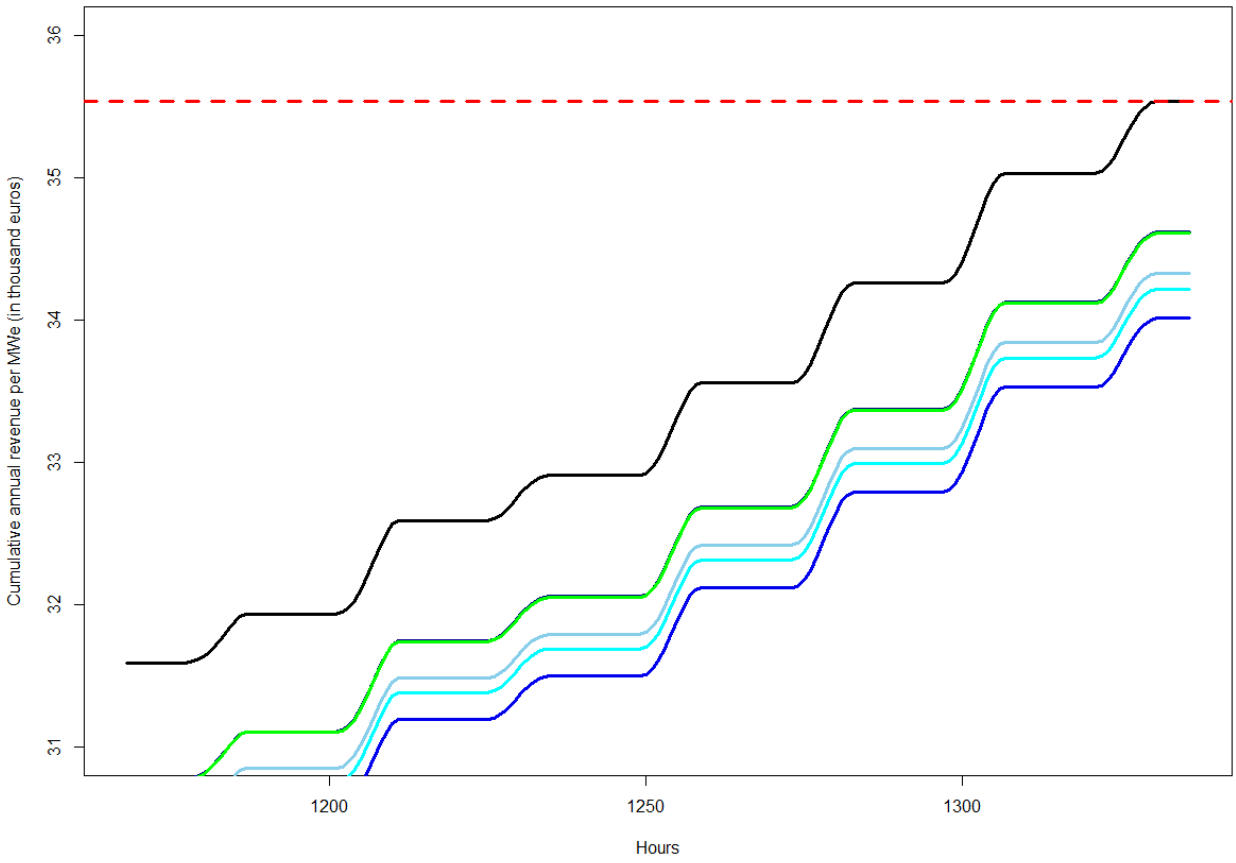

Figure 12.C.: Cumulative total revenue per MWe of installed solar, under various computation basis

Note: The plain black (resp. dark blue, blue, clear blue, cyan and green) line corresponds the cumulative sum of total revenues, including both market remuneration and CfD remuneration, when taking the computation period 2013-2018 (resp. 2014-2018, 2015-2018, 2016-2018, 2017-2018 and 2018). Only the 168 last hours of the set of representative weeks are represented.

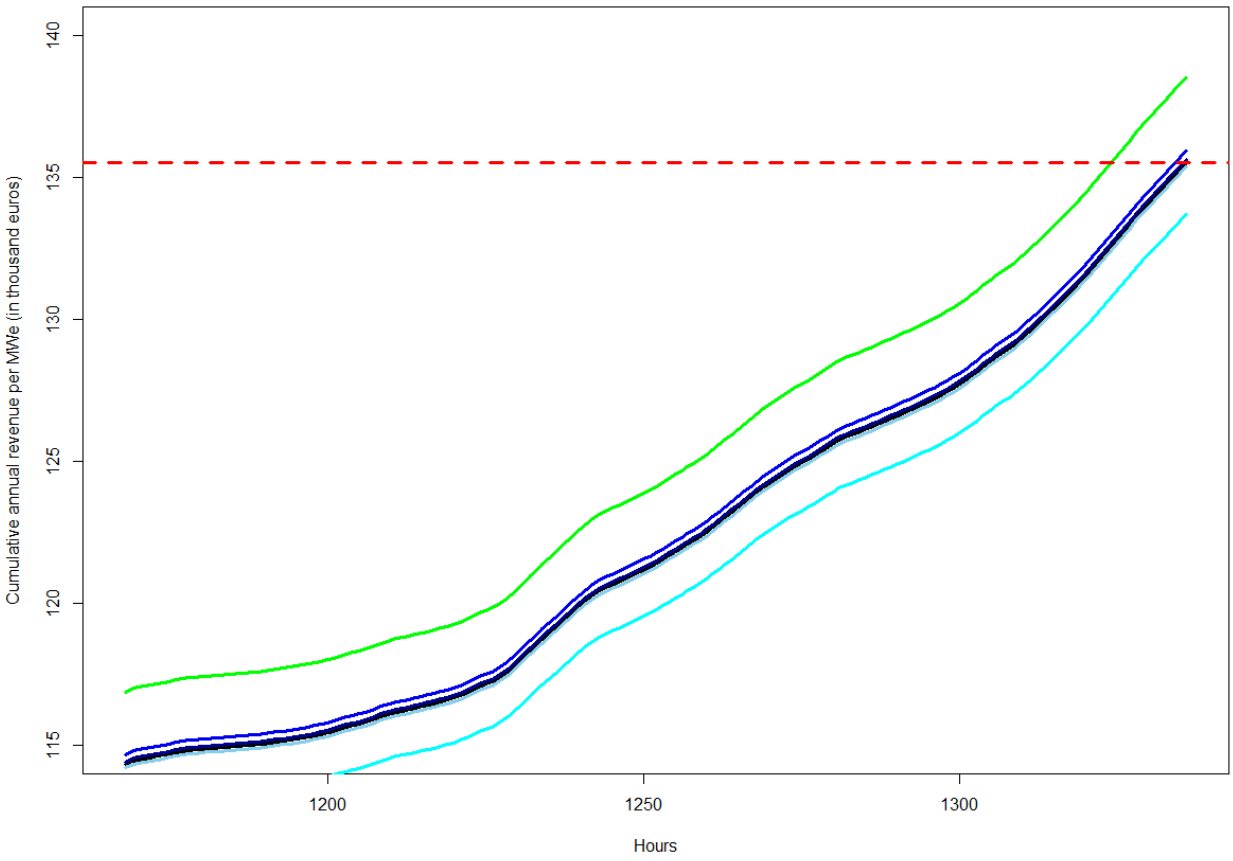

Figure 12.D.: Cumulative total revenue per MWe of installed wind power, under various computation basis

Proof 2:

$$W(\vec{K})^{*} = \sum_{t\in\mathcal{D}} \left(\mathbb{E}_{\mathbb{P}_{\boldsymbol{P}}\times\mathbb{P}_{\boldsymbol{Q}_t}} \left[h_3\left(\boldsymbol{Q}_t, \boldsymbol{\Upsilon}_{\boldsymbol{P},\boldsymbol{K}_t}\right) \right] \right)$$

$$= \sum_{t\in\mathcal{D}} \left(\iint_{\Omega_{\boldsymbol{Q}_t}\times\Omega_{\boldsymbol{P}}} Q_t((K_t^{*} - P)^{+} - \rho(P - K_t^{*})^{+}) d\mathbb{P}_{\boldsymbol{Q}_t,\boldsymbol{P}}(Q_t, P) \right)$$

$$= \sum_{t\in\mathcal{D}} \left(\iint_{\Omega_{\boldsymbol{Q}_t}\times\Omega_{\boldsymbol{P}}} Q_t((K_t^{*} - P)^{+} - \rho(P - K_t^{*})^{+}) g_{\boldsymbol{P},\boldsymbol{Q}_t}(P, Q_t) dP dQ_t \right)$$

$$= \sum_{t\in\mathcal{D}} \left(\int_{\Omega_{\boldsymbol{P}}<K_t^{*}} \left[\int_{\Omega_{Q_t}} Q_t(K_t^{*} - P) g_{\boldsymbol{P},\boldsymbol{Q}_t}(P, Q_t) dQ_t \right] dP - \rho \int_{\Omega_{\boldsymbol{P}}>K_t^{*}} \left[\int_{\Omega_{Q_t}} Q_t(P - K_t^{*}) g_{\boldsymbol{P},\boldsymbol{Q}_t}(P, Q_t) dQ_t \right] dP \right)$$

$$= \sum_{t\in\mathcal{D}} \left(\int_{\Omega_{\boldsymbol{P}}<K_t^*} K_t^* \left[\int_{\Omega_{\boldsymbol{Q}_t}} Q_t g_{\boldsymbol{Q}_t|\boldsymbol{P}=P}(Q_t|P) g_{\boldsymbol{P}}(P) dQ_t \right] dP - \rho K_t^* \int_{\Omega_{\boldsymbol{P}}>K_t^*} \left[\int_{\Omega_{\boldsymbol{Q}_t}} Q_t g_{\boldsymbol{Q}_t|\boldsymbol{P}=P}(Q_t|P) g_{\boldsymbol{P}}(P) dQ_t \right] dP \right.$$
$$\left. - \int_{\Omega_{\boldsymbol{P}}<K_t^*} \left[\int_{\Omega_{\boldsymbol{Q}_t}} Q_t P g_{\boldsymbol{Q}_t|\boldsymbol{P}=P}(Q_t|P) g_{\boldsymbol{P}}(P) dQ_t \right] dP + \rho \int_{\Omega_{\boldsymbol{P}}>K_t^*} \left[\int_{\Omega_{\boldsymbol{Q}_t}} Q_t P g_{\boldsymbol{Q}_t|\boldsymbol{P}=P}(Q_t|P) g_{\boldsymbol{P}}(P) dQ_t \right] \right)$$

$$= \sum_{t\in\mathcal{D}} \left(K_t^* \int_{\Omega_{\boldsymbol{P}}<K_t^*} g_{\boldsymbol{P}}(P) \mathbb{E}_{\mathbb{P}_{\boldsymbol{Q}_t|P=P}}[\boldsymbol{Q}_t|\boldsymbol{P}=P] dP - \rho K_t^* \int_{\Omega_{\boldsymbol{P}}>K_t^*} g_{\boldsymbol{P}}(P) \mathbb{E}_{\mathbb{P}_{\boldsymbol{Q}_t|P=P}}[\boldsymbol{Q}_t|\boldsymbol{P}=P] dP \right.$$
$$\left. - \int_{\Omega_{\boldsymbol{P}}<K_t^*} \left[\int_{\Omega_{\boldsymbol{Q}_t}} Q_t P g_{\boldsymbol{P},\boldsymbol{Q}_t}(P, Q_t) dP dQ_t \right] dP + \rho \int_{\Omega_{\boldsymbol{P}}>K_t^*} \left[\int_{\Omega_{\boldsymbol{Q}_t}} Q_t P g_{\boldsymbol{P},\boldsymbol{Q}_t}(P, Q_t) dP dQ_t \right] \right)$$

$$= \sum_{t\in\mathcal{D}} \left(K_t^* G_{\boldsymbol{P}}(K_t^*) \mathbb{E}_{\mathbb{P}_{\boldsymbol{P}}}[\boldsymbol{P}|\boldsymbol{P} < K_t^*] - \rho K_t^* \left(1 - G_{\boldsymbol{P}}(K_t^*)\right) \mathbb{E}_{\mathbb{P}_{\boldsymbol{P}}}[\boldsymbol{P}|\boldsymbol{P} > K_t^*] - G_{\boldsymbol{P}}(K_t^*) \mathbb{E}_{\mathbb{P}_{\boldsymbol{Q}_t,\mathbb{P}_{\boldsymbol{P}}}}[h_2(\boldsymbol{Q}_t, \boldsymbol{P})|\boldsymbol{P} < K_t^*] \right.$$
$$\left. + \rho \left(1 - G_{\boldsymbol{P}}(K_t^*)\right) \mathbb{E}_{\mathbb{P}_{\boldsymbol{Q}_t},\mathbb{P}_{\boldsymbol{P}}}[h_2(\boldsymbol{Q}_t, \boldsymbol{P})|\boldsymbol{P} > K_t^*] \right)$$

$$= \sum_{t\in\mathcal{D}} \left(K_t^* \left(G_{\boldsymbol{P}}(K_t^*) \mathbb{E}_{\mathbb{P}_{\boldsymbol{P}}}[\boldsymbol{P}|\boldsymbol{P} < K_t^*] - \rho \left(1 - G_{\boldsymbol{P}}(K_t^*)\right) \mathbb{E}_{\mathbb{P}_{\boldsymbol{P}}}[\boldsymbol{P}|\boldsymbol{P} > K_t^*] \right) - G_{\boldsymbol{P}}(K_t^*) \mathbb{E}_{\mathbb{P}_{\boldsymbol{P}}\times\mathbb{P}_{\boldsymbol{Q}_t}}[h_2(\boldsymbol{Q}_t, \boldsymbol{P})|\boldsymbol{P} < K_t^*] \right.$$
$$\left. + \rho \left(1 - G_{\boldsymbol{P}}(K_t^*)\right) \mathbb{E}_{\mathbb{P}_{\boldsymbol{P}}\times\mathbb{P}_{\boldsymbol{Q}_t}}[h_2(\boldsymbol{Q}_t, \boldsymbol{P})|\boldsymbol{P} > K_t^*] \right)$$

The above result greatly simplifies for $\rho = 1$:

$$W(\vec{K})^* = \sum_{t\in\mathcal{D}} \left(\iint_{\Omega_{\boldsymbol{Q}_t}\times\Omega_{\boldsymbol{P}}} Q_t ((K_t^* - P)^+ - (P - K_t^*)^+) g_{\boldsymbol{P},\boldsymbol{Q}_t}(P, Q_t) dP dQ_t \right)$$

$$= \sum_{t\in\mathcal{D}} \left(\int_{\Omega_{\boldsymbol{P}}<K_t} \left[\int_{\Omega_{\boldsymbol{Q}_t}} Q_t (K_t^* - P) g_{\boldsymbol{P},\boldsymbol{Q}_t}(P, Q_t) dQ_t \right] dP - \int_{\Omega_{\boldsymbol{P}}>K_t} \left[\int_{\Omega_{\boldsymbol{Q}_t}} Q_t (P - K_t^*) g_{\boldsymbol{P},\boldsymbol{Q}_t}(P, Q_t) dQ_t \right] dP \right)$$

$$= \sum_{t\in\mathcal{D}} \left(\int_{\Omega_{\boldsymbol{Q}_t}} Q_t K_t^* dQ_t - \left(\int_{\Omega_{\boldsymbol{P}}<K_t^*} \left[\int_{\Omega_{\boldsymbol{Q}_t}} Q_t P g_{\boldsymbol{P},\boldsymbol{Q}_t}(P, Q_t) dQ_t \right] dP + \int_{\Omega_{\boldsymbol{P}}>K_t^*} \left[\int_{\Omega_{\boldsymbol{Q}_t}} Q_t P g_{\boldsymbol{P},\boldsymbol{Q}_t}(P, Q_t) dQ_t \right] dP \right) \right)$$

$$= \sum_{t\in\mathcal{D}} \left(K_t^* \mathbb{E}_{\mathbb{P}_{\boldsymbol{Q}_t}}[\boldsymbol{Q}_t] - \mathbb{E}_{\mathbb{P}_{\boldsymbol{P}}\times\mathbb{P}_{\boldsymbol{Q}_t}}[\boldsymbol{P}\boldsymbol{Q}_t] \right)$$

$$= \sum_{t\in\mathcal{D}} \left(\left(c_t^V + F_t \mathbb{E}_{\mathbb{P}_{\boldsymbol{Q}_t}}[\boldsymbol{Q}_t]^{-1} \right) \mathbb{E}_{\mathbb{P}_{\boldsymbol{Q}_t}}[\boldsymbol{Q}_t] - \mathbb{E}_{\mathbb{P}_{\boldsymbol{P}}\times\mathbb{P}_{\boldsymbol{Q}_t}}[h_2(\boldsymbol{Q}_t, \boldsymbol{P})] \right)$$

$$= \sum_{t\in\mathcal{D}} \left(c_t^V \mathbb{E}_{\mathbb{P}_{\boldsymbol{Q}_t}}[\boldsymbol{Q}_t] + F_t - \mathbb{E}_{\mathbb{P}_{\boldsymbol{P}}\times\mathbb{P}_{\boldsymbol{Q}_t}}[h_2(\boldsymbol{Q}_g, \boldsymbol{P})] \right)$$

7. Bibliography

[1] MACHENAUD Hervé, *La France dans le noir : les méfaits de l'idéologie en politique énergétique*, Manitoba, Entreprise et Société, 2017, 120 p.

[2] SENSFUSS Frank, RAGWITZ Mario, GENOESE Massimo, "The merit-order effect: A detailed analysis of the price effect of renewable energy generation on spot market prices in Germany", *Energy Policy*, vol. 36, n°8, 2008, pp. 3086-3094

[3] PAGNIER Laurent & JACQUOD Philippe, "How fast can one overcome the paradox of the energy transition? A physico-economic model for the European power grid", *Energy*, vol. 157, 2018, pp. 550-560

[4] MARTIN DE LAGARDE Cyril, LANTZ Frédéric, "How renewable production depresses electricity prices: Evidence from the German market", *Energy Policy*, vol. 117, 2018, pp. 263-277

[5] PERCEBOIS Jacques & POMMERET Stanislas, "Coût complet lié à l'injection d'électricité renouvelable intermittente ; approche modélisée sur le marché français « day-ahead »", *Cahiers de recherche du CREDEN*, n°16.07.115, 2016

[6] SHANKER R., "Comments on standard market design: resource adequacy requirements", *FERC*, Docket RM-01-12-000, 2003

[7] LESLIE Gordon W., STERN David I., SHANKER Ashley, HOGAN Michael T., "Designing electricity markets for high penetrations of zero or low marginal cost intermittent energy sources", *The Electricity Journal*, vol. 33, 2020

[8] BILLIMORIA Farhad, POUDINEH Rahmatallah, "Decarbonized Market Design: An Insurance Overlay on Energy-Only Electricity Markets", The Oxford Institute for Energy Studies, OEIS Paper: EL 30, 2018, 26 p.

[9] BESSEC Marie, FOUQUAU Julien, MERITET Sophie, "Forecasting electricity spot prices using time-series models with a double temporal segmentation", 2nd International Symposium on Energy and Finance Issues (ISEFI-2014), March 2014, Paris, France, 34 p.

[10] HIRTH Lion, “The market value of variables renewables: The effect of solar wind power variability on their relative price”, *Energy Economics,* vol. 38, 2013, pp. 218-236

[11] PETITET Marie, FINON Dominique, JANSSEN Tanguy, “Carbon Price instead of Support Schemes: Wind Power Investments by the Electricity Market”, *The Energy Journal,* vol. 37, n°4, 2016

[12] CRAMTON Peter, “Electricity market design”, *Oxford Review of Economic Policy,* vol. 33, n°4, pp. 589-612

[13] BORENSTEIN Severin, “The economics of fixed cost recovery by utilities”, *The Electricity Journal,* n°29, 2016, pp. 5-12

[14] BORENSTEIN Severin, “Understanding competitive pricing and market power in wholesale electricity markets”, *The Electricity Journal,* vol. 13, 2000, pp. 49-57

[15] BORENSTEIN Severin, “The Redistributional Impact of Nonlinear Electricity Pricing”, *American Economic Journal: Economic Policy,* vol. 4, n°3, 2012, pp. 56-90

[16] DE SISTERNES Fernando, “Risk Implications of the Deployment of Renewables for Investments in Electricity Generation”, MIT, May 2014

[17] RUIZ C., CONEJO A. J., GABRIEL S. A., “Pricing non-convexities in an electricity pool”, *IEEE Transactions on Power Sytems,* vol. 27, n°3, 2012, pp. 1334-1342

[18] BATTLE Carlos, HERRERO Ignacio, RODILLA Pablo, “Evolving Bidding Formats and Pricing Schemes in US and Europe Day-Ahead Electricity Markets”, MIT CEEPR Working Paper 2020-013, 38 p.

[19] BLANCO R., ARROYO J., ALGUACIL N., “On the solution of revenue and network constrained day ahead market clearing under marginal pricing – part I: An exact bilevel programming approach”, IEEE Transactions on power systems, vol. 32, 2017, pp. 208-219

[20] HEISTRENE Leena, MISHRA Poonam, LOKHANDE Makarand, “Stochastic Market Clearing With Revenue Sufficiency Constraints”, *Energy Procedia,* vol. 158, 2019, pp. 3840-3845

[21] HEDAYATI-MEHDIABADI Mojgan, ZHANG Junshan, HEDMAN Kory W., “Wind Power Dispatch Margin for Flexible Energy and Reserve Scheduling with Increased Wind Generation”, *IEEE Transaction on Sustainable Energy*, vol. 6, n°4, pp. 1543-1552

[22] PAPAVASILIOU Anthony, “Scarcity pricing and the missing European market for real-time reserve capacity”, *The Electricity Journal*, vol. 33, 2020

[23] YAFFE David P., TABAK Gabriel L., “Why capacity markets are the Fitbits of the electric utility industry”, *The Electricity Journal*, vol. 31, 2018, pp. 32-38

[24] HOGAN Michael T., “Follow the missing money: Ensuring reliability at least cost to consumers in the transition to a low-carbon power system”, *The Electricity Journal*, vol. 30, 2017, pp. 55-61

[25] DAMBRINE Fabrice, “Analyse micro-économique de l’intégration des EnR électriques intermittentes dans un système de production électrique”, *Responsabilité & Environnement*, Annales des Mines, n°93, 2019, pp. 7-14

[26] PERCEBOIS Jacques, “Les défis de la transformation du secteur électrique européen”, *Etudes de l’Ifri*, Ifri, 2019, 52 p.

[27] PERCEBOIS Jacques & POMMERET, “Storage Cost Induced by a Large Substitution of Nuclear by Intermittent Renewable Energies: The French Case”, *Energy Policy*, vol. 135, 2019

[28] BROWN Barbara G., KATZ Richard W., MURPHY Allan H., “Time Series Models to Simulate and Forecast Wind Speed and Wind Power”, *Journal of Climate and Applied Meteorology*, vol. 23, 1984, pp. 1184-1195

[29] PINSON Pierre, *Estimation of the uncertainty in wind power forecasting*, Engineering Sciences [Physics], Ecole Nationale Supérieure des Mines de Paris, 2006, English. NNT: 2006ENMP1432ff. ffpastel00002187

[30] KEAY M. & ROBINSON D., “Market design for a decarbonized electricity market the “two market” approach”, in ROSETTO N. (ed.), *Design the Electricity Market(s) of the Future*, proceedings for the Eurelectric-Florence School of Regulation Conference, 7 June 2017

[31] SILVA-RODRIGUEZ L., SANJAB A., FUMAGALLI E., VIRAG A., GIBESCU M., “Short Term Electricity Market Designs: Identified Challenges and Promising Solutions”, Papers 2011.04587, arXiv.org., 19 p.

[32] HOGAN William H., “Electricity Scarcity Pricing Through Operating Reserves”, *Economics of Energy & Environmental Policy*, vol. 2, n°2, 2013

[33] PERCEBOIS Jacques, “Aides publiques aux énergies éolienne et photovoltaïque”, *Revue française d’économie*, vol. 30, n°4, 2015, pp. 146-186

[34] GREEN Richard J. & LEAUTIER Thomas-Olivier, “Do costs fall faster than revenues? Dynamics of renewables entry into electricity markets”, TSE Working Paper 15-191, Toulouse School of Economics, 2015

[35] SARTOR Olivier & BATAILLE Chris, “Decarbonizing basic materials in Europe: How Carbon Contracts-for-Difference could help bring breakthrough technologies to market”, IDDRI Sustainable Development & International Relations, Sciences Po, n°6, 2019

[36] RICHSTEIN J., “Project-Based Carbon Contracts: A Way to Finance Innovative Low-Carbon Investments”, DIW Discussion Paper n°1714, 2017

[37] MANOVE Michael, “Provider Insurance”, *The Bell Journal of Economics*, vol. 14, n°2, 1983, pp. 489-496

[38] VICKREY William, “Counterspeculation, Auctions, and Competitive Sealed Tenders”, *The Journal of Finance*, vol. 16, n°1, 1961, pp. 8-37

[39] BUSHNELL James, FLAGG Michael, MANSUR Erin, “Capacity Markets at a Crossroads”, Energy Institute at Haas, EI-Haas WP 278, 2017, 59 p.

[40] SCHRÖDER Thomas & KUCKSHINRICHS Wilhelm, “Value of Lost Load: An Efficiency Economic Indicator for Power Supply Security? A Literature Review”, *Frontiers in Energy Research*, vol. 3, 2015

[41] BILLINTON R., TOLLEFSON G., WACKER G., “Assessment of electric service reliability worth”, *International Journal of Electrical Power & Energy Systems*, vol. 15, 1993, pp. 95-100

[42] DE NOOIJ M., KOOPMANS C., BIJVOET C., “The value of supply security. The costs of power interruptions: economic input for damage reduction and investment in networks”, *Energy Economics*, vol. 29, 2007, pp. 275-295